

This electronic thesis or dissertation has been downloaded from the King's Research Portal at <https://kclpure.kcl.ac.uk/portal/>



Cardiac Signalling Processes involving Obscurin and Phospholamban

Koch, Daniel

Awarding institution:
King's College London

The copyright of this thesis rests with the author and no quotation from it or information derived from it may be published without proper acknowledgement.

END USER LICENCE AGREEMENT



Unless another licence is stated on the immediately following page this work is licensed under a Creative Commons Attribution-NonCommercial-NoDerivatives 4.0 International licence. <https://creativecommons.org/licenses/by-nc-nd/4.0/>

You are free to copy, distribute and transmit the work

Under the following conditions:

- Attribution: You must attribute the work in the manner specified by the author (but not in any way that suggests that they endorse you or your use of the work).
- Non Commercial: You may not use this work for commercial purposes.
- No Derivative Works - You may not alter, transform, or build upon this work.

Any of these conditions can be waived if you receive permission from the author. Your fair dealings and other rights are in no way affected by the above.

Take down policy

If you believe that this document breaches copyright please contact librarypure@kcl.ac.uk providing details, and we will remove access to the work immediately and investigate your claim.

**Cardiac Signalling Processes involving
Obscurin and Phospholamban**
Biochemical and Theoretical Studies



Daniel Koch

Randall Centre for Cell & Molecular Biophysics
King's College London

This dissertation is submitted for the degree of
Doctor of Philosophy

September 2021

Abstract

The human heart beats more than two billion times over the average human lifespan. To maintain reliable functioning of this organ throughout a lifetime, the molecular architecture underlying contraction and relaxation of the heart's muscle cells has evolved to withstand the continuous mechanical strain and to dynamically adapt the workload to the oxygen demand of the body. Such adaptation is regulated by biochemical networks which process the information contained in various humoral and mechanical signals.

Among the largest molecules in heart muscle cells is the protein obscurin. It provides a direct physical link between the sarcomere, the contractile machinery of the cell, and the sarcoplasmic reticulum from which the calcium transients originate that control contraction. Obscurin also features multiple, yet barely characterised signalling domains including two kinase domains, an SH3 domain and a DH-PH Rho GEF domain tandem, suggesting obscurin may be involved in complex signalling functions. Although increasing numbers of missense mutations in the obscurin protein have been associated with cardiomyopathies and skeletal muscle diseases, the mechanism of action of these potentially pathogenic variants remains unknown. One of the few genetic variants characterised in more detail is the variant Arg4344Gln in obscurin domain Ig58. Although found in about 1 in 7 African Americans, some scholars argue that this variant is pathogenic because it has been reported to cause dilated cardiomyopathy and cardiac arrhythmias in mice due to a strengthened interaction between obscurin and phospholamban. Phospholamban is among the smallest proteins in heart muscle cells and an important mediator of the "fight-or-flight" response. Under resting conditions, phospholamban inhibits the calcium pump SERCA2a. The binding of catecholamines such as adrenaline to the β -adrenergic receptors of cardiomyocytes leads to activation of protein kinase A which phosphorylates phospholamban and thereby releases SERCA2a inhibition, resulting in faster calcium reuptake into the sarcoplasmic reticulum, faster relaxation and stronger contraction of the heart. Phospholamban, too, can harbour genetic mutations, some of which lead to severe and lethal cardiomyopathies. Phospholamban also forms homo-pentamers whose physiological functions are still unknown.

The present work investigates selected biochemical signal processing aspects of obscurin and phospholamban in the context of cardiomyocyte physiology and genetic mutations.

The first project established the recombinant production of obscurin DH and DH-PH domains and provided a first *in vitro* biochemical characterisation of its catalytic activity, post-translational modification and binding partners. It is found that recombinant DH and DH-PH domains of obscurin purified from *E. coli* do not possess *in vitro* GEF activity towards any classical Rho GTPase but can be phosphorylated and dephosphorylated by several kinases and phosphatases of relevance in cardiac physiology.

A second project systematically investigated the effect of several potentially pathogenic missense mutations in obscurin domains Ig58 and Ig59 on previously reported protein-protein interactions between obscurin and titin, the titin isoform novex-3 and phospholamban. An important finding was that the previously reported interaction with phospholamban is an *in vitro* artefact and that the phenotype observed in Arg4344Gln mice does likely not translate to humans.

A third project studied the potential signal processing abilities of homo-oligomers with a particular emphasis on the physiological role of phospholamban pentamers. Starting with general mathematical models of homo-oligomerisation, it was found that homo-oligomerisation could provide an unanticipated wealth of non-linear dynamics and signal processing functions including

dynamic signal encoding and homeostatic monomer buffering. Furthermore, homo-oligomers are found to constitute pseudo-multisite phosphorylation systems that allow ultrasensitive or bistable steady-state phosphorylation responses in simulations. Applying these concepts to phospholamban demonstrated that phospholamban pentamers indeed cause ultrasensitive and bistable phosphorylation both in numerical simulations and in experiments. Pentamers are moreover found to constitute a substrate competition based low-pass filter for phosphorylation of phospholamban monomers. These mechanisms could contribute to the prevention of cardiac arrhythmias in the context of β -adrenergic stimulation and may be impaired by the pathogenic phospholamban mutation R14del.

Taken together, the presented work contributes to the understanding of several related signal processing functions in heart muscle cells relevant to cardiac physiology and disease.

Acknowledgements

I would like to express my sincere gratitude to everyone who helped or supported me to complete the work presented here.

Firstly, I would like to thank my supervisor, Prof Mathias Gautel, for his support and encouragement during the last 4 years. I would also like to thank him for what could have been an exciting project in which the biochemical characterisation of a Rho GEF is followed up by lots of interesting cell biology in living muscle cells. Alas, nature had other plans and the discovery of the absence of catalytic activity of these domains was followed by a global pandemic, which meant we had not enough time in the lab to develop a completely new experimental approach to this project. All the more, I would like to thank him for giving me the freedom to follow my own ideas and to develop my own, independent projects. Without this scientific freedom, my papers on information processing by homo-oligomers in general and by phospholamban pentamers in particular would not have been possible. For a young scientist, the value of the opportunity to publish papers as single author and as first and corresponding author is hard to overestimate in today's publish-or-perish culture.

I extend my gratitude to all members of the Gautel Group for all their support and the fun times both inside and outside the lab. A special thanks goes to Dr Alexander Alexandrovich without whom I'd still be cloning, expressing and purifying proteins fragments by hand.

Mark Pfuhl, my second supervisor, I would like to thank for helpful advice and for performing the NMR measurements with me.

For many interesting discussions and career advice, I would also like to thank Prof Elisabeth Ehler and Dr Thomas Kampourakis.

For helpful and interesting discussions and advice, I would like to thank Prof Franca Fraternali, Dr Joseph Ng and Dr Stephen Martin.

Dr Florian Funk and Prof Joachim P. Schmitt I would like to thank for their collaboration and many interesting discussions about phospholamban.

The generous studentship and funding of my research throughout the last 4 years by the British Heart Foundation enabled me to completely focus on my research. A big thank you to everyone at the BHF and to all the BHF volunteers who make such brilliant research support possible!

I am very grateful for the support and encouragement from my family and parents throughout my whole studies and for being understanding when I don't find enough time for them!

Finally, I would like to thank Petra, my wife and best friend, for making my life so much brighter. I love you.

Covid-19 impact statement

The impact of the Covid-19 pandemic on this work was a twofold. On the one hand, the restricted access to the laboratory due to social distancing requirements during the year 2020 severely hampered the experimental progress of the obscurin Rho GEF project. Since the results of the *in vitro* approach presented in [chapter 3](#) of this thesis did not reveal any discernible enzymatic activity of the obscurin Rho GEF domains, we planned to complement this line of work by cell biological approaches. For instance, we generated adeno-associated viral constructs of the human obscurin Rho GEF domains for expression and purification of these domains from mammalian cells and for conducting experiments to assess the activity of these domains in living muscle cells using immuno-fluorescence microscopy, pull-down assays and mass-spectrometry based proteomics. However, since time-consuming cell biological experiments were not possible for us during the year 2020, the viral constructs were stored in the ultra-low temperature freezer for >12 months and, unfortunately, lost their biological activity during that time. Similarly, social distancing, reduced supply of cardiomyocytes and reduced access to imaging facilities made experimental testing of the predictions of my phospholamban model more challenging. For instance, planned experiments to test whether hysteresis due to bistable phospholamban phosphorylation can be detected in the calcium transients of living cardiomyocytes could not be done because all training on the microscope required for such experiments was suspended during the year 2020. Moreover, I would have liked to probe hysteretic phospholamban phosphorylation by a more fine-grained concentration range in the isoproterenol dose-response experiments, but a limited supply of cardiomyocytes and time constraints did not allow to conduct more experiments or to further optimise e.g. the separation of phospholamban monomers from other small oligomeric forms.

On the other hand, the limited time spent in the laboratory during the lockdown periods allowed me to dedicate more time to the theoretical concepts and models presented in this thesis, especially the phospholamban model. Furthermore, the circumstances allowed me to write up and publish the work for most of my different projects as peer-reviewed papers timely before submission of this thesis.

Published Articles

Publications which form part of this work:

Koch D. (2020). Homo-Oligomerisation in Signal Transduction: Dynamics, Homeostasis, Ultra-sensitivity, Bistability. *Journal of Theoretical Biology*, 499: 110305.

This paper is the content of chapter 5.

Fukuzawa A., Koch D., Grover S., Rees M., Gautel M. (2021). When is an obscurin variant pathogenic? The impact of Arg4344Gln and Arg4444Trp variants on protein-protein interactions and protein stability. *Human Molecular Genetics*, 30: 1131-1141.

This paper is the content of chapter 4.

Koch D., Alexandrovich A., Funk F., Kho A.L., Schmitt J.P., Gautel M. (2021). Molecular Noise-Filtering in the β -adrenergic Signaling Network by Phospholamban Pentamers. *Cell Reports*, 36: 109448.

This paper is the content of chapter 6.

Contents

Non-standard abbreviations	12
1 Introduction	13
1.1 Background	13
1.2 Anatomy and physiology of the heart	14
1.3 The molecular architecture of cardiomyocytes	16
1.4 Obscurin	16
1.4.1 An obscure muscle giant	16
1.4.2 Localisation of obscurin	18
1.4.3 Functional roles of obscurin	19
1.4.4 Potential functions beyond safeguarding membrane integrity	21
1.4.5 Obscurin in the context of mechanical forces	21
1.5 Signalling processes associated with obscurin	23
1.5.1 Calcium signalling	23
1.5.2 Obscurin kinase domains	23
1.5.3 Obscurin Rho GEF domains	25
1.5.4 Summary of the obscurin interactome	31
1.6 β -adrenergic signalling	31
1.6.1 Regulation of cardiac calcium handling by SERCA and phospholamban in the context of β -adrenergic signalling	32
1.6.2 Phospholamban pentamers and the role of homo-oligomerisation in signalling networks	34
1.7 Medical relevance	35
1.7.1 Heart failure, genetic cardiomyopathies and cardiac arrhythmias	35
1.7.2 Cardiac arrhythmias	39
1.7.3 Current therapy approaches	41
1.7.4 Obscurin in the context of cardiovascular diseases	42
1.7.5 Phospholamban in the context of cardiovascular diseases	43
1.8 Aims and objectives	44
2 Material and Methods	47
2.1 Material	47
2.2 Bioinformatic methods	49
2.2.1 Multiple sequence alignments	49
2.2.2 Evolutionary protein sequence conservation analysis	49

2.2.3	Structure prediction and visualisation	49
2.3	Microbiological and molecular biological methods	50
2.3.1	Transformation of <i>E. coli</i> cells	50
2.3.2	Polymerase chain reaction (PCR)	50
2.3.3	DNA gel-electrophoresis and DNA purification	51
2.3.4	Site-directed mutagenesis	51
2.3.5	Determination of DNA concentration	51
2.3.6	Cloning	52
2.3.7	Preparation of plasmid DNA	52
2.4	Biochemical and biophysical methods	52
2.4.1	Protein expression and affinity-purification	52
2.4.2	Buffer exchange	54
2.4.3	Determination of protein concentration	54
2.4.4	SDS-PAGE	54
2.4.5	Gel staining methods	54
2.4.6	Dot-blotting	54
2.4.7	Measurement of nucleotide exchange kinetics of Rho GTPases	55
2.4.8	Identification of Ser/Thr-kinases that phosphorylation obscurin SH3-DH	56
2.4.9	<i>In vitro</i> phosphorylation of obscurin	56
2.4.10	Identification of the MST2 phosphorylation site in obscurin	56
2.4.11	Dephosphorylation of MST2-phosphorylated obscurin SH3-DH	56
2.4.12	1D-NMR	57
2.4.13	Protein crystallisation trials	57
3	Results	58
3.1	Characterisation of the obscurin Rho GEF domains	58
3.1.1	Introduction	58
3.1.2	Construct design and purification	60
3.1.3	Larger scale purification of two DH domain fragments and analysis of protein folding by NMR	65
3.1.4	Crystallisation trials	65
3.1.5	Catalytic activity of the obscurin Rho GEF domains <i>in vitro</i>	67
3.1.6	Changing species: the potential role of the PH domain	68
3.1.7	Catalytic activity of zebrafish and chimeric ‘mermaid’ obscurin Rho GEF domains <i>in vitro</i>	76
3.1.8	Regulation of the obscurin Rho GEF domains by phosphorylation	77
3.1.9	Discussion	84
4	When is an obscurin variant pathogenic?	87
5	Homo-Oligomerisation in Signal Transduction	99
6	Molecular noise filtering in the β-adrenergic signalling network by phospholamban pentamers	108

7 Conclusion and Outlook	142
7.1 Obscurin Rho GEF domains	142
7.2 Genetic obscurin variants	143
7.3 The potential roles of homo-oligomerisation in biochemical signalling processes – from first principles to preventing cardiac arrhythmias?	144
References	147
Appendix A: Supplementary material for chapter 3	167
A4 Supplementary data	167
A5 Supplementary method details	170
A5.1 Experimental procedure of KinaseFinder screening	175
A5.2 Experimental procedure of phosphorylation site identification	181
Appendix B: Supplementary material for chapter 4	183
Appendix C: Supplementary material for chapter 5	187
Appendix D: Supplementary material for chapter 6	212

List of Figures

1.1	Schematic depiction of the heart from the organ to the subcellular level.	15
1.2	Experimentally confirmed obscurin isoforms and their domain compositions.	17
1.3	Mechanisms of small GTPase signalling.	27
1.4	Obscurin interactome.	31
1.5	Regulation of cardiac calcium cycling by SERCA and phospholamban (PLN).	33
1.6	The hallmarks of heart failure.	37
1.7	Mechanisms of cardiac arrhythmias.	40
3.1	Obscurin Rho GEF domain boundary optimisation for protein expression constructs.	61
3.2	Previously designed constructs of the obscurin Rho GEF domains and their behaviour and properties after large-scale purification.	62
3.3	Design and test-purification of novel obscurin Rho GEF constructs.	63
3.4	Coomassie-stained gel after SDS-PAGE of selected obscurin Rho GEF constructs.	65
3.5	Two-step purification of two obscurin DH domain fragments from 1L <i>E. coli</i> cultures.	66
3.6	Nucleotide exchange of human obscurin Rho GEF fragments towards RhoA, Cdc42, Rac1 and RhoQ at 1.5 μ M [GTPase].	70
3.7	Nucleotide exchange of human obscurin Rho GEF fragments towards RhoB, RhoC, Rac2, Rac3 and RhoG at 1.5 μ M [GTPase].	71
3.8	Catalytic residues at the DH/PH interface.	72
3.9	Chimeric obscurin Rho GEF constructs.	74
3.10	Chimeric and zebrafish obscurin Rho GEF constructs.	75
3.11	Purification of chimeric and zebrafish obscurin Rho GEF constructs.	76
3.12	Nucleotide exchange of chimeric and zebrafish obscurin Rho GEF fragments towards RhoA, Cdc42, Rac1 and RhoQ at 1.5 μ M [GTPase].	78
3.13	Nucleotide exchange activity of zebrafish obscurin DH-PH ₅₈₈₄₋₆₂₁₇ domains towards RhoB, RhoC, Rac2, Rac3 and RhoG at 1.5 μ M.	79
3.14	Identification of kinases that can phosphorylate obscurin Rho GEF domains in a commercial Ser/Thr-kinase screen.	82
3.15	Characterisation of MST2 phosphorylation sites.	83
3.16	Nucleotide exchange of obscurin pThr5798 SH3-DH and pThr5798 DH ₅₆₆₇₋₅₈₈₉ towards RhoA, Cdc42, Rac1 or RhoQ at 1.5 μ M [GTPase].	84
3.17	Comparative sequence analysis of the obscurin DH-PH domains and those of other trio-subfamily GEFs.	86
7.1	Further dynamics resulting from homo-oligomerisation.	144

A2	SDS-PAGE analysis of the purification of LARG and Vav2 DH domains.	167
A3	Results for all kinases in the ProKinase KinaseFinder screen.	168
A4	Nucleotide exchange activity of LARG DH domain in the presence of imidazole towards RhoA at 1.5 μ M [GTPase].	169

List of Tables

2.1	Frequently used chemicals and reagents	47
2.2	Frequently used media	47
2.3	Frequently used protein buffers	48
2.4	Frequently used buffers and stock solutions	49
2.5	Chemically competent <i>E. coli</i> strains used in this study	50
3.1	Crystallisation trials of three obscurin Rho GEF fragments using four different crystal screening suites.	66
A1	Primers used in this study	170
A2	Protein expression constructs used in this study.	172

Non-standard abbreviations

AC: Adenylate cyclase	MWCO: Molecular weight cut-off
ACM: Arrhythmogenic cardiomyopathy	NCX: Sodium-calcium exchanger
AP: Action potential	Ni-NTA: Nickel-nitriloacetic acid
ATP: Adenosine triphosphate	NMR: Nuclear magnetic resonance
CaMK: Calcium/calmodulin dependent kinase	Obsl-1: Obscurin-like 1
cAMP: Cyclic adenosine mono-phosphate	ODE: Ordinary differential equation
DCM: Dilated cardiomyopathy	PCR: Polymerase chain reaction
DH: Dbl homology domain	PH: Pleckstrin homology domain
DHF: Diastolic heart failure	PKA: Protein kinase A
DNA: Deoxyribonucleic acid	PKC: Protein kinase C
DTT: Dithiothreitol	PLN: Phospholamban
ECG: Electro-cardiogram	PP1: Protein phosphatase 1
EDTA: Ethylenediaminetetraacetic acid	PP2A: Protein phosphatase 2A
GAP: GTPase activating protein	ppm: Parts per million (chemical shift in NMR spectra)
GDI: Guanosine-nucleotide dissociation inhibitor protein	PTM: Post-translational modification
GDP: Guanosine diphosphate	RNA: Ribonucleic acid
GEF: Guanosine nucleotide exchange factor	RNAi: Ribonucleic acid interference
GFP: Green fluorescent protein	ROCK: Rho-associated protein kinase
GST: Glutathione-S-transferase	RyR: Ryanodine Receptor
GTP: Guanosine triphosphate	sAnk: Small ankyrin
GTPase: Guanosine triphosphate hydrolase	SDS: Sodium dodecyl sulfate
HCM: Hypertrophic cardiomyopathy	SDS-PAGE: Sodium dodecyl sulfate poly-acrylamide gel-electrophoresis
HEK293 cells: Human embryonic kidney 293 cells	SEC: Size-exclusion chromatography
HF: Heart failure	SERCA: Sarco(endo)-plasmic reticulum Ca^{2+} ATPase
Ig: Immuno-globulin like domain	SH3: Src homology 3 domain
IQ-motif: Isoleucine and glutamine motif	SHF: Systolic heart failure
kDa: kilo-Dalton	siRNA: small interfering ribonucleic acid
Mant-GDP: Methyl-anthraniloyl-guanosine diphosphate	SR: Sarco(endo)-plasmic reticulum
MLCK: Myosin light chain kinase	TEV: Tobacco etch virus
MLCP: Myosin light chain phosphatase	(v/v): Volume per volume
MST: Microscale thermophoresis	(w/v): weight per volume
MST-kinase: Mammalian STE20-like protein kinase	Y2H screen: Yeast-two-hybrid screen
	β 1-AR: β 1-Adrenergic receptor

Chapter 1

Introduction

1.1 Background

The cardiovascular system is responsible for the transport and exchange of gases, metabolites, signal molecules and cellular components between organs and tissues via a continuous circulation of blood. The heart is the muscular pump that maintains the flow of blood through the body's blood vessels via coordinated, periodic contractions throughout an organism's lifetime.

Only by utilising oxygen for ATP synthesis via oxidative phosphorylation can the high energy demands of complex multicellular organisms be met. Since oxygen is normally available at all times in our environment, the capacity of our body to store oxygen or to utilise anaerobic energy production is limited. Under the acute absence of supply, oxygen becomes the limiting factor in cellular ATP production. Without ATP, our cells lack the energy required to maintain their complex organisation and structural integrity: their non-equilibrium organisation disintegrates according to the laws of thermodynamics. Although it is arbitrary to make judgements about the relative importance of the different functions of the cardiovascular system for maintaining physiological homeostasis, its role in supplying oxygen is what makes acute failure lethal.

The relevance of the cardiovascular system for human health is highlighted by the global death statistics: almost a third of all deaths in 2017 were caused by cardiovascular diseases such as ischemic heart disease and stroke (Roth et al. 2018). Although many cases of cardiovascular disease can be attributed to increasing age and lifestyle (unhealthy diet, smoking, lack of exercise), genetic causes for cardiovascular diseases are not uncommon (Eckel 1997; Kannel and McGee 1979; Lavie et al. 2019; North and Sinclair 2012). Familial hypertrophic cardiomyopathy, for instance, affects 1 out of 500 people in the USA and is often caused by genetic mutations impairing the functioning of the sarcomere, i.e. the contractile machinery of heart muscle cells (Alcalai et al. 2008; Marian 2021; Maron and Maron 2013). Even in the absence of monogenic causes, recent evidence from genome-wide association studies showed that the risk for heart diseases such as cardiomyopathy and cardiac arrhythmias is strongly influenced by polygenic factors, i.e. by the presence of multiple (sometimes quite common) genetic variants which can influence how deleterious other mutations will be (Tadros et al. 2021; Roselli et al. 2020; Harper et al. 2021).

At a normal resting heart rate of about 60 to 100 beats per minute, the human heart contracts more than 30 to 50 million times each year, adding up to more than 2 to 3 billion heartbeats over the average human lifespan of 70 years. The continuous mechanical workload and the requirement to dynamically respond to various levels of oxygen demand have shaped the evolution of the

heart including its anatomy and the molecular organisation of its components and regulatory mechanisms. To understand how this biological and molecular organisation regulates and maintains the functioning of the heart with such astonishing fidelity despite its tremendous workload is an ongoing endeavour. Before presenting the questions and aims which motivated the present study, we shall review the required physiological and biochemical context.

1.2 Anatomy and physiology of the heart

A single heartbeat can be subdivided into two main phases: systole and diastole. During systole, the heart contracts, thereby ejecting the blood from the heart chambers into the blood vessels of the circulatory system. During the following diastole, the heart muscle relaxes and dilates so that the heart chambers can refill with blood. To understand how the periodic contraction and relaxation of the heart leads to a unidirectional flow of blood, we will review some basic anatomy of the heart.

The heart consists of four muscular chambers: the left and right ventricle, each of which has a smaller atrial chamber attached to it. The ventricles have strong muscular walls required to eject the blood against the resistance of the connected vessels, whereas the atria have relatively thin walls. Valves between atria and ventricles and valves between ventricles and aorta or pulmonary artery ensure unidirectionality of blood flow (Standring 2016). In order to understand this architecture, it helps to visualise the flow of blood as it passes the different compartments of the heart: deoxygenated blood reaches the heart via the venae cavae (numbers 1 and 2 in Figure 1.1A) and is collected in the right atrium (3). During diastole, the tricuspid valve (4) opens, and blood flows into the right ventricle (5). Oxygenated blood from the lungs reaches the left atrium (9) via the pulmonary veins (8), accordingly. During diastole, the mitral valve (10) opens, allowing the left ventricle (11) to be filled with blood. The valves in the pulmonary artery (6) and aorta (12) are closed during diastole, thereby preventing retrograde blood flow from the lungs or the aorta into the ventricles. During systole, both ventricles contract and build up pressure which closes tricuspid and mitral valves. Once the pressure is high enough, pulmonary and aortic valves give in and blood is ejected from the right ventricle through the pulmonary artery (7) and from the left ventricle via the aorta (13). After systole, the ventricles relax and refilling starts with the next diastole (Hall 2016).

The contractions of the heart are triggered and coordinated by electrical activity: Specialised pace-maker cells localised in the sinoatrial node of the right atrium and the AV-node in the lower interatrial septum of the right atrium before the tricuspid valve generate rhythmic electrical pulses (Hall 2016). These are propagated to the ventricles by the cardiac conduction system consisting of the His-bundle which splits into a left and right bundle branch from which Purkinje-fibres are sprouting, penetrating the depths of the ventricular muscle tissue. The muscle tissue itself is made up of cardiomyocytes, striated muscle cells specific to the heart. Once the electrical activity has reached a cardiomyocyte, it is further propagated to neighbouring cardiomyocytes via gap-junctions which establish electrical coupling between cells (Figure 1.1B) (Hall 2016). Most importantly, cardiomyocytes are responsible for translating the electrical activity of the heart into mechanical activity by contracting. To see how this works, we need to consider their molecular architecture and organisation.

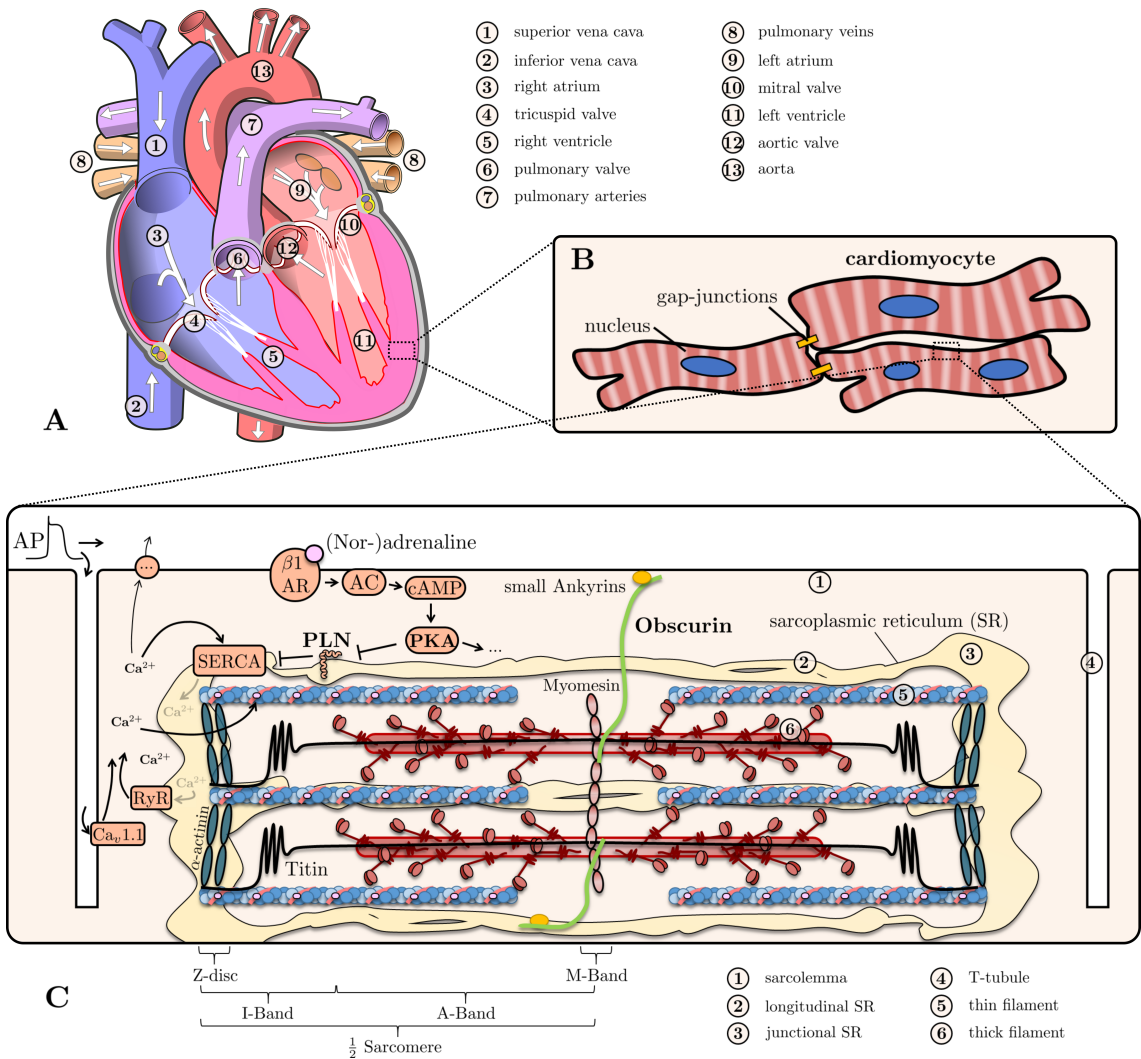


Figure 1.1. Schematic depiction of the heart from the organ to the subcellular level.

A, Anatomy of the heart. Schematic of the fenestrated heart shows the basic four-chamber architecture, afferent and efferent blood vessels and valves. White arrows depict the direction of blood flow. Picture adapted from Wapcaplet, [https://commons.wikimedia.org/wiki/File:Diagram_of_the_human_heart_\(cropped\).svg](https://commons.wikimedia.org/wiki/File:Diagram_of_the_human_heart_(cropped).svg), accessed 18/06/2021, under the Creative Commons Attribution-Share Alike 3.0 Unported licence. **B**, Cardiomyocytes in the heart muscle are responsible for contraction of the heart. Basic features such as their striated appearance and their electrical coupling via gap-junctions are highlighted. **C**, Scheme in the longitudinal axis representing the molecular architecture of cardiomyocytes including the sarcomere, sarcoplasmic reticulum and key molecules involved in excitation-contraction coupling and β -adrenergic signalling. Contraction is initiated by membrane depolarisation which triggers a calcium transient that activates the thin filaments and enables cross-bridge cycling. β -adrenergic stimulation leads to faster relaxation by enhancing SERCA activity via PLN phosphorylation, thereby reducing the time for calcium to be removed after release. The sarcomeric organisation and the positioning of obscurin is essentially identical in skeletal myocytes. Abbreviations: AC = adenylate cyclase, β_1 -AR = β_1 -adrenergic receptor, cAMP = cyclic adenosine mono-phosphate, Ca_v1.1 = voltage-gated L-type calcium channel, PKA = protein kinase A, PLN = phospholamban, RyR = ryanodine receptor, SERCA = sarco(endo)plasmic reticulum calcium ATPase, SR = sarcoplasmic reticulum.

1.3 The molecular architecture of cardiomyocytes

A striking visual hallmark when inspecting cardiomyocytes under a microscope is their striated appearance (Figure 1.1B). These striations result from the highly regular arrangement of myofilaments into sarcomeres (Figure 1.1C). The optical and microscopic appearance resulting from the molecular organisation of its components gave rise to a classification of different sarcomeric regions including Z-disc, I-, A- and M-band. Sarcomeres are the smallest contractile units of muscle fibres and molecular machines responsible for contraction. Among the most prominent structures of sarcomeres are the thin filaments (mainly composed of F-actin) and the thick filaments (mainly consisting of myosin) whose myosin heads are the molecular motors converting the energy stored in the form of ATP into mechanical force. In order to produce force by contraction, however, sarcomeres need to be activated by high intracellular calcium concentration (Ca^{2+}). Importantly, intracellular Ca^{2+} represents the molecular link between the electrical and mechanical activity of the heart (excitation-contraction coupling). If and when electrical activity in form of an action potential (AP) is propagated along the cardiomyocyte membrane (sarcolemma) and into t-tubules, transverse membrane invaginations of the sarcolemma, the membrane depolarisation opens voltage-gated Ca^{2+} -channels (L-type) and allows extracellular Ca^{2+} to enter. The Ca^{2+} influx activates ryanodine receptors (RyRs) on the junctional side of the sarcoplasmic reticulum (SR; the internal calcium storage of cardiomyocytes) which are in juxtaposition to the T-tubular L-Type Ca^{2+} channels (Eisner et al. 2017; Hall 2016). RyR activation triggers further Ca^{2+} efflux from the SR, resulting in a pronounced Ca^{2+} amplitude of up to 600 nM, although local $[\text{Ca}^{2+}]$ can exceed 50 μM (Bers 2002).

Following its release, Ca^{2+} binds to Troponin C of the troponin complex on the thin filaments, resulting in a conformational rearrangement of tropomyosin which leads to the availability of binding sites for myosin heads on the thin filament and thereby enables force production and sarcomeric contraction via cross-bridge cycling (Berg et al. 2015). In order to terminate the contraction, Ca^{2+} needs to be removed from the cytosol again. The sarco(endo)-plasmic reticulum Ca^{2+} ATPase (SERCA) is the calcium pump responsible for removing 70 to >90% of the Ca^{2+} by reuptake into the SR, whereas the remaining Ca^{2+} is removed by the sarcolemmal sodium-calcium exchanger (NCX), the plasma membrane Ca^{2+} -ATPase (PMCA) and mitochondrial uptake (although the latter two mechanisms only account for less than 2% of calcium removal) (Bers 2002). Once enough Ca^{2+} has been removed, the thin filaments switch off and cross-bridge cycling is terminated, the cardiomyocytes relax and become ready for another contraction cycle.

The outlined sequence of mechanisms triggered by electrical stimulation is what is underlying each heart beat on a molecular level. While the molecular details of muscle cell organisation and contraction have been studied for decades, it is becoming increasingly clear that the regulation and maintenance of activity and integrity of the sarcomere and SR requires a multitude of structural and signalling factors.

1.4 Obscurin

1.4.1 An obscure muscle giant

A factor with both structural and putative signalling functions is the giant muscle protein obscurin (Young et al. 2001). Mammalian obscurin has been discovered in 2001 in a yeast-two-hybrid screen

as an interaction partner of the muscle protein titin by Young et al. The protein's unusual name has been chosen by the authors "after the adjective obscure, defined in the New Oxford Dictionary as meaning: (a) difficult to see or make out, (b) not well known, or (c) not easily understood. All three meanings are appropriate to obscurin, which has not been identified previously and has proven difficult to characterise because of its complexity, large size, and relatively low abundance" (Young et al. 2001).

While its interactions with some components of the sarcomere (e.g. titin or myomesin) and SR (small Ankyrin-1) are well established, other interactions (e.g. with phospholamban at the SR) and the role of its signalling domains are still poorly characterised (Fukuzawa et al. 2008; Hu et al. 2017; Kontrogianni-Konstantopoulos et al. 2003; Young et al. 2001). Interestingly, the interaction between obscurin and small ankyrins is the first physical link which has been discovered between the sarcomere and the SR (Kontrogianni-Konstantopoulos et al. 2003; Lange et al. 2012; Desmond et al. 2015). The only physiological function of obscurin understood with some certainty to date is a contribution of this link to the structural integrity of sarcolemmal and SR membranes (Lange et al. 2009; Randazzo et al. 2013a). Considering its complexity of domains, interactions, isoforms and their distinct subcellular localisations during muscle development, it is unlikely, however, that maintenance of membrane integrity is the only function of obscurin.

Obscurin is an exceptionally large protein of which four isoforms have been confirmed experimentally so far: two large isoforms obscurin A and B as well as two smaller isoforms containing different combinations of signalling domains (Fukuzawa et al. 2005). Due to a significant potential for differential splicing, more isoforms may exist (Fukuzawa et al. 2005). Depending on the isoform, obscurin comprises up to 70 Ig-domains, zero to three Fibronectin type 3 domains, an IQ-motif, an SH3 domain, a Rho GEF DH-PH domain tandem and two kinase domains (Figure 1.2) (Fukuzawa et al. 2005). Another protein closely to obscurin is obscurin-like 1 (obsl-1) which is likely the result of a duplication of the original obscurin gene but lacks the signalling domains of obscurin (Figure 1.2) (Geisler et al. 2007).

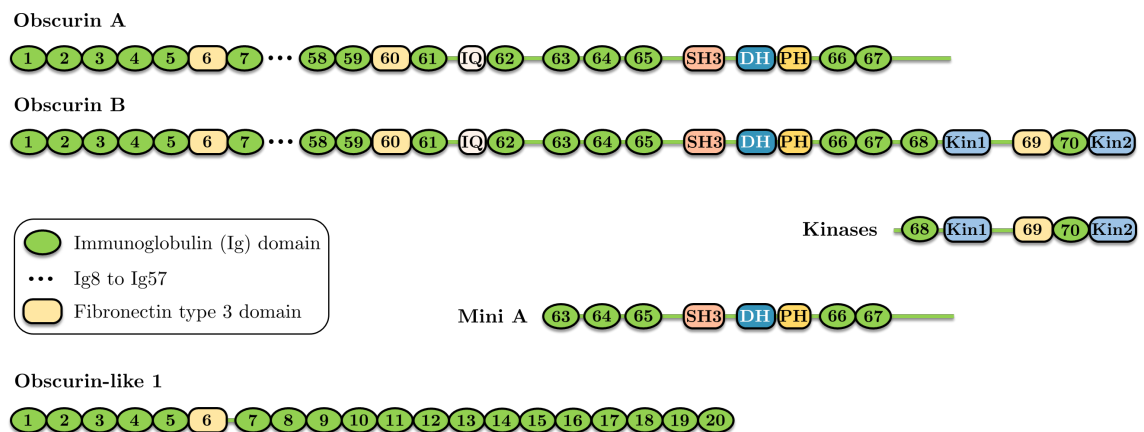


Figure 1.2. Experimentally confirmed obscurin isoforms and their domain compositions.

Large obscurin isoforms A and B consist mainly of Ig- and fibronectin-domains which likely have structural purposes. In addition all isoforms feature multiple signalling domains such as an SH3 domain, Rho GEF domains (DH, PH) or kinase domains (Kin1, Kin2), suggesting obscurin may play complex signalling functions in muscle cells. Obscurin-like 1 is a homologue of obscurin which is essentially identical to the region comprising the first 20 N-terminal domains of large obscurin isoforms and features no signalling domains.

1.4.2 Localisation of obscurin

Where exactly and at what developmental stage different obscurin isoforms are expressed and how this affects the function of obscurin is poorly understood. Using antibodies against a range of different epitopes (Ig19-Ig20, Ig58-Ig59, IQ-motif and DH-domain), consistent M-band staining has been reported in most immuno-fluorescence microscopy studies of mature sarcomeres from multiple species (Young et al. 2001; Carlsson et al. 2008; Fukuzawa et al. 2008). The earliest detectable epitope, however, was Ig58-Ig59 at the Z-disc of chicken cardiomyocytes during the c8-c11 somite stages, whereas the remaining epitopes either exhibited diffuse localisation (IQ- and DH-domain) or were not detectable (Ig19-Ig20) (Young et al. 2001). Carlsson et al. 2008, who used the same Ig58-Ig59 and IQ-domain antibodies from Young et al. 2001 on human skeletal muscle sections, reported that obscurin can additionally be found at the sarcolemma and postsynaptic neuromuscular junctions. Following exercise, the authors could furthermore detect diffuse recruitment of obscurin to sarcomeric lesions (Carlsson et al. 2008). Bang and colleagues studied the localisation of obscurin in cardiomyocytes from rat left ventricular tissue with different antibodies directed against Fn6-Ig7 at the N-terminus of obscurin and against an Ig58-Ig59-Fn60 domain triplet. For the N-terminal Fn6-Ig7 domains of obscurin, the authors reported localisation at both the Z-disc and M-band, whereas the Ig58-Ig59-Fn60 antibody resulted in a signal in the vicinity, but not the centre of the Z-disc, which was further confirmed by the similar localisation pattern of GFP-tagged and transiently transfected obscurin Ig58-Ig59-Fn60 in NRCs (Bang et al. 2001). Another study by Bowman et al. 2007 studied the localisation of obscurin in rat extensor digitorum longus using antibodies against the N-terminal Ig1-Ig2 domains, against the C-terminal ankyrin-binding region in obscurin, against Ig68 N-terminally of the first kinase domain in obscurin B, as well as a different antibody against the DH-domain than used in Young et al. 2001. Clear M-band staining was observed for Ig1-Ig2, the DH-domain and the C-terminus of obscurin A, although the latter was to a lesser extent also localised to the Z-disc (Bowman et al. 2007). In contrast, a broad signal surrounding the Z-disc was obtained with the antibody against Ig68, which was interpreted by the authors as Z/I and I/A junctional localisation (Bowman et al. 2007). Similarly, antibodies against different parts of the inter-kinase region and the N-terminal kinase domain of obscurin resulted in both M-band and Z-disc staining and to a lesser degree to staining of other structures (Hu and Kontrogianni-Konstantopoulos 2013).

The mechanism responsible for targeting obscurin (and obsl-1) to the M-band has been discovered by Fukuzawa et al. who showed that titin, myomesin and obscurin form a ternary complex in which each molecule has a separate binding site for the other two (Ig1 of obscurin/obsl-1 binds to titin M10, whereas Ig3 of obscurin/obsl-1 binds to the interdomain linker between myomesin domains M4 and M5). The functional relevance of these interactions is demonstrated by the fact that overexpression of the minimal binding regions of titin or myomesin can outcompete these interactions and result in the mislocalisation of endogenous obscurin (Fukuzawa et al. 2008).

Unc89, the orthologue of obscurin in *D. melanogaster* and *C. elegans*, localises to the M-band, too, where it covers the whole cross-sectional plane (Katzemich et al. 2012; Qadota et al. 2017). In contrast, cross-sections stained with antibodies against obsl-1 Ig1, obscurin Ig1-Ig2, Ig58-Ig59 and the ankyrin-binding site of obscurin A revealed that vertebrate obscurin is localised at the periphery of the sarcomere, whereas obsl-1 is an intra-sarcomeric protein (Fukuzawa et al. 2008; Kontrogianni-Konstantopoulos et al. 2003). Moreover, the signal obtained for obscurin showed good alignment to the signal obtained with SERCA staining, suggesting spatial vicinity between

parts of obscurin and SERCA (Fukuzawa et al. 2008). Taken together, it therefore appears that obscurin is not an intra-sarcomeric protein but rather attached to the periphery of the M-band.

The domain composition of obscurin A and B implies that both isoforms have the required binding sites to localise to the M-band as well as to the Z-disc. Yet, the published localisation reports are somewhat contradictory. While Bang et al. reported the N-terminus (Ig6-Fn7) of obscurin to be localised simultaneously to the M-band and the Z-disc of adult rat left ventricular sarcomeres, Bowman et al., studying the localisation of obscurin in rat extensor digitorum longus, found the C-terminus of obscurin A to be localised both to M-band and the Z-disc, whereas the N-terminus and the DH-domain were found at the M-band and to a lesser degree at I/A junctions (Bang et al. 2001; Bowman et al. 2007). Z-disc localisation of the large A and B isoforms in adult myocytes is unlikely since both isoforms comprise the majority of epitopes studied so far. Excluding the C-terminal kinase domains and the ankyrin binding region, there are six separate epitopes from different regions (Ig1-Ig2, Ig6-Fn7, Ig19-Ig20, IQ-motif, Ig58-Ig59, and DH-domain) which have been studied by seven antibodies (two against the DH-domain). Z-disc localisation of any large isoform would therefore lead to consistent Z-disc staining by multiple antibodies. Since this is not the case, the observed Z-disc and I/A junctional staining perhaps result from smaller isoforms comprising the kinase or Rho GEF domains (Bowman et al. 2007).

Thus, consistent staining for multiple epitopes renders the M-band the most likely localisation for the large obscurin isoforms. For obscurin A, the localisation and orientation can be further specified by noting that the N-terminus is anchored to the M-band via titin and myomesin and the C-terminus is well established to bind and colocalise to small ankyrins (Fukuzawa et al. 2008; Bagnato et al. 2003; Kontrogianni-Konstantopoulos et al. 2003; Cunha and Mohler 2008). Obscurin A thus creates a direct connection between the M-band and the SR. The localisation of the C-terminus of obscurin B, however, remains an open question. Another question yet to be answered is how the observed localisation shift of the Ig58-Ig59 epitope (present in obscurin A and B) from the embryonic Z-disc to the mature M-band is regulated.

1.4.3 Functional roles of obscurin

When it comes to the functional roles of obscurin, Young et al.'s choice of name remains essentially adequate despite some progress and almost two decades of research.

The first role proposed for obscurin was the regulation of sarcomere assembly. The earliest evidence for an involvement in sarcomere assembly came directly with the discovery of the invertebrate orthologue of obscurin, *unc89*, twenty years before the discovery of human obscurin: *Unc89* was found in a study which searched for genes that determine muscle structure based on screening chemically induced random mutations in *C. elegans* (Waterston et al. 1980). *Unc89* was defined as the genetic locus identified in a mutant strain with missing M-bands and a failure to incorporate thick filaments into A-bands. Animals with these mutations were generally viable but smaller than wild-type animals. Despite these seemingly major structural alterations, the animals were surprisingly unimpaired in their general motility (Waterston et al. 1980). A detailed analysis of the gene sequence showed that *unc89*, similar to obscurin, consists mainly of Ig-domains interspersed by several signalling domains including N-terminal SH3 and DH-PH domains and two C-terminal kinase domains (Benian et al. 1996). In agreement with the context of discovery of *unc89*, many of its domains have been shown to interact with and regulate the localisation of other proteins involved in sarcomere organisation (Katzemich et al. 2015; Qadota et al. 2018; Warner et al. 2013).

Later studies on *C. elegans* and *D. melanogaster* further substantiated that unc89 plays a role in regulating the structure of the sarcomere: the Rho GEF DH-PH domains were found to be important for thick filament organisation in *C. elegans* as mutants lacking these domains or RNAi based downregulation of their putative substrate RHO-1 (an invertebrate orthologue of RhoA) led to a misdistribution of myosin heavy chains (Qadota et al. 2008b). Decreasing the expression levels of unc89 in *D. melanogaster* using the same RNAi based approach resulted in severe sarcomeric aberrations including abnormal length of thin filaments, misaligned H- and missing M-bands and defects of myosin incorporation into A-bands (Katzemich et al. 2012).

After the discovery of vertebrate obscurin, a series of papers from the laboratories of Bloch, Russell and Kontrogianni-Konstantopoulos adopted the concept proposed for unc89 and suggested a similar role in sarcomere assembly and myofibrillogenesis for obscurin. In the first of these studies, the authors used adenoviral gene transfer of the C-terminus of obscurin A into myotubes from rat hind limb and found that obscurin prevented the integration of myosin into A-bands (Kontrogianni-Konstantopoulos et al. 2004). Mechanistically, the authors stipulated that obscurin is responsible for correct myosin targeting based on a direct interaction between obscurin and myosin which they identified using co-immunoprecipitation (Kontrogianni-Konstantopoulos et al. 2004). Three subsequent studies in different species and myocyte types reported that downregulation of obscurin using siRNA and morpholino antisense approaches resulted in blurred or disrupted M-bands, incorrect localisation of titin and myosin heavy chains and lateral misalignment of myofibrils (Borisov et al. 2006; Kontrogianni-Konstantopoulos et al. 2006; Raeker et al. 2006).

In contradiction to the studies postulating a role in myofibril and sarcomere organisation, however, the deletion of large obscurin isoforms A and B in mice had no observable effect on the alignment of myofibrils or on the ultrastructure of sarcomeres (Lange et al. 2009). Furthermore, obscurin knock-out mice were viable, appeared generally healthy and showed no overt pathological phenotype (Lange et al. 2009). Although obscurin deletion led to minor reductions in fibre length and muscle mass, functional parameters of contraction and relaxation were not affected (Lange et al. 2009). One of the few observable effects of deleting large obscurin isoforms, however, was a retraction of the longitudinal SR away from the M-band and towards the junctional SR which was further accompanied by incorrect localisation and reduction of sAnk1.5, the ligand of the C-terminus of obscurin A (Lange et al. 2009; Lange et al. 2012). When forced to run until exhaustion, however, obscurin knock-out mice showed significantly less endurance than their wild-type littermates and demonstrated more signs of muscle damage including fibrosis, leukocyte infiltration, wave-like and disturbed myofibrils and altered Z-discs and M-bands (Randazzo et al. 2017a). More recently, a double knock-out mouse model lacking both obscurin and obsl-1 (a smaller protein encoded by OBSL1 which is homologous to the N-terminus of obscurin A and B) confirmed that even the double-knock-out of obscurin and obsl-1 does not lead to structural alterations of the sarcomere, but to even more pronounced disorganisation of the SR and sarcolemmal membrane complexes (Blondelle et al. 2019).

Taken together, these findings indicate that obscurin is unlikely to be essential for sarcomere assembly or myofibril organisation but is structurally required to tether the longitudinal SR to the M-band and to maintain sarcolemmal membrane integrity, particularly in the context of increased physical strain. The discrepancy between early *in vitro* studies and the findings from the knock-out mice may be explained by multiple aspects: firstly, a limitation of Lange et al. 2009 is that the knock-out mice may not represent a complete loss-of-function model as the smaller kinase isoform of obscurin was still expressed due to alternate promoter usage. Furthermore, compared to humans,

invertebrate and zebrafish exhibit important differences both in obscurin and relevant interaction partners. The invertebrate homologue of obscurin, *unc89*, for instance, differs drastically in the position of the Rho GEF signalling domains: instead of being positioned at the C-terminal third, the SH3, DH and PH domains are found at the very N-terminus of *unc89* in *D. melanogaster* and *C. elegans* (cf. e.g. NCBI reference sequences NM_001103970 and NM_001025814) (Katzemich et al. 2012). Furthermore, *unc89* is found throughout the whole cross-sectional plane of the M-band instead of covering only the periphery like vertebrate obscurin (Katzemich et al. 2012; Qadota et al. 2017). This could be explained by an interaction of the SH3 domain of *unc89* with paramyosin (Qadota et al. 2016). Paramyosin is an invertebrate-specific protein in the core of thick filaments required for correct thick filament assembly (Hooper et al. 2008). Insights about invertebrate muscle, which rely on obscurin's interaction with paramyosin and thick filaments, are therefore unlikely to translate to humans.

Zebrafish, on the other hand, have significantly more members in the Rho-family of small GTPases than humans or mice (zebrafish have e.g. five RhoA homologues) but potentially no homologue of RhoQ, all of which may be putative substrates of obscurin's DH-PH domain tandem (Salas-Vidal et al. 2005). Secondly, siRNA and related downregulation approaches can have "off-target" effects which may impair other processes important for sarcomere or myofibril organisation (Jackson et al. 2006). Finally, due to the nature of the preparation procedure, isolated (cardio-)myocytes necessarily experience a substantial amount of physical stress and typical cell culture conditions only have limited resemblance with the *in vivo* environment in terms of substrate stiffness, extracellular matrix composition, cell type diversity and humoral stimulation. Thus, if obscurin has protective functions, the increased physical stress to which isolated cells are subjected may lead to alterations in sarcomere structure which may be misinterpreted as impaired *de novo* assembly of sarcomeres and myofibrils.

1.4.4 Potential functions beyond safeguarding membrane integrity

The only function established for obscurin without contrary evidence from other studies so far is a role in maintaining the structural organisation and integrity of SR and sarcolemmal membranes (Lange et al. 2009; Blondelle et al. 2019). However, a synopsis of the literature on obscurin reveals that it is at least highly likely that obscurin plays a more general role in the response of cardiomyocytes to mechanical strain. Given that obscurin has several signalling domains, it is also likely that it plays a role in receiving and transducing signals either as a mechano-transducer and/or in other contexts. The following sections review both possibilities.

1.4.5 Obscurin in the context of mechanical forces

The sarcomeres of muscle cells in general and of cardiomyocytes in particular need to withstand the considerable mechanical forces they generate on a molecular level. To fulfil this requirement, sarcomeres require continuous maintenance (Boateng and Goldspink 2008). Multiple independent research groups have reported obscurin to be associated with contexts of increased mechanical strain to the heart and or skeletal muscles. One of the first of such studies reported that mRNA-transcripts of obscurin isoforms containing the Rho GEF domains were significantly increased in mice subjected to aortic banding (which, by reducing the diameter of the aorta, leads to a higher resistance against which the heart has to work during the systolic ejection phase) (Borisov et al. 2003). In human muscle biopsies from healthy volunteers following acute exercise, Carlsson

et al. 2008, as mentioned above, found obscurin to be localised to the site of sarcomeric lesions. Interestingly, this observed recruitment of obscurin to sites of sarcomeric lesions strongly resembles similar patterns reported for filamin C, which is a muscle protein connecting the sarcomeric Z-disc with the sarcolemma (Bönnemann et al. 2003). Upon damage to the sarcomere, however, filamin C is recruited to the sarcomeric lesions where it is proposed to be involved in forming a non-contractile patch and reported to recruit further proteins to initiate the repair of the sarcomere (Leber et al. 2016; Orfanos et al. 2016). The striking similarity between filamin C and obscurin in connecting one of the anchoring planes of the sarcomere with membrane structures and the dynamic recruitment of both proteins to sarcomeric lesions indicates that obscurin could be involved in similar processes as filamin C. Interestingly, a recent study which included a clinical case report indicated that a mutation in obscurin domain Ig59 (Arg4444Trp) accelerated the time of onset in two patients with distal muscular dystrophy caused by a filamin C frameshift mutation (Rossi et al. 2017). More evidence for a role in sarcomeric maintenance or repair after mechanical damage comes from the above-mentioned observation that obscurin knock-out mice exhibited more muscle damage after exhaustive running exercise than their wild-type littermates and also showed altered H-, M-Band and Z-disc structures not observed in the wild-type mice (Randazzo et al. 2017a).

Lastly, a series of reviews stressed the mechanobiological importance of the sarcomeric M-band for striated muscle (Agarkova et al. 2003; Agarkova and Perriard 2005; Agarkova and Ehler 2015; Lange et al. 2005; Lange et al. 2020). In contrast to the Z-disc, the M-band is more elastic which is attributed to flexible and spring-like regions in titin and myomesin (Agarkova and Ehler 2015). The ternary complex between obscurin (or obsl-1), myomesin and titin may be important for these mechanical properties (Fukuzawa et al. 2008; Pernigo et al. 2017). Moreover, based on the in-solution structural characterisation of tandem Ig-domains and molecular dynamics simulations, the Ig-domain organisation has recently been proposed to confer elastic properties to obscurin itself (Whitley et al. 2019). This elasticity of the M-band is believed to provide a buffer to mechanical shear forces which otherwise may damage the sarcomere. Specifically, since the position of the thick myofilaments is considered to be intrinsically unstable, the elasticity of the M-band may help to counterbalance and distribute shear forces to ensure symmetric contraction along the longitudinal axis of the sarcomere (Agarkova et al. 2003). Connections between the sarcomere and the sarcolemma or costameres (see below) could further improve stability (Agarkova et al. 2003). In addition to these mechano-protective roles, the M-band is also considered to be an ideal structure for sensing mechanical forces and translating these into biochemical signals to initiate adaptive processes. One candidate mechanosensor at the M-band is titin-kinase in which an autoinhibitory region obstructing the catalytic site has been demonstrated to be relieved by force in molecular dynamics simulations and experimentally by atomic force microscopy (Gräter et al. 2005; Puchner et al. 2008). The catalytic activity of titin-kinase has been a subject of debate as no substrate has yet been identified and replacing residues in the active site of the invertebrate homologue twitchin-kinase with those found in titin silences the otherwise catalytically active twitchin-kinase (Bogomolovas et al. 2014). Regardless of whether human titin-kinase possesses catalytical activity or not, it may in either case act as force-sensor due to force-dependent availability of binding sites to interaction partners such as nbr1 and MuRF ubiquitin-ligases (Bogomolovas et al. 2014; Agarkova and Ehler 2015; Lange et al. 2020).

Interestingly, obscurin is among a group of proteins strongly phosphorylated in cardiac and skeletal muscle after exercise, although the identity of the responsible kinases is currently unknown (Guo et al. 2017; Potts et al. 2017). In skeletal muscle, the largest fold-change in phosphorylation

after exercise was observed in a serine residue of the linker between the SH3 and DH domain of obscurin, indicating that some of the hypothesized mechanobiological roles of obscurin might be linked to the signalling domains of obscurin. Indeed, mechanical stretch and overexpression of the obscurin Rho GEF domains have been reported to lead to a redistribution of the putative substrate RhoA from the M-band to the Z-disc/I-band (Ford-Speelman et al. 2009).

1.5 Signalling processes associated with obscurin

Several lines of evidence imply obscurin to be involved in signalling processes, although most aspects are only rudiments and require further experimental work.

1.5.1 Calcium signalling

The first line of evidence links obscurin to the regulation of calcium cycling in (cardio-)myocytes. Truncation mutations of large unc89 isoforms in *C. elegans* were reported to lead to significantly attenuated calcium transients, indicating reduced calcium mobilisation (Spooner et al. 2012). Vertebrate obscurin, too, can influence calcium handling. Cardiomyocytes from a mouse model of the human genetic variant Arg4344Gln in obscurin domain Ig58 exhibited increased calcium amplitudes and higher decay constants resulting from the increased function of the SR-calcium pump SERCA, which the authors attributed to increased sequestration of the SERCA inhibitor PLN by obscurin (Hu et al. 2017). In contrast, an obscurin Ig58-Ig59 deletion mouse model resulted in a slower decay of the calcium transient (Grogan et al. 2020). Moreover, mice from both lines developed cardiac arrhythmias and exhibited alterations in expression and phosphorylation levels of calcium handling proteins including SERCA, PLN and RyR, although the effects differed between mouse models and the effects of Ig58-Ig59 deletion were mostly restricted to male mice (Grogan et al. 2020; Hu et al. 2017). While some of these effects could be related to the structural organisation of the longitudinal SR network (Lange et al. 2009; Spooner et al. 2012), it is likely that obscurin is more directly involved in calcium signalling, too. For example, obscurin has at least two independent binding sites for the calcium-binding protein calmodulin: one IQ-motif between domains Ig61 and Ig62, which has been shown to constitutively bind calmodulin, and a basic amphipathic sequence following kinase domain 1 in obscurin B (Young et al. 2001; Fukuzawa et al. 2005). Being a calcium sensor, calmodulin could thus regulate obscurin function in a calcium-dependent manner (Bähler and Rhoads 2002). In addition, obscurin has been reported to interact directly and indirectly with several proteins involved in calcium signalling including the above mentioned PLN, the phosphatase PP2A (which also dephosphorylates PLN) and SERCA1 in skeletal muscle (via sAnk1) (Cunha and Mohler 2008; Desmond et al. 2015; Hu et al. 2017; Qadota et al. 2018). More recently, obscurin kinase domain 1 was predicted to phosphorylate several calcium handling proteins including RyR and multiple calcium channel subunits (Fleming et al. 2021). Although these findings are far from providing a functional, let alone mechanistic understanding, they provide strong cumulative evidence that the regulation of or by calcium likely plays an important role in obscurin function.

1.5.2 Obscurin kinase domains

Both invertebrate unc89 and vertebrate obscurin feature two kinase domains in one of their large and in two of their smaller isoforms. Although often referred to as MLCK subfamily members, this

classification is somewhat misleading as many members in this kinase subfamily neither phosphorylate myosin nor are regulated by calcium/calmodulin (Gautel 2011). The sequence of obscurin kinase domains is most closely related to the two kinase domains of striated muscle preferentially expressed kinase (SPEG) in the MLCK-like subfamily, but also bears significant similarity to the kinase domains of titin and death-associated protein kinases (Fleming et al. 2021; Gautel 2011).

In *C. elegans*, the different kinase-comprising isoforms of unc89 were demonstrated to be controlled by three different promoters and to have non-redundant functions in sarcomere organisation as judged by the characterisation of the muscle structure and phenotype of different knock-out strains (Small et al. 2004). The N-terminal kinase domain of unc89 is likely inactive as its active site deviates in multiple aspects (e.g. lack of a conserved lysine in the active site) from catalytically active kinases and small isoforms furthermore lack the N-terminal lobe (Fukuzawa et al. 2005). The C-terminal kinase domain, in contrast, has all necessary sequence features for catalytic activity, although neither kinase domain demonstrated any *in vitro* activity so far (Small et al. 2004; Xiong et al. 2009). Since the substrate-binding region is more exposed in the N-terminal kinase domain due to the lacking N-terminal lobe, the authors hypothesized that the N-terminal kinase domain might function as a scaffold for protein-protein interactions (Small et al. 2004). Later on, the domain has indeed been demonstrated to interact with *C. elegans* proteins SCPL-1 and LIM-9 in a ternary complex with further links to M-band costameres (Qadota et al. 2008b; Xiong et al. 2009). Costameres are macromolecular complexes consisting of integrins and various other proteins which connect the sarcomere, sarcolemma and the extracellular matrix (Peter et al. 2011). The C-terminal kinase of obscurin, however, seems to be capable of the same interactions (Qadota et al. 2008b; Xiong et al. 2009). While overexpression of SCPL-1 was reported to lead to mislocalisation of unc89, RNA-interference based downregulation of SCPL-1 led to defective functioning of the *C. elegans* egg-laying muscle (Qadota et al. 2008b; Xiong et al. 2009). Interestingly, the mammalian homologue of LIM-9, FHL-2, has also been shown to interact with titin as well as multiple enzymes involved in energy metabolism (e.g. phosphofructokinase), thereby perhaps recruiting metabolic enzymes to subcellular sides of high energetic demand (Lange et al. 2002). In *D. melanogaster*, unc89 kinase domains differ from those in *C. elegans* and mammalian obscurin kinase domains insofar both kinase domains were predicted to be catalytically inactive. Instead, it has been demonstrated that they provide a scaffold for proteins Bällchen and MASK and are necessary for correct sarcomere assembly in the indirect flight muscle of *D. melanogaster* (Katzemich et al. 2015).

Little is known about the kinase domains of mammalian obscurin. The isoforms containing the kinase domains of obscurin were discovered slightly later than the ‘original’ A-isoform (Russell et al. 2002; Fukuzawa et al. 2005). Borisov and colleagues reported that expression of kinase containing isoforms increased during cardiac development in mouse embryos and reported mid-A-bands and Z-disc staining in differentiated mouse cardiomyocytes with an antibody developed against the denatured and refolded C-terminal kinase domain (Borisov et al. 2008). With respect to catalytic activity, the N-terminal kinase domain of obscurin appears to have all necessary sequence features of active Ser/Thr-kinases, whereas the C-terminal kinase domain features a replacement of the conserved active site lysine with an arginine, possibly preventing catalytic activity (Gautel 2011; Small et al. 2004). Hu and Kontrogianni-Konstantopoulos, however, reported that both kinase domains are capable of autophosphorylation and that the N-terminal kinase can additionally phosphorylate a generic histone substrate as well as N-cadherin (Hu and Kontrogianni-Konstantopoulos 2013). Furthermore, they identified multiple binding partners using the kinase domains as baits in

a yeast-two-hybrid screen against a human heart cDNA library. Among these were ISLR, galectin, titin and N-cadherin for the N-terminal kinase and Na/K-ATPase β 1-subunit, galectin, filamin C, fibronectin-1 and FHL-2 for the C-terminal kinase (Hu and Kontrogianni-Konstantopoulos 2013). While the binding to FHL-2 points indicates that this interaction may be evolutionary conserved, an interaction with SCP-1 to SCP-3, the closest mammalian orthologues for the catalytic domain of SCPL-1, has not yet been evaluated. Recently, catalytic activity at least in terms of autophosphorylation of the N-terminal obscurin kinase has been confirmed by the Lange group using mutagenesis and PhosTag-gels. As mentioned above, they further predicted the N-terminal kinase to phosphorylate calcium handling proteins such as RyR and calcium channel subunits (Fleming et al. 2021). Due to the well-established role of the highly similar SPEG-kinases in cardiac calcium handling, it is not unlikely that obscurin kinases are involved in similar regulatory processes (Quick et al. 2017; Huntoon et al. 2018; Quan et al. 2019).

1.5.3 Obscurin Rho GEF domains

In the narrow sense, the Rho GEF domains of obscurin comprise its Dbl-homology (DH) domain and the directly following Pleckstrin-homology (PH) domain, although the SRC homology 3 (SH3) domain is sometimes considered to be part of the Rho GEF domain, too, since it is positioned almost directly N-terminally of the DH domain (Young et al. 2001). This domain composition in which the DH domain is followed by a PH domain is, with very few exceptions, characteristic for all of the approximately 70 members of the Dbl-like Rho GEF family (Rossman et al. 2005; Fort and Blangy 2017). As the name suggests and as will be discussed in more detail below, these domains act as guanosine nucleotide exchange factors (GEFs) for the Rho family of small GTPases: the DH domain can bind to small GTPases and facilitate the exchange of their bound nucleotide (GDP for GTP *in vivo*), thereby enabling the GTPase to interact with downstream effector proteins. The PH-domain typically exerts a positive or negative regulatory role or contributes to localisation. The substrates or targets of Dbl-family GEFs, i.e. Rho GTPases, are involved in a wide spectrum of molecular processes including actin (de-)polymerisation, microtubule dynamics, vesicular trafficking, gene expression and other processes, making Rho GTPases important regulators of cellular functions such as migration and adhesion, polarity, endocytosis, contractility, cell division, morphogenesis and proliferation (Etienne-Manneville and Hall 2002; Burrige and Wennerberg 2004; Jaffe and Hall 2005; Heasman and Ridley 2008). This also applies to the heart and cardiomyocytes, where Rho GTPases are implicated in cardiac development, cardiomyocyte hypertrophy and apoptosis, sarcomere assembly and contractility (via Rho GTPase effectors PAK and ROCK) (Desmond et al. 2015; Nagai et al. 2003; Loirand et al. 2006; Peters and Michel 2007; Rangrez et al. 2013; Loirand et al. 2013; Leung et al. 2014; Shimokawa et al. 2016). Before reviewing previous studies of the obscurin Rho GEF domains, it will be helpful to outline the basic biochemical principles of the regulation of small GTPases by GEFs and other proteins.

Small GTPases of the Ras-superfamily and their regulation by GEFs, GAPs and GDIs in a nutshell

Along with Ras, Rab, Ran and Arf, Rho GTPases belong to the Ras-superfamily of small GTPases of signalling proteins which are involved in numerous different signalling processes but share significant similarities in their structure and regulatory mechanisms (Wennerberg et al. 2005; Wittinghofer and Vetter 2011). A hallmark of small GTPases is their ability to bind guanosine nu-

cleotides GDP and GTP. While GTP-bound, the γ -phosphate exerts attractive forces upon invariant residues in the so-called switch-regions of small GTPases and induces a rigid conformation of these regions (Figure 1.3A,B) (Vetter and Wittinghofer 2001). This renders GTPases biologically active in the sense that the rigid switch-regions allow binding of effector proteins, thereby initiating subsequent signalling events. When GDP-bound, the lack of the γ -phosphate allows the switch-regions to relax into a more flexible conformation in which the GTPases are unable to bind effectors and thus are biologically inactive.

As their name suggests, small GTPases have the intrinsic ability to hydrolyse GTP, thereby transitioning into the GDP-state. They also have the ability to release and rebind nucleotides which on average leads to the transition into the GTP-bound state (as intracellular [GTP] exceeds [GDP]). The transitioning rates between the two states are further accelerated by guanine nucleotide exchange factors (GEFs), which facilitate the GDP \rightarrow GTP transition *in vivo*, and GTPase activating proteins (GAPs), which accelerate the hydrolysis and thus the GTP \rightarrow GDP transition. Although the biochemical mechanism of GEFs can be described by a system of coupled equilibrium reactions in which GEFs can be conceptualised as allosteric regulators, it is often more convenient to treat GEFs – and GAPs for that matter – as enzymes, making them amenable to conventional steady-state kinetic methods (Guo et al. 2005; Klebe et al. 1995; Randazzo et al. 2013b). From this perspective, the GTPase cycle strongly resembles futile cycles of post-translational modifications (PTMs) such as phosphorylation/dephosphorylation cycles. However, most proteins typically do not intrinsically transition between their PTM states (except for autocatalytic enzymes) and many small GTPases are additionally regulated by guanine-nucleotide dissociation inhibitor proteins (GDIs) which solubilise these typically membrane-bound GTPases by extracting and binding their lipid-moiety, thus adding another layer of complexity (Boulter et al. 2011; Cherfils and Zeghouf 2013). The most important steps in the GTPase cycle are summarised in Figure 1.3C.

The intrinsic hydrolysis rate, on the other hand, has been proposed to act as a molecular timer to reduce the variance in the lifetime of the GTP-state (Li and Qian 2002).

Although small GTPases are commonly referred to as “molecular switches” because of their structurally distinct conformations, it is important to emphasize that the switch-like transition between the active and inactive state of individual GTPase molecules is often not representative of the bulk-behaviour of a particular GTPase in the cell. In fact, the biological activity of small GTPases can exhibit complex dynamics and behaviour including graded responses, switch-like or bistable responses, excitable behaviour and sustained oscillations (Conte-Zerial et al. 2008; Tsyganov et al. 2012; Nikonova et al. 2013; Byrne et al. 2016; Graessl et al. 2017; Nobis et al. 2017; Ehrmann et al. 2019; Bezeljak et al. 2020). While small GTPases can intrinsically transition between GDP and GTP states, it is typically the regulators such as GEFs and GAPs, and GDIs which are responsible for the orchestration of specific signalling activities in a given context (Bos et al. 2007; Hodge and Ridley 2016). In the case of Rho GTPases, regulatory proteins from the human Rho GAP and Rho GEF families each have over 60 members which are responsible for controlling only 10 “typical” and often ubiquitously expressed Rho GTPases which cycle between GDP and GTP bound states (Amin et al. 2016; Jaiswal et al. 2013). Accordingly, regulators such as GEFs show more cell-type-specific expression patterns and the Dbl-GEF family shows a clear evolutionary correlation between the complexity in terms of the number of different cell types and size of the Dbl-family of Rho GEFs for a given species (Boureaux et al. 2007; Fort and Blangy 2017).

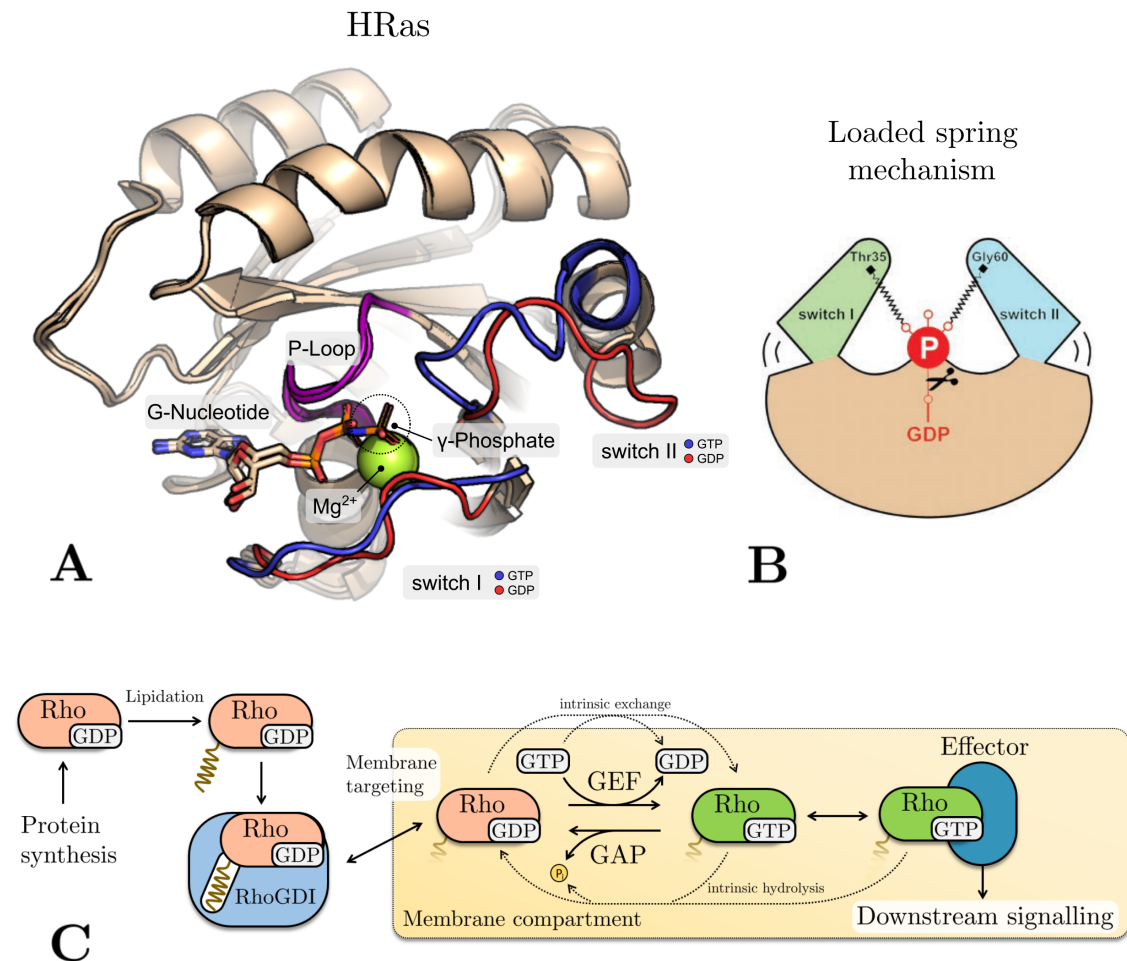


Figure 1.3. Mechanisms of small GTPase signalling.

A, Superimposed 3D-structures of human HRas bound to GDP (PDB-ID: 4Q21) and the non-hydrolysable GTP analogue GppNHp (PDB-ID: 5P21), respectively. Guanosine nucleotides and important elements involved in nucleotide binding (P-Loop, Mg^{2+} -ion) are highlighted as are switch-regions that undergo conformational rearrangement upon changes in the nucleotide state (red = GDP-bound, blue = GTP-bound). **B**, Schematic of the so-called “loaded spring” mechanism, illustrating how the γ -phosphate of GTP induces a rigid conformation of the switch regions. From Vetter IR, Wittinghofer A (2001): The guanine nucleotide-binding switch in three dimensions. *Science*, 294: 1299-1304. Reprinted with permission from AAAS. **C**, Simplified illustration of key steps in the synthesis of functional Rho GTPases and subsequent regulation by GEFs, GAPs and GDIs. Downstream signalling is initiated via recruitment of effector proteins such as kinases to the GTP-bound Rho GTPase.

Unc89 Rho GEF domains in worm and fly

As mentioned above, the SH3, DH and PH domains are positioned at the N-terminus of invertebrate unc89. The unc89 PH domain from *C. elegans* was the first of these domains to be characterised biochemically. Although reported to be intrinsically unstable, Blomberg et al. 2000 succeeded to solve the domain structure of this domain via solution NMR. Interestingly, it was reported that the unc89 PH domain is positioned unusually close to the DH domain and has a strongly negative surface charge compared to other PH domains, suggesting it might not be capable of binding negatively charged phospholipids as many other PH domains do. In agreement with this, Blomberg and colleagues were not able to detect any interaction with inositol(1,4,5)trisphosphate,

a common ligand for PH domains, in ^{15}N HSQC NMR experiments and thus proposed the PH domain may bind to ligands other than phospholipids (Blomberg et al. 2000). A test of the ability of *C. elegans* unc89 to facilitate nucleotide exchange on Rho-family small GTPases was performed by Qadota et al. who used a yeast-based assay in which a putative substrate GTPase was fused to a LexA domain and a known effector was fused to a GAL4-activation domain. Since GTPases only bind their effectors when in the GTP-bound state, significant β -galactosidase activity can only be detected in the presence of GTP-bound GTPases and therefore can be used as a read-out of the nucleotide exchange activity of an overexpressed putative GEF. The authors reported that overexpression of either the DH domain or the DH-PH domain tandem resulted in notable β -galactosidase activity of cells with LexA-RHO-1 (RhoA in mammals), but not for cells with CED-10 (Rac), MIG-2 (RhoG) or CDC-42 (Cdc42), suggesting that the DH domain of unc89 functions as RHO-1 selective GEF (Qadota et al. 2008a). Interestingly, however, all four GTPases were able to bind unc89 DH-PH in pull-down assays (Qadota et al. 2008a). Functionally, both a *C. elegans* mutant lacking the DH-PH domain and worms in which RHO-1 abundance was decreased by RNA interference displayed abnormal organisation of the myosin heavy chain A in the body wall muscle, suggesting unc89 Rho GEF activity is important for correct assembly of thick filaments in *C. elegans* (Qadota et al. 2008a). In a subsequent study, the authors further demonstrated that a newly identified interaction between the SH3 domain of unc89 and the invertebrate protein paramyosin is necessary for targeting paramyosin to the thick filament and that deletion of the SH3 domain leads to similar phenotypes as deletion of the DH-PH domains (Qadota et al. 2018). Reminiscent of the situation with the PH domain, the authors further found that the interaction does not rely on the canonical binding mode between SH3 domains and their ligands because the interaction was found to rely on the coiled-coil domain of paramyosin which lacks a PxxP motif (Qadota et al. 2016). In agreement with this, homology models demonstrated that the PxxP binding groove of the SH3 domain is partly degenerated (Qadota et al. 2016). Although paramyosin has 40% sequence identity to the rod-domain of vertebrate myosin, Qadota and colleagues considered it unlikely that the SH3 of mammalian obscurin interacts with myosin since they estimated the distance between the SH3 domain in obscurin A and myosin in the sarcomere to be approximately 200 nm, but they proposed that the SH3 domain of obscurin to possibly bind other coiled-coil proteins (Qadota et al. 2016). While the steric constraint mentioned in that study does not apply to the small ‘mini A’ isoform of obscurin (see Figure 1.2), it is interesting to note in this context that there are many coiled-coil domain proteins among the effectors of small GTPases (Grosshans et al. 2006; Patel and Côté 2013).

Obscurin Rho GEF domains

The first protein reported to interact with the DH domain of mammalian obscurin was not a small GTPase but a protein called RanBP9/RanBPM, a multi-domain scaffolding protein with many binding partners and reported functions in ubiquitin signalling, apoptosis, transcriptional regulation, motility and development (Bowman et al. 2008; Salemi et al. 2017). The authors further reported RanBP9 to bind to titin and that these surprising interactions are responsible specifically for the integration of the N-terminus of titin into Z-discs as overexpression of RanBP9 was associated with an increased number of myofibrils in which titin was not properly integrated into the Z-disc (Bowman et al. 2008). As the effect was modest in absolute numbers (about 0.5% of control myofibrils compared to about 1.8% of myofibrils overexpressing RanBP9) and since

the complete lack of obscurin does not impair the integration of titin into murine sarcomeres, the physiological significance of these interactions remains to be evaluated (Bowman et al. 2008; Lange et al. 2009). The first putative substrate GTPase of the obscurin Rho GEF domains was identified in two studies by Coisy-Quivy et al. on the role of Rho GTPases in skeletal muscle development and myofibrillogenesis. In the first study, the authors used ascidians (sea squirts) *Ciona intestinalis* and *Ciona savignyi* as model organisms because the evolutionary distance of their Rho GTPase family is closer and their muscle development more similar to vertebrates than invertebrates. Employing constitutively active and inactive mutants, the first study demonstrated RhoA, Cdc42, TC10/RhoQ, Rac1 and Rac2 to have important roles in muscle development and myofibril organisation with respect to cell polarity, lateral fibre alignment and organisation of actin thin-filaments (Coisy-Quivy et al. 2006). TC10/RhoQ mutants displayed some of the most severe phenotypes among the GTPases studied. Specifically, constitutively active TC10/RhoQ mutants led to complete loss of muscle cell polarity, severe reduction in myofibrils and loss of the striated organisation pattern, whereas constitutively inactive TC10/RhoQ mutants displayed a strong reduction of mature myofibrils but not polarity defects (Coisy-Quivy et al. 2006). In a subsequent study, Coisy-Quivy and colleagues identified (human) obscurin to be a GEF for TC10/RhoQ using co-immunoprecipitation and effector-bait based pull-downs as activity assays and further demonstrated TC10/RhoQ and obscurin activity to lead to more autophosphorylation of the TC10/RhoQ effector PAK. In agreement with the role of TC10/RhoQ in ascidians, the authors reported perturbation of TC10/RhoQ activity to impair myofibrillogenesis in human myotubes (Coisy-Quivy et al. 2009). Using essentially the same effector-bait based pulldown and co-immunoprecipitation approach, a study from the Bloch group found evidence for obscurin GEF activity towards RhoA, consistent with the finding that *unc89* can facilitate nucleotide exchange on the RhoA-homologue RHO-1 in *C. elegans* (Ford-Speelman et al. 2009). In addition, the study found obscurin and RhoA to colocalise at the M-band and that overexpression of the obscurin Rho GEF domains or mechanical stretching leads to a redistribution of RhoA from the M-band to the Z-disc/I-band and changes in the localisation of RhoA effectors ROCK and CRIK (Ford-Speelman et al. 2009). A potential interaction between obscurin and RhoA is further confirmed by the observation that RhoA shows a completely diffuse localisation in obscurin knock-out-mice, whereas it exhibits a striated pattern in wild-type mice (Lange et al. 2012). A targeted deletion of the obscurin DH domain via morpholino-antisense technology was reported to lead to a series of developmental and functional defects in zebrafish including cardiac hypoplasia and dilation as well as reduced ejection fraction, stroke volume and heart rate although the structural effects were subtle and limited to moderately less defined M-bands and Z-discs (Raeker et al. 2010). In addition to the involvement of the obscurin Rho GEF domains in developmental processes and GTPase signalling in muscle, the PH-domain of obscurin appears to be involved in another surprising interaction: Shriver et al. reported that the PH-domain of obscurin binds to the SH3-domain of phosphatidylinositol-3-kinase (PI3K) subunit p85 and promotes anti-oncogenic signalling in epithelial cells (Shriver et al. 2016). In a subsequent study from the same laboratory, the PH-domain in two novel small obscurin isoforms was reported to bind both PI3K subunit p85 and – in contrast to the PH-domain from *C. elegans* – to phospholipids and it was suggested that these interactions are important to regulate cardiomyocyte adhesion and size via the Akt/mTOR pathway (Ackermann et al. 2017).

Physiological functions of the obscurin Rho GEF domains

Although these studies do not yet provide a clear concept of the physiological function of the obscurin Rho GEF domains, the preliminary picture drawn by their observations suggests that these domains are an attractive candidate for sensing and/or transducing signals in response to mechanical force in order to initiate or regulate adaptive processes. Indeed, Rho GTPases and their regulators are important and central components of many mechanoresponsive signalling pathways in both non-muscle and muscle cells: Strain exerted onto the actin-cytoskeleton, for instance, has been demonstrated to induce conformational changes in actin-bound filamin A, thereby releasing the filamin-bound FilGAP and allowing it to relocate to the plasma membrane where it inactivates the Rho GTPase Rac (Ehrlicher et al. 2011). Cyclic stretch, on the other hand, has been shown to result in RhoA/ROCK and RhoA/mDia dependent actin stress fibre reorientation in epithelial cells and more than 11 GEFs have been found to be involved in such reorientation processes (Abiko et al. 2015; Kaunas et al. 2005). Applying pulling forces to integrins of REF52 fibroblasts has been reported to lead to increased kinase activity (ERK and FAK) and phosphorylation-dependent activation of GEF-H1 and LARG, resulting in activation of RhoA and stiffening of the cell (Guilluy et al. 2011). Similar as in epithelial cells, cyclic stretching of cardiomyocytes leads to activation and phosphorylation of kinases ERK and FAK (Torsoni et al. 2005). Interestingly, RhoA/ROCK critically contributes to FAK and ERK activation in cardiomyocytes, pointing towards the possibility of a positive feedback-loop between RhoA/ROCK signalling and FAK/ERK signalling (Torsoni et al. 2005). Although it is a subject of debate whether RhoA/ROCK activity is detrimental or beneficial in heart disease, the pathway has received particular attention in cardiovascular research due to an association with hypertensive blood pressure, cardiac hypertrophy and other aspects of cardiovascular pathophysiology (Peters and Michel 2007; Shimokawa et al. 2016; Sah et al. 1999; Brown et al. 2006; Xiang et al. 2011; Miyamoto et al. 2010). Moreover, the pathway is particularly interesting because it can regulate calcium handling via PTEN and SERCA2a and increase sarcomeric contractility via phosphorylation and inhibition of myosin light chain phosphatase (MLCP) and troponin I/T, therefore potentially enabling a mechano-mechanical coupling in which mechanical forces initiate signalling processes to alter the mechanical properties of the cell (Amano et al. 1996; Vahebi et al. 2005; Vlasblom et al. 2009; Lauriol et al. 2014). Interestingly, some of the ROCK-mediated events seem to have opposing effects on contractility: phosphorylation of MLCP increases contractility, whereas phosphorylation of troponins decreases contractility (Lauriol et al. 2014; Vahebi et al. 2005). Moreover, mechanical compression of cardiomyocytes has been reported to inactivate RhoA/ROCK signalling via PKA-mediated phosphorylation of RhoA, resulting in less MLCP phosphorylation, thus less myosin RLC phosphorylation and less contraction (Takemoto et al. 2015). Taken together, this bestows the RhoA/ROCK pathway in principle with the intriguing possibility to distinguish between different mechanical inputs and to respond in a specific manner.

It is currently unclear what role exactly obscurin plays in RhoA/ROCK signalling in cardiomyocytes. Given obscurin's association with mechano-signalling and its localisation at the M-band, it is an attractive hypothesis that activation of the Rho GEF domains e.g. by mechanosensitive kinases may initiate protective processes which for example locally increase or decrease contractility to balance out lateral shear forces and to ensure "force balance" at the M-band – whether via RhoA/ROCK signalling or through other Rho GTPases (Agarkova et al. 2003).

1.5.4 Summary of the obscurin interactome

A summary of the direct interactions cited in previous sections as well as selected indirect associations is given in Figure 1.4.

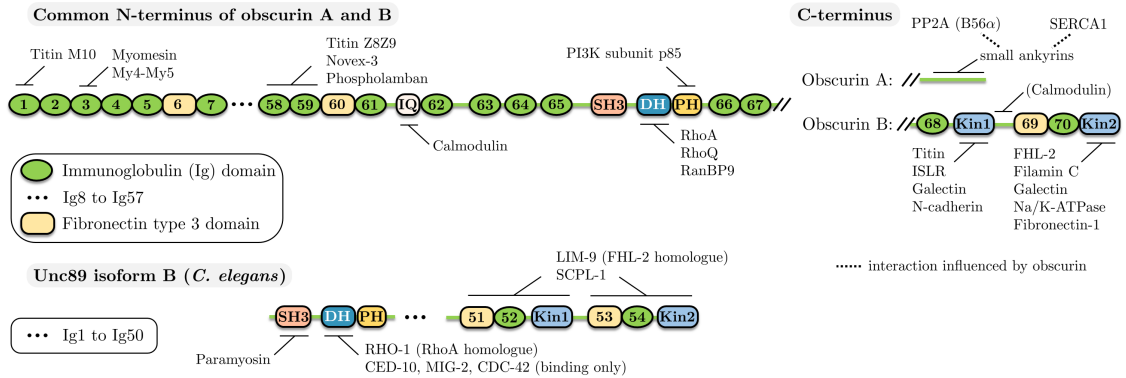


Figure 1.4. Obscurin interactome.

Obscurin is involved in a multitude of protein-protein interactions which are important for structural purposes and to maintain obscurin localisation (e.g. interactions with titin, myosin or small ankyrins). Interactions with signalling molecules such as RhoGTPases, calmodulin or substrates of the kinase domains may play important roles in muscle signalling. Unc89 domain numbering based on (Small et al., 2004). See text for details and references to individual interactions. Not all interactions are supported by the same degree of evidence. While some interactions have been reported by several groups and with multiple methods (e.g. for titin Z8Z9), others were reported only as not further confirmed hit in e.g. in the Y2H-screening assay (e.g. for Galectin).

1.6 β -adrenergic signalling

Cardiac performance and homeostasis are controlled by a multitude of signalling pathways regulating various aspects of cardiomyocyte biology on different time-scales (Hunter and Chien 1999; Molkenin and Dorn 2001; Nakamura and Sadoshima 2018). Many of these pathways feature extensive cross-talk, thereby further complicating the picture (Natarajan et al. 2006). The β -adrenergic signalling cascade is considered to be one of the most important pathways for acute adaption of cardiac performance to increased demand in situations of physiological stress or alert (the “fight-or-flight” response). Binding of catecholamines to β -adrenergic receptors on the cardiomyocyte cell surface results in the activation of adenylate cyclase (AC) via stimulatory G-protein subunits which in turn results in the production of cyclic adenosine mono-phosphate (cAMP) (Lohse et al. 2003). cAMP binds to the regulatory subunits of protein kinase A (PKA), thereby releasing and activating its catalytic subunit (Turnham and Scott 2016). PKA is an important signalling kinase that regulates a plethora of processes in muscle cell physiology. Among its target substrates are well-characterised proteins with crucial roles in cardiac and skeletal muscle such as myosin binding protein C, titin, RyRs, troponin I and phospholamban (Figure 1.1C), whose combined net effect after PKA phosphorylation is the overall increase of cardiomyocyte performance (Kranias and Solaro 1982; Lohse et al. 2003; MacLennan and Kranias 2003; Ponnam et al. 2019; Yamasaki et al. 2002). Local compartmentalisation of cAMP concentration and PKA activity via A-kinase anchoring proteins (AKAPs), phosphodiesterases and other factors allows for differential regulation of these substrates in specific contexts (Bers et al. 2019).

1.6.1 Regulation of cardiac calcium handling by SERCA and phospholamban in the context of β -adrenergic signalling

Cardiac contraction is controlled by membrane depolarisation which triggers the release of calcium from the SR, thereby activating cross-bridge cycling of the sarcomere (Bers 2002; Eisner et al. 2017). For the ventricles to fill with blood again after contraction and ejection, the myocardium needs to relax, requiring calcium to be removed from the cytosol of cardiomyocytes. The activity of the calcium pump SERCA is responsible for removing 70 to >90 % of the Ca^{2+} after contraction, rendering SERCA activity the rate-limiting step of cardiac relaxation (Bers 2002). However, SERCA activity not only determines the rate of cardiac relaxation, but also contributes to regulating the SR calcium concentration and participates in maintaining calcium flux-balance: at steady state, the influx of calcium into the cell and the efflux of calcium out of the cell during contraction cycles need to be equal. Any long-term imbalances would lead to severe net gain or net loss of intracellular calcium which would push the system outside the physiological range of concentrations that allow regulation of the myofilaments, thereby preventing coordinated cardiomyocyte contraction (Eisner et al. 2017; Eisner 2018). Furthermore, dyadic populations of SERCA have been proposed to limit the propagation of spontaneous calcium sparks resulting from high SR load that otherwise could form pro-arrhythmogenic calcium waves (Eisner et al. 2017). Although the influence of SERCA activity on SR calcium concentration generally appears to be moderate at baseline, it is considered to be an important factor during β -adrenergic stimulation as will be further discussed below (Bode et al. 2011). SERCA function is regulated by multiple mechanisms including changes in expression levels and multiple post-translational modifications (Stammers et al. 2015). One of the most prominent and best characterised factors, however, is its regulation by phospholamban (PLN). Being one of the first substrates of PKA to be discovered in heart muscle, it was named after “phosphate” and the Greek word λαμβάνειν, “to receive” (Tada et al. 1975; Katz 1998). PLN is a small 52 amino acid protein embedded in the sarcoplasmic reticulum membrane where it binds and inhibits SERCA by reducing the affinity of SERCA for calcium (Luo et al. 1994; MacLennan and Kranias 2003). The phosphorylation of PLN at serine 16 by PKA leads to a change in the conformation of PLN resulting in the release of SERCA inhibition (Figure 1.1C and Figure 1.5A) (Gustavsson et al. 2013; Traaseth et al. 2006). Comparative studies on PLN, troponin and myosin binding protein C as well as studies on rodents in which PLN was genetically ablated revealed that phosphorylation of PLN mediates the majority of the inotropic (stronger contractions) and lusitropic (faster relaxation) effect of β -adrenergic stimulation (cf. time/force plots shown in Figure 1.5B) (Luo et al. 1994; Garvey et al. 1988; Wolska et al. 1996). In fact, perfused and work-performing hearts isolated from phospholamban-deficient mice exhibited already maximally increased myocardial contractility at baseline which did not improve further upon administration of β -adrenergic agonists, although later studies on single isolated ventricular cardiomyocytes showed some residual effects of β -adrenergic stimulation, indicating that PLN is not solely responsible for the inotropic response (Luo et al. 1994; Wolska et al. 1996). While the positive lusitropy is a direct effect of the faster calcium re-uptake rate upon release of SERCA inhibition via PLN phosphorylation, the positive inotropy is an indirect effect (Bers 2002; MacLennan and Kranias 2003). Increased SERCA activity results in higher SR calcium filling which increases the amplitude of the calcium transient and thereby leads to enhanced myofilament activation and stronger contractions (Bers 2002; Eisner et al. 2017). In addition to phosphorylation by PKA, PLN can also be phosphorylated at threonine 17 by calmodulin-dependent

protein kinase II (CaMKII) and at serine 10 by protein kinase C (PKC), although phosphorylation of PLN at serine 10 has only been observed *in vitro* and not *in vivo* (Simmerman et al. 1986; Wegener et al. 1989; Movsesian et al. 1989; Iwasa and Hosey 1984; Edes and Kranias 1990). Interestingly, calcium-dependent CaMKII activity and thus phosphorylation of PLN at threonine 17 is frequency dependent and mechanistically independent of serine 16 phosphorylation (Koninck and Schulman 1998; Hagemann et al. 2000). Phosphorylation at threonine 17, too, releases SERCA inhibition (Mattiuzzi and Kranias 2014). However, under physiological conditions only less than 5% of total PLN is phosphorylated by CaMKII and thus is expected to contribute little to the PLN-mediated β -adrenergic response (Huke and Bers 2007; Mattiuzzi et al. 2005; Mattiuzzi and Kranias 2014). Despite these relatively low phosphorylation levels, however, PLN phosphorylation by CaMKII has been reported to contribute to the enhanced myocardial contractility at higher heart rates (Wu et al. 2012). Significant phosphorylation of PLN by CaMKII has furthermore been reported under pathophysiological conditions such as cardiomyocyte acidosis or ischemia-reperfusion and can have both beneficial and detrimental effects depending on the balance of various other factors in these contexts (Mattiuzzi and Kranias 2014).

The phosphorylation state of phospholamban is not only regulated by kinases PKA and CaMKII, but also by protein phosphatases 1 and 2A (PP1 and PP2A, respectively) as well as modulatory proteins inhibitor-1 and Hsp20 which can inhibit PP1 after phosphorylation by PKA, thereby constituting feed-forward loops which may amplify the β -adrenergic response (El-Armouche et al. 2003; Macdougall et al. 1991; Nicolaou et al. 2009; Qian et al. 2011; Vafiadaki et al. 2007; Vafiadaki et al. 2013).

PLN is thus embedded in a regulatory network (Figure 1.5B) whose complexity keeps growing in size due to the continued discovery of new components. Interestingly, one of most recently

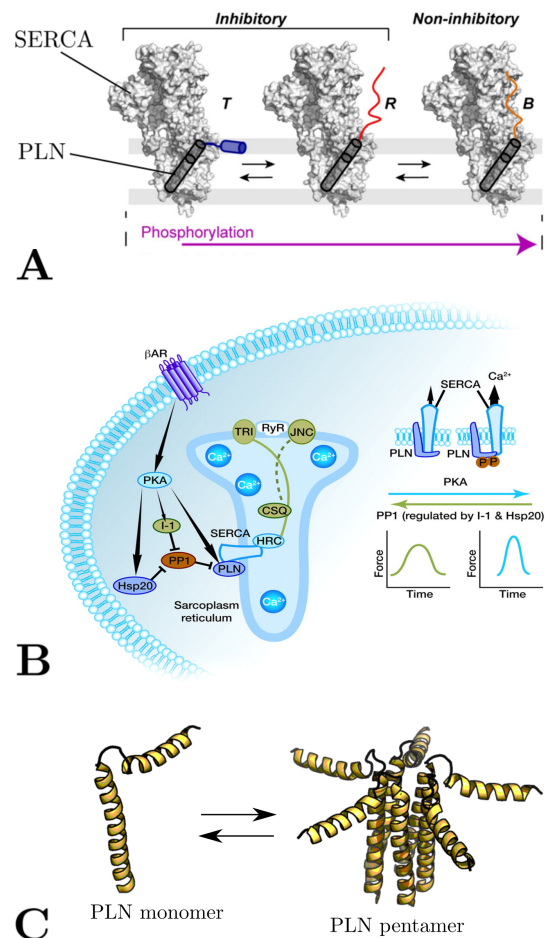


Figure 1.5. Regulation of cardiac calcium cycling by SERCA and phospholamban (PLN)

A, PLN binds and in the unphosphorylated inhibits the SERCA pump (T- and R-state). Phosphorylation of PLN by PKA in the context of β -adrenergic stimulation shifts the conformational equilibrium of the SERCA:PLN complex towards the non-inhibitory B-state with a higher calcium affinity, thereby increasing SERCA activity. Reprinted with permission from Gustavsson M, et al. (2013): Allosteric regulation of SERCA by phosphorylation-mediated conformational shift of phospholamban. PNAS, 110: 17338–17343. **B**, PLN is embedded in a biochemical signalling network with multiple kinases, phosphatases and regulatory proteins which together control PLN phosphorylation and thus SERCA activity and cardiac contractility. Figure reprinted with permission from Kranias EG, Hajjar RJ (2012): Modulation of Cardiac Contractility by the Phospholamban/SERCA2a Regulatome. Circ Res, 110: 1646–1660. **C**, PLN exists in an equilibrium between a monomeric form responsible for binding and inhibiting SERCA, and a pentameric form whose role is currently unclear (PDB-ID: 2KYV).

reported interaction partners for PLN, certainly one of the smallest proteins in cardiac physiology, involves obscurin, one of the largest proteins in heart muscle cells (Hu et al. 2017). Although the basic mechanism of enhancing contractility and relaxation via phosphorylation of PLN are well understood, what role exactly these other network components play in controlling the dynamics, shape and robustness of the physiological β -adrenergic response is less clear.

1.6.2 Phospholamban pentamers and the role of homo-oligomerisation in signalling networks

A good example for a poorly understood aspect of PLN is the assembly of PLN into homo-pentamers. Since their discovery in 1984 by Wegener and Jones, the physiological role of PLN pentamers has remained unclear and controversial (Wegener and Jones 1984). The first hypothesis was introduced by Kovacs et al. who in 1988 observed conductivity for Ca^{2+} and K^+ after addition of PLN to lipid bilayers, which led the authors to propose that PLN pentamers act as ion channels (Kovacs et al. 1988). At first glance, this hypothesis seems to receive further support by the channel-like structure of PLN pentamers with a central pore between PLN's transmembrane helices (cf. Figure 1.5C) (Oxenoid and Chou 2005; Verardi et al. 2011). Based on structural considerations, Oxenoid and Chu proposed PLN pentamers also to potentially be permeable for Cl^- ions (Oxenoid and Chou 2005). Two recent studies by Smeazzetto and colleagues, however, reported that PLN pentamers are selective for small monovalent cations such as K^+ , but not for larger divalent cations such as Ca^{2+} (Smeazzetto et al. 2016; Smeazzetto et al. 2018). In contrast, detailed structural, experimental and theoretical studies by the Veglia group contested the ion-channel hypothesis more generally. Experiments by Becucci et al. demonstrated that PLN pentamers do not conduct Cl^- ions (Becucci et al. 2009). The structural and theoretical considerations from these studies furthermore suggest that conduction of other ions is thermodynamically not feasible due to the small size of the pore and that the pore configuration is generally unsuited to act as selectivity filter for ions (Becucci et al. 2009; Vostrikov et al. 2013). Due to these conflicting studies, the ion-channel hypothesis thus remains controversial. Since artificial monomeric mutants of PLN have furthermore been found to be equally potent inhibitors of SERCA function as wild-type PLN, the prevailing paradigm considers PLN pentamers to be an inactive storage form or buffering reservoir to keep the concentration of active monomers within a physiological range (Becucci et al. 2009; Kimura et al. 1997; Kranias and Hajjar 2012; MacLennan and Kranias 2003; Vostrikov et al. 2013). As SERCA function can already be regulated via numerous mechanisms that operate on different time-scales (including changes in expression levels and multiple post-translational modifications, as mentioned earlier) (Stammers et al. 2015) even without considering PLN monomers, it is not obvious what advantage such buffering by pentamers might offer.

However, a few studies which have received relatively little attention so far indicate that PLN pentamers could play a more active role than currently appreciated. A 1998 study from the Kranias and Bers groups on transgenic mice with wild-type PLN and with the artificial mutation C41F (which prevents pentamerisation) found that pentamers contribute to reduce cardiac contractility at baseline and that the β -adrenergic response is somewhat blunted in the absence of pentamers (Chu et al. 1998). Pentamers also appear to be relevant in the context of phosphorylation and dephosphorylation. Studies from the Colyer laboratory demonstrated that phosphorylation of PLN pentamers by CaMKII and dephosphorylation of PKA-phosphorylated PLN pentamers (likely via PP1) exhibits strong positive cooperativity (Li et al. 1990; Jackson and Colyer 1996; Colyer

1998). Phosphorylation by PKA has also been reported to promote pentamerisation of PLN, although others studies could not confirm this effect (Chu et al. 1998; Cornea et al. 1997; Hou et al. 2008; Wittmann et al. 2015). More recently, Wittmann et al. reported PLN pentamers to be phosphorylated more rapidly than PLN monomers and to attenuate the phosphorylation of the latter at low stimulation levels, which the authors proposed to gradually increase SERCA activity at a slower time-scale than direct monomer phosphorylation (Wittmann et al. 2015).

While these studies suggest that PLN pentamers are likely more than an inactive storage form for monomers, they do not provide a clear picture of their physiological role beyond vague and rather unhelpful notions such as “fine-tuning”. Interestingly, this situation applies more generally to our current understanding of the role of homo-oligomers. Although 30-50% of all proteins in vertebrates can form homo-oligomers, a general understanding of the possible roles and functions oligomerisation can play is currently lacking (Lynch 2012; Marsh and Teichmann 2015). Homo-oligomerisation can often be a quite economic way to form large molecules in the cell e.g. for structural purposes and may be favoured by evolution due to higher error-free transcription rates of small monomeric subunits (Ali and Imperiali 2005; Marianayagam et al. 2004). A well-established concept is that oligomers can allow for allosteric regulation and cooperative binding as for example in the cooperative binding of oxygen by the tetramer haemoglobin (Marianayagam et al. 2004). However, these exemplary functions hardly apply to all homo-oligomers or can account e.g. for the abundance of homo-oligomers among enzymes, two thirds of which form homo-oligomers (Marianayagam et al. 2004). A better understanding of what functions homo-oligomers can perform in the context of signalling networks, including an understanding of how the dynamics of their assembly and disassembly look like or how they influence e.g. the regulation of post-translational modifications, may therefore also enable novel insights into the physiological role of PLN pentamers.

1.7 Medical relevance

Both obscurin and phospholamban have been implicated in the pathophysiology of heart failure and cardiac arrhythmias. This section briefly introduces some of the most relevant aspects of these conditions for the presented work before reviewing the role of phospholamban and obscurin in their pathophysiology.

1.7.1 Heart failure, genetic cardiomyopathies and cardiac arrhythmias

Heart failure

Heart failure (HF) is a common and clinically important issue which, as first approximation, can be characterised as the inability of the heart to properly pump blood (see e.g. the definition by the NHS in its information material for patients at <https://www.nhs.uk/conditions/heart-failure/>, last accessed 07/06/2021). The prevalence of HF is increasing quickly and in 2016 already affected more than 37 Million people globally (Ziaei and Fonarow 2016). The European Society of Cardiology defines HF in their 2016 guidelines as follows:

“HF is a clinical syndrome characterized by typical symptoms (e.g. breathlessness, ankle swelling and fatigue) that may be accompanied by signs (e.g. elevated jugular venous pressure, pulmonary crackles and peripheral oedema) caused by a structural and/or functional cardiac abnormality, resulting in a reduced cardiac output and/or elevated intracardiac pressures at rest or during stress.” (Ponikowski et al. 2016)

Chronic heart failure is a condition that can often be managed effectively with adequate therapy and risk minimisation, although the average 10-year survival probability after diagnosis remains below 30% (Ponikowski et al. 2016; Roger 2013; Taylor et al. 2019). Acute HF, however, is a life-threatening situation that requires urgent intervention and may result from the decompensation of chronic HF or factors such as cardiac arrhythmias, myocardial infarction, drug intoxication, infections (e.g. myocarditis) and others (Ponikowski et al. 2016).

Functionally, HF can further be subdivided into systolic and diastolic HF (SHF and DHF, respectively). While SHF is characterised by a reduced ejection volume and higher end diastolic volume, DHF, in contrast, is primarily characterised by a reduced end diastolic volume, i.e. by impaired filling of the left ventricle (Katz and Rolett 2016). Structurally, DHF is typically preceded and accompanied by a concentric hypertrophy of the left ventricle wall, whereas SHF is accompanied by dilation and eccentric hypertrophy of the left ventricle wall (Figure 1.6A) (Katz and Rolett 2016; Nakamura and Sadoshima 2018). On a cellular level, concentric hypertrophy of cardiomyocytes results from the addition of sarcomeres in parallel, whereas serial addition of sarcomeres is underlying eccentric hypertrophy (Hunter and Chien 1999; Nakamura and Sadoshima 2018). On a biochemical level, cardiac hypertrophy is mediated by altered activity in numerous signalling and gene-regulatory networks in response to mechanical or humoral stimuli including growth factors, interleukins, catecholamines, angiotensin II, and others (Lymperopoulos et al. 2013; Lyon et al. 2015; Molkenkin and Dorn 2001; Nakamura and Sadoshima 2018). The hypertrophic response involves changes to almost all aspects of cell biology such as transcriptional regulation, protein synthesis, calcium handling, cell survival, contractility and energy metabolism (Hunter and Chien 1999; Nakamura and Sadoshima 2018; Tham et al. 2015). The list of pathways, molecules and genes involved in this response is too long for an exhaustive list, but includes the Ras/MAPK/Erk cascade, signalling kinases and phosphatases (AMPK, Akt, CaMKII, PKA, PKC, PKG, PI3K, PP1, PP2A, Calcineurin), small GTPases (RhoA, Rac1, Cdc42) and many more (Figure 1.6B) (Brown et al. 2006; Hunter and Chien 1999; Molkenkin and Dorn 2001; Nakamura and Sadoshima 2018; Tham et al. 2015). Initially, these signals serve to adapt heart function by increasing the contractile and metabolic activity of the myocardium. Both concentric and eccentric hypertrophy offer a temporary solution for haemodynamic challenges of the heart.

Concentric hypertrophy typically results from pressure overload during systole and the increased wall-thickness (h_w) reduces wall tension (T) according to the law of Laplace ($T \sim h_w^{-1}$), thereby improving contractility (Katz and Rolett 2016). Eccentric hypertrophy is a way to accommodate volume overload and at least on short time-scales the increased filling of the left ventricle during diastole leads to higher stroke volumes via the Frank-Starling mechanism (increased filling volumes stretch the muscle fibres which improves their contractility) (Katz and Rolett 2016). Both types of hypertrophy are, however, eventually maladaptive. Concentric hypertrophy can be beneficial to maintain cardiac output even over longer periods but leads to trophic issues that result in cell death, fibrosis and progress towards eccentric hypertrophy and ventricle dilation (Nakamura and Sadoshima 2018; Tham et al. 2015). Eccentric hypertrophy, in contrast, quickly triggers a vicious cycle in which the increased chamber volume increases wall stress, leading to further eccentric hypertrophy, leading to an even larger chamber volume and reduced stroke volumes (Figure 1.6C) (Katz and Rolett 2016).

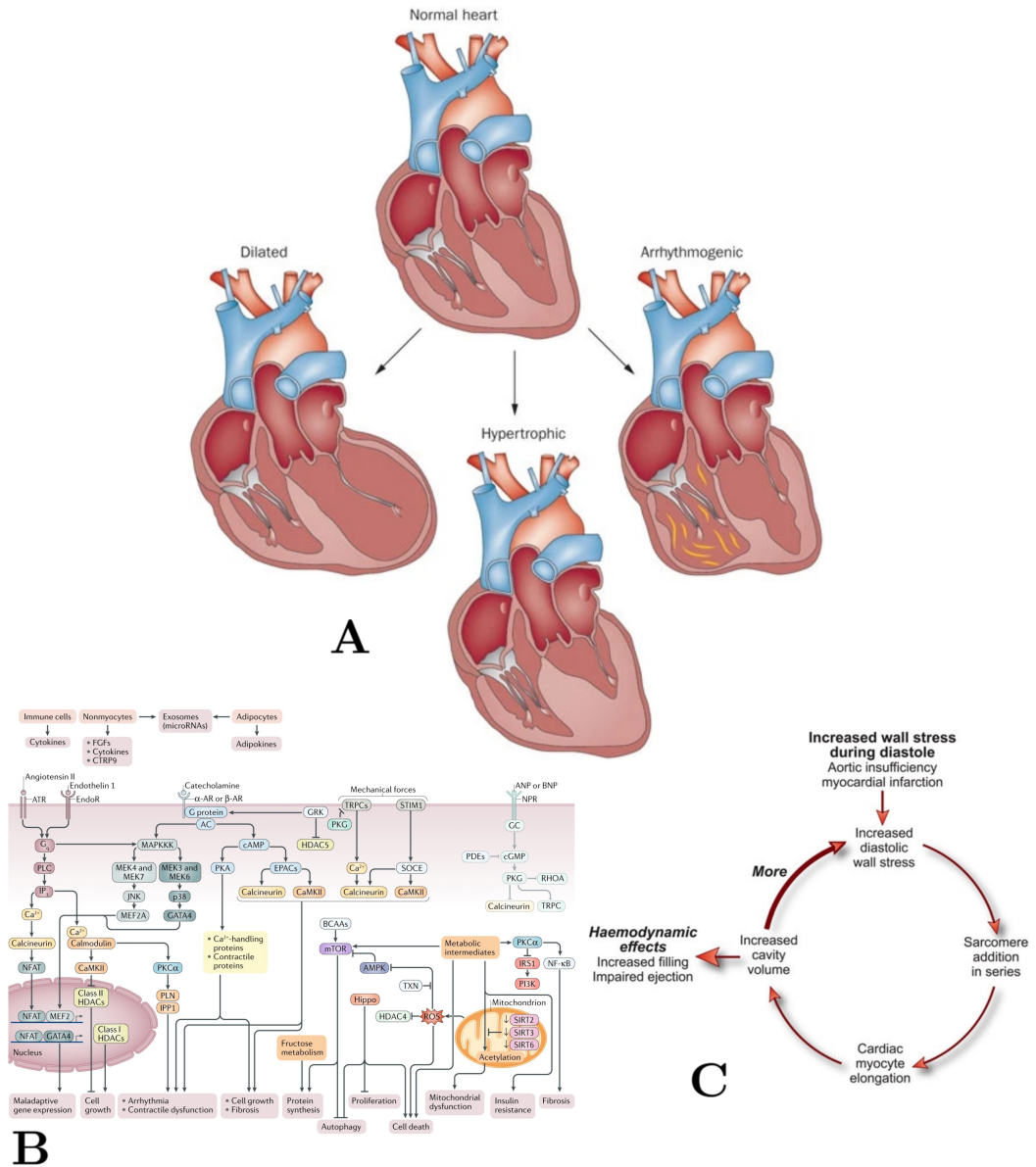


Figure 1.6. The hallmarks of heart failure.

A, Genetic or lifestyle related factors can cause cardiomyopathies which can be subdivided into different categories based on their appearance, hypertrophy patterns and contractile properties. Top: healthy heart. Left: dilated cardiomyopathy is characterised by eccentric hypertrophy and chamber dilation, leading to volume overload and decreased contractility and ejection. Bottom: hypertrophic cardiomyopathy is characterised by concentric hypertrophy and enlarged ventricle walls leading to reduced end-diastolic volumes. Right: other categories such as arrhythmogenic cardiomyopathy are less easily distinguished by anatomical features and also rely on other phenotypical factors (e.g. haemodynamics, arrhythmias). Reprinted by permission from Springer Nature. *Nat. Rev. Cardiol.* Dilated cardiomyopathy: the complexity of a diverse genetic architecture. Hershberger RE, Hedges DJ, Morales A. © 2013, Macmillan Publishers Limited.

B, Signalling pathways integrate information from neurohumoral and mechanical signals leading to changes in cellular processes and behaviour including growth, cell death, gene-expression, calcium handling, metabolic activity, contractility and others. While some of these are initially adaptive and beneficial, they often become maladaptive and lead to deleterious remodelling of the myocardium in the long run. Reprinted by permission from Springer Nature. *Nat. Rev. Cardiol.* Mechanisms of physiological and pathological cardiac hypertrophy. Nakamura M, Sadoshima J. © 2018, Macmillan Publishers Limited.

C, Maladaptive signalling and eccentric hypertrophy during dilated cardiomyopathy quickly triggers a vicious cycle in which lack of contractility and impaired ejection causes more eccentric hypertrophy, thereby further reducing contractility. Reprinted from Katz AM, Rolett EL. Heart failure: when form fails to follow function. *Eur Heart J.* 2016, 37(5): 449-454, by permission of the European Society of Cardiology.

It is not easy to distinguish cause and effect in the molecular pathophysiology of hypertrophy and heart failure. One complicating factor is that the involved signalling processes can differ depending for example on the type of hypertrophy or the cause (primary causes such as genetic mutations or secondary effects such as chronic hypertension) (Brown et al. 2006; Cahill et al. 2013; Nakamura and Sadoshima 2018; Tham et al. 2015). Furthermore, as the initially adaptive, but eventually maladaptive responses illustrate, the consequences of altered signalling activity are often dynamic and the chain of causation cyclical. Enhanced RhoA activity, for instance, initially leads to cardiomyocyte hypertrophy, but prolonged activation results in increased apoptosis and fibrosis (Aoki et al. 1998; Del Re et al. 2007; Lauriol et al. 2014). Similarly, increased β -adrenergic signalling is beneficial in the short run as it improves contractility and cardiac output, but is detrimental when forcing a diseased heart to work beyond its capacity, thereby causing increased apoptosis and fibrosis in the long run (Lohse et al. 2003; Lymperopoulos et al. 2013).

To a considerable extent, the aetiology of HF is based on preventable conditions such as myocardial infarction, hypertension or atrial fibrillation, all of which are strongly predicted by lifestyle related risk factors such as diet, exercise, smoking and alcohol consumption (Djoussé 2009; Ponikowski et al. 2016; Ziaieian and Fonarow 2016). However, genetic causes, too, are among the most frequent causes of HF, particularly genetic cardiomyopathies (Ponikowski et al. 2016; Ziaieian and Fonarow 2016). According to their morphological phenotype, genetic cardiomyopathies can be categorised as hypertrophic cardiomyopathy (HCM; characterised by concentric hypertrophy) or dilated cardiomyopathy (DCM; characterised by eccentric hypertrophy), although less frequent types such as arrhythmogenic (ACM), restrictive and left-ventricular non-compaction cardiomyopathies do exist (Cahill et al. 2013). Some of these, however, are not necessarily different disease entities. DCM and ACM, for instance, have recently been proposed to be poles of a continuum, rather than to be different cardiomyopathies (Zwaag et al. 2012). HCM typically results from single mutations in sarcomeric proteins such as the myosin heavy chain, cMyBPC or Titin and these mutations are often inherited in an autosomal dominant fashion (Cahill et al. 2013; Marian 2021; Marian and Braunwald 2017). The prevalence of HCM is estimated to lie somewhere between 1:300 to 1:600, with 1:500 being one of the most commonly used estimates in the literature (Alcalai et al. 2008; Marian 2021; Maron and Maron 2013). DCM, while not uncommon, only affects about 1 in 2500 people (Kärkkäinen and Peuhkurinen 2007). The molecular genetics of DCM is considered to be more multifactorial, with monogenic causes only accounting for about 25-35% of observed cases and a significant contribution of non-genetic causes (Kärkkäinen and Peuhkurinen 2007; Luk et al. 2009). Like HCM, DCM can result from mutations in sarcomeric proteins (Kärkkäinen and Peuhkurinen 2007; Luk et al. 2009). Interestingly, mutations in genes that are associated with both HCM and DCM often seem to have functionally opposite effects, further supporting the idea that the pathophysiology leading to HF can be disease specific (Cahill et al. 2013; Tadros et al. 2021). In addition, both HCM and especially DCM can result from mutations in non-sarcomeric proteins involved in calcium handling, sarcolemmal integrity, signalling or ion homeostasis (Cahill et al. 2013; Kärkkäinen and Peuhkurinen 2007; Marian 2021; Marian and Braunwald 2017; Maron and Maron 2013).

Although substantial progress has been made in understanding the way how some mutations impair cardiac function and lead to disease (e.g. impairing incorporation of a protein into the sarcomere or reducing force generation), a detailed mechanistic understanding of the physiological roles and how mutations can interfere with them is still lacking for many proteins associated with cardiomyopathies (Cahill et al. 2013; Marian and Braunwald 2017).

1.7.2 Cardiac arrhythmias

Cardiac arrhythmias are deviations from the physiological, rhythmic electrical activity of the heart and can range from harmless occasional extrasystoles without clinical significance to dangerous and immediately life-threatening arrhythmias such as ventricular fibrillation which impedes any coordinated pumping activity of the heart. The classification of arrhythmias can be made along multiple dimensions such as anatomical origin (supra-ventricular vs. ventricular), velocity (brady- vs. tachycard), ECG characteristics (relevant parameters include e.g. the appearance of P-wave, QRS complex or T-wave, duration of specific intervals and others), genetic origin (e.g. inherited vs. secondary, non-genetic cause such as myocardial infarction or intoxication) and others (Brugada et al. 2020; Fu 2015; Padeletti and Bagliani 2017; Priori et al. 2015).

The epidemiological evaluation of cardiac arrhythmias as a whole is challenging not only due to the complexity of the classification but also due to limited data availability for some of these diseases (Offerhaus et al. 2020). However, epidemiological data on just a few types of arrhythmias illustrates that cardiac arrhythmias are an important clinical issue: Congenital long QT-syndrome affects 1:2000 to 1:2500 persons, more than 1 in 500 persons are affected by supraventricular tachycardias and ventricular fibrillation causes between 1100 and 9000 sudden cardiac deaths each year in Europe alone (Brugada et al. 2020; Offerhaus et al. 2020; Priori et al. 2015).

A particular challenge in understanding cardiac arrhythmias arises not only from the inherent non-linear nature of cardiac electrical dynamics, but also from the fact that their emergence and maintenance involves multiple temporal and spatial scales ranging from subcellular to cellular to tissue level processes (Kistamás et al. 2020; Noble 2002; Qu et al. 2014). In a work dedicated to biochemical signalling processes, we can therefore only outline some basic mechanistic principles underlying the emergence of cardiac arrhythmias.

As outlined earlier, the depolarization of the cardiomyocyte cell membrane triggers intracellular calcium waves which regulate sarcomeric cross-bridge cycling. The contractions of the heart are therefore controlled by its electrical activity. From an electrophysiological perspective, cardiac arrhythmias can arise from irregularities both in the generation or conduction of electrical pulses (Cabo and Wit 1997; Gaztañaga et al. 2012). A good example for a condition resulting from irregular impulse generation is the sick sinus syndrome, in which the primary pace-maker of the heart, due to genetic mutations or secondary changes to the sinus node tissue, generates abnormally fast or slow impulse rates (Dobrzynski et al. 2007). Autonomous electrical automaticity in the ventricular tissue, too, constitutes abnormal impulse generation and can trigger arrhythmias (Gaztañaga et al. 2012). Irregular impulse conduction, in contrast, can result from anatomical or functional obstacles which can cause the re-entry of electrical activity into incompletely repolarised but re-excitabile heart tissue (Figure 1.7A) (Gaztañaga et al. 2012; Qu and Weiss 2015). Depending on the circumstances, such re-entry currents can cause various forms of tachycardias or even ventricular fibrillation.

Similar to neurons, the cardiac action potential is generated by changing fluxes mainly of sodium, calcium and potassium ions (Figure 1.7B). Unsurprisingly, many genetic cardiac arrhythmia syndromes result from genes implicated in regulating these fluxes such as ion-channels or transporters (Qu and Weiss 2015). Calcium influences both the cardiac action potential and excitation-contraction coupling. Aberrant calcium handling is thus an important factor in the molecular pathophysiology of cardiac arrhythmias (Kistamás et al. 2020; Landstrom et al. 2017; Opbergen et al. 2017). In fact, dysfunctional calcium handling can cause or contribute to both

impulse generation and conduction problems: Abnormal impulse generation leading to autonomic focal activity is often triggered by early or delayed afterdepolarisations which interrupt the normal repolarisation process (Figure 1.7C) (Kistamás et al. 2020; Landstrom et al. 2017). Early afterdepolarizations, for instance, can arise due to spontaneous calcium release from the SR which in turn activates depolarising currents via the $\text{Na}^+/\text{Ca}^{2+}$ -exchanger (NCX) and can reactivate Ca^{2+} influx via L-type channels during the plateau phase of the action potential (Kistamás et al. 2020). Elevated intracellular calcium concentration can also support the occurrence of early afterdepolarizations, particular in the context of cardiac hypertrophy, heart failure, acidosis, β -adrenergic stimulation and other factors (Kistamás et al. 2020).

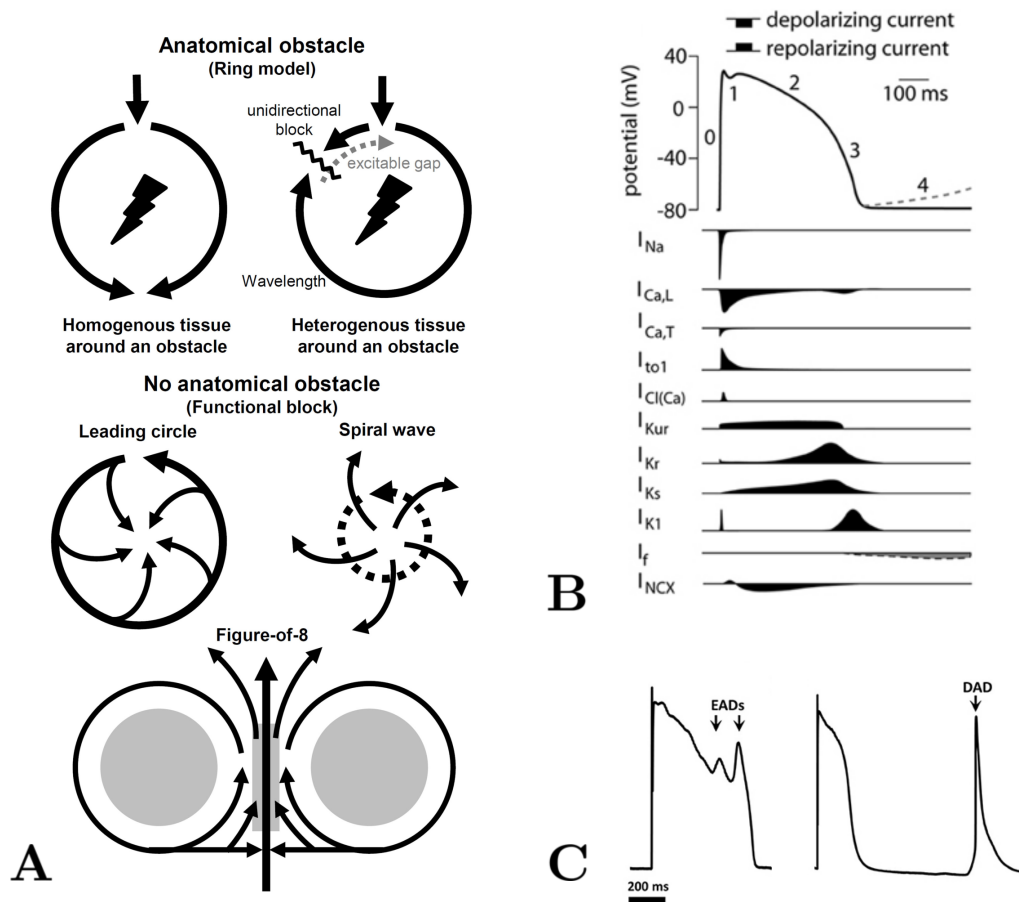


Figure 1.7. Mechanisms of cardiac arrhythmias.

A, Heterogeneities in tissue composition (top) or the electrophysiological properties of cardiomyocytes (middle, bottom) can lead to the re-entry of electrical excitation independent from physiological pacemaker activity. Focal re-entry activity can cause e.g. tachyarrhythmias or ventricular fibrillation. Figure reprinted with permission from Kistamás et al. 2020 under the Creative Commons Attribution License (CC BY). **B**, The cardiac action potential (top) is the result of ionic currents (Na^+ , K^+ and Ca^{2+} ions) regulated by multiple channels and ion pumps (bottom). After initial influx of Na^+ (0) and Na^+ -channel inactivation (1), depolarising Ca^{2+} influx and release from the SR counterbalances early repolarisation, leading to a plateau phase (2). Following Ca^{2+} -channel inactivation, multiple potassium currents further repolarise the cell (3) until resting membrane potential is reached (4). Figure reprinted with permission from Hoekstra et al. 2012 under the Creative Commons Attribution License (CC BY). **C**, On the subcellular level, altered balance of ion concentrations (e.g. calcium) or ion channel/pump function can result in early or delayed afterdepolarizations which are pro-arrhythmogenic. Figure adapted with permission from Denham et al. 2018 under the Creative Commons Attribution License (CC BY).

Impulse conductance, too, can be negatively impacted by reduced gap-junction conductance due to high intracellular calcium (Kistamás et al. 2020). The same factors can also promote delayed afterdepolarisations by increasing the SR calcium load and thus increasing the probability for spontaneous calcium release (Kistamás et al. 2020). Moreover, irregular calcium handling can promote spatially heterogeneous excitation and repolarisation behaviour across the heart tissue (dispersion of excitability and refractoriness) as well as temporal heterogeneity in the calcium transient (termed calcium alternans) which can further lead to variability of action potential duration, and both types of heterogeneity can promote focal activity and re-entrant arrhythmias (Kistamás et al. 2020; Qu et al. 2010; Weiss et al. 2011). Consistent with these findings, mutations in signalling proteins which regulate calcium handling are often pro-arrhythmogenic (Kistamás et al. 2020; Landstrom et al. 2017; Opbergen et al. 2017).

1.7.3 Current therapy approaches

In comparison to the complexity of the specific causes for HF and cardiac arrhythmias, the available therapeutic tools are rather unspecific and mainly directed at preventing further deterioration of the patient's condition. Apart from minimising and adjusting life-style related risk factors (obesity, smoking, etc.), drug therapy of chronic HF plays an important role in reducing the workload of the heart and for preventing or slowing down adverse cardiac remodelling processes. Important key classes of drugs in the therapy of chronic HF include β -blockers, ACE II inhibitors and diuretics (Ponikowski et al. 2016). All of these exert an anti-hypertensive effect, i.e. lower the blood pressure, and improve cardiac haemodynamics, thereby reduce the workload of the heart. β -blockers also have a protective effects against tachyarrhythmias (i.e. arrhythmias which exceed the normal heart rate) and can help the heart to exit or reduce the vicious cycle of chronically increased β -adrenergic tonus due to insufficient cardiac output which leads to further progression of the condition (Lohse et al. 2003). In addition, both β -blockers and ACE II inhibitors have a positive influence on cardiac remodelling (Khattar et al. 2001). Positive inotropes which improve cardiac contractility can offer some short-term symptomatic relief and seem to be a plausible approach to improve cardiac function at first glance (Ponikowski et al. 2016). However, since none of these drugs has been shown to improve survival so far, positive inotropes only have a limited indication in the pharmacotherapy of HF, although the discussion of their potential usefulness has recently received new attention (Ahmad et al. 2019). The therapeutic management of HF can require further drug therapy to minimise other cardiovascular risks such as coronary heart disease or arrhythmias (Ponikowski et al. 2016). If and when pharmacotherapy and life-style related interventions fail, additional interventions such as the implantation of a cardioverter defibrillator or even mechanical circulatory support or heart transplantation can become necessary (Ponikowski et al. 2016).

Anti-arrhythmic drug therapy, too, is highly unspecific. Important classes of molecules include the above mentioned β -blockers, different types of sodium channel blockers (e.g. Procainamide), potassium channel blockers (e.g. Amiodarone), calcium channel blockers (e.g. Diltiazem), and other drugs (Lei et al. 2018). Since conventional anti-arrhythmic pharmacotherapy is often insufficient, additional measures can be required to control the emergence of arrhythmias such as atrial fibrillation (e.g. catheter ablation) and their potential consequences (as atrial fibrillation can cause blood clotting which increases the risk for ischaemic strokes, anticoagulation therapy is typically necessary) (Brugada et al. 2020; Priori et al. 2015). Although current drug therapies for HF and cardiac arrhythmias do improve survival and quality of life, none of the drugs currently in use

typically addresses the underlying cause of the condition. Particularly for inheritable conditions with a specific underlying genetic cause, these general purpose therapies are often not sufficient to compensate the molecular consequences of the mutation. Moreover, antiarrhythmic drugs in particular often suffer from a narrow therapeutic window (Mankad and Kalahasty 2019). The development of novel therapy approaches and drugs are therefore the focus of significant research efforts in the cardiovascular field (Tham et al. 2015).

1.7.4 Obscurin in the context of cardiovascular diseases

Obscurin and mutations in the encoding OBSCN gene have been associated with various neuromuscular, cardiovascular and other diseases such as cancer (Marston 2017; Randazzo et al. 2017b). Here, we will focus mostly on the association with cardiovascular diseases.

One of the earliest evidence for the potential involvement of obscurin in processes relevant to cardiovascular disease came from the observation that obscurin transcript levels comprising the Rho GEF domains showed a significant and sustained increase in mice after aortic banding, pointing towards a role in myocardial hypertrophy (Borisov et al. 2003). Consistent with this idea, two missense-mutations in the OBSCN gene were discovered in 2007 in a 19-year old patient with left-ventricular hypertrophic cardiomyopathy, resulting in a substitution of Arginine 4344 in Ig58 to Glutamine (R4344Q) and Alanine 4444 in Ig59 to Threonine (A4444T) (Arimura et al. 2007). Based on data from luciferase and co-immunoprecipitation binding assays as well as immunofluorescence studies of exogenously expressed obscurin Ig58-Ig59 in neonatal rat cardiomyocytes, the authors reported the R4344Q mutation, but not the A4484T mutation, to impair both binding to titin Z8-Z9 and recruitment of obscurin Ig58-Ig59 to the M-band (Arimura et al. 2007). Ten years later, a study from the Kontrogianni-Konstantopoulos group characterised a mouse model of the R4344Q mutation and reported the mutation to cause aberrant calcium handling, cardiac arrhythmias and, when mice were subjected to aortic banding, a dilated cardiomyopathy like phenotype (Hu et al. 2017). Mechanistically, the authors explained the phenotype to stem from a newly identified interaction between obscurin Ig58 and the cytoplasmic domain of PLN which the authors reported being strengthened by the R4344Q mutation, thereby sequestering monomeric PLN (Hu et al. 2017). Shortly before the completion of this PhD thesis, the same group published another, related study on the deletion of obscurin domains Ig58-Ig59 in mice (Grogan et al. 2020). Deletion of these domains, too, was reported to alter calcium handling, but the effects were mostly opposite to those observed in R4344Q mice and accompanied by changes in the phosphorylation and expression of several calcium-handling proteins including SERCA, RyR and PLN. Phenotypically, these mice demonstrated cardiac hypertrophy and age- and sex-dependent remodelling as well as impaired contractility and arrhythmias, particularly under β -adrenergic stimulation (Grogan et al. 2020). However, as the R4344Q variant is highly common among African Americans (up to 15% of individuals), other research groups have challenged the classification of this variant as pathogenic (Manrai et al. 2016; Marston 2017).

In recent years, an increasing number of novel OBSCN missense-mutations is being associated with various cardiovascular diseases including dilated cardiomyopathy, hypertrophic cardiomyopathy and left ventricular noncompaction and more are expected to be discovered (Marston 2017; Marston et al. 2015; Xu et al. 2015; Rowland et al. 2016). However, the mechanistic effect of these genetic mutations is currently still unclear. As expected from the gene structure, most mutations affect Ig-domains in obscurin, although one dilated cardiomyopathy associated mutation has been

reported to affect the PH-domain of obscurin (Marston et al. 2015). In addition to cardiovascular diseases, obscurin is also associated with skeletal myopathies. A missense mutation leading to an exchange of Arginine 4444 in obscurin domain Ig59 for Tryptophan, for instance, has been reported to impair binding to titin Z8-Z9 and to be associated with earlier and more severe onset of distal muscular dystrophy caused by a filamin C frameshift mutation (Rossi et al. 2017). Moreover, several titin mutations are known to disrupt the interaction between titin and obscurin/obs1-1 at the M-band, contributing to the pathophysiology of several skeletal muscle disorders (Pernigo et al. 2010).

In summary, these studies provide evidence that perturbing the physiological functions of obscurin can contribute to the development of cardiovascular and neuromuscular disease. Although several researchers have already considered it as an interesting pharmacological target (Randazzo et al. 2017b), our understanding of the physiological and pathophysiological roles of obscurin is perhaps still too rudimentary to evaluate the prospects of successful therapeutic interventions.

1.7.5 Phospholamban in the context of cardiovascular diseases

Studies from the 1990s and early 2000s which investigated the effect of ablating PLN from the murine heart showed that deletion of PLN improved cardiac function without compromising the life span, suggesting that loss of PLN is actually beneficial (Luo et al. 1994; Wolska et al. 1996; Slack et al. 2001). Earlier studies which demonstrated that PLN expression relative to SERCA expression is increased during HF and that PLN ablation can rescue the phenotype of DCM mouse models further supported this interpretation (Meyer et al. 1995; Minamisawa et al. 1999). The discovery of one of the first natural PLN mutations, PLN-L39stop, however, challenged this view. Discovered in patients with hereditary HF, the characterisation of this mutation demonstrated that PLN-L39stop patients and HEK293 cell based PLN-L39stop models expressed almost no functional PLN and thus exhibited no SERCA inhibition in the cell models (Haghighi et al. 2003). Homozygous PLN-L39Stop carriers developed severe heart failure and required heart transplantation before the age of 30 (Haghighi et al. 2003). Since the pedigree of patients carrying the mutation left no doubt that this variant is responsible for causing DCM and early HF, this study demonstrated that humans, unlike mice, require PLN and that PLN loss-of-function mutations are highly deleterious for the human heart (Haghighi et al. 2003). Only a month earlier, the Seidman group published their discovery of the first pathogenic PLN mutation, the Arginine to Cysteine substitution at position 9 (R9C), leading to severe DCM and HF at young age, thereby drastically limiting the life expectancy of affected patients (average age of death \approx 25) (Schmitt et al. 2003). Curiously, the R9C-PLN does not inhibit SERCA function itself, but reduces PLN phosphorylation, potentially by “trapping” the kinase PKA (Schmitt et al. 2003).

In the following years, an increasing number of naturally occurring, pathogenic mutations in the PLN gene have been reported: R14del, R9H, R25C and others which are not only associated with DCM, but also HCM and ACM (Haghighi et al. 2006; Landstrom et al. 2011; Liu et al. 2015; Opbergen et al. 2017; Yost et al. 2019; Zwaag et al. 2012). The perhaps most frequently occurring PLN mutation is the R14del mutation. In the Netherlands, where this mutation is particularly prevalent, the R14del mutation accounts for approximately 12% of ACM and 15% of DCM cases, but the R14del mutation have also been identified in Greece, Germany and Spain (Zwaag et al. 2012; Haghighi et al. 2006; Hof et al. 2019; López-Ayala et al. 2015; Posch et al. 2009). Consistent with this, PLN-R14del carriers typically develop a DCM like phenotype with frequent episodes of

cardiac arrhythmias (Haghighi et al. 2006; Hof et al. 2019; Posch et al. 2009). On a molecular level, the mutation has been reported to impair phosphorylation, to destabilise PLN pentamers and to lead to faulty localisation of mutant PLN to the plasma membrane where it interacts with the Na/K-ATPase (Ceholski et al. 2012; Haghighi et al. 2006; Haghighi et al. 2012; Kim et al. 2015). Moreover, it has been reported that PLN-R14del alters calcium cycling parameters in iPSC models and leads to changes in autophagy resulting in increased accumulation of PLN aggregates (Karakikes et al. 2015; Rijdt et al. 2016). Unfortunately, conventional therapies for HF patients appear to have little effect on R14del carriers and patients often die before the age of 50-60 of HF or sudden cardiac death (Eijgenraam et al. 2020; Haghighi et al. 2006; Hof et al. 2019).

In addition to mutations in the PLN gene itself, perturbations to PP1 or inhibitor-1, both of which are part of the signalling network surrounding PLN, have also been reported to change PLN phosphorylation levels and cause cardiac arrhythmias (Alsina et al. 2019; Haghighi et al. 2015).

Taken together, this demonstrates that interfering with the function of PLN or other proteins in this signalling network can cause HF and cardiac arrhythmias and that currently available therapy approaches are not sufficient for patients with mutations in the PLN gene.

1.8 Aims and objectives

The overarching goal of this work is to elucidate hitherto poorly understood and unknown signalling processes at the interface of the sarcomere and the SR and their potential relevance in the pathophysiology of cardiovascular diseases.

The first part of this thesis comprises the work which has been done on the giant muscle protein obscurin within two separate projects. Given the context outlined above, we hypothesize that obscurin, and particularly its Rho GEF domains, play important signalling functions in cardiomyocyte (patho-)physiology. The aim of the first project is to provide a better understanding the obscurin Rho GEF domains. Although cell biological studies have provided evidence that the obscurin Rho GEF domains can activate RhoA and RhoQ/TC10 in skeletal muscle, a solid mechanistic understanding of these interactions is still lacking. The specific goal for this project is therefore to provide a biochemical and structural characterisation of the Rho GEF domains to answer the following questions:

Project 1

1. What is the catalytic activity of obscurin Rho GEF domains and how do they compare to other Rho GEFs?
2. What are the substrates for which obscurin Rho GEF domains shows the highest specificity?
3. How is catalytic activity regulated by adjacent domains and post-translational modifications, specifically phosphorylation?

Mutations which impair obscurin's stability, signalling functions or interaction with other proteins may cause muscle diseases. However, we hypothesize that the R4344Q mutation in the obscurin domain Ig59 is not causative in the pathophysiology of heart or skeletal muscle diseases. The second project thus aims to characterise the influence of disease-associated genetic mutations on protein-protein interactions and biophysical properties such as domain stability with a focus

on variants affecting obscurin domains Ig58 (R4344Q, A4484T), Ig59 (R4444W) and PH domain (D5966N) (Arimura et al. 2007; Marston et al. 2015; Rossi et al. 2017).

To date, mutations R4344Q and A4484T have only been characterised by means of pulldown/co-immunoprecipitation, whereas the mutation D5966N has not yet been characterised. A systematic investigation using quantitative methods to determine e.g. differences in affinities may therefore help to resolve existing controversies particularly concerning the pathogenicity of the R4344Q mutation and could yield new mechanistic insights into the pathophysiology of other variants. Given that the R4344Q variant has a high prevalence among African Americans, we hypothesize that it will have no major effect on biophysical and biochemical properties. The specific questions this project seeks to answer are:

Project 2

1. How do potentially pathogenic obscurin variants alter the thermo-stability of the affected domains?
2. What effect do potentially pathogenic obscurin variants have on the affinities of interactions between obscurin and its binding partners?
3. How can the discrepancy between the population genetics of the R4344Q variant (found in up to 15% of African Americans) and its proposed pathogenicity be explained?

The chapter about the second project consists of the peer-reviewed paper which has been published after completion of this project.

The second part of the thesis is about phospholamban, a small (52 amino acids, ≈ 6 kDa) protein found in the SR membrane. In the unphosphorylated form, phospholamban (PLN) is a constituent inhibitor of the SERCA pump which is responsible for the bulk of Ca^{2+} removal after sarcomeric contraction. The phosphorylation of PLN by PKA relieves SERCA inhibition to accelerate Ca^{2+} reuptake and is a key mechanism of positive lusitropy (faster relaxation) and positive inotropy (stronger contractions) mediated by the β -adrenergic pathway (Kranias and Hajjar 2012; MacLennan and Kranias 2003). Phospholamban also forms homo-pentamers of yet unknown physiological functions. Using dynamical systems approaches and biochemical experiments, this work tries to provide a better understanding of the role of homo-oligomers in biochemical signalling networks in general and of PLN pentamers in particular. We hypothesize that homo-oligomers can markedly alter the dynamics and regulatory modes of interactions and post-translational modifications in which they are involved.

As the potential functions of homo-oligomerisation in biochemical signalling networks have not yet been studied systematically, the first project in this line of work aims to develop and explore general mathematical models of homo-oligomerisation. Specifically, the project aims to answer the following questions:

Project 3

1. What are the dynamics and what is the steady-state behaviour that can be observed in simulations of homo-oligomerisation models?
2. How is the predicted behaviour influenced by the order of oligomerisation?

3. How does oligomerisation affect the dynamics and the steady-states level of post-translational modification?

The findings from this project will then be used in a second project to develop a mathematical model of PLN pentamers in the context of β -adrenergic signalling which will be calibrated with experimental data on oligomerisation and explored by detailed model analyses and numerical simulations. Specifically, the project aims to answer the following questions:

Project 4

1. What are the possible dynamics and the steady-state of PLN pentamer phosphorylation?
2. How do PLN pentamers influence the phosphorylation of PLN monomers?
3. If PLN pentamers influence phosphorylation PLN monomers:
 - (a) What are the functional implications for cardiac physiology?
 - (b) What are the implications for the pathophysiology of cardiovascular diseases such as heart failure or cardiac arrhythmias?

Both projects in the second part have already been completed before thesis submission and the results are therefore presented in the form of published and peer-reviewed papers. Each chapter features a short discussion of technical or biological aspects immediately relevant to the project. A synopsis of the results presented in this thesis, the discussion of their wider implications and an outlook onto potential future work is provided at the end of this thesis.

Chapter 2

Material and Methods

2.1 Material

Table 2.1. Frequently used chemicals and reagents

Chemical/reagent	Source
Carbenicillin	Apollo Scientific, cat. no. BIC0109
cOmplete™, EDTA-free Protease Inhibitor Cocktail Tablets	Roche, cat. no. 11873580001
DTT	Thermo Scientific, cat. no. R0862
EDTA	VWR chemicals, cat. no. 20302.260
GDP	Sigma-Aldrich, cat. no. G7127-100MG
Glycerol	Sigma-Aldrich, cat. no. G5516-1L
Glycine	Sigma-Aldrich, cat. no. G8898-500G
Hepes	Sigma-Aldrich, cat. no. H3375-100G
Imidazole	Sigma-Aldrich, cat. no. I2399-500G
IPTG	Generon, cat. no. GEN-S-02122
L-Glutathione, reduced	Sigma-Aldrich, cat. no. G4251-25G
Lysozyme, from egg white	Fluka Analytical, cat. no. 62971-50G-F
β-Mercaptoethanol	Sigma-Aldrich, cat. no. M3148-250ML
Magnesium chloride (MgCl ₂)	Sigma-Aldrich, cat. no. M2670-500G
Sodium chloride (NaCl)	Sigma-Aldrich, cat. no. S7653-5KG
Sodium dodecyl sulfate (SDS)	Sigma-Aldrich, cat. no. 75746-1KG
Tris base	Sigma-Aldrich, cat. no. T6066-5KG
Triton X-100	Sigma-Aldrich, cat. no. T8787-100ML

Table 2.2. Frequently used media

Medium	Contents
Lysogeny broth (LB), Miller	Ready to use granules, 25 g/L (10 g casein peptone, 5 g yeast extract, 10 g NaCl), Fisher Scientific, cat. no. BP9723-2
LB-agar, Miller	Ready to use granules, 37 g/L (10 g casein peptone, 5 g yeast extract, 10 g NaCl, 12 g agar), Fisher Scientific, cat. no. 1281-1660
Auto-induction medium (AIM)	10 g tryptone, 5 g yeast extract, 1 mL MgSO ₄ , 20 mL 50x 5052 solution, 50 mL 20x NPS solution, ultrapure water ad 1 L. Smaller volumes were made up accordingly by scaling the above amounts.

Table 2.3. Frequently used protein buffers

Rho GTPases	Buffer A: 50 mM Tris-HCl pH 7.5, 300 mM NaCl, 2 mM MgCl ₂ , 1:1000 (v/v) β-mercaptoethanol. Lysis buffer: buffer A + 1 cOmplete protein inhibitor tablet / 50 mL, spiked with 10 μM GDP. Buffer B: like Buffer A + 10 mM glutathione. Buffer C (final): 50 mM Tris-HCl, 100 mM NaCl, 2 mM MgCl ₂ , 2 mM DTT.
Obscurin Rho GEF fragments (affinity purification with HisTrap followed by His-tag cleavage via TEV protease and size-exclusion chromatography)	Buffer A: 50 mM Tris-HCl pH 7.5, 300 mM NaCl, 25 mM imidazole, 1:1000 (v/v) β-mercaptoethanol. Lysis buffer: buffer A + 1 cOmplete protein inhibitor tablet / 50 mL. Buffer B: 50 mM Tris-HCl pH 7.5, 300 mM NaCl, 500 mM imidazole, 1:1000 (v/v) β-mercaptoethanol. Buffer C (final): 30 mM Hepes pH 7.5, 100 mM NaCl, 2 mM DTT, (optional: 5% (v/v) glycerol).
Obscurin Rho GEF fragments (single-step affinity purification with Ni-NTA resin from < 0.5 L cultures)	Buffer A: 1x PBS, 35 mM imidazole, 1:1000 (v/v) β-mercaptoethanol. Lysis buffer: buffer A + 1 cOmplete protein inhibitor tablet / 50 mL. Buffer B: 1x PBS, 600 mM imidazole, 1:1000 (v/v) β-mercaptoethanol. Buffer C (final): 40 mM Hepes pH 7.5, 100 mM NaCl, 2 mM DTT, 5% glycerol.
Obscurin Rho GEF fragments (single-step affinity purification with Ni-NTA resin for solubility screen)	Buffer A: 50 mM Tris-HCl pH 7.5, 300 mM NaCl, 30 mM imidazole, 1 mM DTT. Buffer B: 50 mM Tris-HCl pH 7.5, 300 mM NaCl, 1 M imidazole, 1 mM DTT. Buffer C (final): 30 mM Hepes pH 7.5, 100 mM NaCl, 2 mM DTT.
Vav2 DH and Larg DH (single-step affinity purification with Ni-NTA resin from < 0.5 L cultures)	Buffer A: 30 mM Hepes pH 7.5, 100 mM NaCl, 40 mM imidazole, 1:1000 (v/v) β-mercaptoethanol, 5% glycerol. Lysis buffer: buffer A + 1 cOmplete protein inhibitor tablet / 50 mL. Buffer B: 30 mM Hepes pH 7.5, 100 mM NaCl, 500 mM imidazole, 1:1000 (v/v) β-mercaptoethanol, 5% glycerol. Buffer C (final): 30 mM Hepes pH 7.5, 100 mM NaCl, 2 mM DTT, 5% glycerol.
PP1-β ₆₋₃₂₇ , catalytic subunit (affinity purification with HisTrap followed by size-exclusion chromatography)	Buffer A: 50 mM Tris-HCl pH 8, 700 mM NaCl, 1 mM MnCl ₂ , 25 mM imidazole, 1 mM DTT. Lysis buffer: buffer A + 1 cOmplete protein inhibitor tablet / 25 mL. Buffer B: 50 mM Tris-HCl pH 8, 700 mM NaCl, 1 mM MnCl ₂ , 500 mM imidazole, 1 mM DTT. Buffer C (final): 50 mM Tris-HCl pH 8, 700 mM NaCl, 1 mM MnCl ₂ , 1 mM DTT.

Table 2.4. Frequently used buffers and stock solutions

Medium	Contents
50x 5052 solution	0.5% (v/v) glycerol, 0.2% (w/v) α -lactose, 0.05% (w/v) glucose.
20x NPS solution	6.6 g $(\text{NH}_4)_2\text{SO}_4$, 13.6 g KH_2PO_4 , 14.2 g HNa_2PO_4 , ultrapure water ad 0.1 L.
1x Potassium buffered saline (PBS, Dulbecco's Formulation)	2.7 mM KCl, 1.5 mM KH_2PO_4 , 136.9 mM NaCl, 8.9 mM $\text{Na}_2\text{HPO}_4 \cdot 7\text{H}_2\text{O}$, made with ready to use tablets: 1 tablet/100 mL. Oxoid, cat. no. BR0014G
0.5x TBE	27 g tris base, 14 g boric acid, 2.3 g EDTA, water ad 5 L.

2.2 Bioinformatic methods

2.2.1 Multiple sequence alignments

To align multiple DNA or amino acid sequences, the clustal Omega server v1.2.4. was used (EMBL-EBI, <https://www.ebi.ac.uk/Tools/msa/clustalo/>) (Sievers et al. 2011). Aligned sequences and amino acid properties (e.g. hydrophobicity or percent identity across aligned sequences) were visualised in the UGENE software v1.28.1 (Unipro) (Okonechnikov et al. 2012).

2.2.2 Evolutionary protein sequence conservation analysis

The ConSurf server was used to determine the conservation of a protein's amino acid sequence across different species (<https://consurf.tau.ac.il/>) (Ashkenazy et al. 2010). Parameters: amino acids, no known structures, no MSA upload (sequence was provided in FASTA format), Proteins database: Uniprot, Select homologs for ConSurf analyses: automatically. Other parameters were left at their default settings.

2.2.3 Structure prediction and visualisation

Secondary structure predictions for proteins were obtained from 2018 to 2019 using the PredictProtein (<https://predictprotein.org/>) and PSIPRED 4.0 (<http://bioinf.cs.ucl.ac.uk/psipred/>) servers using default parameters (Buchan and Jones 2019; Yachdav et al. 2014). Tertiary structure models were obtained by homology-modelling using the I-TASSER server (<http://bioinf.cs.ucl.ac.uk/psipred/>) with default parameters (Roy et al. 2010; Yang et al. 2015). Unless stated otherwise, only the model with highest C-Score was used for further analysis. Molecular structure models were visualised using the PyMOL Molecular Graphics System v2.3.4 (<https://pymol.org/2/>, Schrödinger, LLC).

2.3 Microbiological and molecular biological methods

2.3.1 Transformation of *E. coli* cells

50 μL of chemically competent *E. coli* strains (BL21-CodonPlus (DE3)-RIPL or SoluBL21 for protein expression, or One Shot TOP10 for cloning, see Table 2.5) were thawed on ice for 10 min, 0.1 - 0.2 μL plasmid DNA at 50-200 ng/ μL were added and the cells were incubated for further 30 min on ice. Cells were transformed by heat-shock for 30 s at 42°C followed by a 1 min cool down period on ice. The transformation mixture was supplemented with 1 mL of LB- or SOC-medium and incubated for 45-60 min at 37°C in a shaking incubator before cells were either plated out on LB-agar plates (for cloning, cells were always transferred onto LB-agar plates) or transferred to a 50-200 mL pre-culture with appropriate antibiotics for selection and grown at 37°C overnight.

Table 2.5. Chemically competent *E. coli* strains used in this study

Strain	Genotype
BL21-CodonPlus (DE3)-RIPL (Agilent, cat. no. 230280)	<i>E. coli</i> B F- ompT hsdS(rB-mB-) dcm+ TetR gal λ (DE3) endA Hte [argU proL CamR] [argU ileY leuW Step/SpecR]
SoluBL21™ (amsbio, cat. no. C700200)	F- ompT hsdSB (rB- mB-) gal dcm (DE3)†
One Shot™ TOP10 (Invitrogen, cat. no. C404010)	F- mcrA Δ (mrr-hsdRMS-mcrBC) Φ 80lacZ Δ M15 Δ lacX74 recA1 araD139 Δ (araleu)7697 galU galK rpsL (StrR) endA1 nupG

† The SoluBL21 strain contains additional uncharacterised mutations obtained through special selection criteria. These mutations make the strain able to express insoluble proteins in soluble form, fully or partially, in most tests conducted. (From: <https://resources.amsbio.com/Datasheets/C700200.pdf>, accessed 7/7/2021)

2.3.2 Polymerase chain reaction (PCR)

Polymerase chain reaction was carried out to amplify DNA. Briefly, a reaction mixture was set up with the total amount or end concentration of the following components being: 1-5 ng template DNA, 0.5 μM of forward and reverse primers, 200 μM dNTPs, 0.1 U Q5® High-Fidelity DNA Polymerase (NEB, cat. no. M0491S), 1xQ5 reaction buffer. Nuclease free water was added to achieve an end volume of 25 μL . A list of all primers used in this study can be found in the appendix (Table A1). Following set up, 30-35 cycles of steps 2. - 4. from the following PCR programme were run on a conventional thermocycler:

1. Initial denaturation: 98°C, 30 s
2. Denaturation: 98°C, 15 s
3. Annealing: min(ATf,ATr), 30 s
4. Amplification: 72°C, (length of DNA segment to be amplified)[bp]/1000[bp] \times 60 s
5. Final amplification: 72°C, 5 min
6. Hold: 4°C until sample removal,

where ATf and ATr denote the annealing temperatures (in °C) of the forward and reverse primers, respectively. For reactions involving differences in annealing temperatures exceeding 4°C, the above programme was modified by splitting step 3 into two separate annealing steps to reduce unspecific binding of primers with high annealing temperatures:

3. Annealing:
 - (a) $\max(\text{ATf}, \text{ATr})$, 20 s
 - (b) $\min(\text{ATf}, \text{ATr})$, 20 s.

In case the reaction product was used for cloning, the reaction mixture was separated and purified by gel-electrophoresis.

2.3.3 DNA gel-electrophoresis and DNA purification

DNA was separated electrophoretically on a 1% agarose gel in 0.5x TBE (Tris-borate-EDTA) buffer. Bands of appropriate size were cut out and purified with the QIAquick® Gel Extraction Kit (Qiagen, cat. no. 28706).

2.3.4 Site-directed mutagenesis

Point mutations were introduced by site-directed mutagenesis. For each mutation, a single forward primer of the design [5'-end][19-22 bases][XXX][19-22 bases][3'-end], where [XXX] represents the codon for the new amino acid. If possible, G or C were chosen as bases at the 3'/5' end of the primer. A reaction mixture was set up with the total amount or end concentration of the following components being: ≥ 200 ng vector template, 40 nM of the forward primer, 200 μM dNTPs, 0.1 U Q5® High-Fidelity DNA Polymerase. Nuclease free water was added to achieve an end volume of 25 μL . Following set up, 35 cycles of steps 1. - 4. from the following PCR programme were run on a conventional thermocycler:

1. Initial denaturation: 98°C, 30 s
2. Denaturation: 98°C, 15 s
3. Annealing: 78°C, 30 s
4. Amplification: 72°C, (length of DNA segment to be amplified)[bp]/1000[bp]×60 s
5. Final amplification: 72°C, 5 min
6. Hold: 4°C until sample removal.

Following PCR, methylated template DNA was digested for >10h with DpnI (NEB, cat. no. R0176S) according to the manufacturer's instructions. 4 μL of the DpnI treated reaction mixture were used for the transformation of chemically competent *E. coli* cells as described above. Successful mutagenesis was confirmed by sequencing using an external sequencing service (Eurofins genomics, Germany).

2.3.5 Determination of DNA concentration

DNA concentration was determined by the absorbance at 260 nm with a DS-11 FX+ Spectrophotometer (DeNovix) against a blank sample using ultrapure water.

2.3.6 Cloning

Vectors for protein expression in *E. coli* or mammalian cells were generated using the NEBuilder® HiFi DNA Assembly kit (NEB, cat.no. E2621S) or using restriction enzymes and ligation following the manufacturer's instructions. All cloned vectors were validated by sequencing using an external sequencing service (Mix2Seq Kit; eurofins genomics, Germany).

NEBuilder® HiFi DNA Assembly

Briefly, 1 or 2 DNA inserts were combined with the appropriate vector backbone in a 2:1 molar ratio. 2 μL of the combined DNA were mixed with 2 μL of the HiFi DNA Assembly master mix and incubated for 1 hr at 50°C before the whole reaction mixture was used for the transformation of chemically competent *E. coli* cells as described above.

Cloning via restriction enzymes and ligation

Conventional cloning was carried out as follows: first, restriction enzymes XhoI and BamHI (NEB, cat. nos. R0146S and R0136S) were used according to the manufacturer's instructions to prepare the target vector and insert. Cleaved DNA fragments were purified by gel-electrophoresis and vector and insert were joined with T4 DNA ligase (NEB, cat. no. M0202S) according to the manufacturer's instructions.

2.3.7 Preparation of plasmid DNA

For preparation of plasmid DNA, *E. coli* One Shot™ TOP10 cells were transformed and grown over night as described in [subsection 2.3.1](#). On the next day, a single colony was transferred into 5-6 mL LB with appropriate selection antibiotics and grown over night at 37°C in a shaking incubator at 200 rpm. The following day, cultures were pelleted by centrifugation for 10 min at 4500 rpm in a benchtop centrifuge (Allegra X-22R, Beckman Coulter). Plasmid DNA was isolated and purified using the Monarch Plasmid Miniprep Kit (NEB, cat. no. T1010L) according to the manufacturer's instructions.

2.4 Biochemical and biophysical methods

2.4.1 Protein expression and affinity-purification

For the purification of recombinant proteins, *E. coli* cells were transformed with an expression vector carrying the sequence of the target protein and appropriate affinity-tag (GST or hexahistidine) as described in [subsection 2.3.1](#). A list of all protein expression constructs used in this study can be found in the appendix ([Table A2](#)). On the following morning, 0.5 – 2 L of culture medium (LB or autoinduction medium) supplemented with appropriate antibiotics were inoculated with transformed cells scraped directly from agar-plates or with 25-50 mL/L of a pre-culture. For IPTG-induced protein expression the cells were grown in LB-medium at 37°C in a shaking incubator at 180-200 rpm until the culture reached an optical density at 600 nm (OD_{600nm}) of 0.6 – 0.9. Upon reaching this point, the cultures were cooled down for approximately 15 min at 4°C before protein expression was induced by addition of 0.2 mM IPTG and allowed to proceed overnight at 16-20°C. For autoinduction, cells were directly transferred into autoinduction medium in the morning and

grown further at 37°C and 180-200 rpm until the evening, before the temperature was lowered to 18-25°C and the cultures were left to grow further until $OD_{600nm} \approx 8-10$ (typically 48-72 h).

After sufficient time for protein expression, cultures were harvested by centrifugation (15 min, $5000 \times g$, 4°C). Cell pellets were washed in PBS, snap-frozen in liquid nitrogen and stored at -70°C until further use.

Cells were lysed as follows: cell pellets were resuspended in lysis buffer and subjected to 1-2 freeze-thaw cycles followed by the addition of lysozyme. After 30 min incubation on ice and regular mixing by inversion, the cell suspension was supplemented with 0.1% Triton X-100 and left to incubate for further 15 min on ice before sonication (15 pulses, 20 Watt). Genomic DNA was removed by addition of DNase (Sigma-Aldrich, cat. no. 4536282001) and insoluble cell material was removed by centrifugation (20-40 min, $30000 \times g$, 4°C) and subsequent filtration of the supernatant through a 5 µm pore size cellulose acetate membrane (Sartorius, cat. no. 17594). For cultures ≤ 0.5 L, proteins were purified in a single step using 0.5-1 mL of SuperGlu agarose resin for GST-tagged proteins (Generon, cat. no. SuperGlu 25) or 0.5-1 mL of Ni-NTA resin (Qiagen, cat. no. 30410) for His₆-tagged proteins as described as follows: first, the resin was washed three times in 10 resin volumes of lysis buffer. For protein binding, the resin was incubated with the lysate for 45-60 min at 10 rpm inversion in a cold-room at 4°C. After binding, the supernatant was removed and the resin was washed three times in 10-15 resin volumes buffer A. The enriched protein was eluted by incubating the resin in 3-5 resin volumes buffer B. The eluting agent was removed by buffer exchange as described in [subsection 2.4.2](#).

For cultures > 0.5 L, proteins were purified using 2×1 mL affinity columns (HisTrap™ FF or GSTrap™ 4B, GE Healthcare, cat. nos. 17531901 and 29048609) as primary columns. If necessary, proteins were further purified by size-exclusion chromatography using a HiLoad™ 26/600 Superdex™ 75 pg or 200 pg (GE Healthcare, cat. nos. 28-9893-34 and 28-9893-36) column. Purified protein solutions were adjusted to the desired concentration using Amicon™ Centrifugal Filter Units of appropriate MWCO (Millipore, cat. nos. UFC901096, UFC903096, UFC801096 and UFC803096).

For small scale expression and purification of proteins for solubility screening, 4 mL cultures were grown in autoinduction medium in 24 deep well plates (Elkay, cat. no. 43001-0066) for 3-4 days in a shaking incubator at 300 rpm. On day 1, cultures were grown at 37°C for at least 5-6 h, before the temperature was lowered to 30°C. On day 2, the temperature was lowered to 20°C and the cultures were grown for further 1-2 days until control cultures transformed with mCherry / GFP plasmids showed a strongly visible color. Cells were harvested by centrifugation (20 min, $5000 \times g$, 4°C) and lysed with 4 mL B-PER™ Bacterial Protein Extraction Reagent (Thermo Scientific, cat. no. 78243) supplemented with DNase (Sigma-Aldrich, cat. no. 4536282001) for 45-60 min at room temperature and gentle agitation at 60-80 rpm. The lysate was cleared by centrifugation (20 min, $5000 \times g$, 4°C) and 200 µl of Ni-NTA resin (Qiagen, cat. no. 30410) were added to the cleared lysate. Binding was allowed to proceed for about 20 min at room temperature. The lysate was discarded via vacuum suction by transferring the lysate including the resin to a 96-well filtration plate with 25 µm pore size (Porvair, cat. no. 36002). The retained resin was washed two times with 1 ml buffer A on the filtration plate before the protein was eluted with 2×400 µL buffer B. To test for the presence of soluble protein, the eluted sample was analysed by dot-blotting or SDS-PAGE.

2.4.2 Buffer exchange

Desalting columns were used according to the manufacturer's instructions to remove small molecules such as imidazole, GSH or nucleotides from protein samples or to transfer a protein sample into a new buffer: Zeba™ Spin Desalting Columns, 7K MWCO for samples with 30-130 μ L volume (Thermo Scientific™, cat. no. 89882), or illustra™ NAP-5/10/25 columns for samples with \leq 0.5/1/2.5 mL (GE Healthcare, cat. nos. 17-0853-01/17-0854-01/17-0852-01). Larger sample volumes were subjected to size-exclusion chromatography.

2.4.3 Determination of protein concentration

Protein concentration was determined based on absorbance (A) at 280 nm according to the Beer-Lambert law $A = \epsilon lc$, where the ϵ is the extinction coefficient, c the concentration of a molecular species and l the optical path length. Extinction coefficients were calculated using the ProtParam web-tool (<https://web.expasy.org/protparam/>) assuming reduction of all cysteines. Absorbance was measured on a DS-11 FX+ Spectrophoto-/Fluorometer (DeNovix). For proteins without sufficient numbers of aromatic amino acids or for Rho GTPases (whose bound nucleotides interfere with the absorbance measurement) concentration was determined by the Bradford assay (VWR Life Sciences, cat. no. M172-1L) using BSA as a standard.

2.4.4 SDS-PAGE

To separate proteins according to molecular weight, gel electrophoresis was performed essentially as described by Laemmli 1970. Precast 4-20% Mini-PROTEAN® TGX gradient gels (Bio-Rad, cat. no. 456-1096) were mounted into a Mini-PROTEAN® vertical electrophoresis chamber (Bio-Rad, cat. no. 1658004) and samples were separated for approximately 30 min at a constant voltage of 200V in 1 \times SDS running buffer (25 mM Tris, 190 mM Glycin, 0.1% (w/v) SDS). Following separation of proteins by SDS-PAGE, gels were stained following the procedures described below. After staining, gels were imaged on a ChemiDoc™ XRS+ imaging system (Bio-Rad).

2.4.5 Gel staining methods

Quick Coomassie stain

For visualisation of total protein content, gels were stained with Quick Coomassie solution (Protein Ark, cat. no. GEN-QC-STAIN-1L) for up to 16 h followed by two or three 30 min washing cycles in ultrapure water to remove background staining.

Pro-Q™ Diamond Phosphoprotein Gel Stain

For visualisation of phosphorylated proteins, gels were stained with the Pro-Q™ Diamond Phosphoprotein Gel Stain (Invitrogen, cat. no. P33301) according to the manufacturer's instructions.

2.4.6 Dot-blotting

1-2 μ L of protein samples were spotted onto a nitrocellulose membrane of 0.45 μ m pore-size (GE Healthcare, cat. no. 10600002) and allowed to dry for 1-2 h at room temperature. To confirm successful spotting and visualise total protein content, membranes were stained with Ponceau S solution (Sigma Aldrich, cat. no. 6226-79-5). Before application of primary antibodies, the

membrane was incubated for 15-30 min in binding buffer (10 mM Tris base pH 7.4, 9 g/l NaCl, 1 ‰ (v/v) Tween-20, and 5% (w/v) milk powder) at room temperature to prevent or reduce unspecific antibody binding. Primary antibodies (mouse anti-His mAb, 1:1000 dilution; Millipore, cat. no. 70796) were applied for 1 h at room temperature or overnight at 4°C. HRP-conjugated secondary antibodies (rabbit anti-mouse IgG, 1:1000 dilution; Dako, cat. no. P0260) were applied for 1 h at room temperature. Signals were detected by chemiluminescence (Clarity ECL Western Substrate; Bio-Rad, cat. no. 1705061) on a ChemiDocTM XRS+ imaging system (Bio-Rad).

2.4.7 Measurement of nucleotide exchange kinetics of Rho GTPases

Intrinsic or GEF-catalysed kinetics of the nucleotide exchange reaction of Rho GTPases were measured using GTPases bound to fluorescent 2'/3'-O-(N-Methyl-anthraniloyl)-GDP or short mant-GDP. When bound to a GTPase, the fluorescence signal intensity of the mant-GDP nucleotide is higher compared to the fluorescence signal intensity of the free nucleotide. The release of mant-GDP from the GTPase and its replacement with a non-fluorescent nucleotide such as GDP or GTP during the nucleotide exchange reaction therefore results in a decreasing signal amplitude that can be used to describe the kinetics of the reaction.

In a first step, mant-GDP bound GTPases were prepared by incubating the GTPases at a protein concentration of 50-100 μM with a 5-fold molar excess of mant-GDP (Jena Bioscience, cat. no. NU-204S) in the presence of excess EDTA (usually 5 mM). EDTA chelates metal ions and therefore destabilises the GTPase-nucleotide interaction by removing Mg^{2+} from the nucleotide binding pocket, leading to faster nucleotide exchange. GTPases with limited stability were spiked with glycerol to an end concentration of 10-20% (v/v). After 2-4 h incubation at room temperature, EDTA was removed and replaced with MgCl_2 by buffer exchange into GTPase buffer to stabilise the GTPase:mant-GDP complex. After buffer exchange and further concentration to $>50 \mu\text{M}$, the protein was aliquoted, snapfrozen in liquid nitrogen and stored at -70°C until use.

Measurement of nucleotide exchange kinetics was performed at 25°C in 96-well microplates (greiner bio-one, cat. no. 675076 or invitrogen, cat. no. M33089) in a CLARIOstar microplate reader (BMG LABTECH, Germany). Samples were excited at a wavelength of 360 nm and emission was measured every 2-15s at a wavelength of 440 nm. Samples were set up as follows. First, 80 μL of 1.875 μM [GTPase] in reaction buffer (40 mM Hepes pH 7.5, 100 mM NaCl, 5 mM MgCl_2 , 2 mM DTT) were briefly equilibrated at room temperature. Next, the plate was inserted into the microplate reader and signal was recorded sufficiently long to reach a stable line (300 s). To start the nucleotide exchange reaction, 20 μL of GDP or GDP + EDTA or GDP + GEF (final concentrations: [GTPase] = 1.5 μM , [GDP] = 200 μM , [EDTA] = 10 mM, [GEF] = various) were added to the sample and mixed by careful pipetting and the signal was recorded for further 1-2 h.

The obtained traces were normalised by the average fluorescence signal of the first 300 s before start of the reaction. Apparent rate constants were obtained from the normalised traces by fitting the decay phase of the signal to a mono-exponential decay function of the form

$$f(t) = (a_0 - a_{\text{plateau}})e^{-k_{\text{obs}}t} + a_{\text{plateau}}$$

using the GraphPad Prism software v8.3 (GraphPad Software, Inc).

2.4.8 Identification of Ser/Thr-kinases that phosphorylation obscurin SH3-DH

To identify kinases which can phosphorylate obscurin, a commercially available service to screen a protein as a substrate against 245 different Ser/Thr-protein kinases was used (KinaseFinder screen from ProQinase GmbH, now Reaction Biology Europe GmbH). The technical details of the screen can be found in [subsection A5.1](#). Statistical comparison of the validation assay data was performed by comparing the phosphorylation signal in kinase samples to the negative control via T-test using the GraphPad Prism v8.3 software (GraphPad Software, Inc), correcting for multiple comparisons via the Holm-Sidak method. A p-value of <0.05 was considered to be statistically significant.

2.4.9 *In vitro* phosphorylation of obscurin

For analytical *in vitro* phosphorylation of obscurin Rho GEF fragments, 50 μ L reactions were set up containing 0.2 mg/ml obscurin substrate (5-20 μ M, depending on the fragment used) and 200 U PKA (Sigma-Aldrich, cat. no. 539576) or 500 U CaMK II (NEB, cat. no. P6060L) or 25 ng CaMK Id (BioVision, cat. no. 7713-5) or 25 ng MST2 (Millipore, cat. no. 14-524) in kinase reaction buffer (30 mM Hepes pH 7.5, 100 mM NaCl, 2 mM MgCl₂, 300 μ M ATP, 2 mM DTT [+ 1mM CaCl₂ and 1 μ g/ml (approx. 3 μ M) Calmodulin (NEB, cat. no. 6060S) for CaMK II/Id)). Samples were incubated for 3 h at 30°C in a PCR cycler and the reaction was stopped by addition of SDS sample buffer. To visualise phosphorylation, 2 μ g of obscurin substrate were separated by SDS-PAGE and stained with Pro-Q™ Diamond Phosphoprotein Gel Stain as described above.

For preparative MST2-phosphorylation of obscurin, a 200 μ L reaction mixture was set up with 110 μ M obscurin substrate and 500 ng MST2 in kinase reaction buffer. The reaction was allowed to proceed for 5 h at 25°C, followed by further incubation over night at 8°C. The phosphorylated protein was buffer exchanged into 40 mM Hepes pH 7.5, 100 mM NaCl and 2 mM DTT.

2.4.10 Identification of the MST2 phosphorylation site in obscurin

The site in obscurin which is phosphorylated by the kinase MST2 was identified via a commercially available mass spectrometry service. 5 μ g of MST2-phosphorylated obscurin SH3-DH were separated by SDS-PAGE and the coomassie stained protein band was cut out and sent for phosphorylation site analysis to the Metabolomics and Proteomics Laboratory of the Bioscience Technology Facility of the University of York. The technical details of this analysis provided by the responsible staff scientists of this service can be found in [subsection A5.2](#).

2.4.11 Dephosphorylation of MST2-phosphorylated obscurin SH3-DH

A 50 μ L reaction mixture was set up with 0.2 mg/ml MST2-phosphorylated obscurin SH3-DH and 1 μ M of phosphatases PP1 or PP2A (Cayman Chemical, cat. no. 10011237) or 1 U rAPid Alkaline Phosphatase (Roche, cat. no. 4898133001) in 40 mM Hepes pH 7.5, 100 mM NaCl, 5mM MgCl₂ and 2 mM DTT (+ 1mM MnCl₂ for PP1). The reaction was allowed to proceed for 1.5 h at 25°C and was stopped by the addition of SDS sample buffer. To visualise the phosphorylation signal, 2 μ g of obscurin substrate were separated by SDS-PAGE and stained with Pro-Q™ Diamond Phosphoprotein Gel Stain as described above.

2.4.12 1D-NMR

1D-NMR spectroscopy was used to analyse whether or not a purified protein was folded. In this approach, the magnetic spin states of hydrogen nuclei are probed by radiofrequency waves. Since the resonance frequency depends on the chemical environment, the nuclei of ^1H -atoms in a protein resonate at different frequencies which can be visualised in a graph of intensity versus resonance frequency – called the 1D-spectrum (Kwan et al. 2011). For analysis, the analyte protein was buffer exchanged into 25 mM HNa_2PO_4 pH 7.3, 100 mM NaCl, 2 mM DTT and protein concentration was adjusted to at least 60 μM . Spectra were recorded with an Ascend 600 instrument (Bruker Scientific Instruments).

2.4.13 Protein crystallisation trials

For protein crystallisation trials, the purified and concentrated protein solution was used in commercially available protein crystallisation screening suites using the sitting drop method (JCSG++, Jena Bioscience, cat. no. CS-206L; PACT, Jena Bioscience, cat. no. CS-207L; Classics suite; NeXtal, cat. no. 130901; Classics II suite, NeXtal, cat. no. 130923). Briefly, 2 \times 200 nL protein solution were placed into different sub-wells of each well of a 96-well crystallisation plate (MRC 2 Well Crystallization Plate in Polystyrene, Jena Bioscience, cat. no. CPL-153L) using a mosquito[®] crystal liquid handling robot (sptlabtech). Next, 200 and 400 nL assay solution were mixed into the protein drop and the plate was stored at 18°C for at least 4 weeks. Potential crystal formation was checked at week 1, 2 and 4. The number of conditions resulting in precipitation or crystal formation was quantified at week 4.

Chapter 3

Results

3.1 Characterisation of the obscurin Rho GEF domains

3.1.1 Introduction

Obscurin is a fascinating protein with links to many physiologically relevant processes and signalling pathways. However, the mechanistic details and functional implications of these links are largely unclear. The cumulative evidence from the studies mentioned in previous sections suggests that the obscurin Rho GEF domains can activate Rho GTPases RhoA and RhoQ/TC10 and that these interactions are potentially relevant for muscle physiology. Moreover, they are also a highly attractive candidate to mediate mechano-signalling at the M-band. However, independent confirmation of previous results is still lacking and our current biochemical understanding of these processes is severely limited.

How the stipulated GEF activity of obscurin is itself regulated, for example, has not been studied yet. Often, GEF activity is regulated in a complex fashion by adjacent domains. In multiple Dbl-family GEFs adjacent SH3 domains and linker regions are known to autoinhibit the DH domain (Zamarian and Kelly 2003; Mitin et al. 2007; Murayama et al. 2007; Kintscher et al. 2010; Ahmad and Lim 2010; Zhang et al. 2012; Barreira et al. 2014). SH3 domains of Dbl-GEFs domains have also been reported to sometimes interact directly with Rho GTPases and their effectors (Manser et al. 1998; Mott et al. 2005; Hoelz et al. 2006; Klooster et al. 2006). PH-domains of Dbl-GEFs, on the other hand, have been reported to determine membrane localisation, to provide positive feedback by interacting with activated GTPases, to directly contribute to or enhance, or even autoinhibit nucleotide exchange activity (Rossman et al. 2005; Nimmual et al. 1998; Xu et al. 2017; Pruitt et al. 2003; Muroya et al. 2007; Chen et al. 2010; Shankaranarayanan et al. 2010). Autoinhibition, whether through linkers, SH3 or PH-domains is often released by phosphorylation (Hodge and Ridley 2016; Rossman et al. 2005). The potential possibilities of regulating obscurin Rho GEF activity and associated downstream processes are thus immense.

Furthermore, a direct confirmation of obscurin's nucleotide exchange factor activity is still missing and the cell biological approaches applied previously have significant limitations. Pull-down and co-immuno-precipitation experiments, for example, provide only very limited quantitative information on interactions and are prone to unspecific binding, particularly since several of the utilised approaches rely on indirect interactions and stipulated inactivating/activating mutations. The latter point could be particularly problematic as their activating/inactivating effect is in many

cases only an assumption based on the general functioning principles of the structurally conserved G-domain and the exact effects of such mutations for a particular GTPase are rarely studied. It has been demonstrated, however, that this assumption is sometimes violated. A commonly used mutation to render small GTPases constitutively active is the replacement of a conserved glutamine involved in GTP hydrolysis in the switch II region, thereby slowing down GTP hydrolysis and thus theoretically prolonging the biologically active GTP bound state. However, it has been shown that in Rab5, this mutation only impairs intrinsic hydrolysis, not GAP catalysed hydrolysis, thus not significantly changing the activity state in living cells (Langemeyer et al. 2014). For Rab1 and Rab35, in contrast, this mutation can also impair the activation of a GTPase by GEFs, thus making it a functionally inactivating mutation in cellular contexts (Langemeyer et al. 2014). Even more complicating, this effect is sometimes specific for a particular GEF (Langemeyer et al. 2014). Moreover, several small GTPases are known to bind to regions outside the catalytic domains of GEFs and GAPs, sometimes independent of their nucleotide state (Chen et al. 2010; Klooster et al. 2006). Indeed, RhoQ/TC10 has been reported to interact with C-terminal obscurin constructs lacking the DH-PH domain, making such an interaction mode conceivable (Coisy-Quivy et al. 2009).

The gold standard to study both the catalytic activity as well as biochemical and structural regulation of a GEFs is, therefore, to characterise purified recombinant protein fragments by the use of enzymological, biochemical, and biophysical *in vitro* methods. However, this approach was not successful so far due to the lack of soluble and stable recombinant protein fragments of the obscurin DH and PH domain. Although the purification of the obscurin DH and PH domains from *E. coli* via large solubility-enhancing tags such as Glutathione-S-Transferase (GST) has been described in the literature, a rigorous *in vitro* characterisation of their GEF-activity or the regulatory role of these recombinant domains has not been performed (Ackermann et al. 2017; Coisy-Quivy et al. 2009; Ford-Speelman et al. 2009; Shriver et al. 2016).

Previous experience made in the Gautel group indicated that the expression and purification of these domains from *E. coli* with just a Hexa-histidine-tag is not possible due to insolubility of the domains. Unpublished experiments by Dr Atsushi Fukuzawa from our group further showed that when expressed in SF9-insect cells, the DH-domain can be purified as soluble protein but rapidly degrades and precipitates. Taken together, this indicates that both the DH and the PH domain are likely intrinsically unstable and insoluble. This also poses a concern for any data generated by protein fragments artificially solubilised via solubility enhancing tags such as GST, as the biological activity of the solubilised domain is highly uncertain.

The specific objectives of this project with respect to the Rho GEF domains are therefore to:

- Explore ways to improve the solubility and stability of the obscurin DH and PH domains in order to obtain high quantities of pure and high-quality protein for biochemical and structural characterisation
- Explore the feasibility of structural characterisation of the obscurin Rho GEF domains
- Provide a biochemical characterisation of the obscurin GEF activity via enzyme kinetic methods to identify substrate Rho GTPases and characterise the identified substrates via Michaelis-Menten kinetics
- Identify the role of obscurin SH3 and PH domains and explore how SH3 and PH domains regulate GEF activity or downstream signalling

- Identify kinases and phosphatases which are responsible for the (de-)phosphorylation of obscurin Rho GEF domains and explore how phosphorylation influences GEF activity

Achieving these would provide a solid biochemical understanding on which further physiological studies could build upon.

3.1.2 Construct design and purification

The first necessary step in this approach is the purification of soluble and stable recombinant protein in sufficient quantities for biochemical and biophysical experiments. The first constructs of the obscurin Rho GEF domains for recombinant expression were designed previously by Dr Atsushi Fukuzawa and comprised exons 80-83 for the DH domain and exons 80-85 or exons 80 to amino acids ...PDFEEEE of exon 86 for the DH-PH domain tandem in human obscurin B (Figure 3.1, top). However, neither of these protein fragments was expressed solubly in *E. coli*, preventing purification of these protein domains. Although the DH domain could be purified when expressed in insect cells, the protein rapidly degraded and precipitated. Due to this instability, further characterisation of these domains was hitherto not possible (Dr Atsushi Fukuzawa, unpublished results).

To overcome this obstacle, we developed a rationale to design protein constructs that would allow the expression and subsequent purification of soluble and stable obscurin Rho GEF domains. As only the DH domain in isolation and the DH-PH domain tandem domains have been tested for expression and purification so far, we additionally cloned and tested the SH3-DH domain combination before the start of this PhD project. While this domain combination yielded soluble, highly pure, folded and stable protein, it did not exhibit any activity towards previously reported substrate GTPases RhoA and RhoQ in our pilot experiments. Although no activity was observed, these pilot studies indicated that the DH domain might not be intrinsically unstable, but that the previous constructs may have been too short and thus potentially disrupted secondary structure elements, thereby destabilising the DH domain. We furthermore reasoned that the lack of activity could result from an autoinhibitory influence of the SH3-domain as observed for many other DH-PH Rho GEFs (Zamanian and Kelly 2003; Mitin et al. 2007; Murayama et al. 2007; Kintscher et al. 2010; Ahmad and Lim 2010; Zhang et al. 2012; Barreira et al. 2014). Therefore, we decided to use bioinformatic tools to analyse the primary, secondary and tertiary structure of the obscurin Rho GEF domains and systematically design the domain boundaries based on the findings from these analyses.

Specifically, we used the ConSeq-server to identify which residues at the N- and C-terminus of the DH domain are evolutionary highly conserved across species, with the rationale that highly conserved residues are likely to be functionally relevant and, if possible, to be included in the construct design. Since conservation does not inform about structure, we used the two secondary structure prediction servers PredictProtein and PSIPRED as well as the homology-modelling server I-Tasser for 3D-structure prediction. Figure 3.1 shows a summary of the results of these analyses for the N- and C-terminal boundaries of both DH and PH domains. Interestingly, a sequence of four highly conserved residues SE[X]EY in exon 79 is found directly before the N-terminus of the residues encoded by exon 80. Additionally, both secondary structure prediction algorithms predict an alpha-helix whose sequence spans from conserved residues DEY in exon 79 into exon 80. Taken together, this indicates that the previously designed construct for the DH domain, which only included exon 80, might be too short at the N-terminus and thereby disrupts the first alpha-

helix of the DH domain. Similarly, highly conserved residues and secondary structure elements were predicted at the boundaries of exon 83/84 and exon 85/86. Based on these findings, we designed a series of primers and in total cloned 39 different constructs into a modified pET15b vector frequently used in our group for protein expression in *E. coli* and subsequent purification by Ni²⁺-NTA affinity matrices. 21 of these constructs comprised only the DH domain, 12 the DH-PH domain tandem, and 6 the PH domain.

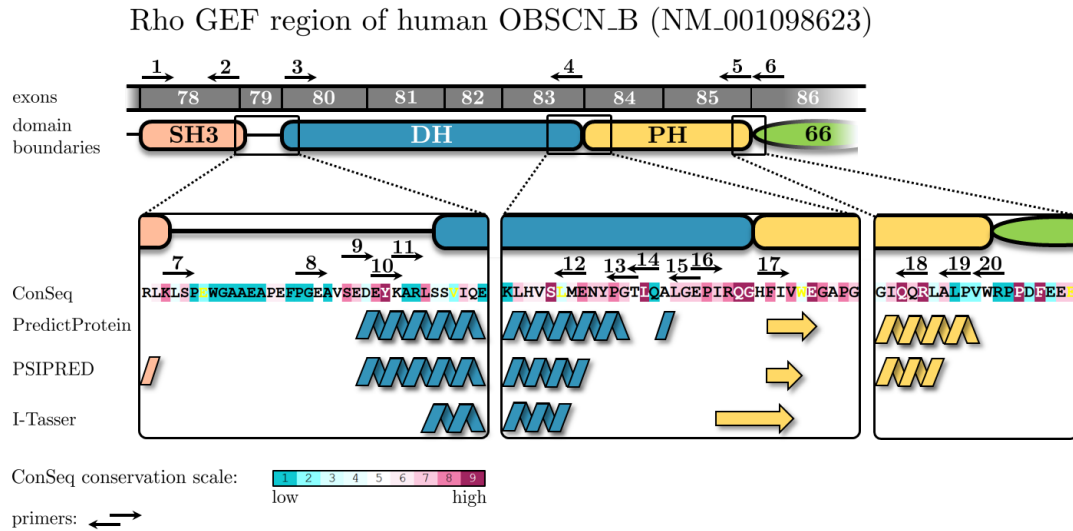


Figure 3.1. Obscurin Rho GEF domain boundary optimisation for protein expression constructs.

Top, exon-based domain boundaries. Bottom, bioinformatic analysis of sequence conservation and prediction of secondary structure elements. The presence of highly conserved amino acids and structure predictions suggest that domain boundaries likely exceed the exon boundaries. Black arrows indicate the position of forward and reverse primers for optimisation of domain boundaries.

To avoid time-consuming expression and purification trials with conventional protein expression and purification approaches, we decided to apply a semi-high-throughput small-scale expression and purification approach developed by Dr Alexander Alexandrovich in our group, which involves growing 4 ml *E. coli* cultures in 24-well plates followed by cell lysis with detergents and a single purification step using Ni²⁺-NTA affinity resin. To evaluate successful purification, eluted samples were first analysed by a rapid dot-blotting procedure with anti-His-tag antibodies and selected samples that yielded high signals in the dot-blot assay were further analysed by SDS-PAGE. We tested this procedure in pilot experiments with 4 previously successful and unsuccessful constructs as a reference and found that the soluble and stable SH3-DH protein fragment yielded a notably higher signal than the samples from the insoluble DH and DH-PH. Interestingly, however, the soluble SH3 domain did not yield a notable signal in the dot-blot, possibly indicating unsuccessful expression (Figure 3.2). As an internal quality control for expression and purification, we further decided to include fluorescent proteins GFP and mCherry for visual confirmation of protein expression in growing *E. coli* cultures as well as the SH3-DH construct as a reference for successful purification in all subsequent experiments.

We next analysed the small-scale expression and purification of the 39 novel Rho GEF constructs. As shown in Figure 3.3, samples from all new DH domain constructs with the longer N-terminus showed a strong signal in the dot-blot, most even exceeding the signal for the solu-












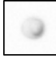


Reference constructs	Purification from ≥ 0.5 l <i>E.coli</i> culture	Primers	Residues (obscurin B)	Dot-blot signal	
				1s	10s
	soluble, multiple milligrams, folded (NMR)	1,2	5601-5667		
	soluble, multiple milligrams, folded (NMR)	1,4	5601-5899		
	expressed but insoluble in DE3 RIPL and Solubl21 strains	3,4	5695-5899		
	expressed but insoluble in DE3 RIPL and Solubl21 strains	3,5	5695-6011		
	expressed but insoluble in DE3 RIPL and Solubl21 strains	3,6	5695-6019	n.d.	
	expressed but insoluble in DE3 RIPL and Solubl21 strains	1,6	5601-6019	n.d.	

Figure 3.2. Previously designed constructs of the obscurin Rho GEF domains and their behaviour and properties after large-scale purification.

The results from the applied small-scale semi-high-throughput expression and purification approach as evaluated by the dot-blot signal are given as a reference for subsequent constructs on the right. n.d. = not determined.

ble and stable SH3-DH reference construct. This suggests that the N-terminal extension of the DH-domain based on the bioinformatic prediction of the first alpha-helix indeed helps to stabilise the DH-fold and thus makes the protein domain soluble. In contrast, samples from constructs of the DH-PH domain tandem resulted in notably weaker signals, whereas samples of the PH domain constructs showed no signal. This suggests that the PH domain of obscurin, despite different boundary designs, is on its own intrinsically unstable even in the presence of the otherwise stable and soluble DH domain.

To confirm successful purification, we performed an SDS-PAGE analysis of selected samples (Figure 3.4). In agreement with the dot-blot data, all analysed samples of the DH domain resulted in a clearly visible band at the expected molecular weight of approximately 25 kDa with little indication for degradation products or contaminations after only a single purification step. In contrast, none of the analysed samples of the DH-PH domain tandem or the PH domain resulted in a visible band at the correct molecular weight (37 and 13 kDa, respectively), again confirming that the PH domain is intrinsically unstable.

In summary, the domain optimisation approach based on bioinformatic analysis of sequence conservation and secondary structure elements enabled us to successfully express and purify the obscurin DH domain, but not the DH-PH domain tandem or the PH domain. As for obscurin, the PH domain of unc89 was also reported to be very unstable, although obviously less so than the obscurin PH domain since the authors were able to purify the unc89 PH domain and solve its structure by NMR (Blomberg et al. 2000). Another, unrelated example is the PH domain of the yeast Rho GAP Bem3, which is insoluble as an individual domain (personal communication with Dr Matthias Müller, TU Dortmund) but soluble and relatively stable when purified together with the N-terminal PX domain (Ali et al. 2018). Taken together, this indicates that the PH-fold may at times be unstable and difficult to purify unless stabilised by additional factors.

Boundary-optimised Rho GEF constructs






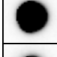


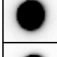


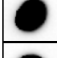


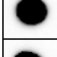

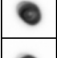
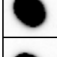

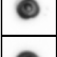
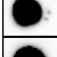

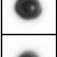
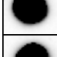

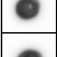
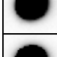

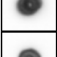
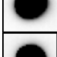

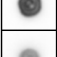









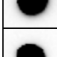


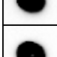


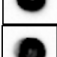











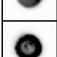




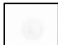





























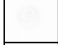


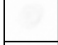








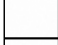


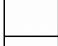
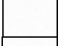

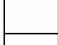
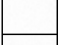


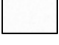
	Nr.	Primers	Residues (obscurin B)	Dot-blot signal	
				1s	10s
	1	7,4	5667-5899		
	2	8,12	5681-5884		
	3	8,13	5681-5889		
	4	8,14	5681-5891		
	5	8,15	5681-5895		
	6	8,4	5681-5899		
	7	9,12	5686-5884		
	8	9,13	5686-5889		
	9	9,14	5686-5891		
	10	9,15	5686-5895		
	11	9,4	5686-5899		
	12	10,12	5689-5884		
	13	10,13	5689-5889		
	14	10,14	5689-5891		
	15	10,15	5689-5895		
	16	10,4	5689-5899		
	17	11,12	5691-5884		
	18	11,13	5691-5889		
	19	11,14	5691-5891		
	20	11,15	5691-5895		
	21	11,4	5691-5899		

Figure 3.3. Design and test-purification of novel obscurin Rho GEF constructs.

Result of the small-scale expression and purification trials as evaluated by dot-blotting shown on the right. Figure continues on the next page.

Boundary-optimised Rho GEF constructs

	Nr.	Primers	Residues (obscurin B)	Dot-blot signal	
				1s	10s
	22	8,18	5681-6005		
	23	8,19	5681-6009		
	24	8,20	5681-6012		
	25	9,18	5686-6005		
	26	9,19	5686-6009		
	27	9,20	5686-6012		
	28	10,18	5689-6005		
	29	10,19	5689-6009		
	30	10,20	5689-6012		
	31	11,18	5691-6005		
	32	11,19	5691-6009		
	33	11,20	5691-6012		
	34	16,18	5895-6005		
	35	16,19	5895-6009		
	36	16,20	5895-6012		
	37	17,18	5901-6005		
	38	17,19	5901-6009		
	39	17,20	5901-6012		

Design and test-purification of novel obscurin Rho GEF constructs (continued). Result of the small-scale expression and purification trials as evaluated by dot-blotting shown on the right.

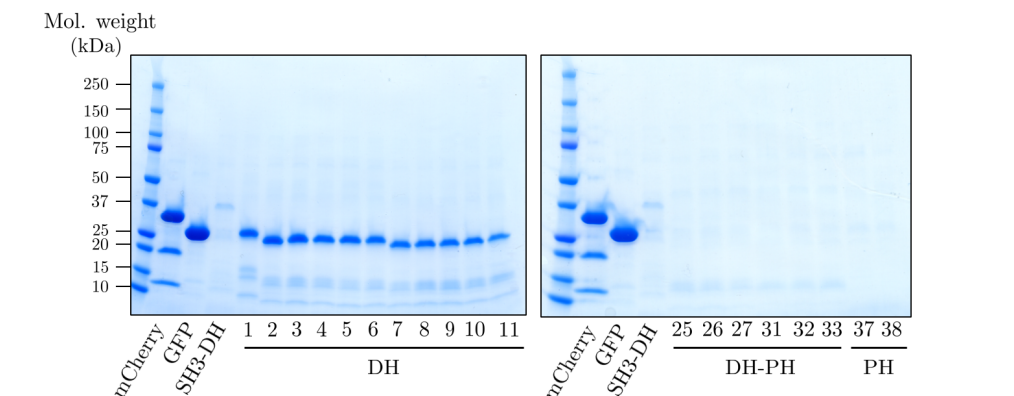


Figure 3.4. Coomassie-stained gel after SDS-PAGE of selected obscurin Rho GEF constructs.

Strongly visible bands running at the height of 20-25 kDa marker bands confirm solubility of DH domain constructs with longer N-terminus.

3.1.3 Larger scale purification of two DH domain fragments and analysis of protein folding by NMR

Although the DH domain is clearly soluble, it is unclear whether the DH domain purified from *E. coli* has a physiological protein fold. To answer this question, we purified the soluble obscurin fragments DH₅₆₈₁₋₅₈₈₉ (comprising only the DH-fold, i.e. all predicted alpha helices) and the longer DH₅₆₆₇₋₅₈₈₉ (additionally comprising the N-terminal linker between SH3 and DH domain) on a larger scale followed by His₆-tag removal via TEV digestion and size-exclusion chromatography on a Superdex 75 column and obtained ≈ 13 and ≈ 22 mg protein at high purity from 1L *E. coli* culture (Figure 3.5A,B). Using these highly pure protein samples, we recorded ^1H 1D-NMR spectra to obtain information about whether or not the protein fragments are folded. The spectra of both protein fragments exhibited a good peak dispersal up to 9.5 and 10 ppm as well as peaks below 0 ppm, indicating the presence of a hydrophobic core (Figure 3.5C, black arrows). Both of these NMR characteristics are hallmarks of folded proteins, suggesting that both DH domain fragments are indeed properly folded.

3.1.4 Crystallisation trials

The availability of highly pure, soluble, stable and folded protein is an important prerequisite for growing protein crystals for structural studies by x-ray crystallography. To explore conditions under which the obscurin Rho GEF domains might form protein crystals, we set up crystallisation trials of obscurin fragments SH3-DH, DH₅₆₈₁₋₅₈₈₉ and DH₅₆₆₇₋₅₈₈₉ at multiple protein concentrations and using several commercial screening suites (Table 3.1). While at higher concentrations approximately 50-60% of conditions resulted in precipitates of varying appearance, none of the tested proteins or conditions resulted in the formation of crystals.

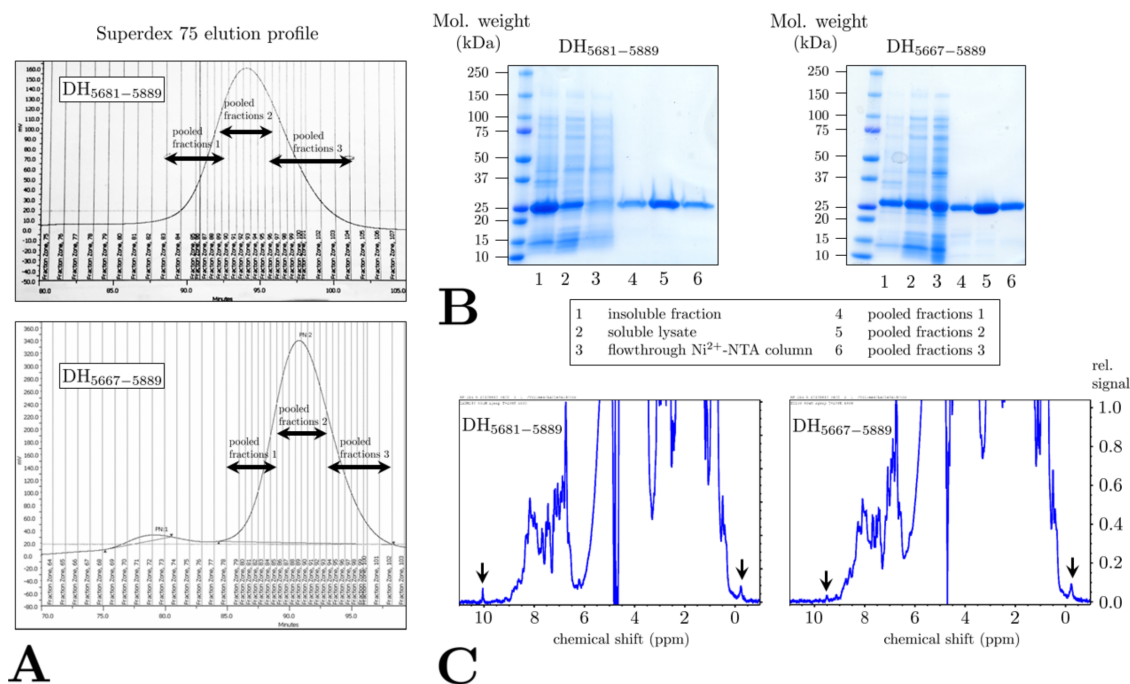


Figure 3.5. Two-step purification of two obscurin DH domain fragments from 1L *E. coli* cultures.

A, size exclusion chromatography profiles and, **B**, SDS-PAGE analyses of purified DH domains show bands at the expected molecular weight. Due to high purity, pooled fractions 1-3 were combined and further concentrated to about 10 mg/ml, snap-frozen and stored at -70°C before further analysis. **C**, ^1H 1D-NMR spectra of purified obscurin DH domain fragments (60 μM) suggest both proteins are folded due to the presence of peaks above 9.5 ppm and below 0 ppm (arrows).

Table 3.1. Crystallisation trials of three obscurin Rho GEF fragments using four different crystal screening suites.

Protein	initial concentration	JCSG++		PACT		Qiagen classics I		Qiagen classics II	
		end dilution		end dilution		end dilution		end dilution	
		$\times \frac{1}{2}$	$\times \frac{1}{3}$	$\times \frac{1}{2}$	$\times \frac{1}{3}$	$\times \frac{1}{2}$	$\times \frac{1}{3}$	$\times \frac{1}{2}$	$\times \frac{1}{3}$
SH3-DH	6.7 mg/ml	P: 58.3% C: 0%	P: 57.3% C: 0%	P: 53.1% C: 0%	P: 53.1% C: 0%	P: 61.5% C: 0%	P: 56.3% C: 0%	P: 64.6% C: 0%	P: 62.5% C: 0%
DH ₅₆₈₁₋₅₈₈₉	9.9 mg/ml	P: yes* C: 0%	P: yes* C: 0%	P: yes* C: 0%	P: yes* C: 0%	P: yes* C: 0%	P: yes* C: 0%	n.d.	n.d.
DH ₅₆₆₇₋₅₈₈₉	10.3 mg/ml	P: yes* C: 0%	P: yes* C: 0%	P: yes* C: 0%	P: yes* C: 0%	P: yes* C: 0%	P: yes* C: 0%	P: yes* C: 0%	P: yes* C: 0%

P = precipitation, C = crystallisation, n.d. = not determined, * = precipitation observed but not quantified

3.1.5 Catalytic activity of the obscurin Rho GEF domains *in vitro*

For many Dbl-family Rho GEFs, the DH domain on its own exerts strong catalytic activity towards Rho GTPases even in absence of the PH domain (Pruitt et al. 2003; Souchet et al. 2002; Kristelly et al. 2004; Heo et al. 2005; Jaiswal et al. 2011). Moreover, the DH domain is also the major determinant of Rho GEF substrate specificity (Snyder et al. 2002; Jaiswal et al. 2011). In agreement with this, Ford-Speelman et al. 2009 reported that the transfection of the obscurin DH domain alone is sufficient to activate RhoA in cellular assays but does not increase the activity of Cdc42 or Rac1. Although the DH-PH domain tandem could not be purified successfully, we thus decided to use the obscurin fragments SH3-DH, DH₅₆₈₁₋₅₈₈₉ and DH₅₆₆₇₋₅₈₈₉ to screen for substrates *in vitro*. Among the 20 Rho GTPases in *homo sapiens*, only 10 are “classical” Rho GTPases in the sense that they are regulated by GEFs and GAPs and thus can be a potential substrate of the obscurin Rho GEF domains: RhoA, RhoB, RhoC, Rac1, Rac2, Rac3, RhoG, Cdc42, RhoQ/TC10, RhoJ/TCL (Amin et al. 2016; Aspenström 2017; Jaiswal et al. 2013; Wennerberg and Der 2004). As mentioned earlier, RhoA and RhoQ/TC10 have been reported to be obscurin substrates based on cellular assays (Coisy-Quivy et al. 2009; Ford-Speelman et al. 2009). In contrast, Jaiswal and colleagues predicted obscurin to have specificity for the Rac subfamily of Rho GTPases based on a systematic characterisation of the activity determinants of multiple Dbl-family GEFs towards all classical Rho GTPases (Jaiswal et al. 2013). To address the question of obscurin’s substrate GTPases experimentally, we opted for a well-established approach to directly monitor the nucleotide exchange reaction in real-time via fluorescent nucleotides. The advantage of this assay is two-fold: first, it is a direct measure of the nucleotide exchange reaction and thus is not subject to potential confounding variables of indirect pull-down methods mentioned earlier. Secondly, it provides precise quantitative information and even a single time-course experiment can sometimes allow one to obtain a good estimate of the specificity constant k_{cat}/K_m for a given GTPase (if $[GTPase] < K_m$). Once a substrate is identified, the same assay can also be conveniently used to perform a complete steady-state kinetic characterisation by repeating the same experiment at different GTPase concentrations. This furthermore provides an accurate tool for studying the regulation of GEF activity by adjacent domains or post-translational modification.

We thus first expressed and purified all 10 classical Rho GTPases as GST-fusion proteins from *E. coli* and subsequently prepared potential substrate GTPases for the assay by performing a preparative nucleotide exchange in which the bound nucleotide is released via chelation of the GTPases’ Mg^{2+} ion by EDTA and replaced by fluorescent 2’/3’-O-(N-Methyl-anthraniloyl)-GDP (mant-GDP). As biological positive controls for our assay, we cloned and purified the DH domain of LARG for Rho-subfamily GTPases and the DH domain of Vav2 as a GEF for Rac- and Cdc42-subfamily GTPases (Abe et al. 2000) (Figure A2). Additionally, since for some of the GTPases neither LARG nor Vav2 show GEF activity, we used 10 mM EDTA as chemical positive control, which releases the bound nucleotide at similar timescales as does an effective biological GEF.

First, we analysed the nucleotide exchange activity of obscurin Rho GEF fragments SH3-DH, DH₅₆₈₁₋₅₈₈₉ and DH₅₆₆₇₋₅₈₈₉ at two different concentrations towards previously reported substrates RhoA and RhoQ as well as towards the well characterised and important Rho GTPases Rac1 and Cdc42. Despite equal (10 μ M) or higher concentrations (25 μ M) of obscurin Rho GEF domains than used for the positive controls ($[Vav2] = 10 \mu$ M, $[LARG] = 0.5 \mu$ M) and despite a >5 to >10 -fold excess of enzyme over substrate concentration, neither of the obscurin Rho GEF fragments exhibited any GEF activity towards the tested GTPases and the recorded kinetic traces perfectly

overlap with the slow intrinsic nucleotide exchange traces of the respective GTPase (Figure 3.6, right panel). In contrast, the kinetic traces for the positive controls show a rapid signal decline and the apparent rate constant (k_{obs}) for the GEF-catalysed or EDTA-induced exchange reaction was 1-2 orders of magnitudes higher than for the intrinsic nucleotide exchange activity (k_{int}) of the respective GTPase (Figure 3.6, left panel).

The lack of GEF activity towards RhoQ and RhoA in our assay contradicts previous studies by Coisy-Quivy et al. 2009 and Ford-Speelman et al. 2009. One potential explanation for this discrepancy is that the reported GEF activity could be an indirect effect of obscurin. Indeed, many small GTPases, including Rho GTPases, are known to activate or inhibit other small GTPases via recruiting or regulating their GEFs or GAPs (Conte-Zerial et al. 2008; Byrne et al. 2016; Nottingham and Pfeffer 2009). Thus, it is possible that obscurin exhibits GEF activity towards other Rho GTPases which in turn activate RhoA and RhoQ *in vivo*, thereby explaining the observed enrichment of active RhoA and RhoQ in pull-down based activity assays from lysates of cells transfected with the obscurin Rho GEF domains.

To test this possibility, we probed the GEF activity of obscurin towards the remaining potential substrate GTPases, i.e. RhoB, RhoC, Rac2, Rac3 and RhoG. We also intended to test activity towards RhoJ, but this GTPase exhibited very poor solubility and stability in our hands and did not generate analysable data in this kind of assay. Therefore, we excluded RhoJ from further experiments. For the sake of feasibility, we further decided to focus only on the obscurin DH domain (residues 5667-5889). However, neither of these GTPases demonstrated an increased nucleotide exchange rate in the presence of the tested obscurin Rho GEF domains (Figure 3.7). In summary, our experiments demonstrate that neither of the tested recombinant obscurin Rho GEF fragments SH3-DH, DH₅₆₈₁₋₅₈₈₉ and DH₅₆₆₇₋₅₈₈₉ had any discernible GEF activity towards Rho GTPases despite being soluble, stable and properly folded.

3.1.6 Changing species: the potential role of the PH domain

The apparent lack of any GEF activity in our assays is surprising given the previously reported activity towards RhoA and RhoQ in pull-down assays (Coisy-Quivy et al. 2009; Ford-Speelman et al. 2009). One potential explanation could be that the Rho GEF domains contain autoinhibitory elements which prevent GEF activity in our assays. While this is certainly a possibility for the tested SH3-DH fragment, this explanation is less likely for the DH₅₆₆₇₋₅₈₈₉ fragment which features the interdomain linker between SH3 and DH domain, and highly implausible for the DH₅₆₈₁₋₅₈₈₉ fragment which, based on the structure predictions outlined above, likely comprises only the DH fold without additional elements. As mentioned earlier and as demonstrated by the data with our positive controls which only feature the DH domains of the GEFs Vav2 and LARG, the isolated DH domain is often sufficient to obtain significant GEF activity (Pruitt et al. 2003; Souchet et al. 2002; Kristelly et al. 2004; Heo et al. 2005; Jaiswal et al. 2011). This agrees with the data from Ford-Speelman et al. who reported that the obscurin DH domain alone is sufficient to activate RhoA in cells (Ford-Speelman et al. 2009).

In other cases, however, the PH domain can significantly contribute to GEF activity and for some GEF/GTPase pairs can even be necessary (Rossman and Campbell 2000; Rossman et al. 2002). Together with the limitations of pull-down based assays, we considered the possibility that the PH domain of obscurin might be necessary for detectable GEF activity. To better understand the molecular reasons for this possibility, we compared the primary sequence and ho-

mology model of the obscurin DH-PH domain tandem with Rho GEFs which are evolutionary close to obscurin and have already been characterised both enzymatically and structurally. Obscurin belongs to the trio-subfamily of Dbl-homology domain Rho GEFs which further includes the “founding” Rho GEF Dbl/MCF as well as the proteins Dbs/MCF2L, drg/MCF2L2, trio, kalirin, p63RhoGEF/ARHGEF25, solo/ ARHGEF40, puratrophin-1/PLEKHG4 and PLEKHG4B (Fort and Blangy 2017). The molecular mechanisms of some subfamily members are well characterised. Particularly for Dbs, detailed structural and kinetic data yielded several key insights into the molecular mechanism of PH domain assisted nucleotide exchange.

It was long known that the DH domains of Dbs, Dbl and trio are much less potent at facilitating nucleotide exchange compared to the DH-PH domain tandem, requiring high enzyme to substrate ratios to observe a significant acceleration of the exchange reaction (Rossman and Campbell 2000). The crystal structures of the Dbs DH-PH domains in complex with RhoA and Cdc42 revealed that three residues of the GEF, which are conserved in the obscurin, Dbl and the N-terminal trio and kalirin DH-PH tandems, interact with the switch II region of the substrate GTPase at the DH-PH interface (Figure 3.8A,B) (Rossman et al. 2002; Snyder et al. 2002). The interaction of these residues (His814 in the C-terminal alpha-helix of the Dbs DH domain as well as Gln834 in the first and Tyr889 in the fourth beta-strand of the PH domain) with a conserved aspartate and arginine of the switch II region likely contributes to remodelling of the binding pocket for nucleotide release from the substrate GTPase (Figure 3.8C). In agreement with this model, mutation of these residues in Dbs or trio drastically reduces catalytic activity (Chhatriwala et al. 2007; Snyder et al. 2002). Dbl, too, requires the presence of the PH domain for efficient nucleotide exchange, further confirming the catalytic significance of these residues (Hart et al. 1994). As the catalytically important residues are present in obscurin (Figure 3.8A)(Chhatriwala et al. 2007; Snyder et al. 2002), we superimposed the obscurin DH-PH homology model and the available Dbs DH-PH/RhoA or Cdc42 crystal structures.

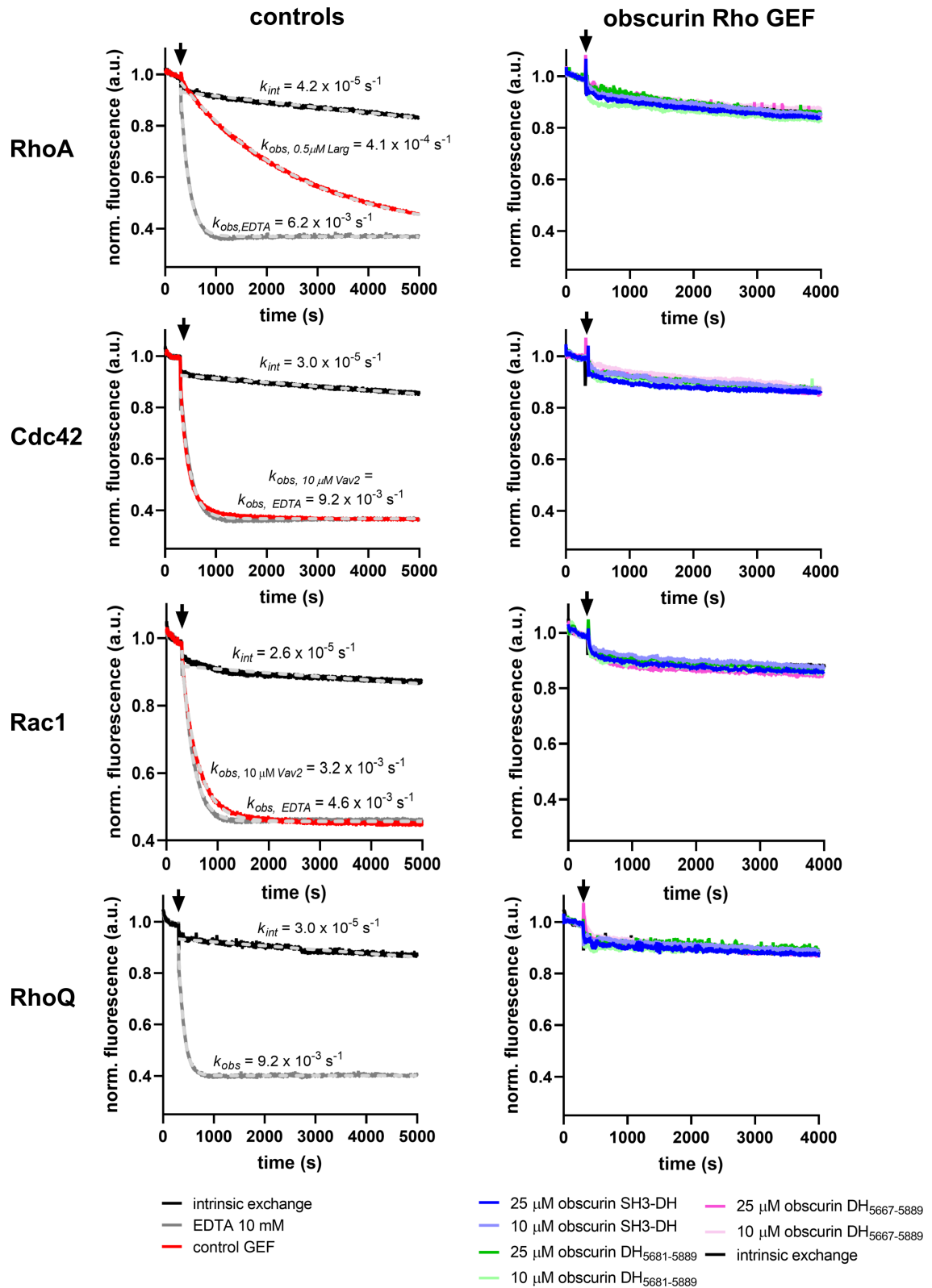


Figure 3.6. Nucleotide exchange of human obscurin Rho GEF fragments towards RhoA, Cdc42, Rac1 and RhoQ at 1.5 μM [GTPase].

Left panel shows intrinsic nucleotide exchange activity and GEF and/or EDTA-induced exchange as positive control. Right panel shows exchange after addition of obscurin Rho GEF domains. No GEF activity was observed for the tested obscurin Rho GEF fragments. Black arrows indicate addition of GEF/EDTA. Curves represent the mean of $n = 3-4$ technical replicates/experiment. Dashed lines indicate fitted decay functions.

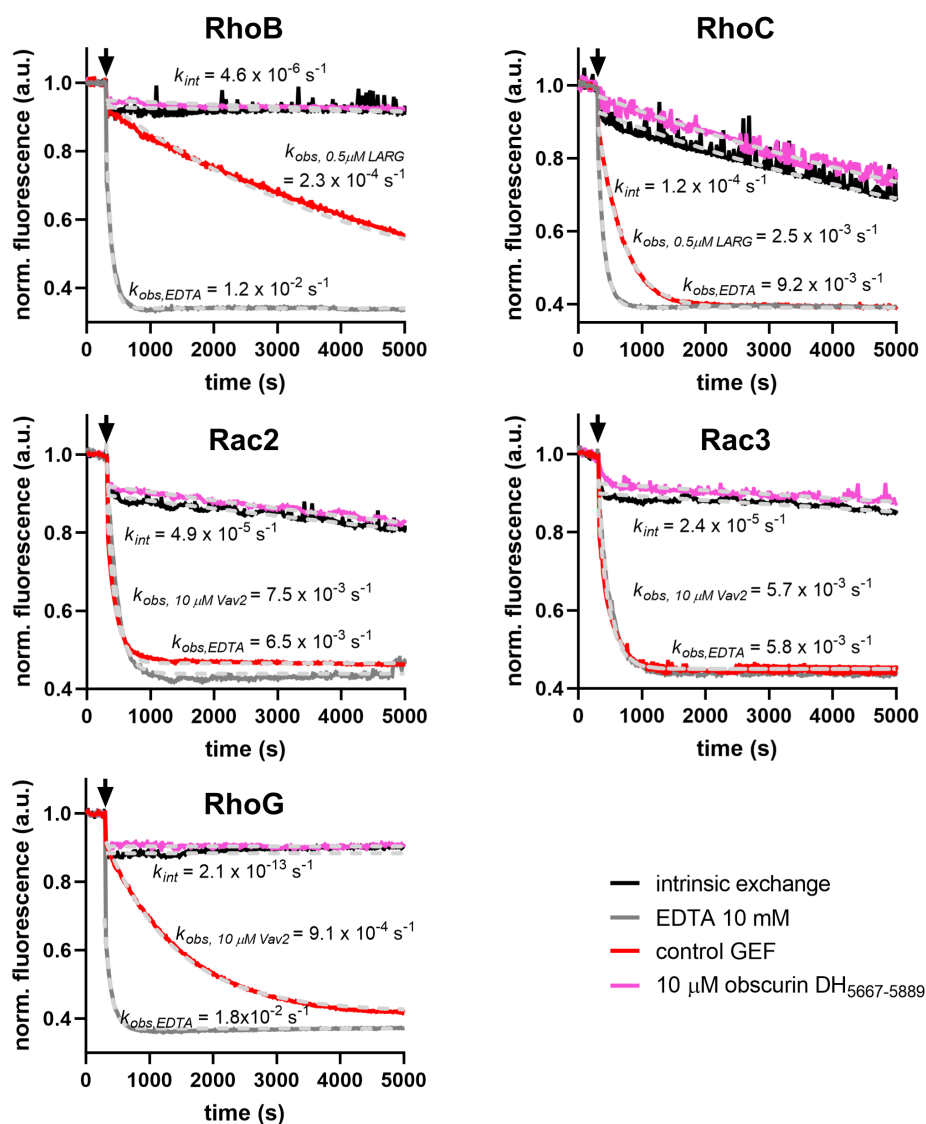


Figure 3.7. Nucleotide exchange of human obscurin Rho GEF fragments towards RhoB, RhoC, Rac2, Rac3 and RhoG at $1.5 \mu\text{M}$ [GTPase].

Red and grey curves show strong acceleration of exchange after addition of EDTA or the control GEF. No GEF activity was observed for the tested obscurin Rho GEF fragment, shown in pink. Black arrows indicate addition of GEF/EDTA. Curves represent the mean of $n = 3-4$ replicates/experiment. Dashed lines indicate fitted single-exponential decay functions.

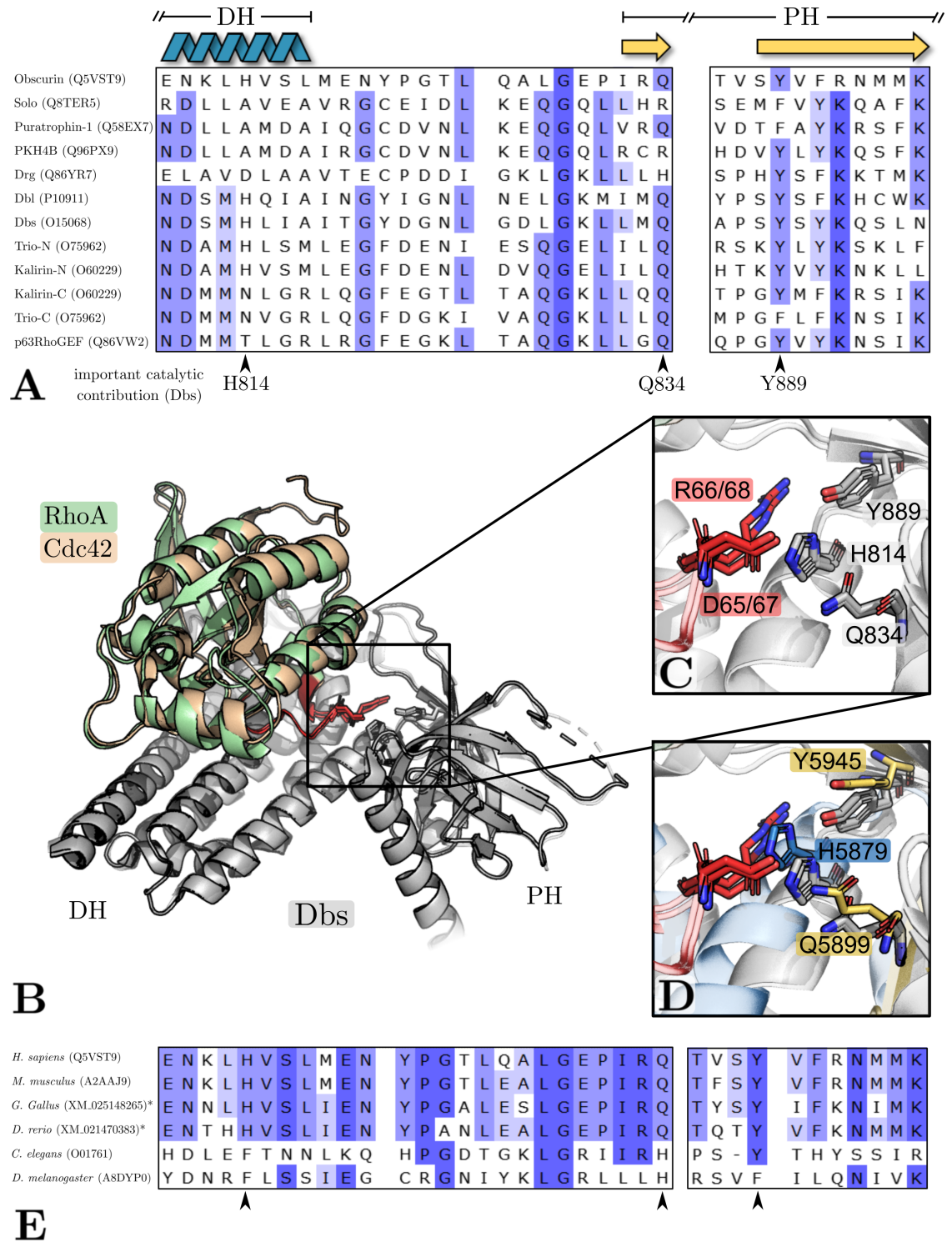


Figure 3.8. Catalytic residues at the DH/PH interface.

A, multiple sequence alignment of DH-PH domain tandems of the Trio-subfamily showing residues at the DH/PH/GTPase interface. Conserved residues are highlighted in blue. Secondary structure elements of the obscurin homology-model are highlighted above. Black arrows indicate catalytically important residues. **B**, aligned complex structures of Dbs bound to RhoA (PDB-ID: 1LB1) and Cdc42 (PDB-ID: 1KZ7). **C**, highlighted residues in the DH and PH domain of Dbs (grey) interact with conserved residues of the switch II region (red) of RhoA and Cdc42, thereby assisting in nucleotide exchange. **D**, superimposition of the obscurin homology model indicates that the interactions between PH domain and GTPase are likely relevant in obscurin. **E**, conservation of obscurin/unc89 residues at the DH/PH/GTPase interface across species. Uniprot-ID or NCBI reference sequence, indicated by *, are given in brackets.

This demonstrated that Gln5899 and Tyr5945 in the homology model of the obscurin PH domain are in a similar position and configuration as in Dbs (Figure 3.8D). Taken together, these data suggest that the PH domain of obscurin could be important for full catalytic activity of the obscurin Rho GEF domains.

Unfortunately, as shown above, the PH domain of human obscurin is intrinsically unstable and it is not possible to express and purify the PH domain from *E. coli* (Figure 3.3 and Figure 3.4). Interestingly, however, the PH domain of unc89 in *C. elegans*, although reported to be of limited stability, is stable enough to be purified as a soluble recombinant protein from *E. coli*, suggesting that the PH domain may be more or less stable depending on the species of origin (Blomberg et al. 2000). We thus wondered whether obscurin from other species may lend itself more easily to an *in vitro* characterisation. Using other species as model systems for human biology is common practice and often a very successful one. Although the Dbl-family of Rho GEFs shows a strong evolutionary increase in complexity (Fort and Blangy 2017), the functionality of individual small GTPases is often strongly conserved. The GTPase Rab1 involved in vesicular trafficking to and in the Golgi-network, for instance, can be replaced with YPT1 from *S. cerevisiae* without loss of functionality, suggesting that the yeast GTPase put into mammalian cells is regulated by the same GEFs and GAPs as the human homologue Rab1 (Segev 2001). Thus, the PH domain from a different species, if stable, may be a solution for obtaining an active obscurin Rho GEF fragment.

To identify suitable species, we performed a multiple sequence alignment of the sequence of the DH-PH domain tandem in humans and several common model organisms (mouse, chicken, zebrafish, nematode, fruit fly). The sequence identity to the human DH-PH domain tandem is: mouse – 91%, chicken – 75%, zebrafish – 58%, nematode – 21%, fruit fly – 20%. Next, we analysed the sequence in the vicinity of the above described catalytically important residues in trio-subfamily GEFs. As shown in Figure 3.8E, these residues are strictly conserved in all included vertebrate species. Interestingly, the included invertebrates exhibit strong deviations. While *D. melanogaster* features neither of these catalytically relevant residues, the nematode *C. elegans* only features the tyrosine in the fourth beta-strand of the PH domain, although the deletion of the preceding residue may alter the spatial configuration of this residue. This suggests that the catalytic assistance by the PH domain may not be evolutionary conserved across the whole animal kingdom.

Based on these analyses we designed and cloned several chimeric obscurin Rho GEF constructs in which the human PH domain is replaced by another PH domain. First, we also used the PH domains of Dbs and Trio as a substitute due to the apparent mechanistic similarity. Additionally, we used the PH domain from other species to substitute the human PH domain of obscurin. We decided not to use mouse obscurin as the high sequence identity makes it unlikely that the PH domain is more stable than the human PH domain. The invertebrate PH domains, on the other hand, are not suitable as they do not feature the catalytically important residues. We thus decided to design human/chicken and human/zebrafish hybrid Rho GEF fragments which we called “harpy” and “mermaid” obscurin, respectively. The sequences of both chicken and zebrafish are different enough from human to be potentially more stable but still feature the catalytically relevant residues. Figure 3.9A shows the design of the chimeric constructs.

As for the human constructs, we performed a small-scale expression and purification trial of the chimeric constructs. The dot-blot analysis of the eluted samples indicated that only the mermaid construct yields soluble and stable protein (Figure 3.9A, right panels). SDS-PAGE analysis of the mermaid sample demonstrated a band at a position consistent with the expected molecular weight

of about 40 kDa, although the band appeared slightly below the 37 kDa marker band due to a smiling effect on the gel (Figure 3.9B).

Due to the successful purification of mermaid obscurin, we decided to design additional, larger constructs as well as non-chimeric constructs of the zebrafish obscurin Rho GEF domains (Figure 3.10A,B). Although zebrafish have an expanded Rho subfamily, most GTPases are highly similar to human ones. For instance, the zebrafish homologues of RhoA, a putative obscurin Rho GEF substrate, share 92-97% sequence identity with human RhoA (Salas-Vidal et al. 2005). If zebrafish obscurin is a functional GEF for RhoA, it is thus very likely that it will also exhibit activity towards human RhoA. SDS-PAGE analysis of the eluted samples demonstrated successful purification due to the presence of a band of correct molecular weight for all novel constructs except ‘mermaid II’ (Figure 3.10).

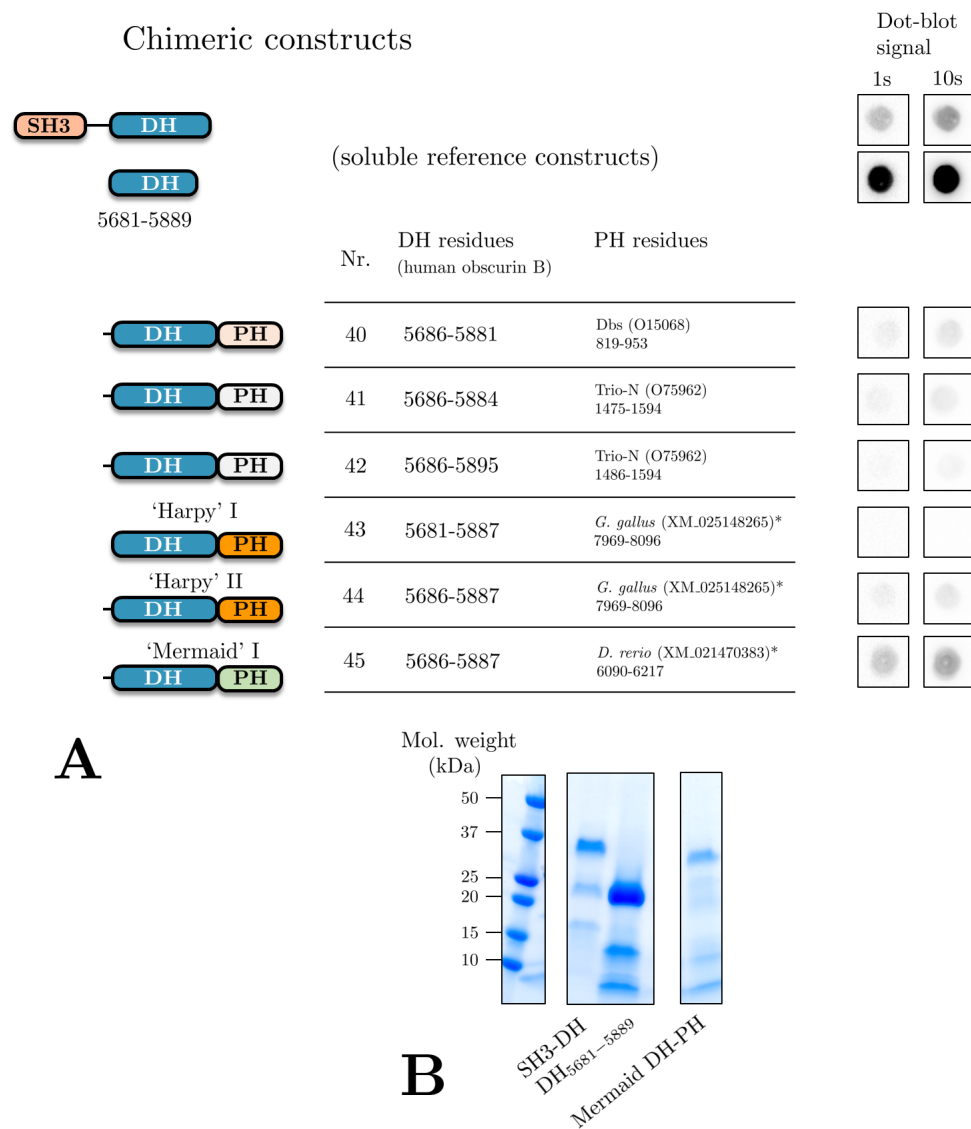


Figure 3.9. Chimeric obscurin Rho GEF constructs.

A, six different chimeric constructs with human DH domain sequence and PH domain sequence from (human) Dbc and Trio (N-terminal PH domain) or from chicken or zebrafish obscurin were designed. Results of small-scale expression and purification trials as evaluated by dot-blotting are shown on the right side. **B**, SDS-PAGE demonstrates successful purification of the human-DH/zebrafish-PH chimera (‘Mermaid’ I; expected molecular weight = 40 kDa).

Chimeric constructs

	Nr.	SH3/DH residues (human obscurin B)	PH residues
	46	5601-5887	<i>D. rerio</i> (XM.021470383)* 6090-6217
	47	5681-5887	<i>D. rerio</i> (XM.021470383)* 6090-6217
	48	5673-5887	<i>D. rerio</i> (XM.021470383)* 6090-6217
	49	5667-5887	<i>D. rerio</i> (XM.021470383)* 6090-6217

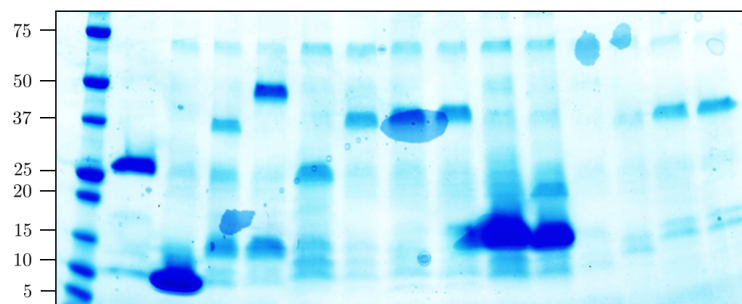
A

Zebrafish constructs (XM.021470383)*

	Nr.	Residues
	50	5806-5872
	51	5806-6101
	52	5806-6217
	53	5884-6091
	54	5884-6217
	55	5879-6217
	56	5872-6217
	57	6084-6217
	58	6094-6217

B

Mol. weight
(kDa)



C

Figure 3.10. Chimeric and zebrafish obscurin Rho GEF constructs.

A,B design of additional chimeric constructs and zebrafish obscurin constructs. **C**, SDS-PAGE analysis demonstrates successful purification by the presence of a band of correct molecular weight for all novel constructs except 'mermaid II' (Nr. 46).

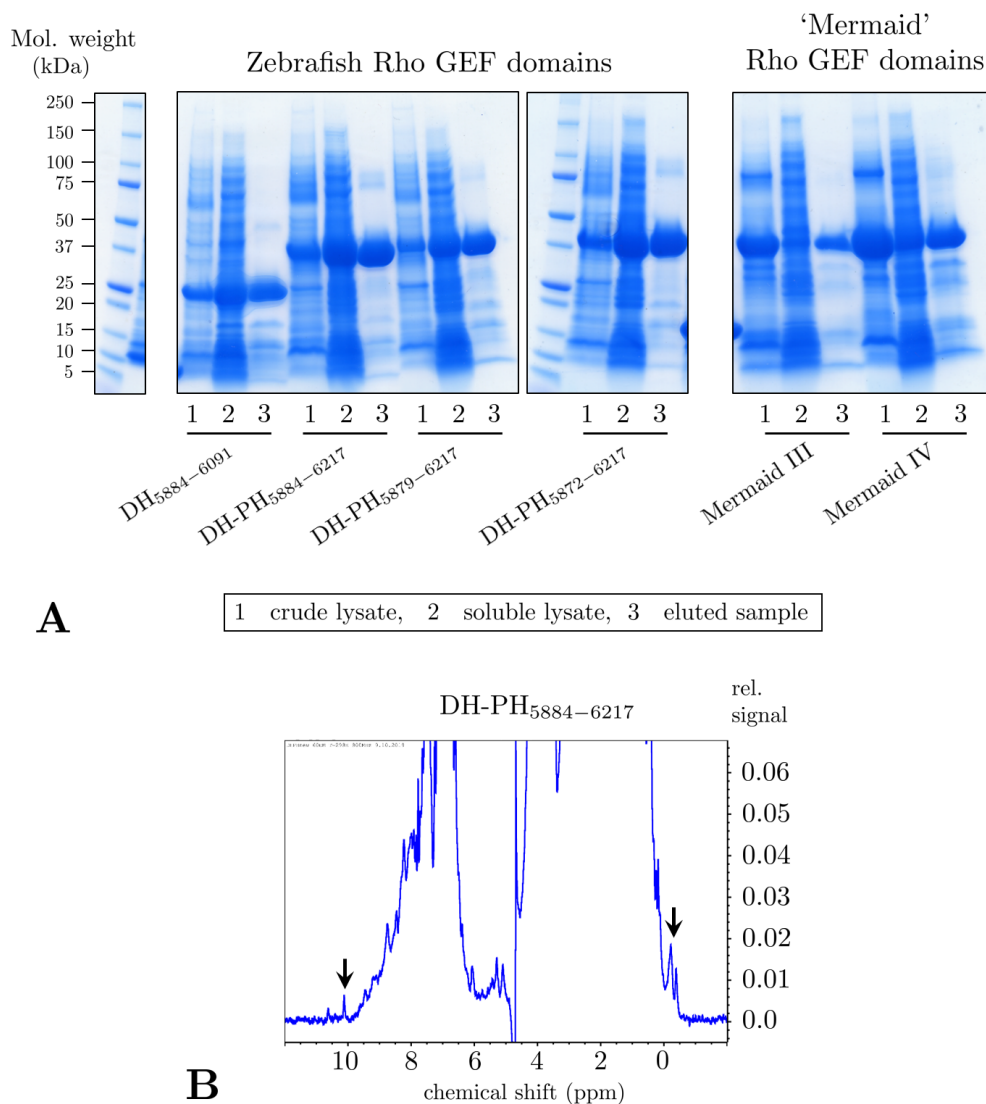


Figure 3.11. Purification of chimeric and zebrafish obscurin Rho GEF constructs.

A, SDS-PAGE analysis of purified zebrafish and chimeric 'mermaid' obscurin Rho GEF domains indicates successful purification. **B**, ^1H 1D-NMR spectrum of the zebrafish DH-PH₅₈₇₉₋₆₂₁₇ fragment (60 μM) suggests the protein is folded.

3.1.7 Catalytic activity of zebrafish and chimeric 'mermaid' obscurin Rho GEF domains *in vitro*

The successful purification of all obscurin Rho GEF domains from a vertebrate species allowed us to further study exchange activity. Specifically, we decided to study the following new zebrafish and 'mermaid' proteins in the GEF activity assays: mermaid III and IV, zebrafish DH₅₈₈₄₋₆₀₉₁ (Nr. 53), DH-PH₅₈₈₄₋₆₂₁₇ (Nr. 54), DH-PH₅₈₇₉₋₆₂₁₇ (Nr. 55) and DH-PH₅₈₇₂₋₆₂₁₇ (Nr. 56). To avoid time-consuming purification procedures, we decided to use a single step batch-purification protocol for medium scale preparation. When the purification is performed under abundant availability of soluble protein, even a single-step purification with Ni-NTA resin can yield protein of >50-90% purity (cf. Figure 3.4 and appendix Figure A2), which is sufficient for the purpose of screening

for enzymatic activity. All novel protein fragments could be successfully purified and resulted in approximately >50-80% pure protein (Figure 3.11A). While the zebrafish fragments were stable and soluble at least within a concentration range of 4-8 mg/ml, the mermaid constructs tended to form visible precipitates at ≈ 1.5 mg/ml (mermaid III) and ≈ 3.8 mg/ml (mermaid IV) and thus were not concentrated beyond this point. We further analysed the zebrafish DH-PH₅₈₈₄₋₆₂₁₇ fragment by 1D-NMR and confirmed these domains to be folded as indicated by peak dispersal beyond 10 ppm as well as peaks below 0 ppm (Figure 3.11B).

Next, we tested whether these novel chimeric and zebrafish obscurin Rho GEF fragments have catalytic activity towards RhoA, Cdc42, Rac1 or RhoQ. None of the novel constructs exerted any activity towards these GTPases (Figure 3.12). We also tested for activity towards RhoB, RhoC, Rac2, Rac3 and RhoG using the zebrafish obscurin DH-PH₅₈₈₄₋₆₂₁₇, but again did not detect any nucleotide exchange activity (Figure 3.13).

3.1.8 Regulation of the obscurin Rho GEF domains by phosphorylation

Since none of the tested obscurin Rho GEF fragments showed any catalytic activity, we wondered whether our experiments might lack important factors that might be necessary for the obscurin Rho GEF domains to be biologically active. Since we have tested multiple fragments with different domain combinations including the DH domain in isolation and a DH-PH domain tandem, it seems unlikely that the observed lack of activity can be explained by auto-inhibition of the DH domain by adjacent domains. Similarly, based on the well-established structural understanding of the nucleotide exchange reaction of Dbs and other trio-subfamily GEFs there is no obvious factor that the chimeric or zebrafish DH-PH fragments are missing compared to a purely human DH-PH fragment. However, many Rho GEFs are regulated by phosphorylation (Hodge and Ridley 2016; Rossman et al. 2005). Although phosphorylation typically releases autoinhibitory elements, other regulatory modes are conceivable. For instance, an unphosphorylated protein might be in an inactive conformation that shifts towards an active conformation upon phosphorylation.

Interestingly, the obscurin Rho GEF domains have been reported to be highly phosphorylated in the context of muscle exercise, supporting the hypothesis that the obscurin Rho GEF domains are regulated by phosphorylation (Potts et al. 2017). However, no kinases which phosphorylate the obscurin Rho GEF domains have been identified yet. In order to identify such kinases, we used the human SH3-DH fragment, the largest soluble Rho GEF fragment of human obscurin, for a commercially available service to screen a protein as a substrate against 245 different Ser/Thr-protein kinases (KinaseFinder screen from ProQinase GmbH, now Reaction Biology Europe GmbH). The screening assay is based on the use of radioactive ATP-isotopes ($[\gamma\text{-}^{33}\text{P}]\text{-ATP}$) and the phosphorylation of the substrate is measured in a microplate scintillation counter as the detectable radioactivity (given in counts per minute, cpm) after sample precipitation and ATP removal. To control for potential autophosphorylation of the kinase, a sample with the respective kinase and $[\gamma\text{-}^{33}\text{P}]\text{-ATP}$ but without substrate is run in parallel to measure the autophosphorylation background and subtract it from the substrate phosphorylation signal. Potentially interesting candidate kinases were identified by an activity ratio > 3 (defined as the phosphorylation signal of the substrate divided by the autophosphorylation signal background).

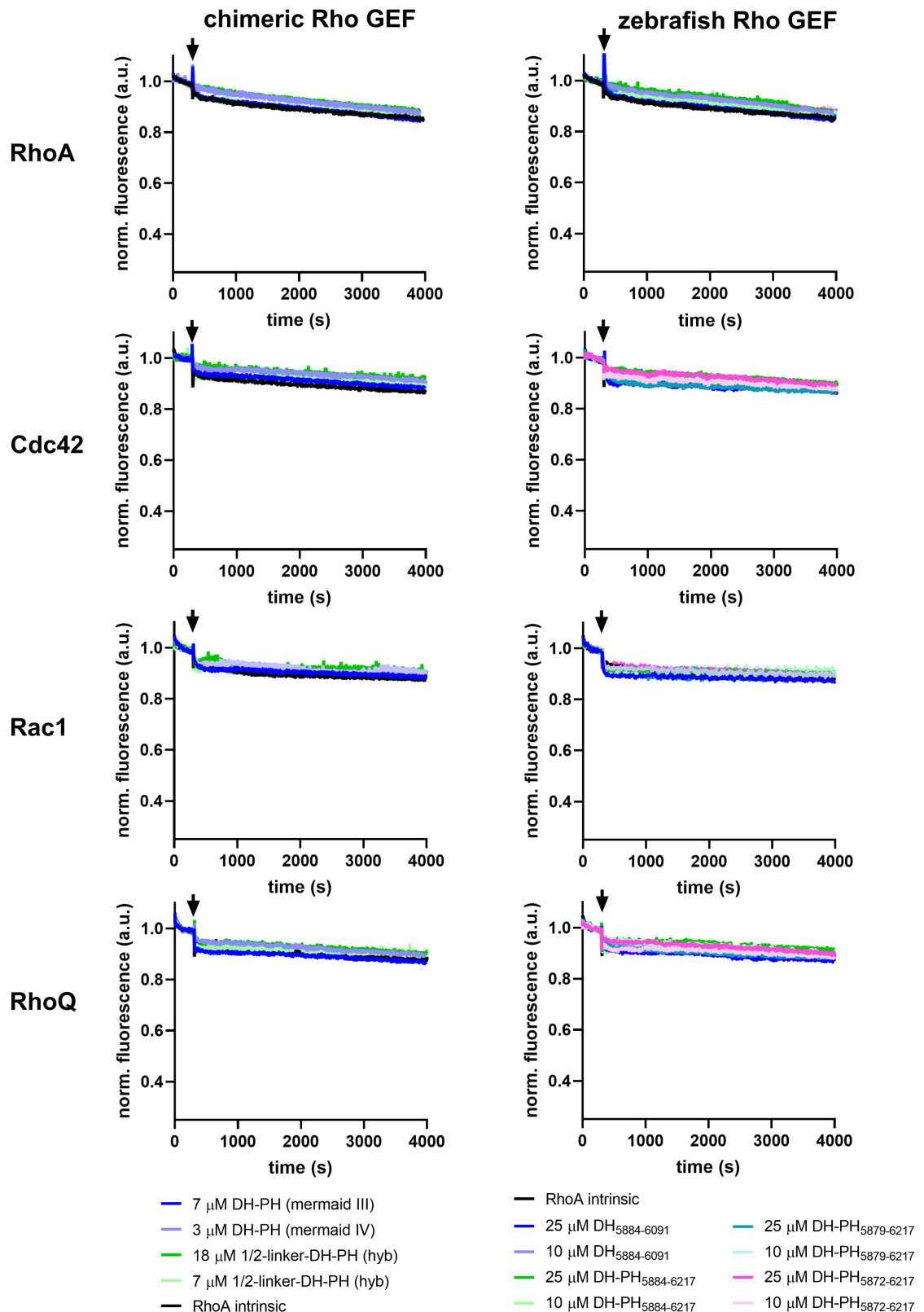


Figure 3.12. Nucleotide exchange of chimeric and zebrafish obscurin Rho GEF fragments towards RhoA, Cdc42, Rac1 and RhoQ at 1.5 μ M [GTPase].

Left and right panel show nucleotide exchange activity of human-zebrafish chimeric (mermaid) and zebrafish obscurin DH-PH proteins, respectively. Black arrows indicate time point of GEF addition. Curves represent the mean of $n = 3-4$ technical replicates/experiment. See Figure 3.6 for positive controls.

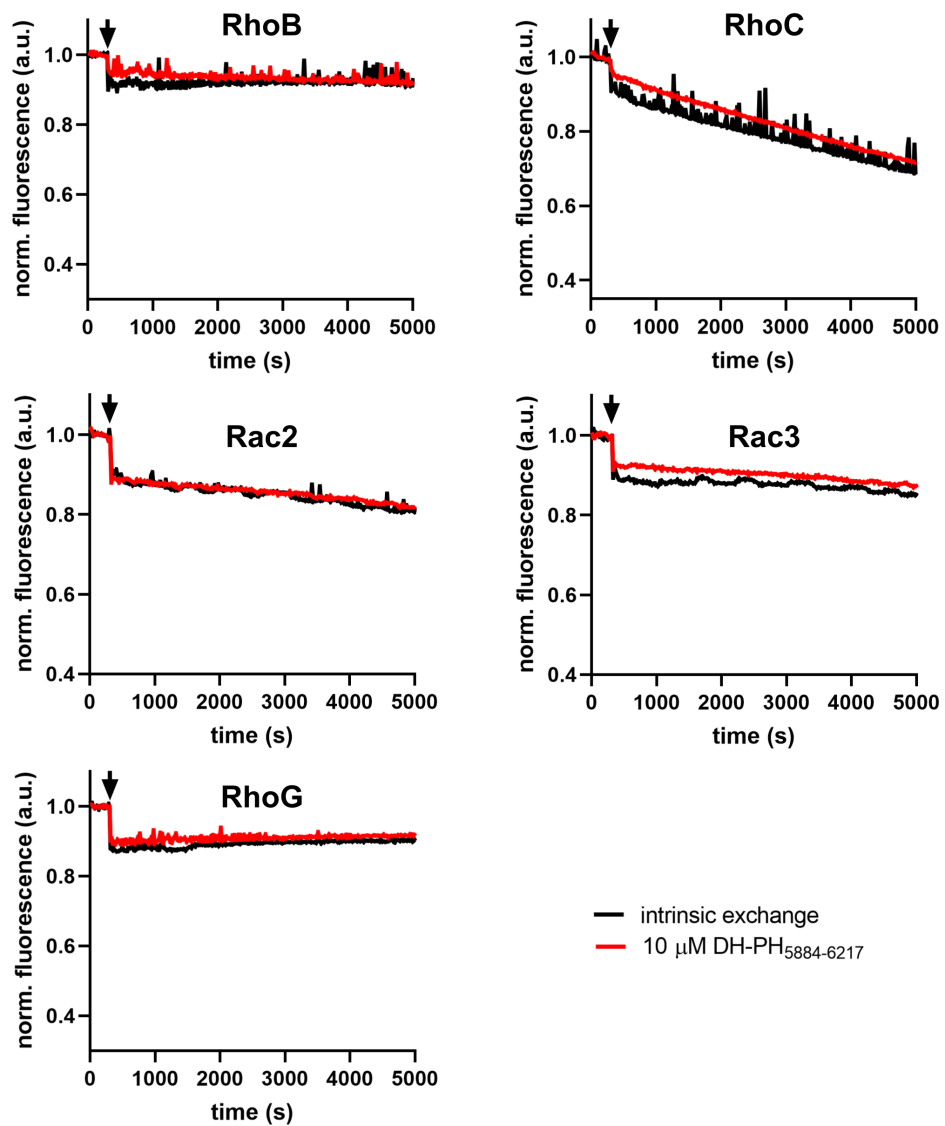


Figure 3.13. Nucleotide exchange activity of zebrafish obscurin DH-PH₅₈₈₄₋₆₂₁₇ domains towards RhoB, RhoC, Rac2, Rac3 and RhoG at 1.5 μM .

Black arrows indicate addition of GEF. Curves represent the mean of $n = 3-4$ technical replicates/experiment. See Figure 3.7 for positive controls.

Figure 3.14A shows the results of this screen for the obscurin SH3-DH fragment as the top 50 kinases with the highest activity ratio (top) as well as the raw values for phosphorylation and autophosphorylation (bottom; see Figure A3 for the all raw values of all kinases). Interestingly, we found multiple members of the calcium/calmodulin-dependent protein kinase family among the kinases with the highest activity ratio, including CaMK1d, CaMMK1, CaMK2b, CaMK2d, CaMKK2, and CaMK4. CaMK family members, especially CaMKII (CaMK2), have well-established and important functions in cardiac physiology and their substrates include PLN, RyRs, L-type calcium channels, and others (Maier and Bers 2007). Given obscurin's potential association with calcium signalling reviewed above, the identification of CaMKs as potential regulators of obscurin is plausible and interesting. Other promising candidates which have been identified in the screen are MST-family kinases MST1, MST2 and MST4. MST-kinases play important roles in the Hippo-pathway during development (Halder and Johnson 2011). In the heart, MST1 and MST2 have been reported to be involved in the regulation of cardiomyocyte proliferation, hypertrophy, fibrosis, and heart development (Heallen et al. 2011; Lee et al. 2015; Zi et al. 2014). Another kinase family of which more than one family member has been identified are HIPK kinases HIPK1 and HIPK2. Since HIPK family kinases appear to be mainly involved in transcriptional regulation and DNA damage response in the cell nucleus, we considered them less promising as regulators of obscurin function (Rinaldo et al. 2008). The kinase with the highest activity ratio in the screen is TBK1, which has been associated with functions in nucleic acid sensing, cancer and the immune system (Zhou et al. 2020).

To validate some of these hits, we selected the kinases with the three highest activity ratios for a confirmation screen at different substrate concentrations in triplicate performed by ProQinase. As shown in Figure 3.14B, all three kinases showed significant activity towards obscurin SH3-DH. However, the absolute phosphorylation by TBK1 appeared to very modest, whereas CaMK4 showed an untypical biphasic response in which higher substrate concentrations seem to inhibit CaMK4 activity. MST2, in contrast, showed strong and robust absolute phosphorylation that saturated at high concentrations. MST2 thus appears to be one of the most promising candidates for a physiological regulator of obscurin. Next, we decided to confirm the activity of MST2 and other CaMK family members towards obscurin with a different method and to identify the phosphorylation sites. Using recombinant MST2, CaMKId or CaMKII from commercial suppliers, we set up kinase reactions using the obscurin Rho GEF fragments SH3, SH3-DH and DH as substrates and visualised phosphorylation by phospho-protein specific ProQ diamond staining (Figure 3.14C). Interestingly, we found that the SH3-DH fragment can only be phosphorylated by MST2, not by CaMKId or CaMKII. Since neither the SH3 domain, nor DH domain alone can be phosphorylated by MST2, the phosphorylation site either lies in the absent interdomain region 5668-5680 in which Ser5669 is the only serine/threonine residue, or the kinase-substrate interaction requires multiple binding sites on different domains/regions of obscurin. While the DH fragment could not be phosphorylated by any of the tested kinases, the SH3 fragment could be phosphorylated by CaMKII. Interestingly, the SH3 domain could not be phosphorylated by CaMKII in the SH3-DH fragment, indicating that the phosphorylation site for CaMKII is sterically unavailable in this fragment. In summary, these experiments confirm that MST2 can phosphorylate obscurin SH3-DH. To our surprise, the SH3-DH fragment could not be phosphorylated by the tested CaMKs, although the SH3 domain alone could be phosphorylated by CaMKII.

The muscle activity dependent phosphorylation sites identified by Potts et al. 2017 were Ser5669 in the SH3-DH interdomain linker region and Thr5798 within the DH domain. To see whether these

sites are evolutionary conserved, we aligned the sequences from different species in the vicinity of these sites. While the phosphorylation motif of Ser5669 seems to be conserved in human, mouse and zebrafish but not in invertebrates, the Thr5798 site is only present in human and mouse, but not in zebrafish or invertebrates (Figure 3.15A). To further narrow down the potential phosphorylation site and the kinase-substrate interaction sites, we tested whether a longer DH domain fragment (residues 5667-5889), comprising the SH3-DH interdomain linker region, or the zebrafish DH-PH domain tandem could be phosphorylated (Figure 3.15B). We found that the longer DH fragment could indeed be phosphorylated, whereas the zebrafish DH-PH fragment could not. This suggests that the SH3-DH interdomain region is indeed necessary for the kinase-substrate interaction and that the MST2 phosphorylation site is unlikely to be Ser5669, as the basic residues at position -5, -4 and -2 which are typical for kinase motifs are not present. If the MST2 site is one of the sites identified by Potts et al., it is therefore likely Thr5798, in agreement with the observation that zebrafish DH-PH cannot be phosphorylated by MST2.

If the MST2 site is a physiological one, we reasoned that the phosphorylation will be reversed by phosphatases. We therefore tested whether PP1 and PP2A, two important phosphatases which are known to be present at the M-band and the SR, can reverse phosphorylation by MST2. As shown in Figure 3.15C, we found that phosphorylation by MST2 can indeed be reversed by PP1 and PP2A. Finally, we decided to directly identify the MST2 phosphorylation site by mass-spectrometry which confirmed that the MST2 phosphorylation site is most likely Thr5798 (Figure 3.15D).

In summary, we have demonstrated that MST2 can phosphorylate the obscurin DH domain at Thr5798 and requires the SH3-DH interdomain region to recognise obscurin as a substrate. Thr5798 is one of the muscle activity dependent sites identified by Potts et al. 2017 and phosphorylation at this site can be reversed by phosphatases relevant to cardiomyocyte biology. Aligning the homology model of the obscurin DH-PH tandem with the Dbs DH-PH/RhoA complex reveals that Thr5798 likely makes no direct contact to obscurin substrate GTPases but is positioned directly at the intersection of multiple alpha-helices (Figure 3.15E). Phosphorylation at this site could therefore plausibly induce significant conformational changes in the DH domain. MST2 is thus a highly promising candidate for physiologically relevant regulation of obscurin Rho GEF function in the context of muscle exercise (Figure 3.15F).

Next, we tested whether phosphorylated obscurin SH3-DH or DH₅₆₆₇₋₅₈₈₉ exhibits GEF activity towards RhoA, RhoQ, Cdc42 or Rac1. As shown in Figure 3.16, neither of the phosphorylated GEF fragments showed any nucleotide exchange activity towards the tested GTPases, indicating that phosphorylation by MST2 does not activate obscurin's GEF activity.

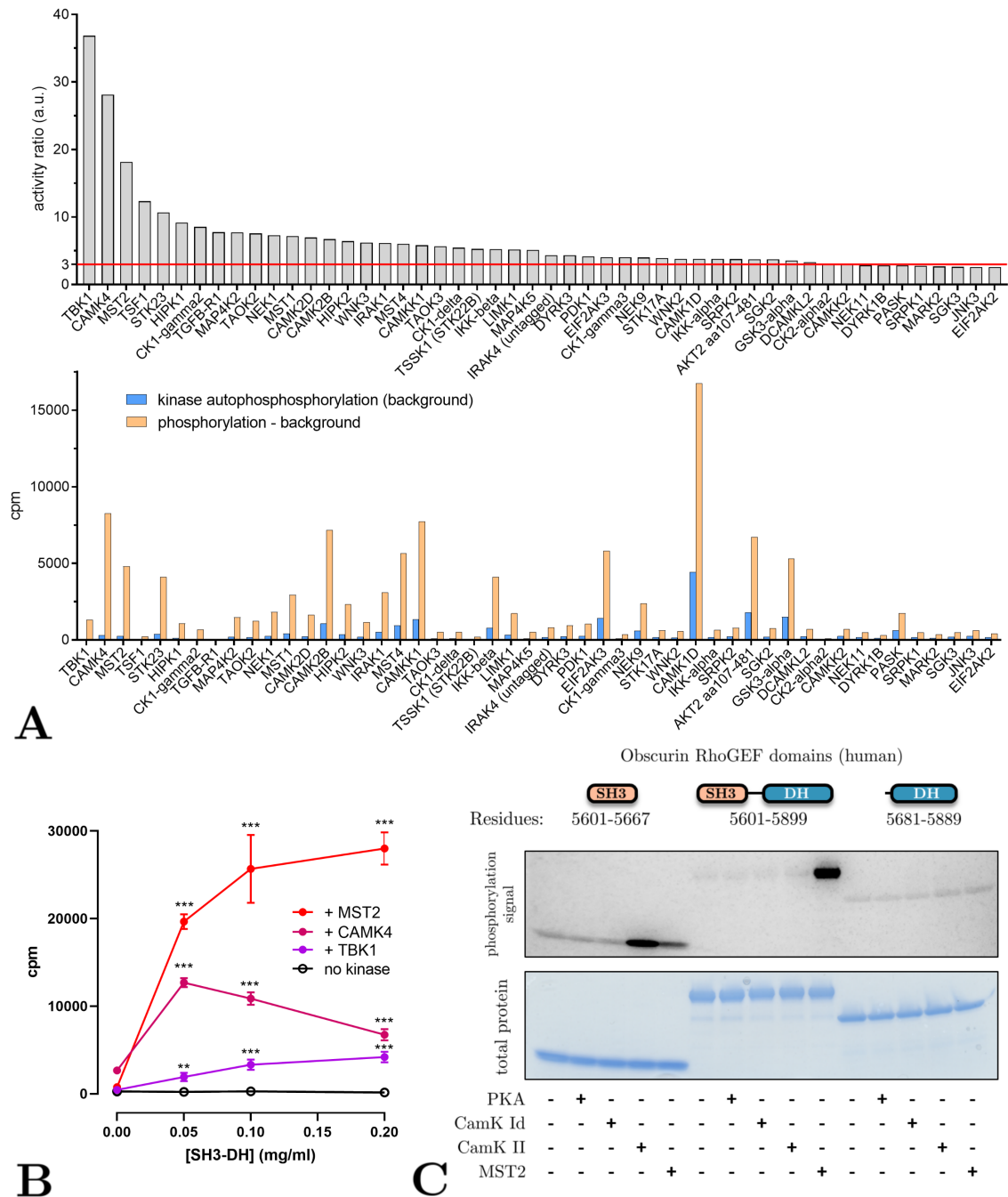


Figure 3.14. Identification of kinases that can phosphorylate obscurin Rho GEF domains in a commercial Ser/Thr-kinase screen.

A, top: 50 kinases with the highest activity ratio (substrate phosphorylation/kinase autophosphorylation) in the obscurin SH3-DH phosphorylation screen. Bottom: absolute values for substrate phosphorylation and autophosphorylation of the top 50 kinases. **B**, confirmation assay for the top 3 kinases validates that MST2, CaMK4 and TBK1 can phosphorylate obscurin SH3-DH. **C**, in-house validation of selected kinases by ProQ™ diamond staining shows that only MST2 can phosphorylate obscurin SH3-DH. CaMKII can phosphorylate SH3 alone but not the SH3-DH fragment. PKA was used as a negative control.

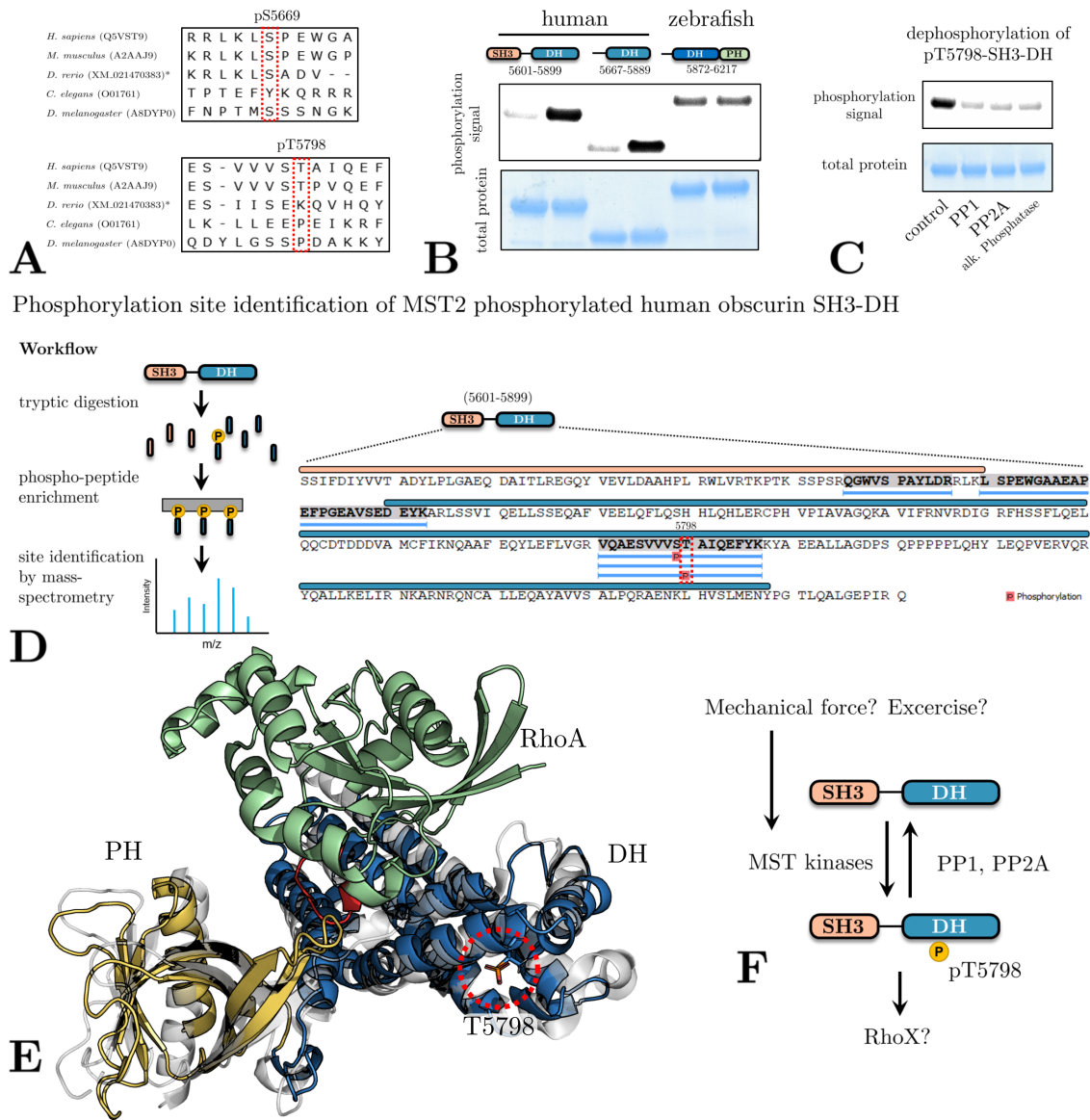


Figure 3.15. Characterisation of MST2 phosphorylation sites.

A, Evolutionary conservation of muscle exercise responsive phosphorylation sites in the obscurin Rho GEF domains identified by Potts et al. 2017. **B**, MST2 dependent phosphorylation of a DH fragment with longer N-terminus (linker region) and the zebrafish DH-PH tandem. **C**, dephosphorylation of MST2-phosphorylated obscurin DH-PH by PP1 and PP2A. Alkaline phosphatase was used as a positive control. **D**, Identification of the MST2-phosphorylation site by mass-spectrometry showed that obscurin is phosphorylated at Thr5798 in the DH domain. **E**, Homology model of obscurin DH-PH aligned to the RhoA/DH-PH complex of Dbs (PDB-ID: 1LB1) shows that Thr5798 is unlikely to participate in direct contacts with the GTPase but is located at the intersection of multiple alpha-helices so that phosphorylation potentially induces conformational changes. **F**, Proposed scheme of how MST-kinases and phosphatases might regulate obscurin Rho GEF activity.

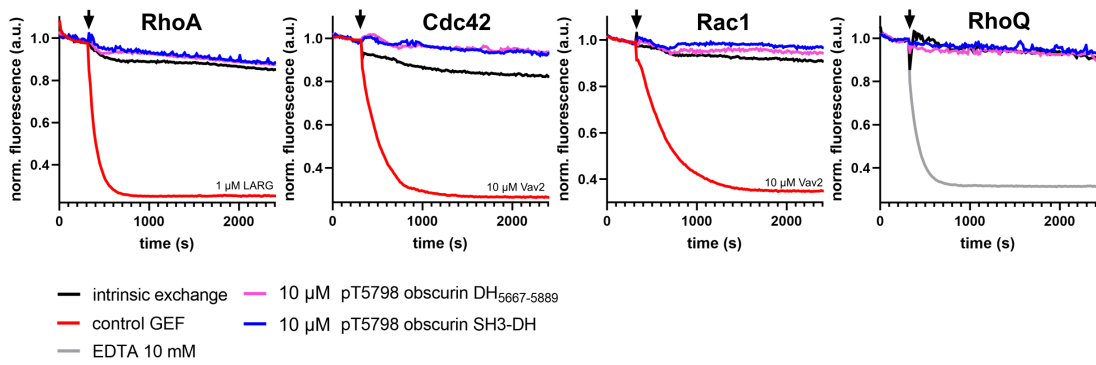


Figure 3.16. Nucleotide exchange of obscurin pThr5798 SH3-DH and pThr5798 DH₅₆₆₇₋₅₈₈₉ towards RhoA, Cdc42, Rac1 or RhoQ at 1.5 μ M [GTPase].

Red and grey curves show strong acceleration of exchange after addition of EDTA or the control GEF. No GEF activity was observed for the phosphorylated obscurin Rho GEF fragments, shown in pink and blue, respectively. Black arrows indicate addition of GEF/EDTA. Curves represent the mean of $n = 2-4$ replicates/experiment.

3.1.9 Discussion

Despite comprehensive testing of multiple obscurin Rho GEF fragments containing different domain combinations (SH3-DH, DH, DH-PH) against almost all potential substrate Rho GTPases (except RhoJ, which was not stable in our hands), we were not able to detect any catalytic activity. Furthermore, we were able to identify kinases that can phosphorylate the obscurin Rho GEF domains at physiologically relevant sites, but even these post-translational modifications were not able to stimulate the catalytic activity of the Rho GEF fragments. Our results are surprising and contradict the previously reported activity of obscurin Rho GEF activity towards RhoA and RhoQ in cell biological experiments. What might account for this discrepancy?

Let us first consider more technical aspects. The obscurin Rho GEF protein fragments were sufficiently pure, stable and folded at least for the time scale of our experiments, so the lack of activity is unlikely a result of insufficient protein quality. The tested substrate GTPases, too, were sufficiently soluble, stable, able to bind nucleotides and nucleotide exchange could be accelerated by addition of other GEFs or EDTA. Another technical aspect to consider is that chimeric and zebrafish Rho GEF fragments have been purified by a single-step purification protocol, and buffer exchange has been performed on desalting columns. It is thus possible that the GEF samples contained micromolar concentrations of imidazole from the elution buffer which may interfere with catalytic activity. However, even high concentrations of imidazole did not interfere with the catalytic activity of Larg, another DH-domain GEF (appendix Figure A4), making this explanation less plausible. Moreover, although our experiments were comprehensive, they were not exhaustive. It is thus possible that we may have missed just the right Rho GEF fragment/GTPase pairs for which nucleotide exchange does show an increased rate. The phosphorylated Rho GEF fragments, for example, have only been tested against RhoA, Cdc42, Rac1 and RhoQ. However, a systematic characterisation of 14 DH-domain GEFs from different subfamilies has shown that all tested GEFs showed significant activity against at least towards one of the “big three” Rho GTPases RhoA, Cdc42 or Rac1, making the explanation of having missed just the right pairs less likely (Jaiswal et al. 2013).

A biologically perhaps slightly more plausible explanation is that the PH domain of human obscurin is strictly necessary and that the zebrafish PH domain is not a valid substitute. However, this would be somewhat surprising given the mechanistic understanding of trio-subfamily GEFs and the fact that all residues with known catalytically important functions are present in the zebrafish PH domain of obscurin (cf. [Figure 3.8E](#)). Since the zebrafish homologues of RhoA are >90% identical to human RhoA, the lack of zebrafish obscurin DH-PH towards human RhoA would also be unexpected.

However, it is furthermore possible that obscurin Rho GEF activity may require an even larger domain combination such as an SH3-DH-PH fragment. Another possibility certainly is that we have not identified the right phosphorylation site and kinase to activate obscurin activity. Ser5669 between the SH3 and DH domain, for instance, shows higher cross-species conservation than Thr5798 and was also identified by Potts et al. [2017](#) to be phosphorylated in the context of muscle exercise. Ser5669, too, is thus a physiologically promising candidate for activating obscurin Rho GEF activity. It is also conceivable that obscurin Rho GEF activity not only requires phosphorylation, but maybe the effect of direct mechanical force. This, however, is difficult to test with currently available *in vitro* methods.

However, even the DH domain of trio-subfamily GEFs which strongly rely on the PH domain for catalytic activity show a significant level of activity at high concentrations without the PH domain or additional phosphorylation (Rossman and Campbell [2000](#)). Given that obscurin is the only trio-subfamily GEF so far which has been demonstrated not to be active *in vitro* even at high enzyme concentrations, neither of these explanations considered so far seems particularly attractive. Interestingly, a closer examination of the DH-PH sequence of obscurin in comparison to the other trio-subfamily GEFs reveals that obscurin has the least average sequence identity to the other GEFs and is the only one not clustering with other GEFs in the heat map representation of sequence identity in the trio-subfamily of Rho GEFs ([Figure 3.17A](#)). This suggests that obscurin might indeed be a rather untypical GEF in the evolution of the trio-subfamily. In a systematic comparison of the crystal structures of 13 DH-domains in complex with their different substrate GTPases, Jaiswal et al. found that the DH domain features 30 positions that are involved in constitutive and non-selective contacts with all GTPases, regardless of their subfamily (Rho, Rac or Cdc42) (Jaiswal et al. [2011](#)). Given obscurin's low sequence identity to other trio-subfamily GEFs, we analysed these residues within the trio-subfamily to see whether the obscurin sequence deviates at these functionally important residues from other members of this subfamily. To identify these residues, we also included the Larg DH-domain which was used as a reference by (Jaiswal et al. [2011](#)). Interestingly, the obscurin DH domain deviates from other trio-subfamily members at 7/30 of these functionally important amino acid positions ([Figure 3.17B](#)). Potentially, these differences might explain the lack of GEF activity for obscurin.

Taken together, our data demonstrate that obscurin is a highly atypical Rho GEF, whose nucleotide exchange mechanism and regulation are likely markedly different from other Rho GEFs. Clearly, more research is needed to identify the function, regulation and interaction partners of obscurin's Rho GEF domains. However, given that our extensive screening revealed no *in vitro* activity so far, it seems prudent to approach these questions with different methods.

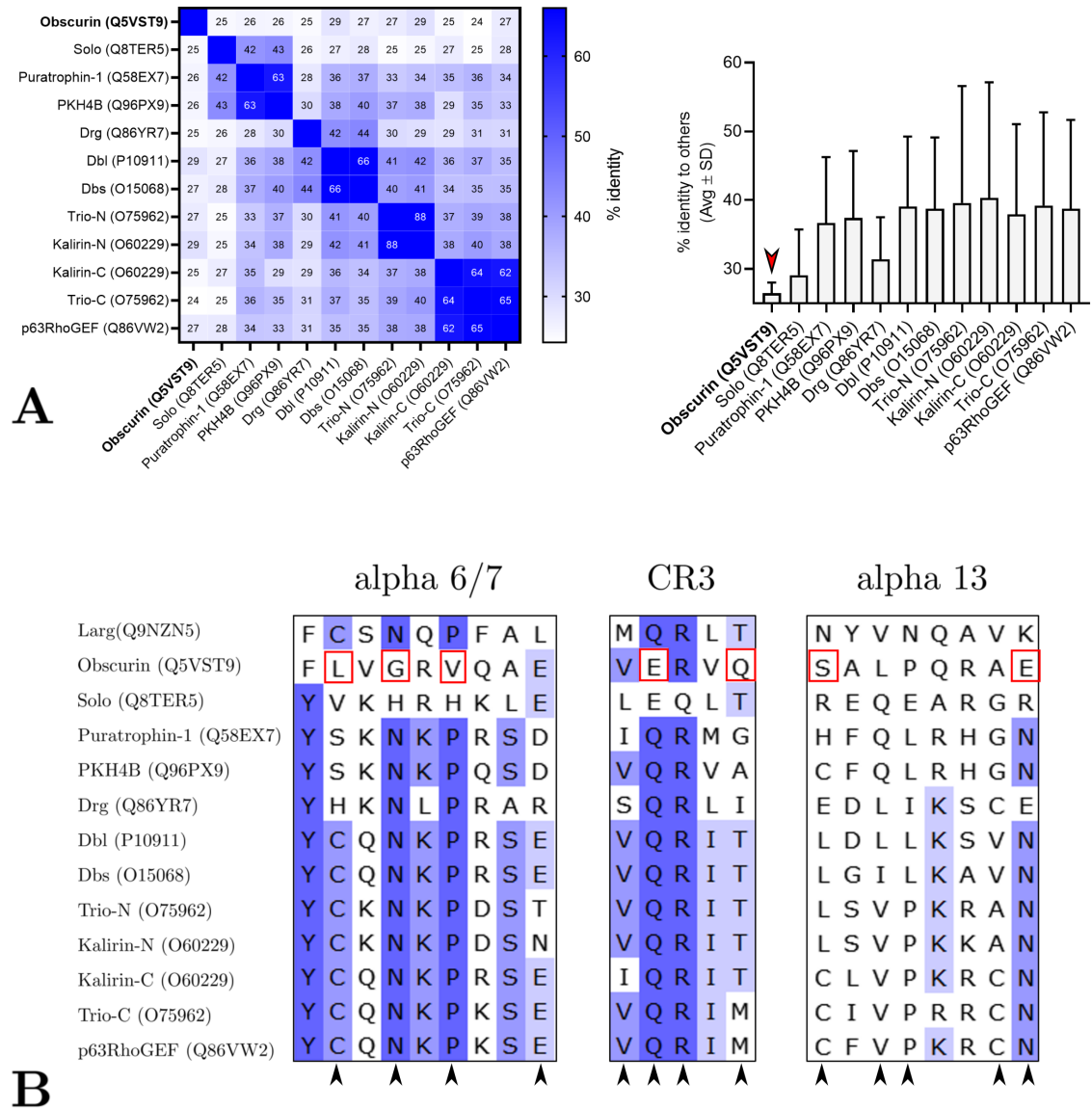


Figure 3.17. Comparative sequence analysis of the obscurin DH-PH domains and those of other trio-subfamily GEFs.

A, comparison of DH-PH sequence identity of the trio-subfamily of Rho GEFs shows that obscurin has the lowest average sequence identity in this subfamily and does not cluster with other family members. **B**, Jaiswal et al. 2011 identified 30 amino acid positions in 13 DH/GTPase complex structures that interact with members of all RhoGT-Pase subfamilies (Rho, Rac, Cdc42), some of which are highlighted by black arrowheads. At 7 of these functionally important positions, the obscurin sequence deviates notably from other trio-subfamily members (highlighted by red rectangles)

Chapter 4

When is an obscurin variant pathogenic?

Several mutations in the obscurin gene have been associated with cardiovascular or musculoskeletal disease. Due to limited mechanistic and quantitative characterisation of the impact of these mutations, it is currently unclear whether these mutations are really disease causing. This applies in particular to the R4344Q mutation which affects about 1 in 7 African Americans.

This chapter addresses this question and consists of the research paper “When is an obscurin variant pathogenic? The impact of Arg4344Gln and Arg4444Trp variants on protein–protein interactions and protein stability” published in the journal *Human Molecular Genetics*. The supplementary material for this study can be found in [chapter A5.2](#).

The idea for the project originated from a discussion in 2019 between Dr Atsushi Fukuzawa, Prof Stephan Lange and myself in the pub “The Miller” close to Guy’s Campus during which we lamented our often frustrating experiences of working on obscurin. Since I had plenty of phospholamban peptide stored in the lab-freezer, Dr Atsushi Fukuzawa and I decided to test whether we can confirm a previously published, but not further characterised interaction between obscurin and phospholamban, speculating that a better mechanistic understanding of this interaction could be interesting in the context of the postulated pathogenicity of the R4344Q mutation. Together with Prof Mathias Gautel, we conceived a project to test and quantify reported obscurin interactions in order to characterise the impact of previously reported genetic mutations. While I wrote the manuscript, conducted the obscurin/PLN pull-down assays and microscale-thermophoresis experiments, Dr Atsushi Fukuzawa performed the cell biological experiments and obscurin/Novex-3 and obscurin/Titin pull-down assays. Sarah Grover and Dr Martin Rees performed the differential scanning fluorimetry experiments.

GENERAL ARTICLE

When is an obscurin variant pathogenic? The impact of Arg4344Gln and Arg4444Trp variants on protein–protein interactions and protein stability

Atsushi Fukuzawa[†], Daniel Koch^{†*}, Sarah Grover, Martin Rees and Mathias Gautel^{1*}

Randall Centre for Cell & Molecular Biophysics, King's College London, 18–20 Newcomen Street, SE1 1UL, UK

[†]To whom correspondence should be addressed at: Randall Centre for Cell & Molecular Biophysics, New Hunt's House, 18–20 Newcomen Street, SE1 1UL, London. Tel: +44 2078486438; Email: daniel.koch@kcl.ac.uk; Randall Centre for Cell & Molecular Biophysics, New Hunt's House, 18–20 Newcomen Street, SE1 1UL, London. Tel: +44 2078486709; Email: mathias.gautel@kcl.ac.uk

Abstract

Obscurin is a giant muscle protein that connects the sarcomere with the sarcoplasmic reticulum, and has poorly understood structural and signalling functions. Increasingly, obscurin variants are implicated in the pathophysiology of cardiovascular diseases. The Arg4344Gln variant (R4344Q) in obscurin domain Ig58, initially discovered in a patient with hypertrophic cardiomyopathy, has been reported to reduce binding to titin domains Z8–Z9, impairing obscurin's Z-disc localization. An R4344Q knock-in mouse developed a cardiomyopathy-like phenotype with abnormal Ca²⁺-handling and arrhythmias, which were attributed to an enhanced affinity of a putative interaction between obscurin Ig58 and phospholamban (PLN) due to the R4344Q variant. However, the R4344Q variant is found in 15% of African Americans, arguing against its pathogenicity. To resolve this apparent paradox, we quantified the influence of the R4344Q variant (alongside another potentially pathogenic variant: Arg4444Trp (R4444W)) on binding to titin Z8–Z9, novex-3 and PLN using pull-down assays and microscale thermophoresis and characterized the influence on domain stability using differential scanning fluorimetry. We found no changes in titin binding and thermostability for both variants and modestly increased affinities of PLN for R4344Q and R4444W. While we could not confirm the novex-3/obscurin interaction, the PLN/obscurin interaction relies on the transmembrane region of PLN and is not reproducible in mammalian cells, suggesting it is an *in vitro* artefact. Without clear clinical evidence for disease involvement, we advise against classifying these obscurin variants as pathogenic.

Introduction

Obscurin is a giant muscle protein that connects the contractile unit of muscle cells, the sarcomere, with their intracellular calcium storage, the sarcoplasmic reticulum (SR) (1,2). Like many other large sarcomeric proteins, it exists as different splicing isoforms (3,4). The two largest isoforms, obscurin A

and obscurin B, are mainly composed of immunoglobulin-like (Ig) domains, but feature several signalling domains in their C-terminal third: a calmodulin binding IQ-motif, an SH3 domain and a DH/PH domain tandem typical for Dbl-family Rho-GEFs (Fig. 1A). Obscurin B additionally features two kinase domains. Obscurin A, in contrast, has putatively unstructured regions at the C-terminus that can bind to small ankyrins in the SR

[†] Authors contributed equally and are listed alphabetically.

Received: October 26, 2020. Revised: December 17, 2020. Accepted: January 4, 2021

© The Author(s) 2021. Published by Oxford University Press.

This is an Open Access article distributed under the terms of the Creative Commons Attribution License (<http://creativecommons.org/licenses/by/4.0/>), which permits unrestricted reuse, distribution, and reproduction in any medium, provided the original work is properly cited.

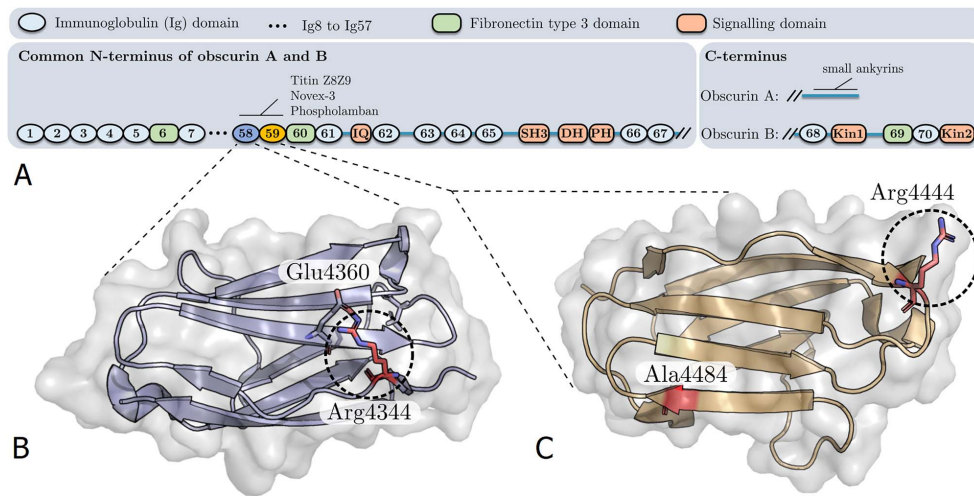


Figure 1. (A) Domain composition of large obscurin isoforms A and B. Position of residues affected by mutation are shown in the Ig58 (B) (PDB-ID: 4RSV) and Ig59 (C) (PDB-ID: 5TZM) structures of obscurin.

membrane, thereby connecting the M-band of the sarcomere with the SR (2,3,5,6). At least two smaller isoforms exist, one of which features the SH3-DH/PH triplet, the other of which contains the kinase domains (3,4). The multitude of domains and interactions (e.g. with titin Z8-Z9 and small ankyrins) (1,5,6) suggests that obscurin has both structural and signalling functions, which are only beginning to emerge. The picture is further complicated by developmentally specific localization patterns and a multitude of post-translational modifications (1,7,8).

Despite our limited understanding of the protein, genetic obscurin variants are increasingly implicated into the pathophysiology of muscular and cardiovascular diseases (9–13). The first variant suggested to be involved in the pathophysiology of cardiomyopathy is the R4344Q mutant in obscurin Ig58. Discovered in a patient with hypertrophic cardiomyopathy by Arimura *et al.*, their data suggested that the R4344Q mutation impairs binding to Titin Z8-Z9 and reduces incorporation of transfected obscurin Ig58-Ig59 into the sarcomeric Z-disc of neonatal rat cardiomyocytes (9). More recently, a homozygous R4344Q knock-in mouse created by the Kontrogianni-Konstantopoulou group developed cardiac arrhythmias under sedentary conditions and a DCM-like phenotype upon pressure overload, which the authors attributed to an increase in the affinity, as judged by co-immunoprecipitation, for a newly identified interaction between obscurin and phospholamban, a small inhibitory peptide of the SERCA pump in the SR membrane (14). A different obscurin mutation in the neighbouring Ig59 domain, R4444W, has also been described to impair the binding to Titin Z8-Z9 and is suggested to increase the penetrance of distal muscular dystrophy when co-inherited with a Filamin-C frameshift mutation (13). Of note, this co-inheritance of two alleles on two different chromosomes would have had to occur over four generations to explain the phenotype in the described family (13).

Crystal structures of obscurin Ig58 and Ig59 are available from the protein data bank. R4344 in Ig58 is surface exposed

and forms a salt bridge with Glu4360 (Fig. 1B). Mutation of arginine to glutamine would result in a loss of the salt bridge, but would not be predicted to affect the folding of the domain. R4444 in Ig59 is also surface exposed, and the side chain does not mediate polar contacts with other residues (Fig. 1C). Mutation to the large, hydrophobic residue tryptophan is not predicted to sterically hinder nearby residues or affect domain folding, but tryptophan is more typically found in the core of proteins.

Curiously, and at odds with the findings of Arimura *et al.* and Hu *et al.*, the R4344Q variant is found in up to 15% of African Americans and has a high overall mean allele frequency of 0.01165, which prompted several researchers to question the pathogenicity of this variant (10,15). To resolve the apparent paradox between the previous *in vitro* findings and the population genetics, we characterized the effect of the R4344Q variant on protein–protein interactions and protein domain stability, using quantitative biochemical and biophysical approaches. We also included the R4444W variant in our study as a comparison, since it was reported to affect some of the same interactions as R4344Q and to be potentially pathogenic. While our data contradict the findings by Arimura *et al.* and Hu *et al.*, it supports the argument that the R4344Q variant is too common to be pathogenic. Our findings should thus help to refine diagnostic fidelity in patients carrying obscurin variants.

Results

Effect of the R4344Q variant on protein–protein interactions

To study and quantify any potential effect of the R4344Q variant on protein–protein interactions, we used microscale thermophoresis (MST), which measures how a binding partner influences the migration of a labelled protein along a temperature gradient (17). We found no significant difference in the affinity

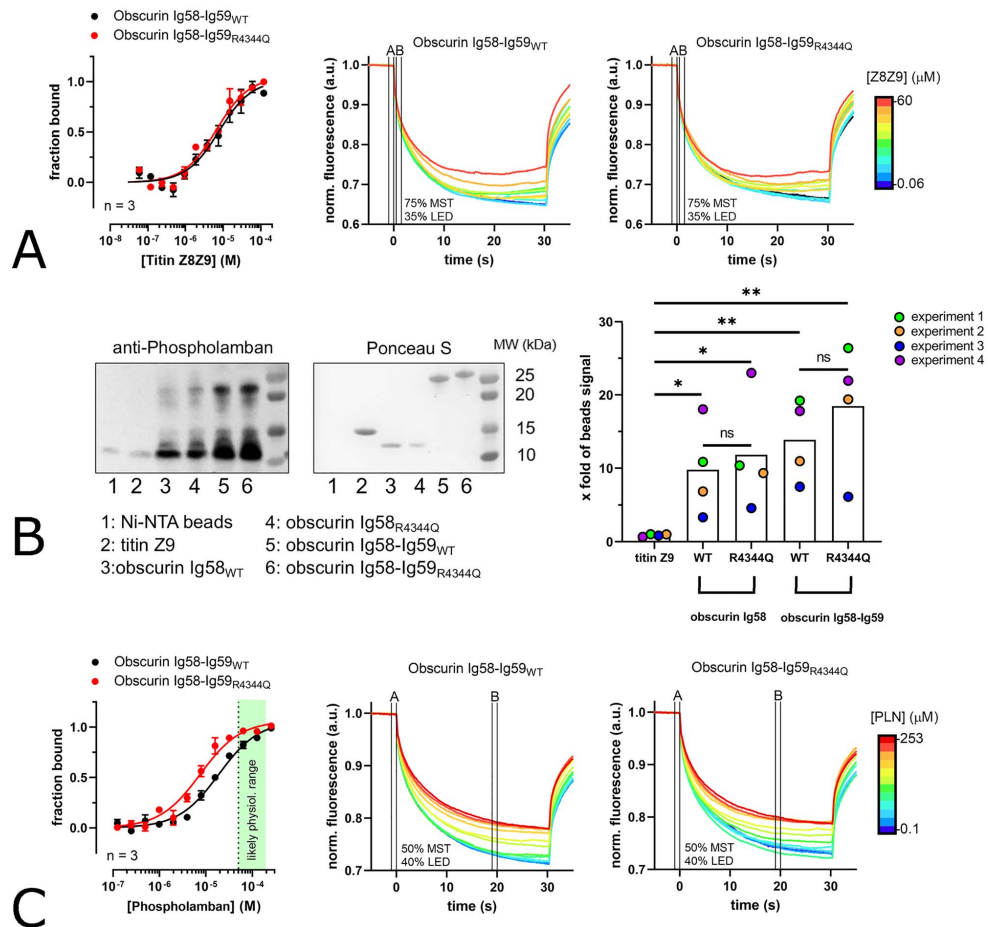


Figure 2. Effect of the obscurin R4344Q variant on protein-protein interactions. (A) MST shows no significant difference between wild-type and R4344Q variant for titin Z8-Z9 binding. Binding curves based on signal at Lane B (MST-laser on) divided by signal at Lane A (MST-laser off) in the MST traces. (B,C) Pull-down and MST data showing binding of human full-length phospholamban to obscurin Ig58 and Ig58-Ig59. MST data show statistically significant but moderate affinity increase for the R4344Q variant.

for titin Z8-Z9 between wild-type obscurin Ig58-Ig59 ($K_d = 7.8 \pm 1.7 \mu\text{M}$) and Ig58-Ig59_{R4344Q} ($K_d = 6.6 \pm 1.2 \mu\text{M}$) (Fig. 2A). We also used isothermal titration calorimetry to verify the affinities based on reaction heat and found similar K_d values (data not shown).

Since obscurin Ig58-Ig59 has been reported to interact with novex-3, a small titin isoform, we also sought to characterize whether the R4344Q variant might influence the affinity towards novex-3 (18). However, we were not able to detect an interaction between obscurin Ig58-Ig59 and the obscurin binding region of novex-3 (ObB, residues 4991 to 5187) by MST (Supplementary Material, Fig. S1) or pull-down assays using novex-3 ObB expressed in HEK293A cells (Supplementary Material, Fig. S2). Bang et al. identified this interaction in the yeast two hybrid

system and then confirmed it in an *in vitro*-transcription/translation pull-down assay, using a cell-free eukaryotic expression system based on reticulocyte lysate for producing novex-3 ObB. Although the ObB sequence used by Bang and colleagues shows only minor differences to our sequence (Supplementary Material, Fig. S3), we cannot rule out that these differences, the different cell types used for producing the ObB (reticulocytes vs. *E. coli* and HEK293A) or other factors play a role for this interaction.

Next, we sought to characterize the binding between obscurin Ig58 or Ig58-Ig59 and phospholamban. First, we tried to replicate the findings by Hu et al. by performing similar pull-down assays with recombinant/synthetic proteins. As shown in Figure 2B, we could confirm an interaction between obscurin

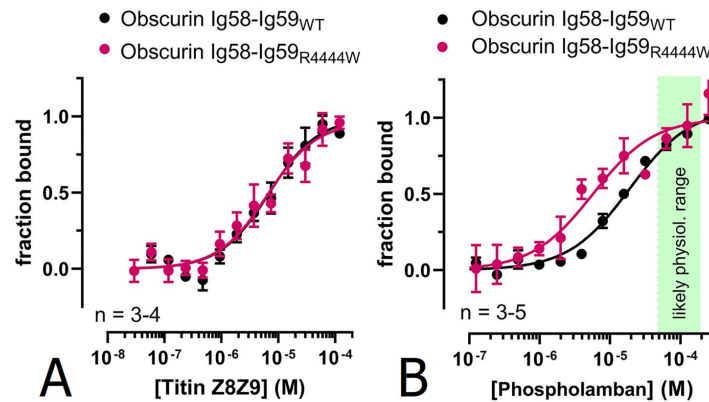


Figure 3. Effect of the obscurin R4444W variant on protein-protein interactions. (A) No effect can be observed on the interaction with titin Z8-Z9 as measured by MST. (B) MST analysis of the interaction between obscurin Ig58-Ig59_{R4444W} and phospholamban reveals an increase in affinity.

Ig58 or Ig58-Ig59 and phospholamban *in vitro*. In contrast to Hu *et al.*, however, we found no significant increase in binding for the R4344Q variant. We also found that Ig58-Ig59 interacts both with monomeric (low MW bands) and pentameric phospholamban (higher MW bands). Quantifying the binding affinities using MST, we found a statistically significant but modest difference amounting to a 2.5-fold decreased K_d for the R4344Q variant (Fig. 2C; K_d wild-type = $18.9 \pm 2 \mu\text{M}$, K_d R4344Q = $7.5 \pm 1 \mu\text{M}$). In agreement with our pull-down data, the binding curve is well described by a single binding-site model, indicating that all phospholamban protomers (i.e. also those in a pentamer) are available for binding obscurin.

Effect of the R4444W variant on protein-protein interactions

The R4444W variant of the obscurin Ig59 domain is reported to weaken the interaction between obscurin Ig58-Ig59 and titin Z8-Z9 (13). We therefore tested the influence of the R4444W variant on the interaction with titin Z8-Z9 and phospholamban. As shown in Figure 3A, we detected no difference in titin Z8-Z9 binding compared to the wild-type protein and Ig58-Ig59_{R4344Q} ($K_d = 6.4 \pm 1.6 \mu\text{M}$). Surprisingly, however, we found that the R4444W variant, too, has a higher affinity for phospholamban ($K_d = 5.7 \pm 1.2 \mu\text{M}$) than wild-type obscurin (Fig. 3B).

Based on structural modelling and computational docking, Hu *et al.* proposed that the R4344Q replacement stabilizes putative electrostatic interactions between obscurin Ig58 and the cytoplasmic region of phospholamban (14). The replacement of a hydrophilic and charged arginine with a hydrophobic tryptophan in the R4444W variant, however, seems inconsistent with such an interaction mode. Therefore, we characterized this interaction in more detail and tested if obscurin Ig58-Ig59 binds phospholamban's cytoplasmic or transmembrane region in isolation. Interestingly, we found that obscurin binds to the transmembrane region (residues 23–52), albeit with a ≈ 3 -fold weaker affinity ($K_d = 58.5 \pm 1.7 \mu\text{M}$) compared to full-length phospholamban. In contrast, we detected no interaction with the cytoplasmic region (residues 1–22) (Fig. 4A). The transmembrane region of phospholamban might not be accessible for obscurin

binding *in vivo* when inserted in membrane. If it is, however, we reasoned that phospholamban might be able to recruit obscurin to membrane structures. To test this hypothesis, we co-transfected HEK293A cells with phospholamban and GFP-tagged obscurin Ig58-Ig59. Confocal microscopy showed that phospholamban is exclusively targeted to membrane structures, most likely ER and/or ER-derived vesicles, whereas obscurin Ig58-Ig59 exhibits unspecific and diffuse localization in both cytoplasm and nuclei (Fig. 4B, panel B1) without colocalizing with phospholamban-positive vesicles. GFP alone and also GFP-tagged titin M2-M3, which we used as a control for two tandem Ig domains, showed very similar, diffuse localizations as obscurin Ig58-Ig59 (Fig. 4B, panels B2 and B3). These results suggest that while the transmembrane region of phospholamban is capable of obscurin binding *in vitro*, when phospholamban is integrated into membrane structures of living cells, this interaction is abolished most likely because the transmembrane region is not accessible to obscurin.

Effect of the R4344Q and the R4444W variant on thermostability

The destabilization of protein domain folding can play a major causative role in the pathogenesis of cardiovascular and other diseases (19,20). Pathogenic destabilizing mutants in titin Ig-domains, for example, typically lead to differences in melting temperatures of $>> 10^\circ\text{C}$ or result in insoluble protein expression (21,22). We therefore probed the influence of the R4344Q and R4444W variants on thermostability using differential scanning fluorimetry (DSF). Both the wild-type and variant domains were solubly expressed, and as shown in Figure 5, neither the R4344Q nor R4444W variant lead to a biologically relevant decrease of the protein's melting temperature when compared to the wild-type protein. Thus, neither variant has a destabilizing effect on domain structure.

Characterization of an R4344Q, A4484T double variant

Although the characterized variants are likely benign in isolation (see discussion), it is interesting to note that in the context of

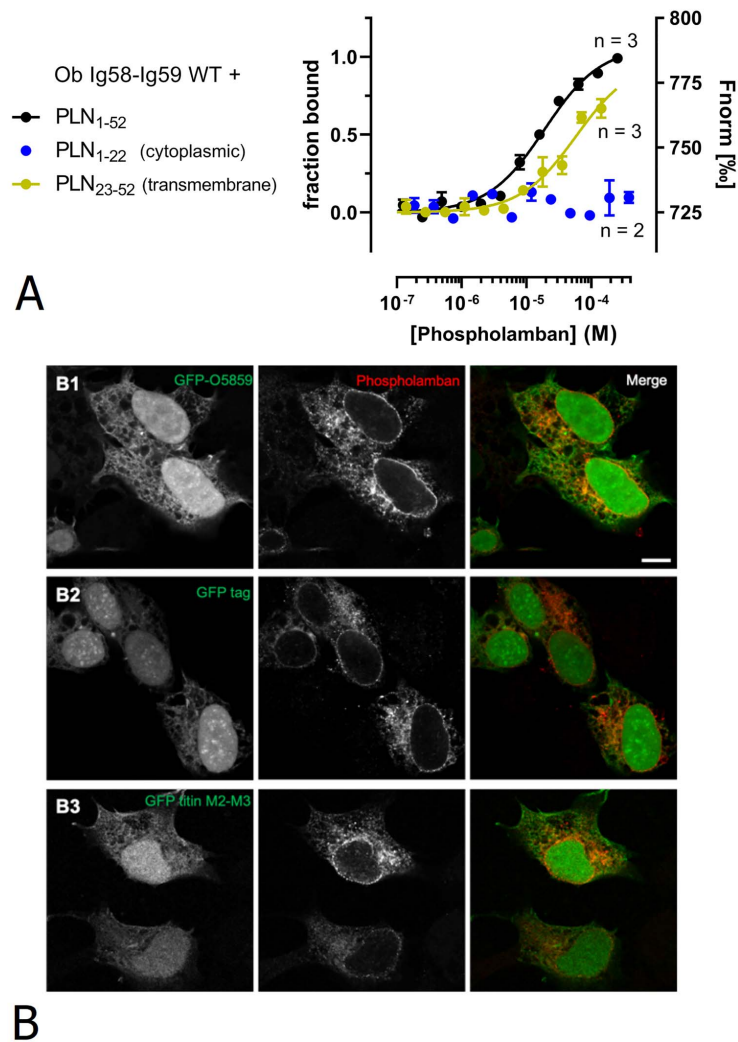


Figure 4. Characterization of the interaction between obscurin and phospholamban. (A) MST analysis using full-length phospholamban, cytoplasmic and transmembrane region. Data for the cytoplasmic region are displayed as normalized fluorescence (F_{norm}) due to absence of binding. (B) Obscurin Ig58-59 did not show significant co-localization with phospholamban. HEK293A cells were co-transfected with phospholamban and B1) GFP-obscurin Ig58-Ig59, B2) GFP-empty or B3) GFP-titin M2-M3. Scale bar: 10 μ m.

their discovery, both the R4344Q and the R4444W variant co-segregated with additional variants (9,13). This raises the possibility that the disease phenotype of the patients, in whom these variants were discovered, is the cumulative effect of multiple variants. For instance, the patient in whom the R4344Q variant was discovered was also a carrier of the A4484T variant on Ig59 in cis (Fig. 6A). Although Arimura *et al.* found no effect of the A4484T variant (9), we decided to test the influence of an R4344Q, A4484T double variant on the interaction with titin Z8-Z9 and on thermostability.

In agreement with Arimura *et al.*, we found that the double variant does not diminish the affinity for binding to titin Z8-Z9 (Fig. 6B). However, we found that the A4484T mutation alters the way how the titin Z8-Z9 ligand changes the MST signal: instead of increased normalized fluorescence upon ligand binding, as observed for obscurin Ig58-Ig59_{WT}, R4344Q and R4444W, the double variant showed a decrease in fluorescence upon titin Z8-Z9 binding (Supplementary Material, Fig. S4A). Since the temperature jump signal that we used for characterizing this interaction is highly dependent on the chemical environment

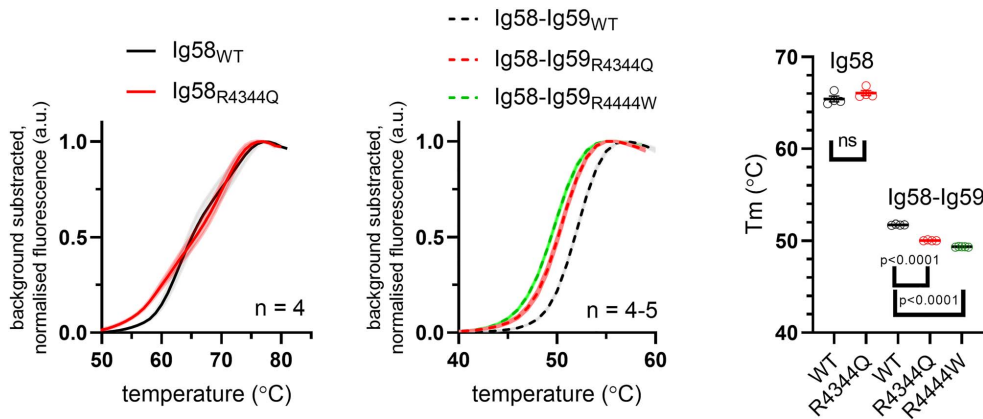


Figure 5. Effect of the obscurin R4344Q and R4444W variants on domain stability. Differential scanning fluorimetry for increasing temperatures shows no biologically relevant increase in protein domain unfolding for either variant when compared to the wild-type protein. Melting temperatures were determined by fitting melting curves to the Boltzmann equation.

of the fluorophore (17), this could either indicate that the 4484 position lies in the vicinity of the labelling site, or that the A4484T substitution locally alters the conformation of the Ig58-Ig59 tandem without impairing the titin interaction. Moreover, we observed a moderate but consistent tendency of the double variant to form aggregates during the MST-assay (Supplementary Material, Fig. S4B). Next, we characterized the thermostability of the A4484T variant and the R4344Q, A4484T double variant. We found that the A4484T variant decreases the melting temperature by 2.7°C, resulting in a cumulatively 5°C lower melting temperature for the R4344Q, A4484T double variant compared to the wild-type protein (Fig. 6C). Although the observed *in vitro* differences are statistically significant, the magnitude of the effect remains far lower than observed in known disease-causing destabilizing mutations (21,22). Taken together, our data suggest that the R4344Q, A4484T double variant is unlikely to be pathogenic.

Discussion

The loss or change of affinity of protein-protein interactions and the destabilization of protein domain folding belong to the major molecular mechanisms linking pathogenic genetic variants to disease phenotypes. In this study, we focused on obscurin domains Ig58-Ig59, which potentially bind to multiple proteins including titin Z8-Z9, phospholamban and novex-3 and for which pathogenic mutations were reported previously.

The R4344Q variant

Taken together, our data suggest that the only influence of the R4344Q variant is a 2.5-fold decreased K_d for the interaction with phospholamban *in vitro*. Interestingly, our data further suggest that this interaction relies primarily on the transmembrane region of phospholamban and that it does not occur in co-transfected mammalian cells. Our findings thus contest the physiological plausibility of this interaction and indicate that it is likely an *in vitro* artefact, as the transmembrane region will not be solvent accessible to a cytoplasmic Ig-domain. Consistent with an unspecific hydrophobic interaction, both obscurin variants substitute a hydrophilic arginine with a less hydrophilic

residue. Even if one would assume that the interaction is physiological, the question arises whether a 2.5-fold decreased K_d would be functionally relevant. At physiological phospholamban concentrations of >50 μM (23), the difference in affinity would result in at most 15% higher fractional saturation of obscurin binding sites with phospholamban (Fig. 2C, green shaded area). Since most obscurin binding sites would be already occupied by phospholamban at such concentrations, it seems implausible that a <15% increase would significantly impair whatever the function of this interaction would be. This is in excellent agreement with the genetic prevalence of this variant. Although Hu *et al.* proposed that this variant might contribute to the higher risk for cardiovascular disease among African Americans, prevailing socio-economic factors and other health risks among African Americans render a genetic ‘*obscurin ex machina*’ an unnecessary explanation (14,24). Comparing the age structure of R4344Q carriers in the gnomAD database to the overall population shows that heterozygous carriers do not die earlier than the rest of the population and while the number of homozygous carriers in the database is too low to draw definite conclusions, the mere fact that it contains dozens of homozygous carriers, many of which live well beyond their sixth decade, argues against any significant pathogenicity (Fig. 7). Why then, on the other hand, do R4344Q knock-in mice develop cardiac arrhythmias and a DCM phenotype upon pressure overload (14)?

Let us assume, for the sake of the argument, that the interaction between phospholamban and obscurin would be a physiological one. An interesting clue to this puzzle then is the observation that there are several quantitative differences between murine and human calcium handling. Firstly, mice seem to have slightly lower phospholamban concentrations than larger species (25–27), thus the difference in fractional saturation of obscurin binding sites could be bigger for the R4344Q variant in mice. Secondly, the SERCA pump, the main regulatory target of phospholamban, is responsible for 70% of calcium removal in human cardiomyocytes, but for >90% of calcium removal in cardiomyocytes of small rodents such as mice (23). Combined with a 10-fold higher resting heart rate, any detrimental effects of the R4344Q variant could be much more pronounced in

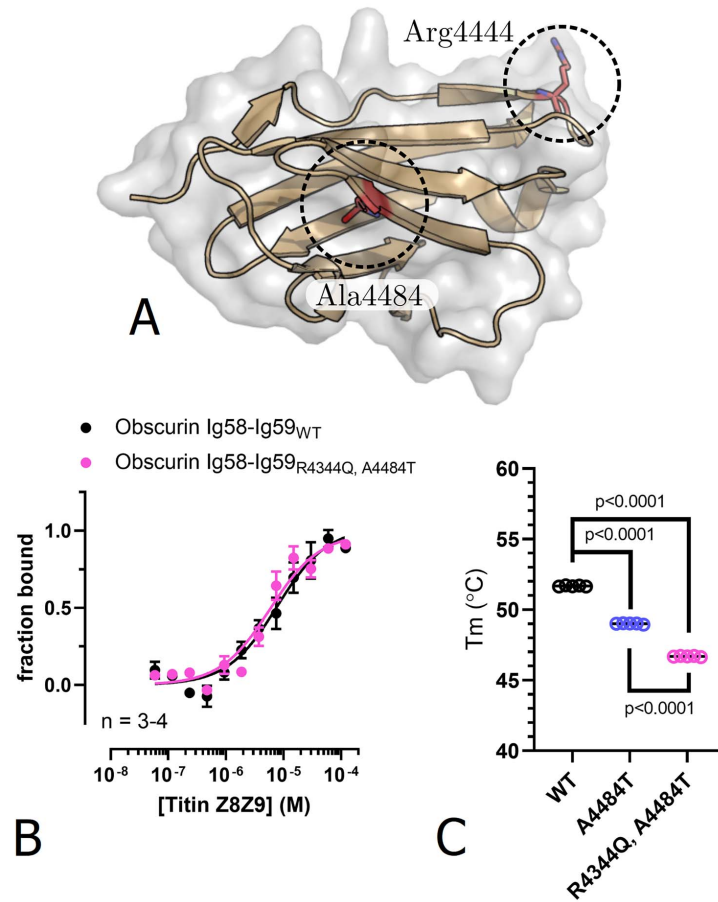


Figure 6. Characterization of the obscurin R4344Q, A4484T double variant. (A) Position of A4484 affected by mutation in the Ig59 structure of obscurin (PDB-ID: 5TZM). (B) No effect can be observed for the affinity to titin Z8-Z9 as measured by MST. (C) Thermostability of obscurin Ig58-Ig59_{WT}, A4484T variant, and R4344Q, A4484T double variant.

the murine heart. We thus speculate that the phenotype observed by Hu *et al.* might be specific to the physiology of the murine heart.

The R4444W variant

The minor allele frequency of the R4444W variant is at 1.2×10^{-4} among the European/American population (13), more consistent with a potentially pathogenic mutation than the frequency of the R4344Q variant. In our hands, however, the R4444W variant did not exhibit any effect on protein-protein interactions either, contrary to the results of Rossi *et al.* who found a 15-fold increased K_d for the interaction with titin Z8-Z9 due to the R4444W variant (13). Having studied this interaction using surface plasmon resonance (SPR), the authors explained this result with a strongly decreased *on*-rate constant based on their

fit to the SPR data. This is surprising for two reasons: first, empirically, many single amino-acid substitutions typically have a far bigger impact on the *off*-rate rather than on the *on*-rate constant of simple binding reactions (28,29). This is intuitively plausible if one assumes binding to be limited by diffusion and orientation but dissociation to be limited by the strength of the molecular interactions between two molecules (30). Secondly, a decreased *on*-rate constant due to a substitution seems plausible if the exchanged residue poses a significant steric hindrance for binding or if the complex formation proceeds via a two-step mechanism, e.g. if it involves a slower conformational transition from an initial low-affinity to a high-affinity complex. In the latter case, a mutation could interfere with the transition rate and thereby increase the time during which the complex remains in its low-affinity state. Both explanations, however, seem not to apply to the obscurin Ig58-Ig59/titin Z8-Z9 complex.

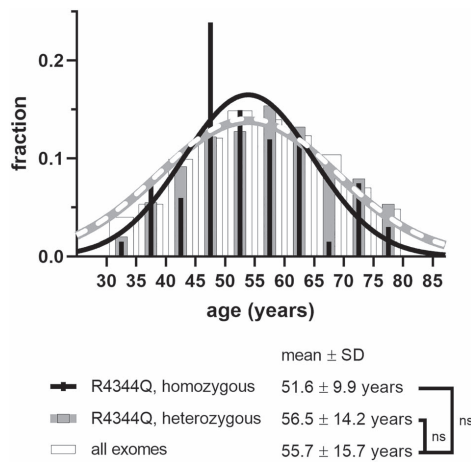


Figure 7. Age structure of homozygous and heterozygous carriers of the R4344Q variant. If the R4344Q variant would lead to significant cardiac disease (such as dilated cardiomyopathy), variant carriers could be expected to die earlier, resulting in a 'left-shift' of the age distribution of variant carriers. The absence of any significant change in the mean age compared to the overall population confirms that carriers of the R4344Q variant do not die earlier, indicating that the variant is not pathogenic.

While we have no kinetic data on the binding mechanism, R4444 is a very peripheral surface residue, and whose substitution by tryptophan exerts only very localized effects on chemical shifts (according to Rossi *et al.*'s NMR data (13)), suggesting that it does not alter the structural dynamics of obscurin Ig59. It is worth pointing out, however, that the SPR dissociation curves presented by Rossi *et al.* are not homogenous and therefore might have affected the quality of the fitting procedure. In agreement with Rossi *et al.*, however, we did not find a biologically relevant effect of the R4444W variant on domain stability.

Conclusion

Our results highlight the importance of interpreting *in vitro* data on potentially disease-causing variants in the context of human physiology and population genetics, and requiring experimental designs with sufficiently quantitative information. Our quantitative biochemical and biophysical characterization of the influence of the R4344Q or R4444W variants on protein-protein interactions and thermostability suggests that these variants are benign. Obviously, we cannot completely exclude the possibility that there are other protein-protein interactions or epistatic effects due to which the R4344Q or R4444W variants could exert a pathogenic influence, but these would not be covered by the mechanistic explanations of their actions on known interactions. For the R4344Q variant, however, this possibility seems unlikely in light of the overwhelming abundance amongst African Americans. Moreover, both variants were discovered in co-segregation with additional variants, suggesting that the disease phenotype observed in these patients could be the effect of multiple, individually benign, but in accumulation pathogenic variants. For the R4444W variant, this seems possible, having been discovered in patients with an FLNC frameshift mutation.

For the R4344Q variant, our *in vitro* data suggest that even co-segregation with the A4484T variant may not lead to major increases in the risk for cardiovascular disease. While this does not rule out a minor risk increase; e.g. in the context of chronic heart disease due to lifestyle or environmental factors, we expect such predisposition not to be discernible without clinical studies of sufficient statistical power.

We, therefore, advise against classifying these variants as pathogenic and highlight the need to view genetic data in light of sufficient clinical and functional evidence that establishes a clear correlation between variants and the occurrence of cardiovascular or neuromuscular disease.

Material and Methods

Constructs used in this work

Obscurin Ig58 and Ig58-Ig59 (residue number 4337–4429 and 4337–4521, based on NCBI Ref. Seq. NM_001098623/NP_001092093, transcript variant B), titin Z8-Z9 and titin M2-M3 (1698 to 1931 and 34258 to 34454 based on NM_001267550/NP_001254479, transcript variant IC) and novex-3 obscurin binding region (ObB) (4991 to 5187 based on NM_133379/NP_596870, transcript variant novex-3) were cloned from a homemade human cardiac cDNA library into a modified pET protein expression vector encoding an N-terminal His₆ tag followed by TEV cleavage site, and pEGFP2 vector for expression in mammalian cells. The Arg4344Gln, Arg4444Trp and Ala4484Thr mutations were introduced by site-directed mutagenesis. pcDNA3-PLN was a kind gift of Dr. Joachim P. Schmitt (HHU Düsseldorf). All constructs were validated by sequencing.

Protein expression and purification

Expression vectors were transformed into BL21-CodonPlus (DE3)-RIPL competent cells (Agilent Technologies), which were grown in 0.5 L of LB medium at 37°C until 0.6–0.7 at OD₆₀₀ before protein expression was induced overnight by addition of 0.3 mM IPTG at 20°C. Cells were harvested by centrifugation and lysed by sonication in PBS supplemented with lysozyme, 1:1000 (v/v) β-mercaptoethanol, 30 mM imidazole, 1x cComplete™ EDTA-free Protease Inhibitor Cocktail (Roche). Proteins were purified using 1ml superflow Ni-NTA resin (Qiagen) according to the manufacturer's instructions and subsequently concentrated to 1.7–12 mg/ml (absorbance at 280 nm) into a final buffer of 30 mM HEPES pH 7.5, 100 mM NaCl and 2 mM DTT. Synthetic human full-length PLN, PLN₁₋₂₂ (cytoplasmic region) and PLN₂₃₋₅₂ (transmembrane region) was obtained from Pepsan (Lelystad, Netherlands) as lyophilized peptides and were resuspended in PBS supplemented with 0.2% (v/v) Triton X-100 and 2 mM DTT, or in 50 mM Tris-HCl pH 7.5, 100 mM NaCl, 0.5 % (v/v) Triton X-100 and 2 mM DTT. Due to interference of Triton X-100 with other methods, peptide concentration was determined densitometrically from SDS-PAGE using a BSA standard of known concentration and Oriole™ Fluorescent Gel Stain (Bio-Rad). All proteins were snap-frozen in liquid N₂ and stored at –80°C until further use.

Cell culture and transfection

HEK293A cells were cultured in DMEM supplemented with 10% foetal calf serum and 1% penicillin/streptomycin in 37°C/5% CO₂ incubator. Around 70 % confluence, cells were transfected with plasmids using Escort IV (Sigma) following the manufacturer's instruction. 24 h after transfection, cells were either fixed with

4% paraformaldehyde (PFA) for imaging, or lysed with lysis buffer for pull-down assays.

Immunostaining and imaging

Cells were fixed with 4% paraformaldehyde (PFA) in PBS for 6 min, permeabilized with 0.1% (v/v) Triton X-100 in PBS for 8 min, blocked with 5% normal goat serum/1% BSA in PBS for 30 min, and then treated with mouse anti-phospholamban antibody (primary, A1, Badrilla, 1:300 dilution) in 1% BSA in PBS for 2 h, followed by washing with PBS. Cells were then treated with Cy3-conjugated goat anti-mouse IgG (H+L) (Jackson ImmunoResearch, 115-165-146) in 1% BSA/PBS for overnight at 4°C. Following sufficient washing with PBS, the sample was mounted in mounting medium (30 mM Tris-HCl pH 9.5, 70% (v/v) glycerol, 5% n-propyl gallate). All procedures were performed at room temperature (RT). Cell images were collected on a Zeiss LSM510 confocal microscope in sequential scanning mode, using an APOCHROMAT 63x oil-immersion objective, instrument zoom rates set to 2 and image size of 1024 × 1024 pixels.

Pull-down experiments

Obscurin: phospholamban interaction. About, 50 µl of superflow Ni-NTA beads (Qjagen) were equilibrated with 0.5 ml of assay buffer (40 mM imidazole in PBS, pH 7.4) three times. 100 µl of 8 nmol of His₆-tagged proteins were mixed with the beads and incubated for 30 min at RT with moderate shaking to promote the binding. Unbound bait protein was removed by washing with 0.5 ml of assay buffer 3 times. 1 mg/ml PLN in 50 mM Tris-HCl pH 7.5, 100 mM NaCl, 2 mM DTT, 0.5 % (v/v) Triton X-100 was diluted with assay buffer to 0.2 mg/ml (32.8 µM), of which 100 µl were mixed with beads coated with bait protein, and then incubated for 1 h at RT with moderate shaking. A sample of the unbound fraction was taken (dilution of 1: 25 in 2x SDS sample buffer), and then beads were washed three times with 0.5 ml of washing buffer (PBS pH 7.2, 10 mM sodium azide, 0.1 % (v/v) Tween 20 as described in (14) supplemented with 40 mM of imidazole to reduce unspecific binding to the beads). The bound fraction samples were prepared by suspending the beads in 50 µl of 2x SDS sample buffer. 10 µl of bound and 3 µl of unbound fractions were loaded and separated by SDS-PAGE, transferred to a nitrocellulose membrane and analyzed by western blotting with mouse anti-PLN (A1, Badrilla, dilution of 1:5000) and HRP-conjugated rabbit anti-mouse IgG (Dako P0260, dilution of 1:1000). The signals of HRP were developed by Amersham™ ECL™ Western Blotting Detection Reagents (GERPN2109) and then imaged on a ChemiDoc™ XRS+ imaging system (Bio-Rad).

Obscurin: Novex-3 interaction. About, 24 h after transfections with pEGFP2 constructs, cells on 35-mm dishes were washed once with PBS and then lysed with 150 µl of lysis buffer (50 mM Tris-HCl pH 7.5, 40 mM imidazole, 100 mM NaCl, 2 mM DTT, 10 % (v/v) glycerol, 0.5 % (v/v) Triton X-100, 1 mM MgCl₂, 2x PhosStop phosphatase inhibitor cocktail (Roche), 0.5 µM Staurosporin, 1x cOmplete™ EDTA-free Protease Inhibitor Cocktail (Roche)). Soluble fractions were collected by centrifugation, 15 000 × g at 4°C for 20 min. 50 µl of His₆-O5859-coated Ni-NTA beads prepared as described above were equilibrated with Novex-3 assay buffer (PBS, 40 mM imidazole, 2 mM MgCl₂, 3.55 mM β-mercaptoethanol, 0.2% (v/v) NP-40, 1x cOmplete™ EDTA-free Protease Inhibitor Cocktail (Roche) and 1x PhosStop phosphatase inhibitor cocktail (Roche)) before mixing with 60 µl of cell lysates. Following incubation at RT with moderate shaking for 1 h, a

sample of the unbound fraction was taken (dilution of 1: 10 in 2x SDS sample buffer), and then beads were washed three times with 0.5 ml of Novex-3 assay buffer. The bound fraction samples were prepared by suspending the beads in 50 µl of 2x SDS sample buffer. All samples were boiled at 95°C for 5 min immediately before gel electrophoresis. About, 8 µl of bound and 4 µl of unbound fractions were loaded and separated by SDS-PAGE, transferred to a nitrocellulose membrane and then analyzed by western blotting with mouse anti-GFP (clones 7.1 and 13.1, Roche 11814460001, dilution of 1:2000), followed by HRP-conjugated rabbit anti-mouse IgG (Dako P0260, dilution of 1:2000). The signals of HRP were developed by Amersham™ ECL™ Western Blotting Detection Reagents (GERPN2109) and then imaged on a ChemiDoc™ XRS+ imaging system (Bio-Rad).

MST

Obscurin Ig58-Ig59, Ig58-Ig59^{R4344Q}, Ig58-Ig59^{R4444W} and Ig58-Ig59^{R4344Q, A4484T} was labelled for MST using the Monolith NT Protein Labeling kit RED-NHS (NanoTemper) according to the manufacturer's instructions. The unlabelled binding partners were diluted serially by a factor of 0.5 in MST-Buffer (PBS, 0.2% (v/v) Triton x-100, 2 mM DTT for PLN and PBS, 2 mM DTT for Titin Z8-Z9 and ObB) and mixed with an appropriate amount of the labelled partner to give a signal of 300–700 fluorescence units (typically 50–100 nM). Thermophoresis was measured on a Monolith NT.115 instrument (NanoTemper) using 10-µl glass capillaries (Brand, cat.no. PIP3114). Data were transformed into fractional saturation and exported using the MO. Affinity Analysis software (NanoTemper) to be fitted to a one-site binding model ($Y = \frac{[X]}{K_d + [X]}$), where Y denotes fractional saturation and [X] the concentration of the free binding partner) using GraphPad Prism software version 8.3. Fitted dissociation constants K_d are expressed as mean ± standard error.

DSF

Purified obscurin Ig58, Ig58^{R4344Q}, Ig58-Ig59, Ig58-Ig59^{R4344Q}, Ig58-Ig59^{R4444W}, Ig58-Ig59^{A4484T}, and Ig58-Ig59^{R4344Q, A4484T} were mixed with SYPRO orange (ThermoFisher) to a final concentration of 20 µM and 20X, respectively. 20 µl of each protein-SYPRO orange mix was pipetted into 4–5 wells of a white 96-well PCR plate (ThermoFisher) covered with optical PCR seals (Bio-Rad) and DSF was run according to Niesen et al.(16); briefly, the plate was loaded into a Stratagene Mx3005p and heated from 25 to 96°C, 1°C per minute, and fluorescent emission of SYPRO orange was measured at each degree °C at 610 nm following excitation at 492 nm. The data relating to the unfolding of the protein were automatically identified using a Microsoft Excel spreadsheet from Niesen et al., with the melting temperature, T_m, calculated in GraphPad Prism (v8.3) by fitting the curve to the Boltzman Equation $Y = LL + \frac{UL - LL}{1 + \exp\left(\frac{T_m - x}{a}\right)}$, where LL and UL refer to the lower and upper fluorescent intensities, T_m is the melting temperature, Y is the fluorescence at x, x is the temperature and a is the slope of the curve at T_m.

Statistical analysis

Statistical significance between two experimental groups was determined in GraphPad Prism (v8.3) using the two-tailed unpaired T-test. Sample sizes are given in the respective figures.

For analysis of the population age structure of R4344Q carriers, data on single nucleotide variant 1-228503566-G-A (GRCh37)

were retrieved from the gnomAD database v2.1.1 (accessed 27 March 2020). Absolute frequencies were transformed into relative frequencies and X/Y bar charts were plotted in GraphPad Prism (v8.3) by assigning X the arithmetic mean of the boundaries of the respective bin (the >80 years bin was assigned the value 90 years). For comparison of the age structure of all exomes, heterozygote and homozygote carriers, the data were fitted to Gaussian distributions and means were compared using the extra square-of-sums *F* test in GraphPad Prism. *P*-values <0.05 were considered significant.

Supplementary Material

Supplementary Material is available at HMG online.

Acknowledgements

We would like to thank Dr. Joachim P. Schmitt for the pCDNA3-PLN plasmid, Dr. Thomas Kampourakis for the PLN transmembrane region peptides and two anonymous referees for constructive comments.

Conflict of Interest statement. The authors have no competing interest to declare.

Funding

The British Heart Foundation (grant nos [FS/17/65/33481] to D.K., [RG/15/8/31480] to M.R. and S.G.); Medical Research Council (grant no. [MR/R003106/1] to M.G. and A.F.). M.G. holds the BHF Chair of Molecular Cardiology.

Author contributions

A.F., D.K. and M.G. conceived the study, A.F. and D.K. designed experiments, A.F., D.K., S.G. and M.R. performed experiments and analyzed the data, D.K. wrote the manuscript with the help of M.G., A.F. and M.R.

References

- Young, P., Ehler, E. and Gautel, M. (2001) Obscurin, a giant sarcomeric Rho guanine nucleotide exchange factor protein involved in sarcomere assembly. *J. Cell Biol.*, **154**, 123–136.
- Bagnato, P., Barone, V., Giacomello, E., Rossi, D. and Sorrentino, V. (2003) Binding of an ankyrin-1 isoform to obscurin suggests a molecular link between the sarcoplasmic reticulum and myofibrils in striated muscles. *J. Cell Biol.*, **160**, 245–253.
- Fukuzawa, A., Idowu, S. and Gautel, M. (2005) Complete human gene structure of obscurin: implications for isoform generation by differential splicing. *J. Muscle Res. Cell Motil.*, **26**, 427–434.
- Russell, M.W., Raeker, M.O., Korytkowski, K.A. and Sonnenman, K.J. (2002) Identification, tissue expression and chromosomal localization of human Obscurin-MLCK, a member of the titin and Dbl families of myosin light chain kinases. *Gene*, **282**, 237–246.
- Kontogianni-Konstantopoulos, A., Jones, E. M., van Rossum, D. B., Bloch, R., J. (2003) Obscurin is a ligand for small ankyrin 1 in skeletal muscle. *Mol. Biol. Cell*, **14**, 1138–1148.
- Borzok, M. A., Catino, D. H., Nicholson, J. D., Kontogianni-Konstantopoulos, A., Bloch, R., J. (2007) Mapping the Binding Site on Small Ankyrin 1 for Obscurin. *J. Biol. Chem.*, **282**, 32384–32396.
- Lange, S., Ehler, E. and Gautel, M. (2006) From A to Z and back? Multicompartment proteins in the sarcomere. *Trends Cell Biol.*, **16**, 11–18.
- Potts, G.K., McNally, R.M., Blanco, R., You, J., Hebert, A.S., Westphall, M.S., Coon, J.J. and Hornberger, T.A. (2017) A map of the phosphoproteomic alterations that occur after a bout of maximal-intensity contractions. *J. Physiol.*, **595**, 5209–5226.
- Arimura, T., Matsumoto, Y., Okazaki, O., Hayashi, T., Takahashi, M., Inagaki, N., Hinohara, K., Ashizawa, N., Yano, K. and Kimura, A. (2007) Structural analysis of obscurin gene in hypertrophic cardiomyopathy. *Biochem. Biophys. Res. Commun.*, **362**, 281–287.
- Marston, S., Montgiraud, C., Munster, A.B., Copeland, O., Choi, O., Dos Remedios, C., Messer, A.E., Ehler, E. and Knöll, R. (2015) OBSCN Mutations Associated with dilated cardiomyopathy and haploinsufficiency. *PLOS ONE*, **10**, e0138568.
- Rowland, T.J., Graw, S.L., Sweet, M.E., Gigli, M., Taylor, M.R. and Mestroni, L. (2016) Obscurin variants in patients with left ventricular noncompaction. *J. Am. Coll. Cardiol.*, **68**, 2237–2238.
- Marston, S. (2017) Obscurin variants and inherited cardiomyopathies. *Biophys. Rev.*, **9**, 239–243.
- Rossi, D., Palmio, J., Evilä, A., Galli, L., Barone, V., Caldwell, T.A., Policke, R.A., Aldkheil, E., Berndsen, C.E., Wright, N.T. et al. (2017) A novel FLNC frameshift and an OBSCN variant in a family with distal muscular dystrophy. *PLOS ONE*, **12**, e0186642.
- Hu, L.-Y.R., Ackermann, M.A., Hecker, P.A., Prosser, B.L., King, B., O'Connell, K.A., Grogan, A., Meyer, L.C., Berndsen, C.E., Wright, N.T. et al. (2017) Deregulated Ca²⁺ cycling underlies the development of arrhythmia and heart disease due to mutant obscurin. *Sci. Adv.*, **3**, e1603081.
- Manrai, A.K., Funke, B.H., Rehm, H.L., Olesen, M.S., Maron, B.A., Szolovits, P., Margulies, D.M., Loscalzo, J. and Kohane, I.S. (2016) Genetic misdiagnoses and the potential for health Disparities. *N. Engl. J. Med.*, **375**, 655–665.
- Niesen, F.H., Berglund, H. and Vedadi, M. (2007) The use of differential scanning fluorimetry to detect ligand interactions that promote protein stability. *Nat. Protoc.*, **2**, 2212–2221.
- Jerabek-Willemsen, M., André, T., Wanner, R., Roth, H.M., Duhr, S., Baske, P. and Breitspacher, D. (2014) MicroScale thermophoresis: interaction analysis and beyond. *J. Mol. Struct.*, **1077**, 101–113.
- Bang, M.-L., Centner, T., Fornoff, F., Geach, A.J., Gotthardt, M., McNabb, M., Witt, C.C., Labeit, D., Gregorio, C.C., Granzier, H. et al. (2001) The complete gene sequence of titin, expression of an unusual ≈700-kDa titin isoform, and its interaction with obscurin identify a novel Z-line to I-band linking system. *Circ. Res.*, **89**, 1065–1072.
- Yue, P., Li, Z. and Moul, J. (2005) Loss of protein structure stability as a major causative factor in monogenic disease. *J. Mol. Biol.*, **353**, 459–473.
- Anderson, B.R., Bogomolovas, J., Labeit, S. and Granzier, H. (2013) Single molecule force spectroscopy on titin implicates immunoglobulin domain stability as a cardiac disease mechanism. *J. Biol. Chem.*, **288**, 5303–5315.
- Rudloff, M.W., Woosley, A.N. and Wright, N.T. (2015) Biophysical characterization of naturally occurring titin M10 mutations. *Prot. Sci.*, **24**, 946–955.
- Rees, M., Nikoipour, R., Fukuzawa, A., Kho, A.L., Fernandez-Garcia, M.A., Wraige, E., Bodi, I., Deshpande, C., Özdemir, Ö., Daimagüler, H.-S. et al. (2021) Making sense of missense variants in TTN-related congenital myopathies. *Acta Neuropathol.* doi: 10.1007/s00401-020-02257-0.

23. Bers, D.M. (2002) Cardiac excitation-contraction coupling. *Nature*, **415**, 198–205.
24. Carnethon, M.R., Pu, J., Howard, G., Albert, M.A., Anderson, C.A.M., Bertoni, A.G., Mujahid, M.S., Palaniappan, L., Taylor, H.A., Jr., Willis, M. et al. (2017) Cardiovascular health in African Americans: a scientific statement from the American Heart Association. *Circulation*, **136**, e393–e423.
25. Mayer, E.J., Savage, G.M. and Johnson, R.G. (1998) A quantitative immunoassay for the measurement of phospholamban levels and phosphorylation states: measurement of phospholamban levels in transgenic mouse hearts. *Ann. N. Y. Acad. Sci.*, **853**, 284–287.
26. Mayer, E.J., Huckle, W., Johnson, R.G., Jr. and McKenna, E. (2000) Characterization and quantitation of phospholamban and its phosphorylation state using antibodies. *Biochem. Biophys. Res. Commun.*, **267**, 40–48.
27. Ablorh, N.-A., Miller, T., Nitu, F., Gruber, S.J., Karim, C. and Thomas, D.D. (2012) Accurate quantitation of phospholamban phosphorylation by immunoblot. *Anal. Biochem.*, **425**, 68–75.
28. Lever, M., Lim, H.-S., Kruger, P., Nguyen, J., Trendel, N., Abu-Shah, E., Maini, P.K., van der Merwe, P.A. and Dushek, O. (2016) Architecture of a minimal signaling pathway explains the T-cell response to a 1 million-fold variation in antigen affinity and dose. *Proc. Natl. Acad. Sci. U.S.A.*, **113**, 6630–6638.
29. Signorelli, S., Santini, S., Yamada, T., Bizzarri, A.R., Beatrice, C.W. and Cannistraro, S. (2017) Binding of amphipathic cell penetrating peptide p28 to wild type and mutated p53 as studied by Raman, atomic force and surface plasmon resonance spectroscopies. *Biochim. Biophys. Acta*, **1861**, 910–921.
30. Schreiber, G., Haran, G. and Zhou, H.-X. (2009) Fundamental aspects of protein–protein association kinetics. *Chem. Rev.*, **109**, 839–860.

Chapter 5

Homo-Oligomerisation in Signal Transduction

This chapter presents the first line of my theoretical work on homo-oligomerisation. The chapter consists of the research paper “Homo-Oligomerisation in Signal Transduction: Dynamics, Homeostasis, Ultrasensitivity, Bistability” published in the *Journal of Theoretical Biology*. The supplementary material for this study can be found in [chapter A5.2](#).

The first mathematical models of phospholamban pentamerisation developed during this work behaved rather unexpectedly insofar as they predicted transients of oligomerisation during post-translational modification despite unchanged rate constants. As this contradicted biochemical intuition, this prompted me to start with simpler models of oligomerisation (dimerisation to tetramerisation), which showed that the surprising transients during post-translational modification were the result of a combinatorial expansion in the model that needs to be counterbalanced. As the literature on the general functions of oligomerisation in biochemical signalling networks was rather limited, these simple models were explored further and revealed an unexpected and surprising variety of behaviour that may be useful in biochemical signalling networks.

Correction note:

On page 101 of this thesis (page 2 of the published paper), the units for the association rate constants of the oligomerisation reactions were incorrectly given as $\text{mol}^{-1}\text{s}^{-1}$ which should be given as $\text{M}^{-1}\text{s}^{-1}$ instead.



Homo-Oligomerisation in Signal Transduction: Dynamics, Homeostasis, Ultrasensitivity, Bistability

Daniel Koch

Randall Centre for Cell & Molecular Biophysics King's College London, London SE1 1UL, United Kingdom



ARTICLE INFO

Article history:

Received 27 December 2019

Revised 26 April 2020

Accepted 27 April 2020

Available online 8 May 2020

Keywords:

Protein complexes

Mathematical modelling

Dynamic signal encoding

Post-translational modifications

Multi-enzyme systems

ABSTRACT

Homo-oligomerisation of proteins is a ubiquitous phenomenon whose exact role remains unclear in many cases. To identify novel functions, this paper provides an exploration of general dynamical mathematical models of homo-oligomerisation. Simulation and analysis of these models show that homo-oligomerisation on its own allows for a remarkable variety of complex dynamic and steady state regulatory behaviour such as transient overshoots or homeostatic control of monomer concentration. If post-translational modifications are considered, however, conventional mass action kinetics lead to thermodynamic inconsistencies due to asymmetric combinatorial expansion of reaction routes. Introducing a conservation principle to balance rate equations re-establishes thermodynamic consistency. Using such balanced models it is shown that oligomerisation can lead to bistability by enabling pseudo-multisite modification and kinetic pseudo-cooperativity via multi-enzyme regulation, thereby constituting a novel motif for bistable modification reactions. Due to these potential signal processing capabilities, homo-oligomerisation could play far more versatile roles in signal transduction than previously appreciated.

© 2020 The Author(s). Published by Elsevier Ltd. This is an open access article under the CC BY license (<http://creativecommons.org/licenses/by/4.0/>).

1. Introduction

Homo-oligomerisation of proteins, i.e. the assembly of supramolecular protein complexes made up from multiple identical subunits, is a ubiquitous phenomenon. In vertebrates, about 30–50% of all proteins form homo-oligomers, most of which are dimers ($\approx 72\%$), tetramers ($\approx 17\%$) and trimers ($\approx 8\%$), while only $\approx 3\%$ form other higher order oligomers (Lynch, 2012; Marsh and Teichmann, 2015). Oligomerisation may offer several advantages: it can be a way to economically assemble larger structures (thereby reducing genome size) and allows for a higher error-free transcription chance for individual subunits. Moreover, it can provide additional regulatory control via allostery and cooperative binding events (hemoglobin being the classical example) (Marianayagam et al., 2004; Ali and Imperiali, 2005). Yet, in many cases the function of homo-oligomerisation remains unclear.

Dynamical mathematical models based on ordinary differential equations (ODEs) have been extensively used to study many important motifs, mechanisms and phenomena in signal transduction networks. To lesser extent, ODE models have also been used to study signal transduction processes involving homo-oligomers. Such theoretical studies have shown that in addition to the well-known role in the emergence of ultrasensitive responses via cooperative binding, oligomerisation can provide an additional layer of

control over such responses. Bouhaddou and Birtwistle, for instance, showed that different oligomerisation routes provide an effective means of tuning ultrasensitive, cooperative responses (Bouhaddou and Birtwistle, 2014). Buchler and Louis showed that homo-oligomerisation itself can lead to modest ultrasensitivity independent from cooperativity (Buchler and Louis, 2008). If coupled to positive feedback, the ultrasensitivity generated e.g. by homo-dimerisation is sufficient for the emergence of bistability (Hsu et al., 2016). For signalling involving dimeric receptors and substrate activation, the presence of a single/dual activation mechanism can lead to complex, non-linear signal dynamics (Vera et al., 2008). Taken together, this highlights the importance of homo-oligomerisation and the use of mathematical modelling as a tool to study its roles in signal transduction.

However, above mentioned studies focussed on specific questions, contexts or systems. A general analysis of homo-oligomerisation in terms of assembly dynamics, steady state behaviour and the potential effects of post-translational modifications (PTMs) is neither covered by classical and popular textbooks on mathematical or system's biology (see e.g. Murray, 2002; Klipp et al., 2005; Keshet-Edelstein, 2005; Voit, 2012; Ingalls, 2013), nor is the author aware of such analysis in the recent research literature. It thus seems that an exploration of general dynamical mathematical models of homo-oligomerisation is still lacking. This paper provides such an exploration. As this study focusses solely

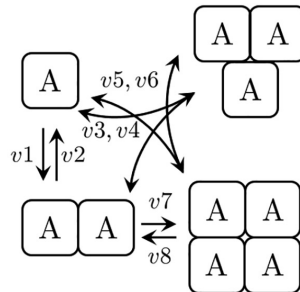
E-mail address: daniel.koch@kcl.ac.uk

<https://doi.org/10.1016/j.jtbi.2020.110305>

0022-5193/© 2020 The Author(s). Published by Elsevier Ltd.

This is an open access article under the CC BY license (<http://creativecommons.org/licenses/by/4.0/>).

Reaction scheme



Individual reactions and rate expressions

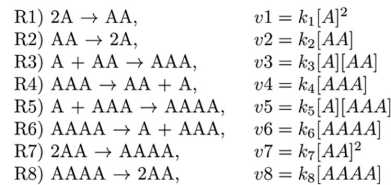


Fig. 1. Model scheme of homo-tetramerisation based on conventional mass action kinetics assuming that all intermediate species (dimers and trimers) are possible in the reaction pathway. See text for the differential equations describing the system.

on homo-oligomerisation, we will often leave out the prefix 'homo-' in the remainder of this article for the sake of brevity.

Beginning with simple mass action kinetics based models of dimerisation to tetramerisation, we will study assembly dynamics and steady state behaviour numerically. Although the first presented models are very simple, it is found that they are capable of complex dynamic and steady state behaviour such as undulations and homeostatic regulation.

Next, PTMs of oligomers are considered. Surprisingly, the application of conventional mass action rate laws easily results in thermodynamically inconsistent models due to combinatorial expansion of the oligomerisation routes upon modification. To keep the focus on biological results, details on this technical issue and how it can be circumvented are discussed in the supplement.

Finally, two novel mechanisms based on oligomerisation leading to ultrasensitive, bistable PTM responses will be presented: pseudo-multisite modification and regulation by multiple enzymes.

The focus of the current work is to demonstrate that oligomerisation enables more complex regulatory behaviour than previously appreciated. While the broad scope of a general analysis of dynamical mathematical models of oligomerisation does not permit an exhaustive treatment of all aspects within the limit of a single article, some of the most important implications and avenues for future research will be outlined in the discussion.

2. Results

2.1. Simple mass action models of oligomerisation: transients and homeostasis

Let us begin by assuming that a general protein A can form symmetric oligomers with a maximum number of n subunits (protomers) per oligomeric complex. We furthermore assume that A can form all intermediate oligomeric species with m subunits (where $m \in \mathbb{N}, 1 < m < n$) and that each oligomeric species is formed through simple one-step, second-order binding reactions described by mass action kinetics. For the remainder of this article, we will study oligomers with a maximum of four protomers or less, i.e. tetramers, trimers and dimers. It is likely that many of the presented findings apply to higher-order oligomers as well.

In the case of tetramers, we therefore assume that tetramers can be formed by the association of two dimers or, alternatively, of a trimer and a monomer. The reaction scheme and the reaction rates for the individual reactions can then be summarised as in Fig. 1. Denoting the monomeric to tetrameric species by $A, \dots, AAAA$ we can now formulate the system's equations:

$$\begin{aligned} \frac{d}{dt}[A] &= 2 \cdot v_2 + v_4 + v_6 - 2 \cdot v_1 - v_3 - v_5 \\ \frac{d}{dt}[AA] &= v_1 + v_4 + 2 \cdot v_8 - v_2 - v_3 - 2 \cdot v_7 \\ \frac{d}{dt}[AAA] &= v_3 + v_6 - v_4 - v_5 \\ \frac{d}{dt}[AAAA] &= v_5 + v_7 - v_6 - v_8 \end{aligned}$$

The total amount of subunits is conserved by the relation $A_{\text{tot}} = [A] + 2 \cdot [AA] + 3 \cdot [AAA] + 4 \cdot [AAAA]$ which can be used to eliminate one of the above equations. Note that models for tri- or dimerisation can be obtained simply by removing reactions R5–R8 or R3–R8, respectively. For the sake of simplicity, we will begin by assuming equal rate constants of $10^6 \text{ mol}^{-1} \text{ s}^{-1}$ for all association reactions and equal rate constants of 0.1 s^{-1} for all dissociation reactions, thereby yielding a K_d value of $0.1 \text{ } \mu\text{M}$ for all reactions, a typical value for many protein–protein interactions.

Time course simulations of the system with initial conditions $[A]_0 = A_{\text{tot}} = 10 \text{ } \mu\text{M}$ show association dynamics typical for binary protein–protein interactions in the case of dimerisation, whereas trimerisation and tetramerisation reactions exhibit a transient overshoot of dimers followed by a slower decrease of dimers and an increase in trimers and tetramers, respectively (Fig. 2A–C). Amplitude and position of such overshoots strongly depend on the monomer concentration at the beginning of the reaction (Fig. 2C, inset). More complex dynamics such as damped oscillations or undulations on different time scales are possible (Fig. 2B, inset). If the individual oligomeric species possess different biological functionality, such dynamics could be a mechanism for dynamic signal encoding as will be outlined in the discussion in more detail.

Numerical steady state analysis shows that the dose–response curves for the individual species meet in a single intersection point (Fig. 2D–F), mirroring the assumption that all reactions have the same K_d value. Local sensitivity analysis at $A_{\text{tot}} = 10 \text{ nM}$ with 2% perturbation yields relative sensitivities $\frac{dS}{dA_{\text{tot}}} \frac{A_{\text{tot}}}{S}$ (where S is the steady state concentration of either $A, \dots, AAAA$) of 0.87 for monomers and 1.76 for dimers in the dimerisation model, 2.58 for trimers in the trimerisation model and 3.46 for tetramers in the tetramerisation model. The analysis confirms again that oligomerisation at concentrations below the K_d can lead to modest ultrasensitivity in response to changes in total protein concentration, and that ultrasensitivity can increase with higher number of protomers per complex (as can also be seen from the increasing slopes in Fig. 2E, F) (Buchler and Louis, 2008).

For many proteins able to form higher order oligomers, the presence of a single or a small subfraction of possible oligomeric species often dominates over other potential intermediate species (Powers and Powers, 2003), indicating that oligomerisation is often

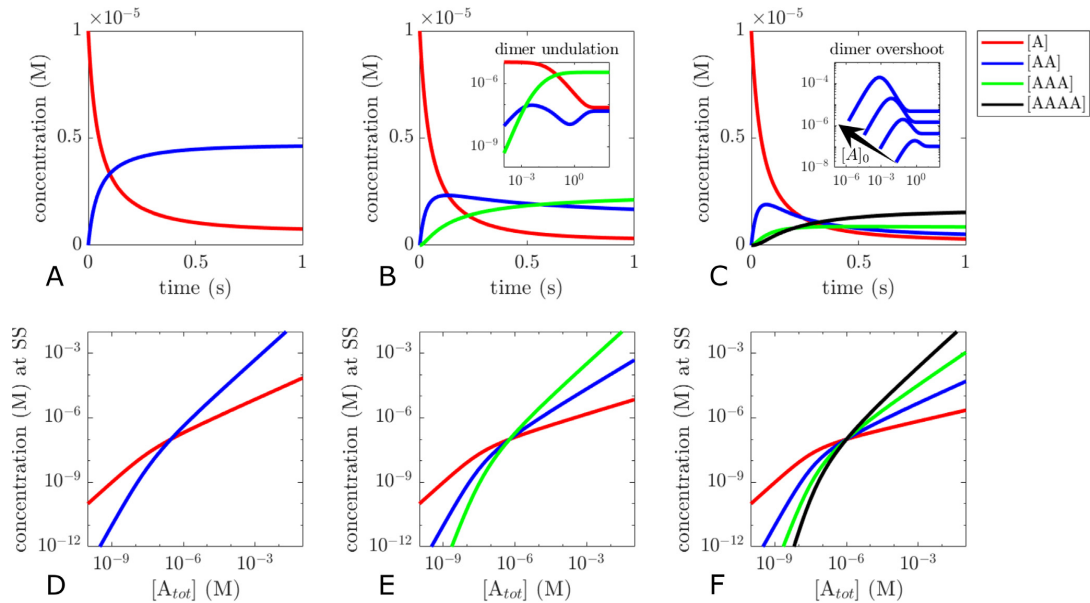


Fig. 2. Time course simulations (A–C) and steady state analysis (D–F) for dimers (A, D), trimers (B, E) and tetramers (C, F). Initial conditions for A–C: $[A]_0 = 10 \mu\text{M}$, $[AA]_0 = [AAA]_0 = [AAAA]_0 = 0 \text{ M}$. Parameters: (A and D) $k_1 = 10^6 \text{ mol}^{-1} \text{ s}^{-1}$, $k_2 = 0.1 \text{ s}^{-1}$, (B and E) $k_1 = k_3 = 10^6 \text{ mol}^{-1} \text{ s}^{-1}$, $k_2 = k_4 = 0.1 \text{ s}^{-1}$, (C and F) $k_1 = k_3 = k_5 = k_7 = 10^6 \text{ mol}^{-1} \text{ s}^{-1}$ (C inset: $k_3 = 10^8 \text{ mol}^{-1} \text{ s}^{-1}$), $k_2 = k_4 = k_6 = k_8 = 0.1 \text{ s}^{-1}$.

cooperative and that K_d values differ for the individual reactions. Varying the model parameters in a way to favour formation of the highest order oligomer in the trimerisation and tetramerisation model (e.g. by increasing association rate constants) can reproduce the dominance of the highest order oligomer over large concentration ranges (Fig. 3A, B). This also leads to a shift of intersection points, resulting in different apparent K_d values between the individual intermediate oligomerisation reactions. Tweaking of the parameters allows to shift the curves for each individual species into almost any direction (data not shown). Parameter variation also highlights the flipside of oligomeric ultrasensitivity. If we consider the monomer concentration at higher total protein concentrations in the inset of Fig. 3B, it becomes apparent that oligomerisation can be an efficient homeostatic regulatory mechanism of the monomer concentration (relative sensitivity of 0.25 for monomers at $A_{tot} = 100 \mu\text{M}$). This would be plausible in situations where monomers are the biologically active species. Note that this mechanism does not require a complex feedback organisation typically associated with homeostasis (Cannon, 1929; Tyson et al., 2003).

2.2. Considering post-translational modification of homo-oligomers

Just like non-oligomeric proteins, oligomeric proteins are subject to various post-translational modifications such as phosphorylation, ubiquitinylation, lipidation and others. Sometimes these modifications can regulate the equilibria between monomeric and oligomeric species via conformational changes or steric hindrance. Other times these modifications are irrelevant to the protein’s oligomerisation behaviour. Even accounting merely for a single PTM makes model formulation of anything higher than dimers unlikely more difficult due to the combinatorial expansion of potential oligomerisation routes.

Unfortunately, combinatorial expansion is not the only challenge when PTMs of oligomers are considered: it is remarkably

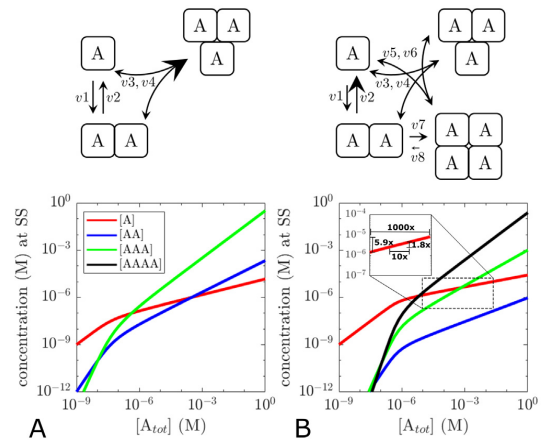


Fig. 3. Steady state analysis of trimerisation and tetramerisation models with varied parameters. The relative change of parameters is visualised in the upper reaction schemes. Parameters: (A) $k_1 = 10^6 \text{ mol}^{-1} \text{ s}^{-1}$, $k_3 = 10^8 \text{ mol}^{-1} \text{ s}^{-1}$, $k_2 = k_4 = 0.1 \text{ s}^{-1}$, (B) $k_1 = 3.2 \times 10^6 \text{ mol}^{-1} \text{ s}^{-1}$, $k_2 = 2400 \text{ s}^{-1}$, $k_3 = 3.45 \times 10^6 \text{ mol}^{-1} \text{ s}^{-1}$, $k_4 = 0.083 \text{ s}^{-1}$, $k_5 = 4.8 \times 10^6 \text{ mol}^{-1} \text{ s}^{-1}$, $k_6 = 0.525 \text{ s}^{-1}$, $k_7 = 3 \times 10^6 \text{ mol}^{-1} \text{ s}^{-1}$, $k_8 = 1.0525 \times 10^{-5} \text{ s}^{-1}$.

easy to slip into thermodynamical inconsistency even with models based purely on conventional mass action kinetics. The reason for this is that PTMs induce a combinatorial asymmetry: for a monomer, a single PTM site results in an either modified or unmodified state. For a n-tamer with the same PTM site, however, $n + 1$ possibilities to modify the n-tamer emerge (assuming that only the total number of PTMs is relevant). A model of dimerisation, for example, thus has to account for a single monomeric and a single dimeric

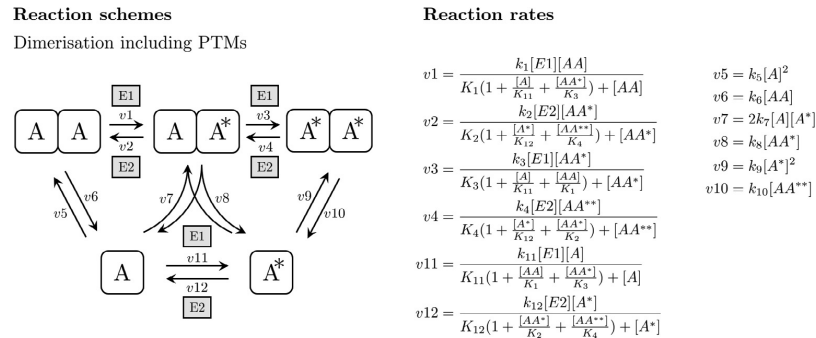


Fig. 4. Reaction scheme and reaction rates for the mass action kinetics model of dimerisation including reversible post-translational modification of a single site.

species if no PTMs are considered. If PTMs are considered, however, there are two monomeric species and three dimeric species (unmodified, singly modified, fully modified) to be accounted for. The model thus ‘grows’ asymmetrically on the n-tamer site. A more detailed description of the problem and how to avoid it can be found in [Supplementary section 1](#). In the following, we shall only consider models which have been balanced according to the procedure outlined there.

To proceed with model formulation, let us suppose an oligomeric protein can be modified by a PTM at a single site. For the sake of simplicity we assume that the site lies remote from the oligomerisation interface and does not alter any of the reaction parameters. Let A^* , AA^* , AA^{**} , ... denote modified monomers, dimers with one and dimers with two modified protomers and so forth. We assume molecules such as A^*A and AA^* are identical due to symmetry. Let $E1$ and $E2$ be a modifying and a demodifying enzyme for A 's PTM site, respectively, both of which operate by a non-cooperative, irreversible and distributive mechanism. We assume that all molecular species, regardless the number of their protomers, are (de-)modified with the same kinetic parameters, i.e. the oligomeric state does not influence the (de-)modification reactions. These assumptions reflect a situation in which a PTM does not induce conformational changes and lies remote from the oligomerisation interface, allowing the enzymes to access the PTM site equally in all oligomeric species. We therefore expect the individual monomeric and oligomeric species to compete for enzymes $E1$ and $E2$. In situations with multiple competing substrates S_1, \dots, S_n , an irreversible Michaelis–Menten type rate law of the form:

$$v_i = \frac{V_{max}S_i}{K_{m_i} \left(1 + \sum_{j \in \mathcal{N}(i)} \frac{S_j}{K_{m_j}} \right) + S_i},$$

where $J = \{1, \dots, n\}$, can be employed to describe the rate of consumption v_i of substrate S_i ([Schäuble et al., 2013](#)). That is, the individual substrates act as competitive inhibitors for each other. Like previous studies, we use a Michaelis–Menten type rate law to limit the number of parameters and reactions to be modelled ([Markevich et al., 2004](#); [Conradi and Mincheva, 2014](#)). Note, however, that modelling a specific signalling pathway with low substrate concentrations can require mass action kinetics ([Salazar and Höfer, 2009](#)). We are now able to formulate reaction schemes, reaction rates and model equations.

[Fig. 4A](#) shows the reaction scheme and rate expressions for a dimerisation model based on mass action kinetics for oligomerisation and mentioned Michaelis–Menten type rate law for addition and removal of PTMs. The equations are:

$$\frac{d}{dt}[A] = 2 \cdot v_6 + v_8 + v_{12} - 2 \cdot v_5 - v_7 - v_{11}$$

$$\frac{d}{dt}[A^*] = v_8 + 2 \cdot v_{10} + v_{11} - v_7 - 2 \cdot v_9 - v_{12}$$

$$\frac{d}{dt}[AA] = v_2 + v_5 - v_1 - v_6$$

$$\frac{d}{dt}[AA^*] = v_1 + v_4 + v_7 - v_2 - v_3 - v_8$$

$$\frac{d}{dt}[AA^{**}] = v_3 + v_9 - v_4 - v_{10}$$

Rate v_7 has been balanced according to the procedure outlined in [Supplementary section 1](#).

2.3. Ultrasensitivity and bistability via pseudo-multisite modification

We will begin exploring the steady state behaviour in the presence of (de-)modifying enzymes $E1, E2$ using the balanced dimer model as an example. The relative fraction of modified dimer and monomer shows pronounced ultrasensitivity in response to increasing concentrations of modifying enzyme $E1$ ([Fig. 5A](#)). On closer examination, this is not very surprising. Apart from some degree of zero-order ultrasensitivity arising from enzyme saturation ([Goldbeter and Koshland, 1981](#)), oligomerisation additionally creates a substrate competition situation between monomeric and oligomeric species for (de-)modification and provides pseudo-multisites for PTMs (i.e. multiple protomers with identical PTM sites). Both motifs are capable of generating ultrasensitivity ([Salazar and Höfer, 2006](#); [Ferrell et al., 2014](#)).

Moreover, multisite modification can in principle generate bi- or multistability if there is a sufficient asymmetry in the sequential modification cycles, i.e. if either the demodification and/or the modification steps exhibit kinetic cooperativity ([Markevich et al., 2004](#); [Ortega et al., 2006](#); [Thomson and Gunawardena, 2009](#)). For dual-site modification of monomeric proteins, [Conradi and Mincheva](#) have proven that in general, bistability must occur for some concentrations of demodifying and modifying enzyme if the product of the rate constants for the first modification and demodification steps is smaller than the product of the rate constants for the second modification and demododification steps ([Conradi and Mincheva, 2014](#)). Without considering the oligomeric nature, introducing positive kinetic cooperativity for the demodification of the dimer, i.e. assuming $k_2 > k_4$, would fulfill this requirement. Indeed, implementing this assumption leads to bistability with respect to the modification status in the dimer model ([Fig. 5B](#)). The range over which bistability occurs depends both on the degree of kinetic cooperativity and on the extend of dimerisation ([Fig. 5C, D](#)). As the bistable range increases with the number of cooperative modification steps ([Ortega et al., 2006](#)), the likelihood for a bistable PTM status will also increase with higher order oligomers.

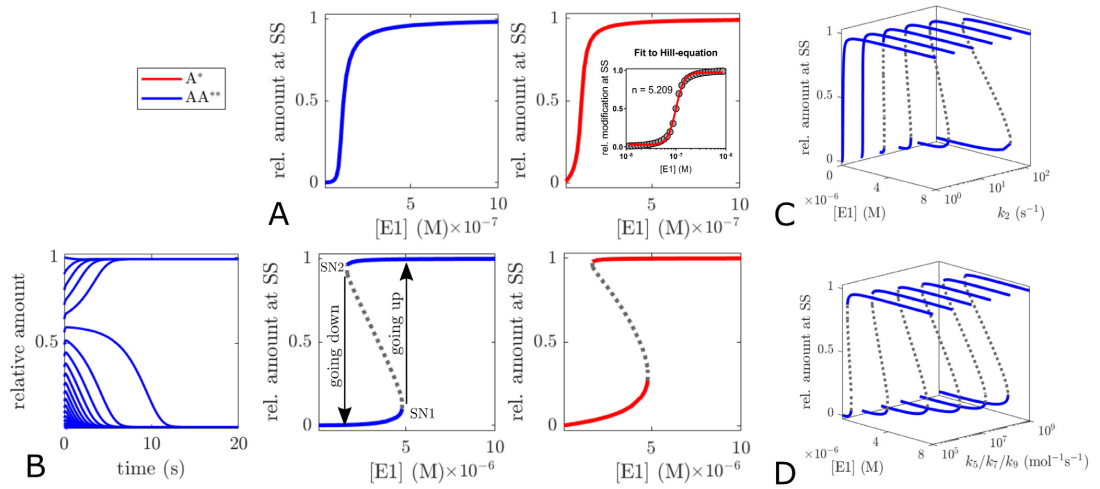


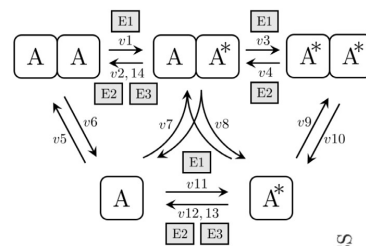
Fig. 5. Ultrasensitivity and Bistability of the modification response. Parameters and initial conditions: $k_5 = k_7 = k_9 = 10^7 \text{ mol}^{-1} \text{ s}^{-1}$, $k_6 = k_8 = k_{10} = 10 \text{ s}^{-1}$, $k_1 = k_2 = k_3 = k_4 = k_{11} = k_{12} = 1 \text{ s}^{-1}$, $K_1 = K_2 = K_3 = K_4 = K_{11} = K_{12} = 1 \mu\text{M}$, $A_{tot} = 10 \mu\text{M}$, $[E_2] = 0.1 \mu\text{M}$ (A) fractional modification of both monomers and dimers in response to increasing concentrations of modifying enzyme E1 is notably ultrasensitive. (B) left, time course simulations demonstrate that the approached steady state is determined by the initial conditions if demodification is assumed to be cooperative. Parameters: $k_2 = 100 \text{ s}^{-1}$, $[E_1] = 3 \mu\text{M}$, different fractional modification at $t = 0$. (B) middle and right, bifurcation diagrams show identical parameter values for saddle node bifurcations of dimer and monomer modification. Unstable steady states are indicated by dotted lines. (C,D) The bistable range of the modification response increases with stronger kinetic cooperativity (C) and dimer formation (D).

Interestingly, not only the dimer, but also the monomer modification exhibits bistability even without multiple sites for PTMs. This becomes less surprising if one considers that the dimer is in equilibrium with the monomer, allowing modified dimers to dissociate into monomers. Furthermore, when dimers are completely (de-)modified, substrate competition for (de-)modification of the monomer abates, allowing for more monomer (de-)modification.

While perhaps not uncommon, kinetic cooperativity might not be the only way to realise bistability in (pseudo-)multisite PTM systems. From a biochemical point of view, asymmetry in the (de-)modification rate of a multisite PTM protein could effectively

be realised, too, if one of the (de-)modification steps would also be catalysed by another enzyme E3. Let us, for instance, assume that in a dually modified dimer each PTM mutually prevents (e.g. due to steric reasons) access to the other PTM for demodifying enzyme E3. Only when one of the PTMs has already been removed by demodifying enzyme E2 (which we assume to catalyse PTM removal from the singly and dually modified dimer equally well), can E3 bind to the singly modified dimer and catalyse the last demodification step. Assuming that E3 can also catalyse demodification of the modified monomer, the scheme for the updated dimer model is shown in Fig. 6A. Using the updated dimer model it is not

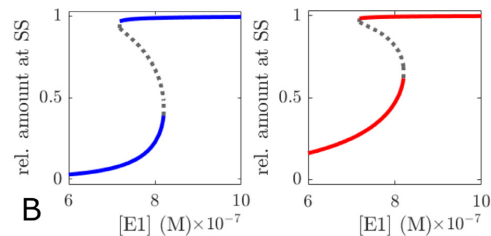
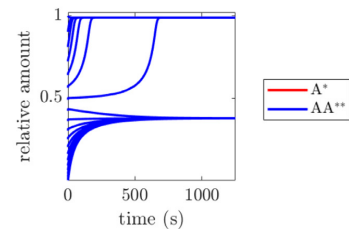
Multi-enzyme demodification



$$v_{13} = \frac{k_{13}[E_3][A^*]}{K_{13}(1 + \frac{[AA^*]}{K_{14}}) + [A^*]}$$

$$v_{14} = \frac{k_{14}[E_3][AA^*]}{K_{14}(1 + \frac{[A^*]}{K_{13}}) + [AA^*]}$$

A



B

Fig. 6. Bistability through multi-enzyme regulation of the modification status of oligomers. (A) scheme of the (balanced) dimer model with additional demodification enzyme E3 which can not catalyse the first step of the dimer demodification. (B) time course simulations and bifurcation plots demonstrating bistability in the dimer model. Parameters: $[E_2] = 10 \text{ nM}$, $[E_3] = 0.1 \mu\text{M}$, $k_{13} = 0.1 \text{ s}^{-1}$, $k_{14} = 100 \text{ s}^{-1}$, $K_{13} = 10 \mu\text{M}$, $K_{14} = 1 \mu\text{M}$, other parameters as specified for Fig. 5.

difficult to find parameter values that lead to bistability (Fig. 6B), showing that multi-enzyme regulation can be an effective alternative for realising the asymmetry required for bistability in multisite PTM systems.

3. Discussion

3.1. Complex dynamics and steady state behaviour

Even simple homo-oligomerisation systems can in principle be capable of surprisingly complex behaviour. Dynamical phenomena such as transient overshoots of dimers followed by a slower increase in higher order oligomers will be relevant to proteins which are not in a constitutive monomer/oligomer equilibrium. Examples include membrane receptors which oligomerise upon ligand binding (Klemm et al., 1998) or proteins which oligomerise upon recruitment to a membrane. If dimers and higher order oligomers have different downstream signalling functions, such transients could be an effective way to encode the duration of the input signal (e.g. ligand presence or membrane recruitment) and thereby lead to different cellular responses for short and prolonged stimuli. The tumor suppressor p53 is a relevant example of a protein with different biological activity for different oligomeric species (Rajagopalan et al., 2011). As p53 is also involved in dynamic signal encoding leading to different cell-fate decisions (Sonnen and Aulehla, 2014), it is tempting to speculate that some of this could be the result of oligomerisation. Another promising candidate for dynamic signal encoding through oligomerisation could be the EGF-receptor for which dimers, trimers and tetramers have been described (Furuuchi et al., 2007; Gan et al., 2007). A considerable list of higher-order homo-oligomers for which various intermediate forms have been observed (and thereby might also be candidates for dynamic signal encoding) can be found in Selwood and Jaffe (2012).

In addition to the previously described but modest ultrasensitivity through oligomerisation (Buchler and Louis, 2008; Hsu et al., 2016), we have seen that oligomerisation could also be an effective homeostatic regulatory mechanism to keep monomer concentration in a narrow range. In contrast to the dynamical phenomena, this more likely applies to proteins which are in a constitutive monomer/oligomer equilibrium. Recently, Frieden proposed oligomerisation as metabolic control mechanism (Frieden, 2019). Given that many enzymes oligomerise, monomer-homeostasis could be a good example. If enzyme function is inhibited e.g. by active site obstruction in an oligomeric complex (Matthews and Sunde, 2012), monomer-homeostasis could ensure a nearly constant performance of a metabolic activity over a wide range of total protein concentration (and therefore cellular conditions such as starvation or different cell cycle phases).

So far, few oligomeric proteins have been studied experimentally extensively enough to validate scenarios such as depicted in Fig. 3B. Since individual species concentrations in the homeostatic scenario often differ by ≥ 2 orders of magnitude, experimental testing of such behaviour would at least require to determine the equilibrium distribution of monomeric and oligomeric species over several orders of magnitude of total protein concentration. Ideally, this would be complemented by kinetic data on oligomer (dis-) assembly. Both types of experiments can be technically challenging and likely need to be analysed via model fitting (Kanno and Levitus, 2014; Parsons et al., 2019).

3.2. Combinatorial complexity

As the order of oligomers increases and/or PTMs are taken into account, the number of species and possible reactions quickly grows. This is a typical situation of 'combinatorial explosion' which

poses a significant challenge for many signal transduction models (Hlavacek et al., 2003; Stefan et al., 2014). If PTMs are not considered and only one oligomeric species is relevant, oligomerisation pathways can be approximated via *generalised mass action* rate laws (i.e. power-laws) provided that the range of total concentrations is sufficiently restricted (data not shown).

Upon inclusion of PTMs, the combinatorial expansion of possible oligomerisation routes posed another unanticipated challenge: ensuring thermodynamic consistency of the model. The rate balancing procedure described in the [Supplementary material](#) offers a solution which is straightforward to apply to mass action kinetics models. An open question is how this procedure fares if PTMs do affect oligomerisation parameters. A plausible conjecture would be that once the balancing coefficients have been introduced into the rate equations, changing parameter values for individual reactions will not affect thermodynamic consistency.

For practical purposes, modelling higher-order oligomers with multiple PTM sites will generally require implicit modelling approaches. Rule-based modelling, for instance, has been applied successfully for modelling EGF-receptor oligomerisation (Kozor et al., 2013).

3.3. Bistability

Ultrasensitivity and bistability are important properties of signal transduction networks for cellular decision making, allowing to respond in a switch-like, binary and sometimes irreversible fashion. Oligomerisation can also lead to ultrasensitivity and bistability by providing pseudo-multisite complexes (i.e. complexes with multiple identical PTM sites). Given previous work on ultrasensitivity and bistability arising via multisite modification from the Kholodenko lab and others (Markevich et al., 2004; Ortega et al., 2006; Salazar and Höfer, 2006; Conradi and Mincheva, 2014), this possibility seems obvious from a biochemical point of view, yet, has not been appreciated before. An interesting and unique twist of this motif is that the bistability resulting from modification of the oligomer extends to the monomer due to intrinsic substrate competition and because both species are in equilibrium with each other. We also demonstrated that kinetic cooperativity of multisite modification systems is not a requirement for bistability. If multiple enzymes regulate the modification steps and if some can only catalyse a subset of the individual modification steps, this leads effectively to the same kinetic asymmetry (Ortega et al., 2006; Conradi and Mincheva, 2014) as kinetic cooperativity. While oligomers might be particularly suited for this mechanism due to their symmetrical quaternary structure, bistability through multi-enzyme regulation could in principle arise in any multisite PTM system.

The relevance of these findings is that they significantly expand the range of contexts in which one should look for biochemical 'switches' as both homo-oligomerisation and multi-enzyme regulation are extremely common. Phosphatases, for example, are known to often act promiscuously on multiple substrates (Shi, 2009). As a consequence, many phosphorylation sites can be dephosphorylated by multiple phosphatases, creating potential situations in which bistability could occur. Alternatively, multi-enzyme regulation of the modification rather than demodification steps is also conceivable. Phosphorylating a protomer within a dimer, for example, could lead to a new binding site for a second kinase facilitating phosphorylation of the same residue in the other protomer. The combination of both mechanisms, oligomerisation and multi-enzyme regulation, therefore represents an interesting novel signalling motif that does not require feedback or kinetic cooperativity to generate bistable responses.

Other biologically relevant examples in which bistability are predicted to play important roles are small GTPase networks

(Barr, 2013; Conte-Zerial et al., 2008), some for which bistability has recently been demonstrated experimentally (Byrne et al., 2016; Bezeljak et al., 2020). Interestingly, many small GTPases homo-dimerise (Chen et al., 2016; Daitoku et al., 2001; Zhang and Zheng, 1998) and are typically inactivated (i.e. converted to the GDP-bound form) by multiple GTPase activating proteins (GAPs) (Müller and Goody, 2018; Lawson and Ridley, 2018). Thus, the motifs presented in this paper might plausibly cause or contribute to the emergence of bistability in small GTPase networks.

3.4. Conclusion

We have demonstrated that homo-oligomers, making up approximately 30–50% of the proteome (Lynch, 2012; Marsh and Teichmann, 2015), offer an even greater variety of regulatory mechanisms than previously appreciated. Since two thirds of all enzymes homo-oligomerise (Marianayagam et al., 2004) and since about 44% of homo-oligomers are involved in signal transduction (Fig. S5), these mechanisms could be relevant to many cellular signalling pathways. Furthermore, it may partly explain why homo-oligomerisation is so commonly found throughout evolution. Hopefully, the presented findings will be helpful to modellers interested in homo-oligomeric signalling proteins and stimulate experimental research into signalling processes to which the presented findings might apply. [Supplementary section 7](#) provides an overview of techniques and suggested experimental designs that could be deployed to test presented predictions.

4. Methods

Details on the computational procedures can be found in the [Supplementary material](#).

Competing Interests

The author has no competing interests to declare.

CRediT authorship contribution statement

Daniel Koch: Conceptualization, Investigation, Formal analysis, Writing - original draft.

Acknowledgements

I thank Thomas Kampourakis, Stephen Martin, Franca Fraternali and Petra Göbbels for helpful discussions and critical reading of the manuscript and Brian Ingalls for his excellent textbook and general modelling advice. I would like to thank Joseph Ng for the bioinformatic estimation of the fraction of oligomeric signalling proteins and an anonymous referee for constructive criticism. I acknowledge the British Heart Foundation for financial support (PhD studentship, grant [FS/17/65/33481]).

Appendix A. Supplementary material

Supplementary material associated with this article can be found, in the online version, at <https://doi.org/10.1016/j.jtbi.2020.110305>.

References

- Ali, M.H., Imperiali, B., 2005. Protein oligomerization: how and why. *Bioorg. Med. Chem.* 13 (17), 5013–5020. URL: <http://www.sciencedirect.com/science/article/pii/S0968089605004748>.
- Barr, F.A., 2013. Rab GTPases and membrane identity: causal or inconsequential?. *J. Cell Biol.* 202 (2), 191–199. <https://doi.org/10.1083/jcb.201306010>.
- Bezeljak, U., Loya, H., Kaczmarek, B., Saunders, T.E., Loose, M., 2020. Stochastic activation and bistability in a Rab GTPase regulatory network. *PNAS*. URL: <https://www.pnas.org/content/early/2020/03/10/1921027117>.
- Bouhaddou, M., Birtwistle, M.R., 2014. Dimerization-based control of cooperativity. *Mol. BioSyst.* 10 (7), 1824–1832. URL: <https://pubs.rsc.org/en/content/articlelanding/2014/mb/c4mb00022f>.
- Buchler, N.E., Louis, M., 2008. Molecular titration and ultrasensitivity in regulatory networks. *J. Mol. Biol.* 384 (5), 1106–1119. URL: <https://linkinghub.elsevier.com/retrieve/pii/S0022283608012485>.
- Byrne, K.M., Monsefi, N., Dawson, J.C., Degasperis, A., Bukowski-Wills, J.-C., Volinsky, N., Dobrzyński, M., Birtwistle, M.R., Tsyganov, M.A., Kiyatkin, A., Kida, K., Finch, A.J., Carragher, N.O., Kolch, W., Nguyen, L.K., von Kriegsheim, A., Kholodenko, B.N., 2016. Bistability in the Rac1, PAK, and RhoA signaling network drives actin cytoskeleton dynamics and cell motility switches. *Cell Syst.* 2 (1), 38–48. URL: [http://www.cell.com/cell-systems/abstract/S2405-4712\(16\)00004-1](http://www.cell.com/cell-systems/abstract/S2405-4712(16)00004-1).
- Cannon, W.B., 1929. Organization for physiological homeostasis. *Physiol. Rev.* 9 (3), 399. URL: <http://physrev.physiology.org/content/9/3/399.abstract>.
- Chen, M., Peters, A., Huang, T., Nan, X., 2016. Ras dimer formation as a new signaling mechanism and potential cancer therapeutic target. *Mini. Rev. Med. Chem.* 16, 391–403. URL: <http://www.eurekaselect.com/135447/article>.
- Comradi, C., Mincheva, M., 2014. Catalytic constants enable the emergence of bistability in dual phosphorylation. *J. R. Soc. Interface* 11 (95), 20140158. URL: <https://royalsocietypublishing.org/doi/full/10.1098/rsif.2014.0158>.
- Conte-Zerial, P.D., Bruschi, L., Rink, J.C., Collinet, C., Kalaidzidis, Y., Zerial, M., Deutsch, A., 2008. Membrane identity and GTPase cascades regulated by toggle and cut-out switches. *Mol. Syst. Biol.* 4 (1), 206. URL: <http://msb.embopress.org/content/4/1/206>.
- Daitoku, H., Isida, J., Fujiwara, K., Nakajima, T., Fukamizu, A., 2001. Dimerization of small GTPase Rab5. *Int. J. Mol. Med.* 8 (4), 397–404. URL: <http://www.spandidos-publications.com/10.3892/ijmm.8.4.397/abstract>.
- Ferrell Jr, J.E., Ha, S.H., 2014. Ultrasensitivity part II: multisite phosphorylation, stoichiometric inhibitors, and positive feedback. *Trends Biochem. Sci.* 39 (11), 556–569. URL: <http://www.sciencedirect.com/science/article/pii/S0968000414001698>.
- Frieden, C., 2019. Protein oligomerization as a metabolic control mechanism: application to apoE. *Protein Sci.* 28 (4), 837–842. URL: <https://onlinelibrary.wiley.com/doi/abs/10.1002/pro.3583>.
- Furuuchi, K., Berezov, A., Kumagai, T., Greene, M.I., 2007. Targeted antireceptor therapy with monoclonal antibodies leads to the formation of inactivated tetrameric forms of ErbB receptors. *J. Immunol.* 178 (2), 1021–1029. URL: <https://www.jimmunol.org/content/178/2/1021>.
- Gan, H.K., Walker, F., Burgess, A.W., Rigopoulos, A., Scott, A.M., Johns, T.G., 2007. The epidermal growth factor receptor (EGFR) tyrosine kinase inhibitor AG1478 increases the formation of inactive untethered EGFR dimers. *J. Biol. Chem.* 282 (5), 2840–2850. URL: <http://www.jbc.org/content/282/5/2840>.
- Goldbeter, A., Koshland, D.E., 1981. An amplified sensitivity arising from covalent modification in biological systems. *PNAS* 78 (11), 6840–6844. URL: <http://www.pnas.org/content/78/11/6840>.
- Hlavacek, W.S., Faeder, J.R., Blinov, M.L., Perelson, A.S., Goldstein, B., 2003. The complexity of complexes in signal transduction. *Biotechnol. Bioeng.* 84 (7), 783–794. <https://doi.org/10.1002/bit.10842>.
- Hsu, C., Jaquet, V., Gencoglu, M., Becskei, A., 2016. Protein dimerization generates bistability in positive feedback loops. *Cell Rep.* 16 (5), 1204–1210. URL: <http://www.sciencedirect.com/science/article/pii/S2211124716308415>.
- Ingalls, B., 2013. *Mathematical Modelling in Systems Biology: An Introduction*. MIT Press, Cambridge MA.
- Kanno, D.M., Levitus, M., 2014. Protein oligomerization equilibria and kinetics investigated by fluorescence correlation spectroscopy: a mathematical treatment. *J. Phys. Chem. B* 118 (43), 12404–12415. URL: <http://pubs.acs.org/doi/10.1021/jp507741r>.
- Keshet-Edelstein, L., 2005. *Mathematical Models in Biology*. SIAM, Philadelphia.
- Klemm, J.D., Schreiber, S.L., Crabtree, G.R., 1998. Dimerization as a regulatory mechanism in signal transduction. *Annu. Rev. Immunol.* 16 (1), 569–592. <https://doi.org/10.1146/annurev.immunol.16.1.569>.
- Klipp, E., Herwig, R., Kowald, A., Wierling, C., Lehrach, H., 2005. *Systems Biology in Practice*. Wiley-VCH, Weinheim.
- Kozer, N., Barua, D., Orchard, S., Nice, E.C., Burgess, A.W., Hlavacek, W.S., Clayton, A.H.A., 2013. Exploring higher-order EGFR oligomerisation and phosphorylation – a combined experimental and theoretical approach. *Mol. BioSyst.* 9 (7), 1849–1863. URL: <https://pubs.rsc.org/en/content/articlelanding/2013/mb/c3mb70073a>.
- Lawson, C.D., Ridley, A.J., 2018. Rho GTPase signaling complexes in cell migration and invasion. *J. Cell Biol.* 217 (2), 447–457. URL: <http://www.jcb.org/lookup/doi/10.1083/jcb.201612069>.
- Lynch, M., 2012. The evolution of multimeric protein assemblages. *Mol. Biol. Evol.* 29 (5), 1353–1366. URL: <https://academic.oup.com/mbe/article/29/5/1353/1034121>.
- Marianayagam, N.J., Sunde, M., Matthews, J.M., 2004. The power of two: protein dimerization in biology. *Trends Biochem. Sci.* 29 (11), 618–625. URL: <http://linkinghub.elsevier.com/retrieve/pii/S0968000404002348>.
- Markevich, N.I., Hoek, J.B., Kholodenko, B.N., 2004. Signaling switches and bistability arising from multisite phosphorylation in protein kinase cascades. *J. Cell Biol.* 164 (3), 353–359. URL: <http://www.jcb.org/lookup/doi/10.1083/jcb.200308060>.

- Marsh, J.A., Teichmann, S.A., 2015. Structure, dynamics, assembly, and evolution of protein complexes. *Annu. Rev. Biochem.* 84 (1), 551–575. <https://doi.org/10.1146/annurev-biochem-060614-034142>.
- Matthews, J.M., Sunde, M., 2012. Dimers, oligomers, everywhere. In: Matthews, J.M. (Ed.), *Protein Dimerization and Oligomerization in Biology*, vol. 747. Springer, New York, pp. 1–18. https://doi.org/10.1007/978-1-4614-3229-6_5.
- Müller, M.P., Goody, R.S., 2018. Molecular control of Rab activity by GEFs, GAPs and GDI. *Small GTPases* 9 (1–2), 5–21. <https://doi.org/10.1080/21541248.2016.1276999>.
- Murray, J.D., 2002. *Mathematical Biology, I. An Introduction*. Springer, Berlin Heidelberg.
- Ortega, F., Garcés, J.L., Mas, F., Kholodenko, B.N., Cascante, M., 2006. Bistability from double phosphorylation in signal transduction. *FEBS J.* 273 (17), 3915–3926. <https://doi.org/10.1111/j.1742-4658.2006.05394.x>.
- Parsons, E.S., Stanley, G.J., Pyne, A.L.B., Hodel, A.W., Nievergelt, A.P., Menny, A., Yon, A.R., Rowley, A., Richter, R.P., Fantner, G.E., Bubeck, D., Hoogenboom, B.W., 2019. Single-molecule kinetics of pore assembly by the membrane attack complex. *Nat. Commun.* 10 (1), 2066. URL: <https://www.nature.com/articles/s41467-019-10058-7>.
- Powers, E.T., Powers, D.L., 2003. A Perspective on Mechanisms of Protein Tetramer Formation. *Biophys. J.* 85 (6), 3587–3599. URL: <http://www.sciencedirect.com/science/article/pii/S0006349503747778>.
- Rajagopalan, S., Huang, F., Fersht, A.R., 2011. Single-Molecule characterization of oligomerization kinetics and equilibria of the tumor suppressor p53. *Nucleic Acids Res.* 39 (6), 2294–2303. URL: <https://www.ncbi.nlm.nih.gov/pmc/articles/PMC3064802/>.
- Salazar, C., Höfer, T., 2006. Competition effects shape the response sensitivity and kinetics of phosphorylation cycles in cell signaling. *Ann. N. Y. Acad. Sci.* 1091 (1), 517–530. <https://doi.org/10.1196/annals.1378.093>.
- Salazar, C., Höfer, T., 2009. Multisite protein phosphorylation – from molecular mechanisms to kinetic models. *FEBS J.* 3177–3198 <https://doi.org/10.1111/j.1742-4658.2009.07027.x>.
- Schäuble, S., Stavrum, A.K., Puntervoll, P., Schuster, S., Heiland, I., 2013. Effect of substrate competition in kinetic models of metabolic networks. *FEBS Lett.* 587 (17), 2818–2824. URL: <http://www.sciencedirect.com/science/article/pii/S0014579313004833>.
- Selwood, T., Jaffe, E.K., 2012. Dynamic dissociating homo-oligomers and the control of protein function. *Arch. Biochem. Biophys.* 519 (2), 131–143. URL: <http://www.sciencedirect.com/science/article/pii/S0003986111003948>.
- Shi, Y., 2009. Serine/threonine phosphatases: mechanism through structure. *Cell* 139 (3), 468–484. URL: <http://www.sciencedirect.com/science/article/pii/S0092867409012549>.
- Sonnen, K.F., Aulehla, A., 2014. Dynamic signal encoding – from cells to organisms. *Semin. Cell. Dev. Biol.* 34, 91–98. URL: <http://www.sciencedirect.com/science/article/pii/S108495211400192X>.
- Stefan, M.L., Bartol, T.M., Sejnowski, T.J., Kennedy, M.B., 2014. Multi-state modeling of biomolecules. *PLoS Comput. Biol.* 10, (9). <https://doi.org/10.1371/journal.pcbi.1003844> e1003844.
- Thomson, M., Gunawardena, J., 2009. Unlimited multistability in multisite phosphorylation systems. *Nature* 460 (7252), 274–277. URL: <https://www.nature.com/articles/nature08102>.
- Tyson, J.J., Chen, K.C., Novak, B., 2003. Sniffers, buzzers, toggles and blinkers: dynamics of regulatory and signaling pathways in the cell. *Curr. Opin. Cell Biol.* 15 (2), 221–231. URL: <http://www.sciencedirect.com/science/article/pii/S0955067403000176>.
- Vera, J., Millat, T., Kolch, W., Wolkenhauer, O., 2008. Dynamics of receptor and protein transducer homodimerisation. *BMC Syst. Biol.* 2 (1), 92. <https://doi.org/10.1186/1752-0509-2-92>.
- Voit, E.O., 2012. *A First Course in Systems Biology*. Garland Science, New York.
- Zhang, B., Zheng, Y., 1998. Negative regulation of rho family GTPases Cdc42 and Rac2 by homodimer formation. *J. Biol. Chem.* 273 (40), 25728–25733. URL: <http://www.jbc.org/content/273/40/25728>.

Chapter 6

Molecular noise filtering in the β -adrenergic signalling network by phospholamban pentamers

In this chapter, the theoretical findings from the previous chapter are applied to the PLN sub-network of the β -adrenergic signalling pathway in order to explore the function of phospholamban pentamers. The chapter consists of the research paper “Molecular noise filtering in the β -adrenergic signaling network by phospholamban pentamers” published in the journal *Cell Reports*. The supplementary material for this study can be found in [chapter A5.2](#).

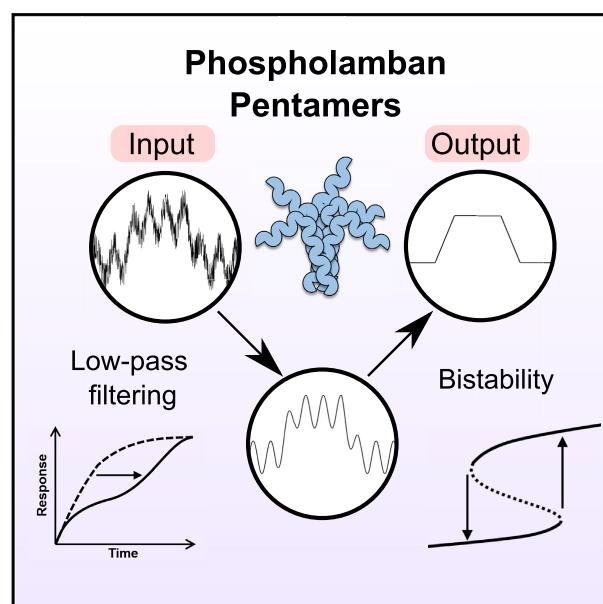
The authors contributed to this work as follows: The project was conceived and designed by me. I developed all models and analyses presented in this chapter and did most experiments. Dr Alexander Alexandrovich helped me over multiple weeks to express and purify recombinant inhibitor-1 and PP1. Interestingly, the Mn^{2+} -ion in the active site of PP1, which is necessary to purify PP1 from *E. coli*, enables this phosphatase to dephosphorylate and thus inactive inhibitor-1 after activation by PKA (data not shown). Attempts to resolve this unphysiological *in vitro* issue using other metal ions (Fe^{2+} , Zn^{2+}) for PP1 purification were unsuccessful. This prevented us to test the model predictions shown in Figure 4. Dr Florian Funk performed the dose-response experiments shown in Figure S3B of [chapter A5.2](#). Dr Ay Lin Kho helped me with the cardiomyocyte cell culture and to perform the hysteresis experiments shown in Figure 5C.

As the motivation and the aims and objectives for this project have already been laid out in [section 1.6](#) and [section 1.8](#), the paper follows without further introduction.

Cell Reports

Molecular noise filtering in the β -adrenergic signaling network by phospholamban pentamers

Graphical abstract



Authors

Daniel Koch, Alexander Alexandrovich, Florian Funk, Ay Lin Kho, Joachim P. Schmitt, Mathias Gautel

Correspondence

dkoch.research@protonmail.com

In brief

While phosphorylation of phospholamban (PLN) is crucial to improve heart function during the β -adrenergic “fight-or-flight” response, the role of PLN pentamers in this context is unclear. By integrating mathematical and experimental approaches, Koch et al. find that PLN pentamers provide complex information-processing capabilities to ensure a consistent phosphorylation response.

Highlights

- A dynamical systems model of the PLN signaling network is developed
- PLN pentamers enable low-pass filtering (LPF) by competing with PLN monomers
- PLN pentamers promote the emergence of bistable PLN phosphorylation
- LPF and bistability filter out simulated signal noise in the β -adrenergic pathway



Koch et al., 2021, Cell Reports 36, 109448
July 27, 2021 © 2021 The Authors.
<https://doi.org/10.1016/j.celrep.2021.109448>



Article

Molecular noise filtering in the β -adrenergic signaling network by phospholamban pentamersDaniel Koch,^{1,3,*} Alexander Alexandrovich,¹ Florian Funk,² Ay Lin Kho,¹ Joachim P. Schmitt,² and Mathias Gautel¹¹Randall Centre for Cell and Molecular Biophysics, King's College London, SE1 1UL London, UK²Institute of Pharmacology and Clinical Pharmacology, and Cardiovascular Research Institute Düsseldorf (CARID), University Hospital Düsseldorf, 40225 Düsseldorf, Germany³Lead contact*Correspondence: dkoch.research@protonmail.com<https://doi.org/10.1016/j.celrep.2021.109448>**SUMMARY**

Phospholamban (PLN) is an important regulator of cardiac calcium handling due to its ability to inhibit the calcium ATPase SERCA. β -Adrenergic stimulation reverses SERCA inhibition via PLN phosphorylation and facilitates fast calcium reuptake. PLN also forms pentamers whose physiological significance has remained elusive. Using mathematical modeling combined with biochemical and cell biological experiments, we show that pentamers regulate both the dynamics and steady-state levels of monomer phosphorylation. Substrate competition by pentamers and a feed-forward loop involving inhibitor-1 can delay monomer phosphorylation by protein kinase A (PKA), whereas cooperative pentamer dephosphorylation enables bistable PLN steady-state phosphorylation. Simulations show that phosphorylation delay and bistability act as complementary filters that reduce the effect of random fluctuations in PKA activity, thereby ensuring consistent monomer phosphorylation and SERCA activity despite noisy upstream signals. Preliminary analyses suggest that the PLN mutation R14del could impair noise filtering, offering a new perspective on how this mutation causes cardiac arrhythmias.

INTRODUCTION

Calcium (Ca^{2+}) currents determine contraction and relaxation of the heart at the cellular level: high Ca^{2+} concentrations enable sarcomeric contraction, whereas low Ca^{2+} concentrations lead to relaxation (Bers, 2002; Eisner et al., 2017). These currents are controlled by the release and reuptake of calcium from and into the sarcoplasmic reticulum (SR), the major storage compartment for intracellular Ca^{2+} . At the molecular level, dozens of proteins regulate Ca^{2+} -handling and excitation-contraction coupling (Bers, 2008). The Ca^{2+} pump sarco/endoplasmic reticulum Ca^{2+} -ATPase (SERCA) mediates ~70%–90% of the Ca^{2+} reuptake into the SR and therefore induces relaxation of the cardiomyocyte (Bers, 2002; MacLennan and Kranias, 2003). SERCA function is inhibited by phospholamban (PLN), a 52-amino acid protein resident in the SR membrane. Phosphorylation of PLN at Ser16 by protein kinase A (PKA) reverses SERCA inhibition in response to β -adrenergic stimulation, thereby accelerating Ca^{2+} removal and cardiomyocyte relaxation (Tada et al., 1975; Kranias and Solaro, 1982; Lindemann et al., 1983; MacLennan and Kranias, 2003; Kranias and Hajjar, 2012). This constitutes an important mechanism to adapt cardiac output to increasing demand and is an integral part of the β -adrenergic “fight-or-flight” response (Simmerman and Jones, 1998; MacLennan and Kranias, 2003; Kranias and Hajjar, 2012). Disruptions in

this part of the β -adrenergic signaling network can have drastic consequences. Multiple mutations in the PLN gene have been discovered in the past two decades, most of which cause severe forms of cardiomyopathy and lead to cardiac arrhythmias or heart failure (Schmitt et al., 2003, 2009; Haghghi et al., 2006; Medeiros et al., 2011; Yost et al., 2019).

In spite of the progress in understanding the structure and function of PLN, many aspects of this protein are still poorly understood and specific therapeutic approaches to manipulate the PLN signaling network are lacking. One of the less-well-understood aspects is the assembly of PLN into homo-pentamers (Wegener and Jones 1984). Although their pinwheel-like structure in lipid environments (Verardi et al., 2011) yields intuitive plausibility to early conjectures and data suggesting that pentameric PLN acts as an ion channel (Kovacs et al., 1988; Smeazzetto et al., 2016), this hypothesis has been contested by multiple experimental, structural, and theoretical studies (Maffeo and Aksimentiev, 2009; Becucci et al., 2009; Vostrikov et al., 2013). Since an artificial monomeric PLN mutant was found to be a similarly potent SERCA inhibitor as wild-type PLN (Kimura et al., 1997), the prevailing paradigm considers pentamers to be a biologically inactive storage form (MacLennan and Kranias, 2003; Becucci et al., 2009; Kranias and Hajjar, 2012). Increasing evidence suggests, however, that PLN pentamers are not entirely passive and influence cardiomyocyte contractility and PLN



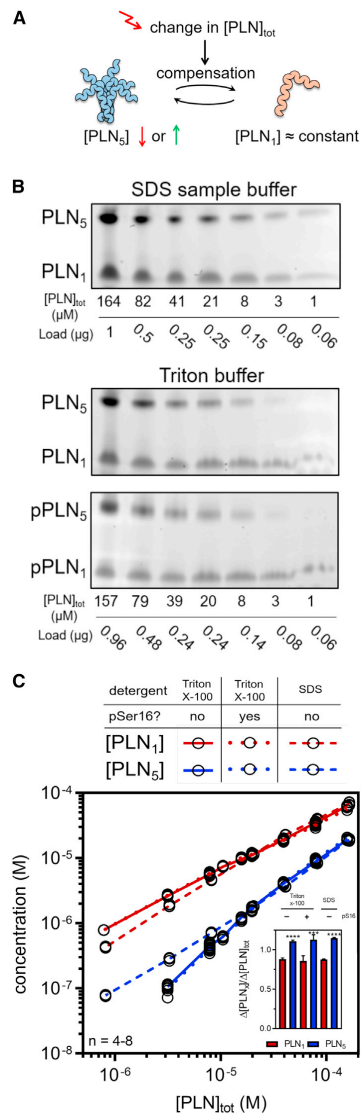


Figure 1. *In vitro* oligomerization
(A) In the prevailing paradigm, pentamers buffer the PLN monomer concentration by compensating changes via association or dissociation.
(B and C) Oligomeric state of PLN in SDS sample or Triton X-100-based buffer (TBB) at different total protein concentrations after dilution.
(B) Oriole-stained gels after semi-native SDS-PAGE.
(C) Quantified monomers and pentamers at different total concentrations. Inset: relative change in monomers and pentamers when comparing the highest 2 total concentrations. *** $p < 0.001$, **** $p < 0.0001$ versus monomers.

phosphorylation dynamics (Colyer, 1993; Chu et al., 1998; Wittmann et al., 2015; Glaves et al., 2019). Vostrikov et al. (2013) proposed that pentamers could act as buffers that fine-tune SERCA regulation via monomeric PLN by keeping it within a physiological window. However, it is not obvious exactly what benefit pentamerization contributes, given that SERCA activity can already be controlled by regulating expression levels and by multiple post-translational modifications of both PLN and SERCA (McTiernan et al., 1999; Stammers et al., 2015; MacLennan and Kranias, 2003). The specific physiological advantage of pentamerization and its role in the pathophysiology of PLN mutations thus remains elusive.

In the present study, we investigated the role of pentamers in the PLN regulatory network. We found that pentamers have only a limited capacity to buffer the concentration of monomeric PLN *in vitro* since the effect is slow and moderate. Based on the hypothesis that the function of pentameric PLN exceeds monomer buffering, we developed a mathematical model of the PLN regulatory network to study the role of pentamers in the context of β -adrenergic stimulation from a dynamical systems perspective. Our results indicate that pentamers are molecular noise filters to ensure consistent PLN phosphorylation in response to noisy β -adrenergic stimulation. A preliminary analysis of the arrhythmic mutation R14del suggests that this mutation could impair noise filtering, indicating that molecular noise filtering in the β -adrenergic signaling network could be important to prevent cardiac arrhythmias.

RESULTS

Pentamers are moderate and slow monomer buffers *in vitro*

The predominant paradigm is that PLN pentamers are a storage or buffering reservoir for monomers (Figure 1A) (MacLennan and Kranias, 2003; Becucci et al., 2009; Kranias and Hajjar, 2012; Vostrikov et al., 2013). The oligomeric state of PLN in tissue or cell homogenates is typically assessed from samples in SDS sample buffer, which does not interfere with oligomerization. However, SDS is a harsh anionic detergent that interferes with the function of many other proteins. We therefore studied PLN oligomerization in both SDS sample buffer and a Triton X-100 based buffer (TBB) at physiological pH and ionic strength, which effectively solubilizes PLN and allows for rapid phosphorylation of PLN at Ser16 by PKA.

To test the hypothesis that PLN pentamers buffer monomer concentration, we analyzed the oligomeric state of PLN (unphosphorylated and phosphorylated) by semi-native SDS-PAGE at various total PLN concentrations after dilution and 2 h of equilibration (Figure 1B). As shown in Figure 1C, the slope of pentameric PLN in TBB is steeper than the slope of monomeric PLN (particularly at low total concentrations), suggesting that changes in total PLN concentration have a larger effect on pentameric than on monomeric PLN. In contrast to the experiments in TBB, pentameric PLN appears not to dissociate upon dilution in SDS sample buffer. In the likely region of physiological PLN concentrations at the SR ($>50 \mu\text{M}$; Star Methods table: review protein concentrations), the change in monomers relative to the change in total PLN is slightly lower than for pentamers,

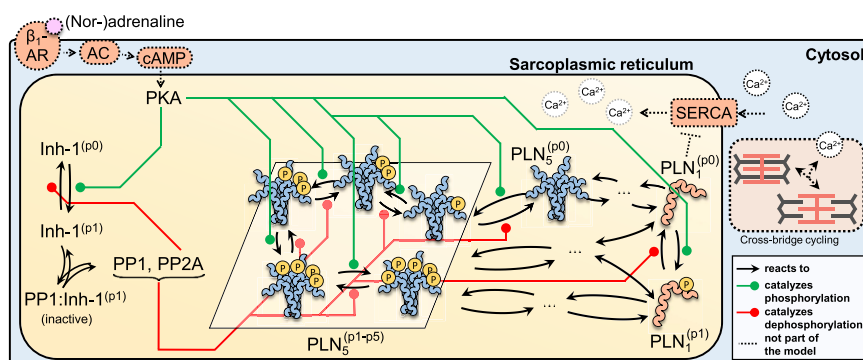


Figure 2. Simplified model scheme

The depicted signaling network controls SERCA activity in response to β -adrenergic stimulation via regulation of PLN phosphorylation. The model captures all of the processes immediately involved in regulating PLN phosphorylation at Ser16. To simplify the scheme, the different oligomerization routes of phosphorylated and unphosphorylated PLN are not shown. See [Method details](#) for model equations and parameter values and [Figure S12A](#) for the complete model scheme.

indicating that pentamers can buffer the concentration of monomers (Figure 1C, inset). However, we found that pentamers dissociate only slowly, with an apparent mean lifetime (k_{obs}^{-1}) of 11.4 min for pentamers (Figure S1A), in good agreement with previous live-cell measurements (Robia et al., 2007). We concluded that under the investigated *in vitro* conditions, PLN pentamers buffer the concentration of PLN monomers only moderately and slowly. We thus hypothesized that PLN pentamers may play further roles.

On a site note, we observed no increased pentamerization upon phosphorylation of PLN in TBB (Figures 1B, 1C, and S1B). The increase in pentamerization upon phosphorylation is sometimes called the dynamic equilibrium of PLN and while its biological significance is unclear, it has been speculated that it might contribute to SERCA regulation (Cornea et al., 1997; Hou et al., 2008; Kranias and Hajjar, 2012). Interestingly, we observed a significant increase in pentamerization after diluting PLN phosphorylated in TBB with SDS sample buffer (Figure S8E), indicating that the effect relies on anionic environments.

A mathematical model of the PLN regulatory network

Mathematical modeling has been paramount to understand the non-linear behavior of signaling networks and how they regulate cellular activities including growth, differentiation, apoptosis, and motility. PLN is also part of a complex signaling network involving multiple kinases, phosphatases, and regulatory complexes, a network that so far remained largely unexplored by mathematical approaches. Although a PLN submodule is part of several models of cardiac Ca^{2+} cycling (Bugenhagen and Beard, 2015) or β -adrenergic signal transduction (Saucerman et al., 2003), no mathematical model has, to our knowledge, considered PLN pentamers or provided a detailed analysis of the network immediately implicated in regulating PLN. Aiming to fill this gap, we set out to develop a mathematical model of the PLN network to study its functionality and the role of pentamers in the context of β -adrenergic stimulation from a dynamical systems perspective.

We began model development by considering several possible models of how PLN forms pentamers and calibrated them using our dilution and dissociation time course data. We found that a model following a monomer \rightarrow dimer \rightarrow tetramer \rightarrow pentamer pathway shows good agreement with our experimental data and outperforms other model variants (see [STAR Methods](#) section “Development of the mathematical model” and Figures S9 and S10). We extended the PLN oligomerization model by including key proteins and reactions of the β -adrenergic signal transduction network involved in regulating the phosphorylation of PLN at Ser16. We accounted for reactions and enzymes responsible for addition (PKA) and removal of the Ser16 phosphate group (phosphatases PP1 and PP2A) (MacDougall et al., 1991; MacLennan and Kranias, 2003). Dephosphorylation of PLN pentamers has been shown to exhibit strong positive cooperativity (Li et al., 1990). Since PP1 is the main phosphatase for reversing Ser16 phosphorylation of PLN (MacDougall et al., 1991; Steenaert et al., 1992), we assumed that the catalytic turnover for dephosphorylation of pentameric PLN by PP1 increases with fewer phosphate groups left on a pentamer. We implemented this assumption by introducing dimensionless parameters ϕ and γ for tuning individual steps of pentamer dephosphorylation by PP1 (Figure S12C). We also included the regulation of PP1 by inhibitor-1 as described in Saucerman et al. (2003). Inhibitor-1 can bind and inhibit PP1 when phosphorylated by PKA at Thr35, whereas phosphorylation at this site is reversed by PP2A (Kranias and Hajjar, 2012; Saucerman et al., 2003). To keep our analysis focused on the regulation of PLN phosphorylation in the context of β -adrenergic stimulation, we treated the concentration of active PKA at the SR as a model input parameter and omitted processes upstream of PKA (e.g., cAMP production and degradation) and downstream of PLN (e.g., SERCA activity, Ca^{2+} handling). Due to the lack of mechanistic and kinetic data, we did not include (de-)phosphorylation of PLN at Ser10 or Thr17.

Figure 2 shows a simplified scheme of the biochemical reactions included in our model. The model comprises 60

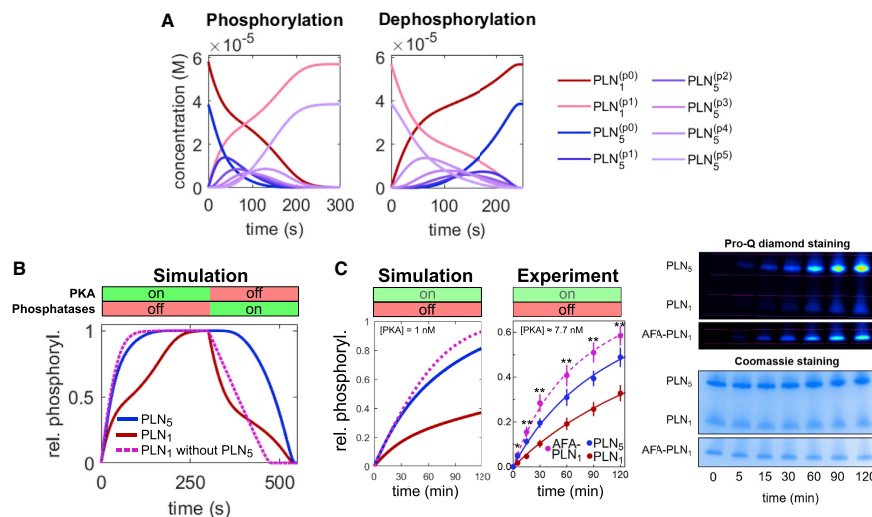


Figure 3. Regulation of phosphorylation dynamics by PLN pentamers

(A) Time course simulations of PLN phosphorylation by 0.1 μ M PKA in the absence of phosphatases (left) and dephosphorylation of completely phosphorylated PLN by PP1 and PP2A in the absence of PKA (right).
 (B) Dynamics of relative phosphorylation levels in a sequential phosphorylation/dephosphorylation simulation in the presence or absence of pentameric PLN.
 (C) Simulated and experimental phosphorylation time course of wild-type PLN ($[\text{PLN}_{\text{tot}}] \approx 157 \mu\text{M}$, at which $[\text{PLN}_1] \approx 52 \mu\text{M}$) and monomeric AFA-PLN₁ ($\approx 52 \mu\text{M}$). A low PKA concentration was chosen to slow down the reaction for easier sampling. Data represent means \pm SEMs. * $p < 0.05$, ** $p < 0.01$, AFA-PLN₁ versus PLN₁.

biochemical reactions between 20 molecular species that are described by a set of 17 ordinary differential and 3 algebraic equations. The additional protein concentrations and model parameters not determined by our own data are based on experimental measurements from the literature.

A more detailed description of how the model was formulated can be found in the [Method details](#) section along with the model equations and parameter values. Having a mathematical description of the processes that regulate PLN phosphorylation at our disposal, we set out to explore the behavior of our model.

Pentamers and the inhibitor-1 feedforward loop delay monomer phosphorylation

In a first simulation, we studied the dynamics of PLN monomer and pentamer phosphorylation by PKA in the absence of phosphatases (Figure 3A, left). The phosphorylation of monomers resembles a hyperbola but features a kink in the middle. Pentamer phosphorylation, however, exhibits dynamics typical for multi-site phosphorylation systems with transient waves of incompletely phosphorylated intermediate forms. Next, we simulated the dephosphorylation of completely phosphorylated PLN in the absence of PKA (Figure 3A, right). As expected, dephosphorylation resembles the phosphorylation dynamics but in reverse order. As expected from the implemented cooperativity of PP1, the accumulation of unphosphorylated pentamers is more abrupt.

To simplify the plots, we decided to focus on relative PLN phosphorylation for the remainder of this study. Interestingly, re-plotting the data from the phosphorylation time course simulations reveals that relative phosphorylation of monomers significantly lags behind the relative phosphorylation of pentamers (Figure 3B). A likely explanation for this delay could be that monomers and pentamers compete against one another as PKA substrates. Performing the same simulation without pentamers but at an equimolar monomer concentration abolishes delayed phosphorylation, confirming that the lag is caused by competing PLN pentamers (Figure 3B, dotted line). Parameters that increase substrate competition or, surprisingly, slow down pentamer phosphorylation, can increase this delay (Figure S2A).

To test the predicted delay experimentally, we carried out PKA-phosphorylation time course experiments using wild-type PLN and AFA-PLN (an artificial monomeric mutant) at equimolar monomer concentrations. In agreement with the simulations, we found monomer phosphorylation to be significantly delayed in the presence of pentamers (Figure 3C).

Substrate competition is not the only network motif able to delay the response to a stimulus. Interestingly, the PLN network contains a second motif with such ability: the inhibition of PP1 by PKA via the phosphorylation of inhibitor-1 constitutes a subgraph that can be described as an elongated version of a coherent type 4 feed-forward loop (FFL) able to cause delays (Figure 4A) (Mangan and Alon, 2003). Simulations show that inhibitor-1 can delay the phosphorylation of PLN monomers and

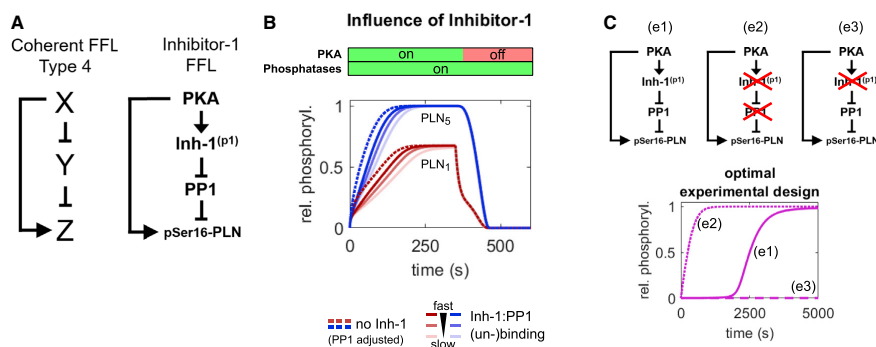


Figure 4. Regulation of phosphorylation dynamics by inhibitor-1
 (A) Left: coherent feed-forward loop (FFL) type 4 in which the full response of Z is delayed until the inhibitory effect of Y is revoked by X. Right: structure of the inhibitor-1 FFL.
 (B) Influence of the inhibitor-1 FFL in simulations of PLN phosphorylation by PKA in the presence of PP1. To ensure equal steady-state phosphatase activity in the absence of inhibitor-1, PP1 levels have been adjusted by the amount in complex with inhibitor-1 in presence of PKA at steady state in the full model.
 (C) Optimal experimental design and controls for detecting PLN phosphorylation delay by the inhibitor-1 FFL is given by $[PKA] < [PP1] < [Inh-1]$ and indicated knockout versions of the FFL.

pentamers if the binding of phosphorylated inhibitor-1 to PP1 is not too fast (Figure 4B). Reducing the PP1 concentration by the fraction that is inhibited by inhibitor-1 at steady state in the presence of PKA and repeating the simulation in the absence of inhibitor-1 shows that PLN phosphorylation approaches the same steady-state levels, but much faster (Figure 4B, dotted lines). For slower inhibitor-1 phosphorylation, the delay becomes more pronounced (Figure S2B). The delay can be uncoupled from pentamer competition by using monomeric AFA-PLN and maximized when $[PKA] < [PP1] < [Inh-1]$. When contrasted to knockout variants of the FFL, this yields an optimal design for future experimental testing of the predicted delay (Figure 4C).

In summary, our simulations predict the existence of two independent response delay elements in the PLN network: pentamers delaying the phosphorylation of monomers and an inhibitor-1 FFL delaying the phosphorylation of both monomers and pentamers.

Bistability in the steady-state phosphorylation of PLN

Mangan and Alon (2003) proposed that response delay elements may act as persistence sensors that reject short input stimuli. Before exploring what the physiological advantage of such persistence sensing in the context of β -adrenergic stimulation may be, we shall first consider how PLN phosphorylation is controlled at steady state.

Multisite phosphorylation systems can exhibit ultrasensitivity and bistability if there is sufficient kinetic asymmetry in the subsequent cycles of phosphorylation and dephosphorylation (e.g., due to cooperativity or multi-enzyme regulation) (Koch, 2020; Markevich et al., 2004). Since cooperativity is present in the dephosphorylation of pentameric PLN (Li et al., 1990), we wondered whether PLN phosphorylation may be bistable at some level of PKA activity. A hallmark of bistability is that the approached steady state depends on the system's history (hyster-

esis). We therefore performed several simulations with identical settings except for different initial levels of relative phosphorylation and found that PLN phosphorylation is indeed bistable at some PKA concentrations (Figure 5A). To better understand the steady-state phosphorylation of PLN, we generated bifurcation diagrams, which visualize how this non-linear system behavior depends on PKA concentration as a control parameter. We found that PLN phosphorylation increases in an abrupt, ultrasensitive fashion as it passes a threshold at approximately one-third of the maximum PKA concentration at the SR ($\approx 0.6 \mu\text{M}$; Saucerman et al., 2003; Figure 5B).

Since ultrasensitivity is considered a prerequisite and indication for bistability, we re-analyzed previous experimental dose-response data by fitting it to the Hill equation and found Hill exponents of ≈ 2 (Figure S3A). The data from Wittmann et al. (2015) suggest that this ultrasensitivity depends on the presence of pentamers (Figure S3A), likely due to the (pseudo-)multisite nature of pentamers (Koch, 2020). We were further able to replicate the ultrasensitive dose-response of PLN Ser16 phosphorylation in transfected HEK293 cells after PKA activation by forskolin (Figure S3B). Despite the experimental uncertainty in the value of the Hill exponents, the data together indicate some degree of ultrasensitivity in PLN phosphorylation. Since these data are based on the average response of the network across cells, it is possible that the Hill exponent at the single-cell level is even higher (Figure S3C).

Next, we sought to determine experimentally whether PLN phosphorylation in cardiomyocytes exhibits hysteresis as predicted by our model. This can be achieved by comparing the steady-state phosphorylation of pre-stimulated/non-pre-stimulated cells. Due to our simulations, we expected hysteresis to most likely occur slightly below but close to the region of highest dose sensitivity. Based on previous dose-response data ($EC_{50} \approx 5 \text{ nM}$ isoproterenol; Kuschel et al., 1999), we chose to test

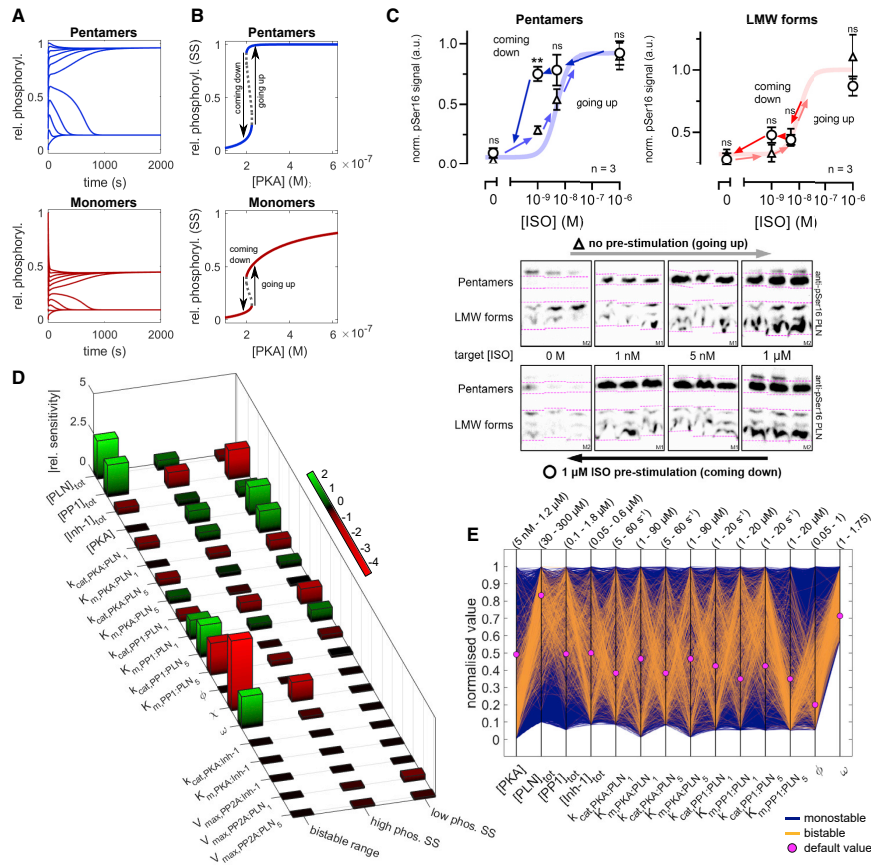


Figure 5. PLN phosphorylation at steady state

(A) Time course simulations with different initial levels of PLN phosphorylation show hysteresis ($[PKA] = 0.21 \mu M$).

(B) Bifurcation diagrams for relative phosphorylation of PLN monomers and pentamers show a bistable region of $\approx 0.025 \mu M$ range.

(C) Western blot analysis of PKA-dependent steady-state PLN phosphorylation confirms the predicted hysteresis in neonatal rat cardiomyocytes. Pre-stimulated cardiomyocytes were treated for 2 min with $1 \mu M$ isoproterenol before the concentration was lowered to the target isoproterenol concentration. Bands shown in logical order; only signals from the same membrane were compared (M1/M2 in bottom corner). Arrows indicate the direction of hysteresis loop. Data represent means \pm SEMs. $**p < 0.01$ pre-stimulated versus non-pre-stimulated.

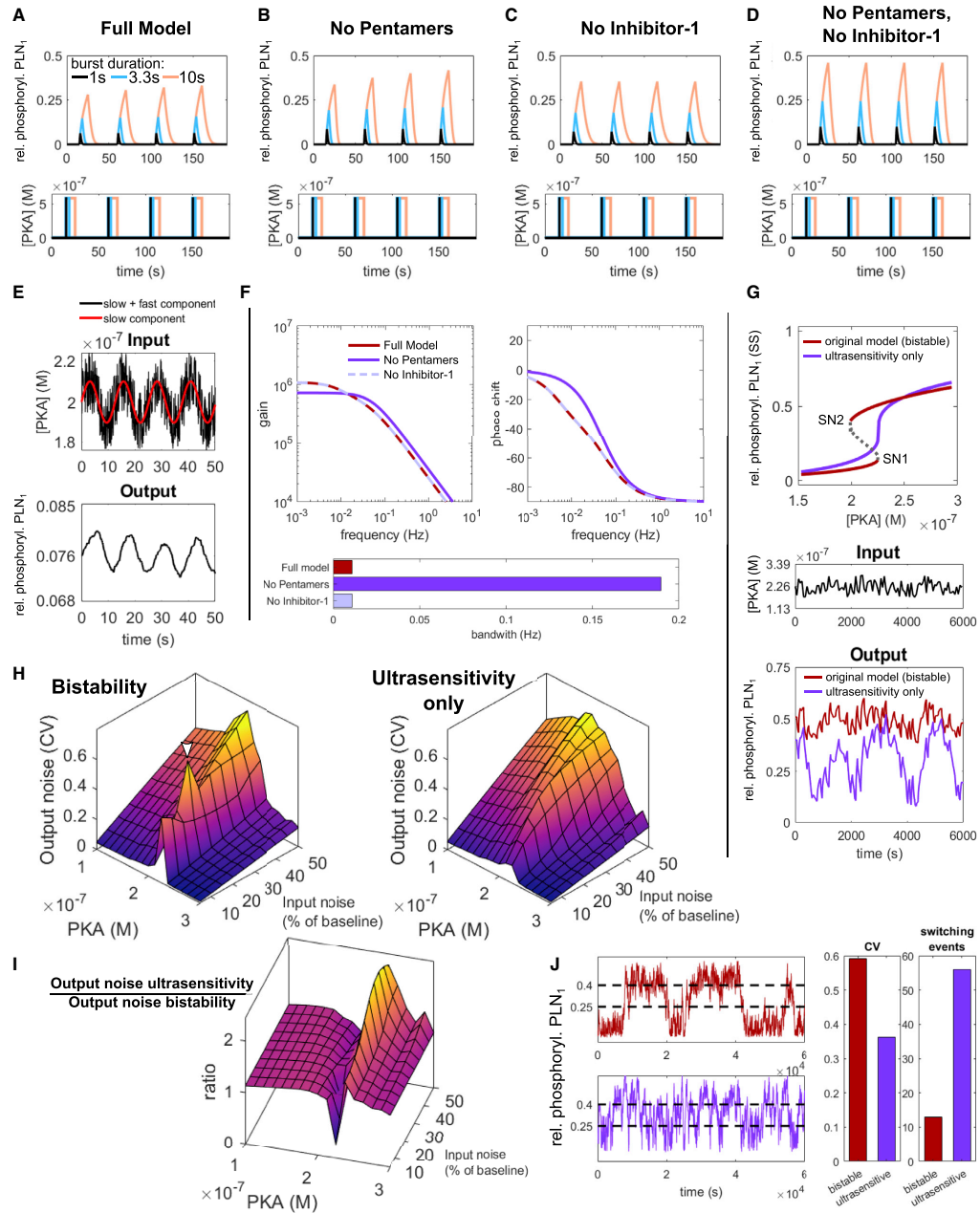
(D) Local sensitivity analysis of low phosphorylation steady state ($[PKA] = 0.13 \mu M$), high phosphorylation steady state ($[PKA] = 0.25 \mu M$), and the range of the bistable region. Relative sensitivities determined at $\Delta p = +1\%$ for high/low phosphorylation steady states and $\Delta p = +10\%$ for bistable range.

(E) Parallel coordinate plot of the model stability behavior for 10,000 random parameter sets.

for hysteresis in the steady-state phosphorylation of PLN at isoproterenol concentrations of 1 and 5 nM by western blotting. As shown in Figure 5C, we found pronounced hysteresis for pentamer steady-state phosphorylation at 1 nM isoproterenol. In contrast, no hysteresis was observed at 0 or $1 \mu M$ isoproterenol, demonstrating that hysteresis is specific to a region of criticality. Unfortunately, monomer bands were poorly separated from other small oligomeric forms and thus were summarized as low-molecular-weight (LMW) forms, but a significant difference

could not be observed. Taken together, our experimental results demonstrate that PLN phosphorylation is ultrasensitive and bistable.

To find out which model parameters exert the most control over PLN phosphorylation at steady state, we performed a local sensitivity analysis of relative monomer phosphorylation (Figure 5D). We found that the low phosphorylation state is generally more sensitive to parameter perturbations than the high phosphorylation state, but both are primarily controlled by



(legend on next page)

concentrations and catalytic constants of PKA and PP1. Parameters associated with inhibitor-1 or PP2A show only a minor influence. The bistable range depends primarily on parameters that influence PP1 cooperativity or substrate competition between PLN monomers and pentamers (e.g., higher concentrations of PLN and PP1 or changes to PP1 dependent dephosphorylation). Interestingly, the cooperative increase in substrate affinity (χ) and the dynamic equilibrium of PLN (ω) show a strong influence on the bistable range. In the default parameter set, we assume PLN turnover (k_{cat}) rather than substrate affinity (K_m) to be regulated cooperatively (i.e., $\chi = 1$ and $\phi < 1$), but the exact nature of cooperative PLN pentamer dephosphorylation is currently unknown. While cooperative increase of k_{cat} is essential for the emergence of bistability, increasing substrate affinity appears to reduce the bistable range. To better understand how parameters ϕ , χ , and ω shape the PLN phosphorylation response curve, we performed further bifurcation analyses. Although low ϕ and χ or high ω values can increase the bistable range, the parameters differ markedly in how they shape other characteristics of the dose-response curve, possibly due to distinct effects on dephosphorylation rates (Figures S4A and S4B).

Local sensitivity analysis permits the study of the influence of parameters only around a nominal steady state, limiting the generality of its conclusions, whereas bifurcation analysis can be challenging and is limited to varying only few parameters simultaneously. We therefore implemented a recently developed method that allows exploring models in a fashion unbiased by a particular parameter set by simultaneously probing an arbitrary subset of the multi-dimensional parameter space and visualizing the resulting stability behavior on parallel coordinate plots (Nguyen et al., 2015). For each analysis, we probed 10,000 randomly sampled parameter sets, focusing on the concentrations of PKA, PP1, PLN, and inhibitor-1, enzymatic constants, cooperativity parameter ϕ , and the dynamic equilibrium of PLN (ω) (Figure 5E). In the absence of cooperative substrate affinity of PLN dephosphorylation ($\chi = 1$), 5.5% of the sampled parameter sets led to bistable phosphorylation responses. The emergence of bistability is favored by high k_{cat} and low K_m values for pentamer dephosphorylation by PP1. In contrast, other PKA and PP1 constants exhibit relatively little influence. Bistability is furthermore associated with low [PKA], high [PLN]_{tot}, and [PP1]_{tot} as well as a strong cooperative increase in k_{cat} of PP1 (low ϕ values) and strong dynamic equilibrium (high ω values). To further study the role

of pentameric PLN and the nature of PP1 cooperativity in pentamer dephosphorylation, we repeated the analysis without pentameric PLN and with cooperative substrate affinity of PLN dephosphorylation ($\chi > 1$), respectively. We found no bistability in the absence of pentameric PLN and markedly fewer (1.1%) parameter sets leading to bistability when $\chi > 1$ (Figures S4C and S4D).

In summary, these analyses show that pentamers, their cooperative dephosphorylation, and the dynamic equilibrium of PLN are important factors in shaping PLN monomer phosphorylation response at steady state.

Phosphorylation delay and bistability are effective noise filters

Like the phosphorylation response delay, the emergence of bistability poses the question what the physiological advantage of such phenomenon may be. Due to the small bistable range, it seems unlikely that PLN phosphorylation is a potent all-or-nothing switch as known for bistable signaling networks controlling (e.g., the cell cycle, apoptosis). In fact, adapting cardiac performance to various levels of demand requires the response to β -adrenergic stimulation to be tunable.

Altered Ca^{2+} handling is a known cause for cardiac arrhythmias (Landstrom et al., 2017). Cardiac arrhythmias such as ventricular tachycardias and fibrillation are also a hallmark of the pathogenic PLN mutation R14del (Haghighi et al., 2006; Posch et al., 2009; van Rijsingen et al., 2012; Hof et al., 2019). We thus speculated that delayed and bistable PLN phosphorylation may play a role in preventing such arrhythmias. If the phosphorylation delay is a persistence sensor (Mangan and Alon, 2003) for β -adrenergic stimulation, then it indicates that the “decision” of a cardiomyocyte to phosphorylate PLN may be a critical one. We hypothesized that by controlling PLN phosphorylation, response delay and bistability are noise-filtering mechanisms to prevent random, uncoordinated β -adrenergic signaling and aberrant Ca^{2+} handling.

To test this hypothesis, we performed a series of different simulations and analyses to characterize the noise-handling behavior of the model in response to random fluctuations of PKA activity. In the first simulations, we explored monomer phosphorylation in response to short bursts (1/3.3/10 s) of maximal PKA activity (0.59 μ M) in the full model, in the absence of either pentamers or inhibitor-1, and in the absence of both pentamers and inhibitor-1 (PP1 levels were adjusted to ensure equal steady-state activity in the absence of inhibitor-1). In the

Figure 6. Noise filtering by the PLN network

- (A–D) Time course simulations of PLN monomer phosphorylation in response to short (1/3.3/10 s) bursts of maximal PKA activity performed with the full model (A) or in the absence of pentameric PLN and/or inhibitor-1 (B–D). To ensure equal steady-state phosphatase activity, PP1 levels in (C) and (D) have been adjusted by the amount in complex with inhibitor-1 in presence of PKA at steady state in the full model.
- (E) Demonstration of the PLN network’s low pass filtering capacity.
- (F) Frequency response analysis (Bode plots) of the linearized input-output systems.
- (G) Comparison of PLN monomer phosphorylation (bottom) in response to a noisy PKA input fluctuating with 25% min^{-1} around a baseline of 0.226 μ M (center) for the original model and a model with similar steady-state response but without bistability (top).
- (H) Output noise as the coefficient of variation σ/μ of monomer phosphorylation for the original (bistable) and ultrasensitive model at different PKA baseline and input noise levels.
- (I) Output noise of the ultrasensitive model relative to the bistable model.
- (J) Comparison of bistable and ultrasensitive model at critical PKA concentrations and a maximum noise amplitude (0.0625 μ M), which enables repeated switching between low/high phosphorylation (dashed lines) in both models.

full model, the first 1/3.3/10 s bursts lead to 6%/13%/28% monomer phosphorylation, respectively (Figure 6A). In the absence of either pentamers or inhibitor-1, the response to such bursts is markedly higher, reaching 10%/23%/46% for 1/3.3/10 s bursts in the absence of both pentamers and inhibitor-1 (Figures 6B–6D). As expected from the response delays, a comparison of the integrated monomer phosphorylation between model versions reveals that relative attenuation is strongest for short bursts (Figure S5A). Interestingly, when inhibitor-1 is present, unbinding and subsequent dephosphorylation of phosphorylated inhibitor-1 occurs more slowly than the dephosphorylation of PLN, leading to the accumulation of the inactive PP1 complex and slightly increasing PLN phosphorylation over multiple bursts (Figures 6A and 6B). These simulations show that the response delay via pentamers and inhibitor-1 can filter out or attenuate short PKA activity bursts while still allowing high phosphorylation upon persistent PKA activity.

Rejecting signals on short timescales while responding to persistent signals is also characteristic of low-pass filters. Simulating the PLN phosphorylation response to a PKA input described by a low-frequency sine wave interspersed with high-frequency random noise confirms that the PLN signaling network has low-pass filtering properties (Figure 6E). Such behavior can be further characterized by a frequency response analysis that permits the determination of the bandwidth (i.e., the frequency above which a system fails to respond adequately). Typical for low-pass filters, the gain Bode plot of our model shows a steady decrease in the gain (roll-off) for frequencies above the bandwidth (Figure 6F). Consistent with our previous analysis, the bandwidth is 17-fold higher in the absence of pentamers (0.196 Hz) compared to the full model (0.011 Hz) (Figure 6F, bar graph), confirming that pentamers contribute to low-pass filtering in the PLN network. Interestingly, the phase shift is also different in the absence of pentamers, further substantiating their role in influencing phosphorylation dynamics.

To our surprise, the absence of inhibitor-1 did not increase the bandwidth (contrary to what would be expected from the demonstrated response delay). The reason for this is that the frequency response is constructed from the reached steady state. Due to the high affinity of inhibitor-1 for PP1, 99.8% of inhibitor-1 at the studied steady state in the full model is already bound to PP1 and does not contribute to low-pass filtering anymore. Unless inhibitor-1 can be dephosphorylated by PP2A while bound to PP1 (which to our knowledge has not been studied yet), its response delay would only apply if the cardiomyocyte has not been exposed to significant β -adrenergic stimulation for some time.

Our simulations and analyses show that the response delay by PLN pentamers and inhibitor-1 can attenuate the response to short bursts of PKA activity and that at least pentamers contribute to low-pass filtering. Next, we explored how bistability may contribute to noise filtering. In general, bistability can make a response more robust and defined: once a system passed a threshold, it can only switch back to its prior state if it passes a second threshold, thus preventing uncontrolled switching (Ferrell and Xiong, 2001). We thus speculated that bistability could reduce noise by preventing repeated switching between low/

high PLN phosphorylation levels. To test this hypothesis, we created a parameter set for which the model shows similar monomer phosphorylation at steady state in terms of sensitivity and critical threshold but without bistability (Figure 6G, top).

Next, we compared the behavior of both parameterizations in response to noisy PKA activity close to the common critical threshold. Fluctuations of 25% with a frequency of 1 min^{-1} have been chosen to make sure the fluctuations are not filtered out by low-pass filtering (Figure 6G, center). As shown in Figure 6G (bottom), the relative PLN monomer phosphorylation of the bistable model (red) fluctuates with small amplitude around a stable baseline of $\sim 50\%$ phosphorylation. In contrast, the non-bistable model (purple) shows dramatic fluctuations between low and high phosphorylation levels. Since PLN monomer phosphorylation directly translates into SERCA activity, such fluctuations could impair coordinated Ca^{2+} -handling.

To investigate the output noise in a more systematic manner, we applied a common definition of signal noise as the coefficient of variation (CV) (Johnston, 2012). By calculating “noise landscapes” for both models based on 150 PKA fluctuations with a frequency of 1 min^{-1} , we visualized how the CV of monomer phosphorylation (output noise) depends both on the baseline PKA activity and amplitude of PKA fluctuations (input noise). While the output noise of bistable and non-bistable model versions is very similar for baseline [PKA] below $\approx 0.2 \mu\text{M}$, the output noise of the bistable model abruptly increases at a baseline [PKA] close to the critical threshold and abruptly decreases at higher [PKA] (Figure 6H, left). The output noise of the non-bistable model follows a more continuous trend and neither shows abrupt increases close to the critical threshold, nor abrupt suppression at higher baseline [PKA] (Figure 6H, right). The relative noise landscape shows that in most circumstances, the bistable model copes better with noisy input than the non-bistable model (Figure 6I). Since we assumed the input noise to be a linear function of the baseline [PKA], we repeated the analyses assuming a constant and a non-linear noise function and came to the same conclusion (Figures S5B–S5D).

Since the bistable model seemingly performs worse in some conditions close to the critical threshold, the question arises whether this could facilitate cardiac arrhythmias in spite of a generally less noisy monomer phosphorylation. To answer this question, we analyzed one of the conditions in which the bistable model seemingly performs worse (white arrowhead in Figure 6H) in more detail. Interestingly, we found that the increased output noise as defined by the CV typically resulted from a single “switching up” event and that in the long run (1,000 fluctuations), the output noise of the bistable model is actually lower than in its non-bistable counterpart (Figure S5E).

Motivated by this finding, we wanted to know how bistable and non-bistable model versions compare at their most vulnerable point for uncontrolled switching between low/high monomer phosphorylation states. We thus designed simulations in which baseline [PKA] was set to the center between both saddle-node bifurcations for the bistable model (i.e., between critical thresholds SN1 and SN2 shown in Figure 6G) or directly to the single threshold in the non-bistable model. In addition, we chose a constant maximum noise amplitude for both models, high enough to surpass both thresholds in the

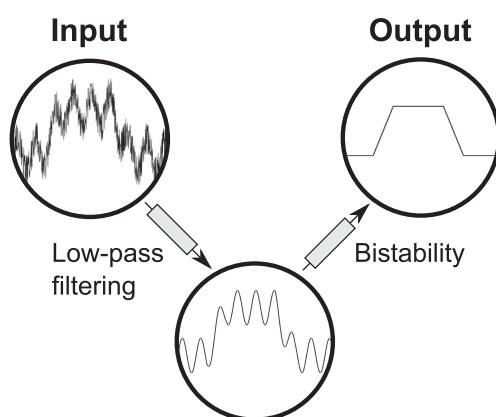


Figure 7. Illustration of proposed noise-filtering principles in the PLN signaling network

Low-pass filtering and bistability reject fluctuations at different timescales in a complementary fashion to ensure defined PLN monomer phosphorylation.

bistable model from its baseline [PKA]. Intriguingly, we found that in spite of a higher CV, monomer phosphorylation is more defined and switches far less frequently in the presence of bistability (Figure 6J).

In summary, these simulations and analyses confirm our hypothesis that phosphorylation delay and bistability can act as molecular noise filters in the β -adrenergic signaling network.

The R14del mutation likely impairs noise filtering

Coordinated functioning of the heart critically depends on the synchronicity of cardiomyocyte contraction and relaxation controlled by intracellular $[Ca^{2+}]$. Since β -adrenergic stimulation is a major regulator of cardiac Ca^{2+} handling, there likely need to be mechanisms in place to prevent arrhythmias triggered by heterogeneous cardiomyocyte responses. By rejecting short random stimuli (low-pass filtering) and by defining the PLN phosphorylation status more clearly (bistability), these noise filters could help to promote synchronicity across the myocardium.

Since cardiac arrhythmias are a major issue for patients with the PLN mutation R14del (Haghighi et al., 2006; Posch et al., 2009; van Rijsingen et al., 2012; Hof et al., 2019), we wanted to know whether noise filtering is impaired if we implement the known molecular effects of this mutation into our model. The consequences reported so far include impaired phosphorylation by PKA (Kim et al., 2015) (although Haghighi et al. [2006, 2012] reported that PLN_{R14del} can still be partly phosphorylated *in vivo*), mistargeting of mutant PLN to the plasma membrane (Haghighi et al., 2012), and destabilization of pentamers (Haghighi et al., 2006). Although all R14del patients are reported to be heterozygous, explicit accounting for both wild-type and mutant PLN molecules requires a model at least three times the complexity of the current model (due to combinatorial expansion of reactions, molecules, and system equations). Since this exceeds the scope of the present study as well as available data on pa-

rameters, we opted for an alternative approach and made qualitative predictions of how known molecular effects of the R14del mutation would individually influence the noise filtering based on the analyses of the original model.

Our qualitative predictions suggested that in a heterozygous setting, mistargeting of R14del PLN, destabilization of pentamers, and potential mutant/wild-type hetero-pentamers would impair both low-pass filtering and bistability (Table S1). Mistargeting and destabilization can be expected to exert a negative effect on noise filtering by reducing the concentration of PLN pentamers. Mutant/wild-type hetero-pentamers would effectively feature fewer phosphorylation sites, thereby reducing the sites that can compete with monomers. As the range of bistability is positively influenced by the number of phosphorylation sites (Ortega et al., 2006), hetero-pentamers can be expected to reduce the bistable range. Thus, the heterozygous R14del situation could be more permissive for short random bursts of PKA activity and lead to higher noise amplitudes, providing an attractive explanation for the susceptibility to cardiac arrhythmias. Since R14del PLN molecules are unresponsive to phosphorylation by PKA, we expect reduced amounts of wild-type pentamers to be the biggest issue for noise filtering.

Although preliminary, our analysis suggests a novel therapeutic strategy: increasing the amount of wild-type pentamers could improve noise filtering and prevent cardiac arrhythmias in patients with the R14del mutation. Potential ways of achieving this include increasing the effective concentration of PLN at the SR, small (and yet to be discovered) molecules that stabilize pentamers without interfering with regulatory enzymes, or metabolically changing the lipid composition of the SR (which regulates PLN pentamerization; cf. Zhang et al., 2005).

DISCUSSION

In the present study, we have demonstrated that at least in our experimental conditions, the buffering effect exerted by PLN pentamers is too moderate and slow to be relevant at the timescale of acute β -adrenergic stimulation. We therefore developed a mathematical model of the PLN regulatory network and studied the role of PLN pentamers in the context of β -adrenergic stimulation from a dynamical systems perspective. Having calibrated the model with own experimental data and experimental parameters from the literature, our simulations predicted delayed phosphorylation responses due to PLN pentamer competition and an inhibitor-1 FFL. Further simulations suggested that PLN phosphorylation could be ultrasensitive and bistable due to cooperative dephosphorylation of PLN pentamers.

Using several different numerical approaches, we have shown that these phenomena can filter out the effect of random fluctuations in PKA activity on PLN monomer phosphorylation; while response delay and persistence sensing constitute a low-pass filter removing fast fluctuations and short stimulus spikes, bistability prevents uncontrolled high-amplitude fluctuations in PLN phosphorylation at critical PKA activity, thereby promoting a well-defined PLN phosphorylation status. Importantly, these noise filters are complementary (Figure 7) and depend largely on PLN pentamers. To our knowledge, this is the first time that

a clearly defined physiological advantage of PLN pentamers has been demonstrated.

While we have provided an optimal design for experimentally testing the FFL functionality (e.g., with cell biological approaches), we have confirmed the delay due to pentamer competition *in vitro*, providing experimental evidence for one of the main mechanisms underlying the predicted low-pass filtering. Similar monomer phosphorylation delays due to pentamers have been observed in transfected HEK293 cells, suggesting that the mechanism can operate in living cells (Wittmann et al., 2015). We further replicated ultrasensitive PLN phosphorylation in transfected HEK293 cells, in agreement with previous dose-response data. While the experimental Hill exponents appear lower than predicted, they are still fully consistent with bistability and low-pass filtering (Figure S6). Importantly, we could experimentally confirm that PLN phosphorylation exhibits hysteresis in primary cardiomyocytes as predicted by our model, demonstrating that PLN phosphorylation is bistable.

In an independent study, we show further that the ability of pentamers to shape the response curve of PLN phosphorylation to β -adrenergic stimulation translates into increased dynamic range and sensitivity of cardiac relaxation and is necessary to cope with increased cardiac pressure (data not shown).

Our results also provide a potential explanation for the frequent emergence of cardiac arrhythmias in patients with the R14del mutation. Although preliminary, a first analysis of the molecular consequences of this mutation points toward impaired noise filtering due to reduced amounts of wild-type pentamers. Since the PLN_{R14del} cardiomyopathy does not respond to conventional heart failure therapy (Eijgenraam et al., 2020), we propose to explore ways to increase the amount of wild-type pentamers in preclinical R14del models as a novel therapeutic approach. A first way to test this concept could be to harness increased pentamerization of the artificial I45A mutant and to determine whether heterozygous R14del/I45A mouse or induced pluripotent stem cell (iPSC) cardiomyocyte models show a lower arrhythmogenic tendency than a heterozygous R14del/wild-type model.

A strength of our model is that it offers new perspectives on multiple and hitherto puzzling phenomena by associating them with a common physiological function: noise filtering. Apart from PLN pentamers, neither their cooperative dephosphorylation (Li et al., 1990; Colyer, 1993) nor the dynamic equilibrium (increased pentamerization upon phosphorylation; Cornea et al., 1997; Hou et al., 2008) were previously known to have clearly defined physiological functions. While pentamers and their cooperative dephosphorylation are necessary in our model for bistability to occur, the dynamic equilibrium makes bistability more robust, potentially by inducing “hidden” feedback loops (Varusai et al., 2015), supporting the emergence of bistability (Figure S7). Interestingly, the recruitment of 14-3-3 proteins to phosphorylated PLN pentamers has recently been found to establish a similar memory of PLN phosphorylation *in vivo* (by slowing down dephosphorylation) and is impaired by R14del (Menzel et al., 2020). This constitutes a double-negative feedback, which may further improve bistability or noise filtering.

Our model also opens a new perspective on the role of inhibitor-1, which is often described as an amplifier for PKA phos-

phorylation (El-Armouche et al., 2003; Wittköpper et al., 2011). Although this is technically not false, the same level of PLN phosphorylation response could in principle be achieved by simpler means such as reduced SR targeting of PP1 (Alsina et al., 2019). Thus, the delayed response dynamics of the inhibitor-1 FFL and the noise filtering capacity demonstrated in our simulations may be equally important as the influence on steady-state phosphorylation levels.

Noise filtering in the β -adrenergic signaling pathway may only be relevant if the network experiences significant fluctuations of pro-arrhythmic potential under some circumstances. While it is known that there is significant electrophysiological variability among individual cardiomyocytes, which can be pro-arrhythmic under conditions of reduced cell-cell coupling (Watanabe et al., 1983; Pueyo et al., 2011), a systematic experimental characterization of the noise at multiple nodes of the β -adrenergic signaling network is, to our knowledge, still lacking. However, studies from the 1980s indicate significant fluctuations at baseline, at least in catecholamines (Linsell et al., 1985; Cameron et al., 1987) and aberrant calcium handling or β -adrenergic signaling are well known for triggering cardiac arrhythmias (Landstrom et al., 2017). In general, many perturbations can have both pro- and anti-arrhythmic components, making the emergence of cardiac arrhythmias a complex (Kistamás et al., 2020). While direct stimulation of, for instance, SERCA activity, has been shown to increase the frequency of spontaneous calcium waves (pro-arrhythmic), it also increased the threshold for wave occurrence and limited wave propagation (anti-arrhythmic), thereby making low SERCA activity potentially pro-arrhythmic in the context of β -adrenergic stimulation (Fernandez-Tenorio and Niggli, 2018). Moreover, several studies have indicated PLN to influence repolarization (abnormal T waves in R14del patients (Hof et al., 2019); variants at the PLN gene locus affect QT interval duration (Pfeuffer et al., 2009)). It is therefore plausible to assume that large fluctuations in PLN phosphorylation could translate into heterogeneous SERCA activity, potentially generating variability in repolarization behavior, calcium transients, and SR calcium load across cell populations, which may trigger pro-arrhythmic activity such as early or delayed after-depolarizations (Kistamás et al., 2020). In this context, a biochemical memory for PLN phosphorylation such as bistability may prevent individual cardiomyocytes from prematurely returning to a potentially pro-arrhythmic low SERCA activity state. As variability on multiple scales ranging from single cells up to whole organisms is increasingly recognized as an important factor for understanding cardiac electrophysiology and arrhythmias (Ni et al., 2018; Gong et al., 2020), noise filtering in the β -adrenergic signaling pathway as an anti-arrhythmic mechanism is a hypothesis worth studying further.

Further experimental and clinical evidence

In agreement with our results, many proteins of the PLN regulatory network are in fact associated with cardiac arrhythmias by both experimental and clinical data. The natural mutation R9H (Medeiros et al., 2011) has recently been shown to cause ventricular arrhythmias in dogs (Yost et al., 2019), indicating that PLN

mutations other than R14del can be arrhythmogenic. Additional evidence that PLN pentamers contribute to noise filtering comes from a mouse model of the natural obscurin variant R4344Q (Hu et al., 2017). Mice carrying this variant developed spontaneous ventricular arrhythmias, which authors attributed to increased SERCA levels and \approx 15% fewer pentamers. Although the pathogenicity of this variant is likely restricted to mice (Fukuzawa et al., 2021), the findings support the idea that pentamers can attenuate cardiac arrhythmias.

A similar mechanism may contribute to the pro-arrhythmic effect of thyroid hormones, which increase SERCA and decrease PLN expression (thus decreasing pentamerization) (Tribulova et al., 2020). Apart from PLN, both PP1 and inhibitor-1 have been shown to be involved in the emergence of arrhythmias (Chiang et al., 2016). Reducing the concentration of PP1 at the SR by ablating its targeting subunit PPP1R3A has been shown to lead to atrial fibrillation (Alcina et al., 2019), which is consistent with a smaller bistable region expected from reducing [PP1] in our model. Interestingly, a mouse model of the human inhibitor-1 variant G109E (showing reduced binding to PP1) and mice expressing a constitutively active version of inhibitor-1 developed severe cardiac arrhythmias in response to β -adrenergic stimulation (Haghighi et al., 2015; Wittköpper et al., 2010). Both mutations interfere with the inhibitor-1 FFL and could make PLN phosphorylation more susceptible to noise, according to our model. Contrary to these findings, complete inhibitor-1 ablation has been shown to protect against catecholamine-induced arrhythmias (El-Armouche et al., 2008), which led to a debate over whether inhibitor-1 is pro- or anti-arrhythmogenic (Nicolaou et al., 2009; Wittköpper et al., 2011). Settling this debate may require a nuanced answer distinguishing between pro- and anti-arrhythmogenic effects (e.g., pro-arrhythmogenic PKC phosphorylation sites versus noise filtering). Moreover, the complete loss of inhibitor-1 may be compensated for by up-regulating FFLs involving, for example, Hsp20 (Kranias and Hajjar 2012).

An intriguing line of evidence that noise filtering may also be upregulated in response to arrhythmic heart activity came from a recent study on arrhythmogenic cardiomyopathy (ACM) patients. In ACM patients without PLN mutation, PLN protein expression was shown to be upregulated more than 2-fold, which the authors hypothesized to be a yet-to-be-elucidated compensatory mechanism (Akdis et al., 2016). As higher PLN concentration leads to increased pentamerization due to mass action, both noise-filtering functions predicted by our model would be enhanced, providing an attractive explanation for this observation.

These studies show that perturbing components that contribute to noise filtering in our model can lead to cardiac arrhythmias, whereas enhancing their functionality may protect against other pro-arrhythmogenic factors.

Limitations and conclusions

Like every modeling study, we had to rely on simplifying assumptions at several points during model development. For example, our model only accounts for a subset of interactions with PLN that we deemed most relevant for our purpose; it assumes that the modeled processes are described well enough by ordinary

differential equations, even though much of the biochemistry takes place on the two-dimensional SR surface; parameters and species concentrations of our model come from different sources (e.g., fitted to our own experimental data, directly measured or fitted parameters from the literature). Furthermore, we have considered noise only in terms of fluctuating PKA activity (representing the input of our model), although extrinsic and intrinsic noise sources affect all molecular processes whose full exploration requires stochastic simulations (Johnston, 2012; Tsimring, 2014). Due to the medical relevance of the R14del mutation, perhaps the most important limitation to highlight is that our analysis of the R14del mutation is preliminary. Since this mutation has been shown to alter additional interactions not currently represented in our model, the model does not yet capture other pathophysiological processes such as (potentially pro-arrhythmogenic) cardiac remodeling (Te Rijdt et al., 2016).

While we have partly addressed some limitations, for example, by performing complementary analyses or systematic explorations of the parameter space, others will need to be addressed in future experimental and theoretical investigations. Despite these limitations, the experimental data support the conclusions from our simulations. We believe our model thus offers a novel and exciting perspective on the physiological role of PLN pentamers and will prove to be a useful starting point for further investigations.

STAR★METHODS

Detailed methods are provided in the online version of this paper and include the following:

- KEY RESOURCES TABLE
- RESOURCE AVAILABILITY
 - Lead contact
 - Materials availability
 - Data and code availability
- EXPERIMENTAL MODEL AND SUBJECT DETAILS
 - Cell culture
- METHOD DETAILS
 - Experimental procedures
 - Development of the mathematical model
 - Reaction rates
 - Computational procedures
- QUANTIFICATION AND STATISTICAL ANALYSIS

SUPPLEMENTAL INFORMATION

Supplemental information can be found online at <https://doi.org/10.1016/j.celrep.2021.109448>.

ACKNOWLEDGMENTS

D.K. is funded by a PhD studentship from the British Heart Foundation (grant [FS/17/65/33481]). J.P.S. received support from the Deutsche Forschungsgemeinschaft (SFB 1116). We thank Jessica Chandler for the cardiomyocyte preparations and Thomas Kampourakis and Martin Rees for helpful feedback on earlier drafts of the manuscript.

AUTHOR CONTRIBUTIONS

D.K. conceived and designed the project, developed the mathematical model, performed the simulations, analyzed the data, and wrote the manuscript. A.A., A.L.K., D.K., and F.F. performed the experiments. J.P.S. and M.G. provided important advice on experimental design.

DECLARATION OF INTERESTS

The authors declare no competing interests.

Received: December 30, 2020

Revised: April 16, 2021

Accepted: July 5, 2021

Published: July 27, 2021

REFERENCES

- Abel, S.M., Roose, J.P., Groves, J.T., Weiss, A., and Chakraborty, A.K. (2012). The membrane environment can promote or suppress bistability in cell signaling networks. *J. Phys. Chem. B* *116*, 3630–3640.
- Akdis, D., Medeiros-Domingo, A., Gaertner-Rommel, A., Kast, J.I., Enseleit, F., Bode, P., Klingel, K., Kandolf, R., Renois, F., Andreoletti, L., et al. (2016). Myocardial expression profiles of candidate molecules in patients with arrhythmogenic right ventricular cardiomyopathy/dysplasia compared to those with dilated cardiomyopathy and healthy controls. *Heart Rhythm* *13*, 731–741.
- Alsina, K.M., Hulsurkar, M., Brandenburg, S., Kownatzki-Danger, D., Lenz, C., Urlaub, H., Abu-Taha, I., Kamler, M., Chiang, D.Y., Lahiri, S.K., et al. (2019). Loss of Protein Phosphatase 1 Regulatory Subunit PPP1R3A Promotes Atrial Fibrillation. *Circulation* *140*, 681–693.
- Becucci, L., Cembran, A., Karim, C.B., Thomas, D.D., Guidelli, R., Gao, J., and Veglia, G. (2009). On the function of pentameric phospholamban: ion channel or storage form? *Biophys. J.* *96*, L60–L62.
- Bers, D.M. (2002). Cardiac excitation-contraction coupling. *Nature* *415*, 198–205.
- Bers, D.M. (2008). Calcium cycling and signaling in cardiac myocytes. *Annu. Rev. Physiol.* *70*, 23–49.
- Bondarenko, V.E. (2014). A compartmentalized mathematical model of the β 1-adrenergic signaling system in mouse ventricular myocytes. *PLoS ONE* *9*, e89113.
- Brittsan, A.G., Carr, A.N., Schmidt, A.G., and Kranias, E.G. (2000). Maximal inhibition of SERCA2 Ca^{2+} affinity by phospholamban in transgenic hearts overexpressing a non-phosphorylatable form of phospholamban. *J. Biol. Chem.* *275*, 12129–12135.
- Bugenhagen, S.M., and Beard, D.A. (2015). Computational analysis of the regulation of Ca^{2+} dynamics in rat ventricular myocytes. *Phys. Biol.* *12*, 056008.
- Cameron, O.G., Curtis, G.C., Zelnik, T., McCann, D., Roth, T., Guire, K., and Huber-Smith, M. (1987). Circadian fluctuation of plasma epinephrine in supine humans. *Psychoneuroendocrinology* *12*, 41–51.
- Chiang, D.Y., Heck, A.J.R., Dobrev, D., and Wehrens, X.H.T. (2016). Regulating the regulator: insights into the cardiac protein phosphatase 1 interactome. *J. Mol. Cell. Cardiol.* *101*, 165–172.
- Chu, G., Li, L., Sato, Y., Harrer, J.M., Kadambi, V.J., Hoyt, B.D., Bers, D.M., and Kranias, E.G. (1998). Pentameric assembly of phospholamban facilitates inhibition of cardiac function *in vivo*. *J. Biol. Chem.* *273*, 33674–33680.
- Colyer, J. (1993). Control of the calcium pump of cardiac sarcoplasmic reticulum. A specific role for the pentameric structure of phospholamban? *Cardiovasc. Res.* *27*, 1766–1771.
- Cornea, R.L., Jones, L.R., Autry, J.M., and Thomas, D.D. (1997). Mutation and phosphorylation change the oligomeric structure of phospholamban in lipid bilayers. *Biochemistry* *36*, 2960–2967.
- Eijgenraam, T.R., Boukens, B.J., Boogerd, C.J., Schouten, E.M., van de Kolk, C.W.A., Stege, N.M., Te Rijdt, W.P., Hoorntje, E.T., van der Zwaag, P.A., van Rooij, E., et al. (2020). The phospholamban p.(Arg14del) pathogenic variant leads to cardiomyopathy with heart failure and is unresponsive to standard heart failure therapy. *Sci. Rep.* *10*, 9819.
- Eisner, D.A., Caldwell, J.L., Kistamás, K., and Trafford, A.W. (2017). Calcium and Excitation-Contraction Coupling in the Heart. *Circ. Res.* *121*, 181–195.
- El-Armouche, A., Rau, T., Zolk, O., Ditz, D., Pamminger, T., Zimmermann, W.H., Jäckel, E., Harding, S.E., Boknik, P., Neumann, J., and Eschenhagen, T. (2003). Evidence for protein phosphatase inhibitor-1 playing an amplifier role in β -adrenergic signaling in cardiac myocytes. *FASEB J.* *17*, 437–439.
- El-Armouche, A., Wittköpper, K., Degenhardt, F., Weinberger, F., Didié, M., Melnychenko, I., Grimm, M., Peeck, M., Zimmermann, W.H., Unsöld, B., et al. (2008). Phosphatase inhibitor-1-deficient mice are protected from catecholamine-induced arrhythmias and myocardial hypertrophy. *Cardiovasc. Res.* *80*, 396–406.
- Fernandez-Tenorio, M., and Niggli, E. (2018). Stabilization of Ca^{2+} signaling in cardiac muscle by stimulation of SERCA. *J. Mol. Cell. Cardiol.* *119*, 87–95.
- Ferrell, J.E., and Xiong, W. (2001). Bistability in cell signaling: how to make continuous processes discontinuous, and reversible processes irreversible. *Chaos* *11*, 227–236.
- Fersht, A. (1999). *Structure and Mechanism in Protein Science: A Guide to Enzyme Catalysis and Protein Folding*, 2nd (W.H. Freeman).
- Flöttmann, M., Schaber, J., Hoops, S., and Klipp, E. (2008). ModelMage: a tool for automatic model generation, selection and management. *Genome Inform.* *20*, 52–63.
- Fukuzawa, A., Koch, D., Grover, S., Rees, M., and Gautel, M. (2021). When is an obscurin variant pathogenic? The impact of Arg4344Gln and Arg4444Trp variants on protein-protein interactions and protein stability. *Hum. Mol. Genet.* *30*, 1131–1141.
- Glaves, J.P., Primeau, J.O., Espinoza-Fonseca, L.M., Lemieux, M.J., and Young, H.S. (2019). The Phospholamban Pentamer Alters Function of the Sarcoplasmic Reticulum Calcium Pump SERCA. *Biophys. J.* *116*, 633–647.
- Gong, J.Q.X., Susilo, M.E., Sher, A., Musante, C.J., and Sobie, E.A. (2020). Quantitative analysis of variability in an integrated model of human ventricular electrophysiology and β -adrenergic signaling. *J. Mol. Cell. Cardiol.* *143*, 96–106.
- Ha, K.N., Masterson, L.R., Hou, Z., Verardi, R., Walsh, N., Veglia, G., and Robia, S.L. (2011). Lethal Arg9Cys phospholamban mutation hinders Ca^{2+} -ATPase regulation and phosphorylation by protein kinase A. *Proc. Natl. Acad. Sci. USA* *108*, 2735–2740.
- Haghighi, K., Kolokathis, F., Gramolini, A.O., Waggoner, J.R., Pater, L., Lynch, R.A., Fan, G.C., Tsiapras, D., Parekh, R.R., Dorn, G.W., 2nd., et al. (2006). A mutation in the human phospholamban gene, deleting arginine 14, results in lethal, hereditary cardiomyopathy. *Proc. Natl. Acad. Sci. USA* *103*, 1388–1393.
- Haghighi, K., Pritchard, T., Bossuyt, J., Waggoner, J.R., Yuan, Q., Fan, G.C., Osinska, H., Anjak, A., Rubinstein, J., Robbins, J., et al. (2012). The human phospholamban Arg14-deletion mutant localizes to plasma membrane and interacts with the Na/K-ATPase. *J. Mol. Cell. Cardiol.* *52*, 773–782.
- Haghighi, K., Pritchard, T.J., Liu, G.S., Singh, V.P., Bidwell, P., Lam, C.K., Vafiadaki, E., Das, P., Ma, J., Kunduri, S., et al. (2015). Human G109E-inhibitor-1 impairs cardiac function and promotes arrhythmias. *J. Mol. Cell. Cardiol.* *89* (Pt B), 349–359.
- Hof, I.E., van der Heijden, J.F., Kranias, E.G., Sanoudou, D., de Boer, R.A., van Tintelen, J.P., van der Zwaag, P.A., and Doevendans, P.A. (2019). Prevalence and cardiac phenotype of patients with a phospholamban mutation. *Neth. Heart J.* *27*, 64–69.
- Hoops, S., Sahle, S., Gauges, R., Lee, C., Pahle, J., Simus, N., Singhal, M., Xu, L., Mendes, P., and Kummer, U. (2006). COPASI—a COmplex PATHway Simulator. *Bioinformatics* *22*, 3067–3074.
- Hou, Z., Kelly, E.M., and Robia, S.L. (2008). Phosphomimetic mutations increase phospholamban oligomerization and alter the structure of its regulatory complex. *J. Biol. Chem.* *283*, 28996–29003.
- Hu, L.R., Ackermann, M.A., Hecker, P.A., Prosser, B.L., King, B., O’Connell, K.A., Grogan, A., Meyer, L.C., Berndsen, C.E., Wright, N.T., et al. (2017).



- Deregulated Ca^{2+} cycling underlies the development of arrhythmia and heart disease due to mutant obscurin. *Sci. Adv.* 3, e1603081.
- Ingalls, B. (2013). *Mathematical Modelling in Systems Biology: An Introduction* (MIT Press).
- Johnston, I. (2012). The chaos within: Exploring noise in cellular biology. *Significance* 9, 17–21.
- Kampourakis, T., Ponnamp, S., Sun, Y.-B., Sevríeva, I., and Irving, M. (2018). Structural and functional effects of myosin-binding protein-C phosphorylation in heart muscle are not mimicked by serine-to-aspartate substitutions. *J. Biol. Chem.* 293, 14270–14275.
- Kim, J., Masterson, L.R., Cembran, A., Verardi, R., Shi, L., Gao, J., Taylor, S.S., and Veglia, G. (2015). Dysfunctional conformational dynamics of protein kinase A induced by a lethal mutant of phospholamban hinder phosphorylation. *Proc. Natl. Acad. Sci. USA* 112, 3716–3721.
- Kimura, Y., Kurzydowski, K., Tada, M., and MacLennan, D.H. (1997). Phospholamban inhibitory function is activated by depolymerization. *J. Biol. Chem.* 272, 15061–15064.
- Kistamás, K., Veress, R., Horváth, B., Bányász, T., Nánási, P.P., and Eisner, D.A. (2020). Calcium Handling Defects and Cardiac Arrhythmia Syndromes. *Front. Pharmacol.* 11, 72.
- Koch, D. (2020). Homo-Oligomerisation in Signal Transduction: Dynamics, Homeostasis, Ultrasensitivity, Bistability. *J. Theor. Biol.* 499, 110305.
- Kovacs, R.J., Nelson, M.T., Simmerman, H.K., and Jones, L.R. (1988). Phospholamban forms Ca^{2+} -selective channels in lipid bilayers. *J. Biol. Chem.* 263, 18364–18368.
- Kranias, E.G., and Hajjar, R.J. (2012). Modulation of cardiac contractility by the phospholamban/SERCA2a regulatome. *Circ. Res.* 110, 1646–1660.
- Kranias, E.G., and Solaro, R.J. (1982). Phosphorylation of troponin I and phospholamban during catecholamine stimulation of rabbit heart. *Nature* 298, 182–184.
- Kuschel, M., Karczewski, P., Hempel, P., Schlegel, W.-P., Krause, E.-G., and Bartel, S. (1999). Ser16 prevails over Thr17 phospholamban phosphorylation in the β -adrenergic regulation of cardiac relaxation. *Am. J. Physiol.* 276, H1625–H1633.
- Landstrom, A.P., Dobrev, D., and Wehrens, X.H.T. (2017). Calcium Signaling and Cardiac Arrhythmias. *Circ. Res.* 120, 1969–1993.
- Legewie, S., Herzei, H., Westerhoff, H.V., and Blüthgen, N. (2008). Recurrent design patterns in the feedback regulation of the mammalian signalling network. *Mol. Syst. Biol.* 4, 190.
- Li, C.F., Wang, J.H., and Colyer, J. (1990). Immunological detection of phospholamban phosphorylation states facilitates the description of the mechanism of phosphorylation and dephosphorylation. *Biochemistry* 29, 4535–4540.
- Lindemann, J.P., Jones, L.R., Hathaway, D.R., Henry, B.G., and Watanabe, A.M. (1983). β -Adrenergic stimulation of phospholamban phosphorylation and Ca^{2+} -ATPase activity in guinea pig ventricles. *J. Biol. Chem.* 258, 464–471.
- Linsell, C.R., Lightman, S.L., Mullen, P.E., Brown, M.J., and Causón, R.C. (1985). Circadian rhythms of epinephrine and norepinephrine in man. *J. Clin. Endocrinol. Metab.* 60, 1210–1215.
- Luby-Phelps, K. (2000). Cytoarchitecture and Physical Properties of Cytoplasm: Volume, Viscosity, Diffusion, Intracellular Surface Area. *Int. Rev. Cytol.* 192, 189–221.
- MacDougall, L.K., Jones, L.R., and Cohen, P. (1991). Identification of the major protein phosphatases in mammalian cardiac muscle which dephosphorylate phospholamban. *Eur. J. Biochem.* 196, 725–734.
- MacLennan, D.H., and Kranias, E.G. (2003). Phospholamban: a crucial regulator of cardiac contractility. *Nat. Rev. Mol. Cell Biol.* 4, 566–577.
- Maffeo, C., and Aksimentiev, A. (2009). Structure, dynamics, and ion conduction of the phospholamban pentamer. *Biophys. J.* 96, 4853–4865.
- Mangan, S., and Alon, U. (2003). Structure and function of the feed-forward loop network motif. *Proc. Natl. Acad. Sci. USA* 100, 11980–11985.
- Markevich, N.I., Hoek, J.B., and Kholodenko, B.N. (2004). Signaling switches and bistability arising from multisite phosphorylation in protein kinase cascades. *J. Cell Biol.* 164, 353–359.
- Masterson, L.R., Yu, T., Shi, L., Wang, Y., Gustavsson, M., Mueller, M.M., and Veglia, G. (2011). cAMP-dependent protein kinase A selects the excited state of the membrane substrate phospholamban. *J. Mol. Biol.* 412, 155–164.
- McTiernan, C.F., Frye, C.S., Lemster, B.H., Kinder, E.A., Ogletree-Hughes, M.L., Moravec, C.S., and Feldman, A.M. (1999). The human phospholamban gene: structure and expression. *J. Mol. Cell. Cardiol.* 31, 679–692.
- Medeiros, A., Biagi, D.G., Sobreira, T.J.P., de Oliveira, P.S.L., Negrão, C.E., Mansur, A.J., Krieger, J.E., Brum, P.C., and Pereira, A.C. (2011). Mutations in the human phospholamban gene in patients with heart failure. *Am. Heart J.* 162, 1088–1095.e1.
- Menzel, J., Kownatzki-Danger, D., Tokar, S., Ballone, A., Unthan-Fechner, K., Kilisch, M., Lenz, C., Urlaub, H., Mori, M., Ottmann, C., et al. (2020). 14-3-3 binding creates a memory of kinase action by stabilizing the modified state of phospholamban. *Sci. Signal.* 13, eaaz4436.
- Nguyen, L.K., Degasperis, A., Cotter, P., and Kholodenko, B.N. (2015). DYVI-PAC: an integrated analysis and visualisation framework to probe multi-dimensional biological networks. *Sci. Rep.* 5, 12569.
- Ni, H., Morotti, S., and Grandi, E. (2018). A Heart for Diversity: Simulating Variability in Cardiac Arrhythmia Research. *Front. Physiol.* 9, 958.
- Nicolaou, P., Hajjar, R.J., and Kranias, E.G. (2009). Role of protein phosphatase-1 inhibitor-1 in cardiac physiology and pathophysiology. *J. Mol. Cell. Cardiol.* 47, 365–371.
- Ortega, F., Garcés, J.L., Mas, F., Kholodenko, B.N., and Cascante, M. (2006). Bistability from double phosphorylation in signal transduction. Kinetic and structural requirements. *FEBS J.* 273, 3915–3926.
- Pfeufer, A., Sanna, S., Arking, D.E., Müller, M., Gateva, V., Fuchsberger, C., Ehret, G.B., Orrù, M., Pattaro, C., Köttgen, A., et al. (2009). Common variants at ten loci modulate the QT interval duration in the QTSCD Study. *Nat. Genet.* 41, 407–414.
- Posch, M.G., Perrot, A., Geier, C., Boldt, L.H., Schmidt, G., Lehmkühl, H.B., Hetzer, R., Dietz, R., Gutberlet, M., Haverkamp, W., and Ozcelik, C. (2009). Genetic deletion of arginine 14 in phospholamban causes dilated cardiomyopathy with attenuated electrocardiographic R amplitudes. *Heart Rhythm* 6, 480–486.
- Pueyo, E., Corriás, A., Virág, L., Jost, N., Széll, T., Varró, A., Szentandrásy, N., Nánási, P.P., Burrage, K., and Rodríguez, B. (2011). A multiscale investigation of repolarization variability and its role in cardiac arrhythmogenesis. *Biophys. J.* 101, 2892–2902.
- Reddy, L.G., Jones, L.R., Cala, S.E., O'Brian, J.J., Tatulian, S.A., and Stokes, D.L. (1995). Functional reconstitution of recombinant phospholamban with rabbit skeletal Ca^{2+} -ATPase. *J. Biol. Chem.* 270, 9390–9397.
- Rigatti, M., Le, A.V., Gerber, C., Moraru, I.I., and Dodge-Kafka, K.L. (2015). Phosphorylation state-dependent interaction between AKAP7 γ and phospholamban increases phospholamban phosphorylation. *Cell. Signal.* 27, 1807–1815.
- Robia, S.L., Campbell, K.S., Kelly, E.M., Hou, Z., Winters, D.L., and Thomas, D.D. (2007). Förster Transfer Recovery Reveals That Phospholamban Exchanges Slowly From Pentamers but Rapidly From the SERCA Regulatory Complex. *Circ. Res.* 101, 1123–1129.
- Saucerman, J.J., Brunton, L.L., Michailova, A.P., and McCulloch, A.D. (2003). Modeling β -adrenergic control of cardiac myocyte contractility in silico. *J. Biol. Chem.* 278, 47997–48003.
- Saucerman, J., Healy, S.N., Belik, M.E., Puglisi, J.L., and McCulloch, A.D. (2004). Proarrhythmic Consequences of a KCNQ1 AKAP-Binding Domain Mutation. *Circ. Res.* 95, 1216–1224.
- Schäuble, S., Stavrum, A.K., Puntervoll, P., Schuster, S., and Heiland, I. (2013). Effect of substrate competition in kinetic models of metabolic networks. *FEBS Lett.* 587, 2818–2824.
- Schmitt, J.P., Kamisago, M., Li, G.H., Ahmad, F., Mende, U., Kranias, E.G., MacLennan, D.H., Seidman, J.G., and Seidman, C.E. (2003). Dilated

- Cardiomyopathy and Heart Failure Caused by a Mutation in Phospholamban. *Science* 299, 1410–1413.
- Schmitt, J.P., Ahmad, F., Lorenz, K., Hein, L., Schulz, S., Asahi, M., MacLennan, D.H., Seidman, C.E., Seidman, J.G., and Lohse, M.J. (2009). Alterations of phospholamban function can exhibit cardiotoxic effects independent of excessive sarcoplasmic reticulum Ca^{2+} -ATPase inhibition. *Circulation* 119, 436–444.
- Schreiber, G., Haran, G., and Zhou, H.-X. (2009). Fundamental aspects of protein-protein association kinetics. *Chem. Rev.* 109, 839–860.
- Simmerman, H.K.B., and Jones, L.R. (1998). Phospholamban: protein structure, mechanism of action, and role in cardiac function. *Physiol. Rev.* 78, 921–947.
- Simpson, P., and Savion, S. (1982). Differentiation of rat myocytes in single cell cultures with and without proliferating nonmyocardial cells. Cross-striations, ultrastructure, and chronotropic response to isoproterenol. *Circ. Res.* 50, 101–116.
- Smeazzetto, S., Tadini-Buoninsegni, F., Thiel, G., Berti, D., and Montis, C. (2016). Phospholamban spontaneously reconstitutes into giant unilamellar vesicles where it generates a cation selective channel. *Phys. Chem. Chem. Phys.* 18, 1629–1636.
- Soltis, A.R., and Saucerman, J.J. (2010). Synergy between CaMKII substrates and β -adrenergic signaling in regulation of cardiac myocyte Ca^{2+} handling. *Biophys. J.* 99, 2038–2047.
- Stammers, A.N., Süsser, S.E., Hamm, N.C., Hlynsky, M.W., Kimber, D.E., Kehler, D.S., and Duhamel, T.A. (2015). The regulation of sarco(endo)plasmic reticulum calcium-ATPases (SERCA). *Can. J. Physiol. Pharmacol.* 93, 843–854.
- Steenart, N.A.E., Ganim, J.R., Di Salvo, J., and Kranias, E.G. (1992). The phospholamban phosphatase associated with cardiac sarcoplasmic reticulum is a type 1 enzyme. *Arch. Biochem. Biophys.* 293, 17–24.
- Tada, M., Kirchberger, M.A., and Katz, A.M. (1975). Phosphorylation of a 22,000-dalton component of the cardiac sarcoplasmic reticulum by adenosine 3':5'-monophosphate-dependent protein kinase. *J. Biol. Chem.* 250, 2640–2647.
- Talosi, L., Edes, I., and Kranias, E.G. (1993). Intracellular mechanisms mediating reversal of beta-adrenergic stimulation in intact beating hearts. *Am. J. Physiol.* 264, H791–H797.
- Te Rijdt, W.P., van Tintelen, J.P., Vink, A., van der Wal, A.C., de Boer, R.A., van den Berg, M.P., and Suurmeijer, A.J.H. (2016). Phospholamban p.Arg14del cardiomyopathy is characterized by phospholamban aggregates, aggregates, and autophagic degradation. *Histopathology* 69, 542–550.
- Tribulova, N., Kurahara, L.H., Hlivak, P., Hirano, K., and Szeiffova Bacova, B. (2020). Pro-Arrhythmic Signaling of Thyroid Hormones and Its Relevance in Subclinical Hyperthyroidism. *Int. J. Mol. Sci.* 21, 2844.
- Tsimring, L.S. (2014). Noise in biology. *Rep. Prog. Phys.* 77, 026601.
- van der Zwaag, P.A., van Rijsingen, I.A.W., Asimaki, A., Jongbloed, J.D.H., van Veldhuisen, D.J., Wiesfeld, A.C.P., Cox, M.G.P.J., van Lochem, L.T., de Boer, R.A., Hofstra, R.M.W., et al. (2012). Phospholamban R14del mutation in patients diagnosed with dilated cardiomyopathy or arrhythmogenic right ventricular cardiomyopathy: evidence supporting the concept of arrhythmogenic cardiomyopathy. *Eur. J. Heart. Fail.* 14, 1199–1207.
- Varusai, T.M., Kolch, W., Kholodenko, B.N., and Nguyen, L.K. (2015). Protein-protein interactions generate hidden feedback and feed-forward loops to trigger bistable switches, oscillations and biphasic dose-responses. *Mol. Biosyst.* 11, 2750–2762.
- Verardi, R., Shi, L., Traaseth, N.J., Walsh, N., and Veglia, G. (2011). Structural topology of phospholamban pentamer in lipid bilayers by a hybrid solution and solid-state NMR method. *Proc. Natl. Acad. Sci. USA* 108, 9101–9106.
- Vostrikov, V.V., Mote, K.R., Verardi, R., and Veglia, G. (2013). Structural dynamics and topology of phosphorylated phospholamban homopentamer reveal its role in the regulation of calcium transport. *Structure* 21, 2119–2130.
- Watanabe, T., Delbridge, L.M., Bustamante, J.O., and McDonald, T.F. (1983). Heterogeneity of the action potential in isolated rat ventricular myocytes and tissue. *Circ. Res.* 52, 280–290.
- Wegener, A.D., and Jones, L.R. (1984). Phosphorylation-induced mobility shift in phospholamban in sodium dodecyl sulfate-polyacrylamide gels. Evidence for a protein structure consisting of multiple identical phosphorylatable subunits. *J. Biol. Chem.* 259, 1834–1841.
- Wittköpper, K., Fabritz, L., Neef, S., Ort, K.R., Grefe, C., Unsöld, B., Kirchhof, P., Maier, L.S., Hasenfuss, G., Dobrev, D., et al. (2010). Constitutively active phosphatase inhibitor-1 improves cardiac contractility in young mice but is deleterious after catecholaminergic stress and with aging. *J. Clin. Invest.* 120, 617–626.
- Wittköpper, K., Dobrev, D., Eschenhagen, T., and El-Armouche, A. (2011). Phosphatase-1 inhibitor-1 in physiological and pathological β -adrenoceptor signalling. *Cardiovasc. Res.* 91, 392–401.
- Wittmann, T., Lohse, M.J., and Schmitt, J.P. (2015). Phospholamban pentamers attenuate PKA-dependent phosphorylation of monomers. *J. Mol. Cell. Cardiol.* 80, 90–97.
- Yost, O., Friedenberg, S.G., Jesty, S.A., Olby, N.J., and Meurs, K.M. (2019). The R9H phospholamban mutation is associated with highly penetrant dilated cardiomyopathy and sudden death in a spontaneous canine model. *Gene* 697, 118–122.
- Zhang, X.-M., Kimura, Y., and Inui, M. (2005). Effects of phospholipids on the oligomeric state of phospholamban of the cardiac sarcoplasmic reticulum. *Circ. J.* 69, 1116–1123.
- Zhang, M., Kho, A.L., Anilkumar, N., Chibber, R., Pagano, P.J., Shah, A.M., and Cave, A.C. (2006). Glycated Proteins Stimulate Reactive Oxygen Species Production in Cardiac Myocytes. *Circulation* 113, 1235–1243.

STAR★METHODS
KEY RESOURCES TABLE

REAGENT or RESOURCE	SOURCE	IDENTIFIER
Antibodies		
Phospholamban (PLN, PLB) (pSer16) pAb	Badrilla	Product code: A010-12AP, RRID: AB_2617047
Phospholamban (PLN, PLB) mAb (clone A1)	Badrilla	Product code: A010-14, RRID: AB_2617049
Goat polyclonal anti-rabbit, HRP coupled	Jackson	Cat# 111-035-003, RRID: AB_2313567
Goat-anti-rabbit IgG (H+L), HRP coupled	Thermo Fischer	Cat# 31460, RRID: AB_228341
Goat-anti-mouse IgG (H+L), HRP coupled	Thermo Fischer	Cat# 31430, RRID: AB_228307
Chemicals, peptides, and recombinant proteins		
Clarity™ ECL Western Substrate	Bio-Rad	Cat# 1705060
Quick Coomassie Stain	Generon	Cat# NB-45-00078-1L
Pro-Q™ Diamond Stain	Thermo Fischer	Cat# P33300
Oriole™ Fluorescent Gel Stain	Bio-Rad	Cat# 161-0496
Ponceau S solution	Sigma-Aldrich	Cat# P7170
Geltrex LDEV-Free, hESC-Qualified, Reduced Growth Factor Basement Membrane Matrix	GIBCO	Cat# A1413302
Human PLN and AFA-PLN peptides	Pepscan	N/A
Collagenase, Type 2	Worthington	Cat# LS004176
Pancreatin	Sigma-Aldrich	Cat# P3292-25G
Dulbecco's Modified Eagle's Medium (DMEM)	Sigma-Aldrich	Cat# D5030
M199	Sigma-Aldrich	Cat# M4530
Fetal Calf Serum (FCS), heat inactivated	Sigma-Aldrich	Cat# F4135
Horse Serum (HS)	Sigma-Aldrich	Cat# H1270
Isoproterenol-hydrochlorid	Sigma-Aldrich	Cat# I5627-25G
Forskolin	Santa Cruz	Cat# sc-3562
Staurosporine	Cambridge Bioscience	Cat# SM97-5
PhosSTOP Inhibitor Cocktail Tablets	Roche	Cat# 04906837001
cOmplete, EDTA-free Protease Inhibitor Cocktail Tablets	Roche	Cat# 11873580001
Benzonase® Nuclease, Purity > 90%	Milipore	Cat# 70746-4
PKA, Catalytic Subunit, Bovine Heart	Sigma-Aldrich (Gift from Dr Thomas Kampourakis)	Cat# 539576
Experimental models: cell lines		
HEK293 cells	ATCC	CRL1573
Experimental models: organisms/strains		
<i>Rattus norvegicus</i> Wistar outbred pups. Strain: Hsd:WI	Envigo	Order code: 001; RRID: RGD_737960
Recombinant DNA		
pCDNA-PLN	Wittmann et al. 2015	N/A
Software and algorithms		
MATLAB R2019b	MathWorks	https://www.mathworks.com/
COPASI v4.26	(Hoops et al., 2006)	http://copasi.org/
GraphPad Prism v8.3	GraphPad Software, Inc.	https://www.graphpad.com
ImageLab v6.0	Bio-Rad	https://www.bio-rad.com/en-us/product/image-lab-software

(Continued on next page)

Continued		
REAGENT or RESOURCE	SOURCE	IDENTIFIER
Bifurcation diagrams	Daniel Koch	https://www.ebi.ac.uk/biomodels/MODEL1910220002
Model code	Daniel Koch	https://www.ebi.ac.uk/biomodels/MODEL2011110001
Other		
4–20% Mini-PROTEAN® TGX™ Precast Protein Gels	Bio-Rad	Cat# 4561096
μ-Dish 35 mm, cell culture dish	Ibidi	Cat# 81156

RESOURCE AVAILABILITY

Lead contact

Further information and requests for resources should be directed to and will be fulfilled by the lead contact, Daniel Koch (dkoch.research@protonmail.com).

Materials availability

This study did not generate new unique reagents.

Data and code availability

The custom code for models and simulations has been deposited in the BioModels database at: <https://www.ebi.ac.uk/biomodels/MODEL2011110001>.

EXPERIMENTAL MODEL AND SUBJECT DETAILS

Cell culture

Neonatal ventricular rat cardiomyocytes (NRCs) were isolated from Wistar rat pups and cultured as described previously (Simpson and Savion, 1982; Zhang et al., 2006). In brief, hearts were isolated from Wistar rat pups at postnatal day 0 to 2 and cut into 4 in ice cold ADS (116 mM NaCl, 20 mM HEPES, 0.8 mM NaH₂PO₄, 5.6 mM glucose, 5.4 mM KCl, 0.8mM MgSO₄). The hearts were enzymatically digested in a sequential manner by incubation in enzyme solution containing collagenase type II (57.5 U/ml) and pancreatin (1.5 mg/ml) for 4–5 times for 15 min in a shaking incubator at 37°C. The supernatant is collected into medium containing 5% FCS and passed through a 70 micron cell strainer (Falcon Corning) before being pelleted at low speed. The cells were pre-plated onto Nunc dishes in plating medium (DMEM, 5% FCS, 10% HS, non-essential amino acids, penicillin/streptomycin (P/S) and L-glutamine) for 2 h to allow non-myocytes to adhere. The non-adherent cardiomyocyte enriched fraction is then plated onto Geltrex (GIBCO) coated ibi-treat 35 mm dishes (Ibidi) and cultured at 37°C and 5% CO₂. Once the cells recovered (2–3 days), the non-adherent cells were washed away with culture medium (M199, DBSSK [116mM NaCl, 1 mM NaH₂PO₄, 0.8 mM MgSO₄, 32.1 mM NaHCO₃, 5.5 mM glucose, 1.8 mM CaCl₂ pH7.2], 4% Horse serum, P/S and L-glutamine) and cultured until day 8–9 for further maturation (medium exchange every 2–3 days).

HEK293 cells were cultured in DMEM medium supplemented with 10%FCS and P/S at 37°C and 5% CO₂ and not used beyond passage 15.

METHOD DETAILS

Experimental procedures

Reconstitution of PLN in detergent micelles

PLN (human wild-type and monomeric 'AFA' mutant C36A, C41F, C46A) was purchased as a synthetic peptide from Pepscan (Leystad, Netherlands). Successful synthesis of the peptide, as indicated by the correct molecular weight, was confirmed by Pepscan via mass-spectrometry (Figure S8A). For further analysis, 1 mg of lyophilized peptide was resolubilized in 1 ml of buffer for 2 h at room temperature under gentle overhead agitation (10 rpm) and subsequently centrifuged in a bench-top centrifuge for 10 min at > 10000 ×g, 4°C to get rid of insoluble residual material. For experiments involving PLN phosphorylation, we tested various detergents in a buffer with physiological ionic strength and pH and found that Triton X-100, which is a milder detergent than the harsh ionic SDS, is excellent at solubilizing PLN at rather low detergent concentrations and allows for effective pentamerization as well as rapid phosphorylation by PKA. We thus used the following Triton X-100 based buffer (TBB) for all experiments involving PLN phosphorylation: 50 mM TRIS-HCl pH 7.5, 100 mM NaCl, 10% (v/v) glycerol, 0.5% (v/v) Triton X-100, 2 mM DTT.

Interestingly, although showing less pentamerization than wild-type PLN, AFA-PLN was not entirely monomeric when kept on ice or even at room temperature. However, short heating for 15 min at 50°C was sufficient to dissociate all pentamers into monomers (Figure S8B). Although some smearing of band was visible after SDS-PAGE, no precipitation in solution was visible even after

45 min at 50 °C and AFA-PLN still appears to be an excellent substrate for PKA after heating, which indicates that heating PLN for 15 min at 50 °C does not seriously denature the protein. Once dissociated, no significant re-oligomerization was observed after incubation at 25 °C for 2 h (the time frame for our phosphorylation experiments) or after snap-freezing and quick thawing.

Semi-native SDS-PAGE

PLN forms stable pentamers even in harsh SDS sample buffer which only dissociate upon sample boiling. As SDS sample buffer is likely to interfere with less stable proteins (e.g., enzymes), all phosphorylation reactions were performed in TBB and analyzed using semi-native SDS-PAGE by directly applying the native samples (e.g., phosphorylated or unphosphorylated PLN in TBB) into the wells of the gels (4%–20% Mini-PROTEAN® TGX™ Precast Protein Gels, Bio-Rad) without addition of other buffers or boiling. All samples contained 10% glycerol to allow samples to settle into the wells and to avoid mixing with running buffer.

Oriole staining and quantification of absolute concentrations

Since conventional Coomassie staining of protein gels only has limited sensitivity and more sensitive silver-staining protocols are typically not suitable for quantitative purposes, we used Oriole™ Fluorescent Gel Stain for detection and quantification of PLN (Bio-Rad). Staining was performed for 90 min according to the manufacturer's instructions. Gels were imaged on a ChemiDoc™ XRS+ imaging system (Bio-Rad). The method shows a wide linear range for PLN and is neither affected by oligomerization or phosphorylation status of PLN (Figures S8C–S8E). Since the Oriole™ signal is not affected by oligomeric state, the signal for an oligomeric species is directly proportional to the number protomers in a complex. Knowing the total PLN concentration of a sample thus allows to calculate the absolute concentrations of monomers and pentamers by $[PLN_x] = \frac{F_{Oriole} \cdot [PLN_{tot}]}{x}$, where F_{Oriole} is the fraction which PLN_x contributes to the total Oriole™ signal. In either SDS-sample buffer or TBB we observed no other PLN forms than monomers and pentamers and occasionally a weak band for dimers at higher concentrations. Since the dimer band was not well demarked and negligible compared to the monomer and pentamer bands, we did not quantify dimers.

Dilution experiments

Samples were diluted in TBB or SDS with end concentrations ranging from ≈ 0.96 mg/ml (undiluted) to 5 μ g/ml in a final volume of 40 μ l. After dilution, samples were left to pre-equilibrate for 45 min at room temperature before being incubated in a PCR machine for 75 min at 37 °C with heated lid at 50 °C to avoid evaporation. To avoid disturbing the pentamerization equilibrium by sample cooling, semi-native SDS-PAGE was performed using SDS-running buffer pre-warmed to 37 °C. Total protein amount for each well was within the determined linear range.

For production of phosphorylated PLN, TBB samples were supplemented with 250 μ M ATP, 5 mM $MgCl_2$ and 3 U/ μ l PKA (Sigma-Aldrich). Phosphorylation was allowed to proceed for 16 h at 4 °C and given another hour at room temperature to approach completion. To avoid differences due to ionic strength, precipitation or evaporation, samples for unphosphorylated PLN in TBB were treated accordingly, but without addition of PKA.

Dissociation time course experiments

To determine pentamer dissociation dynamics, 40 μ l of 0.96 mg/ml PLN in TBB supplemented with 250 μ M ATP and 5 mM $MgCl_2$ were pre-equilibrated for 30 min at RT followed by 30 min at 37 °C. Samples were diluted 20-fold with 37 °C pre-warmed TBB and incubated for up to 15 min at 37 °C. To simultaneously determine the oligomeric status at different time points, dilutions were started in replicates at 1.5, 7.5 and 15 min before semi-native SDS-page (performed with 37 °C pre-warmed running buffer). Samples were processed and loaded to the gel using a multichannel pipette to minimize sample processing time.

In vitro phosphorylation time courses of PLN by PKA

To determine the competitive effect of pentamers on monomer phosphorylation, we compared the phosphorylation dynamics of wild-type PLN and AFA-PLN. To ensure complete dissociation into monomers, AFA-PLN was heated to 50 °C for 15 min followed by 10 min incubation at 25 °C immediately before the experiment. Phosphorylation reactions were performed at 25 °C in a volume of 150 μ l TBB supplemented with 250 μ M ATP, 5 mM $MgCl_2$ and 6.25 U/ μ l (≈ 7.7 nM) PKA (Sigma-Aldrich) with an end concentration of 0.962 mg/ml (≈ 157 μ M) wild-type PLN or 0.32 mg/ml AFA-PLN (at which there is an equimolar monomer concentration of ≈ 52 μ M between wild-type PLN and AFA-PLN). Samples (8 μ l) were taken at 0, 5, 15, 30, 60, 90 and 120 min, snap-frozen and stored in liquid nitrogen until separation by semi-native SDS-PAGE (1.5 μ l/well for wild-type PLN, 2 μ l/well for AFA-PLN). Phosphorylation was detected using Pro-Q™ Diamond staining (Thermo Fisher) according to the manufacturer's instructions (1 h staining step), followed by Quick Coomassie Staining (Generson) to visualize total protein amount. Gels were imaged on a ChemiDoc™ XRS+ imaging system (Bio-Rad) and data were quantified using the ImageLab v6.0 software (Bio-Rad). All monomer phosphorylation data were in the linear range of the Pro-Q™ Diamond stain. The phosphorylation signal of each experiment was corrected by total protein amount as given by the Coomassie signal and by subtracting the background signal at 0 min. Relative phosphorylation levels were calculated by fitting progress curves of wild-type pentamers and AFA-PLN₁ to a hyperbola ($Y(t) = S_{max} * t / (K + t)$) and dividing the corrected phosphorylation signal by S_{max} (the signal expected for complete phosphorylation). Since phosphorylation of wild-type monomers was still linear during the probed reaction period (preventing reliable fitting to a hyperbola), relative phosphorylation was calculated by using S_{max} from wild-type pentamers scaled by $r = 52$ μ M / (157 - 52) μ M, the amount of phosphorylation sites in monomers relative to the amount of phosphorylation sites in pentamers at the given total concentration of PLN.

PKA-dependent phosphorylation of PLN in transfected HEK293 cells (Schmitt lab)

pcDNA3-PLN was expressed in HEK293 cells as described previously (Wittmann et al., 2015). PLN-expressing cells were then treated for 40 min with forskolin (Santa Cruz) in DMEM medium at 37 °C at different concentrations to induce PKA-dependent

phosphorylation of PLN. Cells were washed with PBS before mechanical lysis in PBS containing protease inhibitors and phosphatase inhibitors. Lysates were centrifuged for 20 min at $> 10,000 \times g$ at 4°C and supernatants were used for western blot analysis. Equal amounts of protein (Pierce® BCA Assay Kit, ThermoScientific) were separated on 15% polyacrylamide gels and transferred to PVDF membranes (Immobilon®-P, Millipore) before overnight incubation with primary antibodies in TBS-T / 5% milk (10 mM Tris, 150 mM NaCl, 0.1% Tween 20, pH 7.6, 5% milk) at 4°C . Antigen detection was performed by chemiluminescence using secondary antibodies coupled to horseradish peroxidase (Thermo Fischer) and Luminata Forte Western HRP substrate (Millipore). The following antibodies were used for detection of proteins: anti-PLN (A1, Badrilla, 1:5000 dilution), anti-phospho-PLN (Ser16, Badrilla, 1:5000 dilution). Data were quantified using the ImageLab v6.0 software (Bio-Rad).

Hysteresis detection of PKA-dependent PLN phosphorylation in neonatal rat cardiomyocytes

Hysteresis is defined as the dependence of the state of a system on the history of that system. A common approach for detecting hysteresis in a process ('output') which is triggered by a certain stimulus ('input') is therefore to compare the steady state output at a certain input level when the system had no previous input versus when the system relaxes from a much higher input level: if the output is different, the system exhibits hysteresis. When designing experiments aimed at detecting hysteresis, however, it is important to consider the timescales at which the process under investigation reaches steady state in terms of the time to respond to stimulation, and in terms of the relaxation time after stimulus removal.

PLN phosphorylation in response to β -adrenergic stimulation of intact rat hearts with isoproterenol has been demonstrated to rapidly reach steady state within 1 min both at half-maximal and maximal stimulation (Kuschel et al., 1999). Similarly, dephosphorylation of PLN in isoproterenol stimulated rat hearts after stimulus removal has been reported to be complete within 3 min (Talosi et al., 1993). In agreement with these studies, we found PLN phosphorylation upon $1 \mu\text{M}$ isoproterenol stimulation in isolated NRCs to be complete within 1 min and dephosphorylation after isoproterenol removal to be complete within 2 min (data not shown).

To test for hysteresis in PLN phosphorylation, 8-9 day old NRCs were treated according to either a 'going up' or 'coming down' protocol. *Going up*: all medium was removed from the dishes and replaced with 1 mL culture medium containing the experimental target concentration of isoproterenol ([ISO]). After incubation for 5 min at 37°C , cells were washed in 1 mL PBS + target [ISO] (at room temperature) before all liquid was thoroughly removed. $18 \mu\text{l}$ of ice cold lysis buffer were added to the cells (50 mM Tris pH 7.5, 100 mM NaCl, 1 mM MgCl_2 , 2 mM DTT, 0.5% (v/v) Triton x-100, 10% Glycerol, 2x PhosSTOP, 0.5 μM Staurosporine, 1x cOmplete, EDTA-free Protease Inhibitor Cocktail, Benzonase 1.5 μl / ml buffer). Lysed cells were directly scraped off the dish with a bent 200 μl pipette tip and snapfrozen in liquid nitrogen or briefly stored on ice until the dish was processed. *Coming down*: all medium was removed from the dishes and replaced with 1 mL culture medium containing $1 \mu\text{M}$ [ISO] in which cells were incubated for 2 min at 37°C for pre-stimulation. After pre-stimulation, all medium was removed and cells were washed for 1 min in 1.5 mL culture medium at target [ISO]. After washing out the excess ISO, the medium was replaced again with 1 mL new culture medium at target [ISO] and cells were incubated for 5 min at 37°C to reach steady state before removing the medium and washing the cells in 1 mL PBS + target [ISO] at room temperature. $18 \mu\text{l}$ of ice cold lysis buffer were added to the cells. Lysed cells were directly scraped off the dish with a bent 200 μl pipette tip and snapfrozen in liquid nitrogen or briefly stored on ice until the dish was processed.

Note: the washing step after pre-stimulation is essential and particular care needs to be taken to remove *all* liquid from the dishes after pre-stimulation and washing in order to ensure that non-pre-stimulated and pre-stimulated cells are exposed to the same target [ISO] at steady state. To minimize the impact of environmental parameters such as temperature, dishes were handled on a heating pad at 37°C and medium containing target [ISO] was pre-warmed and kept in 37°C warm water until use. To minimize experimental variation, the same batch of target [ISO] adjusted culture medium was used for non-pre-stimulated and pre-stimulated cells.

Cell lysates were pelleted by centrifugation for 5 min at $>10000 \times g$, 4°C before $13 \mu\text{l}$ of the soluble fraction were separated by semi-native SDS-PAGE followed by wet transfer of the proteins to a nitrocellulose membrane (GE Healthcare) at 100V constant current for 45 min in blotting buffer (3 g/l Tris, 14.5 g/l glycine, 0.1 g/l SDS, 20% (v/v) ethanol). After blotting, membranes were stained with Ponceau S solution to normalize for total protein amount and to confirm successful transfer. Unspecific binding sites on the membrane were blocked for 30 min at room temperature in low-salt binding buffer / 5% milk (10 g/l Tris pH 7.4, 9 g/l NaCl, 1% (v/v) Tween-20, 5% (w/v) milk powder) before the membrane was incubated overnight with primary antibodies (anti-pSer16 PLN, 1:4000 dilution) at 4°C .

Antigen detection was performed by chemiluminescence using secondary antibodies coupled to horseradish peroxidase (goat anti-rabbit pAb, Jackson, 1:1000 dilution) and Clarity ECL Western Substrate (Bio-Rad) on a ChemiDoc™ XRS+ imaging system (Bio-Rad). Data were quantified using the ImageLab v6.0 software (Bio-Rad). All data were in the combined linear range. For analysis, pSer16-PLN signals were corrected by the total protein signal and normalized to the maximum value. To visualize data from different membranes on the same plot, data was scaled by setting the total 'going up'-signal at 5 nM target [ISO] to 0.5 and at $1 \mu\text{M}$ target [ISO] to 1. Statistical comparisons were only made between signals from the same membrane.

Development of the mathematical model

In order to develop a mathematical model of the PLN regulatory network, we first needed to find a mathematical description of how PLN monomers assemble into pentamers. Therefore, we considered several mass action kinetics based possibilities.

A mass action kinetics model of PLN pentamer assembly

The assembly of PLN monomers into pentamers likely follows either of three possible pathways depicted in the scheme on the left side of Figure S9. While model 1 considers all reaction routes possible, model 2 and model 3 assume pentamer assembly to follow a monomer \rightarrow dimer \rightarrow tetramer \rightarrow pentamer or monomer \rightarrow dimer \rightarrow trimer \rightarrow pentamer pathway, respectively. Dimers, trimers and

tetramers have been reported *in vitro* (see e.g., Reddy et al., 1995), but monomers and pentamers are typically the predominantly observed molecular species (including the present study). While this implies that PLN oligomers with < 5 protomers are usually low abundant and transient species, it is difficult to decide between any of the three pathways on *a priori* grounds. We thus formulated mass-action kinetics models for each possibility (Figure S9).

While the schemes for model variant 2 and 3 are linear reaction routes, model 1 contains two cycles. For thermodynamic reasons, model 1 must thus obey the following relations between equilibrium constants:

$$K_{2,3}K_{3,5} = K_{2,4}K_{4,5} \quad (\text{Equation 1})$$

$$K_{1,2}K_{2,4} = K_{2,3}K_{3,4} \quad (\text{Equation 2})$$

$$K_{1,2}K_{3,5} = K_{3,4}K_{4,5} \quad (\text{Equation 3})$$

Replacing equilibrium constants with the rate constants shown in Figure S9 yields:

$$\frac{k_3k_{11}}{k_4k_{12}} = \frac{k_7k_9}{k_8k_{10}} \quad (\text{Equation 4})$$

$$\frac{k_1k_9}{k_2k_{10}} = \frac{k_3k_5}{k_4k_6} \quad (\text{Equation 5})$$

$$\frac{k_1k_{11}}{k_2k_{12}} = \frac{k_5k_7}{k_6k_8} \quad (\text{Equation 6})$$

For parameter estimation, k_7 and k_5 were assigned by solving Equations 4 and 5, respectively. Equation 6 was used as an additional constraint on the parameter space.

After setting up the constraints for model 1, we used the data from our dilution and dissociation time course experiments for calibration of all three models. We found that all three models can reproduce the dissociation time course sufficiently (Figure S10A). Model 1 and model 2 show generally good agreement with the data from dilution experiments apart from small deviations from the measured pentamer concentrations at the lower range of total concentrations (Figure S10B). Model 3, on the other hand, shows a systematic deviation from most experimentally measured pentamer concentrations. Simulated steady-state concentrations of monomers and pentamers are fairly similar for all three model variants (Figure S10C), indicating that the shortcoming of model 3 is a mismatch at the timescale of hours. Also note that at steady state (which in this case is identical to the equilibrium of the reaction) and at $[\text{PLN}]_{\text{tot}} > 100 \mu\text{M}$, there is effective monomer buffering (Figure S10C, red curves).

Moreover, model 3 predicts high trimer concentrations at steady state which should have been clearly visible in our experimental conditions. Taken together, this indicates that model 3, solely relying on the monomer \rightarrow dimer \rightarrow trimer \rightarrow pentamer pathway, cannot account for our experimental data. In contrast, although the available data are not sufficient to identify individual rate constants (Figure S10D), we conclude that both model 1 and 2 can faithfully reproduce most of our experimental data. To choose between models (using their best fit parameter sets), we applied the Akaike Information Criterion (AIC) which ranked model 2 as best performing (AIC scores: model 1 = -735.2 , model 2 = -741.2 , model 3 = -735.9). We, therefore, used model 2 as the basis for the extended model in the remainder of this study.

Before expanding the model, we used our quantitative description of the pentamerization reaction to re-evaluate some of the numbers published on what the effective concentration of PLN in the SR membrane might be and what fraction of SERCA will be occupied at this concentration. In SDS-PAGE analyses of cell/tissue homogenates, 75%–90% of PLN is pentameric (MacLennan and Kranias 2003; Kimura et al., 1997). If oligomerization parameters of PLN in the SR membrane are similar to those in detergent micelles, this would require PLN concentrations of 200 to 600 μM *in vivo* (Figure S11). Although this appears to be very high, PLN is known to be very abundant (*cf.* Table: review protein concentrations) and the required number of molecules to reach high effective concentrations is likely lower on a two-dimensional surface such as the SR membrane than in solution (Abel et al., 2012). Moreover, a PLN concentration of $\approx 250 \mu\text{M}$ would result in a fractional SERCA occupation of about 40%–60% according to published K_d values. This fits well to the observation that about 40% of SERCA activity is functionally regulated by PLN (Brittsan et al., 2000). At a total PLN concentration of 250 μM , the concentration of monomers is $\approx 58 \mu\text{M}$, the concentration of pentamers $\approx 38 \mu\text{M}$, i.e., about 76% of PLN molecules would be in a pentameric complex. *In vivo*, oligomerization of PLN happens in the SR lipid bilayer, an approximately two-dimensional surface. Thus, PLN exists not in a well-mixed solution and its concentration is rather given by molecules per area. For our purposes, however, we assume these processes can be approximated by an effective PLN concentration which allows us to formulate the model with ODEs, similar to previous models (Saucerman et al., 2003).

Full phospholamban model in the context of β -adrenergic stimulation

As outlined in the main text, we extended the mass action kinetics model of pentamerization by accounting for PLN phosphorylation at serine 16. Phosphorylation of phospholamban leads to a combinatorial expansion of oligomeric phospho-isoforms for which we denote the number phosphorylated subunits by a superscript (ρX), e.g., $PLN_1^{(\rho 0)}$ for unphosphorylated monomers or $PLN_5^{(\rho 3)}$ for pentamers with 3 phosphorylated subunits etc. We further included reactions and molecules with a well established role in regulating PLN phosphorylation at serine 16, i.e., enzymes PKA, PP1, PP2A and inhibitor-1. Figure S12A shows the complete reaction scheme of our model. Before substituting rate identifiers with their rate laws, the model equations are as follows:

Model equations

$$\frac{d}{dt} [PLN_1^{(\rho 0)}](t) = 2v_2 + v_4 + v_{20} + v_{24} + v_{28} + v_{32} + v_{36} + v_{40} + v_{41}$$

$$-2v_1 - v_3 - v_{19} - v_{23} - v_{27} - v_{31} - v_{35} - v_{39}$$

$$\frac{d}{dt} [PLN_2^{(\rho 0)}](t) = v_1 + 2v_8 + v_{10} + v_{12} - v_2 - 2v_7 - v_9 - v_{11}$$

$$\frac{d}{dt} [PLN_2^{(\rho 1)}](t) = v_3 + v_{10} + 2v_{14} + v_{16} - v_4 - v_9 - 2v_{13} - v_{15}$$

$$\frac{d}{dt} [PLN_2^{(\rho 2)}](t) = v_5 + v_{12} + v_{16} + 2v_{18} - v_6 - v_{11} - v_{15} - 2v_{17}$$

$$\frac{d}{dt} [PLN_4^{(\rho 0)}](t) = v_7 + v_{20} + v_{22} - v_8 - v_{19} - v_{21}$$

$$\frac{d}{dt} [PLN_4^{(\rho 1)}](t) = v_9 + v_{24} + v_{26} - v_{10} - v_{23} - v_{25}$$

$$\frac{d}{dt} [PLN_4^{(\rho 2)}](t) = v_{11} + v_{13} + v_{28} + v_{30} - v_{12} - v_{14} - v_{27} - v_{29}$$

$$\frac{d}{dt} [PLN_4^{(\rho 3)}](t) = v_{15} + v_{32} + v_{34} - v_{16} - v_{31} - v_{33}$$

$$\frac{d}{dt} [PLN_4^{(\rho 4)}](t) = v_{17} + v_{36} + v_{38} - v_{18} - v_{35} - v_{37}$$

$$\frac{d}{dt} [PLN_5^{(\rho 0)}](t) = v_{19} + v_{43} + v_{44} - v_{20} - v_{42}$$

$$\frac{d}{dt} [PLN_5^{(\rho 1)}](t) = v_{21} + v_{23} + v_{42} + v_{46} + v_{47} - v_{22} - v_{24} - v_{43} - v_{44} - v_{45}$$

$$\frac{d}{dt} [PLN_5^{\rho 2}] (t) = V_{25} + V_{27} + V_{45} + V_{49} + V_{50} - V_{26} - V_{28} - V_{46} - V_{47} - V_{48}$$

$$\frac{d}{dt} [PLN_5^{\rho 3}] (t) = V_{29} + V_{31} + V_{48} + V_{52} + V_{53} - V_{30} - V_{32} - V_{49} - V_{50} - V_{51}$$

$$\frac{d}{dt} [PLN_5^{\rho 4}] (t) = V_{33} + V_{35} + V_{51} + V_{55} + V_{56} - V_{34} - V_{36} - V_{52} - V_{53} - V_{54}$$

$$\frac{d}{dt} [PLN_5^{\rho 5}] (t) = V_{37} + V_{54} - V_{38} - V_{55} - V_{56}$$

$$\frac{d}{dt} [Inh - 1^{(\rho 0)}] (t) = V_{58} - V_{57}$$

$$\frac{d}{dt} [PP1] (t) = V_{60} - V_{59}$$

We do not account for synthesis and degradation of proteins and thus assume the total amounts of PLN, inhibitor-1 and PP1 to be conserved. This allows us to determine three species by the following algebraic equations:

$$[PLN_1^{\rho 1}] (t) = [PLN]_{tot} - [PLN_1^{\rho 0}] (t) - 2([PLN_2^{\rho 0}] (t) + [PLN_2^{\rho 1}] (t) + [PLN_2^{\rho 2}] (t))$$

$$-4([PLN_4^{\rho 0}] (t) + [PLN_4^{\rho 1}] (t) + [PLN_4^{\rho 2}] (t) + [PLN_4^{\rho 3}] (t) + [PLN_4^{\rho 4}] (t))$$

$$-5([PLN_5^{\rho 0}] (t) + [PLN_5^{\rho 1}] (t) + [PLN_5^{\rho 2}] (t) + [PLN_5^{\rho 3}] (t) + [PLN_5^{\rho 4}] (t) + [PLN_5^{\rho 5}] (t))$$

$$[PP1 : Inh - 1^{(\rho 1)}] (t) = [PP1]_{tot} - [PP1] (t)$$

$$[Inh - 1^{(\rho 1)}] (t) = [Inh - 1]_{tot} - [Inh - 1^{(\rho 0)}] (t) - [PP1 : Inh - 1^{(\rho 1)}] (t),$$

where $[PLN]_{tot}$, $[PP1]_{tot}$ and $[Inh - 1]_{tot}$ are the conserved total concentrations of PLN, PP1 and inhibitor-1, respectively.

Other model quantities (relative phosphorylation levels)

For the sake of clarity, only relative phosphorylation levels of PLN monomers and pentamers, defined as $PLN_1^{\rho p} = \frac{[PLN_1^{\rho p}]}{[PLN_1^{\rho 0}] + [PLN_1^{\rho 1}]}$ and $PLN_5^{\rho p} = \frac{[PLN_5^{\rho 1}] + 2[PLN_5^{\rho 2}] + 3[PLN_5^{\rho 3}] + 4[PLN_5^{\rho 4}] + 5[PLN_5^{\rho 5}]}{5([PLN_5^{\rho 0}] + [PLN_5^{\rho 1}] + [PLN_5^{\rho 2}] + [PLN_5^{\rho 3}] + [PLN_5^{\rho 4}] + [PLN_5^{\rho 5}])}$, respectively, have been plotted.

Reaction rates

Oligomerization of PLN

Combinatorial expansion due to phospho-isoforms of oligomeric complexes can lead to thermodynamic inconsistencies if mass action kinetics are applied to the oligomerization reactions as given in a reaction scheme. This can be circumvented by introducing balancing coefficients which account for the effective oligomerization rates regardless of combinatorial effects. We thus modeled oligomerization reactions with balanced mass action kinetics as described in Koch (2020).

Dynamic equilibrium of PLN

How exactly dynamic equilibrium of PLN works on the molecular level is currently not known, although electrostatic interactions (Cornea et al., 1997; Hou et al., 2008) and anionic detergents seem to play an important role. Since electrostatic interactions can increase the association rate constant of an interaction (Schreiber et al., 2009), we assumed this to be the case for phosphorylated PLN. We, therefore, introduced a dimensionless control parameter ω , which increases association

rate constants of oligomerization reactions in an exponential fashion depending on how many phosphorylated subunits are involved.

Enzymatic reactions catalyzed by PKA, PP1 and PP2A

Reactions catalyzed by PKA, PP2A were modeled using a modified Michaelis-Menten rate law, which accounts for competition between multiple substrates S_1, \dots, S_n :

$$v_i = \frac{V_{max} S_i}{K_m \left(1 + \sum_{j \in J \setminus \{i\}} \frac{S_j}{K_m} \right) + S_i}$$

where $J = \{1, \dots, n\}$, and v_i describes the rate of consumption of substrate S_i (Schäuble et al., 2013). Since PLN pentamers and monomers are several orders of magnitude more abundant than dimers or tetramers, the possibility of direct dimer or tetramer (de-)phosphorylation can be ignored and was thus not accounted for in this study. Studying the mechanisms of phosphorylation and dephosphorylation of PLN in native SR membrane preparations, (Li et al., 1990) found that the distribution of pentameric phospho-isoforms after stimulation of PKA follows a binomial pattern, suggesting that PKA utilizes a non-cooperative random mechanism for phosphorylation of PLN pentamers (Li et al., 1990). In contrast, completely unphosphorylated PLN pentamers were the first species to accumulate during dephosphorylation, which led to a strongly U-shaped distribution of pentameric phospho-isoforms, which suggests that dephosphorylation is strongly positive cooperative so that the removal of a phosphate group enhances removal of the next (cf. Figure S12B) (Li et al., 1990). Although the data from Li et al. (1990) did not allow further characterization in terms of identifying kinetic constants for individual steps, it is likely that each dephosphorylation step increases the catalytic rate constant or the substrate affinity (or both) for the subsequent step. To account for the cooperativity observed in PLN pentamer dephosphorylation (Li et al., 1990), we assumed that PP1 (since it is the phosphatase responsible for most PLN dephosphorylation (MacDougall et al., 1991; Steenaert et al., 1992)) dephosphorylates pentamers by a positive cooperative mechanism and introduced two dimensionless control parameters $\phi \leq 1$ and $\chi \geq 1$. For pentamers with $n \geq 1$ phosphorylated subunits, we multiplied $k_{cat,PP1,PLN_n}$ with factor ϕ^{n-1} and $K_{m,PP1,PLN_n}$ with factor χ^{n-1} . For $\phi < 1$ we thus increase the turnover number for each phosphate group removed from a pentamer, with $k_{cat,PP1,PLN_n}$ being an upper limit. For $\chi > 1$ we thus reduce the Michaelis-constant for each phosphate group removed from a pentamer, with $K_{m,PP1,PLN_n}$ representing highest substrate affinity (lowest K_m value). Such modes of cooperativity can be called *v-type* and *k-type* cooperativity, respectively (Fersht, 1999) (see Figure S12C for an illustration). Since *v-type* cooperativity is the simpler assumption (as it does not influence the competition terms determined by the K_m values in the rate laws), the default parameter set assumes only presence of *v-type* cooperativity. Where the influence of *k-type* cooperativity is studied, deviations from this default assumption are explicitly mentioned.

For simplicity and lack of data suggesting otherwise, we assume $K_{m,PP1,PLN_n} = K_{m,PP1,PLN_5}$ and $k_{cat,PP1,PLN_n} = k_{cat,PP1,PLN_5}$, implying that the kinetic constants of monomer dephosphorylation pose an upper efficiency limit for pentamer dephosphorylation. If one assumes that these pose a lower limit for pentamer dephosphorylation, simulated pentamer phosphorylation occurs slower and at lower steady-state levels than monomers (data not shown), contradicting experimental observations (Wittmann et al., 2015). Potentially, this could be amended by assuming higher k_{cat} and lower K_m values for pentamer phosphorylation by PKA compared to monomers. However, since available kinetic data is not sufficient to distinguish between these possibilities, our current implementation of cooperative pentamer dephosphorylation is one of the simplest and requires the fewest assumptions.

Following the outlined rationale of the chosen rate laws, the complete list of the reaction rates of the model is given by:

Oligomer association/dissociation rates

$$v1 = k_1 \cdot [PLN_1^{(p0)}]^2, v2 = k_2 \cdot [PLN_2^{(p0)}], v3 = 2 \cdot k_1 \cdot [PLN_1^{(p0)}] \cdot [PLN_1^{(p1)}],$$

$$v4 = k_2 \cdot [PLN_2^{(p1)}], v5 = k_1 \cdot \omega \cdot [PLN_1^{(p1)}]^2, v6 = k_2 \cdot [PLN_2^{(p2)}],$$

$$v7 = k_3 \cdot [PLN_2^{(p0)}]^2, v8 = k_4 \cdot [PLN_4^{(p0)}], v9 = 2 \cdot k_3 \cdot [PLN_2^{(p0)}] \cdot [PLN_2^{(p1)}],$$

$$v10 = k_4 \cdot [PLN_4^{(p1)}], v11 = 2 \cdot k_3 \cdot [PLN_2^{(p0)}] \cdot [PLN_2^{(p2)}], v12 = \frac{1}{2} \cdot k_4 \cdot [PLN_4^{(p2)}],$$

$$v13 = k_3 \cdot \omega \cdot [PLN_2^{(p1)}]^2, v14 = \frac{1}{2} \cdot k_4 \cdot [PLN_4^{(p2)}], v15 = 2 \cdot k_3 \cdot \omega^2 \cdot [PLN_2^{(p1)}] \cdot [PLN_2^{(p2)}],$$

$$v16 = k_4 \cdot [PLN_4^{(p3)}], v17 = k_3 \cdot \omega^3 \cdot [PLN_2^{(p2)}]^2, v18 = k_4 \cdot [PLN_4^{(p4)}], v19 = k_5 \cdot [PLN_1^{(p0)}] \cdot [PLN_4^{(p0)}],$$

$$v20 = k_6 \cdot [PLN_5^{(p0)}], v21 = k_5 \cdot [PLN_1^{(p1)}] \cdot [PLN_4^{(p0)}], v22 = \frac{1}{2} \cdot k_6 \cdot [PLN_5^{(p1)}],$$

$$v23 = k_5 \cdot [PLN_1^{(p0)}] \cdot [PLN_4^{(p1)}], v24 = \frac{1}{2} \cdot k_6 \cdot [PLN_5^{(p1)}], v25 = k_5 \cdot \omega \cdot [PLN_1^{(p1)}] \cdot [PLN_4^{(p1)}],$$

$$v26 = \frac{1}{2} \cdot k_6 \cdot [PLN_5^{(p2)}], v27 = k_5 \cdot [PLN_1^{(p0)}] \cdot [PLN_4^{(p2)}], v28 = \frac{1}{2} \cdot k_6 \cdot [PLN_5^{(p2)}],$$

$$v29 = k_5 \cdot \omega^2 \cdot [PLN_1^{(p1)}] \cdot [PLN_4^{(p2)}], v30 = \frac{1}{2} \cdot k_6 \cdot [PLN_5^{(p3)}], v31 = k_5 \cdot [PLN_1^{(p0)}] \cdot [PLN_4^{(p3)}],$$

$$v32 = \frac{1}{2} \cdot k_6 \cdot [PLN_5^{(p3)}], v33 = k_5 \cdot \omega^3 \cdot [PLN_1^{(p1)}] \cdot [PLN_4^{(p3)}], v34 = \frac{1}{2} \cdot k_6 \cdot [PLN_5^{(p4)}],$$

$$v35 = k_5 \cdot [PLN_1^{(p0)}] \cdot [PLN_4^{(p4)}], v36 = \frac{1}{2} \cdot k_6 \cdot [PLN_5^{(p4)}], v37 = k_5 \cdot \omega^4 \cdot [PLN_1^{(p1)}] \cdot [PLN_4^{(p4)}],$$

$$v38 = k_6 \cdot [PLN_5^{(p5)}].$$

Phosphorylation and dephosphorylation of PLN

$$v39 = \frac{[PKA]k_{cat,PKA:PLN_1} [PLN_1^{(p0)}]}{K_{m,PKA:PLN_1} \left(1 + \sum_{i \in I} \left(\frac{[PLN_5^{(p1)}]}{K_{m,PKA:PLN_5}} \right) + \frac{[Inh-1^{(p0)}]}{K_{m,PKA:Inh-1}} \right) + [PLN_1^{(p0)}]}$$

$$v40 = \frac{[PP1]k_{cat,PP1:PLN_1} [PLN_1^{(p1)}]}{K_{m,PP1:PLN_1} \left(1 + \sum_{j \in J} \frac{[PLN_5^{(p1)}]}{K_{m,PP1:PLN_5}} \right) + [PLN_1^{(p1)}]}$$

$$v41 = \frac{V_{max,PP2A:PLN_1} [PLN_1^{(p1)}]}{K_{m,PP2A} + [PLN_1^{(p1)}] + \sum_{j \in J} ([PLN_5^{(p1)}]) + [Inh-1^{(p1)}]}$$

$$v42 = \frac{[PKA]k_{cat,PKA:PLN_5} [PLN_5^{(p0)}]}{K_{m,PKA:PLN_5} \left(1 + \frac{[PLN_5^{(p0)}]}{K_{m,PKA:PLN_1}} + \sum_{i \in I \setminus \{0\}} \left(\frac{[PLN_5^{(p1)}]}{K_{m,PKA:PLN_5}} \right) + \frac{[Inh-1^{(p0)}]}{K_{m,PKA:Inh-1}} \right) + [PLN_5^{(p0)}]}$$



$$v43 = \frac{[PP1]k_{cat,PP1,PLN_5} [PLN_5^{(p1)}]}{K_{m,PP1,PLN_5} \left(1 + \frac{[PLN_5^{(p1)}]}{K_{m,PP1,PLN_1}} + \sum_{j \in J \setminus \{1\}} \frac{[PLN_5^{(pj)}]}{\chi^{j-1} K_{m,PP1,PLN_5}} \right) + [PLN_5^{(p1)}]}$$

$$v44 = \frac{V_{max,PP2A,PLN_5} [PLN_5^{(p1)}]}{K_{m,PP2A} + [PLN_1^{(p1)}] + \sum_{j \in J} ([PLN_5^{(pj)}]) + [Inh - 1^{(p1)}]}$$

$$v45 = \frac{[PKA]k_{cat,PKA,PLN_5} [PLN_5^{(p1)}]}{K_{m,PKA,PLN_5} \left(1 + \frac{[PLN_1^{(p0)}]}{K_{m,PKA,PLN_1}} + \sum_{i \in I \setminus \{1\}} \left(\frac{[PLN_5^{(pi)}]}{K_{m,PKA,PLN_5}} \right) + \frac{[Inh-1^{(p0)}]}{K_{m,PKA,Inh-1}} \right) + [PLN_5^{(p1)}]}$$

$$v46 = \frac{\phi [PP1]k_{cat,PP1,PLN_5} [PLN_5^{(p2)}]}{\chi K_{m,PP1,PLN_5} \left(1 + \frac{[PLN_1^{(p1)}]}{K_{m,PP1,PLN_1}} + \sum_{j \in J \setminus \{2\}} \frac{[PLN_5^{(pj)}]}{\chi^{j-1} K_{m,PP1,PLN_5}} \right) + [PLN_5^{(p2)}]}$$

$$v47 = \frac{V_{max,PP2A,PLN_5} [PLN_5^{(p2)}]}{K_{m,PP2A} + [PLN_1^{(p1)}] + \sum_{j \in J} ([PLN_5^{(pj)}]) + [Inh - 1^{(p1)}]}$$

$$v48 = \frac{[PKA]k_{cat,PKA,PLN_5} [PLN_5^{(p2)}]}{K_{m,PKA,PLN_5} \left(1 + \frac{[PLN_1^{(p0)}]}{K_{m,PKA,PLN_1}} + \sum_{i \in I \setminus \{2\}} \left(\frac{[PLN_5^{(pi)}]}{K_{m,PKA,PLN_5}} \right) + \frac{[Inh-1^{(p0)}]}{K_{m,PKA,Inh-1}} \right) + [PLN_5^{(p2)}]}$$

$$v49 = \frac{\phi^2 [PP1]k_{cat,PP1,PLN_5} [PLN_5^{(p3)}]}{\chi^2 K_{m,PP1,PLN_5} \left(1 + \frac{[PLN_1^{(p1)}]}{K_{m,PP1,PLN_1}} + \sum_{j \in J \setminus \{3\}} \frac{[PLN_5^{(pj)}]}{\chi^{j-1} K_{m,PP1,PLN_5}} \right) + [PLN_5^{(p3)}]}$$

$$v50 = \frac{V_{max,PP2A,PLN_5} [PLN_5^{(p3)}]}{K_{m,PP2A} + [PLN_1^{(p1)}] + \sum_{j \in J} ([PLN_5^{(pj)}]) + [Inh - 1^{(p1)}]}$$

$$v51 = \frac{[PKA]k_{cat,PKA,PLN_5} [PLN_5^{(p3)}]}{K_{m,PKA,PLN_5} \left(1 + \frac{[PLN_1^{(p0)}]}{K_{m,PKA,PLN_1}} + \sum_{i \in I \setminus \{3\}} \left(\frac{[PLN_5^{(pi)}]}{K_{m,PKA,PLN_5}} \right) + \frac{[Inh-1^{(p0)}]}{K_{m,PKA,Inh-1}} \right) + [PLN_5^{(p3)}]}$$

$$v52 = \frac{\phi^3 [PP1]k_{cat,PP1,PLN_5} [PLN_5^{(p4)}]}{\chi^3 K_{m,PP1,PLN_5} \left(1 + \frac{[PLN_1^{(p1)}]}{K_{m,PP1,PLN_1}} + \sum_{j \in J \setminus \{4\}} \frac{[PLN_5^{(pj)}]}{\chi^{j-1} K_{m,PP1,PLN_5}} \right) + [PLN_5^{(p4)}]}$$

$$v53 = \frac{V_{max,PP2A,PLN_5} [PLN_5^{(p4)}]}{K_{m,PP2A} + [PLN_1^{(p1)}] + \sum_{j \in J} ([PLN_5^{(pj)}]) + [Inh - 1^{(p1)}]}$$

$$v54 = \frac{[PKA]k_{cat,PKA:PLN_5} [PLN_5^{(p4)}]}{K_{m,PKA:PLN_5} \left(1 + \frac{[PLN_5^{(p0)}]}{K_{m,PKA:PLN_5}} + \sum_{i \in I \setminus \{4\}} \left(\frac{[PLN_5^{(pi)}]}{K_{m,PKA:PLN_5}} \right) + \frac{[Inh-1^{(p0)}]}{K_{m,PKA:Inh-1}} \right) + [PLN_5^{(p4)}]}$$

$$v55 = \frac{\phi^4 [PP1]k_{cat,PP1:PLN_5} [PLN_5^{(p5)}]}{\chi^4 K_{m,PP1:PLN_5} \left(1 + \frac{[PLN_5^{(p1)}]}{K_{m,PP1:PLN_5}} + \sum_{j \in J \setminus \{5\}} \frac{[PLN_5^{(pj)}]}{\chi^{j-1} K_{m,PP1:PLN_5}} \right) + [PLN_5^{(p5)}]}$$

$$v56 = \frac{V_{max,PP2A:PLN_5} [PLN_5^{(p5)}]}{K_{m,PP2A} + [PLN_1^{(p1)}] + \sum_{j \in J} ([PLN_5^{(pj)}]) + [Inh-1^{(p1)}]}$$

Reactions involving inhibitor-1

$$v57 = \frac{[PKA]k_{cat,PKA:Inh-1} [Inh-1^{(p0)}]}{K_{m,PKA:Inh-1} \left(1 + \sum_{i \in I} \left(\frac{[PLN_5^{(pi)}]}{K_{m,PKA:PLN_5}} \right) + \frac{[PLN_5^{(p0)}]}{K_{m,PKA:PLN_5}} \right) + [Inh-1^{(p0)}]}$$

$$v58 = \frac{V_{max,PP2A:Inh-1} [Inh-1^{(p1)}]}{K_{m,PP2A} + [PLN_1^{(p1)}] + \sum_{j \in J} ([PLN_5^{(pj)}]) + [Inh-1^{(p1)}]}$$

$$v59 = k_7 [Inh-1^{(p1)}] [PP1]$$

$$v60 = k_8 [PP1 : Inh-1^{(p1)}]$$

Model parameters and initial conditions

A mathematical model needs parameters and initial conditions to make useful predictions. In order to obtain realistic parameters values and protein concentrations we searched the literature and previously published models related to calcium handling and β -adrenergic signaling in cardiomyocytes, as well as phospholamban, PKA, PP1 and inhibitor-1.

Table: review protein concentrations

Protein concentration	Value	Source	Comments
$[PLN]_{tot}$	$\approx 250 \mu\text{M}$	this study	
	$106 \mu\text{M}$	(Saucerman et al., 2003)	
	$> 50 \mu\text{M}$	(Bers, 2002; Rigatti et al., 2015)	
	$38 \mu\text{M}$	(Soltis and Saucerman 2010)	
$[PKA]$	$0.59 \mu\text{M}$	(Saucerman et al., 2003)	
	$0.5176 \mu\text{M}$	(Bondarenko, 2014)	
	$0.48 \mu\text{M}$	(Saucerman et al., 2004)	
$[PP1]_{tot}$	$0.89 \mu\text{M}$	(Saucerman et al., 2003; Saucerman et al., 2004)	
	$0.2 \mu\text{M}$	(Bondarenko, 2014)	
	$0.5 \mu\text{M}^*$	(Legewie et al., 2008)	(skeletal muscle)
$[Inh-1]_{tot}$	$0.3 \mu\text{M}$	(Saucerman et al., 2003)	
	$0.08543 \mu\text{M}$	(Bondarenko, 2014)	

*Calculated by the number of protein molecules per cell given in the reference and the rule of thumb that in an "average" eukaryotic cell, 1000 molecules of a protein roughly correspond to a cellular concentration of 1 nM (Luby-Phelps, 2000; BioNumbers BNID 104519).

Table: review kinetic and equilibrium constants

Parameter	Value	Source	Comments
$k_{cat,PKA,PLN}$	54 s ⁻¹	(Saucerman et al., 2003)	(k_{cat} for PLN phosphorylation by PKA)
	21 s ⁻¹	(Rigatti et al., 2015)	
	23.4 s ⁻¹	(Ha et al., 2011)	PLN ₁₋₂₀ , no lipid environment
	22.3 – 25 s ⁻¹	(Masterson et al., 2011)	PLN ₁₋₁₉ , different environments
	13 – 21.9 s ⁻¹	(Masterson et al., 2011)	AFA-PLN, different environments
$K_{m,PKA,PLN}$	21 μM	(Saucerman et al., 2003)	(K_m for PLN phosphorylation by PKA)
	12.5 μM	(Rigatti et al., 2015)	
	93.3 μM	(Ha et al., 2011)	PLN ₁₋₂₀ , no lipid environment
	36.4 – 90.1 μM	(Masterson et al., 2011)	PLN ₁₋₁₉ , different environments
$k_{cat,PP1,PLN}$	47.6 – 238.1 s ⁻¹	(Masterson et al., 2011)	AFA-PLN, different environments
$k_{cat,PP1,PLN}$	8.5 s ⁻¹	(Saucerman et al., 2003)	(k_{cat} for PLN phosphorylation by PKA)
$K_{m,PP1,PLN}$	7 μM	(Saucerman et al., 2003)	(K_m for PLN dephosphorylation by PP1)
$V_{max,PP2A,PLN}$	0.708 μM s ⁻¹	(MacDougall et al., 1991)	guesstimate [†] , (V_{max} for PLN dephosphorylation by PP2A)
$V_{max,PP2A,Inh-1}$	14 μM s ⁻¹	(Saucerman et al., 2003)	(V_{max} for inhibitor-1 dephosphorylation by PP2A)
$k_{cat,PKA,Inh-1}$	60 s ⁻¹	(Saucerman et al., 2003)	(k_{cat} for inhibitor-1 phosphorylation by PKA)
$K_{m,PKA,Inh-1}$	1 μM	(Saucerman et al., 2003)	(K_m for inhibitor-1 phosphorylation by PKA)
$K_{m,PP2A}$	1 μM	(Saucerman et al., 2003)	(K_m for inhibitor-1 dephosphorylation by PP2A)
$K_d,PP1,Inh-1^{(e)}$	1 nM	(Saucerman et al., 2003)	(K_d for complex of PP1 and phosphorylated inhibitor-1)

[†]Not included in calculation of median value for default parameter set. # MacDougall et al. (1991) reported that PP1 accounts for 70-90% and PP2A for the remaining dephosphorylation activity toward phospholamban (and to a small extent PP2C, too). We thus assumed that PP2A dephosphorylation accounts for approximately 20% of the total dephosphorylation activity toward phospholamban observed by MacDougall et al. (1991). We furthermore assumed the same K_m value as for inhibitor-1 dephosphorylation.

Parameter ω (dynamic equilibrium of PLN)

Since individual oligomerization steps and the influence of phosphorylation on their rate constants have not been studied before, we used our own data and those from Hou et al. (2008) to obtain a first estimate for ω as described in the subsection 'Parameter estimation and model selection' below.

Parameter	Value	Source	Comments
ω	≈ 1.066	this study	based on data from Figure S8E
	≈ 1.044	(Hou et al., 2008)	see subsection 'Parameter estimation and model selection'

It is important to note, however, that the extend to which this effect can be observed varies considerably. Wittmann et al. (2015), for instance, observed no significant increase in pentamerization upon Ser16 phosphorylation in forskolin stimulated HEK293 cells. Cornea et al. (1997), in contrast, found a near complete pentamerization of Ser16-phosphorylated, recombinant PLN in DOPC lipid bilayers using electron paramagnetic resonance spectroscopy. The effect observed by Hou et al. (2008), could be an underestimation given that phospho-mimetic mutations are not always faithful experimental models for real phosphorylation (Kampourakis et al., 2018). Moreover, the lipid environment, too, plays an important role for both pentamerization (Zhang et al., 2005) and the dynamic equilibrium effect (this study). Taken together, these considerations make it difficult to get a precise estimate from the data so far. We thus decided to opt for a 'guesstimate' of $\omega = 1.25$, which is higher than the estimates based on our or Hou et al. (2008)'s data, but still lower than what one would expect for the near complete pentamerization observed by Cornea et al. (1997).

Cooperative dephosphorylation of pentamers

To the best of our knowledge, no kinetic parameters for the (de-)phosphorylation of pentameric phospholamban have been determined so far. In the absence of better evidence we mostly assumed the parameters to be the same as for monomeric phospholamban. An exception to this is the dephosphorylation of pentameric PLN by PP1. In order to implement the positive cooperativity of dephosphorylation reported by (Li et al., 1990), we assumed a pronounced v-type cooperativity of $\phi = 0.2$ and the absence of k-type cooperativity, i.e., $\chi = 1$.

Set of default parameters and initial conditions

Based on these reviews and considerations we composed a default parameter set, which was used for all simulations and analyses unless specified otherwise in the simulation protocols given below. Oligomerization parameter values are from the best fit parameter set of mass action model 2 calibrated with our experimental data (see subsection 'A mass action kinetics model of PLN pentamer assembly').



Table: default parameter values and initial conditions

Parameter/IC	Value	Comments
$[PLN]_{tot}$	250 μM	
$[PKA]$	0.59 μM	
$[PP1]_{tot}$	0.89 μM	free $[PP1](t=0) = [PP1]_{tot}$ unless stated otherwise
$[Inh-1]_{tot}$	0.3 μM	$[Inh-1]^{(p0)}(t=0) = [Inh-1]_{tot}$ unless stated otherwise
k_1	144724 mol s^{-1}	(rate constant for dimer formation; best fit parameter set)
k_2	5518.45 s^{-1}	(rate constant for dimer dissociation; best fit parameter set)
k_3	72672.8 mol s^{-1}	(rate constant for tetramer formation; best fit parameter set)
k_4	1.20089 s^{-1}	(rate constant for tetramer dissociation; best fit parameter set)
k_5	$1.83 \times 10^8 \text{ mol s}^{-1}$	(rate constant for pentamer formation; best fit parameter set)
k_6	0.13275 s^{-1}	(rate constant for pentamer dissociation; best fit parameter set)
k_7	$5 \times 10^4 \text{ mol s}^{-1}$	(association rate constant for binding of phosphorylated inhibitor-1 to PP1; matched with k_8 to a K_d of 1 nM)
k_8	$5 \times 10^{-5} \text{ s}^{-1}$	(dissociation rate constant of complex between phosphorylated inhibitor-1 and PP1; matched with k_7 to a K_d of 1 nM)
ω	1.25	(increased oligomerization upon PLN phosphorylation)
k_{cat,PKA,PLN_1}	23 s^{-1}	(k_{cat} for PLN_1 phosphorylation by PKA; median of reviewed values)
K_{m,PKA,PLN_1}	42 μM	(K_m for PLN_1 phosphorylation by PKA; median of reviewed values)
k_{cat,PKA,PLN_5}	23 s^{-1}	(k_{cat} for PLN_5 phosphorylation by PKA; assumed equal to monomers)
K_{m,PKA,PLN_5}	42 μM	(K_m for PLN_5 phosphorylation by PKA; assumed equal to monomers)
$k_{cat,PP1,PLN_1}$	8.5 s^{-1}	(k_{cat} for PLN_1 dephosphorylation by PP1)
$K_{m,PP1,PLN_1}$	7 μM	(K_m for PLN_1 dephosphorylation by PP1)
$k_{cat,PP1,PLN_5}$	8.5 s^{-1}	(baseline k_{cat} for PLN_5 dephosphorylation by PP1)
$K_{m,PP1,PLN_5}$	7 μM	(baseline K_m for PLN_5 dephosphorylation by PP1)
$V_{max,PP2A,PLN}$	0.708 $\mu\text{M s}^{-1}$	(V_{max} for PLN dephosphorylation by PP2A)
$V_{max,PP2A,Inh-1}$	14 $\mu\text{M s}^{-1}$	(V_{max} for inhibitor-1 dephosphorylation by PP2A)
$k_{cat,PKA,Inh-1}$	60 s^{-1}	(k_{cat} for inhibitor-1 phosphorylation by PKA)
$K_{m,PKA,Inh-1}$	1 μM	(K_m for inhibitor-1 phosphorylation by PKA)
$K_{m,PP2A}$	1 μM	(K_m for inhibitor-1 and PLN dephosphorylation by PP2A)
$K_d,PP1,Inh-1^{(p1)}$	1 nM	(K_d for complex of PP1 and phosphorylated inhibitor-1)
ϕ	0.2	(v-type cooperativity for PLN_2 dephosphorylation by PP1)
χ	1	(k-type cooperativity for PLN_5 dephosphorylation by PP1)

Computational procedures

Model implementation and software

All models were implemented as MATLAB® (v2019b) scripts for numerical simulation and analysis. Simulations were performed with the ode23s integrator on an Asus® laptop PC with Intel® Corei7-7500U CPU @ 2.70GHz, 2904 Mhz, 2 Core(s) processor, 8GB RAM running under Microsoft® Windows 10 OS. Simulation protocols describing the used parameter values and initial conditions for each simulation shown in the figures of the main text (where deviating from the default parameter set) can be found further below.

Parameter estimation and model selection

Parameter estimation for association and dissociation rate constants of the oligomerization reactions in our mass-action kinetics models was performed in COPASI (v4.26) using the genetic algorithm with 250 generations and a population size of 40. Parameters were constrained by the detailed balance relationships described in subsection 'A mass action kinetics model of PLN pentamer assembly'. Furthermore, association rate constants were constrained to lie between $10^3 \text{ mol} \cdot \text{s}^{-1}$ and $10^9 \text{ mol} \cdot \text{s}^{-1}$, whereas dissociation constants were constrained to lie between 10^{-5} s^{-1} and 10^6 s^{-1} . For each model variant, 30 independent parameter estimation runs with randomized initial values parameters were performed. For model selection, the AIC was calculated as described in Flöttmann et al. (2008) by $AIC = 2 \cdot k + n \cdot \left(\ln \left(\frac{SSE}{n} \right) + 1 \right)$, where k is the number of model parameters, n is the number of experimental observations and SSE is the sum of weighted squared errors for the best fit parameter set of a model. The AIC score balances how well a

model fits the data versus model complexity in number of parameter values and penalizes deviations from experimental data and high number of model parameters. The lower the AIC score, the better. If two models fit the data equally well, the model with fewer parameters is rewarded a lower AIC score because it has less unnecessary complexity.

Estimation of parameter ω to our own data was performed by assuming that the increased pentamerization shown in Figure S8E reflects the steady-state situation and by using the MATLAB® function `nlinfit` to fit the parameter to this data.

Calculation of parameter ω based on the data from Hou et al. (2008) was done as follows. The apparent monomer-pentamer equilibrium in a monomer-dimer-tetramer-pentamer model such as ours can be characterized by the apparent dissociation constant:

$$K_{d,1.5}^{app} = \frac{[PLN_1]^5}{[PLN_5]}$$

Since we have

$$\begin{aligned} [PLN_5] &= K_{4,5}[PLN_4][PLN_1] \\ &= K_{2,4}K_{4,5}[PLN_2]^2[PLN_1] \\ &= K_{1,2}^2K_{2,4}K_{4,5}[PLN_1]^5, \end{aligned}$$

we can write

$$K_{d,1.5}^{app} = \frac{[PLN_1]^5}{[PLN_5]} = \frac{1}{K_{1,2}^2K_{2,4}K_{4,5}} = \frac{k_2^2k_4k_6}{k_1^2k_3k_5}$$

where in the last step the equilibrium constants were substituted with their constitute rate constants. For completely phosphorylated PLN, the derivation of the apparent dissociation constant is identical except for factoring in ω into the individual equilibria:

$$K_{d,1.5}^{app,pPLN} = \frac{[PLN_1^{(p1)}]^5}{[PLN_5^{(p5)}]} = \left(\frac{k_2}{\omega k_1}\right)^2 \left(\frac{k_4}{\omega^3 k_3}\right) \left(\frac{k_6}{\omega^4 k_5}\right) = \frac{1}{\omega^9} \frac{k_2^2k_4k_6}{k_1^2k_3k_5}$$

Using the apparent K_d values from Hou et al. (2008) (given in arbitrary units) for Ser16A PLN (unphosphorylated) and Ser16E PLN (mimicking phosphorylated PLN) we arrive at:

$$\frac{K_{d,1.5}^{app}}{K_{d,1.5}^{app,pPLN}} = \frac{2.2}{1.5} = \frac{\frac{k_2^2k_4k_6}{k_1^2k_3k_5}}{\frac{1}{\omega^9} \frac{k_2^2k_4k_6}{k_1^2k_3k_5}} = \omega^9 \Leftrightarrow \omega = \sqrt[9]{2.2} \approx 1.044$$

Bifurcation diagrams

Bifurcation diagrams were generated using a custom algorithm described previously (Koch, 2020) to make the implementation of bifurcation analysis into the simulation/analysis pipeline easier (e.g., for sensitivity analysis of the bistable range). The algorithm iteratively identifies/approximates the unstable steady states of bistable systems numerically, but does not detect other types of bifurcations (e.g., Hopf-bifurcations). For more details, please refer to: <https://www.ebi.ac.uk/biomodels/MODEL1910220002>.

Local sensitivity analysis

Local sensitivity analyses was performed as described in Ingalls (2013). We analyzed two steady states which were chosen to be sufficiently remote from the saddle node bifurcations SN1 and SN2 of the model: a low relative phosphorylation level ([PKA] = 0.13 μ M), and a high relative phosphorylation level ([PKA] = 0.25 M). Relative sensitivities of (relative) PLN monomer phosphorylation at steady state upon perturbing the nominal value of each parameter p by $dp = 1\%$ at a time were calculated as $s_r(p) = \frac{d[PLN_1^{(p)}]/[PLN_1^{(p)}]}{dp/p}$,

$$\text{where } r[PLN_1^{(p1)}] = \frac{[PLN_1^{(p1)}]}{[PLN_1^{(p5)}] + [PLN_1^{(p1)}]}$$

For bifurcation sensitivity analysis, relative sensitivities were determined in a similar fashion, but instead of focusing on the steady state concentration of relative PLN monomer phosphorylation, relative sensitivities of the bistable range (SN1-SN2) were calculated. In order to obtain well detectable changes in relative sensitivities with a limited granularity of the bifurcation algorithm, a perturbation of $dp = 10\%$ was chosen.

Probing the multi-dimensional parameter space for its influence on bistability

In order to probe how bistability depends on the multi-dimensional parameter space of our model, we decided to perform an analysis developed by Nguyen et al. (2015). First, we used the review of parameter values and protein concentrations to guide the construction of ranges of physiologically plausible values in which the true values are likely to lie. As we could not get our model to be executed by the python implementation provided in Nguyen et al. (2015), we decided to implement the analysis in the MATLAB® code of our

model. However, as our model equations are quite stiff for some combinations of parameters, we first performed a model reduction and replaced one ODE for an algebraic expression in order to speed up the numerical solution of the model. Due to ease of implementation, a quasi-steady-state (QSS) approximation of $PP1$ is particularly suited to replace an ODE with an algebraic expression. Although this can affect the model dynamics (and thereby eliminate e.g., the response delay of the inhibitor-1 FFL), we used the reduced model only for steady state analyses for which the QSS assumption is (trivially) fulfilled (Ingalls, 2013). At steady state we find that:

$$\frac{d}{dt}[PP1](t) = k_8[Inh - 1^{(p1)} : PP1](t) - k_7[Inh - 1^{(p1)}](t)[PP1](t) = 0$$

Assuming that $PP1$ is quasi at steady state compared to the other processes in the reaction network, we denote its concentration in the reduced model by $[PP1]$. From the ODEs, we can identify the following conservation laws:

$$[PP1]_{tot} = [PP1](t) + [PP1 : Inh - 1^{(p1)}](t)$$

$$[Inh - 1]_{tot} = [Inh - 1^{(p0)}](t) + [Inh - 1^{(p1)}](t) + [PP1 : Inh - 1^{(p1)}](t)$$

Applying these to the first equation and solving the resulting quadratic equation for $[PP1]$ using the pq-formula gives (for physical reasons only the positive solution is given):

$$[PP1](t) = - \left(\frac{k_8 + k_7([Inh - 1]_{tot} - [Inh - 1^{(p0)}](t) - [PP1]_{tot})}{2k_7} \right) + \sqrt{\frac{(k_8 + k_7([Inh - 1]_{tot} - [Inh - 1^{(p0)}](t) - [PP1]_{tot}))^2}{4k_7^2} - \frac{k_8[PP1]_{tot}}{k_7}}$$

Having eliminated the ODE for $PP1$ with this algebraic expression, we observed no deviations in the steady state behavior but a marked performance gain.

For the intended analysis, parameters and initial conditions were sampled randomly from a uniform distribution determined by a range of physiologically plausible values. Using the reduced model, two simulations with either completely unphosphorylated or completely phosphorylated PLN (both monomeric and pentameric) as initial conditions were performed with simulation endpoint $t_{end} = 5 \times 10^5$ s. To test whether the model reached steady state, the algorithm checked whether monomer concentration was stable for at least three time points before reaching the end of the simulation. A parameter set was considered bistable if there was a relative difference in phosphorylation levels of $> 10\%$. Parameter sets without a difference in phosphorylation levels or with a difference of $< 10\%$ were considered monostable since we reasoned that marginal differences in steady state phosphorylation might not be of physiological relevance (although technically still bistable). Parameter sets were normalized to the maximum value of the respective parameter range and visualized using parallel coordinate plots.

Frequency response analysis

Frequency response analysis was performed as described in Ingalls (2013). First, the system's jacobian matrix

$$\mathbf{A} = \frac{\partial \mathbf{f}}{\partial \mathbf{x}} = \begin{pmatrix} \frac{\partial f_1}{\partial [PLN_1^{(p0)}]} & \frac{\partial f_1}{\partial [PLN_2^{(p0)}]} & \dots & \frac{\partial f_1}{\partial [PP1]} \\ \frac{\partial f_2}{\partial [PLN_1^{(p0)}]} & \frac{\partial f_2}{\partial [PLN_2^{(p0)}]} & \dots & \frac{\partial f_2}{\partial [PP1]} \\ \vdots & \vdots & \ddots & \vdots \\ \frac{\partial f_{17}}{\partial [PLN_1^{(p0)}]} & \frac{\partial f_{17}}{\partial [PLN_2^{(p0)}]} & \dots & \frac{\partial f_{17}}{\partial [PP1]} \end{pmatrix},$$

was calculated symbolically using MATLAB®, where f_1, \dots, f_{17} (\mathbf{f} in vector notation) denotes the right hand sides of the model ODEs as a function of the model variables $[PLN_1^{(p0)}], \dots, [PP1]$ (\mathbf{x} in vector notation) in the specified order. For the purpose of the frequency response analysis, the model input u was defined as $[PKA]$ and the output h as relative monomer phosphorylation $\frac{[PLN^{(p1)}]}{[PLN^{(p0)}] + [PLN^{(p1)}]}$.

Linearized input and output maps \mathbf{B} and \mathbf{C} were calculated as $\mathbf{B} = \frac{\partial \mathbf{f}}{\partial u}$ and $\mathbf{C} = \frac{\partial h}{\partial \mathbf{x}}$, respectively. The feed-through term D as $\frac{\partial h}{\partial u}$. After evaluating $\mathbf{A}, \mathbf{B}, \mathbf{C}$ and D at a nominal operating point, a linearized input-output system was created using the MATLAB® function `ss2tf`. The linearized input-output system was subsequently used for the evaluation of the system bandwidth and for creating

Bode-diagrams using the MATLAB® functions `bandwidth` and `bode`, respectively, where the gain is defined as the ratio of the amplitude of the response to the amplitude of the input, and phase shift as the ratio of the time difference between response peaks to the period of the input oscillations given in degrees (Ingalls, 2013).

Simulation protocols

To enable reproducibility of our simulations in other software environments, we provide here the simulation protocols, initial conditions and parameter values underlying the presented simulations in the main text. Figure numbers refer to the main text. For specifications of the simulations from the supplementary material, please refer to the published code.

- **Figure 3A, left:** First, 250 μM $[\text{PLN}]_{\text{tot}}$ (unphosphorylated) were simulated until oligomerization reached equilibrium in the absence of any other species (no inhibitor-1, no phosphatases, no PKA). Subsequently, $[\text{PKA}] = 0.1 \mu\text{M}$ and a 300 s phosphorylation time course of PLN species was simulated in the absence of phosphatases and inhibitor-1. Other initial conditions and parameters as listed in [Table: default parameter values and initial conditions](#).

- **Figure 3A, right:** PKA was set to 0 μM and final PLN species concentrations from [Figure 3A](#) (left) were used as initial conditions for PLN. Free PP1 was set 0.1 μM and a 250 s dephosphorylation time course was simulated. Inhibitor-1 was absent. PP2A and other initial conditions and parameters as listed in [Table: default parameter values and initial conditions](#).

- **Figure 3B:** red and blue lines are the same data as in [Figure 3A](#) replotted as relative monomer and pentamer phosphorylation, respectively. For the simulation in the absence of pentamers (dotted purple line), the simulations described for [Figure 3A](#) were repeated with rate constants $k_1 = k_2 = k_3 = k_4 = k_5 = k_6 = 0$ (to prevent oligomerization) and initial PLN concentration equimolar to the monomer concentration of $[\text{PLN}]_{\text{tot}} = 250 \mu\text{M}$ at oligomerization equilibrium ($\approx 58.2 \mu\text{M}$).

- **Figure 3C:** As [Figures 3A](#) and [3B](#), but with $[\text{PKA}] = 1 \text{ nM}$.

- **Figure 4B:** First, 250 μM $[\text{PLN}]_{\text{tot}}$ (unphosphorylated) were simulated until oligomerization reached equilibrium in the absence of any other species (no inhibitor-1, no phosphatases, no PKA). Subsequently, PKA was set to 0.35 μM and a 350 s phosphorylation time course of PLN species was simulated the presence of phosphatases and inhibitor-1 (concentrations as listed in [Table: default parameter values and initial conditions](#)). Subsequently, PKA was set to 0 μM and dephosphorylation was simulated for 250 s. The whole simulation was performed three times with different rate constants for binding of inhibitor-1 to PP1: $k_7 = 1/2 \times 10^4 \text{ mol s}^{-1}$ and $k_8 = 1/2 \times 10^{-5} \text{ s}^{-1}$, respectively. Finally, the simulation was repeated in the absence of inhibitor-1 but with PP1 reduced by the fraction of PP1 bound to inhibitor-1 at steady state from previous simulations (to ensure the same steady state is approached). Other initial conditions and parameters as listed in [Table: default parameter values and initial conditions](#).

- **Figure 4C:** (e1-e3) $[\text{PLN}_1](t=0) = [\text{PLN}]_{\text{tot}} = 55 \mu\text{M}$, $k_1 = k_2 = k_3 = k_4 = k_5 = k_6 = 0$, $V_{\text{max,PP2A-PLN}} = V_{\text{max,PP2A-Inh-1}} = 0$, $k_{\text{cat,PKA-Inh-1}} = 0.25 \text{ s}^{-1}$, $K_{\text{m,PKA-Inh-1}} = 14 \mu\text{M}$, $t_{\text{end}} = 2000 \text{ s}$. (e1) $[\text{PKA}] = 10 \text{ nM}$, $[\text{PP1}](t=0) = [\text{PP1}]_{\text{tot}} = 1 \mu\text{M}$, $[\text{Inh-1}^{(p0)}](t=0) = [\text{Inh-1}]_{\text{tot}} = 10 \mu\text{M}$. (e2) $[\text{PKA}] = 10 \text{ nM}$, $[\text{PP1}](t=0) = [\text{PP1}]_{\text{tot}} = 0 \mu\text{M}$, $[\text{Inh-1}^{(p0)}](t=0) = [\text{Inh-1}]_{\text{tot}} = 0 \mu\text{M}$. (e3) $[\text{PKA}] = 10 \text{ nM}$, $[\text{PP1}](t=0) = [\text{PP1}]_{\text{tot}} = 1 \mu\text{M}$, $[\text{Inh-1}^{(p0)}](t=0) = [\text{Inh-1}]_{\text{tot}} = 0 \mu\text{M}$.

- **Figure 5A:** First, 250 μM $[\text{PLN}]_{\text{tot}}$ (unphosphorylated) were simulated until oligomerization reached equilibrium in the absence of any other species (no inhibitor-1, no phosphatases, no PKA). Next, ten simulations with 0%–100% (in steps of 10%) of monomeric and pentameric PLN from the first step being phosphorylated at $t=0$ were run for 2000s at $[\text{PKA}] = 0.21 \mu\text{M}$ and other initial conditions and parameters as listed in [Table: default parameter values and initial conditions](#).

- **Figure 5B:** Bifurcation plots were calculated as described in subsection ‘[Bifurcation diagrams](#)’. PKA was chosen as bifurcation parameter in the range of 0.1 to 0.6 μM , $t_{\text{end}} = 500000 \text{ s}$ and 30 iterations were allowed for direct identification of unstable steady states before the algorithm switches to approximative identification. When the unstable steady state was approximated, the first 30 integration steps were ignored in order to prevent a bias resulting from smaller integration steps at the beginning of the simulations.

- **Figure 5D:** As described in subsection ‘[Local sensitivity analysis](#)’.

- **Figure 5E:** As described in subsection ‘[Probing the multi-dimensional parameter space for its influence on bistability](#)’.

- **Figure 6A:** First, 250 μM $[\text{PLN}]_{\text{tot}}$ (unphosphorylated) were simulated until oligomerization reached equilibrium in the absence of any other species (no inhibitor-1, no phosphatases, no PKA). Second, except for $[\text{PKA}]$, all species and parameters were set to their default value as listed in [Table: default parameter values and initial conditions](#). Next, a series of short bursts of $[\text{PKA}] = 0.59 \mu\text{M}$, each 45 s apart, was simulated and burst duration was increased for each simulation (1/3.3/10 s).

- **Figure 6B:** As in [Figure 6A](#) but in absence of inhibitor-1 and with PP1 reduced by the fraction of PP1 bound to inhibitor-1 at steady state from previous simulations (to ensure the same steady state is approached).

- **Figure 6C:** As in [Figure 6A](#) but with rate constants $k_1 = k_2 = k_3 = k_4 = k_5 = k_6 = 0$ (to prevent oligomerization) and an initial PLN concentration equimolar to the monomer concentration of $[\text{PLN}]_{\text{tot}} = 250 \mu\text{M}$ at oligomerization equilibrium ($\approx 58.2 \mu\text{M}$).

- **Figure 6D:** combined settings of [Figures 6B](#) and [6C](#).

- **Figure 6E:** First, the model was simulated to steady state with $[\text{PKA}] = 0.2 \mu\text{M}$ and other initial conditions and parameters as listed in [Table: default parameter values and initial conditions](#). From the steady state, we simulated the model for 512 short time intervals of 0.1 s length each, where for the i -th time interval, we set $[\text{PKA}](i) = 0.2 \mu\text{M} + 0.05 \cdot 0.2 \mu\text{M} \cdot \sin(\frac{i-1}{20}) \text{ rand}() \cdot 0.075 \cdot 0.2 \mu\text{M}$, where the last summand represents a fast random noise component.

- **Figure 6F:** First, the model was simulated to steady state with $[\text{PKA}] = 0.2 \mu\text{M}$ and other initial conditions and parameters as listed in [Table: default parameter values and initial conditions](#). Frequency response analysis for the reached steady state was carried out as

described in subsection 'Frequency response analysis'. For frequency response analysis in the absence of pentamers or inhibitor-1, simulation until steady state was modified as described for Figures 6B and 6C.

● **Figure 6G:** The parameters of the parameter set yielding ultrasensitivity without bistability which deviate from default conditions are:

Parameter/IC	Value	Comments
$[PP1]_{tot}$	0.67 μM (default: 0.89 μM)	free $[PP1](t=0) = [PP1]_{tot}$ unless stated otherwise
K_{m,PKA,PLN_1}	55 μM (default: 42 μM)	(K_m for PLN_1 phosphorylation by PKA)
K_{m,PKA,PLN_5}	42.5 μM (default: 42 μM)	(K_m for PLN_5 phosphorylation by PKA)
$k_{cat,PP1,PLN_5}$	9 s^{-1} (default: 8.5 s^{-1})	(baseline k_{cat} for PLN_5 dephosphorylation by PP1)
$K_{m,PP1,PLN_5}$	4 μM (default: 7 μM)	(baseline K_m for PLN_5 dephosphorylation by PP1)
ϕ	0.79 (default: 0.2)	(v-type cooperativity for PLN_5 dephosphorylation by PP1)
χ	1.03 (default: 1)	(k-type cooperativity for PLN_5 dephosphorylation by PP1)

● Bifurcation diagrams were calculated as described for Figure 5B. The response to fluctuations in PKA concentration was determined as follows: First, the model was simulated to steady state with $[PKA] = 0.226 \mu\text{M}$ and other initial conditions and parameters as listed in [Table: default parameter values and initial conditions](#), or as given in the table above for the parameter set leading to ultrasensitivity without bistability. From the steady state, we simulated the model for 100 time intervals of 60 s length each, where for the i -th time interval, we set $[PKA](i) = 0.226 \mu\text{M} \text{rnd}() \cdot 0.25 \cdot 0.226 \mu\text{M}$.

● **Figures 6H and 6I:** Noise-landscapes were calculated as follows. First, the model was simulated to steady state at a given baseline PKA concentration $[PKA]_{bl}$ and other initial conditions and parameters as listed in [Table: default parameter values and initial conditions](#), or as given in the table above for the parameter set leading to ultrasensitivity without bistability. From the steady state, we simulated the model for 150 time intervals of 60 s length each, where for the i -th time interval, we set $[PKA](i) = [PKA]_{bl} \text{rnd}() \cdot n_f \cdot [PKA]_{bl}$, where n_f is the input noise level. From these simulations, the coefficient of variation ($CV = \frac{\sigma}{\mu}$) of relative PLN monomer phosphorylation was determined, where σ and μ denote the standard deviation and mean of the data, respectively. This process was repeated iteratively and the resulting CVs were visualized on a surface plot as function of the indicated ranges of $[PKA]_{bl}$ and input noise levels. For the relative noise landscape shown in Figure 6I, CVs resulting from the parameter set for ultrasensitive without bistability were divided by the CVs resulting from the parameter set for bistability.

● **Figure 6J:** The model was simulated to steady state at a given baseline PKA concentration $[PKA]_{bl}$, where $[PKA]_{bl} = 0.208 \mu\text{M}$ for the parameter set exhibiting bistability or $[PKA]_{bl} = 0.225 \mu\text{M}$ for the parameter set resulting in ultrasensitivity without bistability. Other initial conditions and parameters as listed in [Table: default parameter values and initial conditions](#), or as given in the table above for the parameter set leading to ultrasensitivity without bistability. From the steady state, we simulated the model for 1000 time intervals of 60 s length each, where for the i -th time interval, we set $[PKA](i) = [PKA]_{bl} \text{rnd}() \cdot 0.0625 \mu\text{M}$. A switching event between low and high phosphorylation states was counted when relative monomer phosphorylation changed from ≤ 0.25 to ≥ 0.4 or vice versa.

QUANTIFICATION AND STATISTICAL ANALYSIS

All image-based experimental data were quantified using the ImageLab v6.0 software (Bio-Rad). Statistical comparison between two experimental groups was performed in GraphPad Prism (v8.3) using the two-tailed unpaired t test, corrected for multiple comparisons by the Holm-Sidak method where appropriate. Sample sizes are given in the respective figures. A p value < 0.05 was considered to be statistically significant. Significance levels were encoded as follows: ns = not significant, * $p < 0.05$, ** $p < 0.01$, *** $p < 0.001$, **** $p < 0.0001$.

Chapter 7

Conclusion and Outlook

Many of the aims defined in the introduction of this thesis have been fulfilled. While the characterisation of the function and regulation of the obscurin Rho GEF domains proved more challenging than anticipated, the biochemical and biophysical characterisation of genetic variants in obscurin domains Ig58 and Ig59 proved insightful and demonstrated that the alleged interaction between obscurin and PLN is likely an *in vitro* artefact and that the R4344Q variant is unlikely to be pathogenic. The theoretical investigation of the role of homo-oligomerisation in the context of signalling networks revealed a surprising wealth of potential signal processing functions, some of which have been confirmed in the subsequent project on information processing by PLN pentamers. The combined theoretical and experimental exploration of PLN pentamers in the context of β -adrenergic signalling provided exciting new insights into the mechanisms of how pentamers shape the dynamics and steady state of PLN monomer phosphorylation in ways that are potentially relevant in arrhythmias and heart failure. This chapter highlights and discusses some wider implications of the presented work and provides an outlook on future research avenues.

7.1 Obscurin Rho GEF domains

Our data show that obscurin is quite an atypical member of the trio-subfamily of Rho GEFs. Perhaps obscurin is not even a functional Rho GEF at all: there are many examples of enzymes including kinases, phosphatases and GTPases who have lost their catalytic activity during evolution and occupied new functional roles (Reiterer et al. 2014; Stiegler and Boggon 2020). Such pseudo-enzymes often act as important scaffolds and signal integrators in signalling networks (Reiterer et al. 2014). If the obscurin Rho GEF can still bind GTPases as a scaffold, obscurin may alter the subcellular distribution and regulate the activity of former substrates in an indirect way which may reconcile our *in vitro* data with previous cell biological studies. Interestingly, the kinase domain of the giant muscle protein titin, too, has been proposed to have lost its catalytic activity during evolution, since the invertebrate homologue twitchin kinase exhibits detectable phosphoryl transfer activity, whereas the catalytic activity of titin kinase has not been confirmed yet (Bogomolovas et al. 2014). Since the absence of confirmation is not equivalent to the confirmation of absence, the catalytic activity of titin kinase is still a topic of active debate (Gautel 2011). However, if obscurin has indeed no catalytic Rho GEF activity, this may indicate the existence of a common evolutionary theme in which formerly active catalytic domains of giant muscle proteins are repurposed to play other functions.

Several experiments could be done to further test this hypothesis. Firstly, it might be interesting to probe the catalytic activity of the Rho GEF domains from obscurin homologues in evolutionary more distant species, e.g. the unc89 Rho GEF domains in *C. elegans* or *D. melanogaster*. Another interesting experiment might be to “obscurinise” catalytically active Rho GEFs such as Dbs by replacing functionally important residues like the ones identified in [Figure 3.17B](#) for residues found in obscurin at these positions. Most importantly, however, quantitative cell biological methods such as the use of a Rho GTPase FRET-biosensor could help to directly determine the activity of obscurin’s Rho GEF domains in living cells without the limitations of previous studies (Coisy-Quivy et al. 2009; Ford-Speelman et al. 2009; Pertz and Hahn 2004).

Regardless of obscurin’s Rho GEF activity, our work opens up several interesting avenues for future research. While initial crystallisation trials have been unsuccessful, the availability of pure and stable protein constructs makes further structural characterisation of the obscurin Rho GEF domains e.g. via small-angle x-ray scattering, NMR or cryo-EM feasible. Furthermore, the identification of phosphatases and kinases from the MST- and CaMK-family as potential regulators of obscurin establishes interesting links to the Hippo- and calcium-signalling pathways. While the significance of these discoveries is currently still unclear, the role of these links may be a promising target to explore in future cell biological studies.

7.2 Genetic obscurin variants

Although the functional roles of obscurin still remain poorly understood, several genetic variants in obscurin have been associated with cardiovascular and musculoskeletal diseases. The R4344Q variant in obscurin domain Ig58, for instance, has been discovered in a patient with HCM and was proposed to be disease-causing by altering the parameters of several protein-protein interactions (Arimura et al. 2007; Hu et al. 2017). A recent mouse model seemed to confirm the pathogenicity of the R4344Q variant as transgenic R4344Q mice showed an increased propensity for cardiac arrhythmias and a DCM-like phenotype upon pressure overload (Hu et al. 2017). However, the R4344Q variant is very common among African Americans (about 1 in 7) (Marston 2017). If this variant is indeed disease-causing, would not more African Americans suffer from heart disease and would carriers of the R4344Q variant not be at particular risk? As this seems not generally to be the case, several researchers have contested the pathogenicity of this variant (Manrai et al. 2016).

Due to the increasing resolution of medical imaging techniques, the number of incidental findings that would not have been discovered otherwise has massively increased in recent decades. While the discovery of a lump in the body can be concerning for both patients and physicians, medicine has learned that many of these incidental findings are actually benign and require careful evaluation of the harm that can be caused e.g. by surgical treatment. Similar considerations need to be made in the evaluation of a genetic variant, since the harm that can result from the fear of developing a fatal disease or of passing on such disease to a child can be devastating and influence the outcome of crucial life decisions (Kohane et al. 2006). As important the elucidation of the molecular mechanisms underlying the pathophysiology of diseases is, the classification of a genetic variant as pathogenic requires solid clinical and molecular genetic evidence.

To better understand how previous studies about the molecular effects of this variant can be reconciled with its population genetics, we conducted a systematic biochemical and biophysical characterisation to quantify the influence of the R4344Q and other variants on all known protein-protein interactions and protein stability. In agreement with the population genetics, we found that

the influence of these variants on the studied molecular properties is negligible. We furthermore were not able to confirm a previously reported interaction between obscurin Ig58 and novex-3 and found that the interaction between obscurin Ig58 and PLN is likely an *in vitro* artefact relying on unspecific hydrophobic interactions. In the context of ongoing discussion about the limited reproducibility of published results in the biomedical sciences, our study highlights the advantage of characterising protein-protein interactions with multiple approaches, at least one of which should ideally provide quantitative information about the affinity of an interaction. Since no other clinical evidence currently supports the classification of the R4344Q variant as pathogenic, we concluded that this variant is likely benign.

We also wanted to test the influence of the D5966N mutation in the obscurin PH domain on obscurin function, particularly GEF activity (Marston et al. 2015). However, due to the lack of activity and identified binding partners for the PH domain, characterisation of this mutation was not possible and will require further work.

7.3 The potential roles of homo-oligomerisation in biochemical signalling processes – from first principles to preventing cardiac arrhythmias?

The second strand of work presented in this thesis was motivated by the question of what the function of PLN pentamers is. As the potential roles of homo-oligomerisation in the context of biochemical signalling networks has received relatively little attention, we started with the exploration of the behaviour of very simple mathematical models of reversible homo-oligomerisation. The simulations and analyses of these models revealed an unanticipated and exciting wealth of non-linear dynamics and steady-state behaviour previously not associated with homo-oligomerisation. These include ultrasensitive oligomer and homeostatic monomer response regimes upon changes in total protein concentrations and transients of oligomeric intermediates (“overshoots”) in the assembly dynamics. Building upon previous theoretical work on multisite phosphorylation systems, it was furthermore found that homo-oligomers could constitute pseudo-multisite phosphorylation systems which, similar to conventional multisite phosphorylation systems, allow for the emergence of ultrasensitive and multistable input-output relationships. Such phenomena could allow homo-

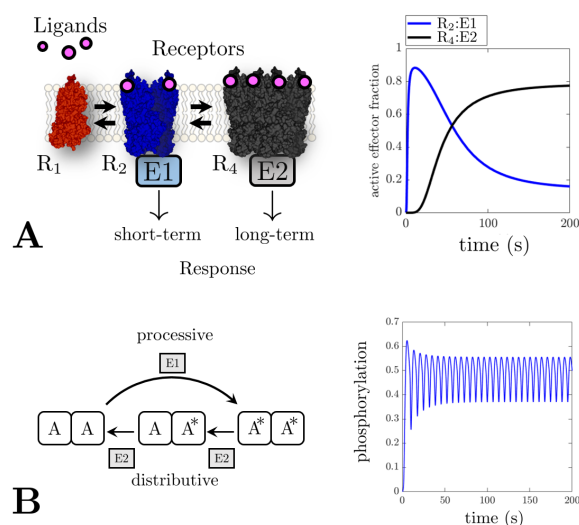


Figure 7.1. Further dynamics resulting from homo-oligomerisation.

A, Separation of a receptor response after ligand binding into early and late phases via different effectors for dimeric (R2) and tetrameric (R4) receptor forms. Effector binding has been assumed to be cooperative and modelled using the Hill-equation with $n_H = 4$. **B**, Simple model of a dimeric protein for which phosphorylation occurs via a processive mechanism, whereas dephosphorylation is processive predicts the emergence of sustained oscillations of the phosphorylation state. For simplicity, oligomerisation reactions are not shown.

oligomerisation to play pivotal functions in biochemical signalling networks. Coupling the dynamics of oligomerisation to different effectors for different oligomeric species could provide a simple, yet elegant and effective mechanism to split the response into an early and a late phase, which seems particularly relevant to cell surface receptors which oligomerise upon ligand binding or oligomeric transcription factors (Figure 7.1A). Transient stimulation of a receptor could for instance lead to short-term adaptive responses mediated via the effector of dimers (e.g. phosphorylation of some metabolic enzymes), whereas prolonged stimulation could lead to different, longer-term responses mediated by higher-order oligomers (e.g. changing the expression levels of metabolic enzymes). Ultrasensitivity and bistability (the simplest case of multistability) play important roles in cellular decision making and allow cells to convert continuous inputs into near-binary outputs and can provide cells with a biochemical memory for a stimulus in the form of hysteresis. Although the discovery of these potential information processing capabilities by homo-oligomers is significant already, the exploration of functions that homo-oligomerisation might offer is likely not exhausted yet. Saddle-node bifurcations, for example, are not the only bifurcations that can arise from multisite phosphorylation. It has been shown, for instance, that if phosphorylation and dephosphorylation proceed via different enzymatic mechanisms (e.g. processive vs. distributive), multiple sites can theoretically lead to sustained oscillations of the phosphorylation state of a protein (Suwanmajo and Krishnan 2015). After some minor modifications of the homo-oligomerisation models presented in chapter 5 to account for such mixed processive-distributive mechanisms, it is indeed not difficult to find parameter regimes that allow sustained oscillations (Figure 7.1B). While oscillatory phosphorylation may seem surprising at first, several proteins have been demonstrated experimentally to exhibit oscillatory phosphorylation states and are a commonly found mechanism to realise molecular clocks for biological rhythms (Hilioti et al. 2008; Rust et al. 2007). In any case, it proves the point that homo-oligomerisation may hold further surprises.

It is astounding that a network motif as simple as homo-oligomerisation can lead to the emergence of so many different and complex dynamics and steady-state responses without any explicit feedback loops. Although many of these predictions still require experimental confirmation in the context of real biochemical signalling networks, these discoveries may partly explain why homo-oligomerisation is such a frequently encountered phenomenon in evolution.

After the general exploration of the signalling functions of homo-oligomers, we applied our findings to the PLN signalling network to better understand the role of PLN pentamers in the context of β -adrenergic stimulation. The mathematical model developed in this work predicted phosphorylation of PLN by PKA to be bistable and PLN monomer phosphorylation to be delayed due to competition with pentamers, thereby adding another component to the regulatory repertoire of homo-oligomerisation. Both predictions have been confirmed experimentally, demonstrating that the mathematical models developed in this work indeed capture essential features of real biological systems. The bistability predicted by the model relies on cooperative dephosphorylation of PLN pentamers by PP1 (Li et al. 1990) which provides the required kinetic asymmetry for the saddle-node bifurcation to manifest (Conradi and Mincheva 2014). In this context, it is worth mentioning that phosphorylation of PLN pentamers by CaMKII has also been reported to exhibit strong positive cooperativity (Jackson and Colyer 1996), raising the possibility that phosphorylation of PLN at Thr17, too, could be bistable. Excitingly, further analyses and numerical simulations demonstrated that the monomer phosphorylation delays due to substrate competition by PLN pentamers and bistability could provide a way to filter out the effects of fluctuating PKA activity. Pentamers thereby may constitute molecular noise-filters that ensure consistent phosphorylation

of monomers. As the phosphorylation state of PLN monomers is a key determinant of SERCA activity, this could play an important role in ensuring coordinated calcium cycling and thus in preventing cardiac arrhythmias. As discussed in [chapter 6](#), this hypothesis is supported by the observation that several mutations that affect model components that contribute to noise-filtering indeed cause cardiac arrhythmias. As the physiological role of PLN pentamers has long been unclear and controversial, our findings provide an important and conceptually novel contribution to this long-standing question. In fact, since previous concepts have remained mostly descriptive and highly vague (“fine-tuning”), our concept of PLN pentamers as molecular noise-filters is the first concept so far to provide a clearly defined physiological advantage. Moreover, SERCA is also regulated by other small peptides such as sarcolipin, dworf, another-regulin and others (Hellstern et al. 2001; Anderson et al. 2015; Anderson et al. 2016; Singh et al. 2019). Since several of these can be phosphorylated and form homo-oligomers, it is possible that the mechanisms described here for PLN also apply to some of these other regulatory peptides (Bhupathy et al. 2007; Singh et al. 2019).

However, despite a better understanding of how PLN pentamers regulate the dynamics of PLN monomer phosphorylation, it is currently unknown what the molecular fluctuations and variability (i.e. the “noise”) in the β -adrenergic signalling networks and in SERCA activity look like in living cardiomyocytes. How exactly fluctuations in SERCA activity may cause cardiac arrhythmias, likewise, is currently unknown, although some potential explanations have been provided in the discussion in [chapter 6](#).

Due to these uncertainties, it remains to be tested whether the noise-filtering postulated to be provided by PLN pentamers can indeed prevent or reduce the development of cardiac arrhythmias in the context of β -adrenergic stimulation. One way to test this experimentally could be to use artificial PLN mutants that slightly disrupt or stabilise pentamers without affecting phosphorylation or SERCA function and to correlate the disruption/stabilisation of pentamers with the frequency or severity of cardiac arrhythmias in rodent or iPSC models. Another promising approach would be to couple the presented model of the PLN signalling networks with mathematical models of cardiomyocyte electrophysiology. In a first approximation, one could use simple phenomenological models that capture essential qualitative aspects of low-pass filtering and bistable PLN phosphorylation and excitable calcium dynamics and study whether noisy upstream signalling leads to irregular calcium dynamics in single cells, or in ensembles of multiple, electrically coupled cells. Furthermore, it may be feasible to integrate the full PLN model into experimentally validated and electrophysiologically realistic models of atrial and ventricular cardiomyocytes which have been developed in the last 10-20 years (Shannon et al. 2004; Grandi et al. 2010; Morotti et al. 2014). Models like these have already proven highly valuable to investigate the effect of β -adrenergic stimulation on arrhythmogenesis and are likely suitable for studying the effect of noisy signals in the β -adrenergic pathway (Soltis and Saucerman 2010; Xie et al. 2014). Such approaches not only hold great promise to better understand the pathophysiology of PLN mutations and other diseases, but also to identify promising therapy approaches (Qu et al. 2014).

References

- Abe K., Rossman K. L., Liu B., Ritola K. D., Chiang D., Campbell S. L., Burrige K., and Der C. J. (2000). “Vav2 Is an Activator of Cdc42, Rac1, and RhoA”. In: *Journal of Biological Chemistry* 275 (14), pp. 10141–10149. DOI: [10.1074/jbc.275.14.10141](https://doi.org/10.1074/jbc.275.14.10141).
- Abiko H., Fujiwara S., Ohashi K., Hiattari R., Mashiko T., Sakamoto N., Sato M., and Mizuno K. (2015). “Rho guanine nucleotide exchange factors involved in cyclic-stretch-induced reorientation of vascular endothelial cells”. In: *J Cell Sci* 128 (9), pp. 1683–1695. DOI: [10.1242/jcs.157503](https://doi.org/10.1242/jcs.157503).
- Ackermann M. A., King B., Lieberman N. A. P., Bobbili P. J., Rudloff M., Berndsen C. E., Wright N. T., Hecker P. A., and Kontogianni-Konstantopoulos A. (2017). “Novel obscurins mediate cardiomyocyte adhesion and size via the PI3K/AKT/mTOR signaling pathway”. In: *Journal of Molecular and Cellular Cardiology* 111, pp. 27–39. DOI: [10.1016/j.yjmcc.2017.08.004](https://doi.org/10.1016/j.yjmcc.2017.08.004).
- Agarkova I. and Ehler E. (2015). “The M-Band: Not Just Inert Glue but Playing an Active Role in the Middle of the Sarcomere”. In: *Cardiac Cytoarchitecture*. Springer, Cham, pp. 125–140. DOI: [10.1007/978-3-319-15263-9_7](https://doi.org/10.1007/978-3-319-15263-9_7).
- Agarkova I., Ehler E., Lange S., Schoenauer R., and Perriard J.-C. (2003). “M-band: a safeguard for sarcomere stability?” In: *Journal of Muscle Research & Cell Motility* 24(2-3), pp. 191–203. DOI: [10.1023/A:1026094924677](https://doi.org/10.1023/A:1026094924677).
- Agarkova I. and Perriard J.-C. (2005). “The M-band: an elastic web that crosslinks thick filaments in the center of the sarcomere”. In: *Trends in Cell Biology* 15 (9), pp. 477–485. DOI: [10.1016/j.tcb.2005.07.001](https://doi.org/10.1016/j.tcb.2005.07.001).
- Ahmad K. F. and Lim W. A. (2010). “The Minimal Autoinhibited Unit of the Guanine Nucleotide Exchange Factor Intersectin”. In: *PLOS ONE* 5 (6), e11291. DOI: [10.1371/journal.pone.0011291](https://doi.org/10.1371/journal.pone.0011291).
- Ahmad T., Miller P. E., McCullough M., et al. (2019). “Why has positive inotropy failed in chronic heart failure? Lessons from prior inotrope trials”. In: *European Journal of Heart Failure* 21 (9), pp. 1064–1078. DOI: <https://doi.org/10.1002/ejhf.1557>.
- Alcalai R., Seidman J. G., and Seidman C. E. (2008). “Genetic Basis of Hypertrophic Cardiomyopathy: From Bench to the Clinics”. In: *Journal of Cardiovascular Electrophysiology* 19 (1), pp. 104–110. DOI: <https://doi.org/10.1111/j.1540-8167.2007.00965.x>.
- Ali I., Eu S., Koch D., Bleimling N., Goody R. S., and Müller M. P. (2018). “Structure of the tandem PX-PH domains of Bem3 from *Saccharomyces cerevisiae*”. In: *Acta Crystallographica Section F: Structural Biology Communications* 74 (5), pp. 315–321. DOI: [10.1107/S2053230X18005915](https://doi.org/10.1107/S2053230X18005915).
- Ali M. H. and Imperiali B. (2005). “Protein oligomerization: How and why”. In: *Bioorganic & Medicinal Chemistry* 13 (17), pp. 5013–5020. DOI: [10.1016/j.bmc.2005.05.037](https://doi.org/10.1016/j.bmc.2005.05.037).
- Alsina K. M., Hulsurkar M., Brandenburg S., et al. (2019). “Loss of Protein Phosphatase 1 Regulatory Subunit PPP1R3A Promotes Atrial Fibrillation”. In: *Circulation* 140 (8), pp. 681–693. DOI: [10.1161/CIRCULATIONAHA.119.039642](https://doi.org/10.1161/CIRCULATIONAHA.119.039642).
- Amano M., Ito M., Kimura K., Fukata Y., Chihara K., Nakano T., Matsuura Y., and Kaibuchi K. (1996). “Phosphorylation and Activation of Myosin by Rho-associated Kinase (Rho-kinase)”. In: *Journal of Biological Chemistry* 271 (34), pp. 20246–20249. DOI: [10.1074/jbc.271.34.20246](https://doi.org/10.1074/jbc.271.34.20246).

- Amin E., Jaiswal M., Derewenda U., et al. (2016). “Deciphering the Molecular and Functional Basis of RHO GAP Family Proteins: a Systematic Approach Toward Selective Inactivation of Rho Family Proteins”. In: *Journal of Biological Chemistry* 291 (39), pp. 20353–20371. DOI: [10.1074/jbc.M116.736967](https://doi.org/10.1074/jbc.M116.736967).
- Anderson D. M., Makarewich C. A., Anderson K. M., Shelton J. M., Bezprozvannaya S., Bassel-Duby R., and Olson E. N. (2016). “Widespread control of calcium signaling by a family of SERCA-inhibiting micropeptides”. In: *Science Signaling* 9 (457), ra119.
- Anderson D., Anderson K., Chang C.-L., et al. (2015). “A Micropeptide Encoded by a Putative Long Noncoding RNA Regulates Muscle Performance”. In: *Cell* 160 (4), pp. 595–606. DOI: [10.1016/j.cell.2015.01.009](https://doi.org/10.1016/j.cell.2015.01.009).
- Aoki H., Izumo S., and Sadoshima J. (1998). “Angiotensin II Activates RhoA in Cardiac Myocytes : A Critical Role of RhoA in Angiotensin II Induced Premyofibril Formation”. In: *Circulation Research* 82 (6), pp. 666–676. DOI: [10.1161/01.RES.82.6.666](https://doi.org/10.1161/01.RES.82.6.666).
- Arimura T., Matsumoto Y., Okazaki O., et al. (2007). “Structural analysis of obscurin gene in hypertrophic cardiomyopathy”. In: *Biochemical and Biophysical Research Communications* 362 (2), pp. 281–287. DOI: [10.1016/j.bbrc.2007.07.183](https://doi.org/10.1016/j.bbrc.2007.07.183).
- El-Armouche A., Rau T., Zolk O., et al. (2003). “Evidence for protein phosphatase inhibitor-1 playing an amplifier role in β -adrenergic signaling in cardiac myocytes”. In: *The FASEB Journal* 17 (3), pp. 437–439. DOI: [10.1096/fj.02-0057fje](https://doi.org/10.1096/fj.02-0057fje).
- Ashkenazy H., Erez E., Martz E., Pupko T., and Ben-Tal N. (2010). “ConSurf 2010: calculating evolutionary conservation in sequence and structure of proteins and nucleic acids”. In: *Nucleic Acids Research* 38, W529–W533. DOI: [10.1093/nar/gkq399](https://doi.org/10.1093/nar/gkq399).
- Aspenström P. (2017). “Fast-cycling Rho GTPases”. In: *Small GTPases* 0 (0), pp. 1–8. DOI: [10.1080/21541248.2017.1391365](https://doi.org/10.1080/21541248.2017.1391365).
- Bagnato P., Barone V., Giacomello E., Rossi D., and Sorrentino V. (2003). “Binding of an ankyrin-1 isoform to obscurin suggests a molecular link between the sarcoplasmic reticulum and myofibrils in striated muscles”. In: *The Journal of Cell Biology* 160 (2), pp. 245–253. DOI: <https://doi.org/10.1083/jcb.200208109>.
- Bähler M. and Rhoads A. (2002). “Calmodulin signaling via the IQ motif”. In: *FEBS Letters* 513 (1), pp. 107–113. DOI: [10.1016/S0014-5793\(01\)03239-2](https://doi.org/10.1016/S0014-5793(01)03239-2).
- Bang M.-L., Centner T., Fornoff F., et al. (2001). “The Complete Gene Sequence of Titin, Expression of an Unusual \approx 700-kDa Titin Isoform, and Its Interaction With Obscurin Identify a Novel Z-Line to I-Band Linking System”. In: *Circulation Research* 89 (11), pp. 1065–1072. DOI: [10.1161/hh2301.100981](https://doi.org/10.1161/hh2301.100981).
- Barreira M., Fabbiano S., Couceiro J. R., Torreira E., Martínez-Torrecaadrada J. L., Montoya G., Llorca O., and Bustelo X. R. (2014). “The C-Terminal SH3 Domain Contributes to the Intramolecular Inhibition of Vav Family Proteins”. In: *Science Signaling* 7 (321), ra35–ra35. DOI: [10.1126/scisignal.2004993](https://doi.org/10.1126/scisignal.2004993).
- Becucci L., Cembran A., Karim C. B., Thomas D. D., Guidelli R., Gao J., and Veglia G. (2009). “On the Function of Pentameric Phospholamban: Ion Channel or Storage Form?” In: *Biophysical Journal* 96 (10), pp. L60–L62. DOI: [10.1016/j.bpj.2009.03.013](https://doi.org/10.1016/j.bpj.2009.03.013).
- Benian G. M., Tinley T. L., Tang X., and Borodovsky M. (1996). “The *Caenorhabditis elegans* gene *unc-89*, required for muscle M-line assembly, encodes a giant modular protein composed of Ig and signal transduction domains.” In: *The Journal of Cell Biology* 132 (5), pp. 835–848. DOI: [10.1083/jcb.132.5.835](https://doi.org/10.1083/jcb.132.5.835).
- Berg J. M., Tymoczko J. L., Gatto Jr G. J., and Stryer L. (2015). *Biochemistry*. 8th edition. New York: W. H. Freeman.
- Bers D. M. (2002). “Cardiac excitation–contraction coupling”. In: *Nature* 415, pp. 198–205. DOI: [10.1038/415198a](https://doi.org/10.1038/415198a).
- Bers D. M., Xiang Y. K., and Zaccolo M. (2019). “Whole-Cell cAMP and PKA Activity are Epiphenomena, Nanodomain Signaling Matters”. In: *Physiology* 34 (4), pp. 240–249. DOI: [10.1152/physiol.00002.2019](https://doi.org/10.1152/physiol.00002.2019).

- Bezeljask U., Loya H., Kaczmarek B., Saunders T. E., and Loose M. (2020). “Stochastic activation and bistability in a Rab GTPase regulatory network”. In: *Proceedings of the National Academy of Sciences* 17 (12), pp. 6540–6549. DOI: [10.1073/pnas.1921027117](https://doi.org/10.1073/pnas.1921027117).
- Bhupathy P., Babu G. J., and Periasamy M. (2007). “Sarcoplipin and Phospholamban as Regulator of Cardiac Sarcoplasmic Reticulum Ca²⁺ ATPase”. In: *Journal of molecular and cellular cardiology* 42 (5), pp. 903–911. DOI: [10.1016/j.yjmcc.2007.03.738](https://doi.org/10.1016/j.yjmcc.2007.03.738).
- Blomberg N., Baraldi E., Sattler M., Saraste M., and Nilges M. (2000). “Structure of a PH Domain from the *C. elegans* Muscle Protein UNC-89 Suggests a Novel Function”. In: *Structure* 8 (10), pp. 1079–1087. DOI: [10.1016/S0969-2126\(00\)00509-8](https://doi.org/10.1016/S0969-2126(00)00509-8).
- Blondelle J., Marrocco V., Clark M., et al. (2019). “Murine obscurin and Obsl1 have functionally redundant roles in sarcolemmal integrity, sarcoplasmic reticulum organization, and muscle metabolism”. In: *Communications Biology* 2 (1), p. 178. DOI: [10.1038/s42003-019-0405-7](https://doi.org/10.1038/s42003-019-0405-7).
- Boateng S. Y. and Goldspink P. H. (2008). “Assembly and maintenance of the sarcomere night and day”. In: *Cardiovascular Research* 77 (4), pp. 667–675. DOI: [10.1093/cvr/cvm048](https://doi.org/10.1093/cvr/cvm048).
- Bode E. F., Briston S. J., Overend C. L., O’Neill S. C., Trafford A. W., and Eisner D. A. (2011). “Changes of SERCA activity have only modest effects on sarcoplasmic reticulum Ca²⁺ content in rat ventricular myocytes”. In: *The Journal of Physiology* 589 (19), pp. 4723–4729. DOI: [10.1113/jphysiol.2011.211052](https://doi.org/10.1113/jphysiol.2011.211052).
- Bogomolovas J., Gasch A., Simkovic F., Rigden D. J., Labeit S., and Mayans O. (2014). “Titin kinase is an inactive pseudokinase scaffold that supports MuRF1 recruitment to the sarcomeric M-line”. In: *Open Biology* 4 (5), p. 140041. DOI: [10.1098/rsob.140041](https://doi.org/10.1098/rsob.140041).
- Bönnemann C. G., Thompson T. G., Ven P. F. M. van der, et al. (2003). “Filamin C accumulation is a strong but nonspecific immunohistochemical marker of core formation in muscle”. In: *Journal of the Neurological Sciences* 206 (1), pp. 71–78. DOI: [10.1016/S0022-510X\(02\)00341-6](https://doi.org/10.1016/S0022-510X(02)00341-6).
- Borisov A. B., Raeker M. O., Kontrogianni-Konstantopoulos A., Yang K., Kurnit D. M., Bloch R. J., and Russell M. W. (2003). “Rapid response of cardiac obscurin gene cluster to aortic stenosis: differential activation of Rho-GEF and MLCK and involvement in hypertrophic growth”. In: *Biochemical and Biophysical Research Communications* 310 (3), pp. 910–918. DOI: [10.1016/j.bbrc.2003.09.035](https://doi.org/10.1016/j.bbrc.2003.09.035).
- Borisov A. B., Raeker M. Ö., and Russell M. W. (2008). “Developmental expression and differential cellular localization of obscurin and obscurin-associated kinase in cardiac muscle cells”. In: *Journal of Cellular Biochemistry* 103 (5), pp. 1621–1635. DOI: [10.1002/jcb.21551](https://doi.org/10.1002/jcb.21551).
- Borisov A. B., Sutter S. B., Kontrogianni-Konstantopoulos A., Bloch R. J., Westfall M. V., and Russell M. W. (2006). “Essential role of obscurin in cardiac myofibrillogenesis and hypertrophic response: evidence from small interfering RNA-mediated gene silencing”. In: *Histochemistry and Cell Biology* 125 (3), p. 227. DOI: [10.1007/s00418-005-0069-x](https://doi.org/10.1007/s00418-005-0069-x).
- Bos J. L., Rehmann H., and Wittinghofer A. (2007). “GEFs and GAPs: Critical Elements in the Control of Small G Proteins”. In: *Cell* 129 (5), pp. 865–877. DOI: [10.1016/j.cell.2007.05.018](https://doi.org/10.1016/j.cell.2007.05.018).
- Boulter E., Burridge K., and Garcia-Mata R. (2011). “The ‘invisible hand’: regulation of RHO GTPases by RHOGDIs”. In: *Nature Reviews Molecular Cell Biology* 12 (8), p. 493. DOI: [10.1038/nrm3153](https://doi.org/10.1038/nrm3153).
- Boureaux A., Vignal E., Faure S., and Fort P. (2007). “Evolution of the Rho Family of Ras-Like GTPases in Eukaryotes”. In: *Molecular Biology and Evolution* 24 (1), pp. 203–216. DOI: [10.1093/molbev/msl145](https://doi.org/10.1093/molbev/msl145).
- Bowman A. L., Catino D. H., Strong J. C., Randall W. R., Kontrogianni-Konstantopoulos A., and Bloch R. J. (2008). “The Rho-Guanine Nucleotide Exchange Factor Domain of Obscurin Regulates Assembly of Titin at the Z-Disk through Interactions with Ran Binding Protein 9”. In: *Molecular Biology of the Cell* 19 (9), pp. 3782–3792. DOI: [10.1091/mbc.E08-03-0237](https://doi.org/10.1091/mbc.E08-03-0237).
- Bowman A. L., Kontrogianni-Konstantopoulos A., Hirsch S. S., Geisler S. B., Gonzalez-Serratos H., Russell M. W., and Bloch R. J. (2007). “Different obscurin isoforms localize to distinct sites at sarcomeres”. In: *FEBS Letters* 581 (8), pp. 1549–1554. DOI: [10.1016/j.febslet.2007.03.011](https://doi.org/10.1016/j.febslet.2007.03.011).

- Brown J. H., Del Re D. P., and Sussman M. A. (2006). “The Rac and Rho hall of fame: a decade of hypertrophic signaling hits”. In: *Circulation Research* 98(6), pp. 730–742. DOI: [10.1161/01.RES.0000216039.75913.9e](https://doi.org/10.1161/01.RES.0000216039.75913.9e).
- Brugada J., Katritsis D. G., Arbelo E., et al. (2020). “2019 ESC Guidelines for the management of patients with supraventricular tachycardia”. In: *European Heart Journal* 41(5), pp. 655–720. DOI: [10.1093/eurheartj/ehz467](https://doi.org/10.1093/eurheartj/ehz467).
- Buchan D. W. A. and Jones D. T. (2019). “The PSIPRED Protein Analysis Workbench: 20 years on”. In: *Nucleic Acids Research* 47(W1), W402–W407. DOI: [10.1093/nar/gkz297](https://doi.org/10.1093/nar/gkz297).
- Burrige K. and Wennerberg K. (2004). “Rho and Rac Take Center Stage”. In: *Cell* 116(2), pp. 167–179. DOI: [10.1016/S0092-8674\(04\)00003-0](https://doi.org/10.1016/S0092-8674(04)00003-0).
- Byrne K. M., Monsefi N., Dawson J. C., et al. (2016). “Bistability in the Rac1, PAK, and RhoA Signaling Network Drives Actin Cytoskeleton Dynamics and Cell Motility Switches”. In: *Cell Systems* 2(1), pp. 38–48. DOI: [10.1016/j.cels.2016.01.003](https://doi.org/10.1016/j.cels.2016.01.003).
- Cabo C. and Wit A. L. (1997). “Cellular Electrophysiologic Mechanisms Of Cardiac Arrhythmias”. In: *Cardiology Clinics* 15(4), pp. 517–538. DOI: [10.1016/S0733-8651\(05\)70360-X](https://doi.org/10.1016/S0733-8651(05)70360-X).
- Cahill T. J., Ashrafian H., and Watkins H. (2013). “Genetic Cardiomyopathies Causing Heart Failure”. In: *Circulation Research* 113(6), pp. 660–675. DOI: [10.1161/CIRCRESAHA.113.300282](https://doi.org/10.1161/CIRCRESAHA.113.300282).
- Carlsson L., Yu J.-G., and Thornell L.-E. (2008). “New aspects of obscurin in human striated muscles”. In: *Histochemistry and Cell Biology* 130(1), pp. 91–103. DOI: [10.1007/s00418-008-0413-z](https://doi.org/10.1007/s00418-008-0413-z).
- Ceholski D. K., Trieber C. A., Holmes C. F. B., and Young H. S. (2012). “Lethal, Hereditary Mutants of Phospholamban Elude Phosphorylation by Protein Kinase A”. In: *Journal of Biological Chemistry* 287(32), pp. 26596–26605. DOI: [10.1074/jbc.M112.382713](https://doi.org/10.1074/jbc.M112.382713).
- Chen Z., Medina F., Liu M.-Y., Thomas C., Sprang S. R., and Sternweis P. C. (2010). “Activated RhoA Binds to the Pleckstrin Homology (PH) Domain of PDZ-RhoGEF, a Potential Site for Autoregulation”. In: *Journal of Biological Chemistry* 285(27), pp. 21070–21081. DOI: [10.1074/jbc.M110.122549](https://doi.org/10.1074/jbc.M110.122549).
- Cherfils J. and Zeghouf M. (2013). “Regulation of small GTPases by GEFs, GAPs, and GDIs.” In: *Physiological reviews* 93(1), pp. 269–309. DOI: [10.1152/physrev.00003.2012](https://doi.org/10.1152/physrev.00003.2012).
- Chhatriwala M. K., Betts L., Worthylake D. K., and Sondek J. (2007). “The DH and PH Domains of Trio Coordinately Engage Rho GTPases for their Efficient Activation”. In: *Journal of Molecular Biology* 368(5), pp. 1307–1320. DOI: [10.1016/j.jmb.2007.02.060](https://doi.org/10.1016/j.jmb.2007.02.060).
- Chu G., Li L., Sato Y., Harrer J. M., Kadambi V. J., Hoit B. D., Bers D. M., and Kranias E. G. (1998). “Pentameric Assembly of Phospholamban Facilitates Inhibition of Cardiac Function *in Vivo*”. In: *Journal of Biological Chemistry* 273(50), pp. 33674–33680. DOI: [10.1074/jbc.273.50.33674](https://doi.org/10.1074/jbc.273.50.33674).
- Coisy-Quivy M., Sanguesa-Ferrer J., Weill M., Johnson D. S., Donnay J.-M., Hipskind R., Fort P., and Philips A. (2006). “Identification of Rho GTPases implicated in terminal differentiation of muscle cells in ascidia”. In: *Biology of the Cell* 98(10), pp. 577–588. DOI: [10.1042/BC20060032](https://doi.org/10.1042/BC20060032).
- Coisy-Quivy M., Touzet O., Bourret A., Hipskind R. A., Mercier J., Fort P., and Philips A. (2009). “TC10 controls human myofibril organization and is activated by the sarcomeric RhoGEF obscurin”. In: *Journal of Cell Science* 122, pp. 947–956. DOI: [10.1242/jcs.040121](https://doi.org/10.1242/jcs.040121).
- Colyer J. (1998). “Phosphorylation States of Phospholamban”. In: *Annals of the New York Academy of Sciences* 853(1), pp. 79–91. DOI: [10.1111/j.1749-6632.1998.tb08258.x](https://doi.org/10.1111/j.1749-6632.1998.tb08258.x).
- Conradi C. and Mincheva M. (2014). “Catalytic constants enable the emergence of bistability in dual phosphorylation”. In: *Journal of The Royal Society Interface* 11(95), p. 20140158. DOI: [10.1098/rsif.2014.0158](https://doi.org/10.1098/rsif.2014.0158).
- Conte-Zerial P. D., Bruschi L., Rink J. C., Collinet C., Kalaidzidis Y., Zerial M., and Deutsch A. (2008). “Membrane identity and GTPase cascades regulated by toggle and cut-out switches”. In: *Molecular Systems Biology* 4(1), p. 206. DOI: [10.1038/msb.2008.45](https://doi.org/10.1038/msb.2008.45).

- Cornea R. L., Jones L. R., Autry J. M., and Thomas D. D. (1997). "Mutation and Phosphorylation Change the Oligomeric Structure of Phospholamban in Lipid Bilayers". In: *Biochemistry* 36 (10), pp. 2960–2967. DOI: [10.1021/bi961955q](https://doi.org/10.1021/bi961955q).
- Cunha S. R. and Mohler P. J. (2008). "Obscurin Targets Ankyrin-B and Protein Phosphatase 2A to the Cardiac M-line". In: *Journal of Biological Chemistry* 283 (46), pp. 31968–31980. DOI: [10.1074/jbc.M806050200](https://doi.org/10.1074/jbc.M806050200).
- Del Re D. P., Miyamoto S., and Brown J. H. (2007). "RhoA/Rho Kinase Up-regulate Bax to Activate a Mitochondrial Death Pathway and Induce Cardiomyocyte Apoptosis". In: *Journal of Biological Chemistry* 282 (11), pp. 8069–8078. DOI: [10.1074/jbc.M604298200](https://doi.org/10.1074/jbc.M604298200).
- Desmond P. F., Muriel J., Markwardt M. L., Rizzo M. A., and Bloch R. J. (2015). "Identification of Small Ankyrin 1 as a Novel Sarco(endo)plasmic Reticulum Ca²⁺-ATPase 1 (SERCA1) Regulatory Protein in Skeletal Muscle". In: *Journal of Biological Chemistry* 290 (46), pp. 27854–27867. DOI: [10.1074/jbc.M115.676585](https://doi.org/10.1074/jbc.M115.676585).
- Djoussé L. (2009). "Relation Between Modifiable Lifestyle Factors and Lifetime Risk of Heart Failure". In: *JAMA* 302 (4), p. 394. DOI: [10.1001/jama.2009.1062](https://doi.org/10.1001/jama.2009.1062).
- Dobrzynski H., Boyett M. R., and Anderson R. H. (2007). "New Insights Into Pacemaker Activity". In: *Circulation* 115 (14), pp. 1921–1932. DOI: [10.1161/CIRCULATIONAHA.106.616011](https://doi.org/10.1161/CIRCULATIONAHA.106.616011).
- Eckel R. H. (1997). "Obesity and Heart Disease". In: *Circulation* 96 (9), pp. 3248–3250. DOI: [10.1161/01.CIR.96.9.3248](https://doi.org/10.1161/01.CIR.96.9.3248).
- Edes I. and Kranias E. G. (1990). "Phospholamban and troponin I are substrates for protein kinase C in vitro but not in intact beating guinea pig hearts." In: *Circulation Research* 67 (2), pp. 394–400. DOI: [10.1161/01.RES.67.2.394](https://doi.org/10.1161/01.RES.67.2.394).
- Ehrlicher A. J., Nakamura F., Hartwig J. H., Weitz D. A., and Stossel T. P. (2011). "Mechanical strain in actin networks regulates FilGAP and integrin binding to filamin A". In: *Nature* 478 (7368), pp. 260–263. DOI: [10.1038/nature10430](https://doi.org/10.1038/nature10430).
- Ehrmann A., Nguyen B., and Seifert U. (2019). "Interlinked GTPase cascades provide a motif for both robust switches and oscillators". In: *Journal of The Royal Society Interface* 16 (157), p. 20190198. DOI: [10.1098/rsif.2019.0198](https://doi.org/10.1098/rsif.2019.0198).
- Eijgenraam T. R., Boukens B. J., Boogerd C. J., et al. (2020). "The phospholamban p.(Arg14del) pathogenic variant leads to cardiomyopathy with heart failure and is unresponsive to standard heart failure therapy". In: *Scientific Reports* 10 (1), p. 9819. DOI: [10.1038/s41598-020-66656-9](https://doi.org/10.1038/s41598-020-66656-9).
- Eisner D. A. (2018). "Ups and downs of calcium in the heart". In: *The Journal of Physiology* 596 (1), pp. 19–30. DOI: [10.1113/JP275130](https://doi.org/10.1113/JP275130).
- Eisner D. A., Caldwell J. L., Kistamás K., and Trafford A. W. (2017). "Calcium and Excitation-Contraction Coupling in the Heart". In: *Circulation Research* 121 (2), pp. 181–195. DOI: [10.1161/CIRCRESAHA.117.310230](https://doi.org/10.1161/CIRCRESAHA.117.310230).
- Etienne-Manneville S. and Hall A. (2002). "Rho GTPases in cell biology". In: *Nature* 420 (6916), pp. 629–635. DOI: [10.1038/nature01148](https://doi.org/10.1038/nature01148).
- Fleming J. R., Rani A., Kraft J., Zenker S., Börgeson E., and Lange S. (2021). "Exploring Obscurin and SPEG Kinase Biology". In: *Journal of Clinical Medicine* 10 (5), p. 984. DOI: [10.3390/jcm10050984](https://doi.org/10.3390/jcm10050984).
- Ford-Speelman D. L., Roche J. A., Bowman A. L., and Bloch R. J. (2009). "The rho-guanine nucleotide exchange factor domain of obscurin activates rhoA signaling in skeletal muscle." In: *Molecular biology of the cell* 20 (17), pp. 3905–3917. DOI: [10.1091/mbc.E08-10-1029](https://doi.org/10.1091/mbc.E08-10-1029).
- Fort P. and Blangy A. (2017). "The Evolutionary Landscape of Dbl-Like RhoGEF Families: Adapting Eukaryotic Cells to Environmental Signals". In: *Genome Biology and Evolution* 9 (6), pp. 1471–1486. DOI: [10.1093/gbe/evx100](https://doi.org/10.1093/gbe/evx100).
- Fu D.-G. (2015). "Cardiac Arrhythmias: Diagnosis, Symptoms, and Treatments". In: *Cell Biochemistry and Biophysics* 73 (2), pp. 291–296. DOI: [10.1007/s12013-015-0626-4](https://doi.org/10.1007/s12013-015-0626-4).

- Fukuzawa A., Idowu S., and Gautel M. (2005). “Complete human gene structure of obscurin: implications for isoform generation by differential splicing”. In: *Journal of Muscle Research & Cell Motility* 26 (6-8), pp. 427–434. DOI: [10.1007/s10974-005-9025-6](https://doi.org/10.1007/s10974-005-9025-6).
- Fukuzawa A., Lange S., Holt M., Vihola A., Carmignac V., Ferreiro A., Udd B., and Gautel M. (2008). “Interactions with titin and myomesin target obscurin and obscurin-like 1 to the M-band – implications for hereditary myopathies”. In: *Journal of Cell Science* 121 (11), p. 1841. DOI: [10.1242/jcs.028019](https://doi.org/10.1242/jcs.028019).
- Garvey J. L., Kranias E. G., and Solaro R. J. (1988). “Phosphorylation of C-protein, troponin I and phospholamban in isolated rabbit hearts”. In: *Biochemical Journal* 249 (3), pp. 709–714. DOI: [10.1042/bj2490709](https://doi.org/10.1042/bj2490709).
- Gautel M. (2011). “Cytoskeletal protein kinases: titin and its relations in mechanosensing”. In: *Pflügers Archiv - European Journal of Physiology* 462 (1), pp. 119–134. DOI: [10.1007/s00424-011-0946-1](https://doi.org/10.1007/s00424-011-0946-1).
- Gaztañaga L., Marchlinski F. E., and Betensky B. P. (2012). “Mechanisms of Cardiac Arrhythmias”. In: *Revista Española de Cardiología (English Edition)* 65 (2), pp. 174–185. DOI: [10.1016/j.rec.2011.09.020](https://doi.org/10.1016/j.rec.2011.09.020).
- Geisler S. B., Robinson D., Hauringa M., Raeker M. O., Borisov A. B., Westfall M. V., and Russell M. W. (2007). “Obscurin-like 1, OBSL1, is a novel cytoskeletal protein related to obscurin”. In: *Genomics* 89 (4), pp. 521–531. DOI: [10.1016/j.ygeno.2006.12.004](https://doi.org/10.1016/j.ygeno.2006.12.004).
- Graessl M., Koch J., Calderon A., et al. (2017). “An excitable Rho GTPase signaling network generates dynamic subcellular contraction patterns”. In: *J Cell Biol* 216 (12), pp. 4271–4285. DOI: [10.1083/jcb.201706052](https://doi.org/10.1083/jcb.201706052).
- Grandi E., Pasqualini F. S., and Bers D. M. (2010). “A novel computational model of the human ventricular action potential and Ca transient”. In: *Journal of Molecular and Cellular Cardiology* 48 (1), pp. 112–121. DOI: [10.1016/j.yjmcc.2009.09.019](https://doi.org/10.1016/j.yjmcc.2009.09.019).
- Gräter F., Shen J., Jiang H., Gautel M., and Grubmüller H. (2005). “Mechanically Induced Titin Kinase Activation Studied by Force-Probe Molecular Dynamics Simulations”. In: *Biophysical Journal* 88 (2), pp. 790–804. DOI: [10.1529/biophysj.104.052423](https://doi.org/10.1529/biophysj.104.052423).
- Grogan A., Coleman A., Joca H., Granzier H., Russel M. W., Ward C. W., and Kontrogianni-Konstantopoulos A. (2020). “Deletion of obscurin immunoglobulin domains Ig58/59 leads to age-dependent cardiac remodeling and arrhythmia”. In: *Basic Research in Cardiology* 115 (6), p. 60. DOI: [10.1007/s00395-020-00818-8](https://doi.org/10.1007/s00395-020-00818-8).
- Grosshans B. L., Ortiz D., and Novick P. (2006). “Rabs and their effectors: Achieving specificity in membrane traffic”. In: *Proceedings of the National Academy of Sciences* 103 (32), pp. 11821–11827. DOI: [10.1073/pnas.0601617103](https://doi.org/10.1073/pnas.0601617103).
- Guilluy C., Swaminathan V., Garcia-Mata R., O’Brien E. T., Superfine R., and Burridge K. (2011). “The Rho GEFs LARG and GEF-H1 regulate the mechanical response to force on integrins”. In: *Nature Cell Biology* 13 (6), pp. 722–727. DOI: [10.1038/ncb2254](https://doi.org/10.1038/ncb2254).
- Guo H., Isserlin R., Emili A., and Burniston J. G. (2017). “Exercise-responsive phosphoproteins in the heart”. In: *Journal of Molecular and Cellular Cardiology* 111, pp. 61–68. DOI: [10.1016/j.yjmcc.2017.08.001](https://doi.org/10.1016/j.yjmcc.2017.08.001).
- Guo Z., Ahmadian M. R., and Goody R. S. (2005). “Guanine Nucleotide Exchange Factors Operate by a Simple Allosteric Competitive Mechanism”. In: *Biochemistry* 44 (47), pp. 15423–15429. DOI: [10.1021/bi0518601](https://doi.org/10.1021/bi0518601).
- Gustavsson M., Verardi R., Mullen D. G., Mote K. R., Traaseth N. J., Gopinath T., and Veglia G. (2013). “Allosteric regulation of SERCA by phosphorylation-mediated conformational shift of phospholamban”. In: *Proceedings of the National Academy of Sciences* 110 (43), pp. 17338–17343. DOI: [10.1073/pnas.1303006110](https://doi.org/10.1073/pnas.1303006110).
- Hagemann D., Kuschel M., Kuramochi T., Zhu W., Cheng H., and Xiao R.-P. (2000). “Frequency-encoding Thr17 Phospholamban Phosphorylation Is Independent of Ser16 Phosphorylation in Cardiac Myocytes”. In: *Journal of Biological Chemistry* 275 (29), pp. 22532–22536. DOI: [10.1074/jbc.C000253200](https://doi.org/10.1074/jbc.C000253200).

- Haghighi K., Kolokathis F., Gramolini A. O., et al. (2006). "A mutation in the human phospholamban gene, deleting arginine 14, results in lethal, hereditary cardiomyopathy". In: *Proceedings of the National Academy of Sciences* 103 (5), pp. 1388–1393. DOI: [10.1073/pnas.0510519103](https://doi.org/10.1073/pnas.0510519103).
- Haghighi K., Kolokathis F., Pater L., et al. (2003). "Human phospholamban null results in lethal dilated cardiomyopathy revealing a critical difference between mouse and human". In: *The Journal of Clinical Investigation* 111 (6), pp. 869–876. DOI: [10.1172/JCI17892](https://doi.org/10.1172/JCI17892).
- Haghighi K., Pritchard T., Bossuyt J., et al. (2012). "The human phospholamban Arg14-deletion mutant localizes to plasma membrane and interacts with the Na/K-ATPase". In: *Journal of Molecular and Cellular Cardiology* 52 (3), pp. 773–782. DOI: [10.1016/j.yjmcc.2011.11.012](https://doi.org/10.1016/j.yjmcc.2011.11.012).
- Haghighi K., Pritchard T. J., Liu G.-S., et al. (2015). "Human G109E-inhibitor-1 impairs cardiac function and promotes arrhythmias". In: *Journal of Molecular and Cellular Cardiology* 89, pp. 349–359. DOI: [10.1016/j.yjmcc.2015.10.004](https://doi.org/10.1016/j.yjmcc.2015.10.004).
- Halder G. and Johnson R. L. (2011). "Hippo signaling: growth control and beyond". In: *Development* 138 (1), pp. 9–22. DOI: [10.1242/dev.045500](https://doi.org/10.1242/dev.045500).
- Hall J. E. (2016). *Guyton and Hall Textbook of Medical Physiology*. 13th. Elsevier.
- Harper A. R., Goel A., Grace C., et al. (2021). "Common genetic variants and modifiable risk factors underpin hypertrophic cardiomyopathy susceptibility and expressivity". In: *Nature Genetics* 53 (2), pp. 135–142. DOI: [10.1038/s41588-020-00764-0](https://doi.org/10.1038/s41588-020-00764-0).
- Hart M. J., Eva A., Zangrilli D., Aaronson S. A., Evans T., Cerione R. A., and Zheng Y. (1994). "Cellular transformation and guanine nucleotide exchange activity are catalyzed by a common domain on the dbl oncogene product." In: *Journal of Biological Chemistry* 269 (1), pp. 62–65.
- Heallen T., Zhang M., Wang J., Bonilla-Claudio M., Klysik E., Johnson R. L., and Martin J. F. (2011). "Hippo Pathway Inhibits Wnt Signaling to Restrain Cardiomyocyte Proliferation and Heart Size". In: *Science* 332 (6028), pp. 458–461. DOI: [10.1126/science.1199010](https://doi.org/10.1126/science.1199010).
- Heasman S. J. and Ridley A. J. (2008). "Mammalian Rho GTPases: new insights into their functions from in vivo studies". In: 9, p. 690.
- Hellstern S., Pegoraro S., Karim C. B., Lustig A., Thomas D. D., Moroder L., and Engel J. (2001). "Sarcolipin, the Shorter Homologue of Phospholamban, Forms Oligomeric Structures in Detergent Micelles and in Liposomes". In: *Journal of Biological Chemistry* 276 (33), pp. 30845–30852. DOI: [10.1074/jbc.M102495200](https://doi.org/10.1074/jbc.M102495200).
- Heo J., Thapar R., and Campbell S. L. (2005). "Recognition and Activation of Rho GTPases by Vav1 and Vav2 Guanine Nucleotide Exchange Factors". In: *Biochemistry* 44 (17), pp. 6573–6585. DOI: [10.1021/bi047443q](https://doi.org/10.1021/bi047443q).
- Hilioti Z., Sabbagh W., Paliwal S., Bergmann A., Goncalves M. D., Bardwell L., and Levchenko A. (2008). "Oscillatory Phosphorylation of Yeast Fus3 MAP Kinase Controls Periodic Gene Expression and Morphogenesis". In: *Current Biology* 18 (21), pp. 1700–1706. DOI: [10.1016/j.cub.2008.09.027](https://doi.org/10.1016/j.cub.2008.09.027).
- Hodge R. G. and Ridley A. J. (2016). "Regulating Rho GTPases and their regulators". In: *Nature Reviews Molecular Cell Biology* 17 (8), pp. 496–510. DOI: [10.1038/nrm.2016.67](https://doi.org/10.1038/nrm.2016.67).
- Hoelz A., Janz J. M., Lawrie S. D., Corwin B., Lee A., and Sakmar T. P. (2006). "Crystal structure of the SH3 domain of betaPIX in complex with a high affinity peptide from PAK2". In: *Journal of Molecular Biology* 358 (2), pp. 509–522. DOI: [10.1016/j.jmb.2006.02.027](https://doi.org/10.1016/j.jmb.2006.02.027).
- Hof I. E., Heijden J. F. van der, Kranias E. G., Sanoudou D., Boer R. A. de, Tintelen J. P. van, Zwaag P. A. van der, and Doevendans P. A. (2019). "Prevalence and cardiac phenotype of patients with a phospholamban mutation". In: *Netherlands Heart Journal* 27 (2), pp. 64–69. DOI: [10.1007/s12471-018-1211-4](https://doi.org/10.1007/s12471-018-1211-4).
- Hooper S. L., Hobbs K. H., and Thuma J. B. (2008). "Invertebrate muscles: thin and thick filament structure; molecular basis of contraction and its regulation, catch and asynchronous muscle". In: *Progress in neurobiology* 86 (2), pp. 72–127. DOI: [10.1016/j.pneurobio.2008.06.004](https://doi.org/10.1016/j.pneurobio.2008.06.004).

- Hou Z., Kelly E. M., and Robia S. L. (2008). “Phosphomimetic Mutations Increase Phospholamban Oligomerization and Alter the Structure of Its Regulatory Complex”. In: *Journal of Biological Chemistry* 283 (43), pp. 28996–29003. DOI: [10.1074/jbc.M804782200](https://doi.org/10.1074/jbc.M804782200).
- Hu L.-Y. R., Ackermann M. A., Hecker P. A., et al. (2017). “Deregulated Ca²⁺ cycling underlies the development of arrhythmia and heart disease due to mutant obscurin”. In: *Science Advances* 3 (6), e1603081. DOI: [10.1126/sciadv.1603081](https://doi.org/10.1126/sciadv.1603081).
- Hu L.-Y. R. and Kontrogianni-Konstantopoulos A. (2013). “The kinase domains of obscurin interact with intercellular adhesion proteins”. In: *The FASEB Journal* 27 (5), pp. 2001–2012. DOI: [10.1096/fj.12-221317](https://doi.org/10.1096/fj.12-221317).
- Huke S. and Bers D. M. (2007). “Temporal dissociation of frequency-dependent acceleration of relaxation and protein phosphorylation by CaMKII”. In: *Journal of Molecular and Cellular Cardiology* 42 (3), pp. 590–599. DOI: [10.1016/j.yjmcc.2006.12.007](https://doi.org/10.1016/j.yjmcc.2006.12.007).
- Hunter J. J. and Chien K. R. (1999). “Signaling Pathways for Cardiac Hypertrophy and Failure”. In: *New England Journal of Medicine* 341 (17), pp. 1276–1283. DOI: [10.1056/NEJM199910213411706](https://doi.org/10.1056/NEJM199910213411706).
- Huntoon V., Widrick J. J., Sanchez C., et al. (2018). “SPEG-deficient skeletal muscles exhibit abnormal triad and defective calcium handling”. In: *Human Molecular Genetics* 27 (9), pp. 1608–1617. DOI: [10.1093/hmg/ddy068](https://doi.org/10.1093/hmg/ddy068).
- Iwasa Y. and Hosey M. M. (1984). “Phosphorylation of cardiac sarcolemma proteins by the calcium-activated phospholipid-dependent protein kinase.” In: *Journal of Biological Chemistry* 259 (1), pp. 534–540. DOI: [10.1016/S0021-9258\(17\)43694-5](https://doi.org/10.1016/S0021-9258(17)43694-5).
- Jackson A. L., Burchard J., Schelter J., Chau B. N., Cleary M., Lim L., and Linsley P. S. (2006). “Widespread siRNA ‘off-target’ transcript silencing mediated by seed region sequence complementarity”. In: *RNA* 12 (7), pp. 1179–1187. DOI: [10.1261/rna.25706](https://doi.org/10.1261/rna.25706).
- Jackson W. A. and Colyer J. (1996). “Translation of Ser16 and Thr17 phosphorylation of phospholamban into Ca²⁺-pump stimulation”. In: *Biochemical Journal* 316, pp. 201–207.
- Jaffe A. B. and Hall A. (2005). “RHO GTPASES: Biochemistry and Biology”. In: *Annual Review of Cell and Developmental Biology* 21 (1), pp. 247–269. DOI: [10.1146/annurev.cellbio.21.020604.150721](https://doi.org/10.1146/annurev.cellbio.21.020604.150721).
- Jaiswal M., Dvorsky R., and Ahmadian M. R. (2013). “Deciphering the Molecular and Functional Basis of Dbl Family Proteins: A Novel Systematic Approach Toward Classification of Selective Activation of the Rho Family Proteins”. In: *Journal of Biological Chemistry* 288 (6), pp. 4486–4500. DOI: [10.1074/jbc.M112.429746](https://doi.org/10.1074/jbc.M112.429746).
- Jaiswal M., Gremer L., Dvorsky R., Haeusler L. C., Cirstea I. C., Uhlenbrock K., and Ahmadian M. R. (2011). “Mechanistic Insights into Specificity, Activity, and Regulatory Elements of the Regulator of G-protein Signaling (RGS)-containing Rho-specific Guanine Nucleotide Exchange Factors (GEFs) p115, PDZ-RhoGEF (PRG), and Leukemia-associated RhoGEF (LARG)”. In: *Journal of Biological Chemistry* 286 (20), pp. 18202–18212. DOI: [10.1074/jbc.M111.226431](https://doi.org/10.1074/jbc.M111.226431).
- Kannel W. B. and McGee D. L. (1979). “Diabetes and cardiovascular risk factors: the Framingham study.” In: *Circulation* 59 (1), pp. 8–13. DOI: [10.1161/01.CIR.59.1.8](https://doi.org/10.1161/01.CIR.59.1.8).
- Karakikes I., Stillitano F., Nonnenmacher M., et al. (2015). “Correction of human phospholamban R14del mutation associated with cardiomyopathy using targeted nucleases and combination therapy”. In: *Nature Communications* 6, p. 6955. DOI: [10.1038/ncomms7955](https://doi.org/10.1038/ncomms7955).
- Kärkkäinen S. and Peuhkurinen K. (2007). “Genetics of dilated cardiomyopathy”. In: *Annals of Medicine* 39 (2), pp. 91–107. DOI: [10.1080/07853890601145821](https://doi.org/10.1080/07853890601145821).
- Katz A. M. (1998). “Discovery of Phospholamban: A Personal History”. In: *Annals of the New York Academy of Sciences* 853 (1), pp. 9–19. DOI: <https://doi.org/10.1111/j.1749-6632.1998.tb08252.x>.
- Katz A. M. and Rolett E. L. (2016). “Heart failure: when form fails to follow function”. In: *European Heart Journal* 37 (5), pp. 449–454. DOI: [10.1093/eurheartj/ehv548](https://doi.org/10.1093/eurheartj/ehv548).

- Katzemich A., Kreisköther N., Alexandrovich A., Elliott C., Schöck F., Leonard K., Sparrow J., and Bullard B. (2012). “The function of the M-line protein obscurin in controlling the symmetry of the sarcomere in the flight muscle of *Drosophila*”. In: *J Cell Sci* 125 (14), pp. 3367–3379. DOI: [10.1242/jcs.097345](https://doi.org/10.1242/jcs.097345).
- Katzemich A., West R. J. H., Fukuzawa A., Sweeney S. T., Gautel M., Sparrow J., and Bullard B. (2015). “Binding partners of the kinase domains in *Drosophila* obscurin and their effect on the structure of the flight muscle”. In: *J Cell Sci* 128 (18), pp. 3386–3397. DOI: [10.1242/jcs.170639](https://doi.org/10.1242/jcs.170639).
- Kaunas R., Nguyen P., Usami S., and Chien S. (2005). “Cooperative effects of Rho and mechanical stretch on stress fiber organization”. In: *Proceedings of the National Academy of Sciences* 102 (44), pp. 15895–15900. DOI: [10.1073/pnas.0506041102](https://doi.org/10.1073/pnas.0506041102).
- Khattar R. S., Senior R., Soman P., Does R. van der, and Lahiri A. (2001). “Regression of left ventricular remodeling in chronic heart failure: Comparative and combined effects of captopril and carvedilol”. In: *American Heart Journal* 142 (4), pp. 704–713. DOI: [10.1067/mhj.2001.116768](https://doi.org/10.1067/mhj.2001.116768).
- Kim J., Masterson L. R., Cembran A., Verardi R., Shi L., Gao J., Taylor S. S., and Veglia G. (2015). “Dysfunctional conformational dynamics of protein kinase A induced by a lethal mutant of phospholamban hinder phosphorylation”. In: *Proceedings of the National Academy of Sciences* 112 (12), pp. 3716–3721. DOI: [10.1073/pnas.1502299112](https://doi.org/10.1073/pnas.1502299112).
- Kimura Y., Kurzydowski K., Tada M., and MacLennan D. H. (1997). “Phospholamban Inhibitory Function Is Activated by Depolymerization”. In: *Journal of Biological Chemistry* 272 (24), pp. 15061–15064. DOI: [10.1074/jbc.272.24.15061](https://doi.org/10.1074/jbc.272.24.15061).
- Kintscher C., Wuertenberger S., Eysten R., Uhlendorf T., and Groemping Y. (2010). “Autoinhibition of GEF activity in Intersectin 1 is mediated by the short SH3-DH domain linker”. In: *Protein Science: A Publication of the Protein Society* 19 (11), pp. 2164–2174. DOI: [10.1002/pro.500](https://doi.org/10.1002/pro.500).
- Kistamás K., Veress R., Horváth B., Bányász T., Nánási P. P., and Eisner D. A. (2020). “Calcium Handling Defects and Cardiac Arrhythmia Syndromes”. In: *Frontiers in Pharmacology* 11 (72). DOI: [10.3389/fphar.2020.00072](https://doi.org/10.3389/fphar.2020.00072).
- Klebe C., Prinz H., Wittinghofer A., and Goody R. S. (1995). “The Kinetic Mechanism of Ran-Nucleotide Exchange Catalyzed by RCC1”. In: *Biochemistry* 34 (39), pp. 12543–12552. DOI: [10.1021/bi00039a008](https://doi.org/10.1021/bi00039a008).
- Klooster J. P. ten, Jaffer Z. M., Chernoff J., and Hordijk P. L. (2006). “Targeting and activation of Rac1 are mediated by the exchange factor beta-Pix”. In: *The Journal of Cell Biology* 172 (5), pp. 759–769. DOI: [10.1083/jcb.200509096](https://doi.org/10.1083/jcb.200509096).
- Kohane I. S., Masys D. R., and Altman R. B. (2006). “The Incidentalome. A Threat to Genomic Medicine.” In: *JAMA* 296 (2), pp. 212–215. DOI: [10.1001/jama.296.2.212](https://doi.org/10.1001/jama.296.2.212).
- Koninck P. D. and Schulman H. (1998). “Sensitivity of CaM Kinase II to the Frequency of Ca²⁺ Oscillations”. In: *Science* 279 (5348), pp. 227–230. DOI: [10.1126/science.279.5348.227](https://doi.org/10.1126/science.279.5348.227).
- Kontogianni-Konstantopoulos A., Catino D. H., Strong J. C., Randall W. R., and Bloch R. J. (2004). “Obscurin regulates the organization of myosin into A bands”. In: *American Journal of Physiology-Cell Physiology* 287 (1), pp. C209–C217. DOI: [10.1152/ajpcell.00497.2003](https://doi.org/10.1152/ajpcell.00497.2003).
- Kontogianni-Konstantopoulos A., Catino D. H., Strong J. C., Sutter S., Borisov A. B., Pumplin D. W., Russell M. W., and Bloch R. J. (2006). “Obscurin modulates the assembly and organization of sarcomeres and the sarcoplasmic reticulum”. In: *The FASEB Journal* 20 (12), pp. 2102–2111. DOI: [10.1096/fj.06-5761.com](https://doi.org/10.1096/fj.06-5761.com).
- Kontogianni-Konstantopoulos A., Jones E. M., Rossum D. B. v., and Bloch R. J. (2003). “Obscurin Is a Ligand for Small Ankyrin 1 in Skeletal Muscle”. In: *Molecular Biology of the Cell* 14 (3), pp. 1138–1148. DOI: [10.1091/mbc.E02-07-0411](https://doi.org/10.1091/mbc.E02-07-0411).
- Kovacs R. J., Nelson M. T., Simmerman H. K., and Jones L. R. (1988). “Phospholamban forms Ca²⁺-selective channels in lipid bilayers.” In: *Journal of Biological Chemistry* 263 (34), pp. 18364–18368.
- Kranias E. G. and Solaro R. J. (1982). “Phosphorylation of troponin I and phospholamban during catecholamine stimulation of rabbit heart”. In: *Nature* 298 (5870), pp. 182–184. DOI: [10.1038/298182a0](https://doi.org/10.1038/298182a0).

- Kranias E. G. and Hajjar R. J. (2012). “Modulation of Cardiac Contractility by the Phospholamban/SERCA2a Regulatome”. In: *Circulation Research* 110 (12), pp. 1646–1660. DOI: [10.1161/CIRCRESAHA.111.259754](https://doi.org/10.1161/CIRCRESAHA.111.259754).
- Kristelly R., Gao G., and Tesmer J. J. G. (2004). “Structural Determinants of RhoA Binding and Nucleotide Exchange in Leukemia-associated Rho Guanine-Nucleotide Exchange Factor”. In: *Journal of Biological Chemistry* 279 (45), pp. 47352–47362. DOI: [10.1074/jbc.M406056200](https://doi.org/10.1074/jbc.M406056200).
- Kwan A. H., Mobli M., Gooley P. R., King G. F., and Mackay J. P. (2011). “Macromolecular NMR spectroscopy for the non-spectroscopist”. In: *FEBS Journal* 278 (5), pp. 687–703. DOI: [10.1111/j.1742-4658.2011.08004.x](https://doi.org/10.1111/j.1742-4658.2011.08004.x).
- Laemmli U. K. (1970). “Cleavage of Structural Proteins during the Assembly of the Head of Bacteriophage T4”. In: *Nature* 227 (5259), pp. 680–685. DOI: [10.1038/227680a0](https://doi.org/10.1038/227680a0).
- Landstrom A. P., Adekola B. A., Bos J. M., Ommen S. R., and Ackerman M. J. (2011). “PLN-encoded phospholamban mutation in a large cohort of hypertrophic cardiomyopathy cases: Summary of the literature and implications for genetic testing”. In: *American Heart Journal* 161 (1), pp. 165–171. DOI: [10.1016/j.ahj.2010.08.001](https://doi.org/10.1016/j.ahj.2010.08.001).
- Landstrom A. P., Dobrev D., and Wehrens X. H. (2017). “Calcium Signaling and Cardiac Arrhythmias”. In: *Circulation Research* 120 (12), pp. 1969–1993. DOI: [10.1161/CIRCRESAHA.117.310083](https://doi.org/10.1161/CIRCRESAHA.117.310083).
- Lange S., Agarkova I., Perriard J.-C., and Ehler E. (2005). “The sarcomeric M-band during development and in disease”. In: *Journal of Muscle Research & Cell Motility* 26 (6-8), pp. 375–379. DOI: [10.1007/s10974-005-9019-4](https://doi.org/10.1007/s10974-005-9019-4).
- Lange S., Auerbach D., McLoughlin P., Perriard E., Schäfer B. W., Perriard J.-C., and Ehler E. (2002). “Subcellular targeting of metabolic enzymes to titin in heart muscle may be mediated by DRAL/FHL-2”. In: *Journal of Cell Science* 115 (24), pp. 4925–4936. DOI: [10.1242/jcs.00181](https://doi.org/10.1242/jcs.00181).
- Lange S., Ouyang K., Meyer G., Cui L., Cheng H., Lieber R. L., and Chen J. (2009). “Obscurin determines the architecture of the longitudinal sarcoplasmic reticulum”. In: *Journal of Cell Science* 122 (15), p. 2640. DOI: [10.1242/jcs.046193](https://doi.org/10.1242/jcs.046193).
- Lange S., Perera S., Teh P., Chen J., and Tansey W. P. (2012). “Obscurin and KCTD6 regulate cullin-dependent small ankyrin-1 (sAnk1.5) protein turnover”. In: *Molecular Biology of the Cell* 23 (13), pp. 2490–2504. DOI: [10.1091/mbc.e12-01-0052](https://doi.org/10.1091/mbc.e12-01-0052).
- Lange S., Pinotsis N., Agarkova I., and Ehler E. (2020). “The M-band: The underestimated part of the sarcomere”. In: *Biochimica et Biophysica Acta (BBA) - Molecular Cell Research* 1867 (3), p. 118440. DOI: [10.1016/j.bbamcr.2019.02.003](https://doi.org/10.1016/j.bbamcr.2019.02.003).
- Langemeyer L., Bastos R. N., Cai Y., Itzen A., Reinisch K. M., and Barr F. A. (2014). “Diversity and plasticity in Rab GTPase nucleotide release mechanism has consequences for Rab activation and inactivation”. In: *eLife* 3, e01623.
- Lauriol J., Keith K., Jaffré F., et al. (2014). “RhoA signaling in cardiomyocytes protects against stress-induced heart failure but facilitates cardiac fibrosis”. In: *Science Signaling* 7 (348), ra100–ra100. DOI: [10.1126/scisignal.2005262](https://doi.org/10.1126/scisignal.2005262).
- Lavie C. J., Ozemek C., Carbone S., Katzmarzyk P. T., and Blair S. N. (2019). “Sedentary Behavior, Exercise, and Cardiovascular Health”. In: *Circulation Research* 124 (5), pp. 799–815. DOI: [10.1161/CIRCRESAHA.118.312669](https://doi.org/10.1161/CIRCRESAHA.118.312669).
- Leber Y., Ruparelia A. A., Kirfel G., Ven V. D., F.m P., Hoffmann B., Merkel R., Bryson-Richardson R. J., and Fürst D. O. (2016). “Filamin C is a highly dynamic protein associated with fast repair of myofibrillar microdamage”. In: *Human Molecular Genetics* 25 (13), pp. 2776–2788. DOI: [10.1093/hmg/ddw135](https://doi.org/10.1093/hmg/ddw135).
- Lee G. J., Yan L., Vatner D. E., and Vatner S. F. (2015). “Mst1 inhibition rescues β 1-adrenergic cardiomyopathy by reducing myocyte necrosis and non-myocyte apoptosis rather than myocyte apoptosis”. In: *Basic Research in Cardiology* 110 (2), p. 7. DOI: [10.1007/s00395-015-0461-1](https://doi.org/10.1007/s00395-015-0461-1).
- Lei M., Wu L., Terrar D. A., and Huang C. L.-H. (2018). “Modernized Classification of Cardiac Antiarrhythmic Drugs”. In: *Circulation* 138 (17), pp. 1879–1896. DOI: [10.1161/CIRCULATIONAHA.118.035455](https://doi.org/10.1161/CIRCULATIONAHA.118.035455).

- Leung C., Lu X., Liu M., and Feng Q. (2014). "Rac1 Signaling Is Critical to Cardiomyocyte Polarity and Embryonic Heart Development". In: *Journal of the American Heart Association* 3 (5), e001271. DOI: [10.1161/JAHA.114.001271](https://doi.org/10.1161/JAHA.114.001271).
- Li C., Wang J. H., and Colyer J. (1990). "Immunological detection of phospholamban phosphorylation states facilitates the description of the mechanism of phosphorylation and dephosphorylation". In: *Biochemistry* 29 (19), pp. 4535–4540. DOI: [10.1021/bi00471a005](https://doi.org/10.1021/bi00471a005).
- Li G. and Qian H. (2002). "Kinetic Timing: A Novel Mechanism That Improves the Accuracy of GTPase Timers in Endosome Fusion and Other Biological Processes". In: *Traffic* 3 (4), pp. 249–255. DOI: [10.1034/j.1600-0854.2002.030402.x](https://doi.org/10.1034/j.1600-0854.2002.030402.x).
- Liu G.-S., Morales A., Vafiadaki E., Lam C. K., Cai W.-F., Haghighi K., Adly G., Hershberger R. E., and Kranias E. G. (2015). "A novel human R25C-phospholamban mutation is associated with super-inhibition of calcium cycling and ventricular arrhythmia". In: *Cardiovascular Research* 107 (1), pp. 164–174. DOI: [10.1093/cvr/cvv127](https://doi.org/10.1093/cvr/cvv127).
- Lohse M. J., Engelhardt S., and Eschenhagen T. (2003). "What Is the Role of β -Adrenergic Signaling in Heart Failure?" In: *Circulation Research* 93 (10), pp. 896–906. DOI: [10.1161/01.RES.0000102042.83024.CA](https://doi.org/10.1161/01.RES.0000102042.83024.CA).
- Loirand G., Guerin P., and Pacaud P. (2006). "Rho Kinases in Cardiovascular Physiology and Pathophysiology". In: *Circulation Research* 98 (3), pp. 322–334. DOI: [10.1161/01.RES.0000201960.04223.3c](https://doi.org/10.1161/01.RES.0000201960.04223.3c).
- Loirand G., Sauzeau V., and Pacaud P. (2013). "Small G Proteins in the Cardiovascular System: Physiological and Pathological Aspects". In: *Physiological Reviews* 93 (4), pp. 1659–1720. DOI: [10.1152/physrev.00021.2012](https://doi.org/10.1152/physrev.00021.2012).
- López-Ayala J. M., Boven L., Wijngaard A. van den, Peñafiel-Verdú P., Tintelen J. P. van, and Gimeno J. R. (2015). "Phospholamban p.arg14del Mutation in a Spanish Family With Arrhythmogenic Cardiomyopathy: Evidence for a European Founder Mutation". In: *Revista Española de Cardiología (English Edition)* 68 (4), pp. 346–349. DOI: [10.1016/j.rec.2014.11.012](https://doi.org/10.1016/j.rec.2014.11.012).
- Luk A., Ahn E., Soor G. S., and Butany J. (2009). "Dilated cardiomyopathy: a review". In: *Journal of Clinical Pathology* 62 (3), pp. 219–225. DOI: [10.1136/jcp.2008.060731](https://doi.org/10.1136/jcp.2008.060731).
- Luo W., Grupp I., Harrer J., Ponniah S., Grupp G., Duffy J., Doetschman T., and Kranias E. (1994). "Targeted ablation of the phospholamban gene is associated with markedly enhanced myocardial contractility and loss of beta-agonist stimulation." In: *Circulation Research* 75 (3), pp. 401–409. DOI: [10.1161/01.RES.75.3.401](https://doi.org/10.1161/01.RES.75.3.401).
- Lymperopoulos A., Rengo G., and Koch W. J. (2013). "Adrenergic Nervous System in Heart Failure". In: *Circulation Research* 113 (6), pp. 739–753. DOI: [10.1161/CIRCRESAHA.113.300308](https://doi.org/10.1161/CIRCRESAHA.113.300308).
- Lynch M. (2012). "The Evolution of Multimeric Protein Assemblages". In: *Molecular Biology and Evolution* 29 (5), pp. 1353–1366. DOI: [10.1093/molbev/msr300](https://doi.org/10.1093/molbev/msr300).
- Lyon R. C., Zanella F., Omens J. H., and Sheikh F. (2015). "Mechanotransduction in Cardiac Hypertrophy and Failure". In: *Circulation Research* 116 (8), pp. 1462–1476. DOI: [10.1161/CIRCRESAHA.116.304937](https://doi.org/10.1161/CIRCRESAHA.116.304937).
- Macdougall L. K., Jones L. R., and Cohen P. (1991). "Identification of the major protein phosphatases in mammalian cardiac muscle which dephosphorylate phospholamban". In: *European Journal of Biochemistry* 196 (3), pp. 725–734. DOI: [10.1111/j.1432-1033.1991.tb15871.x](https://doi.org/10.1111/j.1432-1033.1991.tb15871.x).
- MacLennan D. H. and Kranias E. G. (2003). "Phospholamban: a crucial regulator of cardiac contractility". In: *Nature Reviews Molecular Cell Biology* 4 (7), pp. 566–577. DOI: [10.1038/nrm1151](https://doi.org/10.1038/nrm1151).
- Maier L. S. and Bers D. M. (2007). "Role of Ca²⁺/calmodulin-dependent protein kinase (CaMK) in excitation-contraction coupling in the heart". In: *Cardiovascular Research* 73 (4), pp. 631–640. DOI: [10.1016/j.cardiores.2006.11.005](https://doi.org/10.1016/j.cardiores.2006.11.005).
- Mankad P. and Kalahasty G. (2019). "Antiarrhythmic Drugs: Risks and Benefits". In: *The Medical Clinics of North America* 103 (5), pp. 821–834. DOI: [10.1016/j.mcna.2019.05.004](https://doi.org/10.1016/j.mcna.2019.05.004).

- Manrai A. K., Funke B. H., Rehm H. L., Olesen M. S., Maron B. A., Szolovits P., Margulies D. M., Loscalzo J., and Kohane I. S. (2016). "Genetic Misdiagnoses and the Potential for Health Disparities". In: *New England Journal of Medicine* 375 (7), pp. 655–665. DOI: [10.1056/NEJMs1507092](https://doi.org/10.1056/NEJMs1507092).
- Manser E., Loo T.-H., Koh C.-G., Zhao Z.-S., Chen X.-Q., Tan L., Tan I., Leung T., and Lim L. (1998). "PAK Kinases Are Directly Coupled to the PIX Family of Nucleotide Exchange Factors". In: *Molecular Cell* 1 (2), pp. 183–192. DOI: [10.1016/S1097-2765\(00\)80019-2](https://doi.org/10.1016/S1097-2765(00)80019-2).
- Marian A. (2021). "Molecular Genetic Basis of Hypertrophic Cardiomyopathy". In: *Circulation Research* 128 (10), pp. 1533–1553. DOI: [10.1161/CIRCRESAHA.121.318346](https://doi.org/10.1161/CIRCRESAHA.121.318346).
- Marian A. J. and Braunwald E. (2017). "Hypertrophic Cardiomyopathy". In: *Circulation Research* 121 (7), pp. 749–770. DOI: [10.1161/CIRCRESAHA.117.311059](https://doi.org/10.1161/CIRCRESAHA.117.311059).
- Marianayagam N. J., Sunde M., and Matthews J. M. (2004). "The power of two: protein dimerization in biology". In: *Trends in Biochemical Sciences* 29 (11), pp. 618–625. DOI: [10.1016/j.tibs.2004.09.006](https://doi.org/10.1016/j.tibs.2004.09.006).
- Maron B. J. and Maron M. S. (2013). "Hypertrophic cardiomyopathy". In: *The Lancet* 381 (9862), pp. 242–255. DOI: [10.1016/S0140-6736\(12\)60397-3](https://doi.org/10.1016/S0140-6736(12)60397-3).
- Marsh J. A. and Teichmann S. A. (2015). "Structure, Dynamics, Assembly, and Evolution of Protein Complexes". In: *Annual Review of Biochemistry* 84 (1), pp. 551–575. DOI: [10.1146/annurev-biochem-060614-034142](https://doi.org/10.1146/annurev-biochem-060614-034142).
- Marston S. (2017). "Obscurin variants and inherited cardiomyopathies". In: *Biophysical Reviews* 9 (3), pp. 239–243. DOI: [10.1007/s12551-017-0264-8](https://doi.org/10.1007/s12551-017-0264-8).
- Marston S., Montgiraud C., Munster A. B., Copeland O., Choi O., Remedios C. dos, Messer A. E., Ehler E., and Knöll R. (2015). "OBSCN Mutations Associated with Dilated Cardiomyopathy and Haploinsufficiency". In: *PLOS ONE* 10 (9), e0138568. DOI: [10.1371/journal.pone.0138568](https://doi.org/10.1371/journal.pone.0138568).
- Mattiazzi A. and Kranias E. (2014). "The role of CaMKII regulation of phospholamban activity in heart disease". In: *Frontiers in Pharmacology* 5. DOI: [10.3389/fphar.2014.00005](https://doi.org/10.3389/fphar.2014.00005).
- Mattiazzi A., Mundiña-Weilenmann C., Guoxiang C., Vittone L., and Kranias E. (2005). "Role of phospholamban phosphorylation on Thr17 in cardiac physiological and pathological conditions". In: *Cardiovascular Research* 68 (3), pp. 366–375. DOI: [10.1016/j.cardiores.2005.08.010](https://doi.org/10.1016/j.cardiores.2005.08.010).
- Meyer M., Schillinger W., Pieske B., et al. (1995). "Alterations of Sarcoplasmic Reticulum Proteins in Failing Human Dilated Cardiomyopathy". In: *Circulation* 92 (4), pp. 778–784. DOI: [10.1161/01.CIR.92.4.778](https://doi.org/10.1161/01.CIR.92.4.778).
- Minamisawa S., Hoshijima M., Chu G., et al. (1999). "Chronic Phospholamban-Sarcoplasmic Reticulum Calcium ATPase Interaction Is the Critical Calcium Cycling Defect in Dilated Cardiomyopathy". In: *Cell* 99 (3), pp. 313–322. DOI: [10.1016/S0092-8674\(00\)81662-1](https://doi.org/10.1016/S0092-8674(00)81662-1).
- Mitin N., Betts L., Yohe M. E., Der C. J., Sondek J., and Rossman K. L. (2007). "Release of autoinhibition of ASEF by APC leads to CDC42 activation and tumor suppression". In: *Nature Structural & Molecular Biology* 14 (9), p. 814. DOI: [10.1038/nsmb1290](https://doi.org/10.1038/nsmb1290).
- Miyamoto S., Del Re D. P., Xiang S. Y., Zhao X., Florholmen G., and Brown J. H. (2010). "Revisited and revised: is RhoA always a villain in cardiac pathophysiology?" In: *Journal of Cardiovascular Translational Research* 3 (4), pp. 330–343. DOI: [10.1007/s12265-010-9192-8](https://doi.org/10.1007/s12265-010-9192-8).
- Molkentin J. D. and Dorn G. W. I. (2001). "Cytoplasmic Signaling Pathways That Regulate Cardiac Hypertrophy". In: *Annual Review of Physiology* 63 (1), pp. 391–426. DOI: [10.1146/annurev.physiol.63.1.391](https://doi.org/10.1146/annurev.physiol.63.1.391).
- Morotti S., Edwards A. G., McCulloch A. D., Bers D. M., and Grandi E. (2014). "A novel computational model of mouse myocyte electrophysiology to assess the synergy between Na⁺ loading and CaMKII". In: *The Journal of Physiology* 592 (6), pp. 1181–1197. DOI: [10.1113/jphysiol.2013.266676](https://doi.org/10.1113/jphysiol.2013.266676).
- Mott H. R., Nietlispach D., Evetts K. A., and Owen D. (2005). "Structural analysis of the SH3 domain of beta-PIX and its interaction with alpha-p21 activated kinase (PAK)". In: *Biochemistry* 44 (33), pp. 10977–10983. DOI: [10.1021/bi050374a](https://doi.org/10.1021/bi050374a).

- Movsesian M. A., Bristow M. R., and Krall J. (1989). "Ca²⁺ uptake by cardiac sarcoplasmic reticulum from patients with idiopathic dilated cardiomyopathy." In: *Circulation Research* 65 (4), pp. 1141–1144. DOI: [10.1161/01.RES.65.4.1141](https://doi.org/10.1161/01.RES.65.4.1141).
- Murayama K., Shirouzu M., Kawasaki Y., et al. (2007). "Crystal Structure of the Rac Activator, Asef, Reveals Its Autoinhibitory Mechanism". In: *Journal of Biological Chemistry* 282 (7), pp. 4238–4242. DOI: [10.1074/jbc.C600234200](https://doi.org/10.1074/jbc.C600234200).
- Muroya K., Kawasaki Y., Hayashi T., Ohwada S., and Akiyama T. (2007). "PH domain-mediated membrane targeting of Asef". In: *Biochemical and Biophysical Research Communications* 355 (1), pp. 85–88. DOI: [10.1016/j.bbrc.2007.01.131](https://doi.org/10.1016/j.bbrc.2007.01.131).
- Nagai T., Tanaka-Ishikawa M., Aikawa R., Ishihara H., Zhu W., Yazaki Y., Nagai R., and Komuro I. (2003). "Cdc42 plays a critical role in assembly of sarcomere units in series of cardiac myocytes". In: *Biochemical and Biophysical Research Communications* 305 (4), pp. 806–810. DOI: [10.1016/S0006-291X\(03\)00838-6](https://doi.org/10.1016/S0006-291X(03)00838-6).
- Nakamura M. and Sadoshima J. (2018). "Mechanisms of physiological and pathological cardiac hypertrophy". In: *Nature Reviews Cardiology*, p. 1. DOI: [10.1038/s41569-018-0007-y](https://doi.org/10.1038/s41569-018-0007-y).
- Natarajan M., Lin K.-M., Hsueh R. C., Sternweis P. C., and Ranganathan R. (2006). "A global analysis of cross-talk in a mammalian cellular signalling network". In: *Nature Cell Biology* 8 (6), pp. 571–580. DOI: [10.1038/ncb1418](https://doi.org/10.1038/ncb1418).
- Nicolaou P., Hajjar R. J., and Kranias E. G. (2009). "Role of protein phosphatase-1 inhibitor-1 in cardiac physiology and pathophysiology". In: *Journal of Molecular and Cellular Cardiology* 47 (3), pp. 365–371. DOI: [10.1016/j.yjmcc.2009.05.010](https://doi.org/10.1016/j.yjmcc.2009.05.010).
- Nikonova E., Tsyganov M. A., Kolch W., Fey D., and Kholodenko B. N. (2013). "Control of the G-protein cascade dynamics by GDP dissociation inhibitors". In: *Molecular BioSystems* 9 (10), pp. 2454–2462. DOI: [10.1039/C3MB70152B](https://doi.org/10.1039/C3MB70152B).
- Nimnual A. S., Yatsula B. A., and Bar-Sagi D. (1998). "Coupling of Ras and Rac Guanosine Triphosphatases Through the Ras Exchanger Sos". In: *Science* 279 (5350), pp. 560–563. DOI: [10.1126/science.279.5350.560](https://doi.org/10.1126/science.279.5350.560).
- Nobis M., Herrmann D., Warren S. C., et al. (2017). "A RhoA-FRET Biosensor Mouse for Intravital Imaging in Normal Tissue Homeostasis and Disease Contexts". In: *Cell Reports* 21 (1), pp. 274–288. DOI: [10.1016/j.celrep.2017.09.022](https://doi.org/10.1016/j.celrep.2017.09.022).
- Noble D. (2002). "Unraveling the genetics and mechanisms of cardiac arrhythmia". In: *Proceedings of the National Academy of Sciences* 99 (9), pp. 5755–5756. DOI: [10.1073/pnas.102171699](https://doi.org/10.1073/pnas.102171699).
- North B. J. and Sinclair D. A. (2012). "The Intersection Between Aging and Cardiovascular Disease". In: *Circulation Research* 110 (8), pp. 1097–1108. DOI: [10.1161/CIRCRESAHA.111.246876](https://doi.org/10.1161/CIRCRESAHA.111.246876).
- Nottingham R. M. and Pfeffer S. R. (2009). "Defining the boundaries: Rab GEFs and GAPs". In: *Proc Natl Acad Sci USA* 106 (36), pp. 14185–14186.
- Offerhaus J. A., Bezzina C. R., and Wilde A. A. M. (2020). "Epidemiology of inherited arrhythmias". In: *Nature Reviews Cardiology* 17 (4), pp. 205–215. DOI: [10.1038/s41569-019-0266-2](https://doi.org/10.1038/s41569-019-0266-2).
- Okonechnikov K., Golosova O., Fursov M., and the UGENE team (2012). "Unipro UGENE: a unified bioinformatics toolkit". In: *Bioinformatics* 28 (8), pp. 1166–1167. DOI: [10.1093/bioinformatics/bts091](https://doi.org/10.1093/bioinformatics/bts091).
- Opbergen C. J. M. van, Delmar M., and Veen T. A. B. van (2017). "Potential new mechanisms of pro-arrhythmia in arrhythmogenic cardiomyopathy: focus on calcium sensitive pathways". In: *Netherlands Heart Journal* 25 (3), pp. 157–169. DOI: [10.1007/s12471-017-0946-7](https://doi.org/10.1007/s12471-017-0946-7).
- Orfanos Z., Gödderz M. P. O., Soroka E., Gödderz T., Rumyantseva A., van der Ven P. F. M., Hawke T. J., and Fürst D. O. (2016). "Breaking sarcomeres by in vitro exercise". In: *Scientific Reports* 6, p. 19614. DOI: [10.1038/srep19614](https://doi.org/10.1038/srep19614).

- Oxenoid K. and Chou J. J. (2005). "The structure of phospholamban pentamer reveals a channel-like architecture in membranes". In: *Proceedings of the National Academy of Sciences* 102 (31), pp. 10870–10875. DOI: [10.1073/pnas.0504920102](https://doi.org/10.1073/pnas.0504920102).
- Padeletti L. and Bagliani G. (2017). "General Introduction, Classification, and Electrocardiographic Diagnosis of Cardiac Arrhythmias". In: *Cardiac Electrophysiology Clinics* 9 (3), pp. 345–363. DOI: [10.1016/j.ccep.2017.05.009](https://doi.org/10.1016/j.ccep.2017.05.009).
- Patel M. and Côté J.-F. (2013). "Ras GTPases' interaction with effector domains". In: *Communicative & Integrative Biology* 6 (4), e24298. DOI: [10.4161/cib.24298](https://doi.org/10.4161/cib.24298).
- Pernigo S., Fukuzawa A., Beedle A. E. M., Holt M., Round A., Pandini A., Garcia-Manyes S., Gautel M., and Steiner R. A. (2017). "Binding of Myomesin to Obscurin-Like-1 at the Muscle M-Band Provides a Strategy for Isoform-Specific Mechanical Protection". In: *Structure* 25 (1), pp. 107–120. DOI: [10.1016/j.str.2016.11.015](https://doi.org/10.1016/j.str.2016.11.015).
- Pernigo S., Fukuzawa A., Bertz M., Holt M., Rief M., Steiner R. A., and Gautel M. (2010). "Structural insight into M-band assembly and mechanics from the titin-obscurin-like-1 complex". In: *Proceedings of the National Academy of Sciences* 107 (7), pp. 2908–2913. DOI: [10.1073/pnas.0913736107](https://doi.org/10.1073/pnas.0913736107).
- Pertz O. and Hahn K. M. (2004). "Designing biosensors for Rho family proteins – deciphering the dynamics of Rho family GTPase activation in living cells". In: *Journal of Cell Science* 117 (8), p. 1313. DOI: [10.1242/jcs.01117](https://doi.org/10.1242/jcs.01117).
- Peter A. K., Cheng H., Ross R. S., Knowlton K. U., and Chen J. (2011). "The costamere bridges sarcomeres to the sarcolemma in striated muscle". In: *Progress in Pediatric Cardiology* 31 (2), pp. 83–88. DOI: [10.1016/j.ppedcard.2011.02.003](https://doi.org/10.1016/j.ppedcard.2011.02.003).
- Peters S. L. M. and Michel M. C. (2007). "The RhoA/Rho kinase pathway in the myocardium". In: *Cardiovascular Research* 75 (1), pp. 3–4. DOI: [10.1016/j.cardiores.2007.04.016](https://doi.org/10.1016/j.cardiores.2007.04.016).
- Ponikowski P., Voors A. A., Anker S. D., et al. (2016). "2016 ESC Guidelines for the diagnosis and treatment of acute and chronic heart failure: The Task Force for the diagnosis and treatment of acute and chronic heart failure of the European Society of Cardiology (ESC) Developed with the special contribution of the Heart Failure Association (HFA) of the ESC". In: *European Heart Journal* 37 (27), pp. 2129–2200. DOI: [10.1093/eurheartj/ehw128](https://doi.org/10.1093/eurheartj/ehw128).
- Ponnam S., Sevrieva I., Sun Y.-B., Irving M., and Kambourakis T. (2019). "Site-specific phosphorylation of myosin binding protein-C coordinates thin and thick filament activation in cardiac muscle". In: *Proceedings of the National Academy of Sciences* 116 (31), pp. 15485–15494. DOI: [10.1073/pnas.1903033116](https://doi.org/10.1073/pnas.1903033116).
- Posch M. G., Perrot A., Geier C., et al. (2009). "Genetic deletion of arginine 14 in phospholamban causes dilated cardiomyopathy with attenuated electrocardiographic R amplitudes". In: *Heart Rhythm* 6 (4), pp. 480–486. DOI: [10.1016/j.hrthm.2009.01.016](https://doi.org/10.1016/j.hrthm.2009.01.016).
- Potts G. K., McNally R. M., Blanco R., You J.-S., Hebert A. S., Westphall M. S., Coon J. J., and Hornberger T. A. (2017). "A map of the phosphoproteomic alterations that occur after a bout of maximal-intensity contractions". In: *The Journal of Physiology* 595 (15), pp. 5209–5226. DOI: [10.1113/JP273904](https://doi.org/10.1113/JP273904).
- Priori S. G., Blomström-Lundqvist C., Mazzanti A., et al. (2015). "2015 ESC Guidelines for the management of patients with ventricular arrhythmias and the prevention of sudden cardiac death: The Task Force for the Management of Patients with Ventricular Arrhythmias and the Prevention of Sudden Cardiac Death of the European Society of Cardiology (ESC) Endorsed by: Association for European Paediatric and Congenital Cardiology (AEPC)". In: *European Heart Journal* 36 (41), pp. 2793–2867. DOI: [10.1093/eurheartj/ehv316](https://doi.org/10.1093/eurheartj/ehv316).
- Pruitt W. M., Karnoub A. E., Rakauskas A. C., et al. (2003). "Role of the pleckstrin homology domain in intersectin-L Dbl homology domain activation of Cdc42 and signaling". In: *Biochimica et Biophysica Acta (BBA) - Molecular Cell Research* 1640 (1), pp. 61–68. DOI: [10.1016/S0167-4889\(03\)00002-8](https://doi.org/10.1016/S0167-4889(03)00002-8).

- Puchner E. M., Alexandrovich A., Kho A. L., et al. (2008). “Mechanoenzymatics of titin kinase”. In: *Proceedings of the National Academy of Sciences* 105 (36), pp. 13385–13390. DOI: [10.1073/pnas.0805034105](https://doi.org/10.1073/pnas.0805034105).
- Qadota H., Blangy A., Xiong G., and Benian G. M. (2008a). “The DH-PH Region of the Giant Protein UNC-89 Activates RHO-1 GTPase in *Caenorhabditis elegans* Body Wall Muscle”. In: *Journal of Molecular Biology* 383 (4), pp. 747–752. DOI: [10.1016/j.jmb.2008.08.083](https://doi.org/10.1016/j.jmb.2008.08.083).
- Qadota H., Matsunaga Y., Bagchi P., et al. (2018). “Protein phosphatase 2A is crucial for sarcomere organization in *C. elegans* striated muscle”. In: *Molecular Biology of the Cell*, mbc.E18–03–0192. DOI: [10.1091/mbc.E18-03-0192](https://doi.org/10.1091/mbc.E18-03-0192).
- Qadota H., Matsunaga Y., Nguyen K. C. Q., Mattheyses A., Hall D. H., and Benian G. M. (2017). “High-resolution imaging of muscle attachment structures in *Caenorhabditis elegans*”. In: *Cytoskeleton* 74 (11), pp. 426–442. DOI: [10.1002/cm.21410](https://doi.org/10.1002/cm.21410).
- Qadota H., Mayans O., Matsunaga Y., et al. (2016). “The SH3 domain of UNC-89 (obscurin) interacts with paramyosin, a coiled-coil protein, in *Caenorhabditis elegans* muscle”. In: *Molecular Biology of the Cell* 27 (10), pp. 1606–1620. DOI: [10.1091/mbc.e15-09-0675](https://doi.org/10.1091/mbc.e15-09-0675).
- Qadota H., McGaha L. A., Mercer K. B., Stark T. J., Ferrara T. M., Benian G. M., and Holzbaur E. (2008b). “A Novel Protein Phosphatase is a Binding Partner for the Protein Kinase Domains of UNC-89 (Obscurin) in *Caenorhabditis elegans*”. In: *Molecular Biology of the Cell* 19 (6), pp. 2424–2432. DOI: [10.1091/mbc.e08-01-0053](https://doi.org/10.1091/mbc.e08-01-0053).
- Qian J., Vafiadaki E., Florea S. M., et al. (2011). “Small Heat Shock Protein 20 Interacts With Protein Phosphatase-1 and Enhances Sarcoplasmic Reticulum Calcium Cycling”. In: *Circulation Research* 108 (12), pp. 1429–1438. DOI: [10.1161/CIRCRESAHA.110.237644](https://doi.org/10.1161/CIRCRESAHA.110.237644).
- Qu Z., Hu G., Garfinkel A., and Weiss J. N. (2014). “Nonlinear and stochastic dynamics in the heart”. In: *Physics Reports* 543 (2), pp. 61–162. DOI: [10.1016/j.physrep.2014.05.002](https://doi.org/10.1016/j.physrep.2014.05.002).
- Qu Z. and Weiss J. N. (2015). “Mechanisms of Ventricular Arrhythmias: From Molecular Fluctuations to Electrical Turbulence”. In: *Annual Review of Physiology* 77 (1), pp. 29–55. DOI: [10.1146/annurev-physiol-021014-071622](https://doi.org/10.1146/annurev-physiol-021014-071622).
- Qu Z., Xie Y., Garfinkel A., and Weiss J. N. (2010). “T-Wave Alternans and Arrhythmogenesis in Cardiac Diseases”. In: *Frontiers in Physiology* 1. DOI: [10.3389/fphys.2010.00154](https://doi.org/10.3389/fphys.2010.00154).
- Quan C., Li M., Du Q., et al. (2019). “SPEG Controls Calcium Reuptake Into the Sarcoplasmic Reticulum Through Regulating SERCA2a by Its Second Kinase-Domain”. In: *Circulation Research* 124 (5), pp. 712–726. DOI: [10.1161/CIRCRESAHA.118.313916](https://doi.org/10.1161/CIRCRESAHA.118.313916).
- Quick A. P., Wang Q., Philippen L. E., et al. (2017). “SPEG (Striated Muscle Preferentially Expressed Protein Kinase) Is Essential for Cardiac Function by Regulating Junctional Membrane Complex Activity”. In: *Circulation Research* 120 (1), pp. 110–119. DOI: [10.1161/CIRCRESAHA.116.309977](https://doi.org/10.1161/CIRCRESAHA.116.309977).
- Raeker M. Ö., Su F., Geisler S. B., Borisov A. B., Kontrogianni-Konstantopoulos A., Lyons S. E., and Russell M. W. (2006). “Obscurin is required for the lateral alignment of striated myofibrils in zebrafish”. In: *Developmental Dynamics* 235 (8), pp. 2018–2029. DOI: [10.1002/dvdy.20812](https://doi.org/10.1002/dvdy.20812).
- Raeker M. Ö., Bieniek A. N., Ryan A. S., Tsai H.-J., Zahn K. M., and Russell M. W. (2010). “Targeted deletion of the zebrafish obscurin A RhoGEF domain affects heart, skeletal muscle and brain development”. In: *Developmental Biology* 337 (2), pp. 432–443. DOI: [10.1016/j.ydbio.2009.11.018](https://doi.org/10.1016/j.ydbio.2009.11.018).
- Randazzo D., Giacomello E., Lorenzini S., et al. (2013a). “Obscurin is required for ankyrinB-dependent dystrophin localization and sarcolemma integrity”. In: *Journal of Cell Biology* 200, pp. 523–536.
- Randazzo D., Blaauw B., Paolini C., et al. (2017a). “Exercise-induced alterations and loss of sarcomeric M-line organization in the diaphragm muscle of obscurin knockout mice”. In: *American Journal of Physiology - Cell Physiology* 312 (1), pp. C16–C28. DOI: [10.1152/ajpcell.00098.2016](https://doi.org/10.1152/ajpcell.00098.2016).
- Randazzo D., Pierantozzi E., Rossi D., and Sorrentino V. (2017b). “The potential of obscurin as a therapeutic target in muscle disorders”. In: *Expert Opinion on Therapeutic Targets* 21 (9), pp. 897–910. DOI: [10.1080/14728222.2017.1361931](https://doi.org/10.1080/14728222.2017.1361931).

- Randazzo P. A., Jian X., Chen P.-W., Zhai P., Soubias O., and Northup J. K. (2013b). “Quantitative Analysis of Guanine Nucleotide Exchange Factors (GEFs) as Enzymes”. In: *Cellular Logistics* 3 (1), e27609. DOI: [10.4161/cl.27609](https://doi.org/10.4161/cl.27609).
- Rangrez A. Y., Bernt A., Poyanmehr R., Harazin V., Boomgaarden I., Kuhn C., Rohrbeck A., Frank D., and Frey N. (2013). “Dysbindin is a potent inducer of RhoA–SRF-mediated cardiomyocyte hypertrophy”. In: *J Cell Biol* 203 (4), pp. 643–656. DOI: [10.1083/jcb.201303052](https://doi.org/10.1083/jcb.201303052).
- Reiterer V., Eysers P. A., and Farhan H. (2014). “Day of the dead: pseudokinases and pseudophosphatases in physiology and disease”. In: *Trends in Cell Biology* 24 (9), pp. 489–505. DOI: [10.1016/j.tcb.2014.03.008](https://doi.org/10.1016/j.tcb.2014.03.008).
- Rijdt W. P. t., Tintelen J. P. v., Vink A., Wal A. C. v. d., Boer R. A. d., Berg M. P. v. d., and Surmeijer A. J. H. (2016). “Phospholamban p.Arg14del cardiomyopathy is characterized by phospholamban aggregates, aggresomes, and autophagic degradation”. In: *Histopathology* 69 (4), pp. 542–550. DOI: [10.1111/his.12963](https://doi.org/10.1111/his.12963).
- Rinaldo C., Siepi F., Prodosmo A., and Soddu S. (2008). “HIPKs: Jack of all trades in basic nuclear activities”. In: *Biochimica et Biophysica Acta (BBA) - Molecular Cell Research* 1783 (11), pp. 2124–2129. DOI: [10.1016/j.bbamcr.2008.06.006](https://doi.org/10.1016/j.bbamcr.2008.06.006).
- Roger V. L. (2013). “Epidemiology of Heart Failure”. In: *Circulation Research* 113 (6), pp. 646–659. DOI: [10.1161/CIRCRESAHA.113.300268](https://doi.org/10.1161/CIRCRESAHA.113.300268).
- Roselli C., Rienstra M., and Ellinor P. T. (2020). “Genetics of Atrial Fibrillation in 2020”. In: *Circulation Research* 127 (1), pp. 21–33. DOI: [10.1161/CIRCRESAHA.120.316575](https://doi.org/10.1161/CIRCRESAHA.120.316575).
- Rossi D., Palmio J., Evilä A., et al. (2017). “A novel FLNC frameshift and an OBSCN variant in a family with distal muscular dystrophy”. In: *PLOS ONE* 12 (10), e0186642. DOI: [10.1371/journal.pone.0186642](https://doi.org/10.1371/journal.pone.0186642).
- Rossmann K. L. and Campbell S. L. (2000). “Bacterial expressed DH and DH/PH domains”. In: *Methods in Enzymology*. Ed. by W. E. Balch, C. J. Der, and A. Hall. Vol. 325. Academic Press, pp. 25–38. DOI: [10.1016/S0076-6879\(00\)25428-1](https://doi.org/10.1016/S0076-6879(00)25428-1).
- Rossmann K. L., Der C. J., and Sondek J. (2005). “GEF means go: turning on RHO GTPases with guanine nucleotide-exchange factors”. In: 6, p. 167.
- Rossmann K. L., Worthylake D. K., Snyder J. T., Siderovski D. P., Campbell S. L., and Sondek J. (2002). “A crystallographic view of interactions between Dbs and Cdc42: PH domain-assisted guanine nucleotide exchange”. In: *The EMBO Journal* 21 (6), pp. 1315–1326. DOI: [10.1093/emboj/21.6.1315](https://doi.org/10.1093/emboj/21.6.1315).
- Roth G. A., Abate D., Abate K. H., et al. (2018). “Global, regional, and national age-sex-specific mortality for 282 causes of death in 195 countries and territories, 1980–2017: a systematic analysis for the Global Burden of Disease Study 2017”. In: *The Lancet* 392 (10159), pp. 1736–1788. DOI: [10.1016/S0140-6736\(18\)32203-7](https://doi.org/10.1016/S0140-6736(18)32203-7).
- Rowland T. J., Graw S. L., Sweet M. E., Gigli M., Taylor M. R. G., and Mestroni L. (2016). “Obscurin Variants in Patients With Left Ventricular Noncompaction”. In: *Journal of the American College of Cardiology* 68 (20), pp. 2237–2238. DOI: [10.1016/j.jacc.2016.08.052](https://doi.org/10.1016/j.jacc.2016.08.052).
- Roy A., Kucukural A., and Zhang Y. (2010). “I-TASSER: a unified platform for automated protein structure and function prediction.” In: *Nature protocols* 5 (4), pp. 725–738. DOI: [10.1038/nprot.2010.5](https://doi.org/10.1038/nprot.2010.5).
- Russell M. W., Raeker M. O., Korytkowski K. A., and Sonneman K. J. (2002). “Identification, tissue expression and chromosomal localization of human Obscurin-MLCK, a member of the titin and Dbl families of myosin light chain kinases”. In: *Gene* 282 (1), pp. 237–246. DOI: [10.1016/S0378-1119\(01\)00795-8](https://doi.org/10.1016/S0378-1119(01)00795-8).
- Rust M. J., Markson J. S., Lane W. S., Fisher D. S., and O’Shea E. K. (2007). “Ordered Phosphorylation Governs Oscillation of a Three-Protein Circadian Clock”. In: *Science* 318 (5851), pp. 809–812. DOI: [10.1126/science.1148596](https://doi.org/10.1126/science.1148596).
- Sah V. P., Minamisawa S., Tam S. P., Wu T. H., Dorn G. W., Ross J., Chien K. R., and Brown J. H. (1999). “Cardiac-specific overexpression of RhoA results in sinus and atrioventricular nodal dysfunction and

- contractile failure". In: *The Journal of Clinical Investigation* 103(12), pp. 1627–1634. DOI: [10.1172/JCI6842](https://doi.org/10.1172/JCI6842).
- Salas-Vidal E., Meijer A. H., Cheng X., and Spaink H. P. (2005). "Genomic annotation and expression analysis of the zebrafish Rho small GTPase family during development and bacterial infection". In: *Genomics* 86(1), pp. 25–37. DOI: [10.1016/j.ygeno.2005.03.010](https://doi.org/10.1016/j.ygeno.2005.03.010).
- Salemi L. M., Maitland M. E. R., McTavish C. J., and Schild-Poulter C. (2017). "Cell signalling pathway regulation by RanBPM: molecular insights and disease implications". In: *Open Biology* 7(6), p. 170081. DOI: [10.1098/rsob.170081](https://doi.org/10.1098/rsob.170081).
- Schmitt J. P., Kamisago M., Asahi M., et al. (2003). "Dilated Cardiomyopathy and Heart Failure Caused by a Mutation in Phospholamban". In: *Science* 299(5611), pp. 1410–1413. DOI: [10.1126/science.1081578](https://doi.org/10.1126/science.1081578).
- Segev N. (2001). "Ypt/Rab GTPases: Regulators of Protein Trafficking". In: *Science Signaling* 100.
- Shankaranarayanan A., Boguth C. A., Lutz S., Vettel C., Uhlemann F., Aittaleb M., Wieland T., and Tesmer J. J. G. (2010). "Gαq allosterically activates and relieves autoinhibition of p63RhoGEF". In: *Cellular Signalling* 22(7), pp. 1114–1123. DOI: [10.1016/j.cellsig.2010.03.006](https://doi.org/10.1016/j.cellsig.2010.03.006).
- Shannon T. R., Wang F., Puglisi J., Weber C., and Bers D. M. (2004). "A Mathematical Treatment of Integrated Ca Dynamics within the Ventricular Myocyte". In: *Biophysical Journal* 87(5), pp. 3351–3371. DOI: [10.1529/biophysj.104.047449](https://doi.org/10.1529/biophysj.104.047449).
- Shimokawa H., Sunamura S., and Satoh K. (2016). "RhoA/Rho-Kinase in the Cardiovascular System". In: *Circulation Research* 118(2), pp. 352–366. DOI: [10.1161/CIRCRESAHA.115.306532](https://doi.org/10.1161/CIRCRESAHA.115.306532).
- Shriver M., Marimuthu S., Paul C., Geist J., Seale T., Konstantopoulos K., and Konstantopoulos A. K. (2016). "Giant obscurins regulate the PI3K cascade in breast epithelial cells via direct binding to the PI3K/p85 regulatory subunit". In: *Oncotarget* 7(29), pp. 45414–45428. DOI: [10.18632/oncotarget.9985](https://doi.org/10.18632/oncotarget.9985).
- Sievers F., Wilm A., Dineen D., et al. (2011). "Fast, scalable generation of high-quality protein multiple sequence alignments using Clustal Omega". In: *Molecular Systems Biology* 7(1), p. 539. DOI: [10.1038/msb.2011.75](https://doi.org/10.1038/msb.2011.75).
- Simmerman H. K., Collins J. H., Theibert J. L., Wegener A. D., and Jones L. R. (1986). "Sequence analysis of phospholamban. Identification of phosphorylation sites and two major structural domains." In: *Journal of Biological Chemistry* 261(28), pp. 13333–13341. DOI: [10.1016/S0021-9258\(18\)69309-3](https://doi.org/10.1016/S0021-9258(18)69309-3).
- Singh D. R., Dalton M. P., Cho E. E., Pribadi M. P., Zak T. J., Seřlová J., Makarewich C. A., Olson E. N., and Robia S. L. (2019). "Newly Discovered Micropeptide Regulators of SERCA Form Oligomers but Bind to the Pump as Monomers". In: *Journal of Molecular Biology*. DOI: [10.1016/j.jmb.2019.07.037](https://doi.org/10.1016/j.jmb.2019.07.037).
- Slack J. P., Grupp I. L., Dash R., et al. (2001). "The Enhanced Contractility of the Phospholamban-deficient Mouse Heart Persists with Aging". In: *Journal of Molecular and Cellular Cardiology* 33(5), pp. 1031–1040. DOI: [10.1006/jmcc.2001.1370](https://doi.org/10.1006/jmcc.2001.1370).
- Small T. M., Gernert K. M., Flaherty D. B., Mercer K. B., Borodovsky M., and Benian G. M. (2004). "Three New Isoforms of *Caenorhabditis elegans* UNC-89 Containing MLCK-like Protein Kinase Domains". In: *Journal of Molecular Biology* 342(1), pp. 91–108. DOI: [10.1016/j.jmb.2004.07.006](https://doi.org/10.1016/j.jmb.2004.07.006).
- Smeazzetto S., Tadini-Buoninsegni F., Thiel G., Berti D., and Montis C. (2016). "Phospholamban spontaneously reconstitutes into giant unilamellar vesicles where it generates a cation selective channel". In: *Physical Chemistry Chemical Physics* 18(3), pp. 1629–1636. DOI: [10.1039/C5CP05893G](https://doi.org/10.1039/C5CP05893G).
- Smeazzetto S., Tadini-Buoninsegni F., Thiel G., and Moncelli M. R. (2018). "Selectivity of the phospholamban ion channel investigated by single channel measurements". In: *Journal of Electroanalytical Chemistry* 812, pp. 244–248. DOI: [10.1016/j.jelechem.2018.01.028](https://doi.org/10.1016/j.jelechem.2018.01.028).
- Snyder J. T., Worthylake D. K., Rossman K. L., Betts L., Pruitt W. M., Siderovski D. P., Der C. J., and Sondek J. (2002). "Structural basis for the selective activation of Rho GTPases by Dbl exchange factors". In: 9, p. 468.

- Soltis A. R. and Saucerman J. J. (2010). “Synergy between CaMKII Substrates and β -Adrenergic Signaling in Regulation of Cardiac Myocyte Ca^{2+} Handling”. In: *Biophysical Journal* 99 (7), pp. 2038–2047. DOI: [10.1016/j.bpj.2010.08.016](https://doi.org/10.1016/j.bpj.2010.08.016).
- Souchet M., Portales-Casamar E., Mazurais D., et al. (2002). “Human p63RhoGEF, a novel RhoA-specific guanine nucleotide exchange factor, is localized in cardiac sarcomere”. In: *Journal of Cell Science* 115 (3), p. 629.
- Spooner P. M., Bonner J., Maricq A. V., Benian G. M., and Norman K. R. (2012). “Large Isoforms of UNC-89 (Obscurin) Are Required for Muscle Cell Architecture and Optimal Calcium Release in *Caenorhabditis elegans*”. In: *PLoS ONE* 7 (7), e40182. DOI: [10.1371/journal.pone.0040182](https://doi.org/10.1371/journal.pone.0040182).
- Stammers A. N., Susser S. E., Hamm N. C., Hlynsky M. W., Kimber D. E., Kehler D. S., and Duhamel T. A. (2015). “The regulation of sarco(endo)plasmic reticulum calcium-ATPases (SERCA)”. In: *Canadian Journal of Physiology and Pharmacology* 93 (10), pp. 843–854. DOI: [10.1139/cjpp-2014-0463](https://doi.org/10.1139/cjpp-2014-0463).
- Standring S. (2016). *Gray's Anatomy: The Anatomical Basis of Clinical Practice*. 41st. Elsevier.
- Stiegler A. L. and Boggon T. J. (2020). “The pseudoGTPase group of pseudoenzymes”. In: *The FEBS Journal* 287 (19), pp. 4232–4245. DOI: <https://doi.org/10.1111/febs.15554>.
- Suwanmajo T. and Krishnan J. (2015). “Mixed mechanisms of multi-site phosphorylation”. In: *Journal of The Royal Society Interface* 12 (107), p. 20141405. DOI: [10.1098/rsif.2014.1405](https://doi.org/10.1098/rsif.2014.1405).
- Tada M., Kirchberger M. A., and Katz A. M. (1975). “Phosphorylation of a 22,000-dalton component of the cardiac sarcoplasmic reticulum by adenosine 3':5'-monophosphate-dependent protein kinase.” In: *Journal of Biological Chemistry* 250 (7), pp. 2640–2647.
- Tadros R., Francis C., Xu X., et al. (2021). “Shared genetic pathways contribute to risk of hypertrophic and dilated cardiomyopathies with opposite directions of effect”. In: *Nature Genetics* 53 (2), pp. 128–134. DOI: [10.1038/s41588-020-00762-2](https://doi.org/10.1038/s41588-020-00762-2).
- Takemoto K., Ishihara S., Mizutani T., Kawabata K., and Haga H. (2015). “Compressive Stress Induces Dephosphorylation of the Myosin Regulatory Light Chain via RhoA Phosphorylation by the Adenyl Cyclase/Protein Kinase A Signaling Pathway”. In: *PLoS ONE* 10 (3), e0117937. DOI: [10.1371/journal.pone.0117937](https://doi.org/10.1371/journal.pone.0117937).
- Taylor C. J., Ordóñez-Mena J. M., Roalfe A. K., Lay-Flurrie S., Jones N. R., Marshall T., and Hobbs F. D. R. (2019). “Trends in survival after a diagnosis of heart failure in the United Kingdom 2000-2017: population based cohort study”. In: *British Medical Journal* 364, p. 1223. DOI: [10.1136/bmj.1223](https://doi.org/10.1136/bmj.1223).
- Tham Y. K., Bernardo B. C., Ooi J. Y. Y., Weeks K. L., and McMullen J. R. (2015). “Pathophysiology of cardiac hypertrophy and heart failure: signaling pathways and novel therapeutic targets”. In: *Archives of Toxicology* 89 (9), pp. 1401–1438. DOI: [10.1007/s00204-015-1477-x](https://doi.org/10.1007/s00204-015-1477-x).
- Torsoni A. S., Marin T. M., Velloso L. A., and Franchini K. G. (2005). “RhoA/ROCK signaling is critical to FAK activation by cyclic stretch in cardiac myocytes”. In: *American Journal of Physiology. Heart and Circulatory Physiology* 289 (4), H1488–1496. DOI: [10.1152/ajpheart.00692.2004](https://doi.org/10.1152/ajpheart.00692.2004).
- Traaseth N. J., Thomas D. D., and Veglia G. (2006). “Effects of Ser16 Phosphorylation on the Allosteric Transitions of Phospholamban/ Ca^{2+} -ATPase Complex”. In: *Journal of Molecular Biology* 358 (4), pp. 1041–1050. DOI: [10.1016/j.jmb.2006.02.047](https://doi.org/10.1016/j.jmb.2006.02.047).
- Tsyganov M. A., Kolch W., and Kholodenko B. N. (2012). “The topology design principles that determine the spatiotemporal dynamics of G-protein cascades”. In: *Molecular BioSystems* 8 (3), pp. 730–743. DOI: [10.1039/C2MB05375F](https://doi.org/10.1039/C2MB05375F).
- Turnham R. E. and Scott J. D. (2016). “Protein kinase A catalytic subunit isoform PRKACA; History, function and physiology”. In: *Gene* 577 (2), pp. 101–108. DOI: [10.1016/j.gene.2015.11.052](https://doi.org/10.1016/j.gene.2015.11.052).
- Vafiadaki E., Arvanitis D. A., Sanoudou D., and Kranias E. G. (2013). “Identification of a Protein Phosphatase-1/Phospholamban Complex That Is Regulated by cAMP-Dependent Phosphorylation”. In: *PLoS ONE* 8 (11), e80867. DOI: [10.1371/journal.pone.0080867](https://doi.org/10.1371/journal.pone.0080867).

- Vafiadaki E., Sanoudou D., Arvanitis D. A., Catino D. H., Kranias E. G., and Kontrogianni-Konstantopoulos A. (2007). “Phospholamban Interacts with HAX-1, a Mitochondrial Protein with Anti-apoptotic Function”. In: *Journal of Molecular Biology* 367 (1), pp. 65–79. DOI: [10.1016/j.jmb.2006.10.057](https://doi.org/10.1016/j.jmb.2006.10.057).
- Vahebi S., Kobayashi T., Warren C. M., Tombe P. P. d., and Solaro R. J. (2005). “Functional Effects of Rho-Kinase-Dependent Phosphorylation of Specific Sites on Cardiac Troponin”. In: *Circulation Research* 96 (7), pp. 740–747. DOI: [10.1161/01.RES.0000162457.56568.7d](https://doi.org/10.1161/01.RES.0000162457.56568.7d).
- Verardi R., Shi L., Traaseth N. J., Walsh N., and Veglia G. (2011). “Structural topology of phospholamban pentamer in lipid bilayers by a hybrid solution and solid-state NMR method”. In: *Proceedings of the National Academy of Sciences* 108 (22), pp. 9101–9106. DOI: [10.1073/pnas.1016535108](https://doi.org/10.1073/pnas.1016535108).
- Vetter I. R. and Wittinghofer A. (2001). “The guanine nucleotide-binding switch in three dimensions.” In: *Science* 294 (5545), pp. 1299–1304. DOI: [10.1126/science.1062023](https://doi.org/10.1126/science.1062023).
- Vlasblom R., Muller A., Beckers C. M. L., Amerongen G. P. v. N., Zuidwijk M. J., Hardeveld C. v., Paulus W. J., and Simonides W. S. (2009). “RhoA-ROCK signaling is involved in contraction-mediated inhibition of SERCA2a expression in cardiomyocytes”. In: *Pflügers Archiv - European Journal of Physiology* 458 (4), pp. 785–793. DOI: [10.1007/s00424-009-0659-x](https://doi.org/10.1007/s00424-009-0659-x).
- Vostrikov V., Mote K., Verardi R., and Veglia G. (2013). “Structural Dynamics and Topology of Phosphorylated Phospholamban Homopentamer Reveal Its Role in the Regulation of Calcium Transport”. In: *Structure* 21 (12), pp. 2119–2130. DOI: [10.1016/j.str.2013.09.008](https://doi.org/10.1016/j.str.2013.09.008).
- Warner A., Xiong G., Qadota H., Rogalski T., Vogl A. W., Moerman D. G., Benian G. M., and Hardin J. D. (2013). “CPNA-1, a copine domain protein, is located at integrin adhesion sites and is required for myofilament stability in *Caenorhabditis elegans*”. In: *Molecular Biology of the Cell* 24 (5), pp. 601–616. DOI: [10.1091/mbc.e12-06-0478](https://doi.org/10.1091/mbc.e12-06-0478).
- Waterston R. H., Thomson J. N., and Brenner S. (1980). “Mutants with altered muscle structure in *Caenorhabditis elegans*”. In: *Developmental Biology* 77 (2), pp. 271–302. DOI: [10.1016/0012-1606\(80\)90475-3](https://doi.org/10.1016/0012-1606(80)90475-3).
- Wegener A. D. and Jones L. R. (1984). “Phosphorylation-induced mobility shift in phospholamban in sodium dodecyl sulfate-polyacrylamide gels. Evidence for a protein structure consisting of multiple identical phosphorylatable subunits.” In: *Journal of Biological Chemistry* 259 (3), pp. 1834–1841.
- Wegener A. D., Simmerman H. K., Lindemann J. P., and Jones L. R. (1989). “Phospholamban phosphorylation in intact ventricles. Phosphorylation of serine 16 and threonine 17 in response to beta-adrenergic stimulation.” In: *Journal of Biological Chemistry* 264 (19), pp. 11468–11474.
- Weiss J. N., Nivala M., Garfinkel A., Qu Z., and Winslow R. (2011). “Alternans and Arrhythmias”. In: *Circulation Research* 108 (1), pp. 98–112. DOI: [10.1161/CIRCRESAHA.110.223586](https://doi.org/10.1161/CIRCRESAHA.110.223586).
- Wennerberg K. and Der C. J. (2004). “Rho-family GTPases: it’s not only Rac and Rho (and I like it)”. In: *Journal of Cell Science* 117 (8), pp. 1301–1312. DOI: [10.1242/jcs.01118](https://doi.org/10.1242/jcs.01118).
- Wennerberg K., Rossmann K. L., and Der C. J. (2005). “The Ras superfamily at a glance”. In: *Journal of cell science*.
- Whitley J. A., Ex-Willey A. M., Marzolf D. R., Ackermann M. A., Tongen A. L., Kokhan O., and Wright N. T. (2019). “Obscurin is a semi-flexible molecule in solution”. In: *Protein Science* 28 (4), pp. 717–726. DOI: <https://doi.org/10.1002/pro.3578>.
- Wittinghofer A. and Vetter I. R. (2011). “Structure-Function Relationships of the G Domain, a Canonical Switch Motif”. In: *Annu. Rev. Biochem.* 80, pp. 943–971.
- Wittmann T., Lohse M. J., and Schmitt J. P. (2015). “Phospholamban pentamers attenuate PKA-dependent phosphorylation of monomers”. In: *Journal of Molecular and Cellular Cardiology* 80, pp. 90–97. DOI: [10.1016/j.yjmcc.2014.12.020](https://doi.org/10.1016/j.yjmcc.2014.12.020).
- Wolska B. M., Stojanovic M. O., Luo W., Kranias E. G., and Solaro R. J. (1996). “Effect of ablation of phospholamban on dynamics of cardiac myocyte contraction and intracellular Ca²⁺”. In: *American Journal of Physiology-Cell Physiology* 271 (1), pp. C391–C397. DOI: [10.1152/ajpcell.1996.271.1.C391](https://doi.org/10.1152/ajpcell.1996.271.1.C391).

- Wu Y., Luczak E. D., Lee E.-J., et al. (2012). “CaMKII effects on inotropic but not lusitropic force frequency responses require phospholamban”. In: *Journal of Molecular and Cellular Cardiology* 53 (3), pp. 429–436. DOI: [10.1016/j.yjmcc.2012.06.019](https://doi.org/10.1016/j.yjmcc.2012.06.019).
- Xiang S. Y., Vanhoutte D., Re D. P. D., et al. (2011). “RhoA protects the mouse heart against ischemia/reperfusion injury”. In: *The Journal of Clinical Investigation* 121 (8), pp. 3269–3276. DOI: [10.1172/JCI44371](https://doi.org/10.1172/JCI44371).
- Xie Y., Grandi E., Bers D. M., and Sato D. (2014). “How does β -adrenergic signalling affect the transitions from ventricular tachycardia to ventricular fibrillation?” In: *EP Europace* 16 (3), pp. 452–457. DOI: [10.1093/europace/eut412](https://doi.org/10.1093/europace/eut412).
- Xiong G., Qadota H., Mercer K. B., McGaha L. A., Oberhauser A. F., and Benian G. M. (2009). “A LIM-9 (FHL) / SCPL-1 (SCP) Complex Interacts with the C-terminal Protein Kinase Regions of UNC-89 (Obscurin) in *Caenorhabditis elegans* Muscle”. In: *Journal of Molecular Biology* 386 (4), pp. 976–988. DOI: [10.1016/j.jmb.2009.01.016](https://doi.org/10.1016/j.jmb.2009.01.016).
- Xu J., Li Z., Ren X., et al. (2015). “Investigation of Pathogenic Genes in Chinese sporadic Hypertrophic Cardiomyopathy Patients by Whole Exome Sequencing”. In: *Scientific Reports* 5 (1), pp. 1–13. DOI: [10.1038/srep16609](https://doi.org/10.1038/srep16609).
- Xu Z., Gakhar L., Bain F. E., Spies M., and Fuentes E. J. (2017). “The Tiam1 guanine nucleotide exchange factor is auto-inhibited by its pleckstrin homology coiled-coil extension domain”. In: *Journal of Biological Chemistry* 292 (43), pp. 17777–17793. DOI: [10.1074/jbc.M117.799114](https://doi.org/10.1074/jbc.M117.799114).
- Yachdav G., Kloppmann E., Kajan L., et al. (2014). “PredictProtein—an open resource for online prediction of protein structural and functional features”. In: *Nucleic Acids Research* 42 (W1), W337–W343. DOI: [10.1093/nar/gku366](https://doi.org/10.1093/nar/gku366).
- Yamasaki R., Wu Y., McNabb M., Greaser M., Labeit S., and Granzier H. (2002). “Protein kinase A phosphorylates titin’s cardiac-specific N2B domain and reduces passive tension in rat cardiac myocytes”. In: *Circulation Research* 90 (11), pp. 1181–1188. DOI: [10.1161/01.res.0000021115.24712.99](https://doi.org/10.1161/01.res.0000021115.24712.99).
- Yang J., Yan R., Roy A., Xu D., Poisson J., and Zhang Y. (2015). “The I-TASSER Suite: protein structure and function prediction”. In: *Nature Methods* 12 (1), pp. 7–8. DOI: [10.1038/nmeth.3213](https://doi.org/10.1038/nmeth.3213).
- Yost O., FriedenberG S. G., Jesty S. A., Olby N. J., and Meurs K. M. (2019). “The R9H phospholamban mutation is associated with highly penetrant dilated cardiomyopathy and sudden death in a spontaneous canine model”. In: *Gene* 697, pp. 118–122. DOI: [10.1016/j.gene.2019.02.022](https://doi.org/10.1016/j.gene.2019.02.022).
- Young P., Ehler E., and Gautel M. (2001). “Obscurin, a giant sarcomeric Rho guanine nucleotide exchange factor protein involved in sarcomere assembly”. In: *The Journal of Cell Biology* 154 (1), pp. 123–136. DOI: [10.1083/jcb.200102110](https://doi.org/10.1083/jcb.200102110).
- Zamanian J. L. and Kelly R. B. (2003). “Intersectin 1L Guanine Nucleotide Exchange Activity Is Regulated by Adjacent src Homology 3 Domains That Are Also Involved in Endocytosis”. In: *Molecular Biology of the Cell* 14 (4), pp. 1624–1637. DOI: [10.1091/mbc.E02-08-0494](https://doi.org/10.1091/mbc.E02-08-0494).
- Zhang Z., Chen L., Gao L., et al. (2012). “Structural basis for the recognition of Asef by adenomatous polyposis coli”. In: *Cell Research* 22 (2), p. 372. DOI: [10.1038/cr.2011.119](https://doi.org/10.1038/cr.2011.119).
- Zhou R., Zhang Q., and Xu P. (2020). “TBK1, a central kinase in innate immune sensing of nucleic acids and beyond”. In: *Acta Biochimica et Biophysica Sinica* 52 (7), pp. 757–767. DOI: [10.1093/abbs/gmaa051](https://doi.org/10.1093/abbs/gmaa051).
- Zi M., Maqsood A., Prehar S., et al. (2014). “The Mammalian Ste20-like Kinase 2 (Mst2) Modulates Stress-induced Cardiac Hypertrophy”. In: *Journal of Biological Chemistry* 289 (35), pp. 24275–24288. DOI: [10.1074/jbc.M114.562405](https://doi.org/10.1074/jbc.M114.562405).
- Ziaieian B. and Fonarow G. C. (2016). “Epidemiology and aetiology of heart failure”. In: *Nature Reviews Cardiology* 13 (6), pp. 368–378. DOI: [10.1038/nrcardio.2016.25](https://doi.org/10.1038/nrcardio.2016.25).
- Zwaag P. A. v. d., Rijsingen I. A. W. v., Asimaki A., et al. (2012). “Phospholamban R14del mutation in patients diagnosed with dilated cardiomyopathy or arrhythmogenic right ventricular cardiomyopathy: evidence supporting the concept of arrhythmogenic cardiomyopathy”. In: *European Journal of Heart Failure* 14 (11), pp. 1199–1207. DOI: [10.1093/eurjhf/hfs119](https://doi.org/10.1093/eurjhf/hfs119).

Appendix A: Supplementary material for **chapter 3**

A4 Supplementary data

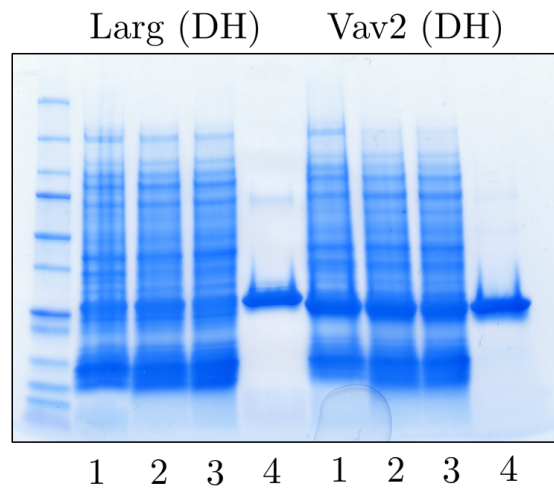


Figure A2. SDS-PAGE analysis of the purification of Larg and Vav2 DH domains.

1: Crude lysate. 2: Soluble fraction. 3: Flow-through. 4: Eluted fraction after buffer exchange and concentration.

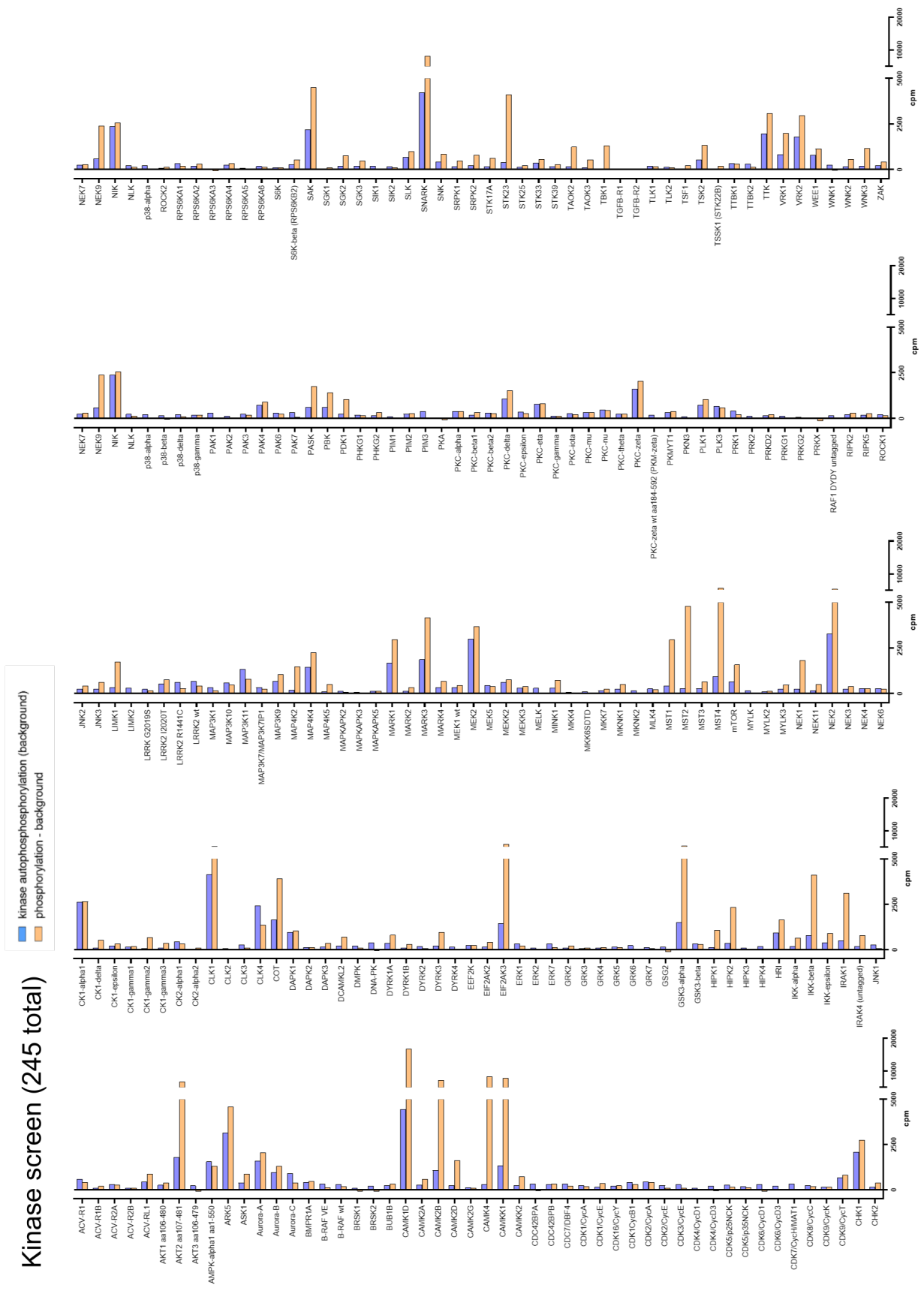


Figure A3. Results for all kinases in the ProQinase KinaseFinder screen. Bars represent corrected absolute values for phosphorylation of obscurin SH3-DH substrate and kinase autophosphorylation background.

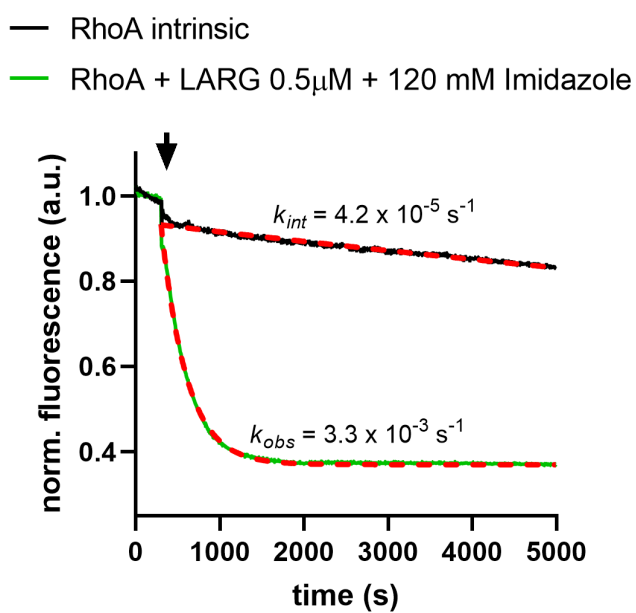


Figure A4. Nucleotide exchange activity of Larg DH domain in the presence of imidazole towards RhoA at 1.5 μ M [GTPase].

The presence of imidazole does not impair the nucleotide exchange activity as the GEF-catalysed exchange rate in the presence of imidazole is still about two orders of magnitude higher than the intrinsic exchange rate. Curves represent the mean of $n = 3-4$ technical replicates/experiment. Dashed lines indicate fitted decay functions.

A5 Supplementary method details

Table A1. Primers used in this study

Capital letters denote regions overlapping with other DNA fragments for the purpose of HiFi-DNA assembly. Underlined and bold letters denote altered codons in mutagenesis primers. T_m was calculated with the NEB web-tool: <http://tcalculator.neb.com/> (parameters: Q5 Hot-start, 400nM [primer]). n.d. = not determined.

Primer	Sequence (5'->3')	T _m (°C)	Comment
1-3, 5-6	-	-	Not used in this study (cf. Figure 8)
4	CACGCGTGGATCCTTActggcggatgggctc	66	Obscurin 5899 reverse, 5' overlap with pET6HtevC2
7	TATTTTCAGGGCTCGAGCaagctgtcacctgaggg	64	Obscurin 5667 forward, 5' overlap with pET6HtevC2
8	TATTTTCAGGGCTCGAGCctctggggaggctg	62	Obscurin 5681 forward, 5' overlap with pET6HtevC2
9	TATTTTCAGGGCTCGAGCtctgaagacgaatacaaggc	62	Obscurin 5686 forward, 5' overlap with pET6HtevC2
10	TATTTTCAGGGCTCGAGCgaatacaaggcaagcctgag	63	Obscurin 5689 forward, 5' overlap with pET6HtevC2
11	TATTTTCAGGGCTCGAGCaaggcaaggctgagctc	65	Obscurin 5691 forward, 5' overlap with pET6HtevC2
12	CACGCGTGGATCCTTActcctatgaggacacgtg	65	Obscurin 5884 reverse, 5' overlap with pET6HtevC2
13	CACGCGTGGATCCTTAggtgctctggtagttctc	65	Obscurin 5889 reverse, 5' overlap with pET6HtevC2
14	CACGCGTGGATCCTTActcagggtgcctg	63	Obscurin 5891 reverse, 5' overlap with pET6HtevC2
15	CACGCGTGGATCCTTActcggccagggc	62	Obscurin 5895 reverse, 5' overlap with pET6HtevC2
16	TATTTTCAGGGCTCGAGCgagccatccg	63	Obscurin 5895 forward, 5' overlap with pET6HtevC2
17	TATTTTCAGGGCTCGAGCcacttcatctgtgtg	63	Obscurin 5901 forward, 5' overlap with pET6HtevC2
18	CACGCGTGGATCCTTAacgctgtctgatgc	62	Obscurin 6005 reverse, 5' overlap with pET6HtevC2
19	CACGCGTGGATCCTTAaggcagggccagac	64	Obscurin 6009 reverse, 5' overlap with pET6HtevC2
20	CACGCGTGGATCCTTAccgcccacacaggc	64	Obscurin 6012 reverse, 5' overlap with pET6HtevC2
21	tggtgattctccatgagg	63	Obscurin 5887 reverse
22	ctccatgagggacacg	62	Obscurin 5884 reverse
23	ctcggccagggc	62	Obscurin 5895 reverse
24	CGTGTCCCTCATGGAGggctatgacgggaatctc	62	Dbs 787 forward, 5' overlap with human obscurin
25	CACGCGTGGATCCTTAttcttacaagcctgcagc	64	Dbs 921 reverse, 5' overlap with pET6HtevC2
26	CGTGTCCCTCATGGAGgggtttgatgaaaacattgag	63	Trio 1475 forward, 5' overlap with human obscurin
27	CAGGCCCTGGGCGAGctcatcctacaggaatc	64	Trio 1486 forward, 5' overlap with human obscurin
28	CACGCGTGGATCCTTAcgtccgctctctgatg	65	Trio 1594 reverse, 5' overlap with pET6HtevC2
29	CTCATGGAGAACTACCCAgg	64	Obscurin (chicken) 7963 forward, 5' overlap with human obscurin
30	CACGCGTGGATCCTTAgctctggaggatccagac	64	Obscurin (chicken) 8096 reverse, 5' overlap with pET6HtevC2
31	CTCATGGAGAACTACCCAgccaatc	69	Obscurin (zebrafish) 6090 forward, 5' overlap with human obscurin
32	CACGCGTGGATCCTTAatctggagagcaccatgttg	64	Obscurin (zebrafish) 6217 reverse, 5' overlap with pET6HtevC2
33	TTCAGGGCTCGAGCatg	65	TEV-site + start codon forward

34	GAGGGATCCTGTTTCTCAagttaaaatggctatg atagcc	64	RhoQ 185 reverse, overlap with pGEXtev
35	TTCAGGGCTCGAGCatgcagacaattaagtgtgtg ttg	63	Cdc42 forward, overlap with pGEXtev
36	GAGGGATCCTGTTTCTCActcgagggcagctag g	64	Cdc42 178 reverse, overlap with pGEXtev
37	TTCAGGGCTCGAGCatgaactgcaagagggaa c	62	RhoJ forward, overlap with pGEXtev
38	GAGGGATCCTGTTTCTCAGgtgaggattgctca tc	60	RhoJ 193 reverse, overlap with pGEXtev
39	TTCAGGGCTCGAGCatgcaggc	63	Rac1 forward, overlap with pGEXtev
40	GAGGGATCCTGTTTCTCAGaggactgctcgat c	63	Rac1 177 reverse, overlap with pGEXtev
41	TTCAGGGCTCGAGCatgcaggccatcaagtgtg	65	Rac2 forward, overlap with pGEXtev
42	GAGGGATCCTGTTTCTCAcagcacggccc	63	Rac2 177 reverse, overlap with pGEXtev
43	TTCAGGGCTCGAGCatgcaggccatcaagtgc	66	Rac3 forward, overlap with pGEXtev
44	GAGGGATCCTGTTTCTCAGagcaccgcgc	64	Rac3 177 reverse, overlap with pGEXtev
45	TTCAGGGCTCGAGCatgcagagcatcaagtgc	63	RhoG forward, overlap with pGEXtev
46	GAGGGATCCTGTTTCTCAGagcacagcccgg	63	RhoG 177 reverse, overlap with pGEXtev
47	TTCAGGGCTCGAGCatggcggccatccg	66	RhoB forward, overlap with pGEXtev
48	GAGGGATCCTGTTTCTCAGccgttctgggagcc	66	RhoB 188 reverse, overlap with pGEXtev
49	TTCAGGGCTCGAGCatggctgcaatccgaaag	63	RhoC forward, overlap with pGEXtev
50	GAGGGATCCTGTTTCTCAGacctggaggccag c	66	RhoC 181 reverse, overlap with pGEXtev
51	ggaaagacatgctgctcatagtc <u>aac</u> agcaaggacgagt tcccagagg	n.d.	RhoB F25N mutagenesis
52	gggaagacctgcctcctcatcgtc <u>aac</u> agcaaggatcagttt ccggagg	n.d.	RhoC F25N mutagenesis
53	taaggatccacgcgtgaggaattttg	69	pET6HtevC2 backbone forward
54	gctcgagccctgaaaatacagg	68	pET6HtevC2 backbone reverse
55	gctcgagccctgaaaatacaggttttcggtcgacgagccatc cgattttgaggatggtc	64	pGEXC2MG backbone reverse, replaces thrombin- with TEV-site for protein cleavage
56	gaaacaggatccctctagataaaattcatc	64	pGEXC2MG backbone forward

Table A2. Protein expression constructs used in this study.

The vectors pGEXteV and pET6HtevC2 are custom vectors from the Gautel lab in which the thrombin-site has been replaced with a TEV-site for cleavage of the affinity-tag. They are based on the vectors pGEX-2TK (GE Healthcare) and pET15b (Novagen), respectively. Species abbreviations: (hs) = *homo sapiens*, (gg) = *gallus gallus*, (dr) = *danio rerio*.

Plasmid	Expressed in	Comment
pGEXteV RhoA _{1-181, F25N}	BL21(DE3) RIPL	C-terminus deletion and F25N mutation introduced to enhance solubility and stability. Generated by Daniel Koch (DK).
pGEXteV RhoB _{1-188, F25N}	BL21(DE3) RIPL	C-terminus deletion and F25N mutation introduced to enhance solubility and stability. Generated by DK.
pGEXteV RhoC _{1-181, F25N}	BL21(DE3) RIPL	C-terminus deletion and F25N mutation introduced to enhance solubility and stability. Generated by DK.
pGEXteV Cdc42 ₁₋₁₇₈	BL21(DE3) RIPL	C-terminus deleted to enhance solubility and stability. Generated by DK.
pGEXteV RhoQ ₁₋₁₈₅	BL21(DE3) RIPL	C-terminus deleted to enhance solubility and stability. Generated by DK.
pGEXteV RhoJ ₁₋₁₉₃	BL21(DE3) RIPL	C-terminus deleted to enhance solubility and stability. Generated by DK.
pGEXteV Rac1 ₁₋₁₇₇	BL21(DE3) RIPL	C-terminus deleted to enhance solubility and stability. Generated by DK.
pGEXteV Rac2 ₁₋₁₇₇	BL21(DE3) RIPL	C-terminus deleted to enhance solubility and stability. Generated by DK.
pGEXteV Rac3 ₁₋₁₇₇	BL21(DE3) RIPL	C-terminus deleted to enhance solubility and stability. Generated by DK.
pGEXteV RhoG ₁₋₁₇₇	BL21(DE3) RIPL	C-terminus deleted to enhance solubility and stability. Generated by DK.
pET6HtevC2 Obscurin (hs) SH3	BL21(DE3) RIPL	Generated by Atsushi Fukuzawa (AF).
pET6HtevC2 Obscurin (hs) SH3-DH	BL21(DE3) RIPL, SoluBL21	Generated by DK.
pET6HtevC2 Obscurin (hs) DH ₅₆₉₅₋₅₈₉₉	BL21(DE3) RIPL, SoluBL21	Generated by AF.
pET6HtevC2 Obscurin (hs) DH-PH ₅₆₉₅₋₆₀₁₁	BL21(DE3) RIPL, SoluBL21	Generated by AF.
pET6HtevC2 Obscurin (hs) DH-PH ₅₆₉₅₋₆₀₁₉	BL21(DE3) RIPL, SoluBL21	Generated by AF.
pET6HtevC2 Obscurin (hs) SH3-DH-PH	BL21(DE3) RIPL, SoluBL21	Generated by AF.
pET6HtevC2 Obscurin (hs) SH3-DH	BL21(DE3) RIPL	Generated by DK.
pET6HtevC2 Obscurin (hs) DH ₅₆₆₇₋₅₈₉₉	BL21(DE3) RIPL	Generated by DK.
pET6HtevC2 Obscurin (hs) DH ₅₆₈₁₋₅₈₈₄	BL21(DE3) RIPL	Generated by DK.
pET6HtevC2 Obscurin (hs) DH ₅₆₈₁₋₅₈₈₉	BL21(DE3) RIPL	Generated by DK.
pET6HtevC2 Obscurin (hs) DH ₅₆₈₁₋₅₈₉₁	BL21(DE3) RIPL	Generated by DK.
pET6HtevC2 Obscurin (hs) DH ₅₆₈₁₋₅₈₉₅	BL21(DE3) RIPL	Generated by DK.
pET6HtevC2 Obscurin (hs) DH ₅₆₈₁₋₅₈₉₉	BL21(DE3) RIPL	Generated by DK.
pET6HtevC2 Obscurin (hs) DH ₅₆₈₆₋₅₈₈₄	BL21(DE3) RIPL	Generated by DK.
pET6HtevC2 Obscurin (hs) DH ₅₆₈₆₋₅₈₈₉	BL21(DE3) RIPL	Generated by DK.
pET6HtevC2 Obscurin (hs) DH ₅₆₈₆₋₅₈₉₁	BL21(DE3) RIPL	Generated by DK.
pET6HtevC2 Obscurin (hs) DH ₅₆₈₆₋₅₈₉₅	BL21(DE3) RIPL	Generated by DK.
pET6HtevC2 Obscurin (hs) DH ₅₆₈₆₋₅₈₉₉	BL21(DE3) RIPL	Generated by DK.
pET6HtevC2 Obscurin (hs) DH ₅₆₈₉₋₅₈₈₄	BL21(DE3) RIPL	Generated by DK.
pET6HtevC2 Obscurin (hs) DH ₅₆₈₉₋₅₈₈₉	BL21(DE3) RIPL	Generated by DK.
pET6HtevC2 Obscurin (hs) DH ₅₆₈₉₋₅₈₉₁	BL21(DE3) RIPL	Generated by DK.

pET6HtevC2 Obscurin (hs) DH ₅₆₈₉₋₅₈₉₅	BL21(DE3) RIPL	Generated by DK.
pET6HtevC2 Obscurin (hs) DH ₅₆₈₉₋₅₈₉₉	BL21(DE3) RIPL	Generated by DK.
pET6HtevC2 Obscurin (hs) DH ₅₆₉₁₋₅₈₈₄	BL21(DE3) RIPL	Generated by DK.
pET6HtevC2 Obscurin (hs) DH- PH ₅₆₈₁₋₆₀₀₅	BL21(DE3) RIPL	Generated by DK.
pET6HtevC2 Obscurin (hs) DH- PH ₅₆₈₁₋₆₀₀₉	BL21(DE3) RIPL	Generated by DK.
pET6HtevC2 Obscurin (hs) DH- PH ₅₆₈₁₋₆₀₁₂	BL21(DE3) RIPL	Generated by DK.
pET6HtevC2 Obscurin (hs) DH- PH ₅₆₈₆₋₆₀₀₅	BL21(DE3) RIPL	Generated by DK.
pET6HtevC2 Obscurin (hs) DH- PH ₅₆₈₆₋₆₀₀₉	BL21(DE3) RIPL	Generated by DK.
pET6HtevC2 Obscurin (hs) DH- PH ₅₆₈₆₋₆₀₁₂	BL21(DE3) RIPL	Generated by DK.
pET6HtevC2 Obscurin (hs) DH- PH ₅₆₈₉₋₆₀₀₅	BL21(DE3) RIPL	Generated by DK.
pET6HtevC2 Obscurin (hs) DH- PH ₅₆₈₉₋₆₀₀₉	BL21(DE3) RIPL	Generated by DK.
pET6HtevC2 Obscurin (hs) DH- PH ₅₆₈₉₋₆₀₁₂	BL21(DE3) RIPL	Generated by DK.
pET6HtevC2 Obscurin (hs) DH- PH ₅₆₉₁₋₆₀₀₅	BL21(DE3) RIPL	Generated by DK.
pET6HtevC2 Obscurin (hs) DH- PH ₅₆₉₁₋₆₀₀₉	BL21(DE3) RIPL	Generated by DK.
pET6HtevC2 Obscurin (hs) DH- PH ₅₆₉₁₋₆₀₁₂	BL21(DE3) RIPL	Generated by DK.
pET6HtevC2 Obscurin (hs) PH ₅₈₉₅₋₆₀₀₅	BL21(DE3) RIPL	Generated by DK.
pET6HtevC2 Obscurin (hs) PH ₅₈₉₅₋₆₀₀₉	BL21(DE3) RIPL	Generated by DK.
pET6HtevC2 Obscurin (hs) PH ₅₈₉₅₋₆₀₁₂	BL21(DE3) RIPL	Generated by DK.
pET6HtevC2 Obscurin (hs) PH ₅₉₀₁₋₆₀₀₅	BL21(DE3) RIPL	Generated by DK.
pET6HtevC2 Obscurin (hs) PH ₅₉₀₁₋₆₀₀₉	BL21(DE3) RIPL	Generated by DK.
pET6HtevC2 Obscurin (hs) PH ₅₉₀₁₋₆₀₁₂	BL21(DE3) RIPL	Generated by DK.
pET6HtevC2 Obscurin (hs) DH ₅₆₈₆₋₅₈₈₁ Dbs PH ₈₁₉₋₉₅₃	BL21(DE3) RIPL	Generated by DK.
pET6HtevC2 Obscurin (hs) DH ₅₆₈₆₋₅₈₈₄ Trio PH ₁₄₇₅₋₁₅₉₄	BL21(DE3) RIPL	Generated by DK.
pET6HtevC2 Obscurin (hs) DH ₅₆₈₆₋₅₈₉₅ Trio PH ₁₄₈₆₋₁₅₉₄	BL21(DE3) RIPL	Generated by DK.
pET6HtevC2 Obscurin DH ₅₆₈₁₋₅₈₈₇ (hs) PH ₇₉₆₉₋₈₀₉₆ (gg)	BL21(DE3) RIPL	Generated by DK.
pET6HtevC2 Obscurin DH ₅₆₈₆₋₅₈₈₇ (hs) PH ₇₉₆₉₋₈₀₉₆ (gg)	BL21(DE3) RIPL	Generated by DK.
pET6HtevC2 Obscurin DH ₅₆₈₆₋₅₈₈₇ (hs) PH ₆₀₉₀₋₆₂₁₇ (dr)	BL21(DE3) RIPL	Generated by DK.
pET6HtevC2 Obscurin SH3-DH ₅₆₀₁₋₅₈₈₇ (hs) PH ₆₀₉₀₋₆₂₁₇ (dr)	BL21(DE3) RIPL	Designed by DK, cloned by Bio Basic Inc (Canada).
pET6HtevC2 Obscurin DH ₅₆₈₁₋₅₈₈₇ (hs) PH ₆₀₉₀₋₆₂₁₇ (dr)	BL21(DE3) RIPL	Designed by DK, cloned by Bio Basic Inc (Canada).
pET6HtevC2 Obscurin DH ₅₆₇₃₋₅₈₈₇ (hs) PH ₆₀₉₀₋₆₂₁₇ (dr)	BL21(DE3) RIPL	Designed by DK, cloned by Bio Basic Inc (Canada).
pET6HtevC2 Obscurin DH ₅₆₆₇₋₅₈₈₇ (hs) PH ₆₀₉₀₋₆₂₁₇ (dr)	BL21(DE3) RIPL	Designed by DK, cloned by Bio Basic Inc (Canada).
pET6HtevC2 Obscurin (dr) SH3	BL21(DE3) RIPL	Designed by DK, cloned by Bio Basic Inc (Canada).

pET6HtevC2 Obscurin (dr) SH3-DH	BL21(DE3) RIPL	Designed by DK, cloned by Bio Basic Inc (Canada).
pET6HtevC2 Obscurin (dr) SH3-DH-PH ₅₈₀₆₋₆₂₁₇	BL21(DE3) RIPL	Designed by DK, cloned by Bio Basic Inc (Canada).
pET6HtevC2 Obscurin (dr) SH3-DH-PH ₅₈₀₆₋₆₂₁₇	BL21(DE3) RIPL	Designed by DK, cloned by Bio Basic Inc (Canada).
pET6HtevC2 Obscurin (dr) DH ₅₈₈₄₋₆₀₉₁	BL21(DE3) RIPL	Designed by DK, cloned by Bio Basic Inc (Canada).
pET6HtevC2 Obscurin (dr) DH-PH ₅₈₈₄₋₆₂₁₇	BL21(DE3) RIPL	Designed by DK, cloned by Bio Basic Inc (Canada).
pET6HtevC2 Obscurin (dr) DH-PH ₅₈₇₉₋₆₂₁₇	BL21(DE3) RIPL	Designed by DK, cloned by Bio Basic Inc (Canada).
pET6HtevC2 Obscurin (dr) DH-PH ₅₈₇₂₋₆₂₁₇	BL21(DE3) RIPL	Designed by DK, cloned by Bio Basic Inc (Canada).
pET6HtevC2 Obscurin (dr) PH ₆₀₈₄₋₆₂₁₇	BL21(DE3) RIPL	Designed by DK, cloned by Bio Basic Inc (Canada).
pET6HtevC2 Obscurin (dr) PH ₆₀₉₄₋₆₂₁₇	BL21(DE3) RIPL	Designed by DK, cloned by Bio Basic Inc (Canada).
pET6HtevC2 Larg DH ₇₆₅₋₉₈₆	BL21(DE3) RIPL	Designed by DK, cloned by Bio Basic Inc (Canada).
pET6HtevC2 Vav2 DH ₁₉₁₋₄₀₂	BL21(DE3) RIPL	Designed by DK, cloned by Bio Basic Inc (Canada).
pET6HtevC2 PP1- β ₆₋₃₂₇ , catalytic subunit	SoluBL21	Designed by DK, cloned by Bio Basic Inc (Canada).

A5.1 Experimental procedure of KinaseFinder screening



Info Sheet KinaseFinder

(Version 16)

Purpose of the KinaseFinder Service

The KinaseFinder Service is intended to identify protein kinases, which accept a given test sample (protein or biotinylated peptide) as a substrate in ProQinase's radiometric ³³PanQinase® Assay.

1. Submission of Test Samples

1.1 Protein Samples

Please provide the indicated volumes of a 1 mg/ml stock solution in H₂O or 50 mM HEPES, pH 7.5. Glycerol up to 10%, beta-mercaptoethanol/DTT up to 5 mM and NaCl up to 300 mM are tolerable. The buffer must not contain detergents or imidazole above 50 mM since these will interfere with the assay. If your test sample is not soluble in aqueous solution please contact us. We recommend to ship samples on dry ice to avoid damage of the proteins during transport.

Primary screening will be performed at 5 µg/50 µl sample assay concentration (100 µg/ml).

Hit confirmation will be performed at 2.5 µg/50 µl, 5 µg/50 µl and 10 µg/50 µl sample assay concentration.

Please note: The sample(s) may be returned at customer's expense. From the date of report, the sample(s) will be stored at -20° Celsius for 6 months and will then be discarded without further notice.

KinaseFinder with 1 assay plate (Tyr version):

- 1 ml ⇨ primary hit finding and hit confirmation with max. 3 hits
- 1.5 ml ⇨ primary hit finding and hit confirmation with max. 7 hits

KinaseFinder with 3 assay plates (Ser/Thr version):

- 2.40 ml ⇨ primary hit finding and hit confirmation with max. 3 hits
- 3.25 ml ⇨ primary hit finding and hit confirmation with max. 7 hits

KinaseFinder with 4 assay plates (complete version):

- 3.25 ml ⇨ primary hit finding and hit confirmation with max. 3 hits
- 3.75 ml ⇨ primary hit finding and hit confirmation with max. 7 hits

Protein stock solutions of other concentrations:

Primary screening will be performed at a sample assay concentration 10 fold lower than the provided sample stock solution concentration.

Hit confirmation will be performed at sample assay concentrations 20-fold, 10-fold and 5-fold lower than the sample stock solution concentration.

1.2 Biotinylated Peptide Samples

Please provide a 200 μM stock solution of the biotinylated peptide, depending on the assay setup, see section 2) in H_2O or 50 mM HEPES, pH 7.5. If your test sample is not soluble in aqueous solution please contact us. Volumes required are a tenth of the volumes indicated above for protein test samples. We recommend to ship samples on dry ice to avoid damage of the peptides during transport.

Primary screening will be performed at 1 μM sample assay concentration.

Hit confirmation will be performed at 1 μM , 0.5 μM and 0.25 μM sample assay concentration.

Please note: The sample(s) may be returned at customer's expense. From the date of report, the sample(s) will be stored at -20° Celsius for 6 months and will then be discarded without further notice.

Peptide stock solutions of other concentrations:

Primary screening will be performed at a sample assay concentration which is 200-fold lower than the sample stock solution concentration.

Hit confirmation will be performed at a sample assay concentration which is 200-fold, 400-fold and 800-fold lower than the sample stock solution concentration.

Please note: Testing of biotinylated peptides above 1 μM assay concentration is not possible, due to the limited binding capacity of the streptavidine-coated HTS Plus FlashPlates.

2. Assay Conditions

The KinaseFinder experiments are performed with a radiometric filter plate assay (protein samples) or a radiometric assay based on streptavidin-coated FlashPlate® HTS PLUS plates (biotinylated peptide samples).

2.1 Phosphorylation reaction

The samples are tested against each kinase in singlicate in a 96-well polypropylene microtiter plate in a 50 μ l reaction volume. The reaction cocktail is pipetted in the following order:

- 10 μ l of kinase
- 40 μ l of buffer/ATP/test sample mixture

The reaction cocktail contains 60 mM HEPES-NaOH, pH 7.5, 3 mM MgCl₂, 3 mM MnCl₂, 3 μ M Na-orthovanadate, 1.2 mM DTT, 1 μ M ATP/[γ -³³P]-ATP (approx. 7.5×10^5 cpm per well), protein kinase (1-300 ng/50 μ l, according to the ³³PanQinase[®] screening assay concentration of the respective kinase/kinase lot) and the protein/peptide of interest.

All PKC assays (except the PKC-mu and the PKC-nu assay) additionally contained 1 mM CaCl₂, 4 mM EDTA, 5 μ g/ml Phosphatidylserine and 1 μ g/ml 1,2-Dioleoyl-glycerol.

The CAMK1D, CAMK2A, CAMK2B, CAMK2D, CAMK4, CAMKK1, CAMKK2, DAPK2, EEF2K, MYLK, MYLK2 and MYLK3 assays additionally contained 1 μ g/ml Calmodulin and 0.5 mM CaCl₂.

The PRKG1 and PRKG2 assays additionally contained 1 μ M cGMP.

The DNA-PK assay additionally contained 2.5 μ g/ml DNA.

The reaction cocktails are incubated at 30° C for 60 minutes.

Subsequently, depending on the type of test sample (protein or biotinylated peptide), the reaction cocktails are processed differently (see below).

2.2 Detection of phosphorylated proteins

Reaction cocktails with a protein or peptide as potential substrate are stopped with 20 μ l of 10% (v/s) H₃PO₄. Subsequently, the reaction cocktails are transferred to pre-wetted 96-well filter plates (Millipore MSFC glass filter), followed by 10 min incubation at room temperature. Subsequently, the plates are washed three times with 250 μ l of 150 mM H₃PO₄ and once with 20 μ l of 100% ethanol. After drying the plates for 30 min at 40° C, 50 μ l of scintillator are added and incorporation of ³³P_i ("counting of cpm") is determined with a microplate scintillation counter.

2.3 Detection of phosphorylated, biotinylated peptides

Reaction cocktails with a biotinylated peptide are stopped with 20 μ l of 4.7 M NaCl/35 mM EDTA. Subsequently, the reaction cocktails are transferred to streptavidin-coated FlashPlate[®] HTS PLUS plates followed by 30 min incubation at room temperature on a shaker. Then, the plates are washed three times with 250 μ l of 0.9% NaCl. Incorporation of ³³P_i ("counting of cpm") is determined with a microplate scintillation counter.

3. Evaluation of Raw Data

For evaluation of the results of the filter assay (testing of protein or peptide test samples), kinase autophosphorylation has previously been determined in three independent experiments and a mean autophosphorylation value has been calculated for each kinase. These values (normalized on the radioactivity input of the current experiment) are subtracted from the corresponding raw data obtained with each kinase. Moreover, the median of three background values (sample protein without enzyme) is subtracted from the raw data.

For evaluation of the results from the streptavidin-coated FlashPlate® HTS PLUS plate assay, the activity value (raw counts of the kinase assay plus biotinylated sample peptide as measured in the FlashPlate® HTS PLUS plate assay), the corresponding kinase background value (kinase w/o sample peptide) and the median of three background values of the sample peptide (sample peptide w/o enzyme) are measured. The median of three background values is subtracted from the raw data of the results of the testings of biotinylated sample peptide plus kinase.

4. Hit confirmation

Hits detected in a KinaseFinder experiment can be verified in a hit confirmation experiment, where the test sample will be tested at three different concentrations in triplicate (see section 1.1 and 1.2) at enzyme concentrations according to the standard ³³PanQinase® screening assay concentration of the respective kinase/kinase lot.

5. Protein Kinases

All kinases currently available for the KinaseFinder Service are listed on the following pages.

5.1 Ser/Thr Kinases

No.	Kinase Name	No.	Kinase Name	No.	Kinase Name	No.	Kinase Name
1	ACV-R1	63	COT	125	MEK2	187	PKMYT1
2	ACV-R1B	64	DAPK1	126	MEK5	188	PKN3
3	ACV-R2A	65	DAPK2	127	MEKK2	189	PLK1
4	ACV-R2B	66	DAPK3	128	MEKK3	190	PLK3
5	ACV-RL1	67	DCAMKL2	129	MELK	191	PRK1
6	AKT1	68	DMPK	130	MINK1	192	PRK2
7	AKT2	69	DNA-PK	131	MKK4	193	PRKD2
8	AKT3	70	DYRK1A	132	MKK6SDTD	194	PRKG1
9	AMPK-alpha1	71	DYRK1B	133	MKK7	195	PRKG2
10	ARK5	72	DYRK2	134	MKNK1	196	PRKX
11	ASK1	73	DYRK3	135	MKNK2	197	RAF1 YDYD
12	Aurora-A	74	DYRK4	136	MLK4	198	RIPK2
13	Aurora-B	75	EEF2K	137	MST1	199	RIPK5
14	Aurora-C	76	EIF2AK2	138	MST2	200	ROCK1
15	BMPR1A	77	EIF2AK3	139	MST3	201	ROCK2
16	B-RAF VE	78	ERK1	140	MST4	202	RPS6KA1
17	B-RAF wt	79	ERK2	141	mTOR	203	RPS6KA2
18	BRSK1	80	ERK7	142	MYLK	204	RPS6KA3
19	BRSK2	81	GRK2	143	MYLK2	205	RPS6KA4
20	BUB1B	82	GRK3	144	MYLK3	206	RPS6KA5
21	CAMK1D	83	GRK4	145	NEK1	207	RPS6KA6
22	CAMK2A	84	GRK5	146	NEK11	208	S6K
23	CAMK2B	85	GRK6	147	NEK2	209	S6K-beta
24	CAMK2D	86	GRK7	148	NEK3	210	SAK
25	CAMK2G	87	GSG2	149	NEK4	211	SGK1
26	CAMK4	88	GSK3-alpha	150	NEK6	212	SGK2
27	CAMKK1	89	GSK3-beta	151	NEK7	213	SGK3
28	CAMKK2	90	HIPK1	152	NEK9	214	SIK1 aa1-350
29	CDC42BPA	91	HIPK2	153	NIK	215	SIK2
30	CDC42BPB	92	HIPK3	154	NLK	216	SLK
31	CDC7/ASK	93	HIPK4	155	p38-alpha	217	SNARK
32	CDK1/CycA	94	HRI	156	p38-beta	218	SNK
33	CDK1/CycE	95	IKK-alpha	157	p38-delta	219	SRPK1
34	CDK16/CycK	96	IKK-beta	158	p38-gamma	220	SRPK2
35	CDK1/CycB1	97	IKK-epsilon	159	PAK1	221	STK17A
36	CDK2/CycA	98	IRAK1	160	PAK2	222	STK23
37	CDK2/CycE	99	IRAK4	161	PAK3	223	STK25
38	CDK3/CycE	100	JNK1	162	PAK4	224	STK33
39	CDK4/CycD1	101	JNK2	163	PAK6	225	STK39
40	CDK4/CycD3	102	JNK3	164	PAK7	226	TAOK2
41	CDK5/p25NCK	103	LIMK1	165	PASK	227	TAOK3
42	CDK5/p35NCK	104	LIMK2	166	PBK	228	TBK1
43	CDK6/CycD1	105	LRRK G2019S	167	PDK1	229	TGFB-R1
44	CDK6/CycD3	106	LRRK2 I2020T	168	PHKG1	230	TGFB-R2
45	CDK7/CycH	107	LRRK2 R1441C	169	PHKG2	231	TLK1
46	CDK8/CycC	108	LRRK2 wt	170	PIM1	232	TLK2
47	CDK9/CycK	109	MAP3K1	171	PIM2	233	TSF1
48	CDK9/CycT	110	MAP3K10	172	PIM3	234	TSK2
49	CHK1	111	MAP3K11	173	PKA	235	TSSK1
50	CHK2	112	MAP3K7/MAP3K7IP1	174	PKC-alpha	236	TTBK1
51	CK1-alpha1	113	MAP3K9	175	PKC-beta1	237	TTBK2
52	CK1-delta	114	MAP4K2	176	PKC-beta2	238	TTK
53	CK1-epsilon	115	MAP4K4	177	PKC-delta	239	VRK1
54	CK1-gamma1	116	MAP4K5	178	PKC-epsilon	240	VRK2
55	CK1-gamma2	117	MAPKAPK2	179	PKC-eta	241	WEE1
56	CK1-gamma3	118	MAPKAPK3	180	PKC-gamma	242	WNK1
57	CK2-alpha1	119	MAPKAPK5	181	PKC-iota	243	WNK2
58	CK2-alpha2	120	MARK1	182	PKC-mu	244	WNK3
59	CLK1	121	MARK2	183	PKC-nu	245	ZAK
60	CLK2	122	MARK3	184	PKC-theta		
61	CLK3	123	MARK4	185	PKC-zeta		
62	CLK4	124	MEK1 wt	186	PKC-zeta wt aa184-592		

5.2 Tyr Kinases

No.	Kinase Name	No.	Kinase Name
1	ABL1 T315I	63	MERTK
2	ABL1 wt	64	MET T1250M
3	ABL2	65	MET wt
4	ACK1	66	MET Y1235D
5	ALK F1174L (GST-HIS-tag)	67	MUSK
6	ALK L1196M (GST-HIS-tag)	68	PDGFR-alpha D842V
7	ALK wt	69	PDGFR-alpha wt
8	AXL	70	PDGFR-beta
9	BLK	71	PYK2
10	BMX	72	RET V804M
11	BRK	73	RET wt
12	BTK	74	RON
13	CSF1-R	75	ROS
14	CSK	76	SRC
15	DDR2 T654M	77	SRMS
16	DDR2 wt	78	SYK
17	EGF-R T790M	79	TEC
18	EGF-R wt	80	TIE2 wt
19	EPHA1	81	TIE2 Y897S
20	EPHA2	82	TNK1
21	EPHA3	83	TRK-A
22	EPHA4	84	TRK-B
23	EPHA5	85	TRK-C
24	EPHA6	86	TXK
25	EPHA7	87	TYK2
26	EPHA8	88	TYRO3
27	EPHB1	89	VEGF-R1
28	EPHB2	90	VEGF-R2
29	EPHB3	91	VEGF-R3
30	EPHB4	92	WEE1
31	ERBB2 wt	93	YES
32	ERBB4	94	ZAP70
33	FAK		
34	FER		
35	FES		
36	FGF-R1 V561M		
37	FGF-R1 wt		
38	FGF-R2		
39	FGF-R3 K650E		
40	FGF-R3 wt		
41	FGF-R4		
42	FGR		
43	FLT3 D835Y		
44	FLT3 ITD		
45	FLT3 wt		
46	FRK		
47	FYN		
48	HCK		
49	IGF1-R		
50	INS-R		
51	INSR-R		
52	ITK		
53	JAK1		
54	JAK2		
55	JAK3		
56	KIT D816V		
57	KIT T670I		
58	KIT wt		
59	LCK		
60	LTK		
61	LYN		
62	MATK		

A5.2 Experimental procedure of phosphorylation site identification

The following technical specifications were provided by the Metabolomics and Proteomics Laboratory of the Bioscience Technology Facility of the University of York:

The coomassie stained bands have been analysed for phosphopeptide identification as requested. Briefly, protein was digested with trypsin in-gel, following reduction with DTE and alkylation with iodoacetamide. Peptides were extracted from gel before phosphopeptide enrichment using MagReSyn titanium dioxide microparticles. Enriched phosphopeptides were loaded onto a 50 cm EN C18 PepMap column with elution over a 1 h acquisition driven by a Waters mClass nanoUPLC. Eluted peptides were measured using a Thermo Orbitrap Fusion Tribrid mass spectrometer, with MS spectra acquired in the Orbitrap and MS2 spectra acquired in parallel, following HCD fragmentation, in the linear ion trap.

Data were searched against the protein sequence provided, appended with common proteomic contaminants, using PEAKS Studio X Pro. Carbamidomethylation of Cys was set as a fixed modification and oxidation of Met and phosphorylation of Ser, Thr and Tyr were all set as variable.

Peptide matches were filtered to require individual peptide assignments to have a $-\log_{10}P$ score of >20 , which equates to $p < 0.01$. When assessed at this threshold against a decoy database search, all searches yielded an empirical false discovery rate of $<1\%$. In all three cases the expected protein identification was made. Phosphorylated peptides are also detected in all three samples.

Please find a summary of the results attached, listing all identified peptides. There is a separate tab in the file for each sample.

When assessing the results please note the final column "Ascore = $-\log_{10}P$ site localisation prob.". Here you will find the site localisation probability for each PTM detected. (...) The probability for the peptide identification including a single phosphorylation is given in row C as $-\log_{10}P$ ID prob. (...). Looking at column Q you will see (...) the site localisation probability for the phosphorylation to sit at the Ser annotated (...). Below each table of peptide identifications there is a visual representation of the peptides and phosphorylation identified, as also presented below:

ID filter = -10logP >20, q1weid FDR <1%

Protein Accession	Peptide	"-10logP ID prob."	Mass (Da)	Length	ppm	m/z	Charge	RT	Area SH3DH	Fraction	Scan	#Feature	Start	End	PTM	"Ascore = -10logP site localisation prob."
protein1 D528_b	R.QGVVSPAYLDR	80.15	1290.6356	11	-0.6	646.32	2	47.54	5.76E+03	1	13994	1	56	66		
protein1 D528_b	R.VQAESVWVSTAIQEFYK	76.38	1896.9833	17	-1.1	633.33	3	50.96	5.14E+03	1	14748	2	191	207		
protein1 D528_b	R.VQAESVWVSTI+79.97 AIQEFYK	72.85	1976.9496	17	-0.3	989.48	2	51.28	0	1	14840	0	191	207	Phosphorylation (STY)	T10:Phosphorylation (STY):8.69
protein1 D528_b	K.IPEWGAAEPEPFGAVSEDFYK	72.01	2607.1653	24	-1.9	1304.6	2	49.77	6.61E+04	1	14490	2	70	93		
protein1 D528_b	R.VQAESVWVSI+79.97 AIQEFYK	55.31	1976.9496	17	-2.1	989.48	2	50.89	1.42E+03	1	14735	1	191	207	Phosphorylation (STY)	S9:Phosphorylation (STY):0.00

1 SSIFDIYVVT ADYLPGLGAEQ DAITLREGQY VEVLDAHPL RMLVETKTK SPSRSQQWVS **PAYIDRRRLK** **SPFWRGAEP** ■ Phosphorylation (STY) (+79.97)

81 **EPFGAVSED EYKARLSSVI** QELLSSEQAF VEELQFQSH HLQHLERCPH VFIAVAGQKA VIFRNRVDIG RPHSSFLQEL

161 QCCDTDDVA MCFIKNQAAF EQYLEFLVGR **VOAESVWVST AIQEFYK**KYA EEALLAGDES QPPPPPLQHY LEQFEVRFQR

241 YQALLKELIR NKARNQNC A LLEQAYAVS ALPQRAENKL HVSLMENYPG TLQALGEPIR Q

In these images peptide identifications are also filtered to $-10\log_{10}P > 20$. Phosphorylation annotated above the line of amino acids represents those with site localisation Ascores > 20 .

Please note that it is common for site localisation to be more confident where potential phosphosites are more spread out. Where sites are very close together they can be harder to distinguish. Also you should consider the possibility that both sites may be detected within the same spectrum as different phosphorylation on adjacent or near adjacent residues may change the retention time very little and if they are not resolved by LC will have identical MS1 masses and so appear in the same chimeric spectrum.

Appendix B: Supplementary
material for [chapter 4](#)

SUPPLEMENTAL DATA

When is an obscurin variant pathogenic?
The impact of Arg4344Gln and Arg4444Trp variants on protein-
protein interactions and protein stability

Atsushi Fukuzawa^{1,†}, Daniel Koch^{1,†,*}, Sarah Grover¹,
Martin Rees¹, Mathias Gautel^{1,*}

¹Randall Centre for Cell & Molecular Biophysics, King's College London, United Kingdom

[†] authors contributed equally and are listed alphabetically.

* corresponding author: daniel.koch@kcl.ac.uk, Randall Centre for Cell & Molecular Biophysics,
New Hunt's House, 18-20 Newcomen Street, London SE1 1UL. Phone: +44 2078486438.

* corresponding author: mathias.gautel@kcl.ac.uk, Randall Centre for Cell & Molecular
Biophysics, New Hunt's House, 18-20 Newcomen Street, London SE1 1UL. Phone: +44 2078486709.

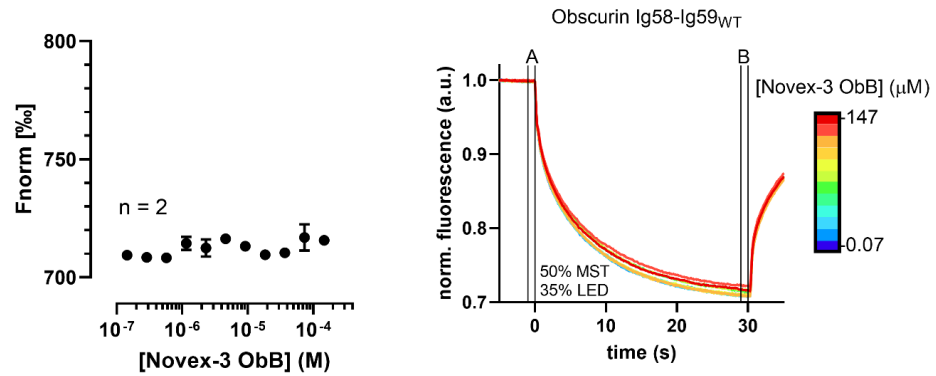


Figure S1: MST showed no binding between obscurin Ig58-Ig59 and recombinant novex-3 obscurin binding region (ObB). Dose response graph (left) based on signal at Lane B (MST-laser on) divided by signal at Lane A (MST-laser off) in the MST traces (right).

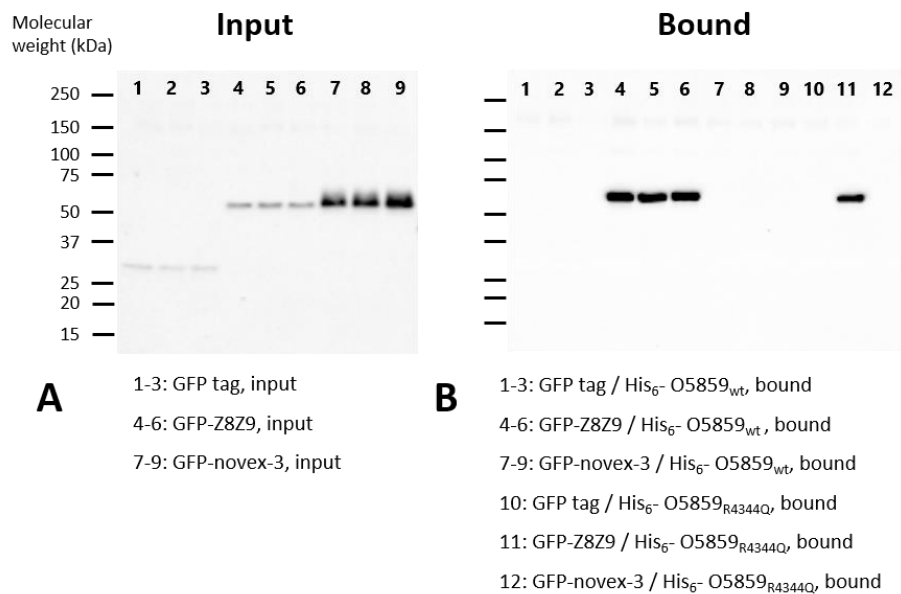


Figure S2: Ni-NTA beads pull down assay. Titin novex-3 isoform showed no interaction with obscurin Ig58-Ig59. A) Cell lysates from HEK293A cells transfected with GFP-empty (lane1-3; negative control), GFP-Z8Z9 (lane4-6; positive control) or GFP-novex-3 ObB (lane7-9) were applied to Ni-NTA beads coated with His₆-O5859 wild type or R4344Q mutant. B) Bound fractions. Assays with His₆-O5859 wild type were triplicated.

CLUSTAL O(1.2.4) multiple sequence alignment

```

Bang et al. 2001  PPSSVEYFESPKSPDLYFNPSDITKQSSIHSGETVERYSTPLGEVAERYSTPSEGEVGE 60
This study      -PPSSVEYFESPKSPDLYFNPSDITKQSSIHSGETVERYSTPLGEVAERYSTPSEGEVGE 59
                *****
                ↑
Bang et al. 2001  RYSTPPGETLERYSTPPGETLERYSTPPGETLERYSTPPGETLERYSTPPGETLERYSTP 120
This study      RYSTPPGETLERYSTPPGETLERYSTPPGETLERYSTPPGETLERYSTPPGETLERYSTP 119
                *****

Bang et al. 2001  PGEALERYSIPTGGPNPTGTFKTYPSKIEREDGTPNEHFYTPTEERGSAYEIWRSDSFGT 180
This study      PGEALERYSIPTGGPNPTGTFKTYPSKIEREDGTPNEHFYTPTEERGSAYEIWRSDSFGT 179
                *****
                ↑

Bang et al. 2001  PNEAIEPKDNEMPPSFIE 198
This study      PNEAIEPKDNEMPPSFIE 197
                *****

```

Figure S3: Alignment of the ObB sequence from novex-3 used in Bang *et al.* 2001 versus the sequence used in this study. While our sequence is shorter by one N-terminal proline (first arrow), the ObB sequence used in Bang *et al.* 2001 features a methionine at position 5139 instead of arginine. This residue is arginine in NM_133379 (transcript variant novex-3, titin) and methionine is reported as missense variant (dbSNP ID = rs66677602, AGG > ATG, minor allele frequency = 0.0773, ClinVar evaluation = benign).

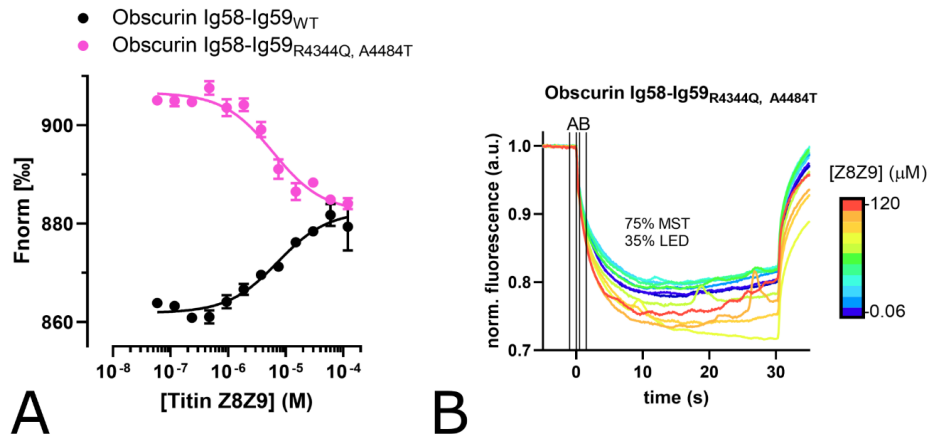


Figure S4: (A) The A4484T variant (pink) causes a decrease in the normalised fluorescence of the temperature jump signal upon ligand binding, whereas WT (black) and R4344Q and R4444W variants (not shown) lead to increased fluorescence upon ligand binding. (B) Bumpy segments in the later parts of the MST traces indicate formation of aggregates

Supplementary references:

Bang, M-L., Centner, T., Fornoff, F., Geach, A. J., Gotthardt, M., McNabb, M., Witt, C. C., Labeit, D., Gregorio, C. C., Granzier, H., et al. (2001) The Complete Gene Sequence of Titin, Expression of an Unusual \approx 700-kDa Titin Isoform, and Its Interaction With Obscurin Identify a Novel Z-Line to I-Band Linking System. *Circ. Res.*, **89**, 1065–1072.

Appendix C: Supplementary
material for [chapter 5](#)

- Supplementary Information -
Homo-Oligomerisation in Signal Transduction:
Dynamics, Homeostasis, Ultrasensitivity, Bistability

Daniel Koch

 orcid.org/0000-0002-4893-1774

Randall Centre for Cell & Molecular Biophysics,
King's College London, London SE1 1UL, United Kingdom
E-mail: daniel.koch@kcl.ac.uk

Contents

1	Ensuring thermodynamical consistency in models of homo-oligomers subject to post-translational modification	2
2	Proof: conservation of oligomerisation rates	10
3	Reaction rates and ODEs for unbalanced trimerisation model including PTMs	13
4	Balancing rates of the trimerisation model including PTMs	15
5	Computational methods	17
6	Other supplementary figures	17
7	Experimental techniques and designs for testing model predictions	19
8	References	23

1 Ensuring thermodynamical consistency in models of homo-oligomers subject to post-translational modification

As outlined in the main text, consideration of PTMs in models of homo-oligomerisation can lead to thermodynamic inconsistencies. Before we incorporate PTMs into our models we will therefore formulate some biochemical intuitions and expectations which will later guide us to avoid such inconsistencies. Let us suppose an oligomeric protein can be modified by a PTM at a single site. For the sake of simplicity, we assume that the site lies remote from the oligomerisation interface and does not alter any of the reaction parameters. Intuitively, we would then expect the following to be true:

- (a) The association rate constants (a1), dissociation rate constants (a2) and therefore equilibrium and dissociation constants (a3) are identical for the following oligomerisation reactions:
 - only unmodified protein
 - only modified protein
 - modified with unmodified protein
- (b) If the modifying enzyme is added to an equilibrated mixture of completely unmodified monomers and oligomers, both monomers and oligomers will be modified over time, yet the total concentrations of monomers and oligomers remains constant.
- (c) There are $\binom{2+n-1}{n}$ possibilities to combine unmodified/modified monomers into symmetric n-tamers. Thus, if equal parts of unmodified/modified monomers are mixed to form n-tamers, the isoform distribution of n-tamers with $0 \leq i \leq n$ modified subunits will be binomial.

The notation and assumptions introduced in the main text are repeated for convenience: Let A^* , AA^* , AA^{**} , ... denote modified monomers, dimers with one and dimers with two modified protomers and so forth. Due to assumed symmetry, molecules such as A^*A and AA^* are identical. Keeping the assumption that each oligomeric species is formed through binary association reactions, it follows from (a1)-(c1) that each pair of molecular species X,Y which is able to associate in the absence of any PTMs is also able to associate with identical reaction parameters regardless of how many protomers of X or Y are modified. We will assume that there is a modifying enzyme $E1$ and a demodifying enzyme $E2$ which operate by a non-cooperative, irreversible and distributive mechanism and that all molecular species, regardless the number of their protomers, are (de-)modified with the same kinetic parameters, i.e. the oligomeric state does not influence the (de-)modification reactions. These assumptions reflect

the situation where a PTM does not induce conformational changes and lies remote from the oligomerisation interface, allowing the enzymes to access the PTM site equally in all oligomeric species. We therefore expect the individual monomeric and oligomeric species to compete for enzymes $E1$ and $E2$. In situations with multiple competing substrates S_1, \dots, S_n an irreversible Michaelis-Menten type rate law of the form:

$$v_i = \frac{V_{max}S_i}{K_{m_i}(1 + \sum_{j \in J \setminus \{i\}} \frac{S_j}{K_{m_j}}) + S_i},$$

where $J = \{1, \dots, n\}$, can be employed to describe the rate of consumption v_i of substrate S_i [1]. That is, the individual substrates act as competitive inhibitors for each other. We are now able to formulate reaction schemes, reaction rates and model equations.

Figure S1A shows the reaction scheme and rate expressions for the dimerisation model based on mass action kinetics for oligomerisation and mentioned Michaelis-Menten type rate law for addition and removal of PTMs. The equations are:

$$\begin{aligned} \frac{d}{dt}[A] &= 2 \cdot v6 + v8 + v12 - 2 \cdot v5 - v7 - v11, & \frac{d}{dt}[A^*] &= v8 + 2 \cdot v10 + v11 - v7 - 2 \cdot v9 - v12, \\ \frac{d}{dt}[AA] &= v2 + v5 - v1 - v6, & \frac{d}{dt}[AA^*] &= v1 + v4 + v7 - v2 - v3 - v8, \\ \frac{d}{dt}[AA^{**}] &= v3 + v9 - v4 - v10. \end{aligned}$$

Figure S1B shows the reaction scheme for the trimerisation model including PTMs. See supplementary section 3 for reaction rates and model equations. Note that the reaction scheme for trimerisation and a single PTM is already more complex than the tetramerisation scheme without PTMs. For oligomerisation, we will use the following parameter values: $10^7 \text{ mol}^{-1} \text{ s}^{-1}$ for dimer formation, $10^9 \text{ mol}^{-1} \text{ s}^{-1}$ for trimer formation, 10 s^{-1} for dissociation of dimers and trimers. We chose catalytic rate constants to be $k_{cat} = 1 \text{ s}^{-1}$ and Michaelis constants to be $K_m = 1 \mu\text{M}$ for all (de-)modification reactions in both models.

Let us first consider the effects of adding catalytic concentrations of E1 to an equilibrated mixture of monomers and oligomers. Interestingly, as the modification reaction proceeds, transient changes in the total concentrations of monomeric and oligomeric species occur (Figure S2A; the total concentrations being the sum of concentrations of all modified isoforms for a given monomeric or oligomeric species). The amplitude and direction of these transients appear to be influenced by the maximum number of protomers. Intuitively, the phenomenon results from the accessibility of additional oligomerisation routes during the modification reaction. Consider for example the dimerisation reaction scheme (Figure S1A). If A is either completely unmodified or modified, a single reaction route between a monomeric and a dimeric species is available. If a mixture of A and A^* is present, a third route appears: the reaction between A and A^* to

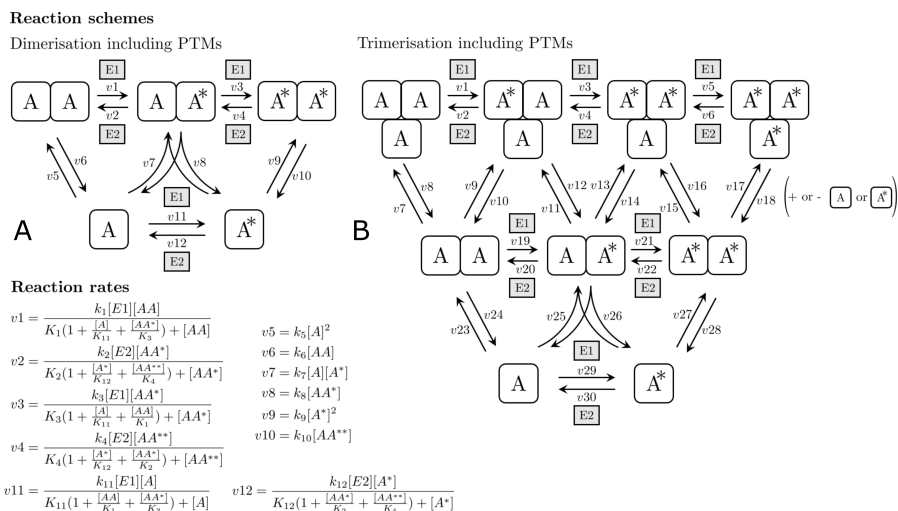
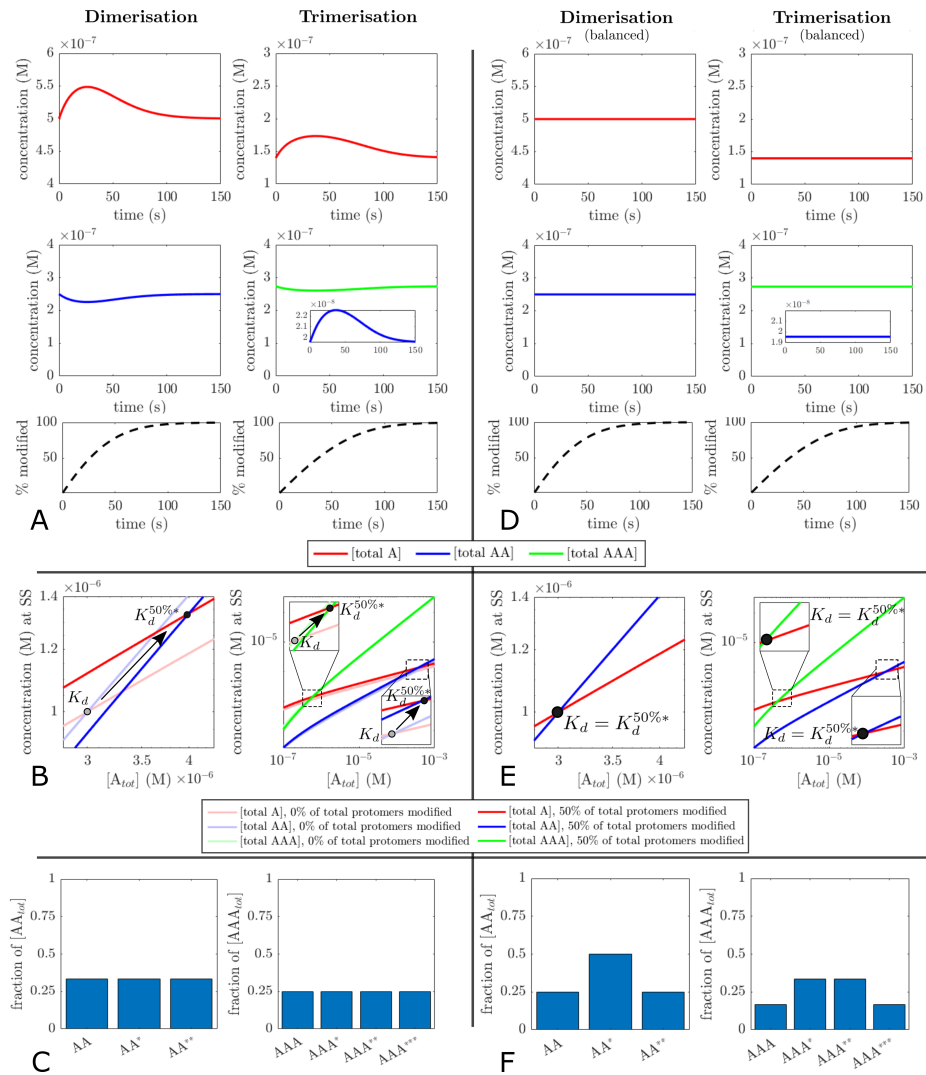


Figure S1 Reaction schemes for the mass action kinetics models of dimerisation (A) and trimerisation (B) including reversible post-translational modifications. See supplementary section 3 for reaction rates and ODEs of the trimerisation model.

AA^* . We would therefore expect that decreasing the velocity of oligomerisation/dissociation or increasing the speed of modification would diminish the effect, as both changes would limit A 's capacity to change its oligomerisation state during the transition time from completely unmodified protein to complete modification. Indeed, while decreasing the velocity of oligomerisation/dissociation reduces the amplitude, increasing the enzyme concentration limits the peak width of the amplitude (Figure S4).

Clearly, these transient changes contradict expectation (b) and no experimental data so far (as far as the author is aware) reported transient alterations of the oligomerisation state upon post-translation without affecting association/dissociation rates. To further explore the models and to test whether the transient changes could be a modelling artefact, let us see what happens if equimolar mixtures of modified and unmodified A are simulated to steady state. According to (a3) we would expect K_d values to be identical to that of completely unmodified and completely modified A . We would furthermore expect a binomial distribution of modified oligomers according to (c). However, both models show altered K_d values (Figure S2B) and a uniform distribution of modified oligomers (Figure S2C). Taken together, this suggests that the transient changes are indeed a modelling artefact resulting from thermodynamic inconsistency.

**Figure S2**

Behaviour of di- and trimerisation models upon post-translational modification. (A,D) timecourses of total monomer and total oligomer concentrations after addition of $50nM$ $[E1]$ starting with $A_{tot} = 10\mu M$ at equilibrium. Dimerisation rate constants: $10^7 mol^{-1}s^{-1}$, trimerisation rate constants: $10^9 mol^{-1}s^{-1}$, dissociation rate constants of dimers and trimers: $10s^{-1}$. Black-dotted curves show progress of the modification reaction. (B,E) apparent dissociation constants and (C,F) distribution of PTM isoforms of the highest order oligomer in equimolar mixtures of modified and unmodified protein at equilibrium.

Where did we go astray if using simple mass action kinetics, arguably the most established deterministic modelling approach for chemical reactions, leads to thermodynamic inconsistency? The answer is: naively deriving ordinary differential equations by applying mass action kinetics and stoichiometrical balancing to reaction schemes such as in [Figure S1](#). To circumvent this issue, we need to introduce a more general notation for oligomeric species and formulate a further expectation.

Let A_n^m denote a m -times modified n -tamer, i.e. an oligomeric complex with $n \in \mathbb{N}^{\geq 1}$ identical subunits of which $0 \leq m \leq n$ carry a PTM at site x . Let $j \in \mathbb{N}^{\geq 1}$ be the number of reversible bimolecular association reactions between lower-order complexes A_r^p and A_s^q able to form A_n^m , where $r + s = n$.

Next, let $I(A_n) = \{\{r_1, s_1\}, \{r_2, s_2\}, \dots\}$ define the set of actually occurring combinations of oligomeric orders of A_n 's educts $A_{r_i}^p$ and $A_{s_i}^q$, where $p + q \leq n$ and $r_i + s_i = n$. For example, if a hexamer can be assembled from dimers with tetramers and from monomers with pentamers (of any PTM status), $I(A_6)$ would be the set $\{\{2, 4\}, \{1, 5\}\}$.

From (a1) and (a2) it follows that all forward steps between $A_{r_i}^p$ and $A_{s_i}^q$ producing A_n^m have the same association rate constant k_i and each corresponding reverse step has the same dissociation rate constant k_i' for all possible values of m, p and q . Unaltered rate constants imply unaltered equilibrium constants. Therefore, we expect that

- (d) the PTM status is irrelevant for the equilibrium. Thus, the equilibrium is solely determined by the total concentrations of each n -tamer, i.e. the sum of all PTM-isoforms of A_n :

$$[A_{n,tot}] = \sum_{m=0}^n [A_n^m]$$

In other words: from the perspective of the oligomerisation equilibrium, all PTM isoforms of a n -tamer are treated as a single species. [Figure S3](#) illustrates these definitions and the equilibrium situation.

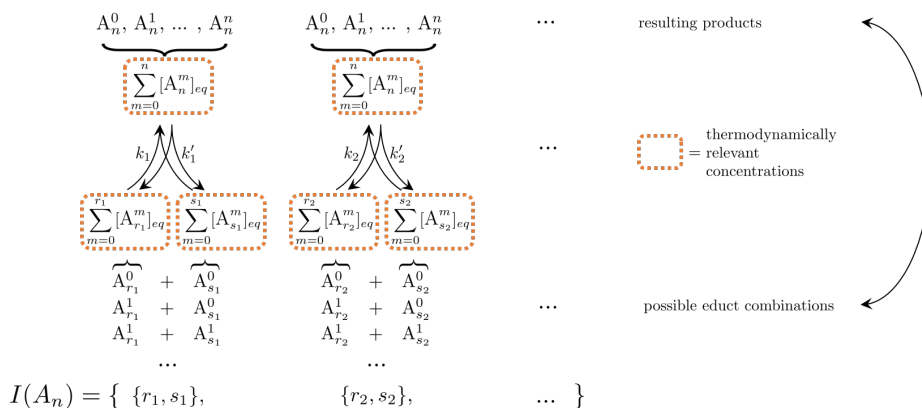
**Figure S3**

Illustration of the n-tamer equilibrium situation if a PTM does not influence the oligomerisation reaction. According to expectation (d) in the main text, we expect the equilibrium to be solely determined by the total n-tamer concentrations $\sum_{m=0}^n [A_n^m]_{eq}$ if the PTM status does not influence oligomerisation. The set $I(A_n)$ denotes the actually occurring combinations of oligomeric orders of A_n 's educts, i.e. $|I(A_n)|$ is the number of reversible reactions that would produce/consume A_n if PTMs were not taken into consideration.

We can now formulate the following principle:

Conservation of oligomerisation rates

If a PTM does not influence the parameters of an oligomerisation reaction, the sum of all rates v_i , $1 \leq i \leq j$, of reactions leading to a n-tamer A_n of any modification status is equal to the association rates based on the total concentrations of A_n 's educts (i.e. all modification isoforms). Conversely, the sum of all rates v'_i , $1 \leq i \leq j$, of reactions dissociating A_n of any modification status is equal to the dissociation rate based on A_n 's total concentration. That is at all times

$$\sum_{i=1}^j v_i = \sum_{i \in I} (k_i \cdot \sum_{m=0}^r [A_{r_i}^m] \cdot \sum_{m=0}^s [A_{s_i}^m]),$$

and

$$\sum_{i=1}^j v'_i = \sum_{i \in I} (k'_i \cdot \sum_{m=0}^n [A_n^m]).$$

We call the right-hand side of each identity the *effective rates*.

The principle's name is chosen in analogy to the conservation of mass as it conserves the reaction rates at given total concentrations of educts regardless the distribution of PTM isoforms. Although it might appear complicated, it is straightforward to illustrate the principle using

dimerisation as an example. Applying it to [Figure S1A](#) yields $I(A_2) = \{\{1, 1\}\}$ and thus

$$v_5 + v_7 + v_9 = k([A] + [A^*])^2 \quad (1)$$

and

$$\begin{aligned} v_6 + v_8 + v_{10} = \\ k'([AA] + [AA^*] + [AA^{**}]) \end{aligned} \quad (2)$$

for association rate constants $k = k_5 = k_7 = k_9$ and dissociation rate constants $k' = k_6 = k_8 = k_{10}$.

How does this principle help us to avoid thermodynamic inconsistency? The principle relates the j reaction rates from the reaction scheme (left-hand side (LHS) of (1) and (2)) to the thermodynamically expected effective rates (right-hand side (RHS) of (1) and (2)). Instead of assigning *a priori* rate expressions based on mass action kinetics, we will assign rates only after making sure the principle is not violated. In the first step of this check, we will expand the RHS of the rate conservation identity. In a second step, we will substitute the rates on the LHS with their mass action kinetics expression. Next, we will compare both sides: if they are equal, all rates can readily be identified with their mass action kinetics expression. If they are not equal, we balance the terms on the LHS where the discrepancy occurs by introducing coefficients that ensure the validity of the identity. Lastly, we identify the respective rates with the balanced terms. Let us illustrate this using equations (1) and (2) derived from the dimerisation scheme:

(1) \rightarrow *expanding RHS, substituting LHS:*

$$\begin{aligned} k[A]^2 + k[A][A^*] + k[A^*]^2 \\ = k[A]^2 + 2k[A][A^*] + k[A^*]^2 \end{aligned}$$

\rightarrow *balancing deviating terms in LHS:*

$$\begin{aligned} k[A]^2 + \mathbf{2} \cdot k[A][A^*] + k_1[A^*]^2 \\ = k[A]^2 + 2k[A][A^*] + k[A^*]^2 \end{aligned}$$

\rightarrow *assigning reaction rates:*

$$\begin{aligned} v_5 = k[A]^2, v_7 = 2k[A][A^*] \\ v_9 = k[A^*]^2 \end{aligned}$$

Optionally, we can reintroduce the reaction indices for the rate constants at this stage.

(2) → *expanding RHS, substituting LHS:*

$$\begin{aligned} & k'[AA] + k'[AA^*] + k'[AA^{**}] \\ & = k'[AA] + k'[AA^*] + k'[AA^{**}] \end{aligned}$$

→ *no balancing necessary*

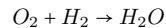
→ *assigning reaction rates:*

$$\begin{aligned} v_6 &= k'[AA], v_8 = k'[AA^*] \\ v_{10} &= k'[AA^{**}] \end{aligned}$$

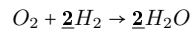
It is straightforward to apply the same procedure to the trimerisation model (cf. supplementary section 4). Other things being equal, the dimerisation and trimerisation model updated with the balanced rate expressions exhibit neither transient changes in the oligomerisation upon modification (Figure S2D), nor shifts in the apparent K_d of equimolar mixtures of unmodified/modified A (Figure S2E). The distribution of PTM isoforms at equilibrium is binomial (Figure S2F). Taken together, this indicates that the balanced models are indeed thermodynamically consistent.

The postulated rate conservation principle is no fundamental law and can readily be proven using the principle of detailed balance [5] as lemma (cf. suppl. section 2).

For a more intuitive understanding of this balancing procedure, it might be helpful to appreciate its similarity to stoichiometric balancing. Consider, for example, the chemical equation for the reaction of oxygen with hydrogen to water:



As the reader will have spotted, there are two oxygen atoms on the LHS, but only one on the RHS of the equation. As this violates the law of conservation of mass, we need to balance the equation by adding stoichiometric coefficients:



The rate balancing procedure presented in this paper is conceptually identical: As the PTM is assumed not to influence oligomerisation, we know that total formation and dissociation rates of oligomers are conserved; they must be the same as for unmodified protein. However, the PTM increases the number of possible oligomeric species due to combinatorial expansion. This expansion is asymmetric because there are more possibilities to combine modified and unmodified subunits to a n -tamer the higher its order: two for a monomer, three for a dimer, four for a trimer and so forth (cf. Figure S1B). This creates additional oligomerisation routes and alters the net rates of oligomer formation and dissociation, thereby violating the rate conservation principle. To avoid this, we need to balance this purely combinatorial effect by introducing balancing coefficients for the rate expressions.

2 Proof: conservation of oligomerisation rates

To show the validity of the principle of conservation of oligomerisation rates, we require the principle of detailed balance. While it has often been treated as a fundamental postulate, it can be derived from microscopic reversibility in physics, which is why we treat it as a lemma [3,4].

Lemma: principle of detailed balance

“When a system is at equilibrium this means that the forward rate of a molecular process has to be equal to the reverse rate of that process. Applying this to a chemical reaction observed on a macroscopic scale means that at equilibrium, the forward rate of each step is equal to the reverse rate of that step; this is the principle of detailed balance.” [5]

For a system in which some molecular species S can be formed by $j \in \mathbb{N}^{\geq 1}$ reversible reactions this means at equilibrium:

$$\sum_{i=1}^j v_i = \sum_{i=1}^j v'_i, \quad (3)$$

where v_i is the forward rate and v'_i the reverse rate of reaction i .

Although the multitude of sums might give the impression of being complicated, the idea for the principle’s proof itself is simple: we find that applying the principle of detailed balance and the assumption that the PTM does not influence oligomerisation (expectation (e) from the main text) to the n-tamer equilibrium concentrations results in the same equations as given by the postulated conservation principle but restricted to equilibrium. We can then prove the principle by contradiction. If we assume that the conservation principle would be false and apply the resulting inequalities to the equilibrium situation, we obtain direct contradictions to the before derived equations describing the equilibrium. For convenience, the principle to be proven is repeated in summarized form below:

Conservation of oligomerisation rates

Let A_n be an oligomeric complex with $n \in \mathbb{N}^{\geq 1}$ protomers¹ which can be formed through $j \in \mathbb{N}^{\geq 1}$ reversible bimolecular association reactions between lower-order complexes $A_{r_i}^p$ and $A_{s_i}^q$, where $p + q \leq n$ and $r_i + s_i = n$, $i \in I(A_n)$. The PTM does not influence the oligomerisation reaction.

It follows that at all times, the sum of all rates v_i , $1 \leq i \leq j$, of reactions leading to A_n of any modification status is the association rate based on the total concentrations (i.e. all modification isoforms) of A_n 's educts. The sum of all rates v'_i , $1 \leq i \leq j$, of reactions dissociating A_n of any modification status is equal to the dissociation rate based on A_n 's total concentration. That is

$$\sum_{i=1}^j v_i = \sum_{i \in I} (k_i \cdot \sum_{m=0}^{r_i} [A_{r_i}^m] \cdot \sum_{m=0}^{s_i} [A_{s_i}^m]), \quad (4)$$

and

$$\sum_{i=1}^j v'_i = \sum_{i \in I} (k'_i \cdot \sum_{m=0}^n [A_n^m]). \quad (5)$$

Proof: For the construction of the contradiction it is necessary to consider the situation at equilibrium. By assumption, the PTM does not influence oligomerisation. From (a1) and (a2) it follows that all forward steps between $A_{r_i}^p$ and $A_{s_i}^q$ producing A_n^m have the same association rate constant k_i and each corresponding reverse step has the same dissociation rate constant k'_i for all possible values of m, p and q . According to (d), equilibrium is only determined by the total concentration of each oligomeric complex, i.e. the relevant educt concentrations are $\sum_{m=0}^{r_i} [A_{r_i}^m]_{eq}$ and $\sum_{m=0}^{s_i} [A_{s_i}^m]_{eq}$, whereas the relevant product concentration is $\sum_{m=0}^n [A_n^m]_{eq}$. Thus, the expressions for forward and reverse rates are

$$k_i \cdot \sum_{m=0}^{r_i} [A_{r_i}^m]_{eq} \cdot \sum_{m=0}^{s_i} [A_{s_i}^m]_{eq}$$

and

$$k'_i \cdot \sum_{m=0}^n [A_n^m]_{eq},$$

respectively, for all $i \in I$. Applying the principle of detailed balance (3) to the formation and dissociation of A_n at equilibrium and substituting above rate expressions therefore gives:

$$\sum_{i=1}^j v_i = \sum_{i \in I} (k_i \cdot \sum_{m=0}^{r_i} [A_{r_i}^m]_{eq} \cdot \sum_{m=0}^{s_i} [A_{s_i}^m]_{eq}) = \sum_{i \in I} (k'_i \cdot \sum_{m=0}^n [A_n^m]_{eq}) = \sum_{i=1}^j v'_i. \quad (6)$$

¹ Monomers are considered as oligomers for purely formal reasons.

Separating (4) into its first and last identity yields

$$\sum_{i=1}^j v_i = \sum_{i \in I} (k_i \cdot \sum_{m=0}^r [A_{r_i}^m]_{eq} \cdot \sum_{m=0}^s [A_{s_i}^m]_{eq}), \quad (7)$$

and

$$\sum_{i=1}^j v'_i = \sum_{i \in I} (k'_i \cdot \sum_{m=0}^n [A_n^m]_{eq}). \quad (8)$$

Let us for a moment assume that the conservation of oligomerisation rates would not be true. We have to distinguish three cases: equation (4) is false, equation (5) is false, both (4) and (5) are false.

Case 1: equation (4) is false, i.e.

$$\begin{aligned} \sum_{i=1}^j v_i &\neq \sum_{i \in I} (k_i \cdot \sum_{m=0}^r [A_{r_i}^m] \cdot \sum_{m=0}^s [A_{s_i}^m]), \\ \text{at equilibrium } \sum_{i=1}^j v_i &\neq \sum_{i \in I} (k_i \cdot \sum_{m=0}^r [A_{r_i}^m]_{eq} \cdot \sum_{m=0}^s [A_{s_i}^m]_{eq}), \end{aligned}$$

in contradiction to (7).

Case 2: equation (5) is false, i.e.

$$\begin{aligned} \sum_{i=1}^j v'_i &\neq \sum_{i \in I} (k'_i \cdot \sum_{m=0}^n [A_n^m]), \\ \text{at equilibrium } \sum_{i=1}^j v'_i &\neq \sum_{i \in I} (k'_i \cdot \sum_{m=0}^n [A_n^m]_{eq}), \end{aligned}$$

in contradiction to (8).

Case 3: Both (4) and (5) are false. The contradiction follows from case 1 and case 2.

□

3 Reaction rates and ODEs for unbalanced trimerisation model including PTMs

This section contains the reaction rates and ODEs for the trimer reaction scheme presented in Figure S1B.

Reaction rates

association & dissociation reactions

$$\begin{aligned}
 v7 &= k_7[A][AA] & v8 &= k_8[AAA] \\
 v9 &= k_9[A^*][AA] & v10 &= k_{10}[AAA^*] \\
 v11 &= k_{11}[A][AA^*] & v12 &= k_{12}[AAA^*] \\
 v13 &= k_{13}[A^*][AA^*] & v14 &= k_{14}[AAA^{**}] \\
 v15 &= k_{15}[A][AA^{**}] & v16 &= k_{16}[AAA^{**}] \\
 v17 &= k_{17}[A^*][AA^{**}] & v18 &= k_{18}[AAA^{***}] \\
 v23 &= k_{23}[A]^2 & v24 &= k_{24}[AA] \\
 v25 &= k_{25}[A][A^*] & v26 &= k_{26}[AA^*] \\
 v27 &= k_{27}[A^*]^2 & v28 &= k_{28}[AA^{**}]
 \end{aligned}$$

modification reactions

$$\begin{aligned}
 v1 &= \frac{k_1[E1][AAA]}{K_1(1 + \frac{[A]}{K_{29}} + \frac{[AA]}{K_{19}} + \frac{[AA^*]}{K_{21}} + \frac{[AAA^*]}{K_3} + \frac{[AAA^{**}]}{K_5}) + [AAA]} \\
 v3 &= \frac{k_3[E1][AA^*]}{K_3(1 + \frac{[A]}{K_{29}} + \frac{[AA]}{K_{19}} + \frac{[AA^*]}{K_{21}} + \frac{[AAA]}{K_1} + \frac{[AAA^*]}{K_5}) + [AA^*]} \\
 v5 &= \frac{k_5[E1][AA^{**}]}{K_5(1 + \frac{[A]}{K_{29}} + \frac{[AA]}{K_{19}} + \frac{[AA^*]}{K_{21}} + \frac{[AAA]}{K_1} + \frac{[AAA^*]}{K_3}) + [AA^{**}]} \\
 v19 &= \frac{k_{19}[E1][AA]}{K_{19}(1 + \frac{[A]}{K_{29}} + \frac{[AA^*]}{K_{21}} + \frac{[AAA]}{K_1} + \frac{[AAA^*]}{K_3} + \frac{[AAA^{**}]}{K_5}) + [AA]} \\
 v21 &= \frac{k_{21}[E1][AA^*]}{K_{21}(1 + \frac{[A]}{K_{29}} + \frac{[AA]}{K_{19}} + \frac{[AAA]}{K_1} + \frac{[AAA^*]}{K_3} + \frac{[AAA^{**}]}{K_5}) + [AA^*]} \\
 v29 &= \frac{k_{29}[E1][A]}{K_{29}(1 + \frac{[AA]}{K_{19}} + \frac{[AA^*]}{K_{21}} + \frac{[AAA]}{K_1} + \frac{[AAA^*]}{K_3} + \frac{[AAA^{**}]}{K_5}) + [A]}
 \end{aligned}$$

demodification reactions

$$\begin{aligned}
 v2 &= \frac{k_2[E2][AAA^*]}{K_2(1 + \frac{[A^*]}{K_{30}} + \frac{[AA^*]}{K_{20}} + \frac{[AA^{**}]}{K_{22}} + \frac{[AAA^*]}{K_4} + \frac{[AAA^{**}]}{K_6}) + [AAA^*]} \\
 v4 &= \frac{k_4[E2][AAA^{**}]}{K_4(1 + \frac{[A^*]}{K_{30}} + \frac{[AA^*]}{K_{20}} + \frac{[AA^{**}]}{K_{22}} + \frac{[AAA^*]}{K_2} + \frac{[AAA^{**}]}{K_6}) + [AAA^{**}]} \\
 v6 &= \frac{k_6[E2][AAA^{***}]}{K_6(1 + \frac{[A^*]}{K_{30}} + \frac{[AA^*]}{K_{20}} + \frac{[AA^{**}]}{K_{22}} + \frac{[AAA^*]}{K_2} + \frac{[AAA^{**}]}{K_4}) + [AAA^{***}]} \\
 v20 &= \frac{k_{20}[E2][AA^*]}{K_{20}(1 + \frac{[A^*]}{K_{30}} + \frac{[AA^{**}]}{K_{22}} + \frac{[AAA^*]}{K_4} + \frac{[AAA^{**}]}{K_6}) + [AA^*]} \\
 v22 &= \frac{k_{22}[E2][AA^{**}]}{K_{22}(1 + \frac{[A^*]}{K_{30}} + \frac{[AA^*]}{K_{20}} + \frac{[AA^{**}]}{K_2} + \frac{[AAA^*]}{K_4} + \frac{[AAA^{**}]}{K_6}) + [AA^{**}]} \\
 v30 &= \frac{k_{30}[E2][A^*]}{K_{30}(1 + \frac{[AA^*]}{K_{20}} + \frac{[AA^{**}]}{K_{22}} + \frac{[AAA^*]}{K_2} + \frac{[AAA^{**}]}{K_4} + \frac{[AAA^{***}]}{K_6}) + [A^*]}
 \end{aligned}$$

The ODE system is:

$$\begin{aligned} \frac{d}{dt}[A] &= v_8 + v_{12} + v_{16} + 2 \cdot v_{24} + v_{26} + v_{30} - v_7 - v_{11} - v_{15} - 2 \cdot v_{23} - v_{25} - v_{29} \\ \frac{d}{dt}[A^*] &= v_{10} + v_{14} + v_{18} + 2 \cdot v_{28} + v_{26} + v_{29} - v_9 - v_{13} - v_{17} - 2 \cdot v_{27} - v_{25} - v_{30} \\ \frac{d}{dt}[AA] &= v_8 + v_{10} + v_{20} + v_{23} - v_7 - v_9 - v_{19} - v_{24} \\ \frac{d}{dt}[AA^*] &= v_{12} + v_{14} + v_{19} + v_{22} + v_{25} - v_{11} - v_{13} - v_{20} - v_{21} - v_{26} \\ \frac{d}{dt}[AA^{**}] &= v_{16} + v_{18} + v_{21} + v_{27} - v_{15} - v_{17} - v_{22} - v_{28} \\ \frac{d}{dt}[AAA] &= v_2 + v_7 - v_1 - v_8 \\ \frac{d}{dt}[AAA^*] &= v_1 + v_4 + v_9 + v_{11} - v_2 - v_3 - v_{10} - v_{12} \\ \frac{d}{dt}[AAA^{**}] &= v_3 + v_6 + v_{13} + v_{15} - v_4 - v_5 - v_{14} - v_{16} \\ \frac{d}{dt}[AAA^{***}] &= v_5 + v_{17} - v_6 - v_{18} \end{aligned}$$

4 Balancing rates of the trimerisation model including PTMs

As for the dimer model, we work under the assumption that all association steps leading to an oligomeric complex A_n have the same rate constant k_i and all dissociation steps have the same rate constant k'_i . As trimers can only be formed by association of dimers and monomers (i.e. $I(A_3) = \{\{1, 2\}\}$), we leave out the index $i \in I$ for convenience. We begin the rate balancing of the trimerisation model by noticing that the lower part of the trimerisation scheme depicted in [Figure S1B](#) is structurally identical to the dimerisation scheme in [Figure S1A](#). We thus can use the same rate balancing coefficients for the dimerisation steps in the trimer model, i.e. we balance v_{25} by multiplying it with 2 to obtain $v_{25} = 2k[A][A^*]$. We next apply the rate conservation principle to the formation of trimers and obtain:

$$v_7 + v_9 + v_{11} + v_{13} + v_{15} + v_{17} = k[A_t][AA_t] = k([A] + [A^*]) \cdot ([AA] + [AA^*] + [AA^{**}])$$

→ *expanding RHS, substituting LHS:*

$$\begin{aligned} & k[AA][A] + k[AA][A^*] + k[AA^*][A] + k[AA^*][A^*] + k[AA^{**}][A] + k[AA^{**}][A^*] \\ & = k[AA][A] + k[AA][A^*] + k[AA^*][A] + k[AA^*][A^*] + k[AA^{**}][A] + k[AA^{**}][A^*] \end{aligned}$$

→ *no balancing necessary*

→ *assigning reaction rates:*

$$\begin{aligned} v_7 &= k[AA][A] \\ v_9 &= k[AA][A^*] \\ v_{11} &= k[AA^*][A] \\ v_{13} &= k[AA^*][A^*] \\ v_{15} &= k[AA^{**}][A] \\ v_{17} &= k[AA^{**}][A^*] \end{aligned}$$

Applying the rate conservation principle to the dissociation of trimers we obtain:

$$v_8 + v_{10} + v_{12} + v_{14} + v_{16} + v_{18} = k'[AAA_t] = k'([AAA] + [AAA^*] + [AAA^{**}] + [AAA^{***}])$$

→ *expanding RHS, substituting LHS:*

$$\begin{aligned} & k'[AAA] + k'[AAA^*] + k'[AAA^*] + k'[AAA^{**}] + k'[AAA^{**}] + k'[AAA^{***}] \\ & = k'[AAA] + k'[AAA^*] + k'[AAA^{**}] + k'[AAA^{***}] \end{aligned}$$

We notice that the dissociation rates for singly and dually modified trimers appear twice in the LHS, but only once in the RHS. We therefore need to

→ *balance deviating terms in LHS:*

$$\begin{aligned} k'[AAA] + \frac{1}{2}k'[AAA^*] + \frac{1}{2}k'[AAA^*] + \frac{1}{2}k'[AAA^{**}] + \frac{1}{2}k'[AAA^{**}] + k'[AAA^{***}] \\ = k'[AAA] + k'[AAA^*] + k'[AAA^{**}] + k'[AAA^{***}] \end{aligned}$$

→ *assigning reaction rates:*

$$\begin{aligned} v_8 &= k'[AAA] \\ v_{10} &= \frac{1}{2}k'[AAA^*] \\ v_{12} &= \frac{1}{2}k'[AAA^*] \\ v_{14} &= \frac{1}{2}k'[AAA^{**}] \\ v_{16} &= \frac{1}{2}k'[AAA^{**}] \\ v_{18} &= k'[AAA^{***}] \end{aligned}$$

5 Computational methods

Presented models have been implemented as MATLAB[®] scripts for numerical simulation and model analysis. All simulations were performed using the ode23s integrator. Sensitivity analysis has been performed as described in [2]. All model code is accessible in the BioModels database under: <https://www.ebi.ac.uk/biomodels/MODEL2003160001>.

Bifurcation diagrams have been generated using a custom algorithm that iteratively identifies the unstable steady states. If the algorithm does not converge within the specified number of iterations, it approximates the unstable steady state. The approximation is based on the distribution of concentrations from all time courses taking advantage of the fact that simulations very close to the unstable steady state take a long time until they eventually tip to either of the stable steady states. For more details, please refer to: <https://www.ebi.ac.uk/biomodels/MODEL1910220002>.

6 Other supplementary figures

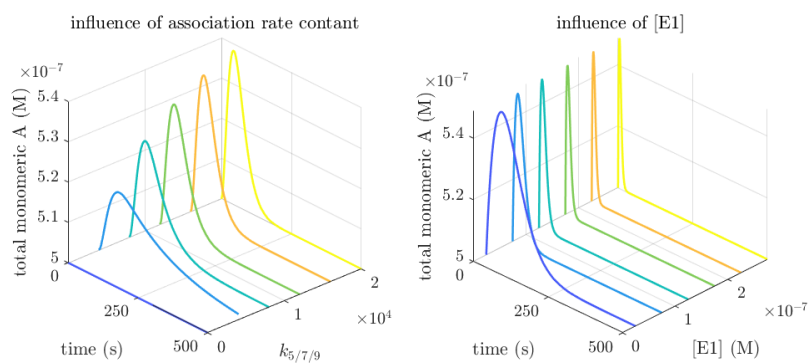
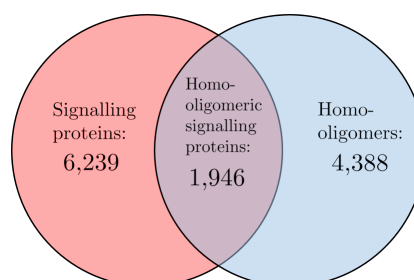


Figure S4
Dependence of transient changes in the mass action dimerisation model on association rate constants and concentration of the modifying enzyme.

**Figure S5**

Bioinformatic analysis of the intersection between homo-oligomerisation and signalling. Proteins annotated with the Gene Ontology (GO) term 'Signal Transduction' (GO:0007165) are considered signalling proteins. For proteins which homo-oligomerise, this is estimated from a large human protein-protein interaction network compiled from various databases and published experiments (see [6]). 'self loops' (i.e. edges in the network which connects a protein to itself) are considered as homo-oligomerisation. The number of proteins which homo-oligomerise is simply the number of 'self loops' in this network. The number of oligomeric signalling proteins is then the number of unique protein IDs associated with the above mentioned GO-term that also feature a self loop.

7 Experimental techniques and designs for testing model predictions

Since I am not aware of published experimental data that confirms the presented model predictions for a specific signalling protein or pathway, this section contains a brief overview of suitable methods and experimental designs that could be used to test the model predictions presented in this paper for a specific context.

Methods for detecting the oligomeric state of proteins

A variety of methods for detecting the oligomeric state of proteins exists, ranging from measuring populations of molecules *in vitro* to single molecule techniques allowing to measure individual binding/unbinding events in living cells. For a more detailed discussion of advantages and disadvantages of individual techniques the reader is referred to [7, 8]. An instructive example of a study analysing a protein's oligomeric state using multiple approaches can be found in [9]. The following table gives an overview and refers to reviews or studies which have applied the respective method:

Method	Description	References
Size exclusion chromatography	Simple and widely available method for separating proteins by their hydrodynamic radius. Molecular weight of fractions can be estimated from retention standards, relative oligomer distribution can be approximated by peak integration. When combined with light scattering measurements, absolute molecular weights and thus oligomeric order can be determined. Low temporal resolution, unsuited for complex analytes.	[10, 11]
Analytical ultracentrifugation	Allows for the determination of the absolute molecular weight of oligomeric complexes as well as equilibrium constants of the oligomerisation reaction.	[12]
Native PAGE	Polyacrylamide gel electrophoresis method that preserves the oligomeric state (since samples are not diluted and boiled in SDS sample buffer). If combined with Western-blotting, the oligomeric state of a protein can be determined even in complex solutions such as cell homogenates.	[13, 14]

Method	Description	References
Fluorescence correlation spectroscopy	Powerful technique which allows to determine both rate constants and equilibrium constants of oligomerisation reactions. Applicable both <i>in vitro</i> and in live cells. Data analysis can be difficult and might require itself some modelling.	[15–17]
Others	Other techniques which can give information about oligomeric complexes are mass-spectrometry, single-particle tracking and quantitative imaging approaches such as FRET-, BRET- and TIRF-microscopy. More details can be found in the listed references.	[18–21]

Methods for detecting the PTM status of proteins

The probably most common approach for detecting the PTM status of a protein is the use of PTM specific antibodies which are commercially available for many better characterised proteins. If used for Western-blotting in combination with native PAGE, this should allow to resolve the modification status for different oligomeric species (and even to estimate the fraction of modified protomers if a linear standard is used alongside). In case of phosphorylations, the PTM status can alternatively be determined by using the Phos-tagTM reagent in combination with native PAGE if no PTM-specific antibody is available [22]. If recombinant proteins are used, the phosphorylation status of a protein can also be visualised e.g. by ProQTM diamond stain.

Analysing the modification status in homogenates can blur the real behaviour of a signalling network taking place at the single-cell level, making it harder to detect phenomena such as ultrasensitivity and bistability [23]. If an antibody is suited for immunofluorescence imaging or FACS, it is possible to resolve the PTM at a single cell level, although the analysis of many conditions (e.g. stimulus doses) can be laborious and material-consuming. This and the limited temporal resolution of immunofluorescence imaging or FACS make these approaches unsuitable for studying the dynamics of a PTM status in live cells. Increasingly sophisticated biosensors for PTMs can overcome this issue and have been applied successfully for quantitative biology purposes [24, 25], although a suitable biosensor design for a protein of interest is a significant challenge on its own.

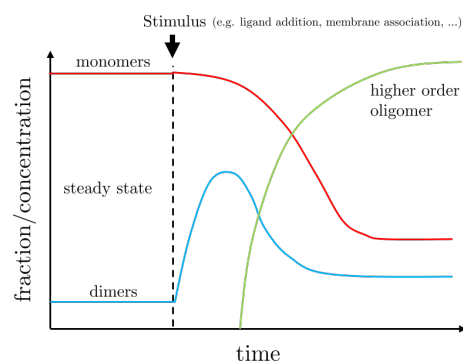
Experimental designs

This subsection discusses possible experimental designs to detect oligomerisation transients as a means of dynamic signal encoding, monomer homeostasis and ultrasensitivity/bistability in a context of interest.

Oligomerisation transients

As this phenomenon is mainly expected for proteins which oligomerise upon some stimulus (e.g. ligand binding to a receptor or recruitment to a membrane), suitable experiments to test this prediction will begin to monitor the oligomeric state of the protein of interest in the absence of any stimulus. If the protein is approximately at a steady state, the oligomerisation stimulus is added (e.g. a ligand, drug, or liposomes) and changes in oligomeric states are monitored (cf. Figure S6). The phenomenon would be confirmed if at least one oligomeric species shows a significant increase, followed by a significant decrease and increase in higher order oligomers. Key requirements for these experiments are a technique that can distinguish between different oligomeric species with sufficient temporal resolution (fluorescence correlation spectroscopy, single molecule techniques, FRET, perhaps even native PAGE if the process is not too fast) and the possibility to apply the oligomerisation stimulus in the experimental setting.

To evaluate whether the transient is involved in dynamic signal encoding, further functional studies that can assign distinct biological activities to different oligomeric forms (e.g. binding to interaction partners, enzymatic activity) will be necessary.

**Figure S6**

Experimental design to test oligomerisation transients.

Monomer homeostasis

The experimental design for testing whether or not monomer homeostasis occurs is in principle straightforward: measuring the equilibrium concentrations of different oligomeric species at different total protein concentrations. Ideally, this would be done with recombinant purified protein of a known concentration. Size exclusion chromatography, analytical ultracentrifugation, fluorescence correlation spectroscopy and native PAGE should in principle all be suitable techniques for this. Ideally, the range of total protein concentration would be varied by 3-5 orders of magnitude to get a clear picture of the oligomerisation curves on a double-logarithmic

scale. This could pose a challenge for the dynamic range of many methods. If native PAGE is applied as illustrated in Figure S7, the gel can be stained with OrioleTM Fluorescent Gel Stain which can show good linearity for >2 orders of magnitude of total protein amount (personal experience of the author).

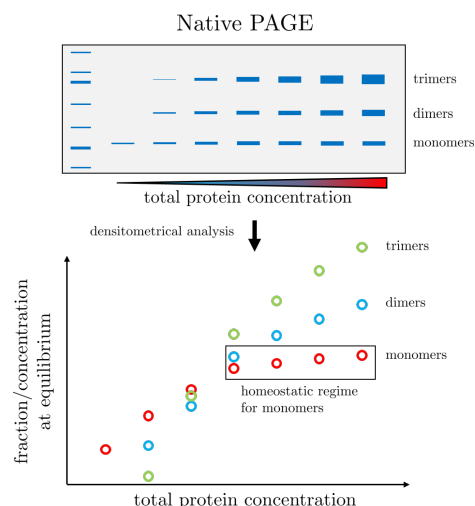


Figure S7

Experimental design to test monomer homeostasis as illustrated for native PAGE.

Ultrasensitivity and bistability

Detecting ultrasensitivity in the PTM status of an oligomer can be simply performed by dose-response experiments in which changes of the stimulus dose lead to changes in the PTM status. The confirmation of bistability ultimately relies on the detection of hysteresis, i.e. dependence of the steady state on the initial conditions of the system. While the general design of such experiments is illustrated in Figure S8, the reader is referred to studies featuring experimental confirmations of bistability for more details [24, 26–28]. Since bistability also occurs for monomers in the models (via equilibration and substrate competition), it may not be necessary to resolve the individual oligomeric species in these experiments, i.e. it would be sufficient to focus on the total modification across oligomeric species.

Ideally, oligomerisation deficient mutants would serve as a negative control. Since ultrasensitivity and bistability in the presented models rely on pseudo-multisite modification in oligomers, preventing oligomerisation should diminish/abolish ultrasensitivity and bistability in the experiments.

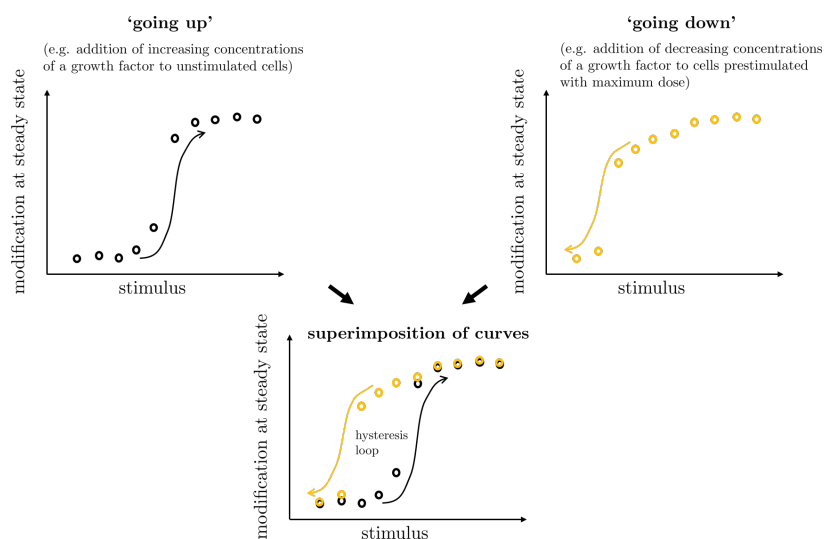


Figure S8
General experimental design to test for bistability: the signalling network has a biochemical ‘memory’ for its previous modification state (hysteresis).

8 References

- Schäuble S, Stavrum AK, Puntervoll P, Schuster S, Heiland I. Effect of substrate competition in kinetic models of metabolic networks. *FEBS Letters*. 2013, 587: 2818–2824.
- Ingalls B. *Mathematical Modeling in Systems Biology: An Introduction*. MIT Press, Cambridge MA. 2013.
- Mahan BH. Microscopic reversibility and detailed balance. An analysis. *J Chem Educ*. 1975, 52: 299–302.
- Gorban AN. Detailed balance in micro- and macrokinetics and micro-distinguishability of macro-processes. *Results in Physics*. 2014, 4: 142–147
- Alberty RA. Principle of Detailed Balance in Kinetics. *J Chem Educ*. 2004, 81: 1206–1209.
- Chung SS, Laddach A, NShaun BT, Fraternali F. Short loop motif profiling of protein interaction networks in acute myeloid leukaemia. *bioArxiv*. 2018, doi: <https://doi.org/10.1101/306886>.
- Gell DA, Grant RP, Mackay JP. The detection and quantitation of protein oligomerization. In: Matthews JM, editor. *Protein Dimerization and Oligomerization in Biology*. Springer, New York. 2012.
- Okamoto K, Hiroshima M, Sako Y. Single-molecule fluorescence-based analysis of protein conformation, interaction, and oligomerization in cellular systems. *Biophys Rev*. 2018, 10: 317–326.
- Cardarelli S, Miele AE, Zamparelli C, Biagioni S, Naro F, Malatesta F, et al. The oligomeric assembly of the phosphodiesterase-5 is a mixture of dimers and tetramers: A putative role in the regulation of function. *BBA - Gen Sub*. 2018, 1862: 2183–2190.

10. Moulintraffort L, Bruneaux M, Nazabal A, Allegro D, Giudice E, Zal F, et al. Biochemical and Biophysical Characterization of the Mg²⁺-induced 90-kDa Heat Shock Protein Oligomers. *J Biol Chem.* 2010, 285: 15100–15110.
11. Folta-Stogniew E. Oligomeric States of Proteins Determined by Size-Exclusion Chromatography Coupled With Light Scattering, Absorbance, and Refractive Index Detectors. In: Nedelkov D, Nelson RW, editors. *New and Emerging Proteomic Techniques*. Totowa, NJ: Humana Press; 2006.
12. Taylor IA, Eccleston JF, Rittinger K. Sedimentation Equilibrium Studies. In: Fu H, editor. *Protein-Protein Interactions: Methods and Applications*. Totowa, NJ: Humana Press; 2004.
13. Wittig I, Braun H-P, Schägger H. Blue native PAGE. *Nat Protoc.* 2006, 1: 418–428.
14. Niepmann M. Discontinuous native protein gel electrophoresis: pros and cons. *Expert Rev Proteomic.* 2007, 4: 355–361.
15. Thompson NL, Lieto AM, Allen NW. Recent advances in fluorescence correlation spectroscopy. *Curr Opin Struct Biol.* 2002, 12: 634–641.
16. Rajagopalan S, Huang F, Fersht AR. Single-Molecule characterization of oligomerization kinetics and equilibria of the tumor suppressor p53. *Nucleic Acids Res.* 2011, 39:2294–2303.
17. Kanno DM, Levitus M. Protein Oligomerization Equilibria and Kinetics Investigated by Fluorescence Correlation Spectroscopy: A Mathematical Treatment. *J Phys Chem B.* 2014, 118: 12404–12415.
18. Guo H, An S, Ward R, Yang Y, Liu Y, Guo X-X, et al. Methods used to study the oligomeric structure of G-protein-coupled receptors. *Biosci Rep.* 2017, 37.
19. Castell OK, Dijkman PM, Wiseman DN, Goddard AD. Single molecule fluorescence for membrane proteins. *Methods.* 2018, 147: 221–228.
20. Chakraborty H, Chattopadhyay A. Excitements and Challenges in GPCR Oligomerization: Molecular Insight from FRET. *ACS Chem Neurosci.* 2015, 6: 199–206.
21. Cai X, Bai B, Zhang R, Wang C, Chen J. Apelin receptor homodimer-oligomers revealed by single-molecule imaging and novel G protein-dependent signaling. *Sci Rep.* 2017, 7: 40335.
22. Deswal S, Beck-García K, Blumenthal B, Dopfer EP, Schamel WWA Detection of phosphorylated T and B cell antigen receptor species by Phos-tag SDS- and Blue Native-PAGE. *Immunol Lett.* 2010, 130, 51–56.
23. Purvis JE, Lahav G. Encoding and Decoding Cellular Information through Signaling Dynamics. *Cell.* 2013, 152: 945–956.
24. Mochida S, Rata S, Hino H, Nagai T, Novák B. Two Bistable Switches Govern M Phase Entry. *Curr Biol.* 2016, 26: 3361–3367.
25. Damayanti NP, Buno K, Narayanan N, Harbin SLV, Deng M, Irudayaraj JMK. Monitoring focal adhesion kinase phosphorylation dynamics in live cells. *Analyst.* 2017, 142: 2713–2716.
26. Pomerening JR, Sontag ED, Ferrell Jr JE. Building a cell cycle oscillator: hysteresis and bistability in the activation of Cdc2. *Nat Cell Biol.* 2003, 5: 346–351.
27. Byrne KM, Monsefi N, Dawson JC, Degasperis A, Bukowski-Wills J-C, Volinsky N, et al. Bistability in the Rac1, PAK, and RhoA Signaling Network Drives Actin Cytoskeleton Dynamics and Cell Motility Switches. *Cell Syst.* 2016, 2: 38–48.
28. Rata S, Rodriguez MFSP, Joseph S, Peter N, Iturra FE, Yang F, et al. Two Interlinked Bistable Switches Govern Mitotic Control in Mammalian Cells. *newblock Curr Biol.* 2018, 28: 3824–3832.

Appendix D: Supplementary
material for [chapter 6](#)

Cell Reports, Volume 36

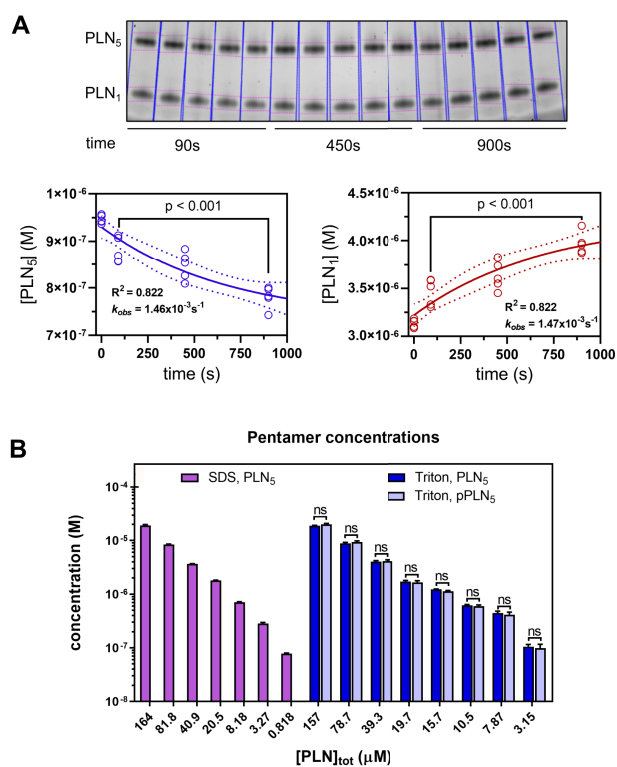
Supplemental information

**Molecular noise filtering in the
 β -adrenergic signaling network
by phospholamban pentamers**

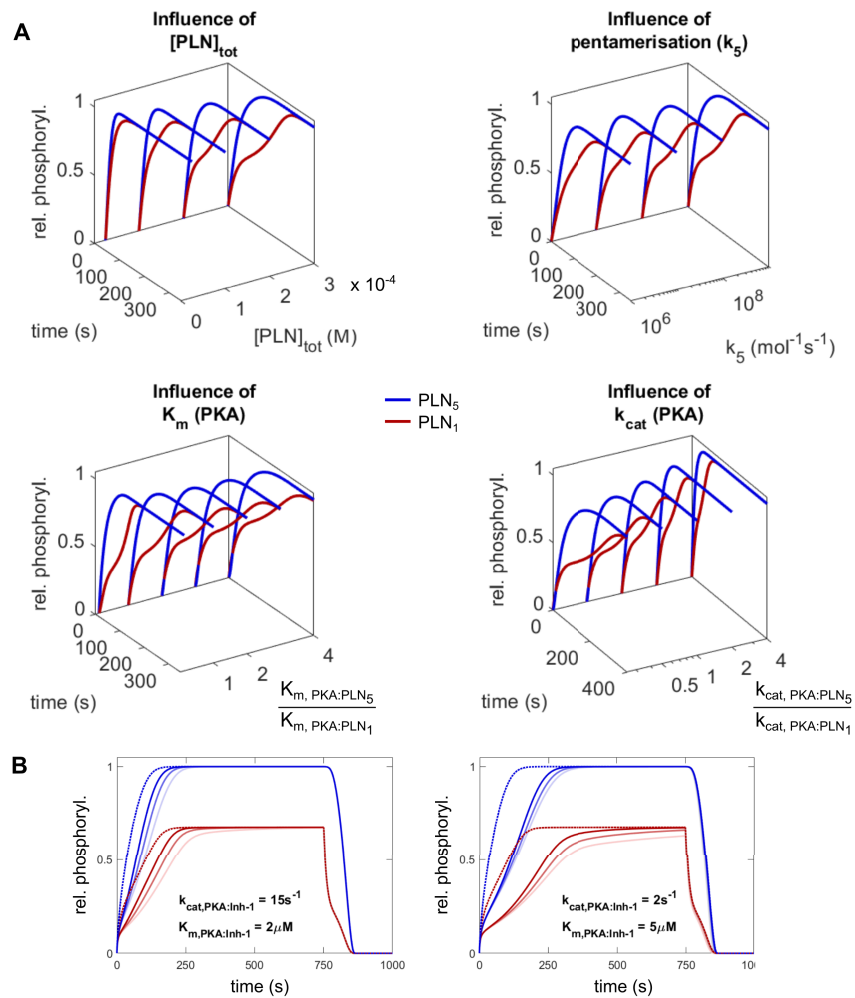
Daniel Koch, Alexander Alexandrovich, Florian Funk, Ay Lin Kho, Joachim P. Schmitt, and Mathias Gautel

Supplemental Information

Supplemental Figures

**Figure S1**

Dissociation dynamics and influence of phosphorylation on pentamerization in TBB. (A) PLN dissociation time course. Top: pre-equilibrated PLN at a concentration of ≈ 1 mg/ml was diluted 20-fold and dissociation was allowed to proceed for 90 to 900 s (each experiment was started at different time points to ensure a simultaneous endpoint). Bottom: quantification shows a very slow, but statistically significant ($p < 0.001$) pentamer dissociation and monomer accumulation. Concentrations at $t = 0$ s were calculated from the equilibrium concentration of PLN at 1 mg/ml by division through 20, i.e. assuming no dissociation directly after dilution at $t = 0$ s. **(B)** PLN pentamer concentrations at different total PLN concentrations show no significant differences between unphosphorylated and phosphorylated PLN in TBB (same data as in Figure 1 from the main text). Bars represent mean \pm SD.



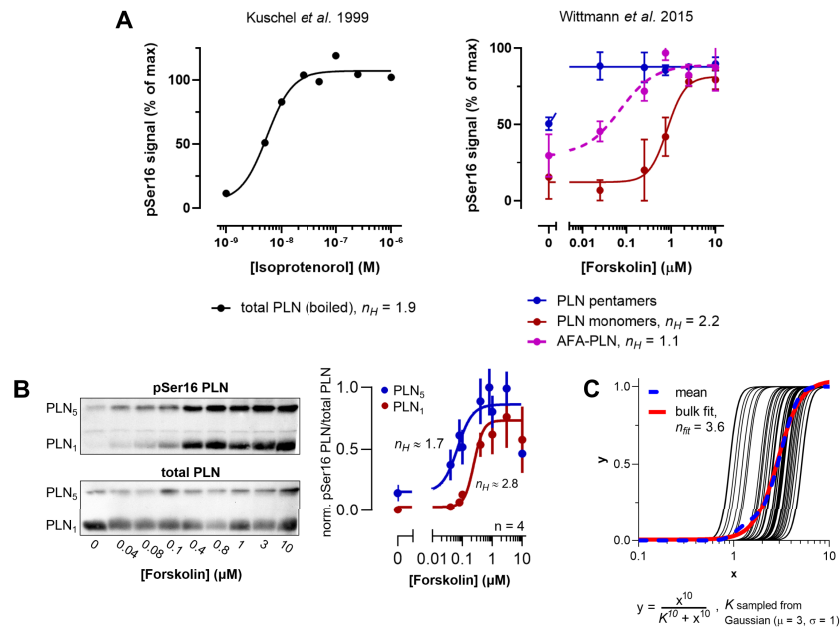


Figure S3

Ultrasensitive PLN phosphorylation. (A) Dose-response data on PLN phosphorylation from the literature was fitted to the Hill-equation with offset. Left: Phosphorylation of total PLN (pentamers were dissociated by boiling) in rat hearts. Right: Differential phosphorylation of PLN monomers and pentamers in transfected and forskolin stimulated HEK293 cells. Note that high Hill-exponents depend on the presence of pentamers. (B) Replication of ultrasensitive PLN phosphorylation in transfected and forskolin stimulated HEK293 cells (this study). Data points represent mean \pm SEM. (C) Although fitted Hill-exponents of experimental data indicate some degree of ultrasensitivity ($n_H \approx 2$), the true response on single cell level could be blunted due to averaging across cells: black lines show 50 Hill-curves generated with $n_H = 10$ and slight variation in the half-saturation constant K . The bulk fit of all curves can lead to reduced Hill-exponents (here: $n_H = 3.6$).

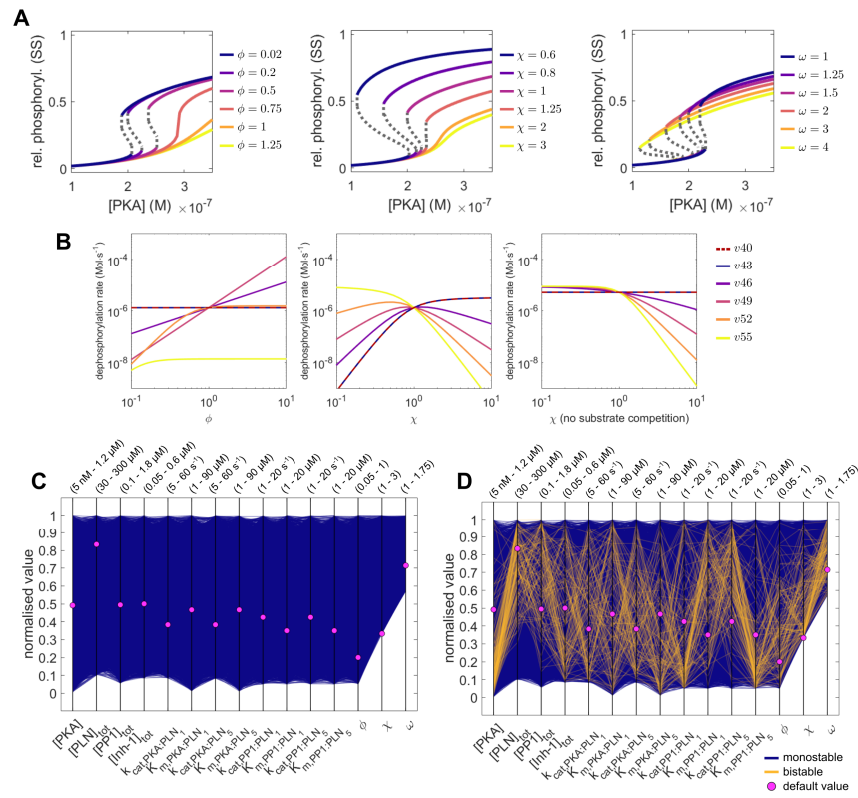


Figure S4

Influence of model parameters on bistability. (A) Bifurcation plots of relative PLN monomer phosphorylation for different strengths and types of PP1 cooperativity (ϕ , χ) and for the dynamic equilibrium of PLN (ω). Parameters, which were not varied, are equal to their default value. (B) PP1 dependent dephosphorylation rates for monomeric and pentameric PLN as a function of parameters ϕ and χ . (C,D) Random sampling of parameters. (C) No bistability could be observed in the absence of pentamers regardless of the values for other kinetic parameters or protein concentrations. (D) Implementing k-type cooperativity (parameter χ) reduces the probability for a parameter set to be bistable as only 1.1% of tested parameter sets showed bistability.

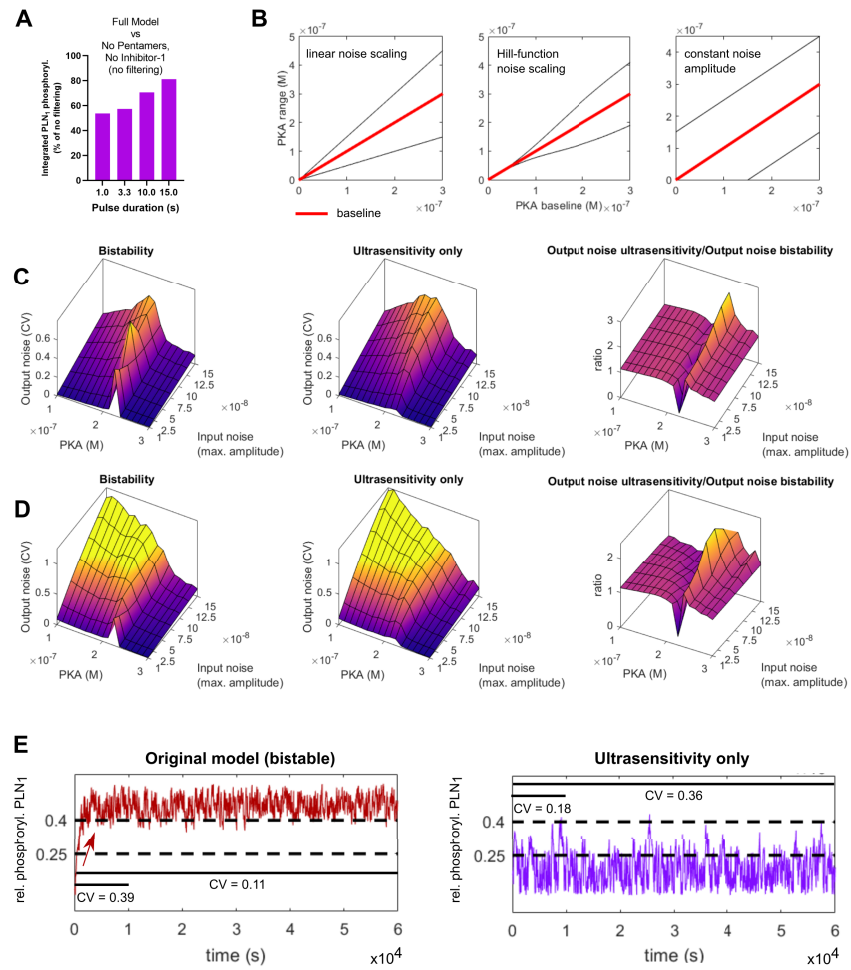


Figure S5

Additional noise-filtering analyses. (A) Comparison of the integrated PLN₁ phosphorylation for 4 subsequent bursts/pulses and different pulse durations in the full model vs the model version without pentamers and inhibitor-1. The difference between the model versions becomes smaller for longer pulses. (B) Alternative noise functions. Left: linear noise underlying the noise landscapes in the main text. Middle: non-linear noise amplitude as a Hill-function of the baseline [PKA] with $K = 2 \times 10^{-7}$ M and $n_H = 2.5$. Right: constant noise amplitude. (C) Absolute and relative noise landscapes with Hill noise. (D) Absolute and relative noise landscapes with constant noise amplitude. (E) Simulation of 1000 fluctuations at 0.225 μM baseline [PKA] and input noise levels of 20% of baseline [PKA] (frequency: 1 min⁻¹). The higher output noise of the bistable model compared to the only ultrasensitive model in short simulations (150 fluctuations) is typically caused by a single switching event (red arrow) and is attenuated in prolonged simulations.

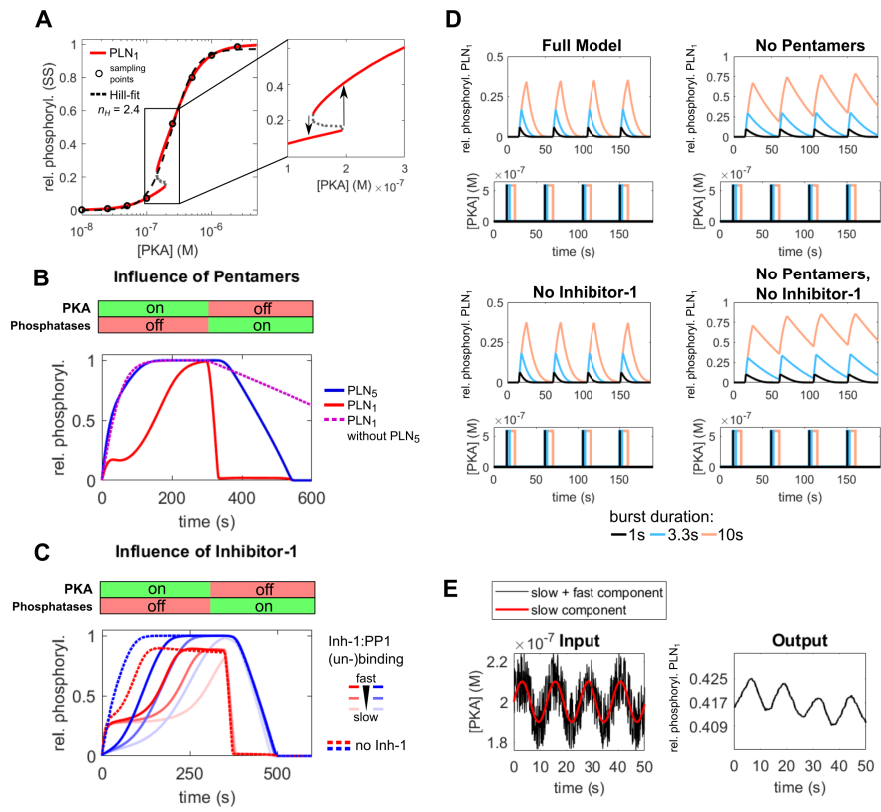


Figure S6

Alternative parameter set with lower ultrasensitivity. (A) Sampling the bifurcation diagram at 8 different points leads to a fitted dose-response curve with a Hill-exponent of $n_H = 2.4$ similar to experimental dose-response data. The parameter set still allows for bistability (with even higher bistable range than with the default parameters) and thus is able to filter out small fluctuations close to the critical threshold. (B,C) The alternative parameter set leads to stronger phosphorylation delay capacities than the default parameter set. Consequently, short PKA activity bursts are filtered out (D) and the PLN network can still act as a low-pass filter (E).

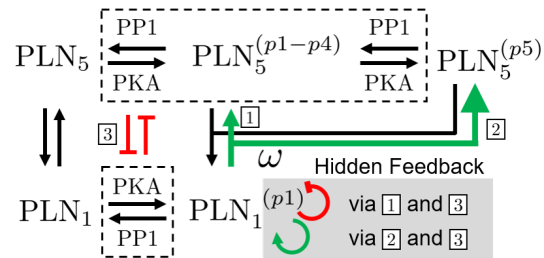


Figure S7

Hidden feedback loops. Since PLN monomers and pentamers compete with each other to be (de-)phosphorylated by PKA and PP1 (3), the dynamic equilibrium could potentially induce hidden feedback loops. First, oligomerization of phosphorylated monomers is in itself a negative auto-loop reducing the amount phosphorylated monomers. If incompletely phosphorylated pentamers are formed (1), monomer phosphorylation could be further decreased due to more pentamers competing with monomers for PKA (3). However, pentamers also compete with monomers for PP1 and could decrease monomer dephosphorylation - particularly if completely phosphorylated pentamers are formed (2). Which of these loops dominates likely depends on the relative reaction velocities among phosphorylation/dephosphorylation steps in a given situation. Hidden feedback loops have been proposed to support the emergence of bistability (see main text for references).

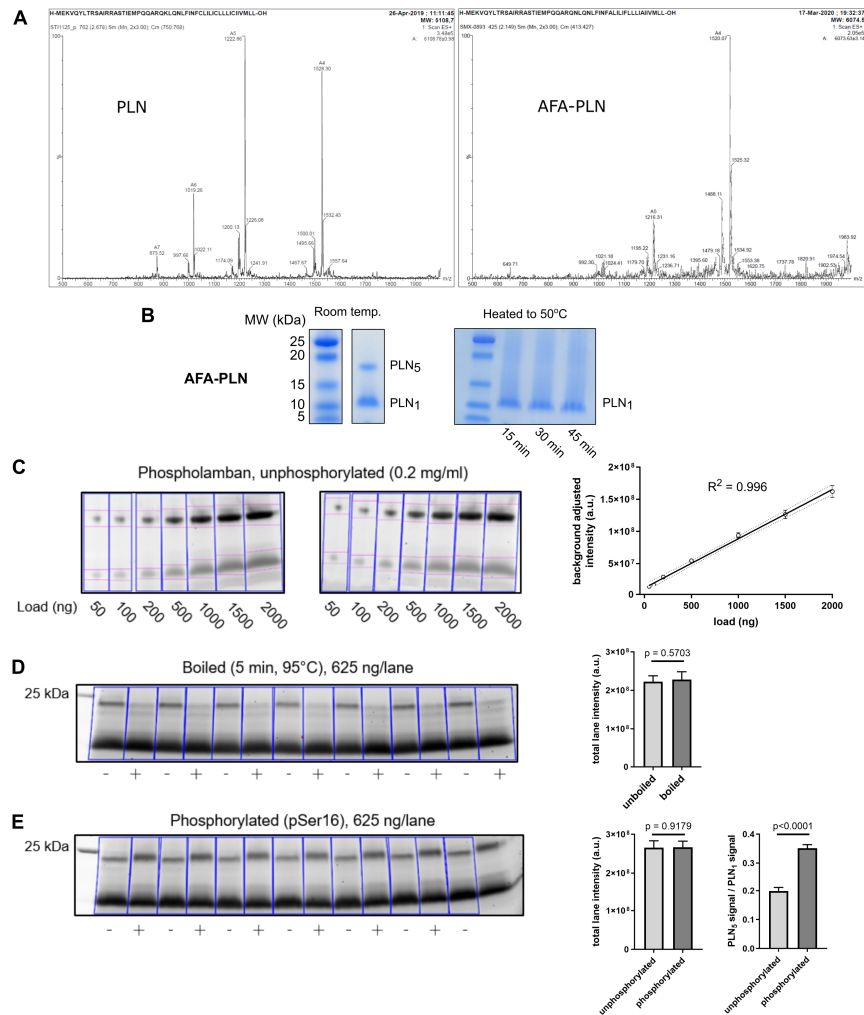


Figure S8

Characterization of synthetic PLN peptides and their quantification via Oriole™ Fluorescent Gel Stain. (A) ES-MS spectra of human wild-type PLN (left) and AFA-PLN (right) show correct molecular weight. **(B)** The Oriole signal of total PLN (monomers + pentamers) in TBB shows excellent linearity for the probed range (50-2000 ng). **(C)** 1 mg/ml of boiled/unboiled PLN in TBB was diluted to 0.05 mg/ml in 1x Laemmli buffer and loaded to the gel. Quantification of total lane intensities suggests that the oligomeric state of PLN does not influence the signal intensity. **(D)** 1 mg/ml of phosphorylated/unphosphorylated PLN in TBB was diluted to 0.05 mg/ml in 1x SDS-sample buffer and loaded to the gel. Quantification of total lane intensities suggests that the phosphorylation state of PLN does not influence the signal intensity. The increased pentamer/monomer signal ratio suggests that Ser16 phosphorylation leads to increased pentamerization in mixed SDS/Triton X-100 micelles. **(E)** SDS-PAGE analysis of the oligomeric status of AFA-PLN at different temperatures and incubation times. 0.33 mg/ml protein concentration, loaded 2 μ l per lane. Bars represent mean \pm SD.

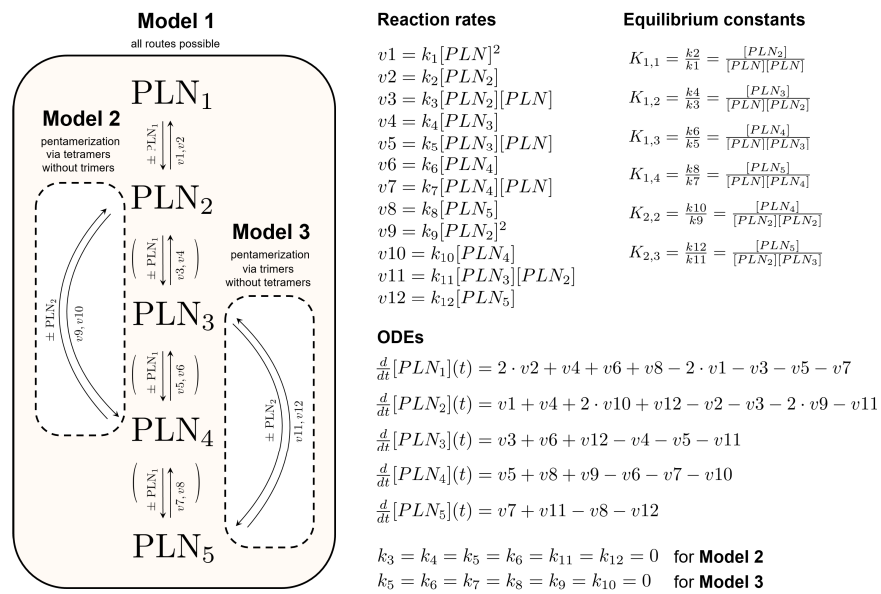


Figure S9
Mass action kinetics based models of PLN pentamerization. The index denotes different oligomer size, PLN_1 for monomers, PLN_2 for dimers and so forth. Model 1 considers all reaction routes possible, whereas model 2 assumes a monomer→dimer→tetramer→pentamer and model 3 a monomer→dimer→trimer→pentamer pathway.

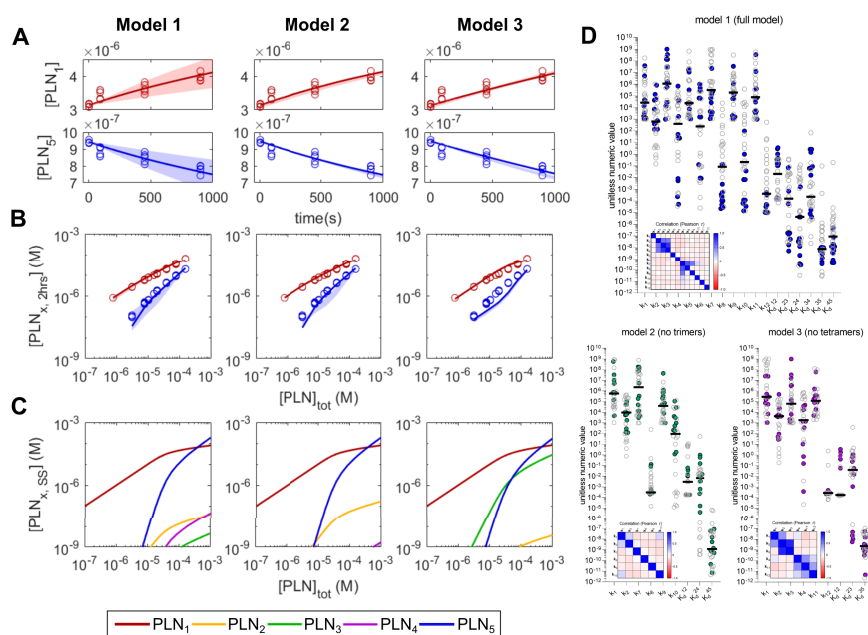


Figure S10

Calibration of the mass action kinetics models. Model fits to experimental dissociation time-course (A) and dilution (B) data. Continuous lines represent results from the best fit parameter sets, circles are experimental data points, shaded areas represent 95% confidence intervals from the ten best parameter sets. (C) Simulated equilibrium concentrations of monomeric and oligomeric PLN at different total PLN concentrations using the best fit parameter set for each model. (D) Distribution of fitted parameter values of 30 independent parameter estimation runs for model 1-3. Parameter values associated with the ten best fits are highlighted in colour. Inset shows correlation matrix of the estimated rate constants.

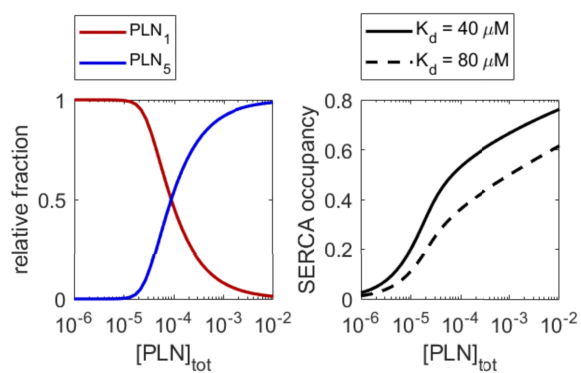


Figure S11
Oligomerization and SERCA occupancy as a function of total PLN concentration. Left: relative fraction of monomers and pentamers as a function of total PLN concentration based on the best fit parameter set for pentamerization model 2. Right: SERCA occupancy by PLN assuming only monomers bind SERCA and that $[SERCA] \ll [PLN]$ so that SERCA binding does not influence pentamerization.

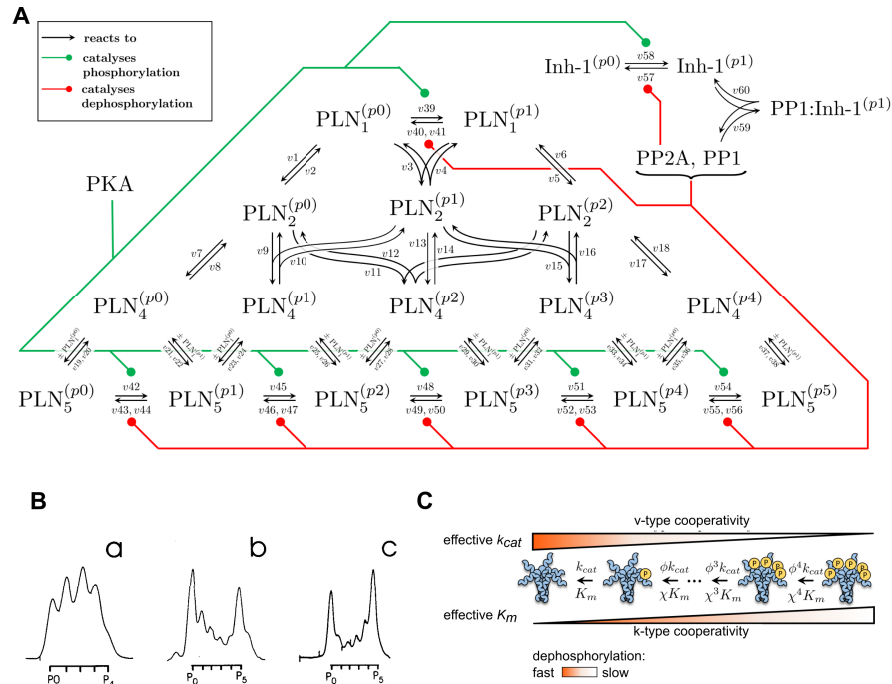


Figure S12

Scheme of the PLN signaling network and kinetic properties of PLN pentamers. (A) Complete reaction scheme of the phospholamban model. (B) Distribution of phosphorylated pentamer species indicated non-cooperative and random phosphorylation of pentamers by PKA (a), but strong positive cooperativity for PLN pentamer phosphorylation by CamKII at Thr17 (b) and dephosphorylation of pentamers after PKA phosphorylation (c). Figure reprinted with permission from Colyer, J. (1998). Phosphorylation States of Phospholamban. *Ann.N.Y.Acad.Sci.* 853, 79-91. (C) Illustration of how positive cooperativity of PLN₅ dephosphorylation is implemented in the model. Positive cooperativity denotes an enhanced reaction velocity after each dephosphorylation step, which could be a result of faster catalytic turnover (v-type cooperativity, i.e. the value of k_{cat} increases after each step) or higher substrate affinity (k-type cooperativity, i.e. the value of K_m increases after each step). For each phosphate group present in a pentamer which is dephosphorylated by PP1, the effective k_{cat} in the model was thus scaled by a factor $\phi < 1$ and/or the effective K_m was scaled by a factor $\chi > 1$.

Supplemental Tables

Table S1

Qualitative predictions for the expected influence of R14del effects on noise-filtering.

R14del effect	Low-pass filtering	Bistability	Based on
Mistargeting of R14del PLN → lower $[PLN]_{tot}$ at SR → lower $[PLN_5]$	↓	↓	sensitivity analysis, Figure S2
destabilization of pentamers → lower $[PLN_5]$	↓	↓	sensitivity analysis, Figure S2
(wildtype/R14del hetero-pentamers → fewer phosphorylation sites)	(↓)	(↓)	(Ortega <i>et al.</i> 2006)